APS SCIENCE 2013

RESEARCH AND ENGINEERING HIGHLIGHTS
FROM THE
ADVANCED PHOTON SOURCE
AT
ARGONNE NATIONAL LABORATORY

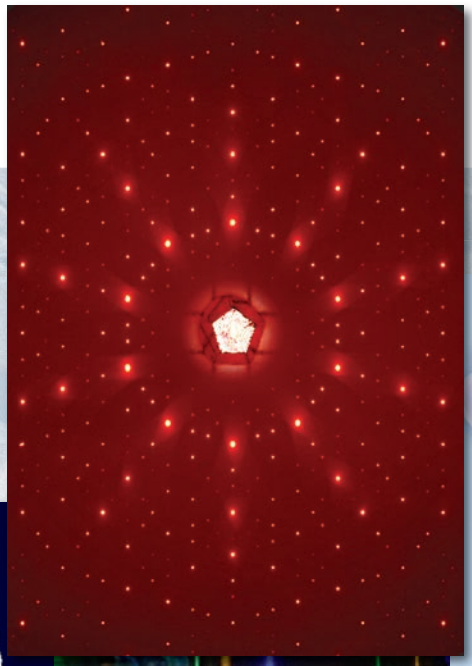

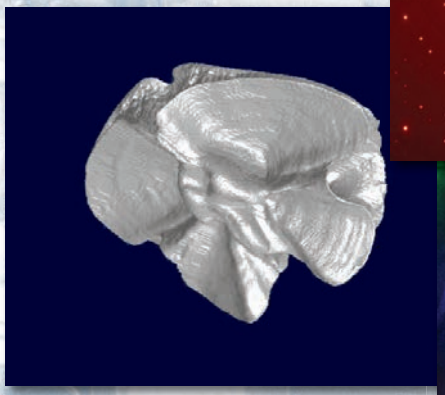

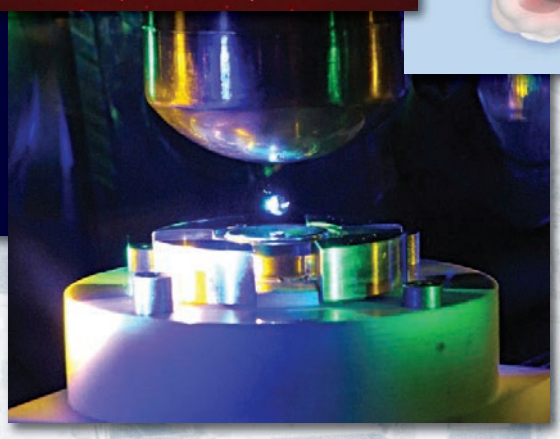

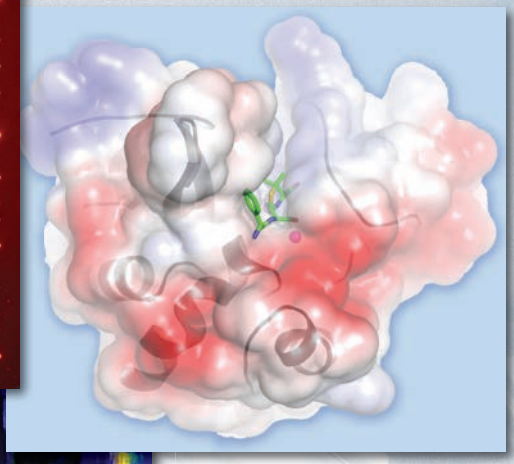

ANL-14/04
ISSN 1931-5015
May 2014

Argonne NATIONAL LABORATORY

ANL-14/04
ISSN 1931-5007
May 2014

The Advanced Photon Source at Argonne National Laboratory is supported by the U.S. Department of Energy, Office of Science, Office of Basic Energy Sciences, under Contract No. DE-ACO2-06CH11357.

About Argonne National Laboratory

Argonne is a U.S. Department of Energy laboratory managed by UChicago Argonne, LLC under contract DE-AC02-06CH11357. The Laboratory's main facility is outside Chicago, at 9700 South Cass Avenue, Argonne, Illinois 60439. For information about Argonne and its pioneering science and technology programs, see www.anl.gov.

See the inside back cover for the key to the cover graphics.

ANL-14/04
ISSN 1931-5007
May 2014

APS SCIENCE

Research and Engineering Highlights from the Advanced Photon Source at Argonne National Laboratory

2013

Argonne NATIONAL LABORATORY

Argonne is a U.S. Department of Energy laboratory managed by UChicago Argonne, LLC
The Advanced Photon Source is an Office of Science User Facility operated for the U.S. Department of Energy Office of Science by Argonne National Laboratory

Table of Contents

APS Organization Chart

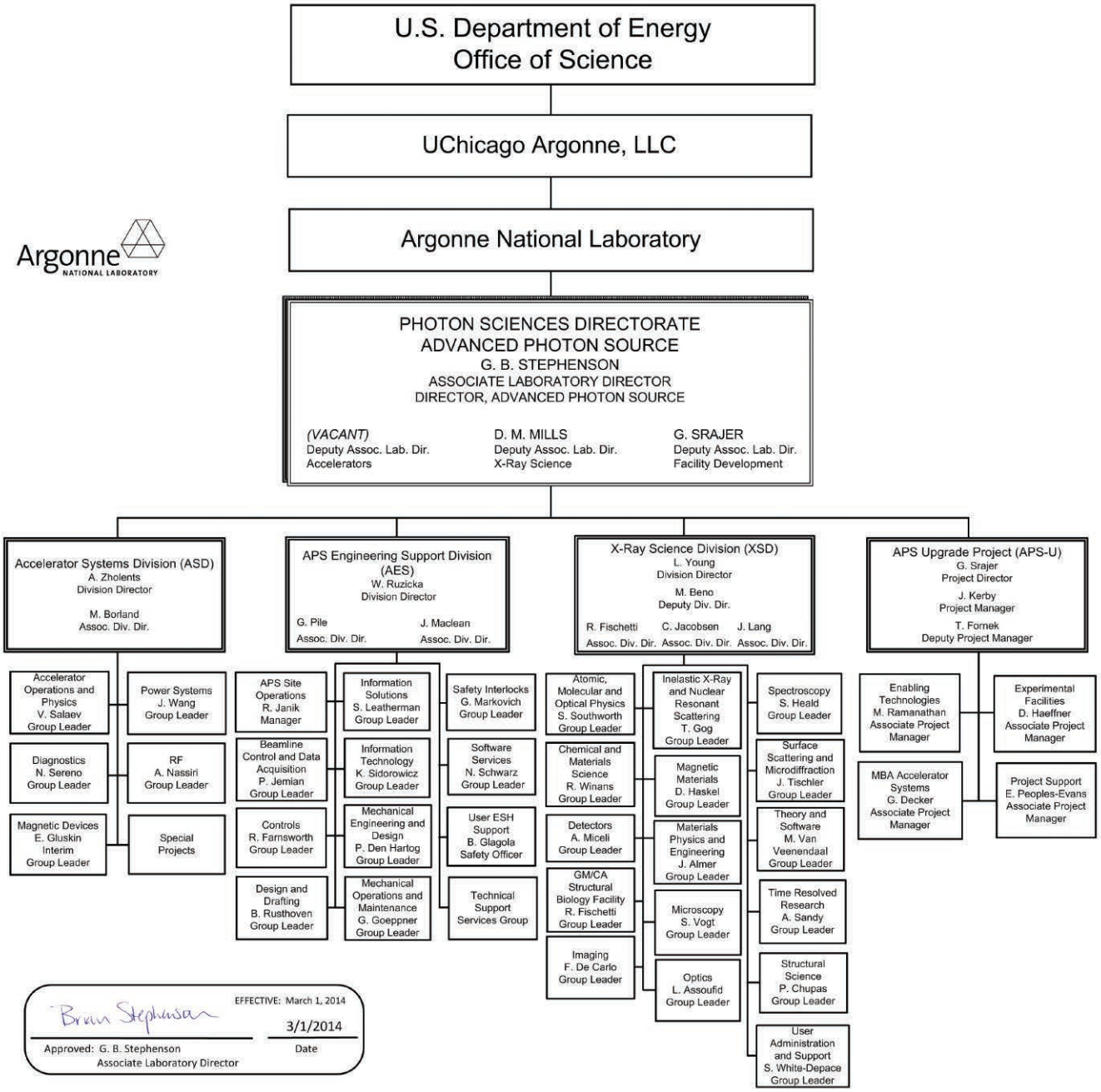

Acronyms for Argonne divisions

AES - APS Engineering Support Division
ASD - Accelerator Systems Division
CEP - Communications, Education, and Public Affairs Division
CSE - Chemical Sciences and Engineering Division
XSD - X-ray Science Division

The Advanced Photon Source Facility at Argonne National Laboratory as of June 2010

The Advanced Photon Source (APS) occupies an 80-acre site on the Argonne National Laboratory campus, about 25 miles from downtown Chicago, Illinois.
For directions to Argonne, see http://www.anl.gov/directions-and-visitor-information.

The APS, a national synchrotron radiation research facility operated by Argonne for the U.S. Department of Energy (DOE) Office of Science, provides this nation's brightest high-energy x-ray beams for science. Research by APS users extends from the center of the Earth to outer space, from new information on combustion engines and microcircuits to new drugs and nanotechnologies whose scale is measured in billionths of a meter. The APS helps researchers illuminate answers to the challenges of our high-tech world, from developing new forms of energy, to sustaining our nation's technological and economic competitiveness, to pushing back against the ravages of disease. Research at the APS promises to have far-reaching impact on our technology, our economy, our health, and fundamental knowledge of the materials that make up our world.

Contact us

For more information about the APS or to order additional copies of this, or previous, issues of *APS Science*, send an email to apsinfo@aps.anl.gov, or write to APS Info, Bldg. 401, Rm. A4115, Argonne National Laboratory, 9700 S. Cass Ave., Argonne, IL 60439, or go to http://www.aps.anl.gov/Science/Reports/ to download PDF versions.

Visit the APS on the Web at www.aps.anl.gov

For links to online content including animations, videos, etc., look for URLs or (for readers of the print version of this book) QR codes (as below). QR codes quickly link smartphone users to the content.
A code reader can be downloaded from, for instance, http://www.quickmark.com.tw/En/basic/download.asp
Adobe Flash may be required for some films.

Welcome

Brian Stephenson

Stephen Streiffer

May 2014

The year 2013 at the Advanced Photon Source (APS) has been a year marked by scientific breakthroughs and capability expansions, making it a highly productive and rewarding year for our staff and users. We have made great progress toward expanding user capabilities, including installing a prototype of a novel superconducting undulator, the first of its kind operated at a third-generation synchrotron x-ray facility (see "First X-rays from the APS Superconducting Undulator," *APS Science 2013*, page 168). Soon after it was turned on, the boost it gave to the APS's high-energy brightness contributed to a groundbreaking discovery by researchers from Ames Lab and Iowa State University of a new type of binary magnetic quasicrystal (page 32).

This was just one of many research breakthroughs from a prolific APS user community that generated about one publication a day in high-impact journals. Complementing the plethora of user publications was an equally impressive string of national awards recognizing the world-leading talent of our users, scientists, and engineers; see page 198 for some examples.

Throughout this report we try to give you a taste of the exciting and boundary-pushing work done by APS users and staff. It is impossible to capture in a single report all of the things that make the APS and its users special, but we hope this will give you at least a small glimpse into the many diverse efforts that go into making the APS a world leader in x-ray science and the nation's most frequented user research facility.

Among the highlights from a busy year: In March, one of the few remaining open sectors in the APS experiment hall was selected as the site for President Obama's visit to Argonne (see page 12), where he presented ideas for future energy research initiatives. Energy research is a major emphasis for Argonne and for experimenters coming to the APS. This issue features some of these results, including investigations into the advantages of mixed-anion iron oxyfluoride conversion electrodes (page 40); new composite materials for life-increasing electrodes in rechargeable lithium-ion (Li-ion) batteries (page 42); and the underlying causes of silicon degradation, silicon being a potentially useful candidate for Li-ion electrodes (page 44). Other battery-related highlights (many in collaboration with the Argonne Center for Nanoscale Materials) are on pages 50, 64, and 66, while solar cells get their due on page 52.

Others delve into the molecular energy contributions to insect flight (page 100); macromolecular crystallography (MX) studies that may result in new vaccines against the human immunodeficiency virus (pages 118 and 120); the role of rusty pipes in the release of strontium into our drinking water (page 156); examinations in the lab of conditions at the center of the Earth (page 164); research on potential anti-cancer therapies (page 170); and, with the Argonne Electron Microscopy Center, a look at new catalysts (page 90).

We strive to give our users the best opportunities possible to create transformational science. In the long term, some fantastic opportunities will come from the proposed APS Upgrade Project, providing a factor of 100 or more in brightness and coherent flux and enabling nanoscale imaging with the full range of powerful x-ray contrast modes. In the near term, continued improvement and innovation will keep expanding the productivity frontier of our existing beamlines. Just a few recent examples of are the installation of a high-energy monochromator at Sector 11, the optimization of the detector and optics at Sector 12, and the upgrade to new state-of-the-art detectors at MX beamlines at sectors 14, 17, 22, 23, and 24.

Construction was finished in 2013 on the $34.5-M, 60,000-sq-ft Advanced Protein Characterization Facility (APCF) adjacent to the APS's suite of MX beamlines. It opened for initial research in March 2014 and will provide state-of-the-art crystallization and robotic systems for the production and structural and functional characterization of proteins and macromolecular

The completed Advanced Protein Characterization Facility. Inset: the APCF main hallway. The APCF will house state-of-the-art robotics for gene cloning, protein expression, protein purification, and protein crystallization.

complexes. This is the only facility of its kind and scale connected to a light source.

Hutches and a laboratory space were built out this year at Sector 35 for the Dynamic Compression Sector (DCS), which will undergo commissioning and have first experiments in mid-2014 (page 194). The shockwave studies enabled here will establish a new paradigm for understanding dynamic compression of materials at multiple length scales. This first-of-its-kind facility will address long-standing scientific challenges with the potential for unprecedented scientific payoff in the areas of structural changes, deformation, fracture, and chemical reactions.

Next year, we'll upgrade areas around the APS ring to offer the tools users have requested to optimize their research. Four new beamlines are expected to enter user operations: DCS at 35-ID, the Intermediate Energy X-ray beamline at 29-ID, the Resonant Inelastic X-ray Scattering beamline at 27-ID (page 188), and the High-Energy Diffraction beamline at 6-BM.

This is the last edition of our *APS Science* highlights book during my term as APS Director. It has been an honor and pleasure to spend the last 3-1/2 years in this role, working with the extraordinary community that makes the APS a global scientific powerhouse. It has also been exciting as the community has enthusiastically joined together to chart the future of the upgraded APS. I'm looking forward to getting back to doing science myself as a user of the APS, which I haven't had much chance to do recently. I leave the APS in the more-than-capable hands of Stephen Streiffer, who will serve as interim during the search for a new director. Stephen is a long-time user of the APS who has been serving as Argonne Deputy Associate Laboratory Director for Physical Sciences and Engineering. I know all of our users and staff will welcome Stephen in his new role and offer him the same support and counsel that has been provided to me. I anticipate reading next year's *APS Science* report as a user and continuing to take inspiration from the creativity, dedication, and passion that this community brings to its research every day.

Brian Stephenson
Argonne National Laboratory
Associate Laboratory Director,
Photon Sciences;
and Director, Advanced Photon Source

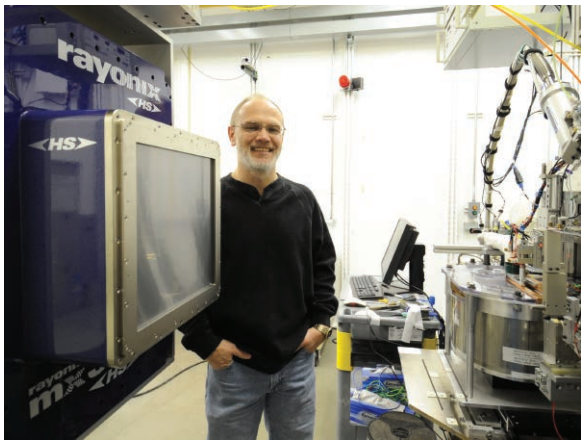

John Chrzas, Sector Manager, SER-CAT, with the Rayonix MX300-HS detector in the 22-BM-D research station. The detector is being commissioned on the bending magnet beamline before being moved to the insertion device line.

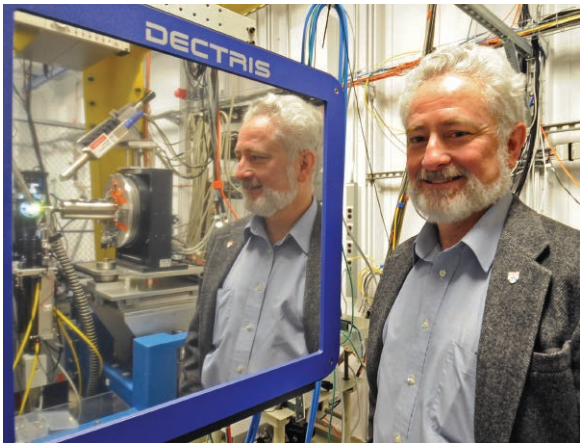

Robert Fischetti, Associate Division Director and Group Leader, GM/CA-XSD, in the 23-ID-D research station with the Pilatus3 6M detector.

The Advanced Photon Source Upgrade Project

George Srajer

May 2014

For several years, accelerator physicists at the APS have been considering the potential benefits of an ultra-low-emittance multi-bend achromat (MBA) lattice for the APS storage ring or other future light source. In July 2013, a joint report by scientists from the x-ray community, the APS, and other U.S. Department of Energy Office of Science light sources — the Advanced Light Source (ALS) at Lawrence Berkeley National Laboratory, the National Synchrotron Light Source-II (NSLS-II) at Brookhaven National Laboratory, and the Stanford Synchrotron Radiation Lightsource at the SLAC National Accelerator Laboratory — outlined the future opportunities from such a highly coherent x-ray source. The report was presented to the Basic Energy Science Advisory Committee Subcommittee on Future X-ray Light Sources. The report of that committee recommended that this new technology be considered for incorporation into the scope of the ongoing APS Upgrade (APS-U). With this endorsement, the APS has moved into high gear, working with our user community to optimize the scientific benefits of such a design and to develop a proposal for an MBA lattice for the APS.

The proposed design for the MBA lattice upgrade will ensure that the APS will remain internationally competitive for many decades to come. The new MBA technology will provide three key improvements over the current APS:

- The ability to focus the full x-ray beam to nanometer-size spots;
- A 100 to 1,000 times increase in coherent flux, thus revolutionizing new capabilities, such as coherent diffraction imaging techniques; and
- A 100 to 1,000 times increase in brightness.

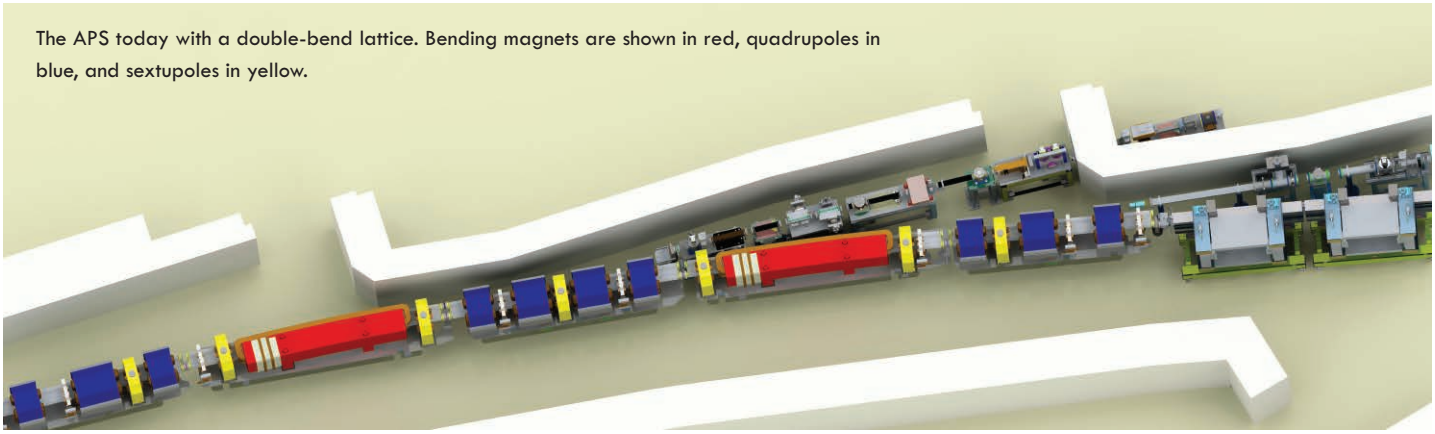

The APS today with a double-bend lattice. Bending magnets are shown in red, quadrupoles in blue, and sextupoles in yellow.

Discussions with the research community have made it clear how these improvements will provide unprecedented opportunities in many areas of science and technology, and the APS user community has embraced the MBA upgrade path. In early October of 2013, we organized more than a dozen meetings with user groups to evaluate the opportunities for using the MBA lattice. We also held several tutorials on the characteristics and capabilities of this new accelerator source. The constructive ideas garnered from these meetings helped focus the topics of discussion at the inaugural "Workshop on Scientific Opportunities Provided by a Multi-bend Achromat Lattice" at the APS held at the end of October. Many ideas for truly transformational science were proposed and collected into a preliminary workshop report that is now available at the APS Upgrade web site: http://www.aps.anl.gov/Upgrade/Workshops/2013/MBA-Technology/includes/aps%20workshop%20report.pdf

At the December 2013 international "Workshop on Diffraction Limited Storage Rings" held at the SLAC National Accelerator Laboratory, the APS Upgrade was a frequent topic of conversation. Discussions in accelerator sessions supported the current approach to developing the APS-U MBA lattice design. In the photon science sessions, the community confirmed the scientific opportunities brought about by this technology and talked about at the APS workshop.

Early 2014 has been very busy with many technical reviews organized by the APS Upgrade Project. The primary goal of these reviews has been to assess whether major components of the accelerator reached the conceptual design level. The topic of the first review in February was on APS MBA lattice beam physics. A committee made up of experts from the European Synchrotron Radiation Facility (France), MAX-IV (Sweden), Soleil (France), Diamond (UK), and NSLS-II and ALS concluded that "the team has made outstanding progress in a short time period towards the conceptual design." While the committee mentioned the

need for continuing studies, it also validated the general approach of the MBA lattice, the choice of the basic technologies, and the current trade-off and boundary conditions. Additional technical reviews in March and April on diagnostic controls, vacuum systems, storage ring installation, magnet and mechanical support, power supplies, and pulsed injection systems generated equally positive comments. Reviewers specifically pointed out the importance of prototyping critical magnets, vacuum systems, and power supplies, and further commented that the integration of beam-physics requirements and engineering solutions is critical to the success of an MBA design. We plan to incorporate the feedback and recommendations from these reviews into technical designs.

We will capture the integration of the new technology into the APS-U plan and describe how it aligns very well with the original science mission. The overarching themes, which were developed in a series of earlier science planning workshops with the community, are:

- Studying real materials under real conditions in real time, and
- Mastering structures across length scales from millimeters to nanometers through x-ray imaging.

Currently, the overall lattice design has converged to a ~70-pm emittance with an integrated three-pole wiggler serving bending magnet beamlines, and an electron energy of 6 GeV. The stored beam current has increased to 200 mA while maintaining the ability to have high flux from individual pulses for dynamics studies. The latest design (http://www.aps.anl.gov/Upgrade/Documents/multi-bend-achromat-lattice.pdf) has improved nonlinear dynamics with a larger injection aperture and longer beam lifetime.

We plan to continue strong interaction with our users through workshops, meetings, and updates in order to optimize the benefits to the different research communities and to provide input into the accelerator design. Concurrently, we are working on developing a revised Science Case for the upgraded APS that will highlight how the MBA lattice technology can push the APS-U capabilities further to answer scientific and technological challenges that today remain beyond our reach.

The coming year promises to be just as exciting and full of successes as 2013. The APS staff are hard at work fine-tuning the accelerator design with input from representatives of sister lightsources in the U.S., Europe, and Asia. Working groups established in the areas of magnets, vacuum, support structures, power supplies, fast injection kickers, controls, diagnostics, radio-frequency systems, tolerances, mechanical systems integration, and electrical systems integration have been meeting on a weekly basis. In addition, system engineering, storage ring installation, supply chain management, and infrastructure are also being addressed at a high level. We are studying various ways to minimize installation time, such as replacing storage ring components simultaneously and implementing other accelerator complex upgrades prior to storage ring installation. Our goal is to execute installation in 12 months. Progress continues on paving the path to a smooth transition through partnerships with sister laboratories to provide user access during the installation time.

The excitement generated by the maturation of this long-awaited technology and the chance to create a fourth-generation storage ring lightsource has made 2013 a year to remember. Incorporation of the MBA lattice really offers once-in-a-lifetime opportunities for the APS and for our user community. With our users' input, we will make sure that we take advantage of the two-to-three orders-of-magnitude increase in brightness to develop and build legacy-making science programs at the APS for decades to come.

I would like to thank the entire APS community, both staff and users, for the support that they have given me over the past two years. It has been a privilege to serve as the Director of the APS Upgrade Project. As we now move into a phase with strong emphasis on accelerator design and construction, we are very happy that Stuart Henderson, a highly respected accelerator expert, has agreed to take over the reins as Project Director on June 1, 2014. Stuart's background and expertise add to the strength of the team and best positions the APS Upgrade to reach its goals. I will remain strongly engaged with the user community in my new role as a deputy to the new interim APS director, Stephen Streiffer. The APS Upgrade is the future of APS and I am excited to do all I can to make it a success.

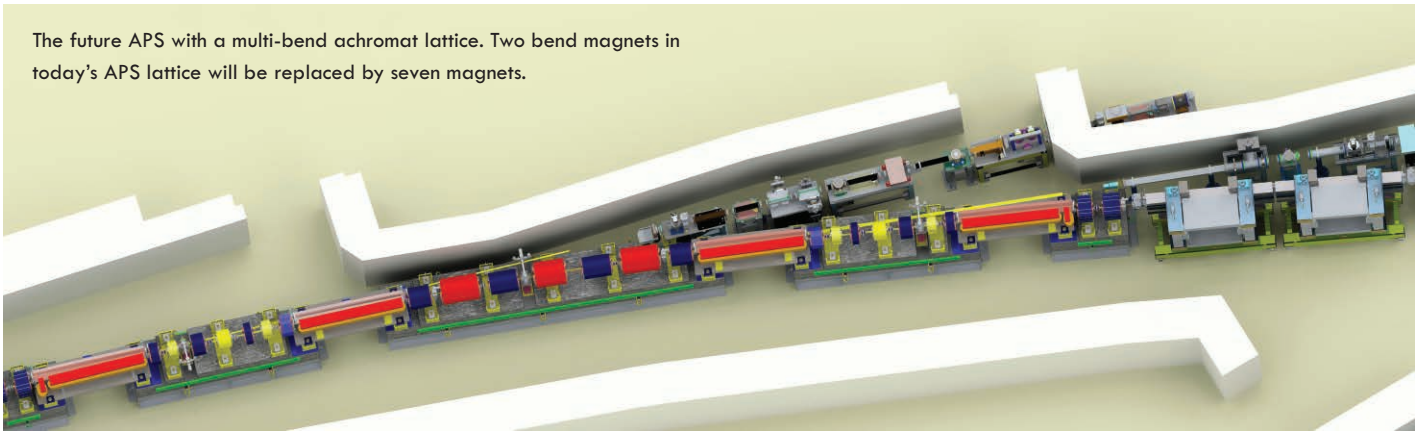

The future APS with a multi-bend achromat lattice. Two bend magnets in today's APS lattice will be replaced by seven magnets.

George Srajer
Argonne National Laboratory
Deputy Associate Laboratory Director, Facility Development, Photon Sciences; and Director, Advanced Photon Source Upgrade Project

The APS Upgrade Project is funded by the U.S. Department of Energy Office of Science under Contract No. DE-AC02-06CH11

Access to Beam Time at the APS

All beam time at the APS must be requested each cycle through the web-based Beam Time Request System. Five types of requests are possible: General User (a researcher not associated with a particular beamline), Partner User (a member of a collaborative access team [CAT], a Partner User proposer, or a member of a collaborative development team), CAT member, CAT staff, and APS staff. Each beam time request (BTR) must be associated with a proposal, but the requirements for each proposal type differ.

The APS User Portal (http://www.aps.anl.gov/Users/aps_userPortal.html) provides access to comprehensive information for prospective and current APS users.

General User proposals and BTRs

Proposals are peer reviewed and scored by a General User Proposal Review Panel, and time is allocated on the basis of scores and feasibility. A new BTR must be submitted each cycle, and for each cycle, allocation is competitive. Proposals expire in two years or when the number of shifts recommended in the peer review has been utilized, whichever comes first.

Partner User proposals and BTRs

Proposals are peer reviewed by a General User Proposal Review Panel and reviewed further by a subcommittee of the APS Scientific Advisory Committee; the final decision on acceptance is made by the APS Deputy Director. Although a new BTR must be submitted each cycle, a specific amount of beam time is guaranteed for up to three years.

CAT member proposals and BTRs

Proposals from CAT members are much shorter, do not expire, and are reviewed by processes developed by individual CATs. A new BTR must be submitted against these proposals for each cycle during which the proposal needs beam time, and allocation/scheduling is determined by the CAT.

CAT and APS staff member proposals and BTRs

These proposals are also very short, do not expire, and are reviewed through processes developed by either the CAT or the APS. A new BTR must be submitted against such proposals for each cycle during which the proposal needs beam time. Each CAT/beamline determines how these BTRs are allocated/scheduled.

ARGONNE NATIONAL LABORATORY 400-AREA FACILITIES

ADVANCED PHOTON SOURCE

(Beamlines, Disciplines, and Source Configuration)

ADVANCED PROTEIN CHARACTERIZATION FACILITY

CENTER FOR NANOSCALE MATERIALS

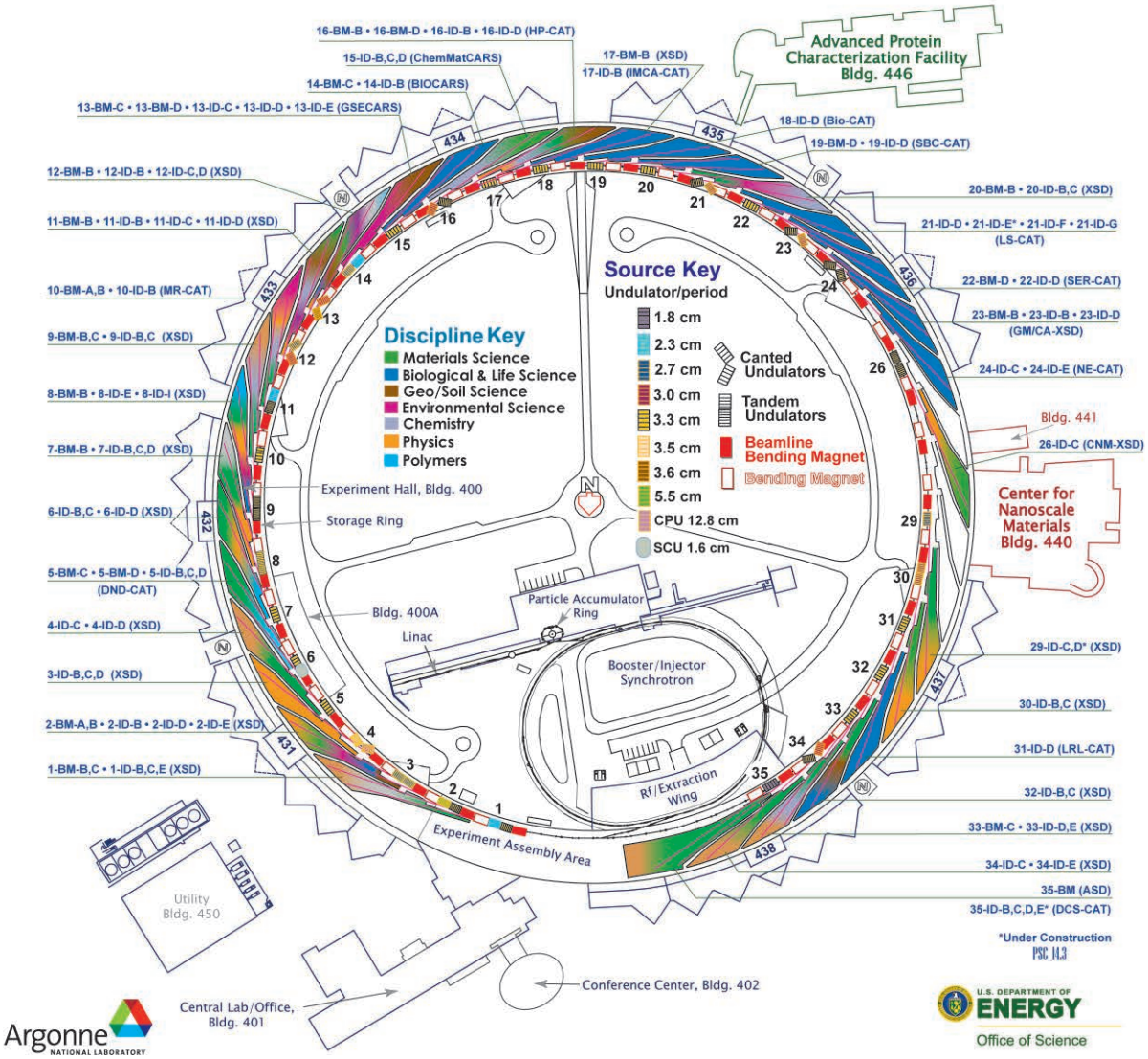

APS SECTORS: At the APS, a "sector" comprises the radiation sources (one bending magnet and nominally one insertion device, although the number of insertion devices in the straight sections of the storage ring can vary), and the beamlines, enclosures, and instrumentation that are associated with a particular storage ring sector. The APS has 35 sectors dedicated to user science and experimental apparatus. **X-ray Science Division (XSD)** sectors comprise those beamlines operated by the APS. **Collaborative access team (CAT)** sectors comprise beamlines operated by independent groups made up of scientists from universities, industry, and/or research laboratories.

Key to the beamline descriptions that accompany each science highlight: Beamline designation • Sector operator • Disciplines • Techniques • Radiation source energy • User access mode(s) • General user status •

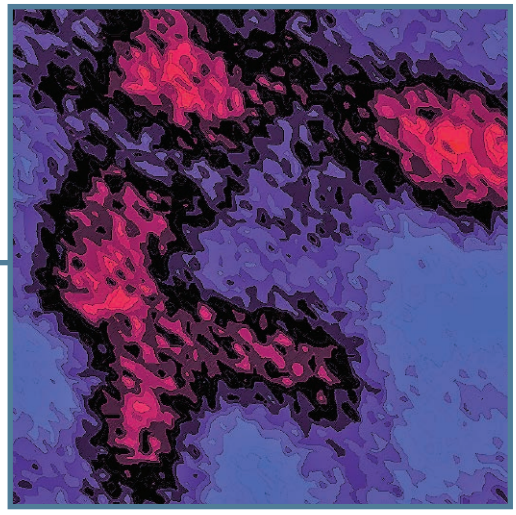

Humanities

X-rays Paint a Picture of Picasso's Pigments

Pablo Picasso is widely regarded as one of the most influential artists of the twentieth century, having pioneered a variety of new styles in painting, sculpture, and other artistic forms. Besides introducing avant-garde art styles, he also innovated in the use of non-traditional materials. For example, a widely-held view has been that Picasso employed the ordinary house paint Ripolin in place of conventional artists' paints in some of his artwork. Over the years art historians have used different approaches in attempting to determine which of Picasso's paintings (if any) incorporate Ripolin. This task is not as straightforward as one might suppose, because many of the ingredients in Ripolin were also present in the artists' paints used by Picasso. A recent collaborative effort between the Art Institute of Chicago and Argonne has demonstrated conclusively that pigment from one of Picasso's paintings is, indeed, derived from the Ripolin-brand house paint of that era. Moreover, x-ray characterization of paint chemical composition can help historians learn about trade movements in ancient times and better determine when an artwork was created. In a broader context, new information about how materials are structured on the molecular level and how chemicals react at the nano-level is pertinent to the development of new materials and technologies.

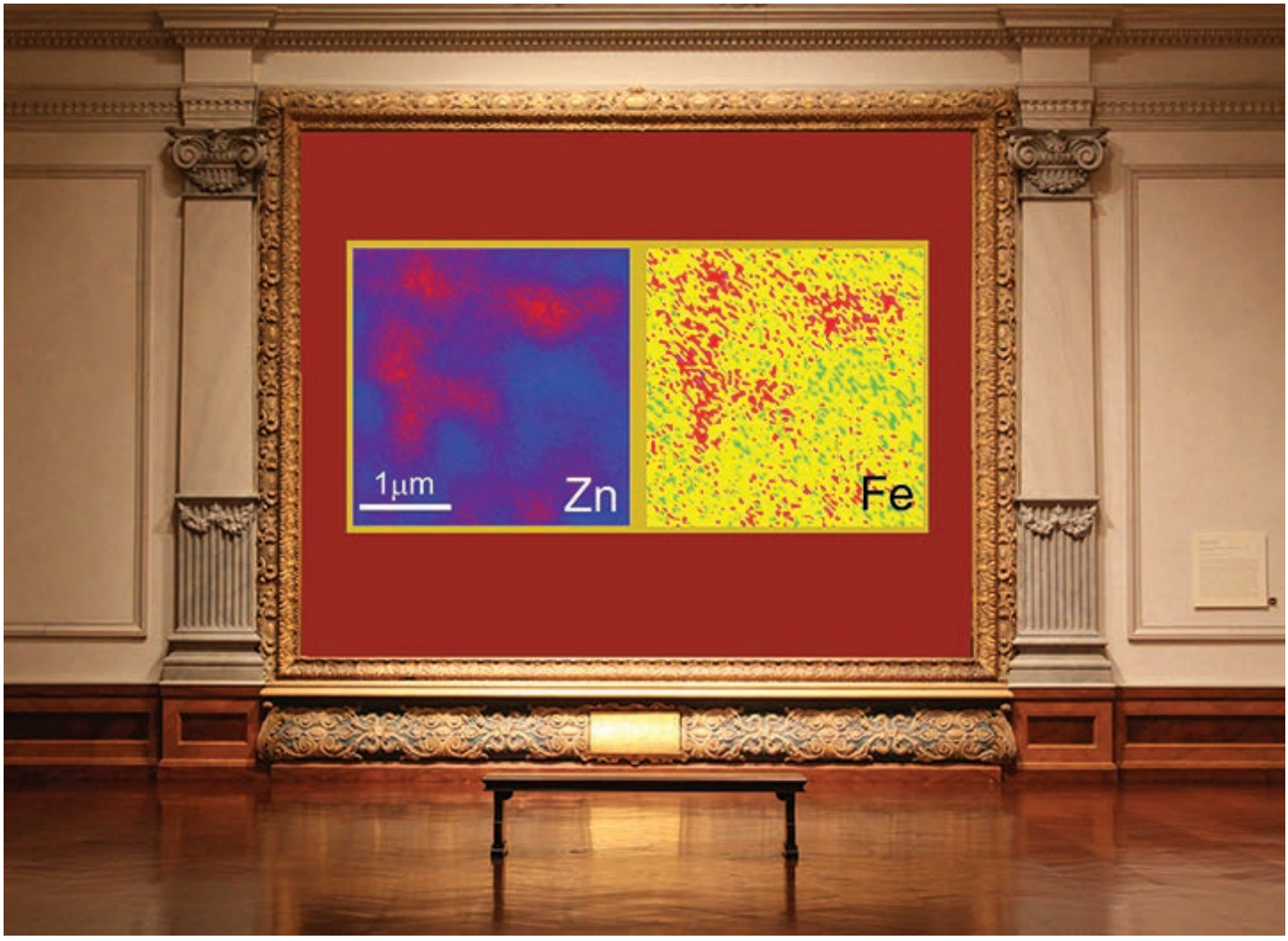

Fig. 1. Fluorescence maps showing the correlation of zinc oxide pigments (labeled Zn) and iron (Fe) impurities in the house paint "Ripolin blanc de neige," originally sold in France in the early twentieth century and used by Pablo Picasso in his artwotks. Background photo: the Rubens Gallery at The John and Mable Ringling Museum of Art by Taty2007. Source: Wikimedia Commons.

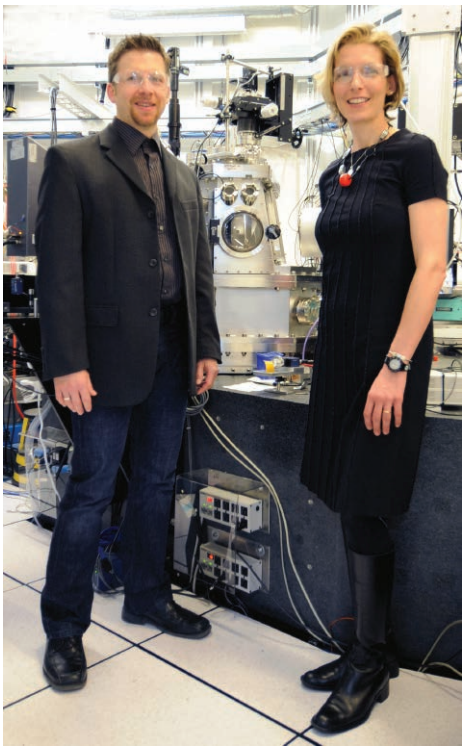

Volker Rose (Argonne) and Francesca Casadio (Art Institute of Chicago) in the Hard X-ray Nanoprobe research station at APS Sector 26. The microscope allowed the scientists to learn that the chemical makeup of paint used by Picasso matched the chemical makeup of the first commercial house paint, Ripolin.

The paints artists utilize normally contain a binder made of synthetic or natural polymers, that imparts a characteristic liquid or pasty consistency so they can easily cover and adhere to a surface. Other paint ingredients include pigments (for color), and additives and fillers that may impart specific characteristics like abrasion resistance or reduced drying time. The binder, pigments, and additives are dispersed throughout a solvent, such as water or mineral spirits, which evaporates as the paint dries.

A specific type and brand of paint can be determined by the proportion and distribution of elements within its ingredients. Many techniques are available for identifying the composition of paintings: multi-spectral imaging (utilizing multiple frequencies of light); portable x-ray fluorescence imaging; x-ray diffraction performed at synchrotron facilities; and several others. None of these techniques, however, has proven capable of discerning the composition and distribution of elements within the pigment particles found in many paints. Zinc oxide pigments, for instance, range in size from 200 to 1,000 nm (0.2 to 1 μm). Conventional analytical and imaging techniques are often incapable of determining whether a particular element resides in the fillers, additives, or pigments of a particular paint.

The Hard X-ray Nanoprobe, situated on the 26-ID beamline of the APS and operated jointly by the APS and the Argonne Center for Nanoscale Materials, is capable of determining element distribution with exquisite precision. Combining the trace element sensitivity of x-ray fluorescence and a highly-precise positioning system, the nanoprobe can map the distribution of elements at spatial resolutions down to 30 nm. With such high resolving power and chemical sensitivity, the distribution of elements within individual pigment particles can be precisely determined.

X-ray fluorescence generally relies on exciting the electrons close to an atom's nucleus. For this research a monochromator was utilized to select x-ray photons possessing an energy of 10 keV, which is slightly over the *K*-shell binding energy of zinc (*K*-shell electrons are closest to the nucleus). Any *K*-shell electrons absorbing photons of this energy were ejected from their zinc atoms; subsequently, an electron from a more distant orbital shell "jumped down" to fill the *K*-shell, releasing a photon with energy equaling the difference in the two shells' binding energies. An x-ray detector registered these fluorescence photons. This same technique was also utilized to measure and quantify the distribution of other elements present in the paint samples.

An extremely small sample of paint (less than 0.5 mm) extracted from the front of a Picasso painting thought to contain Ripolin, titled *Still Life with Three Fish, Moray Eel and Lime on White Ground*, was examined using the nanoprobe. Also examined were artists' paints of French origin, along with samples of Ripolin house paints from France and the United States, all dating from roughly the same era.

Results showed that zinc oxide particles of French origin contained small amounts of iron (Fig. 1), with no measurable cadmium or lead. This high purity level is indicative of chemically-derived pigments, which were present in the French-manufactured zinc oxide particles in both artists' and Ripolin house paints. The artists' paints, however, possessed additional pigments and fillers — for instance, significant amounts of calcium particles — that were absent from the Ripolin. This evidence shows that paint from Picasso's *Still Life…* most closely matches the composition of Ripolin sold in France at that time.

Interestingly, U.S.-manufactured Ripolin house paint featured zinc oxide particles with a significant lead component, indicating a less-refined mineral source for its zinc oxide pigment.

The researchers involved in this project see the Hard X-ray Nanoprobe as an important new tool that complements the results of more conventional methods in the nanoscale analysis of historical artwork. At the same time, the scientists also learned about the role of impurities in zinc oxide, offering important clues to how zinc oxide could be modified to improve performance in a variety of products, including sensors, light-emitting diodes, and energy-saving windows, as well as liquid-crystal displays for computers, TVs, and instrument panels. *— Philip Koth*

See: Francesca Casadio[1]* and Volker Rose[2]**, "High-resolution fluorescence mapping of impurities in historical zinc oxide pigments: hard X-ray nanoprobe applications to the paints of Pablo Picasso," Appl. Phys. A **111**, 1 (2013). DOI:10.1007/s00339-012-7534-x

Author affiliations: [1]The Art Institute of Chicago, [2]Argonne National Laboratory
Correspondence: *fcasadio@artic.edu, ** vrose@anl.gov

Scientific research at the Art Institute of Chicago is generously supported by the A.W. Mellon Foundation, the Grainger Foundation, the Barker Welfare Foundation, and the Stockman Family Foundation. Use of the Advanced Photon Source and the Center for Nanoscale Materials, Office of Science User Facilities operated for the U.S. Department of Energy (DOE) Office of Science by Argonne National Laboratory, was supported by the U.S. DOE under Contract No. DE-AC02-06CH11357.

26-ID-C • CNM/XSD • Physics, materials science • Nanofluorescence imaging, microdiffraction, nanotomography • 8-12 keV • On-site • Accepting general users •

PRESIDENT OBAMA AT THE ADVANCED PHOTON SOURCE

President Obama in the APS experiment hall.

President Barack Obama visited Argonne National Laboratory on Friday, March 15, 2013, where, according to a story that appeared in *The New York Times* he "spoke inside a building housing a giant X-ray [machine] known as the Advanced Photon Source, described by Argonne officials as the brightest source of X-rays in the Western Hemisphere. The facility allows scientists to explore materials on a nanoscale and to study ways to improve engine combustion."

An article and video of the President's visit can be found on the Argonne Web site at http://www.anl.gov/articles/president-calls-new-energy-security-trust-during-argonne-visit.

More Argonne photos of the visit are at: http://www.flickr.com/photos/argonne/sets/72157632993416759/

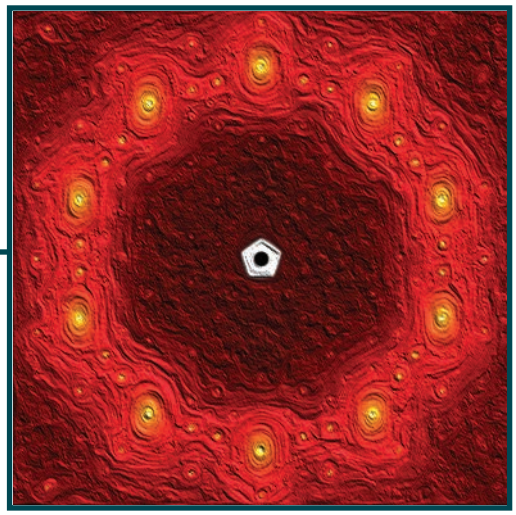

Electronic & Magnetic Materials

Teasing Out the Nature of Structural Instabilities in Ceramic Compounds

For some time, materials scientists have been preparing artificial ceramic systems that simply do not exist in nature, allowing scientists to engineer particularly interesting and even technologically applicable behaviors. But sometimes nature itself finds ingenious solutions to physical problems that we have not been able to solve. An international team of researchers utilized high-brightness x-rays from the APS, as well as a European Synchrotron Radiation Facility (ESRF) beamline, to study the rare-earth magnetic material europium titanate ($EuTiO_3$). In a magnetic field, the (near) optical properties of $EuTiO_3$ change quite dramatically, presenting hope of a strong magneto-electric material often dreamed of by engineers for use in combining magnetic and charge parameters for many memory, processing, and sensor devices.

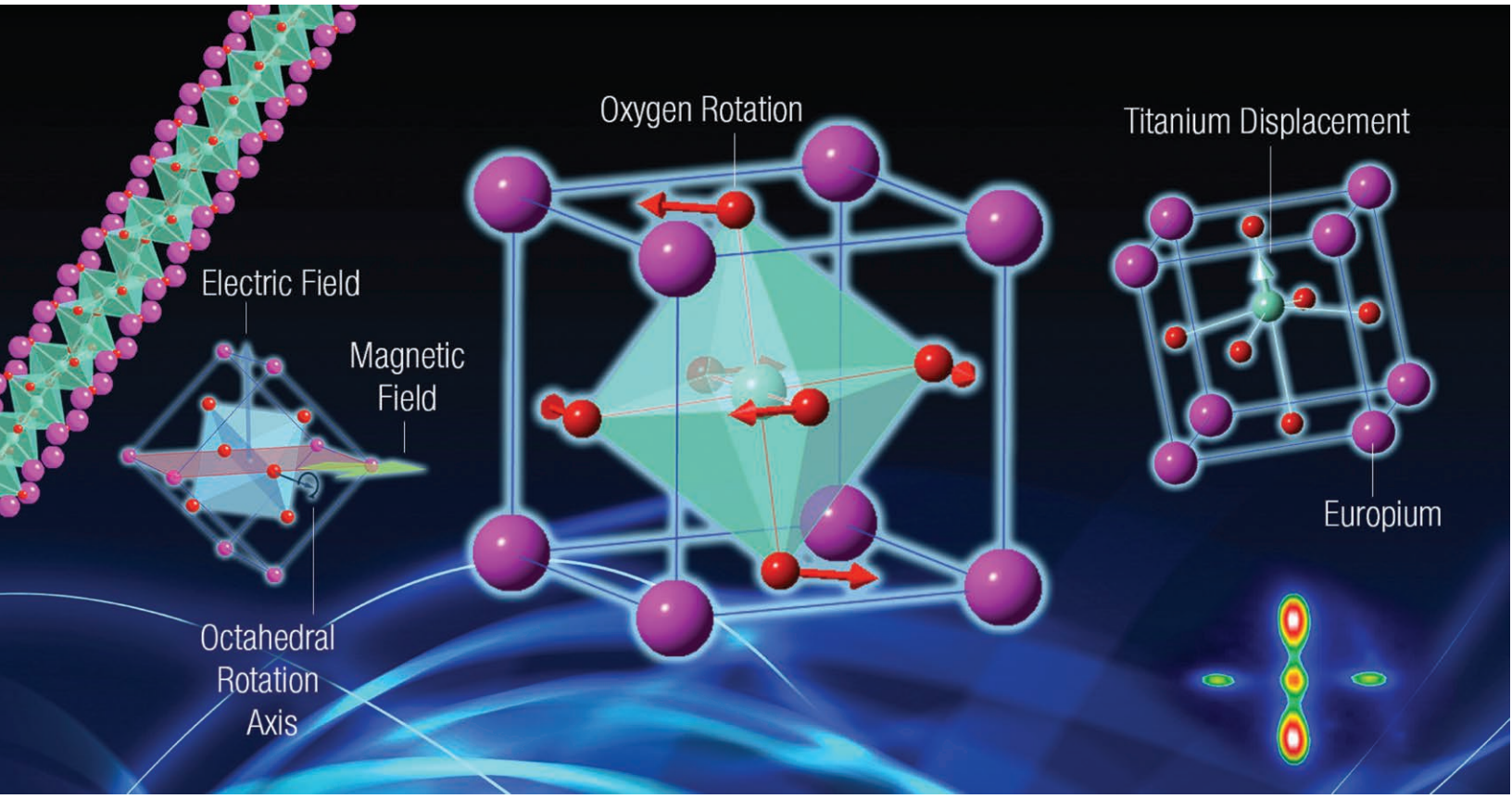

Fig. 1. The simple perovskite structure of $EuTiO_3$ illustrated above shows the essential competing structural instabilities. At the center of the figure is the oxygen cage rotation, and to the right is the central titanium displacement. X-ray diffraction studies showed that, to accommodate the incompatibility of these distortions, they naturally form a long, inter-digitized superstructure (illustrated at far left), which allows them to coexist. Ultimately, this research demonstrates that when both electric and magnetic fields are applied as the europium spins align, the oxygen cage responds, mediating communication between the titanium electric and europium magnetic parameters. Illustration by Renee Carlson, CEPA, Argonne.

Emerging ceramic materials are displaying a tantalizing array of characteristics that could find application in existing and new technologies including magnetic, piezoelectric, ferroelectric, metal insulator transitions, and even superconductivity. Most interesting to physicists is the delicate nature balancing the underlying parameters that drive each quality. If one introduces a different mix of materials, perhaps replacing one element with another or even slightly distorting the structure, then one parameter disappears while another emerges. How all the separate electronic orbits behave and interact with respect to, and with, each other is a fascinating arena for scientists seeking to understand ceramics, a well-known and ancient material family.

A small subgroup referred to as the "tetravalent titanium pseudo-perovskites" have a particularly interesting and well known characteristic. Typically, they fall into either ferroelectric (a permanent electric polarization by application of an electric field) or paraelectric (a temporary electric polarization via an electric field) categories. This division is driven by two prominent phonon instabilities, which generally compete to dominate the materials structure and thus its electric behavior.

Some of the more ubiquitous members of this family include strontium titanate ($SrTiO_3$), calcium titanate ($CaTiO_3$), lead titanate ($PbTiO_3$), and barium titanate ($BaTiO_3$). The first two ($SrTiO_3$ and $CaTiO_3$) are very common and prototypical of the perovskite structure. Both of these systems experience a structural response whereby the oxygen cage tilts and or rotates within the cubic unit cell.

On the other hand, the latter two examples ($PbTiO_3$ and $BaTiO_3$) do not exhibit oxygen distortion but rather the central atom, the titanium, moves away from the center of the sample unit cell. This shift generates a non-neutral electric polarity and with it an internal electric field. Moreover, by applying an electric field, all the titanium atoms can be switched across the center, changing the direction of the polarity and making it a true ferroelectric material.

The researchers in this study, from Argonne, the University of Liverpool (England), the ESRF (France), Universidad de Castilla-la Mancha (Spain), and the Swiss Federal Laboratories for Materials Science and Technology studied a less common member of the same family, europium titanate ($EuTiO_3$), utilizing x-ray diffraction measurements performed on the XSD beamline 6-ID-B,C beamline at the APS and the XMaS beam line at the ESRF. This rare-earth magnetic version has the additional oddity that it demonstrates an anomalous magneto-dielectric character: In a magnetic field, the (near) optical properties change quite dramatically. This presented hope of a strong magneto-electric material often dreamed of by engineers for use in combining magnetic and charge parameters for many memory, processing, and sensor devices.

Ferroelectricity is a very useful commodity, and the oxygen octahedral rotations can inhibit the potential for generating ferroelectricity. But how do these structural instabilities interact and through what mechanism are they coupled?

What surprised the team was evidence of both an oxygen cage structural distortion and a titanium displacement coexisting. What they found was a scenario whereby the two instabilities were well balanced and the system as a whole didn't reconcile a preferred state (Fig. 1).

The result of a complicated superstructure allowing both parameters — in a sense, inter-digitized and therefore spatially separated — resolves the issue of how the competing mechanisms exist in one structure.

Ultimately, the team demonstrated that, with coupled electric and magnetic field application one could monitor the structural response of the oxygen cage rotation, suggesting that the oxygen ion itself plays a role in mediating the magnetism of the europium ions and the electric parameter of the titanium ions and is not, as previously thought, a passive player in the magneto-dielectric phenomenon. — *Philip J. Ryan*

See: Jong-Woo Kim[1]*, Paul Thompson[2], Simon Brown[2], Peter S. Normile[3], John A. Schlueter[1], Andrey Shkabko[4], Anke Weidenkaff[5], and Philip J. Ryan[1]**, "Emergent Superstructural Dynamic Order Due to Competing Antiferroelectric and Antiferrodistortive Instabilities in Bulk $EuTiO_3$" Phys, Rev. Lett. **110**, 027201 (2013). DOI:10.1103/PhysRevLett.110.027201
Author affiliations: [1]Argonne National Laboratory, [2]University of Liverpool and European Synchrotron Radiation Facility, [3]Universidad de Castilla-la Mancha, [4]Swiss Federal Laboratories for Materials Science and Technology
Correspondence:
** pryan@aps.anl.gov,
* jwkim@aps.anl.gov

Work at Argonne and use of the Advanced Photon Source was supported by the U.S. Department of Energy Office of Science under Contract No. DE-AC02-06CH11357. Funding for sample growth is provided by Schweizerischer Nationalfonds National Centre of Competence in Research MaNEP. P.J. Ryan acknowledges additional funding from the University of Liverpool and Aer Lingus Group Plc.

6-ID-B,C • XSD • Physics, materials science • Magnetic x-ray scattering, anomalous and resonant scattering (hard x-ray), general diffraction, grazing incidence diffraction, surface diffraction (UHV) • 3.2-38 keV • On-site • Accepting general users •

$PbTiO_3/SrTiO_3$ Superlattice Components Respond Differently in an Electric Field

A ferroelectric-dielectric superlattice is a precisely formed stack of atoms created by depositing alternating ultrathin layers of a ferroelectric material, such as lead titanate ($PbTiO_3$), and a dielectric material such as strontium titanate ($SrTiO_3$). Researchers utilized the APS to conduct *in situ* time-resolved x-ray microdiffraction experiments in which the changes occurring in the domain pattern and atomic structure of a superlattice were probed with a resolution of 100 ps. Among the key results of this study, the researchers found that the ferroelectric and dielectric components responded differently to the applied field in reaching the uniformly polarized state. Insight into the origin of the time-domain properties of superlattices has the potential to extend the functionalities of complex oxides by providing the means to tune the field and time dependences of their electronic properties, perhaps paving the way for their use in new, multifunctional microelectronic devices.

In weakly coupled $PbTiO_3/SrTiO_3$ (PTO/STO) superlattices, the electrical polarization arising from the crystal structure is distributed unequally between the component layers. The unequal distribution leads to formation of a complex domain pattern consisting of a series of nanoscale stripes of differing polarization. An applied electric field distorts the domain structure and ultimately transforms the superlattice to a uniformly polarized state containing no domains. The changes in the polarization-domain configuration and atomic structure within each component layer during the application of the electric field are not yet understood, partly because the transformation to a uniform polarization state takes place over a nanosecond time scale.

The researchers from the University of Wisconsin-Madison, Stony Brook University, and Argonne considered the structural changes following application of the electric field as occurring in two time regimes. In the first regime, which persists for durations of 1 ns to 100 ns after the onset of the electric field, the striped domain geometry remains but becomes metastable. In the second intermediate regime, the superlattices transform to a uniformly polarized state in some areas while remaining as metastable striped domains in other areas (Fig. 1).

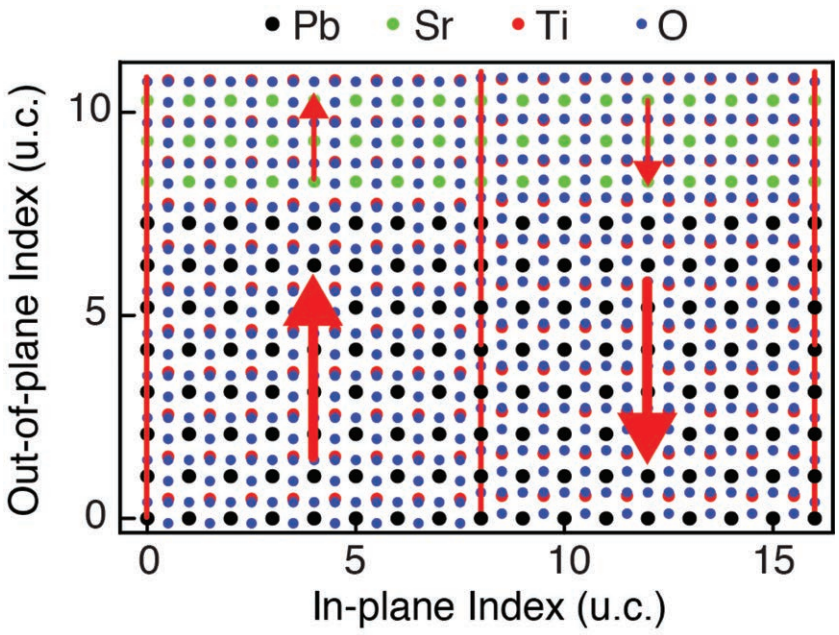

Fig. 1. The atomic arrangement within a PTO/STO SL showing the striped domain pattern. As indicated by the arrows, the polarization is distributed unequally between the component layers, having a smaller magnitude within the STO component.

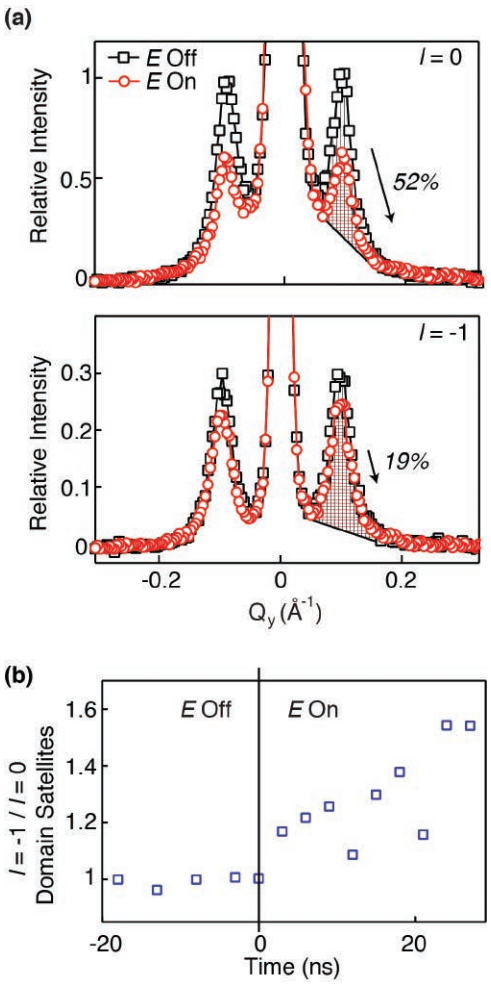

Fig. 2. (a) The striped domains of the superlattice are represented by pairs of domain-related x-ray diffuse scattering peaks, offset from the intense structural reflections at the center of the plots. The domain-related intensity of the satellites decreases more rapidly for the $l = 0$ peak under an electric field. (b) The evolution of the domains is captured by the changes of the domain satellites having different Miller indices. The ratio of the intensities of the $m = 2, l = 1$ to $m = 2, l = 0$ domain satellites increases under the application of a 2.12 MV/cm electric field.

In the first time regime, the intensity of the domain-related x-ray scattering decreased gradually as the overall domain population declined. The experimenters found, however, that the rate of this decrease depended on the Miller indices (a notation system in crystallography for planes in crystal lattices) of the planes associated with the satellite reflections, indicating that additional structural changes accompanied the transformation (Fig. 2).

The researchers gained insight into the structural changes occurring in the domains by carrying out time-resolved x-ray microdiffraction experiments at XSD beamline 7-ID-B,C,D of the APS and analyzing the electric field-induced changes in x-ray intensities in terms of a kinematic x-ray diffraction simulation. Such an analysis showed that the initial distortion of the domains is consistent with the development of polarization in the STO layers.

During the initial 20 ns after application of the electric field, the domain structure responded with a distortion that increased the polarization in the STO layers but not in the PTO layers. Two mechanisms that could lead to the increased polarization in the STO layers were considered: (1) the walls between the nanodomains within the STO layers shifted due to the applied electric field, or (2) the relative positions of the atoms within the STO layers changed in the field. In both cases, the electric field would change the average polarization of the STO and produce intensity changes of the domain satellites that were consistent with the x-ray measurement.

At later times, the domain pattern disappeared and only structural superlattice x-ray reflections remained. The annihilation of the domain walls removed a mechanical constraint that suppressed piezoelectric distortion within the striped domains. With the constraint lifted, the superlattices exhibited an out-of-plane lattice expansion.

In addition, the intensity of the superlattice structural reflections changed in a way that depended on the distribution of piezoelectric distortions within the repeating units of the superlattices. By comparing the empirical results to predictions from a range of structural models, the researchers found that the intensity variation in the superlattice structural reflections showed that the STO layers expanded more than the PTO layers in applied electric fields. The larger piezoelectric distortion in the STO layers matched the expectation that the electric field increases the initially small polarization of STO and produces a correspond- ingly larger piezoelectric expansion.

Taken together, these two results show that the relatively weak polarization of the STO layers in a PTO/STO superlattice has important effects on the evolution of the domain pattern and atomic structure in applied electric fields.

The layer-dependent evolution of the nanometer-scale polarization configuration and the associated structural distortion were both consistent with theoretical predictions that applied fields lead to large increases in the polarization of the STO component.

— Vic Comello

See: Pice Chen[1], Margaret P. Cosgriff[1], Qingteng Zhang[1], Sara J. Callori[2], Bernhard W. Adams[3], Eric M. Dufresne[3], Matthew Dawber[2], and Paul G. Evans[1]*, "Field-Dependent Domain Distortion and Interlayer Polarization Distribution in $PbTiO_3/SrTiO_3$ Superlattices," Phys. Rev. Lett. **110**, 047601 (2013).
DOI:10.1103/PhysRevLett.110.047601
Author affiliations: [1]University of Wisconsin-Madison, [2]Stony Brook University, [3]Argonne National Laboratory
Correspondence:
* evans@engr.wisc.edu

This research was supported by the U.S. Department of Energy Office of Science, Basic Energy Sciences, Division of Materials Sciences and Engineering under Grant No. DE-FG02- 10ER46147 (P.E.). M.D. acknowledges support from the National Science Foundation through Grant No. DMR-1055413. Use of the Advanced Photon Source at Argonne National Laboratory was supported by the U.S. Department of Energy Office of Science under Contract No. DE-AC02-06CH11357.

7-ID-B,C,D • XSD • Materials science, atomic physics, chemistry • Time-resolved x-ray scattering, time-resolved x-ray absorption fine structure, phase contrast imaging • 6-21 keV • On-site • Accepting general users •

The Electronic Origin of Photoinduced Strain

Multiferroics are in a class of materials that exhibits more than one ferroic order simultaneously. One of the prototypical multiferroics is $BiFeO_3$, an important material because it is one of a few that exhibit both ferroelectricity and magnetism at room temperature. The interaction of $BiFeO_3$ with light has attracted great attention because optical control of either magnetism, ferroelectricity, or both has implications for future electronic devices. The origin of a large photoexcited structural change in $BiFeO_3$ was not well understood because of the lack of direct experimental evidence, preventing a rational design for future optomechanical and optoelectrical applications using ferroelectric and multiferroic materials. But research at the APS has revealed the electronic origin of the interaction between optical light using a nanometer-thick layer of BFO at the atomic level and ultrafast time scales.

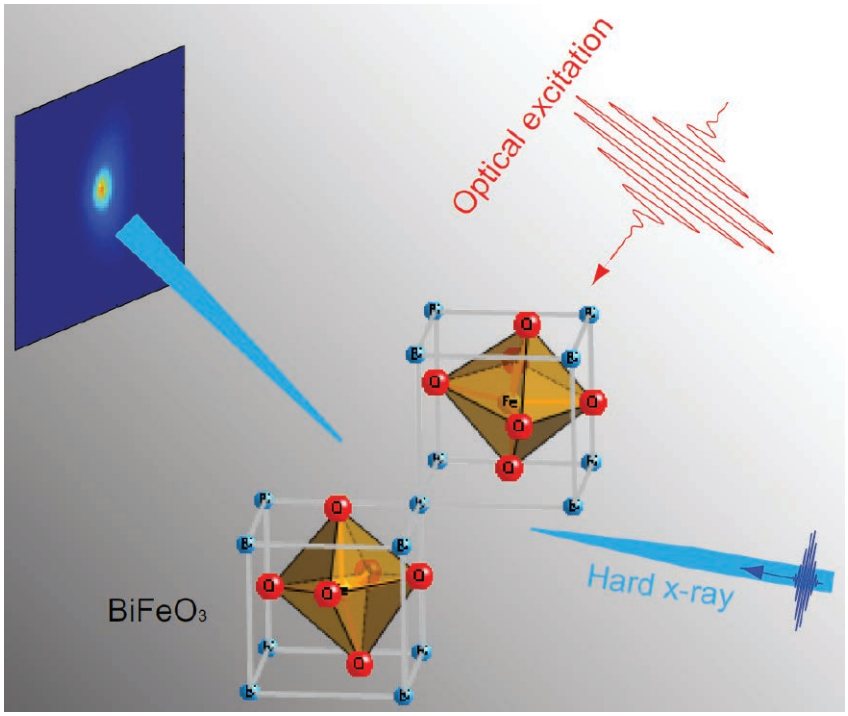

Fig. 1. The dynamics of the lattice structure of a $BiFeO_3$ thin film upon optical excitation was measured with atomic accuracy by a time-resolved x-ray diffraction probe.

Under illumination with light, these multiferroics respond by creating a large electric current, termed a photocurrent, and can also change their atomic structure, both of which are potentially useful in applications.

One of the central problems is how the physical processes associated with the absorption of light in multiferroics leads to these potentially useful properties.

Utilizing state-of-art tools readily available at Argonne, a new approach was employed by the researchers, from the University of Wisconsin-Madison, Cornell University, Northwestern University, Sandia National Laboratories, the Kavli Institute at Cornell for Nanoscale Science and Argonne, to study what happens after $BiFeO_3$ is excited by an intense pulse of light. Structural studies were conducted using the XSD 7-ID-B,C,D ultrafast x-ray diffraction beamline at the APS (Fig. 1). These structural results were compared with the electronic response measured at the ultrafast spectroscopy lab at the Center for Nanoscale Materials.

The large, optically induced strain decays within several billionths of a second, which turned out to be the same rate as the excited electrons return to their initial state. This key insight showed that the structural rearrangements after optical excitation were largely driven by electronic processes.

Faster data storage devices with lower power consumption can result from optical control of electronic and structural properties. This understanding of how that light can induce simultaneous structural and electronic effects now enables optical control of ferroelectric and multiferroic materials without requiring electrical contacts.

The large, optically induced strain opens a new route for ultrafast strain engineering of multifunctional complex oxides and new opportunities for manipulation of magnetism for spintronic applications. *— John Freeland*

See: Haidan Wen[1], Pice Chen[2], Margaret P. Cosgriff[2], Donald A. Walko[1], June Hyuk Lee[1], Carolina Adamo[3], Richard D. Schaller[4,5], Jon F. Ihlefeld[6], Eric M. Dufresne[1], Darrell G. Schlom[3,7], Paul G. Evans[2], John W. Freeland[1], and Yuelin Li[1]*, "Electronic Origin of Ultrafast Photoinduced Strain in $BiFeO_3$," Phys. Rev. Lett **110**, 037601 (2013). DOI:10.1103/PhysRevLett.110.037601

Author affiliations: [1]Argonne National Laboratory, [2]University of Wisconsin–Madison, [3]Cornell University, [4]Northwestern University, [5]Sandia National Laboratories, [6]Kavli Institute at Cornell for Nanoscale Science.

Corresponding author:

* ylli@aps.anl.gov

Work at Argonne, including use of the Advanced Photon Source and the Center for Nanoscale Materials, was supported by the U.S Department of Energy Office of Science under Contract No. DE-AC02-06CH11357.

7-ID-B,C,D • XSD • Materials science, atomic physics, chemistry • Time-resolved x-ray scattering, time-resolved x-ray absorption fine structure, phase contrast imaging • 6-21 keV • On-site • Accepting general users •

Speeding Up Superionic Switching

Superionic conductivity, in which the ions of certain solid materials become mobile above a certain temperature, might sound exotic, but it is nothing new: Michael Faraday first described it back in 1833. In the nineteenth century it was merely an intriguing phenomenon, but it holds important promise for the twenty-first century. Superionic conductors could lead to an array of faster and more efficient electronic devices — if we can understand, and perhaps even control, the mechanisms of superionicity. A team of scientists carrying out experiments at the APS and two other U.S. Department of Energy Office of Science synchrotron x-ray facilities has captured the phase transition associated with superionic conductivity in copper sulfide (Cu_2S) with unprecedented temporal resolution. They discovered that light can be used to drive the transition on time scales that are orders of magnitude faster than previously observed, while also unraveling the processes that determine the switching time. Their work provides a never-before-seen look into the dynamics of superionicity and opens possibilities for the development of novel, superfast resistive switching devices, memory chips, and more-efficient solid-state rechargeable batteries, among other applications that would have awed even Michael Faraday.

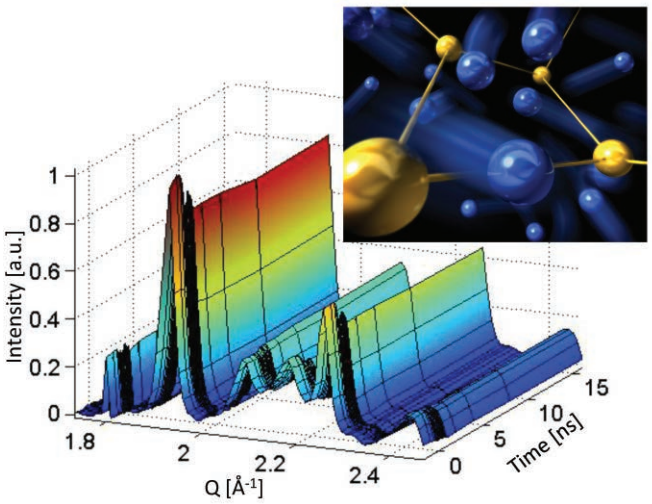

Fig. 1. Main plot: The full time-resolved x-ray diffraction pattern of nanocrystalline copper (I) sulfide nanodisks as revealed by time-resolved x-ray diffraction studies at the APS. Inset: Illustration of high-mobility Cu ions moving through the fixed sublattice of the sulfur atoms in Cu_2S.

Superionic conductors are compounds in which one atomic species is present in a rigid crystalline lattice and another type of atom fills the interstitial spaces. At a specific critical temperature, the cage-like lattice expands and changes shape, allowing ions of the second atomic species to move freely. In effect, the material then behaves more like an electrolytic fluid than a solid. In copper sulfide, this transition temperature is normally around 103˚ C, but recent experiments at the nanoscale have demonstrated that the temperature is reduced in very small pieces of Cu_2S.

The experimenters from Stanford University, Argonne, and the SLAC National Accelerator Laboratory examined Cu_2S nanodisks of ~10-nm diameter using various techniques including ultrafast x-ray diffraction along with near-edge x-ray absorption fine structure (NEXAFS) at the XSD 7-ID-B,C,D beamline of the APS and at the DOE-SC's Stanford Synchrotron Radiation Lightsource; and femtosecond near-edge spectroscopy at the DOE-SC's Advanced Light Source at Lawrence Berkeley National Laboratory.

As demonstrated by Fig. 1, the Cu_2S structure consists of a sulfur lattice with copper atoms at the interstitial sites. The researchers found that the phase transition from a low-temperature monoclinic structure with three unequal axes to a hexagonal, close-packed, high-temperature structure with superionicity occurred at about 70˚ C in the nanodisks. The dynamic capabilities of the techniques they used allowed the resolution of the actual atomic motion during the switching process so that the ionic diffusion processes could be distinguished from crystallographic changes in the lattice.

The transformation to the superionic phase is indicated by a slight red shift in the copper L_3 edge detected by x-ray spectroscopy, or by the appearance and disappearance of diffraction peaks associated with the low- or high-temperature structural phases.

Laser excitation induced the phase transition to occur much faster than previously observed, down to time scales of approximately 20 psec. The researchers note that the time for the transition to the superionic state is determined by the speed with which the copper ions diffuse as the crystal system changes. This ionic hopping time is the key quantity that underlies ionic transport processes in batteries and electrochemical devices.

— Mark Wolverton

See: T.A. Miller[1], J.S. Wittenberg[1], H. Wen[2], S. Connor[1], Y. Cui[1], and A.M. Lindenberg[1,3]*, "The mechanism of ultrafast structural switching in superionic copper (I) sulphide nano crystals," Nat. Commun. **4**, 1369 (22 January 2013). DOI:10.1038/ncomms2385

Author affiliations: [1]Stanford University, [2]Argonne National Laboratory, [3]SLAC National Accelerator Laboratory

Correspondence:

* aaronl@stanford.edu

This research was supported by the U. S. Department of Energy, Basic Energy Sciences, Materials Sciences and Engineering Division. Use of the Advanced Photon Source at Argonne National Laboratory was supported by the U.S. Department of Energy Office of Science under Contract No. DE-AC02-06CH11357.

7-ID-B,C,D • XSD • Materials science, atomic physics, chemistry • Time-resolved x-ray scattering, time-resolved x-ray absorption fine structure, phase contrast imaging • 6-21 keV • On-site • Accepting general users •

New Physics in a Copper-Iridium Compound

An unexpected magnetic behavior within Sr_3CuIrO_6, a transition-metal compound (TMC) that combines the transition metal copper with the transition metal iridium, has been revealed via theoretical calculations complimented by x-ray measurements carried out at the XSD 9-ID-B,C beamline at the APS. These results, which characterize the source of the unusual magnetism, indicate that mixing certain transition metal systems can yield TMCs with surprising physical properties unattainable with these systems alone, and may eventually lead to new materials for applications such as electronic memory devices and quantum computation.

Scientists are drawn to the unusual properties exhibited by TMCs (copper oxide, for instance, is a key ingredient in many high-temperature superconductors). These compounds typically contain oxygen and a transition metal. Transition metals reside in the middle portion of the Periodic Table of Elements in groups 3 through 12. The interest in TMCs has largely focused on compounds containing transition metals with lower atomic numbers, specifically the elements scandium through zinc. These elements all lie in the third period of the table, and are collectively referred to as 3*d* transition metals (indicating their highest electron energy level).

Transition metals form the *d*-block within the periodic table, characterized by the unfilled electron *d*-sublevels of these elements. Iron, for instance, is a 3*d* transition metal. Since a full *d*-sublevel has 10 electrons, the 6 electrons in iron's *d*-sublevel means it is only partially filled. Elements in the *d*-block with higher atomic numbers (like iridium) possess additional electrons. For these elements the 3*d*-sublevel electrons stay much closer to the nucleus than those in the 5*d*-sublevel where the transition metal iridium is found.

This means the atom's 3*d* electrons experience a strong repulsive electrostatic interaction with the other 3*d* electrons, preventing them from hopping to neighboring atoms in TMCs, so the 3*d* electrons cannot freely move through the compounds and are said to be strongly correlated.

A primary process in TMCs featuring 3*d* transition metals like copper is the exchange of two electrons between two 3*d*-sublevel atoms, which does not change the number of 3*d* electrons on any 3*d* atom, avoiding the large penalty associated with the repulsive interaction. This exchange process, in which the physical quality that changes is not charge but electron spin or orbital orientation, explains the magnetic properties in 3*d* TMCs.

The highly-correlated electrons found in many compounds containing only 3*d* transition metals are absent in materials containing 4*d* and 5*d* transition metals. The spatially-extended orbitals of the 5*d* electrons weaken the repulsive electron-electron interaction and facilitate their hopping to neighboring atoms when incorporated into TMCs. This “Coulomb screening effect” prevents iridium and other 5*d*-based TMCs from employing exchange to achieve the type of strong electron correlation seen in 3*d*-based TMCs.

But recent research has shown that, in spite of Coulomb screening, a phenomenon called “spin-orbit coupling” (SOC) can impart significant electron correlation to 5*d*-based TMCs. For instance, spin-orbit coupling causes the 5*d* compound Sr_2IrO_4 to exhibit magnetic ordering similar to that of some 3*d* copper oxides. The strength of SOC is positively correlated with the size of the atom, so SOC is relatively negligible in 3*d* TMCs but is strong in noble metals and 5*d* TMCs. Its effects on magnetism in 5*d* TMCs are just beginning to be explored.

The key microscopic structure of the mixed 3*d*-5*d* Sr_3CuIrO_6 compound is depicted in Fig. 1 (a). This microscopic structure was probed using resonant inelastic x-ray scattering (RIXS), performed at beamline 9-ID. In the RIXS technique, highly-tuned x-rays are utilized to excite closely-bound electrons from the iridium cations onto a 5*d*-sublevel; when another 5*d*-sublevel electron transitions into the electron vacancy, a characteristic x-ray is emitted that provides information about the state of the material.

The x-ray data revealed excited magnetic states (magnons) within the Sr_3CuIrO_6 sample, characterized by a large spectral gap — Fig. 1(b) — which means that substantial energy is required to create a single magnon. This was unexpected since the material was modeled by a simple isotropic (uniform in all directions) Heisenberg model, implying a gapless magnon spectrum, so the observed large gap indicates the existence of strong anisotropy (direction-dependence). SOC is a natural way to account for the anisotropy because SOC breaks the rotational symmetry of the spins by coupling them to the d orbitals, which are directional. But this effect is usually small.

This unexpected magnetic anisotropy motivated the development of a new theory in which the antiferromagnetic and ferromagnetic exchanges mix, depending on which iridium-5*d* orbital is coupled with the copper-3*d* orbital. These different types of exchange interactions usually compete.

But amazingly, in the 3*d*-5*d* Sr_3CuIrO_6 compound they cooperate because the strong SOC on the iridium ion anti-parallelizes the orbital and spin angular momenta — Fig. 1(c) — leading to an effective ferromagnetic exchange between the copper's electronic spins and the iridium's total angular mo-

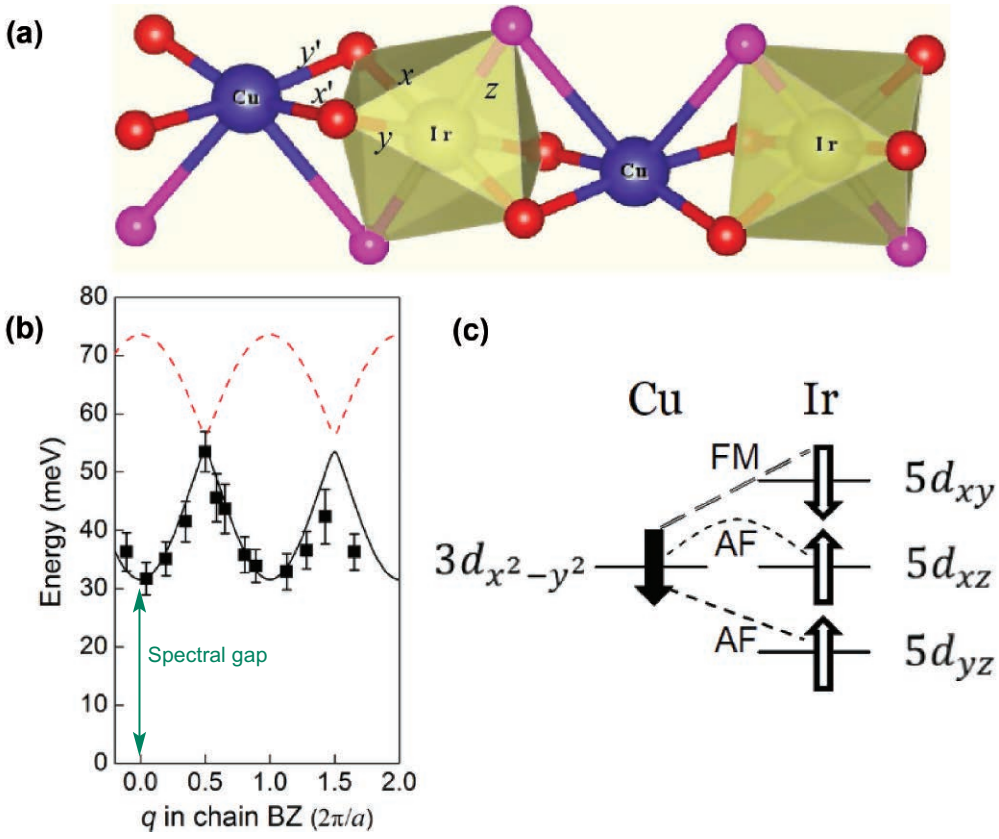

Fig. 1. (a) Cu-Ir chain of Sr_3CuIrO_6. Oxygen atoms surround both copper (Cu^{2+}) and iridium (Ir^{4+}) cations (ions positively charged due to the loss of electrons to the oxygen atoms, which become negatively-charged anions). The copper cation forms a planar arrangement with the surrounding oxygen anions, while the iridium cation resides at the center of an octahedral arrangement of oxygen anions. (b) Magnon dispersion obtained from experiment (solid squares) and theory (lines). (c) Unusual antiferromagnetic (AF) and ferromagnetic (FM) exchange mix between Cu and Ir. They cooperate because SOC anti-parallelizes the *5dxy* and *5dxz/5dyz* spins on the Ir ion. The latter is also effectively prohibited from flipping due to quantum inference, leading to the easy-z-axis exchange anisotropy.

mentum, with the strong exchange anisotropy being induced by the antiferromagnetic exchange.

The theory also predicts a higher energy branch of the magnon dispersion (the red broken line in Fig. 1b), which was not seen in the present RIXS experiment at the Ir L_3 edge (~11.216 keV). But it was predicted to be seen when the incoming x-ray is tuned to the Cu L_3 edge (~0.933 keV). The group of researchers planned to verify this in the near future (when the practical energy resolution of RIXS at Cu L_3 edge is improved from the current 130 meV to about 50 meV).

The promising results derived from this research are anticipated to open the way for the further development of mixed 3*d*-5*d* transition metal systems.

The direction of this exchange anisotropy depends on how the iridium and copper atoms are connected. By arranging the 3*d* and 5*d* atoms, researchers hope to develop advanced materials with specific spin orientations or spin frustration with the use of competing anisotropies. *— Philip Koth*

See: Wei-Guo Yin[1]*, X. Liu[1,2], A.M. Tsvelik[1], M.P.M. Dean[1], M.H. Upton[3], Jungho Kim[3], D. Casa[3], A. Said[3], T. Gog[3], T.F. Qi[4], G. Cao[4], and J.P. Hill[1], "Ferromagnetic Exchange Anisotropy from Antiferromagnetic Superexchange in the Mixed 3*d*-5*d* Transition-Metal Compound Sr_3CuIrO_6", Phys. Rev. Lett. **111**, 057202 (2013). DOI:10.1103/PhysRevLett.111.057202

Author affiliations: [1]Brookhaven National Laboratory, [2]Chinese Academy of Sciences, [3]Argonne National Laboratory, [4]University of Kentucky
Correspondence: *wyin@bnl.gov

This work was supported by the U.S. Department of Energy (DOE), Division of Materials Science, under Contract No. DE-AC02-98CH10886. T.F.Q and G.C. were supported by the National Science Foundation through grant No. DMR-0856234. Use of the Advanced Photon Source was supported by the U.S. Department of Energy Office of Science under Contract No. DE-AC02-06CH11357.

9-ID-B,C • XSD • Physics, materials science • Resonant inelastic x-ray scattering, inelastic x-ray scattering, liquid scattering • 4.5-24 keV • On-site • Accepting general users

Superconductivity with Stripes

The physics of low-temperature superconductivity is fairly well understood, but the ultimate goal of achieving the phenomenon at much higher temperatures remains tantalizingly elusive. The most promising high-temperature superconductor candidates are generally considered to be cuprates with perovskite structures, but it is unclear what mechanisms allow these materials to become superconducting — and how the superconducting temperatures (T_c) can be increased. By examining the stripe-ordering in $La_{1.875}Ba_{0.125}CuO_4$ (LBCO) under high pressure at the APS, a team of researchers probed those questions, specifically the relationship between stripe ordering and superconductivity. Their work reveals the interplay between stripes, lattice structure, and the superconductivity of LBCO in unprecedented detail and is an important step in understanding high-T_c superconductivity and eventually achieving practical room-temperature superconductors.

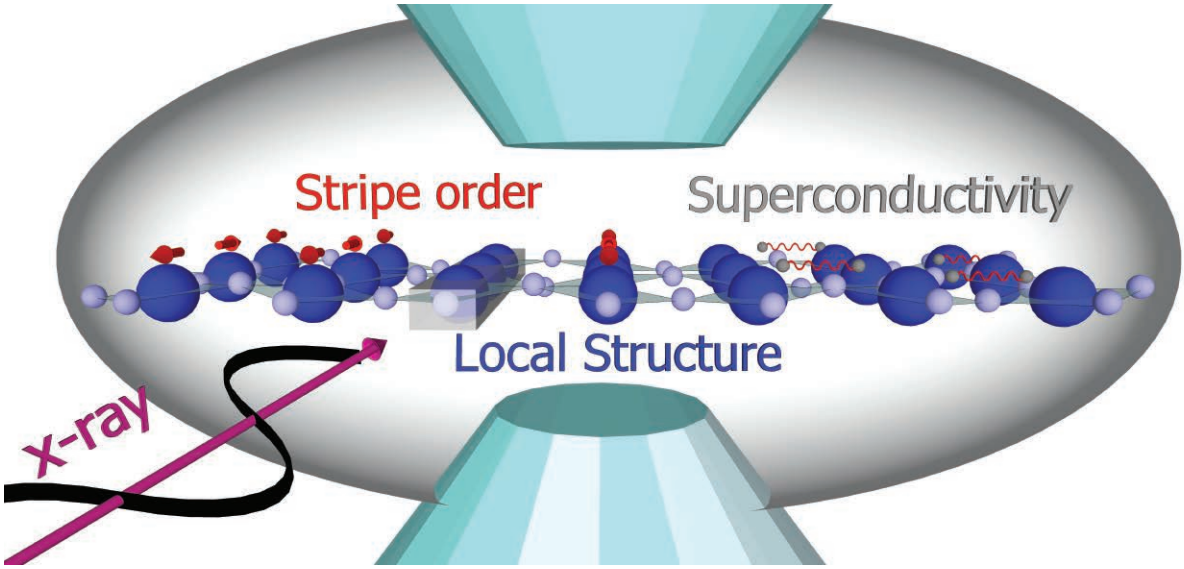

The interplay between stripe correlations, local structure, and superconductivity in $La_{1.875}Ba_{0.125}CuO_4$ was studied at the APS using polarized high-brightness x-ray beams for x-ray absorption fine structure and x-ray diffraction measurements at high pressure.

> Left to right: Paul Ehrenfest, Hendrik Lorentz, Niels Bohr, and Heike Kamerlingh Onnes (1919) in the Cryogenics Laboratory in Leiden, the Netherlands. Onnes, the discoverer of superconductivity, "the gentleman of absolute zero," had as his motto, "Door meten tot weten" ("Knowledge through measurement"). Read more at the source: APS Physics, http://www.aps.org/publications/apsnews/200704/history.cfm. Photo: Wikipedia, http://en.wikipedia.org/wiki/File:Ehrenfest_Lorentz_Bohr_Kamerlingh_Onnes.jpg

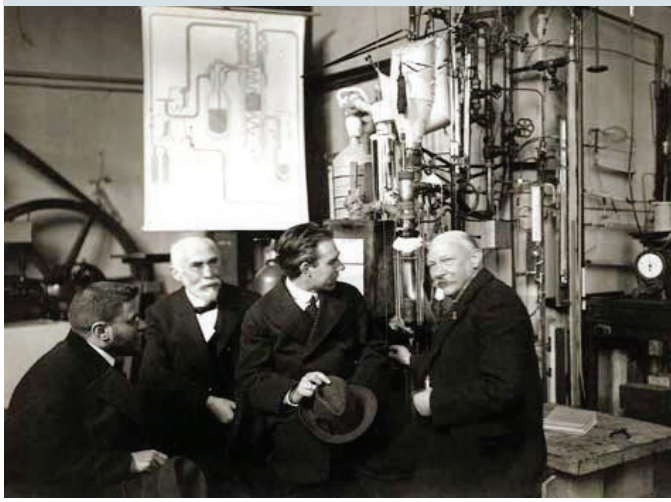

Understanding the behavior of the high-T_c superconductors is challenging in part due to strong correlations between electronic charges and spins. In addition to superconducting "pairing" correlations, these charges and spins can develop myriad order states and phases, dependent upon chemical doping.

For the 0.125 barium concentration (1/8 hole doping) of this particular compound, static "stripe" order is observed where hole charges segregate between spin-order regions in a periodic pattern. The static stripe order is reinforced by the tilt pattern of CuO_6 octahedra in this material's low-temperature tetragonal (LTT) structure. This static stripe ordering at ambient pressure appears to strongly compete with three-dimensional (3-D) superconductivity.

The researchers in this study from Argonne, Washington University in St. Louis, and Brookhaven National Laboratory (BNL) investigated what happens when the ground state of $LBCO_{1/8}$ is manipulated with applied pressure, which is known to enhance three-dimensional superconductivity. Previous work by the BNL co-authors had shown that charge order was able to survive the disappearance of long-range CuO_6 octahedral LTT tilting with the shift to a high-temperature tetragonal (HTT) phase under pressure, and that this charge order coexisted with a marginally enhanced superconducting phase at 2 GPa. Limitations in pressure range prevented suppression of the charge-order phase.

The current experiments extended the pressure range farther into the HTT phase, where diffraction measurements utilizing high-energy x-ray beams at the XSD 4-ID-D beamline of the APS revealed that static charge order completely disappears at 3.6 GPa. With the charge ordering no longer pinned to the lattice structure, superconductivity should again be unhindered. But the experiment team found otherwise, with superconductivity remaining suppressed well below optimal values.

To address this conundrum, high-pressure polarized XAFS (x-ray absorption fine structure) measurements were carried out, also at beamline 4-ID-D, in which the electric field of synchrotron x-rays was oriented along selected crystalline axes. The technique, which allows probing atomic correlations at very short time and length scales, revealed that short-range LTT tilting remains present in the high-pressure HTT phase.

Since LTT tilts pin stripes, and since superconductivity remained suppressed, the natural conclusion is that the local LTT tilts are a manifestation of the presence of dynamic stripe correlations sufficiently strong to limit 3-D superconductivity.

The extreme sensitivity and fine resolution of the polarized XAFS technique made it possible to uncover these persistent short-range LTT tilts, invisible to longer-range diffraction probes. The challenges of obtaining high-quality polarized XAFS from a single crystal in a diamond anvil cell are daunting, but the research team was able to demonstrate this capability for the first time.

The next step involves examining different dopings, pressure ranges, and phases to firmly establish the correlation of stripe order and high-temperature superconductivity. The interplay between stripe order and superconductivity remains a matter of debate. The present results provide indirect evidence that at high pressure, the two may be present simultaneously in a dynamic phase with intertwined order parameters.

This work is an important step in the quest to understand the mechanism of high-T_c superconductivity and eventually achieving practical room-temperature superconductors.

— Mark Wolverton

See: G. Fabbris[1,2], M. Hücker[3], G.D. Gu[3], J.M. Tranquada[3], and D. Haskel[1]*, "Local structure, stripe pinning, and superconductivity in $La_{1.875}Ba_{0.125}CuO_4$ at high pressure," Phys. Rev. B **88** (R), 060507 (2013). DOI:10.1103/PhysRevB.88.060507

Author affiliations: [1]Argonne National Laboratory, [2]Washington University in St. Louis, [3]Brookhaven National Laboratory

Correspondence: *haskel@aps.anl.gov

Work at Argonne National Laboratory and use of the Advanced Photon Source at Argonne was supported by the U.S. Department of Energy Office of Science under Contract No. DE-AC02-06CH11357.

4-ID-D • XSD • Physics, materials science • Anomalous and resonant scattering (hard x-ray), magnetic x-ray scattering, magnetic circular dichroism • 2.7-40 keV • On-site • Accepting general users •

The Secrets of Electron Behavior in High-Temperature Superconductors

More than 25 years after they were discovered, high-temperature superconductors retain a good deal of mystery. Their superconductivity arises from the formation of Cooper pairs of electrons, but the mechanism that stabilizes the pairs is still unknown. By means of high-resolution x-ray scattering studies at the APS, a team of scientists has probed with unprecedented detail the competition between two kinds of electron ordering in a typical high-temperature superconductor. The results shed light on the complex interplay between electron behavior, lattice structure, and superconductivity.

Argonne physicists and XSD beamline scientists Ayman Said (left) and Bogdan Leu with the HERIX instrument in the 30-ID enclosure.

Previous research has shown that high-temperature superconductors with the composition $YBa_2Cu_3O_{6+x}$ (YBCO) develop charge density waves (CDW) at temperatures above the critical temperature for the onset of superconductivity. These materials have planar CuO_2 bilayers separated by layers that include one-dimensional Cu-O chains. In these structures, CDWs take the form of periodic modulations of the electron density that are in antiphase in adjacent CuO_2 layers. As YBCO is cooled to the point where it becomes superconducting, the CDWs diminish. Conversely, if a sample is placed in a magnetic field that suppresses superconductivity, the CDWs strengthen. The two kinds of electron ordering responsible for CDWs and superconductivity evidently compete with each other, although whether the susceptibility to CDW formation is a prerequisite for superconductivity is unclear.

To further investigate the competition between CDWs and superconductivity, a research team from the University of Birmingham (UK), Ecole Polytechnique Féderale de Lausanne (Switzerland), Argonne, the University of British Columbia (Canada), the Canadian Institute for Advanced Research, and the University of Bristol (UK) studied a high-quality single crystal of $YBa_2Cu_3O_{6.54}$ made by the University of British Columbia group. With this specific composition, lattice locations for the Cu-O chains are alternately occupied and empty.

The high-resolution inelastic x-ray scattering (HERIX) instrument at XSD beamline 30-ID-B,C makes it possible to measure separately the momentum and energy transfer of inelastically scattered x rays with an energy resolution of 1.5 meV. Earlier experiments that detected CDWs integrated the scattering at each momentum transfer over a broad range of energy transfer, so that Bragg peaks and phonon scattering would also have contributed to the signals. Measurements using HERIX allowed the team to tease apart these different contributions.

CDWs reveal themselves through the presence of satellite peaks on either side of the normal lattice Bragg peaks, with separation equal to the CDW wavevector. The team found that CDWs appeared at about 155K, in line with previous experiments, and strengthened as the temperature of the crystal was reduced to 55K, when superconductivity sets in. At lower temperatures, the magnitude of the CDWs weakened as electron ordering in the superconducting regime took over.

Because of electron-phonon interactions, the presence of CDWs in a lattice affects the phonon dispersion spectrum. In a strictly one-dimensional model, it is possible for the frequency of a phonon coupled to a CDW to go to zero at a certain temperature. In effect, the phonon "freezes" into a stationary lattice distortion that's also coupled to the charge density modulation. In higher dimensional systems, freezing is not possible, but a phonon may still "soften" dramatically to a lower frequency. In a number of non-superconducting materials, this phenomenon has been observed at the CDW onset temperature.

In $YBa_2Cu_3O_{6.54}$, the researchers found a phonon broadening expected to lead to just such a softening. Simultaneously, the electron ordering embodied in the CDW became static, to within the measurement resolution of the experiment (Fig. 1). The results indicate, however, that the softening happens close to 55K, the superconducting transition temperature, rather than at 155K, the CDW onset temperature. Additional measurements have now confirmed directly the occurrence of softening at the lower temperature.

These results add to the evidence that CDW behavior is strongly linked to the mechanism for superconductivity in YBCO. Comparison with evidence from some other studies, and with theoretical analyses, suggests a connection to observed anomalies in the dielectric properties of the CuO2 layers. But putting all the evidence together to create a true theory of high temperature superconductivity remains a challenge.

— David Lindley

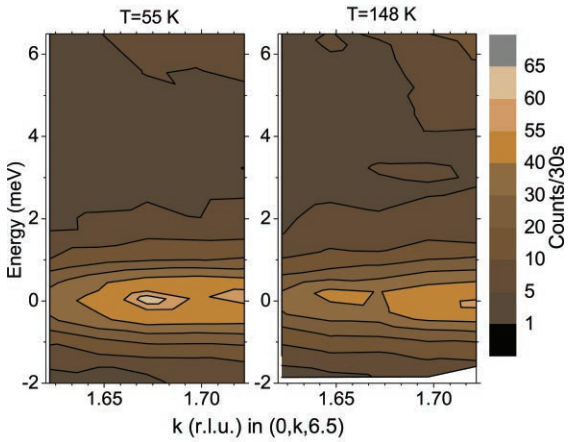

Fig. 1. Intensity of x-ray scattering from a single crystal of $YB_2Cu_3O_{6.54}$, plotted against energy transfer and wavevector (in relative lattice units). At 148K (right), just below the onset of charge density wave ordering, the small ridge of scattering at zero energy is due to lattice disorder. At 55K (left), near the onset of superconductivity, there is a prominent Bragg peak due to the CDW. From E. Blackburn et al., Phys. Rev B **88**, 054506 (2013). ©2013 American Physical Society.

See: E. Blackburn[1]*, J. Chang[2], A.H. Said[3], B.M. Leu[3], Ruixing Liang[4,5], D.A. Bonn[4,5], W.N. Hardy[4,5], E.M. Forgan[1], and S.M. Hayden[6], "Inelastic x-ray study of phonon broadening and charge-density wave formation in ortho-II-ordered $YBa_2Cu_3O_{6.54}$," Phys. Rev B **88**, 054506 (2013). DOI:10.1103/PhysRevB.88.054506

Author affiliations: [1]University of Birmingham, [2]Ecole Polytechnique Féderale de Lausanne, [3]Argonne National Laboratory, [4]University of British Columbia, [5]Canadian Institute for Advanced Research, [6]University of Bristol

Correspondence:

*e.blackburn@bham.ac.uk

This work was supported by the UK Engineering and Physical Sciences Research Council (Grant No. EP/J015423/1 & No. EP/J016977/1), the Swiss National Science Foundation through Nationale Centre of Competence in Research-Materials with Novel Electronic Properties and Grant No. PZ00P2_142434, the Canadian Natural Sciences and Engineering Research Council, and the Canada Foundation for Innovations. Use of the Advanced Photon Source at Argonne was supported by the U.S. Department of Energy Office of Science under Contract No. DE-AC02-06CH11357.

30-ID-B,C • XSD • Physics, materials science • Inelastic x-ray scattering, resonant inelastic x-ray scattering • 5-14 keV, 5-30 keV, 23.7-23.9 keV • On-site• Accepting general users •

Imaging Ferroelectric Domains

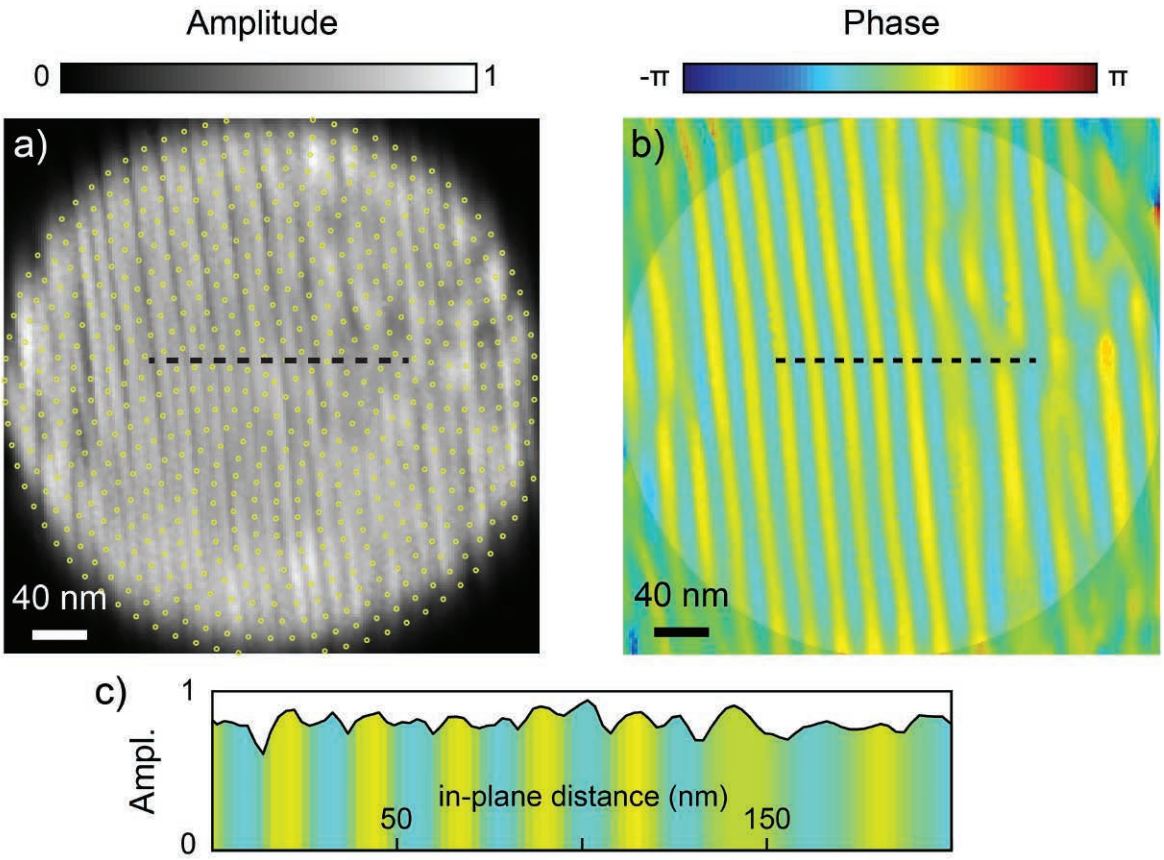

Fig. 1. The striped domains of thin-film lead titanate ($PbTiO_3$) imaged using x-ray Bragg projection ptychography. a) The amplitude of the reconstructed film, where the yellow dots represent the positions of the beam. b) The phase of the reconstructed film, clearly showing the striped pattern of polarization. c) An amplitude cross-section along the dotted line in a), colored with the phase of the dotted line in b).

When thin films of ferroelectric materials are grown on single-crystal substrates, they can develop regions of aligned polarization — called "domains" — that often adopt complex patterns. Manipulation of ferroelectric domains can lead to advances in a number of technologies. However, in order to manipulate the domains, it is important to study their natural development. Previous studies have shown that interfacial strain and electrical boundary conditions play a large role. Accurate measurements of the local polarization can help science learn more. By changing the properties of the substrate and the interfaces of the ferroelectric materials, one can control the size and shape of the domains and thus influence the behavior of the material. At the APS, researchers utilized Bragg projection ptychography (BPP) for ferroelectric domain imaging, potentially improving critical technologies such as memory storage.

X-ray BPP had previously been utilized to measure strain in semiconductor devices. Now, a team of scientists from Argonne, the Korea Advanced Institute of Science and Technology, Northern Illinois University, and La Trobe University (Australia) carrying out studies at the APS and the Argonne Center for Nanoscale Materials (CNM) found another application for BPP: imaging local polarization in ferroelectric thin films. In the future, this technique can help scientists study how domains develop in ferroelectric thin films, and thus how to manipulate them, potentially improving critical technologies such as memory storage.

First, the researchers utilized chemical vapor deposition to grow a 25-nm-thick film of the ferroelectric material lead titanate, or $PbTiO_3$. When $PbTiO_3$ is grown on a certain perfect single-crystal substrates, the domains will normally be distributed in a serpentine pattern. However, by controlling the surface properties of the substrate, these domain patterns can be influenced and controlled.

In this case, the researchers utilized substrates of strontium titanate, or $SrTiO_3$, which had surface miscut steps spaced about 22-nm apart. Using a growth chamber at the Argonne Materials Science Division, they deposited $PbTiO_3$ on the substrates, creating thin films with striped domain patterns.

That is where Bragg projection ptychography comes in. At the CNM/XSD beamline 26-ID-C, the researchers produced a focused coherent x-ray beam about 35-nm wide. When the beam hit the $PbTiO_3$ film at a specific position and angle, it produced a coherent Bragg diffraction pattern — a sort of fingerprint of the local domain structure.

This process was repeated at about 650 points on the film, marked as yellow dots in part (a) of Fig. 1. Because the x-ray beam was larger than the change in position, the information from all 650 points formed an overlapped data set.

Next, the team utilized a ptychographic algorithm, which simultaneously considered all the diffraction patterns from each overlapped point. With appropriate constraints, the algorithm converged to the correct answer in real space, converting the data from reciprocal space. Based on the resulting nanoscale map, the researchers created an image of the film's polarization, as shown in part (b) of Fig. 1. The striped domain pattern they found was consistent with the structure of the $PbTiO_3$ film's underlying $SrTiO_3$ substrate.

To check the accuracy of the BPP reconstruction, the researchers also measured the local polarization of the $PbTiO_3$ film with piezoresponse force microscopy. This method runs a scanning probe over the surface of the film to extract local polarization information.

Both techniques returned similar information about the domain pattern. However, piezoresponse force microscopy has a disadvantage: it requires direct access to the surface it is measuring. If a ferroelectric film was used as a memory device, it would be surrounded by layers of other electronic components, and this method of measuring polarization would be impossible.

BPP, on the other hand, can be performed from a distance, which means it can measure thin films in corrosive or enclosed environments where imaging with other techniques would be difficult or impossible. This makes BPP a promising tool for measuring how materials change under high temperatures and pressures. *— Sophie Bushwick*

See: S.O. Hruszkewycz[1]*, M.J. Highland[1], M.V. Holt[1], Dongjin Kim[1,2], C.M. Folkman[1], Carol Thompson[3], A. Tripathi[4], G.B. Stephenson[1], Seungbum Hong[1,2], and P.H. Fuoss[1], "Imaging Local Polarization in Ferroelectric Thin Films by Coherent X-Ray Bragg Projection Ptychography," Phys Rev. Lett. **110**, 177601 (2013). DOI:10.1103/PhysRevLett.110.177601
Author affiliations: [1]Argonne National Laboratory, [2]Korea Advanced Institute of Science and Technology, [3]Northern Illinois University, [4]La Trobe University
Correspondence: * shrus@anl.gov

This work, including use of the Center for Nanoscale Materials and the Advanced Photon Source, was supported by the U.S. Department of Energy Office of Science, Basic Energy Sciences, under Contract No. DEAC02-06CH11357. S.O.H., M.J.H., D.K., C.M.F., S.H., and P.H.F. were supported by U.S. Department of Energy, Basic Energy Sciences, Materials Sciences and Engineering Division.

26-ID-C • CNM/XSD • Physics, materials science • Nanofluorescence imaging, microdiffraction, nanotomography • 8-12 keV • On-site • Accepting general users •

A Search for Spin Currents Finds a Magnetic Oddity Instead

They were looking for clear-cut evidence of spin currents traveling through magnetic heterostructures, the tiny sandwiches of metal on silicon that make up the guts of a computer hard drive. Instead, researchers utilizing the APS found a magnetic mystery. When applying a microwave magnetic field to a heterostructure containing two different ferromagnets, the magnetic fields of the two varied in phase for several nanoseconds. Puzzled at first, the researchers later found the reason for the phase difference, and showed how to infer the phase of light within a structured material in a synchrotron. Their findings show that as hard drives get faster and their heterostructures get thinner, we can no longer treat the magnetic fields in each layer as identical. These results should smooth the path to hard drives and spintronic devices with gigahertz data speeds.

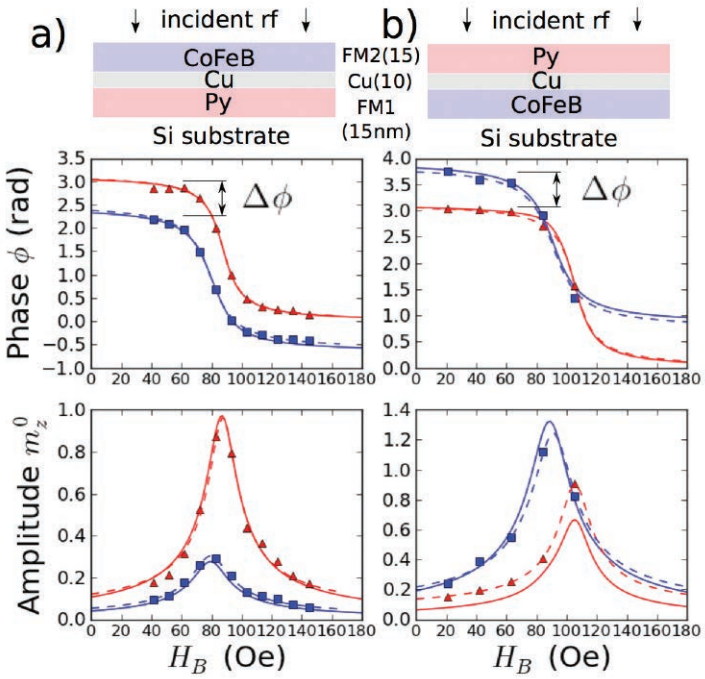

Fig. 1. The phase and amplitude of the magnetization precession, two ways. This page: (a) The experimental magnetization phase and amplitude for the substrate/permalloy/copper/CoFeB heterostructure driven at 2.694 GHz. (b) For the same heterostructure in reversed order of substrate/CoFeB/copper/permalloy, driven at 2.961GHz, and the phase offset (delta theta). Red indicates the nickel (permalloy) resonance, blue the cobalt (CoFeB) resonance. (c, facing page) The calculated magnetic fields driving the precession; the solid arrows trace the magnetic moments' motion over a full cycle. The green line indicates the phase offset. From W.E. Bailey et al., Nat. Commun. **4**, 2025 (26 July 2013).

4-ID-C • XSD • Physics, materials science • Magnetic circular dichroism, x-ray magnetic linear dichroism, x-ray photoemission spectroscopy, x-ray photoemission electron microscopy, anomalous and resonant scattering • 500-2800 eV • On-site • Accepting general users •

The heterostructure used was made of thin layers of cobalt iron boron ($Co_{60}Fe_{20}B_{20}$) and permalloy ($Ni_{81}Fe_{19}$), separated by a layer of copper. Both cobalt iron boron and permalloy are ferromagnets. When placed in a magnetic field, their magnetic moments will precess — that is, spin and wobble like a top — for a few nanoseconds before spinning into alignment with the applied field. When one ferromagnet is set into motion, the precession of its magnetic field should pump a spin current through the copper and into the other ferromagnet, setting its magnetic field into precession as well.

That was what the researchers from Columbia University, Uppsala University (Sweden), Spintec (France), and the Argonne and Brookhaven national laboratories hoped to see. In fact, they hoped to pump it, matching the frequency of the exterior magnetic field to the frequency of the precession to get a stronger spin current. Spin currents transport electrons with spin up in one direction and spin down in the other. They can act over longer distances and at higher speeds than a conventional charge current. The emerging technology of spintronic devices has received a lot of attention from the electronics industry.

To get a good look at the precessing magnetic moments, the researchers used the XSD 4-ID-C circularly polarizing undulator beamline at the APS to make time-resolved x-ray magnetic circular dichroism (TR-XMCD) measurements on the heterostructures. The beamline flashed x-rays every 12 nsec, with each pulse lasting just 40 psec. The APS is one of very few places in the world with this kind of stroboscopic x-ray capability.

Precise tuning of the x-rays allowed the researchers to individually detect the cobalt and nickel magnetic moments, revealing the magnetic field precession of each ferromagnet separately. When they plotted the precessions over time, they noticed something odd. Instead of being nearly synchronous, the precessions of the two ferromagnets were out of phase by about 40º. And the phase difference depended only on position in the stack; when the permalloy was closest to the substrate, its precession was 40º ahead of the cobalt iron boron. When the cobalt iron boron was closest to the substrate, its phase was 40º ahead of the permalloy.

This was unexpected, because each ferromagnet was supposedly exposed to the same exterior magnetic field. The wavelength of the microwave magnetic field was around a centimeter, and each layer of the heterostructure was a mere 15-nm thick, not nearly thick enough to induce metal skin effects. But the phase variation between the two ferromagnets showed that the microwaves that reached them were very different in phase and amplitude.

The explanation turned out to involve the conductivity of the silicon substrate. Although much thicker than the other layers, the silicon that supports the trilayer heterostructure is typically disregarded in calculations.

The researchers found that when magnetic fields are applied at data rates of a few gigahertz, the precessing ferromagnets never come into alignment while the fields are applied. The conductivity of the silicon substrate must be taken into account in order to calculate the magnetic fields which drive the ferromagnets' precession (Fig. 1).

Precise understanding of the substrate effect is one of the keys to designing hard drives, and possibly spintronic devices, with gigahertz rates.

— Kim Krieger

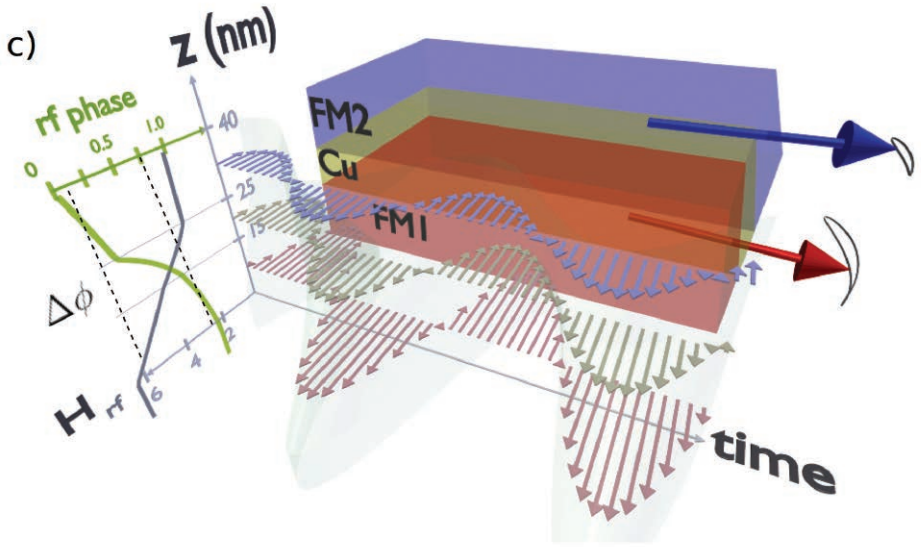

See: W.E. Bailey[1]*, C. Cheng[1], R. Knut[2], O. Karis[2], S. Auffret[3], S. Zohar[1,4], D. Keavney[4], P. Warnicke[5,‡], J.-S. Lee[5,‡‡], and D.A. Arena[5], "Detection of microwave phase variation in nanometre-scale magnetic heterostructures," Nat. Commun. **4**, 2025 (26 July 2013). DOI:10.1038/ncomms3025

Author affiliations: [1]Columbia University, [2]Uppsala University, [3]CEA/CNRS/UJF, [4]Argonne National Laboratory, [5]Brookhaven National Laboratory. Present addresses: ‡Paul Scherrer Institut, ‡‡Stanford Synchrotron Radiation Laboratory

Correspondence:

*web54@columbia.edu

This research was funded by National Science Foundation grant ECCS-0925829. Use of the Advanced Photon Source at Argonne National Laboratory was supported by the U.S. Department of Energy Office of Science under Contract No. DE-AC02-06CH11357.

Conducting Electrons Buried Under Topological Insulator Thin Films

In recent years, the workings of topological insulators (TIs) have been the subject of intense research in condensed matter physics. Much of the fascination comes from the apparently paradoxical nature of TIs: How can a material effortlessly conduct electrons only at its surface while otherwise remaining an insulator? Trying to answer that question has led to a great deal of research on topological surface states (TSSs), i.e., the massless conducting electrons at the vacuum-exposed surface, because it is at the surface where most of the action seems to be in TIs. But the catch in exploiting these resistance-free electrons is that they degrade in air, affecting their utilization in practical applications. A team of researchers has taken an alternative approach, exploring deeply-buried TSSs at the interface between a TI thin film and silicon, the most ubiquitous semiconductor substrate material. Utilizing strongly-penetrating hard x-rays from the APS, the team garnered important information on these buried electrons that is generally inaccessible with conventional methods. Their work has implications for the evolution of semiconductor electronic devices and other TI device applications.

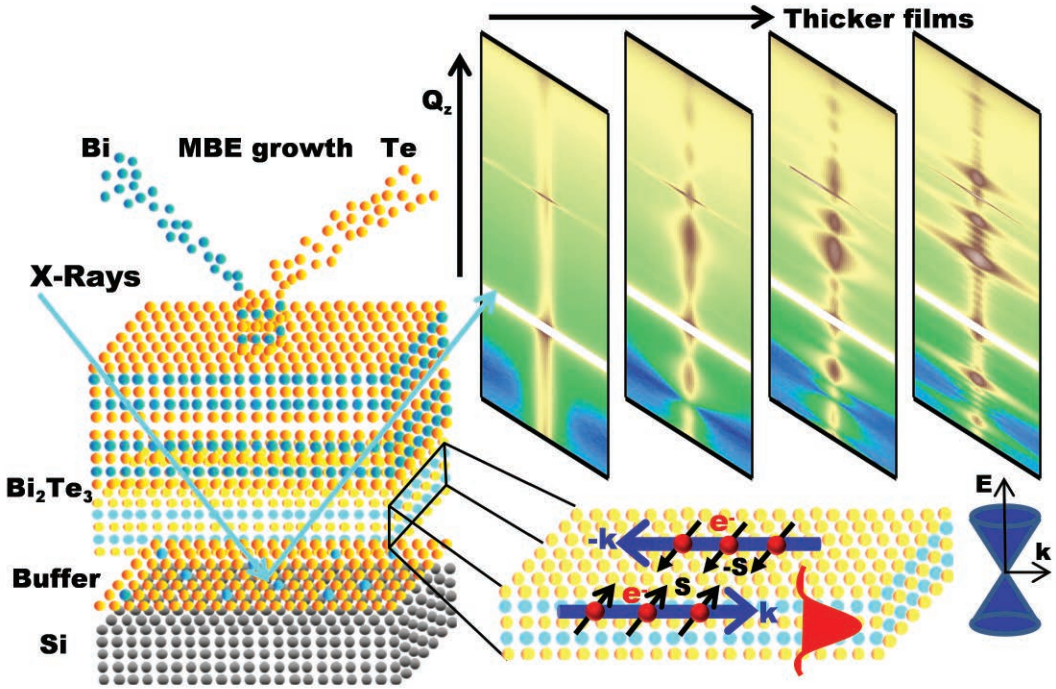

Working at the XSD 33-ID-D,E beamline at the APS, the researchers from Argonne, the University of Illinois at Urbana-Champaign, and the Chinese Academy of Sciences measured x-ray scattering intensities from Bi_2Te_3 thin films grown in vacuum using molecular beam epitaxy (MBE, Fig. 1). Unlike most previous *ex situ* structural studies, this *in situ* method allows real-time measurements without any surface contamination.

Observing the epitaxial growth process, the researchers discovered a rather nontrivial interface featuring the formation of a buffer layer composed mostly of Te, roughly 2.7 Å above the topmost layer of the Si(111) substrate. Quintuple layers (QLs) grow atop the buffer, with the bottom QL both slightly relaxed and partially strained, and the other QLs more bulk-like in structure.

The existence of a buffer layer indicates that the bonding between the interfacial layers is fairly weak and dominated mostly by van der Walls forces, relatively weak electric forces that attract neutral molecules to one another in gases, in liquefied and solidified gases, and in almost all organic liquids and solids. This explains the relaxed yet slightly strained bottom QL, and also indicates that the TI film is largely decoupled electronically from the Si substrate. Detailed first-principles calculation confirms that conducting electrons at this deep interface exhibit similar properties as those at the vacuum exposed surface, experiencing little disturbance from the substrate electrons.

A direct consequence of this kinship between surface and interface TSSs is the emergence of the quantum tunneling effect (quantum-mechanical-allowed transitioning through a classically-forbidden energy state), which happens when the TI films are very thin, allowing crosstalk between these two surfaces. Such quantum coherence could disrupt the TSSs at both surfaces, causing the entire system to revert to an insulating state. This thickness-dependent phase transition (from metallic to insulating) at the surface has been observed by complementary photoemission measurement. In Bi_2Te_3, past experiments have demonstrated that at least four QLs are needed between the surface and interfacial layers to avoid these tunneling gaps and retain the topological conducting electrons. This insight establishes a thickness limit for device architecture based on TI thin films.

The *in situ* study of the TI film interfacial layers presented in this work helps to highlight the importance of this often-neglected component of topological insulators. As the investigators point out, the interfacial topological states can sometimes be more important than those at the TI surface, because the interface is isolated from, and thus unaffected by changes in the ambient environment that readily influence the surface.

Yet interfacial layers are also easy to adjust through the controlled application of voltage or charge, an obvious advantage when considering the practical use of TI films in semiconductor electronic devices. But such control would require the precise knowledge of the interfacial layer structure demonstrated in this work. The successful growth of high quality epitaxial TI films by MBE techniques also paves the way towards TI device applications.

While Bi_2Te_3 is one of the most significant TI materials known, many others exist, or are yet to be discovered, each with different structural and electronic characteristics. The research team is looking toward studying other TI systems, such as those with stronger coupling between the interface layers, with an eye toward achieving a more comprehensive understanding of the workings of this fascinating phase of matter and its potential uses.

— Mark Wolverton

< Fig. 1. *In situ* x-ray scattering of Bi_2Te_3 thin films grown on Si(111) with molecular beam epitaxy. Bi_2Te_3 is a topological insulator with predicted conducting electrons at the interface, but the detailed property of the interface is beyond the detection of conventional experimental probes. Using synchrotron hard x-ray scattering, the interface structure and properties have been determined. The results reveal that the interface hosts massless spin-polarized conducting electrons identical to those on the vacuum-exposed surface.

See: Y. Liu[1]*, H.-H. Wang[2,3], G. Bian[2], Z. Zhang[1], S.S. Lee[1], P.A. Fenter[1], J.Z. Tischler[1], H. Hong[1], and T.-C. Chiang[2]**, "Interfacial Bonding and Structure of Bi_2Te_3 Topological Insulator Films on Si(111) Determined by Surface X-Ray Scattering," Phys. Rev. Lett. **110**, 226103 (2013).
DOI:10.1103/PhysRevLett.110.226103
Author affiliations: [1]Argonne National Laboratory, [2]University of Illinois at Urbana-Champaign, [3]Chinese Academy of Sciences
Correspondence:
* yangliu3@aps.anl.gov,
** tcchiang@illinois.edu

This work is supported by the U.S. Department of Energy Office of Science, Basic Energy Sciences, under Grant No. DE-FG02-07ER46383 (T.-C.C.), and Contract No. DE-AC02-06CH11357 (for operation of the Advanced Photon Source at Argonne, and for P.F. and S.S.L., who are funded by the U.S. Department of Energy Basic Energy Sciences Geochemistry Research Program).

33-ID-D,E • XSD • Materials science, physics, chemistry, geoscience, environmental science • Anomalous and resonant scattering (hard x-ray), diffuse x-ray scattering, general diffraction, surface diffraction, surface diffraction (UHV), x-ray standing waves, x-ray reflectivity • 4-40 keV, 6-25 keV • On-site • Accepting general users •

Making Aperiodic Structure Crystal Clear

Precious gems owe much of their beauty to their periodic crystalline structure, the regular, repeating molecular pattern that orders their atoms and creates the faceted shape exposed by a gem cutter's chisel. Many mundane objects also have periodic crystalline structures, from the salt on your table to the silicon in your cell phone. Such internal structures can affect a material's properties; whether it is ferromagnetic or electrically conductive depends on the atomic arrangement. Teasing apart the effects of crystal symmetry on material properties is difficult, though. To gain insight, some researchers have turned to quasicrystals, compounds whose atomic-scale structures are just as well ordered as crystals, but aperiodic, allowing new rotational symmetries forbidden to periodic crystals. Some quasicrystals have sister compounds with periodic structures that make experimental comparisons possible. A group of researchers used the high-brightness x-rays from the APS to image such a quasicrystal, utilizing diffraction techniques to probe its structure (and, at the Ames Laboratory, its magnetic properties). They found that even though the quasicrystal and its periodic sister shared similar structural motifs, the quasicrystal does not order antiferromagnetically as does the sister compound. Their results could lead to a better understanding of the relationship between crystal structure and material properties, particularly in the field of complex metallic alloys.

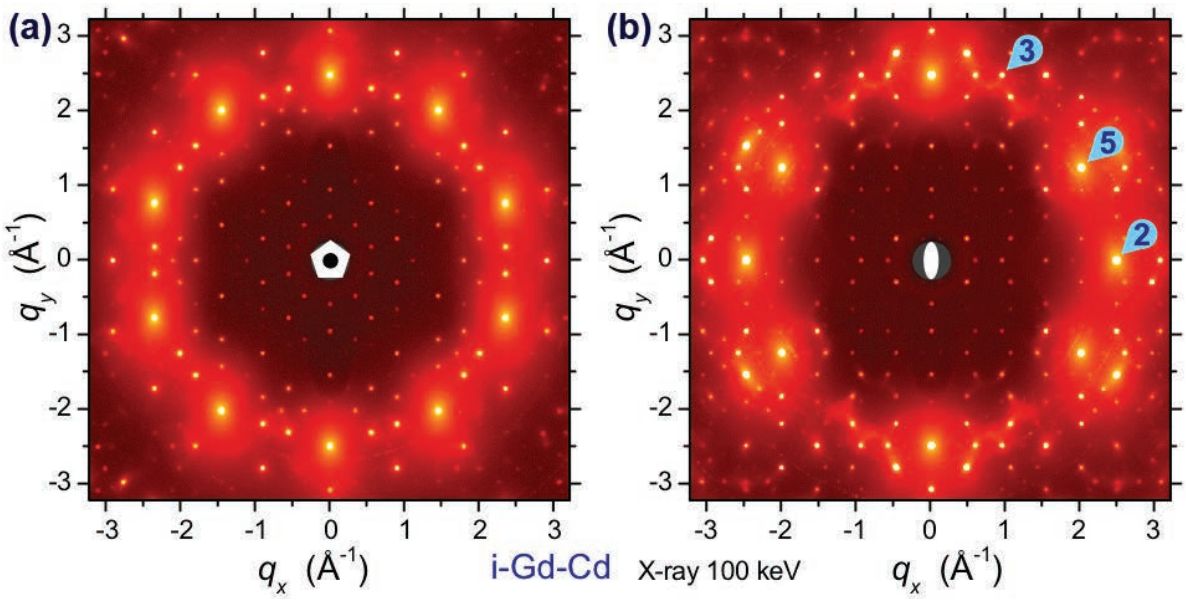

Fig. 1. High-energy x-ray diffraction patterns from a single grain of i-Gd–Cd taken with the x-ray beam parallel to the five-fold (a) and two-fold (b) axes. From A.I. Goldman et al., Nat. Mater. **12,** 714 (August 2013).

The cover of *Nature Materials* showing a high-energy x-ray diffraction pattern from a single grain of icosahedral rare-earth-cadmium quasicrystal, taken with x-ray beam from the APS superconducting undulator at beamline 6-ID-D.

Materials scientists call the periodic sister compounds of quasicrystal "approximants." When the researchers in this study, from the Ames Laboratory and Iowa State University set out to explore how quasiperiodicity affects magnetism, they wanted a very simple approximant, one that contained just two elements. They chose RCd$_6$ (R = Rare earth), a body-centered cubic compound with icosahedral clusters of atoms at the corners and body center of the cube. This structural motif is also found in the respective binary quasicrystals discovered at the Ames Laboratory.

They created a series of alloy melts with rare earths and cadmium. The compositions were very similar to RCd$_6$, but differing slightly in the concentration of cadmium, following an algorithm that previously led to success in the Zn-Sc system.

Ther researchers employed a newly developed x-ray precession technique at the XSD 6-ID-D x-ray beamline at the APS to confirm that the resulting R-Cd compounds were indeed quasicrystalline with five-fold symmetry (Fig. 1), and to characterize their structural properties. The 6-ID-D beamline was chosen because of its high-energy capabilities, which allow one to study the bulk of the crystal rather than just the near-surface region.

The researchers found differences in the magnetic behavior as well when they probed the magnetic properties of the rare earth-cadmium quasicrystals. Many of the RCd$_6$ approximants order antiferromagnetically, but their quasicrystalline analogs do not. Instead, the quasicrystals appear to be spin glasses with their magnetic moments frozen in a disordered state.

Typically, this means that there are many different possible magnetic ground states all with the same energy, so that when they are cooled down the magnetic moments do not favor a specific ordered arrangement.

The researchers in the study were disappointed —They had hoped to find an antiferromagnetic quasicrystal. Theoretical calculations suggested it was possible.

But the spin-glass result is significant in its own right. It gives insight into complex systems and potentially into the properties of complex metallic alloys. Their complex structures on the molecular scale often lead to unusual physics and chemical properties, and researchers are exploring complex metallic alloys for their potential as structural engineering materials and thermoelectric components.

Now that they know it can be done, the researchers intend to continue to search the phase diagram around binary approximants for additional quasicrystals, and probe their magnetic properties for more insight into just what quasiperiodicity brings to the table. *— Kim Krieger*

See: Alan I. Goldman[1,2*], Tai Kong[1,2], Andreas Kreyssig[1,2], Anton Jesche[1,2], Mehmet Ramazanoglu[1,2], KevinW. Dennis[1], Sergey L. Bud'ko[1,2], and Paul C. Canfield[1,2**], "A family of binary magnetic icosahedral quasicrystals based on rare earths and cadmium," Nat. Mater. **12**, 714 (August 2013). DOI:10.1038/NMAT3672
Author affiliations: [1]Ames Laboratory, [2]Iowa State University
Correspondence:
*goldman@ameslab.gov,
**canfield@ameslab.gov

The research was supported by Basic Energy Sciences, Materials Sciences Division, U.S. DOE. Ames Laboratory is operated for DOE by Iowa State University under Contract No. DE-AC02-07CH11358. Use of the Advanced Photon Source at Argonne National Laboratory was supported by the U.S. Department of Energy Office of Science under Contract No. DE-AC02-06CH11357.

6-ID-D • XSD • Physics, materials science • Magnetic x-ray scattering, high-energy x-ray diffraction, powder diffraction, pair distribution function • 50-100 keV, 70-130 keV • On-site • Accepting general users •

Electron Cooperation Leads to Antiferromagnetism

In a ferromagnet, electron spins associated with different atoms line up in the same direction to produce a macroscopic magnetic moment. In an antiferromagnetic material, whose atoms also have net individual magnetic moments, the electron spins align in an alternating fashion so that they cancel each other out. The forces that determine whether spins correlate or anti-correlate can be complex and subtle, depending on details of how electrons interact in a given crystal lattice. Using a combination of macroscopic and microscopic techniques, including x-ray diffraction studies at the APS, a team of scientists has shown that antiferromagnetism in gadolinium monosilicide (GdSi) arises through a cooperative interplay of two distinct electron spin interactions. This insight has implications for the origin of electron correlations in a variety of related materials.

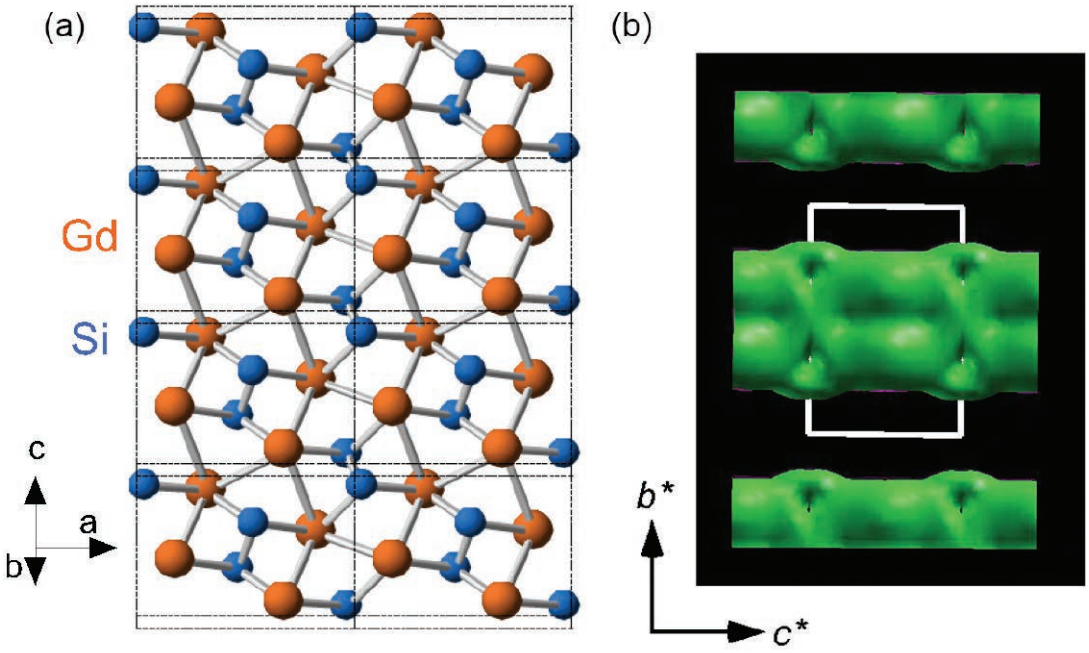

Fig. 1. (a) Lattice structure of GdSi. (b) Band structure calculation reveals a major Fermi surface that is approximately flat, making possible the nesting effect required to form incommensurate SDW order.

Like other rare-earth elements, gadolinium has electrons in its localized $4f$-orbitals that give the atom a magnetic moment. Uniquely, gadolinium's $4f$ electrons possess no overall orbital angular momentum, making it a clean subject for studying phenomena arising purely from electron spins. The compound GdSi is known to transition from a paramagnet to an antiferromagnet at temperatures below about 55K, but both the spin structure and the mechanism responsible for producing the necessary correlation among spins have been unclear.

The microscopic nature of antiferromagnetism is elucidated by resolving the spin structure. By means of x-ray magnetic diffraction observations derived from studies at the XSD beamline 4-ID-D and high-resolution x-ray powder diffraction experiments performed at XSD beamline 11-BM-B, both at the APS, the researchers from Argonne, The University of Chicago, Los Alamos National Laboratory, the University of Tennessee, and Oak Ridge National Laboratory searched for and found the emergence of incommensurate spin structures when GdSi makes the transition to antiferromagnetic behavior (Fig. 1), meaning the periodicity of the correlated spins bears no simple relationship to any periodicity in the GdSi lattice.

At the antiferromagnetic transition temperature, the team also observed drastic changes in the resistivity of GdSi, and in both the signs and magnitudes of its Hall coefficients. These changes indicate a significant restructuring of the material's Fermi surface, and that the antiferromagnetic transition is accompanied by the appearance of an energy gap. Electrons at the Fermi surface thus have settled into a new, lower-energy ground state associated with the magnetic ordering. The change in electron density of states at the Fermi surface was independently verified by band-structure calculations in association with ultraviolet photon emission spectroscopy.

All these observations and inferences still do not pin down the cause of the incommensurate spin structure in GdSi. In metals, correlations among localized spins, such as the $4f$-electrons in GdSi, are typically mediated by itinerant or conduction electrons via the Ruderman-Kittel-Kasuya-Yosida (RKKY) interaction. On the other hand, changes at the Fermi surface are often indicative of a formation of a spin density wave (SDW) – a periodic modulation of the itinerant spins. The relationship between these two organizing principles has not been addressed in the scientific literature, and it has been hard to determine whether interaction or competition between them can stabilize spin structure.

Sifting through all their evidence, the researchers conclude that antiferromagnetism arises in GdSi through cooperation between SDW and RKKY mechanisms.

The key insights include observations of asymmetrically shaped magnetic x ray diffraction lines that are indicative of the spin susceptibility and can be traced to Fermi surfaces with a quasi-one-dimensional form. This is a strong evidence of nested Fermi surfaces that are needed for SDWs to occur.

An equally important realization is that the interaction between nested itinerant electron spins could be mediated by RKKY-organized local spins rather than by lattice vibrations, or phonons. Here, the SDW formation determines the magnetic order wave vector and organizes local spins through RKKY interaction to generate a complementary ordered structure. This cooperative mechanism is analogous to what happens in the formation of a charge density wave, in which an incommensurate charge distribution of itinerant electrons is stabilized by an ordered displacement of lattice ions.

Although the absence of interference from orbital spins in GdSi makes the cooperation between SDW and RKKY easier to discern, the team suggests that the mechanism is rather generic and could be common in other rare earth compounds with similar structures. *— David Lindley*

See: Yejun Feng [1,2*], Jiyang Wang[2], D.M. Silevitch[2], B. Mihaila[3], J.W. Kim[1], J.-Q. Yan[4,5], R.K. Schulze[3], Nayoon Woo[2], A. Palmer[2], Y. Ren[1], Jasper van Wezel[1,‡], P.B. Littlewood[1,2], and T.F. Rosenbaum[2**], "Incommensurate antiferromagnetism in a pure spin system via cooperative organization of local and itinerant moments," Proc. Nat. Acad. Sci. USA **110**, 3287 (2013). DOI:10.1073/pnas.1217292110
Author affiliations: [1]Argonne National Laboratory, [2]The University of Chicago, [3]Los Alamos National Laboratory, [4]University of Tennessee, [5]Oak Ridge National Laboratory. [‡]Present address: University of Bristol
Correspondence: * yejun@aps.anl.gov, ** t-rosenbaum@uchicago.edu

P.B.L. was supported by the U.S. Department of Energy Office of Science -Basic Energy Sciences (DOE SC-BES) under FWP70069. B.M. and R.K.S. were supported in part by the U.S. DOE under the Los Alamos National Laboratory-Lab Director Research and Development program. A.P. is supported in part by DOE-SC Graduate Fellowship Program under Contract No. DE-AC05-06OR23100. Work at the Advanced Photon Source and the Materials Science Division of Argonne National Laboratory was supported by the DOE SC-BES under Contract NEAC02-06CH11357.

4-ID-D • XSD • Physics, materials science • Anomalous and resonant scattering (hard x-ray), magnetic x-ray scattering, magnetic circular dichroism • 2.7-40 keV • On-site • Accepting general users •

11-BM-B • XSD • Chemistry, materials science, physics • Powder diffraction • 15-35 keV • On-site, mail-in • Accepting general users •

An Emergent Spin Filter in Oxide Electronics

The field of spintronics is the study of how the spin of a material's electrons, and thus its magnetic moment, contributes to its electronic behavior. One device used in this research is a magnetic tunnel junction, in which an insulating material is sandwiched between two layers of a ferromagnetic one. Electrons can tunnel through the insulating layer, traveling from one ferromagnetic layer to the other. Scientists from Argonne, the Universidad Complutense de Madrid (Spain), and Los Alamos National Laboratory utilizing experimental tools including an APS x-ray beamline characterized a magnetic tunnel junction structure made from all-oxide materials. By tuning the magnetic properties of oxides, spintronics researchers may be able to produce next-generation electronic devices that are faster and use less energy.

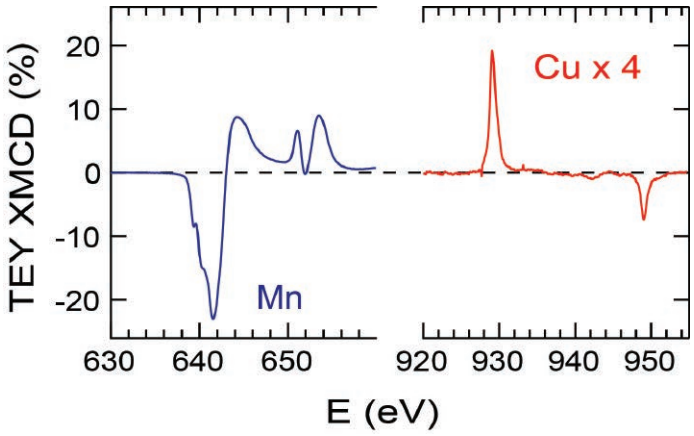

Fig. 1. XMCD spectra taken at the L-edges of manganese and copper, showing an induced copper magnetization that is antiparallel to the manganese magnetization.

The devices contained a layer of insulating cuprate ($PrBa_2Cu_3O_7$) between two layers of ferromagnetic manganite ($La_{0.7}Ca_{0.3}MnO_3$), which has a high spin polarization. At low temperatures, the spin of nearly all of the manganite's electrons that contribute to the charge transport point in the same direction. At the interface between cuprate and manganite, the cuprate, which normally has zero net magnetic moment, acquires an induced magnetic moment. Past research has measured this type of interfacial induced magnetization, but not how it affected electron transport.

The electrons' ability to tunnel through the insulating cuprate layer, known as the device's tunnel magnetoresistance, was measured at Spain's Complutense University of Madrid. As the Spanish members of the team decreased the temperature of the device, the spin polarization of the manganite increased. This was expected to enhance the tunnel magnetoresistance, and it did: As temperature decreased, magnetoresistance increased. However, at low temperatures--between 60K and 90K — the magnetoresistance stopped increasing, peaked, and began decreasing instead. This anomalous decrease had never before been reported in all-oxide magnetic tunnel junctions.

To understand the unexpected change, the researchers examined the magnetization of the manganite layers at Los Alamos National Laboratory. Using polarized neutron reflectometry, a technique that can probe magnetization in thin films and quantitatively determine its value at different depths, they found the magnetization to be equal to that in bulk materials, even at the lowest temperature. They observed no reduction close to the interfaces, as occurs in several other thin films structures, and concluded the decrease in magnetoresistance was not caused by deterioration of the manganite layers' magnetization.

Next, the researchers examined the magnetic tunnel junctions utilizing the XSD beamline 4-ID-C at the APS, employing circularly polarized x-rays to measure the sample's x-ray magnetic circular dichroism, or XMCD (Fig. 1). This spectrum, which contains information about a material's magnetic moment, let researchers distinguish between the magnetic moment of the manganese ions in the manganite and that of the copper ions in the cuprate. They saw that magnetization in the cuprate is induced by and linked to the magnetization of the manganite in the interfacial region. This induced net

"Emergent" cont'd. on page 38

X-Ray Peaks Point the Way to Understanding Helical Behavior

Titanium diselenide (1*T*-$TiSe_2$) consists of hexagonal layers of titanium (Ti) lying between similar layers of selenium (Se), thus forming Se-Ti-Se sandwiches separated by relatively large gaps. Despite this simple lattice structure, 1*T*-$TiSe_2$ exhibits complex behavior at low temperatures due to the emergence of charge-ordered states resulting from electron shifts that give rise to a chiral (helical) charge density distribution. To learn more about the transition from the normal state to the chiral charge-ordered state, researchers subjected single crystals of $TiSe_2$ to 80-keV x-rays at the XSD 6-ID-D beamline of the APS and followed up with analyses of the temperature dependences of the specific heat, resistivity, and resistance anisotropy of the crystals. The research indicated that the normal state gives way to a nonchiral charge density wave state at about 190K, before transforming to a chiral charge-ordered state at about 183K.

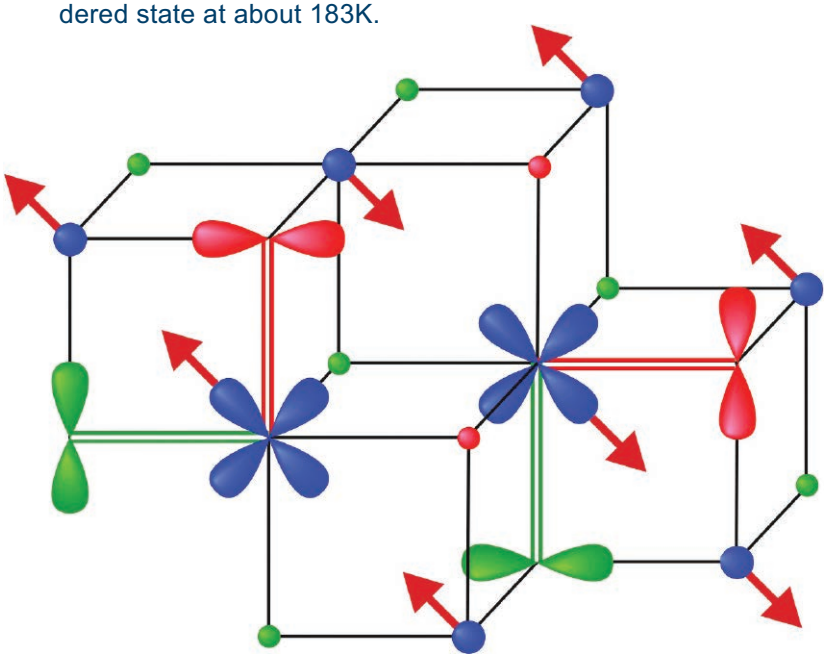

Fig. 1. One of the three components contributing to the proposed chiral CDW state in $TiSe_2$. The specific orbitals involved in the charge transfer process for this component are indicated (in blue for Ti and red and green for Se). The combination of orbital order and CDW formation allows the formation of the chiral charge and orbital ordered state.

$TiSe_2$ has long intrigued scientists because it exhibits so-called charge density waves (CDWs) at low temperatures, whose origin is still being debated. In the CDW phase, a three-component variation in the charge density occurs, with each component being related to a charge transfer process between one particular Ti-3*d* orbital and two Se-4*p* orbitals (Fig. 1). This charge ordering is accompanied by lattice distortions. If the three components of the variation superimpose without any relative phase differences between them, a nonchiral CDW state is produced. When there are phase shifts, the three components superimpose to form chiral lattice distortions.

Detailed order parameter measurements of the transition from the normal state to the charge-ordered phase showed that a nonchiral CDW phase transition occurs at T_{CDW} = 190K. The researchers then discovered previously unobserved x ray diffraction peaks having intensities about fifty times weaker than the primary CDW peaks, while searching for evidence of the emergence of helical ordering below T_{CDW}. Measurements of one of the weak peaks indicated that it evolved differently with decreasing temperature than the primary CDW peaks, suggesting the onset of a different type of order at $T_{chiral} \approx$ 183K.

The temperature dependence of the specific heat of $TiSe_2$ crystals cut from the same samples used in the x-ray diffraction experiments showed an anomaly around 190K related to the nonchiral CDW transition. Below this temperature, the specific heat changed linearly with temperature until about 182K, when a change in slope was seen, indicating a change in the thermodynamic state of the sample.

The two principal components of the resistivity were also measured as a function of temperature. The derivatives of both curves displayed sharp minima at T_{CDW}. Moreover, the resistivity anisotropy showed a sharp peak at 183K.

The researchers in this study, from the University of Bristol (UK), Drexel University, Cornell University, and Argonne concluded that the low-temperature chiral charge-ordered state in 1*T*-$TiSe_2$ arises in a sequence of two

"Peaks" cont'd. on page 38

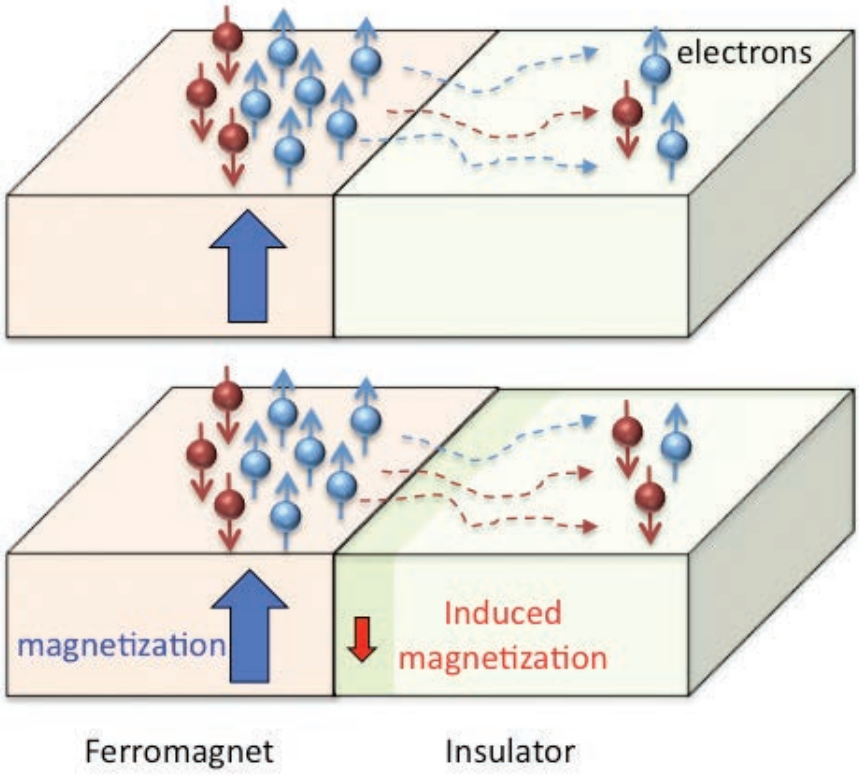

Fig. 2. The effect of induced magnetization on electron tunneling. (Top) The populations of spin-up and spin-down electrons are reduced as electrons tunnel from the ferromagnetic manganite layer on the left into the insulating cuprate layer on the right. (Bottom) The ratio between spin-up and spin-down is strongly affected by the induced magnetization at the cuprate's interface and can even be reversed, as shown here.

"Emergent" cont'd. from page 36
magnetization is antiparallel to the magnetization of the manganite.

The cuprate's antiparallel magnetization makes it harder for the manganite's majority-spin electrons to tunnel through, so more minority-spin electrons reach the other side (Fig. 2). By acting as a negative spin filter, the interfacial region of the cuprate comes into competition with the manganite's high positive spin polarization. This competition gives the magnetoresistance of the magnetic tunnel junction a more complex temperature dependence than had previously been suspected, causing an overall decrease at low temperatures.

Knowing how the induced magnetization affects the transport of electrons may have valuable spintronic applications. By tuning the interface's magnetization, researchers can construct oxide structures with desirable electronic properties. *— Sophie Bushwick*

See: Yaohua Liu[1], F. A. Cuellar[2], Z. Sefrioui[2], J.W. Freeland[1], M.R. Fitzsimmons[3], C. Leon[2], J. Santamaria[2], and S.G.E. te Velthuis[1]*, "Emergent Spin Filter at the Interface between Ferromagnetic and Insulating Layered Oxides," Phys. Rev. Lett. **111**, 247203 (2013).
DOI:10.1103/PhysRevLett.111.247203
Author affiliations: [1]Argonne National Laboratory, [2]Universidad Complutense de Madrid, [3]Los Alamos National Laboratory
Correspondence: * tevelthuis@anl.gov

Work at Universidad Complutense de Madrid was supported by the Spanish MICINN through Grant No.MAT2011-27470-C02, Consolider Ingenio 2010 - CSD2009-00013 (Imagine), and by CAM through Grant No. S2009/MAT-1756 (Phama). Work at Argonne National Laboratory and use of the Advanced Photon Source was supported by the U.S. Department of Energy Office of Science-Basic Energy Sciences under Contract No. DE-AC02-06CH11357.

4-ID-C • XSD • Physics, materials science • Magnetic circular dichroism, x-ray magnetic linear dichroism, x-ray photoemission spectroscopy, x-ray photoemission electron microscopy, anomalous and resonant scattering • 500-2800 eV • On-site • Accepting general users •

"Peaks" cont'd. from page 37
closely separated phase transitions. The first transition, at $T_{CDW} \approx 190$K, involves the onset of a nonchiral charge-ordered state. The second transition, which the researchers identified to occur at $T_{chiral} \approx 183$K, is characterized by the emergence of previously unobserved diffraction peaks, a sudden change in slope of the specific heat, and a sharp peak in the resistivity anisotropy.

This sequence of two transitions leading first from the normal state to the nonchiral CDW state and only then to the chiral charge-ordered state agrees with theoretical predictions put forward previously by one of the authors. In that theoretical model, the possibility of forming the novel chiral CDW state in $TiSe_2$ is explained by the simultaneous formation of orbital order. A direct prediction of the theory of coupled charge and orbital order is that the chiral state cannot emerge directly from the disordered state, but rather has to go through a sequence of two closely separated phase transitions, as observed in the current experiments.

— Vic Comello

See: John-Paul Castellan[1], Stephan Rosenkranz[1], Ray Osborn[1], Qing'an Li[1], K.E. Gray[1], X. Luo[1], U. Welp[1], Goran Karapetrov[1,2], J.P.C. Ruff[1,3], and Jasper van Wezel[1,4]*, Chiral Phase Transition in Charge Ordered 1*T*-$TiSe_2$," Phys. Rev. Lett. **110**, 196404 (2013).
DOI: 10.1103/PhysRevLett.110.196404
Affiliations: [1]Argonne National Laboratory, [2]Drexel University, [3]Cornell University, [4]University of Bristol
Correspondence:
* Jasper.vanWezel@bristol.ac.uk

Work at the Advanced Photon Source and Materials Science Division of Argonne National Laboratory was supported by the U.S. Department of Energy Office of Science, Basic Energy Sciences under Contract No. NE-AC02-06CH11357.

6-ID-D • XSD • Physics, materials science • Magnetic x-ray scattering, high-energy x-ray diffraction, powder diffraction, pair distribution function • 50-100 keV, 70-130 keV • On-site • Accepting general users •

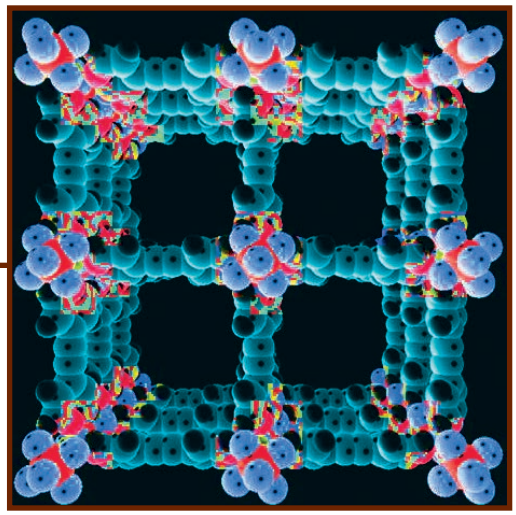

Engineering Materials & Applications

The Superpower behind Iron Oxyfluoride Battery Electrodes

A team of scientists utilized the high-energy x-rays available at the APS to investigate the fundamental basis for the performance advantage offered by mixed-anion iron oxyfluoride (FeOF) conversion electrodes over electrodes made of simple oxide or fluoride phases. This research represents the first-of-a-kind application of *operando* pair distribution function (PDF) methods that probe the structure of battery electrodes *in situ* while they are being cycled, in order to study electrochemical reactions in batteries. The PDF measurements provided exceptionally precise insight into the atom-atom bond distances, the proportion of each type of atom-atom bond, and how these evolve over dozens of points during the electrochemical reaction. This represents significant milestones in both understanding electrochemical reactions in battery electrodes and in the experimental tools available to investigate such reactions.

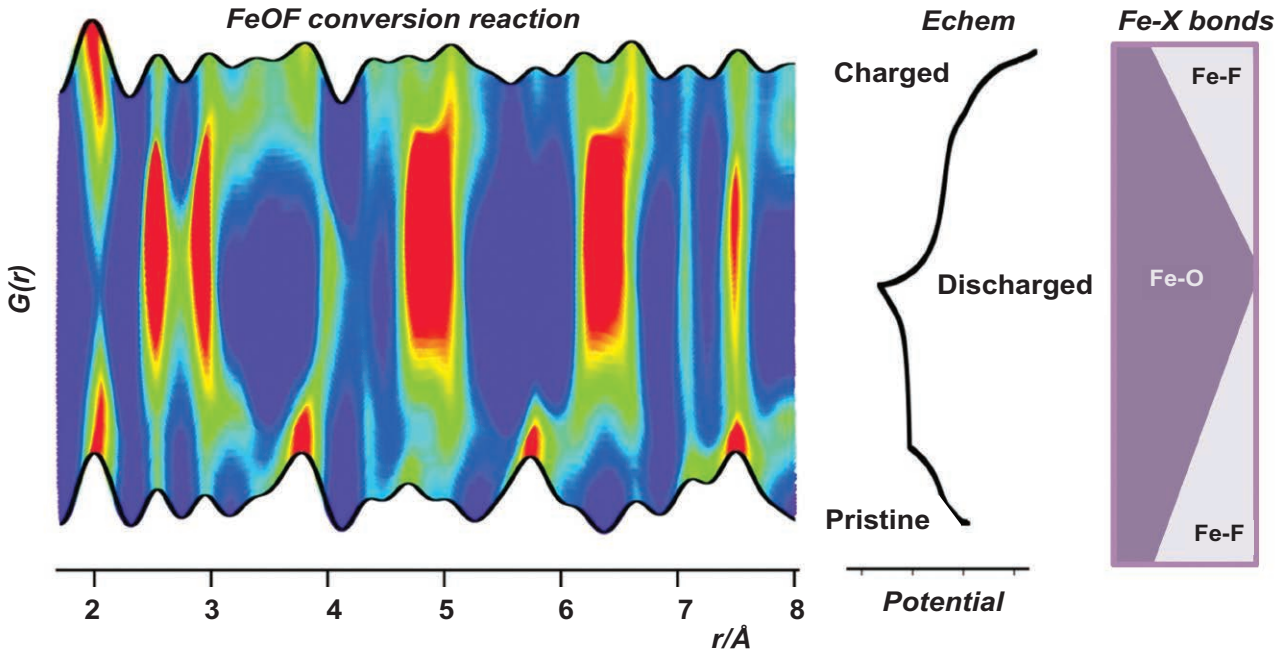

Fig. 1. Structural changes probed using *operando* PDF analysis indicates a partitioning of a FeOF-based electrode into fluorine- and oxygen-rich phases, with different reactivity for each component.

Innovative materials chemistries continue to drive advances in lithium-ion batteries — the state-of-the-art in rechargeable energy storage. While many different battery components contribute to their performance, the largest gains may be achieved through the development of new electrode materials that can power portable electronics longer and propel electronic vehicles farther. Electrodes based on so-called "conversion chemistry" have the potential to double energy storage capacities compared to electrodes in existing rechargeable batteries. This higher energy storage capacity is achieved because each metal atom can react with several electrons in conversion systems, compared to the single electron limit of conventional electrodes. Although these new materials initially deliver higher capacities, their capacities often diminish with repeated charging and discharging. Nevertheless, unusually good long-term performances, with consistently high capacities, have been found with mixed-anion systems such as oxyfluorides. Although they combine the favorable performance characteristics of simple oxides and fluorides, the electrochemical reactions giving rise to the improved performance of these more complex materials remain a mystery.

Scientists from Argonne, the University of Cambridge, Stony Brook University, Rutgers University, and CIC Energigune (Spain) carried out their studies at XSD beamline 11-ID-B at the APS. A notable result was that the evolution of oxygen (O) and fluorine (F) species could be separated despite their nearly identical contributions to the x-ray measurements. These element-specific insights were recovered based

on the distinct chemical bonding characteristics of these anions, with the bond lengths and coordination numbers within the electrodes being specified with high precision by the PDF data.

The PDF study (in combination with solid-state nuclear magnetic resonance spectroscopy) enabled the elucidation of a complex nanoscale transformation mechanism and provided new insights into the functionality of FeOF. Several critical insights emerged from the work that will impact the design of new battery materials:

- There is a preferential reaction of the fluoride component during both discharge and charge.
- The active electrode does not consist of the single-phase oxyfluoride of the pristine uncycled electrode, but rather contains multiple electrochemically active phases—an O-rich rock salt phase and a F-rich rutile phase (Fig. 1).
- Competition between electrochemical reactions involving the rock salt and rutile components in the active electrode and frustration in O/F ordering within these phases may favor the nanosized composite electrode structure that contributes to enhanced cyclability.

These results have important implications for producing other mixed-anion systems, suggesting a possible cost- and time-saving shortcut to achieving exemplary electrochemical performance. There may be no need to go to the trouble of preparing a single-phase oxyfluoride, because simply mixing an oxide with a fluoride could yield similar performance improvements, which is an entirely unexplored route for the development of new battery materials. This is particularly important in systems where oxyfluoride phases are not known (such as nickel).

The *operando* x-ray PDF studies were made possible by a newly developed electrochemical cell that is compatible with PDF measurements and a broad range of other x-ray scattering and spectroscopic methods. Argonne's Multi-Purpose *In-situ* X-ray (AMPIX) electrochemical cell [1] provides reliable electrochemical cycling without compromising the x-ray measurement. The suitability of the AMPIX cell for a broad range of synchrotron-based x-ray scattering and spectroscopic measurements has been demonstrated with studies at eight APS beamlines to date. Compatible techniques include PDF analysis, high-resolution powder diffraction, small-angle scattering, and x-ray absorption spectroscopy. These techniques probe a broad range of electronic, structural, and morphological features relevant to battery materials.

The AMPIX cell enables experiments providing greater insight into the complex processes that occur in operating batteries by allowing the electrochemical reactions to be probed at fine reaction intervals with greater consistency (within the charge-discharge cycle and between different methodologies) with the potential for new time-dependent kinetic studies or studies of transient species. — *Vic Comello*

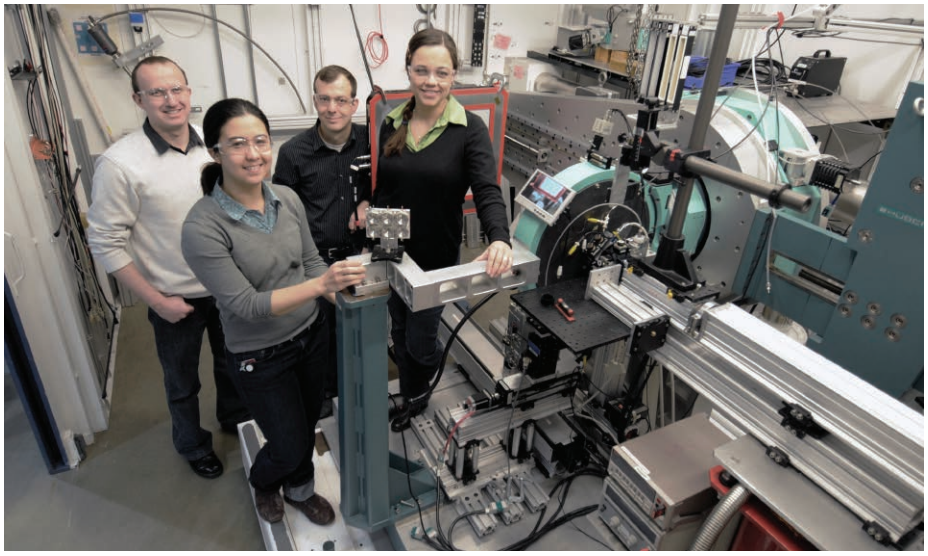

Researchers and journal article co-authors in the 11-ID-B research station. Left to right: XSD postdoc Olaf Borkiewicz, XSD chemists Karena Chapman and Peter Chupas, and XSD postdoc Kamila Wiaderek. Borkiewicz and Wiaderek worked with Chapman and Chupas in the XSD Structural Science Group. Next to Chapman's hand is a multicell holder with six AMPIX electrochemical cells.

Reference

[1] Olaf J. Borkiewicz, Badri Shyam, Kamila M. Wiaderek, Charles Kurtz, Peter J. Chupas, and Karena W. Chapman, "The AMPIX electrochemical cell: a versatile apparatus for i*n situ* x-ray scattering and spectroscopic measurements," J. Appl. Cryst. **45** (2012) 1261. DOI:10.1107/ S0021889812042720

See: Kamila M. Wiaderek[1], Olaf J. Borkiewicz[1], Elizabeth Castillo-Martínez[2,3], Rosa Robert[2,4,‡], Nathalie Pereira[5], Glenn G. Amatucci[5], Clare P. Grey[2,4], Peter J. Chupas[1], and Karena W. Chapman[1]*, "Comprehensive Insights into the Structural and Chemical Changes in Mixed-Anion FeOF Electrodes by Using *Operando* PDF and NMR Spectroscopy," J. Am. Chem. Soc. **135**(10), 4070 (March 13, 2013). DOI:10.1021/ja400229v

Author affiliations: [1]Argonne National Laboratory, [2]University of Cambridge, [3]CIC Energigune, [4]Stony Brook University, [5]Rutgers University. ‡Present address: Paul Scherrer Institute

Correspondence: *chapmank@aps.anl.gov

This work was supported as part of the Northeastern Center for Chemical Energy Storage at Stony Brook University, an Energy Frontier Research Center funded by the U.S. Department of Energy Office of Science (DOE-SC) under Award Number DE-SC0001294. Work done at Argonne and use of the Advanced Photon Source at Argonne National Laboratory were supported by the U.S. DOE-SC under Contract No. DE-AC02-06CH11357. The Generalitat de Catalunya is acknowledged for the postdoctoral research grant awarded to R. Robert (BP-DGR 2008).

11-ID-B • XSD • Chemistry, environmental science, materials science • Pair distribution function • 58-60 keV, 90-91 keV • On-site • Accepting general users •

Composite Battery Boost

New composite materials based on selenium (Se) sulfides that act as the positive electrode in a rechargeable lithium-ion (Li-ion) battery could boost the range of electric vehicles by up to five times, according to groundbreaking research carried out at the XSD 9-BM-B,C, 11-ID-C, and 20-BM-B beamlines at the APS. The studies of the materials demonstrated that they have the potential to pack five times the energy density of conventional batteries.

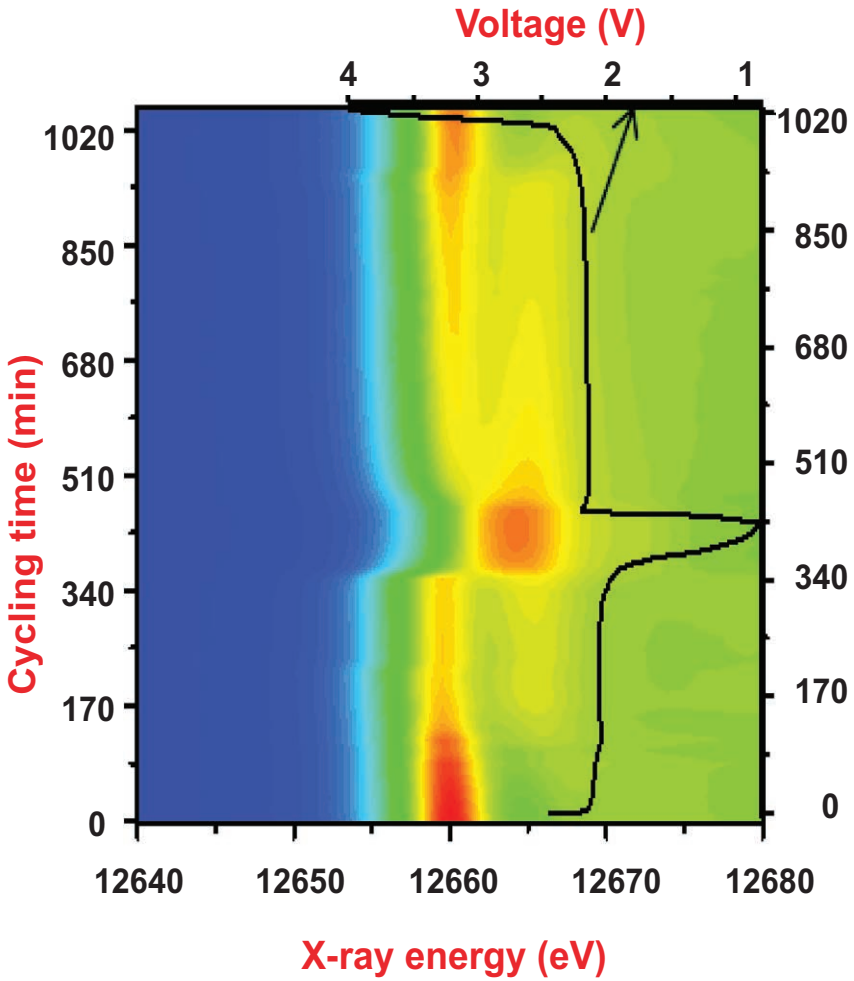

Fig. 1. Normalized XANES spectra of Li/Se cell during cycling. The black line is the battery voltage profile.

Lithium-ion batteries are ubiquitous in rechargeable gadgets such as cell phones, tablet PCs, and GPS devices, as well as early electric vehicles. As any user of these technologies will testify, the amount of energy that Li-ion batteries can hold between recharges can stand improvement, and all-electric vehicles in particular will benefit from a longer-lasting battery. The problem is that existing electrode materials, while relatively effective, cannot pack much electrical energy into a small volume and so range is limited.

Now, researchers from Argonne and King Abdulaziz University (Saudi Arabia) hope to remedy that problem. They have focused on carbon-selenium sulfide composites as an alternative material to the conventional lithium transition metal oxide positive electrode material in standard batteries. These composites are anticipated to have an energy density five times higher than conventional batteries. This could mean up to five times greater range between charging stations.

The researchers point out that in a typical lithium battery, electrical capacity is between 120- and 160-mAh per gram of material. The use of the novel composite materials can boost that capacity to around 678-mAh per gram. While such a boost is theoretically very attractive, understanding the nature of the electrochemical changes taking place when these materials are used (instead of conventional lithium-metal oxide electrodes) is vital to ensure they will be viable in future batteries.

Using the 11-ID-C beamline at the APS, the team carried out *in situ* synchrotron high-energy x-ray diffraction (HEXRD) studies and complementary, selenium *K*-edge x-ray absorption near-edge structure (XANES) analysis to observe the chemical changes that take place in these novel electrode materials as they charge and discharge a battery (Fig. 1).

These measurements, which were undertaken at more than 12-keV energy, were also done in transmission mode on the bending-magnet beamlines 9-BM-B,C and 20-BM-B at the APS. This technique allowed the team to hone in on the changing chemistry of the selenium atoms in the electrode and how they shift between crystalline and non-crystalline phases as current and lithium ions flow through the experimental battery's ether-based electrolyte. Raman microscopy at Argonne's Center for Nanoscale Materials provided additional information about the Li_2Se that was observed on the Li anode of the charged cells.

The power of HEXRD and XANES available on these x-ray beamlines allowed instantaneous monitoring of the phase changes in the electrode materials under charge and discharge states. The team could observe exactly what intermediate stages the materials went through as well as detecting their chemical oxidation states. Such details are critical to the development of a new stable electrode material that might be charged and discharged many hundreds, if not thousands, of repetitions in its lifetime.

The team discovered that it is the chemical composition of the electrolyte — the fluid that bathes the electrodes and through which the charge-carrying positive lithium ions flow — that seems to have the most impact on the changes that take place. The researchers suggest it might be possible to tune the efficiency of a battery based on these new composites by optimizing the electrolyte and so improve battery performance still further.

The x-ray studies and analysis of the electrochemistry of the electrode as it operates have also allowed the team to discover a plausible chemical mechanism for the processes involved in discharging the battery. They explain that the composite electrode is reduced to form lithium polyselenide with more than four selenium atoms per lithium atom; additional discharging to lower voltage leads to chemical species containing two lithium ions per selenium atom. Charging involves the reverse process. This mechanism is first proposed and experimentally proven by the team, and it is similar to that seen in experimental lithium-sulfur electrodes.

— David Bradley

See: Yanjie Cui[1], Ali Abouimrane*[1], Jun Lu[1], Trudy Bolin[1], Yang Ren[1], Wei Weng[1], Chengjun Sun[1], Victor A. Maroni[1], Steve M. Heald[1], and Khalil Amine[1,2], "(De)Lithiation Mechanism of Li/SeS_x (x = 0−7) Batteries Determined by *in situ* Synchrotron X-ray Diffraction and X-ray Absorption Spectroscopy," J. Am. Chem. Soc. **135**, 8047 (2013). DOI:10.1021/ja402597g

Author affiliations: [1]Argonne National Laboratory, [2]King Abdulaziz University

Correspondence:

*abouimrane@anl.gov

Work done at Argonne and use of the Advanced Photon Source and the Center for Nanoscale Materials at Argonne National Laboratory were supported by the U.S. Department of Energy Office of Science under Contract No. DE-AC02-06CH11357. J. Lu was supported by the Department of Energy Office of Energy Efficiency and Renewable Energy (EERE) Postdoctoral Research Award under the EERE Vehicles Technology Program administered by the Oak Ridge Institute for Science and Education for the Department of Energy. APS Sector 20, which is managed by XSD in partnership with the Canadian Light Source (CLS), is funded by the U.S. Department of Energy Office of Science, and by the Natural Sciences and Engineering Research Council of Canada and the University of Washington via the CLS.

9-BM-B,C • XSD • Materials science, chemistry • X-ray absorption fine structure • 2.1-23 keV • On-site • Accepting general users •

11-ID-C • XSD • Materials science • High-energy x-ray diffraction, diffuse x-ray scattering, Pair distribution function • 115 keV • On-site • Accepting general users •

20-BM-B • XSD • Materials science, environmental science, chemistry • X-ray absorption fine structure, microfluorescence (hard x-ray), micro x-ray absorption fine structure, diffraction anomalous fine structure • 2.7-25 keV, 2.7-30 keV, 2.7-35 keV • On-site • Accepting general users •

X-ray Diffraction Imaging of Silicon Microposts for Lithium-Ion Batteries

Due to its impressive performance characteristics, such as high charge density and long-term cycling capability, lithium-ion (Li-ion) battery technology is increasingly being incorporated in diverse energy storage applications, including the automotive and aeronautical arenas. One key to improving Li-ion battery performance lies in enhancing the efficiency of its electrodes. Silicon is a very promising anode material in this regard. Unfortunately, crystalline silicon typically degrades quickly when used as a Li-ion battery terminal. This is due to silicon's decrystallization from the repeated uptake (lithiation) and expulsion of lithium ions over multiple charge/discharge cycles. This degradation can be reduced by utilizing silicon microstructures, like patterned thin films and arrays of micro-sized "posts" (microposts). This study examined microposts before and after electrical charging/discharging. To quantify the degree of lithiation and decrystallization in the microposts, researchers conducted x-ray reflection interfacial microscopy (XRIM) experiments at the APS. Besides their important experimental findings, the research team expects these experimental techniques will be used to examine a variety of processes at solid/liquid interfaces, ranging from battery materials to the behavior of complex oxides and geochemical processes.

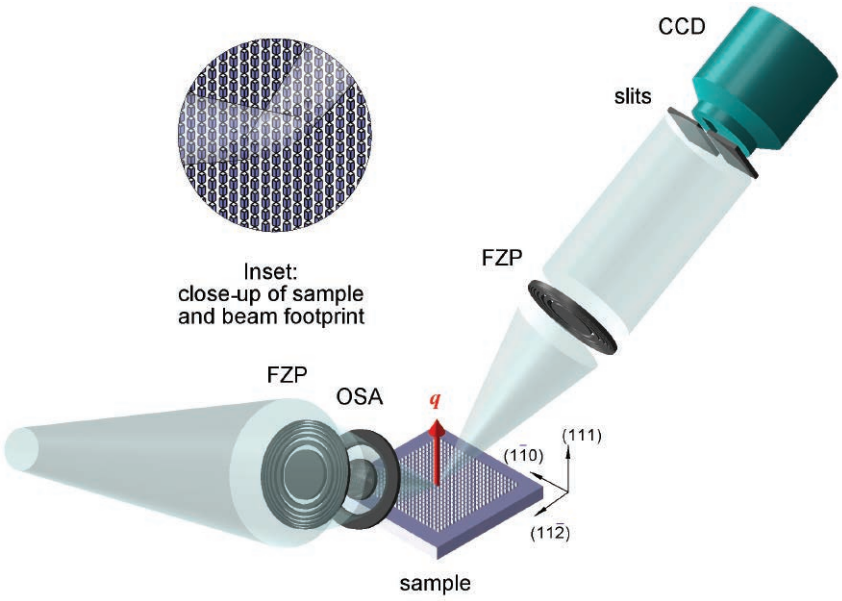

Fig. 1. The XRIM experimental setup. The micropost-array sample is shown at lower center; the crystallographic directions shown next to the sample indicate the lattice planes of the low-index silicon. Also shown are collimating slits and the charge-coupled device (CCD) detector (upper right), and the focusing optics: the Fresnel zone plates (FZPs) and order sorting aperture (OSA) [the OSA is basically a pinhole that reduces higher diffraction orders]. The circular inset depicts the x-ray beam footprint on the micropost array.

Silicon's advantage as a battery terminal material lies in its robust charge capacity, since a single silicon atom can covalently bind four lithium atoms. The ability to bind multiple lithium atoms, however, results in crystalline silicon swelling fourfold during its very first charging cycle. Microposts fabricated from (111)-oriented silicon wafers were previously found to preferentially lithiate laterally, expanding from the (110)-faceted sidewalls. The degree of lithiation can be controlled by adjusting the size and spacing of the posts, preventing their delamination from the underlying metal electrode.

In previous studies, electron microscopy was used to examine silicon microposts following their removal from a simulated battery environment that had been subjected to repeated charge/discharge cycles. The microscopy measurements revealed that some of the silicon remained lithiated, accompanied by partial decrystallization. Electron microscopy also confirmed that lithiation was preferentially initiated along the silicon's (110) facet. These measurements, however, could not directly reveal the amount of decrystallization within the silicon microposts, nor could electron microscopy be performed on microposts while immersed in a Li-ion electrolyte.

Exploiting the penetrating power of synchrotron x-rays at the APS, the research team from Argonne and the University of Illi-

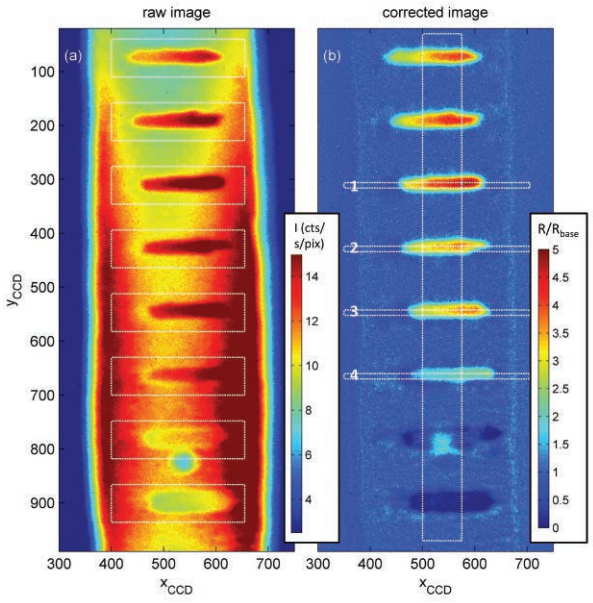

Fig. 2. (a) A raw (uncorrected) CCD image of partially lithiated microposts. The dashed lines around each micropost indicate areas excluded from the interpolated background. (b) In the background-subtracted (or "residual") images, zero intensity corresponds to the average reflectivity of the wafer (or basal plane) upon which the microposts rest. The intensity was then scaled such that zero corresponds to the minimum reflectivity, while the basal plane reflectivity is 1. Note the faint outline of the edges of the slits (see Fig. 1) used to collimate the reflected x-ray beam.

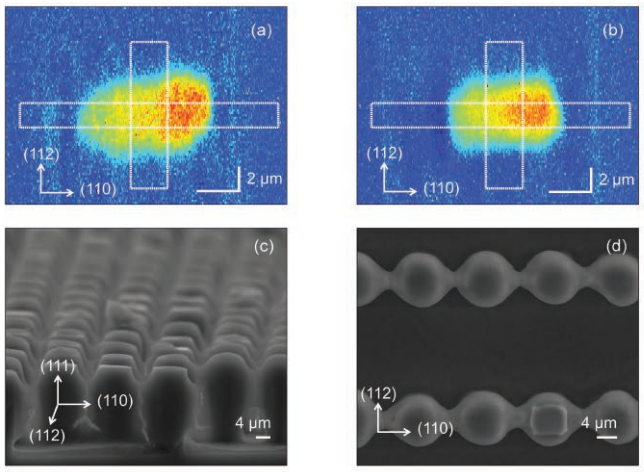

Fig. 3. XRIM images of a single micropost shown before (a) and after (b) partial lithiation. (The dashed lines delineate the areas used to analyze the crystallinity decrease from pre- to post-lithiation. Distance scale bars, and the orientation of the silicon's crystal planes, appear near the bottom of each panel.) Panels (c) and (d) are scanning electron micrographs of micropost arrays taken after the XRIM measurement. Panel (c) is a cross-sectional view. Panel (d) is taken from above (plan view), which matches the perspective used for the single micropost of panels (a) and (b). Lithiation is clearly seen in both (c) and (d) as a lateral bulging of the microposts.

nois at Urbana-Champaign was able to quantify the extent of decrystallization and lithiation of silicon microposts. The XRIM measurements were performed utilizing XSD beamline 33-ID-D,E at the APS on the evenly-spaced microposts shown in Fig. 3(c). Situated atop a silicon wafer (or basal plane), each micropost was fabricated with sides of 6 μm x 6 μm and a height of 10 μm. Within the basal plane, the posts were spaced 10 μm apart in one direction, and 17 μm apart in the other. The high-resolution x-ray measurements (170 nm — well below the microposts' dimensions) were performed before and after lithiation of the crystalline-silicon microposts, following exposure to a sustained electrical current.

The experimental setup is shown in Fig. 1. The x-ray data was background-subtracted to correct for the inhomogeneous illumination of the focused x-ray beam. Figure 2 depicts x-ray data before and after mathematical refinement, obtained using x-rays reflected from a row of microposts. X-ray reflections from the tops of the microposts clearly stand out in the corrected image [Fig. 2(b)].

Figure 3 depicts x-ray reflections off the top of a single micropost, both before [3(a)] and after [3(b)] lithiation. The reduced lateral extent of the micropost's effective size in Fig. 3b indicates a reduction in silicon crystallinity in the partly-lithiated micropost, which further analysis determined to constitute a 5% reduction in crystallinity in the vertical (the up-and-down direction in the image), and 13% horizontally (side-to-side). Since the image is taken from above, this shows a reduction in crystallinity in the lateral directions; in contrast, the x-ray data indicates that the top of the micropost experienced almost no decrystallization. The lateral lithiation of the microposts is clearly seen in the electron micrograph of Fig. 3(d).

The researchers anticipate that with additional improvements in XRIM instrumentation, dramatic new information about the morphology of diverse types of silicon microstructures will be uncovered. Improvements in resolution from 170 nm to 60 nm, as well as faster imaging rates due to extensive changes in the XRIM setup, will provide more detailed measurements of microposts and other materials.

— Philip Koth and William A. Atkins

See: Tim T. Fister[1]*, Jason L. Goldman[2], Brandon R. Long[1,2], Ralph G. Nuzzo[2], Andrew A. Gewirth[2], and Paul A. Fenter[1], "X-ray diffraction microscopy of lithiated silicon microstructures," Appl. Phys. Lett. **102**, 131903 (2013). DOI:10.1063/1.4798554
Author affiliations: [1]Argonne National Laboratory, [2]University of Illinois at Urbana-Champaign
Correspondence: * fister@anl.gov

Use of the Advanced Photon Source at Argonne National Laboratory was supported by the U.S. Department of Energy Office of Science under Contract No. DE-AC02-06CH11357.

33-ID-D,E • XSD • Materials science, physics, chemistry, geoscience, environmental science • Anomalous and resonant scattering (hard x-ray), diffuse x-ray scattering, general diffraction, surface diffraction, surface diffraction (UHV), x-ray standing waves, x-ray reflectivity • 4-40 keV, 6-25 keV • On-site • Accepting general users •

Strain Effects in VO_2 Microcrystals

Metal-insulator transitions (MITs) were first observed in metal oxides more than 50 years ago. These temperature-dependent transitions often change a material's crystalline phase and result in a shift between the electrically-conducting metallic and non-conducting insulator states. This transition can dramatically alter the material's optical characteristics, magnetic properties, etc. Such MIT phenomena have been exploited in many sensor and switching applications. Researchers from Oak Ridge National Laboratory, Southern Illinois University at Carbondale, Argonne, and North Carolina State University utilized x-ray microdiffraction — with micron-sized x-ray beams — to probe inside individual micro-sized crystals (microcrystals) of the important MIT material vanadium dioxide (VO_2). In most technical applications, the VO_2 consists of a thin film deposited on a substrate (i.e., as an epitaxial thin film). The microcrystals were imaged using both monochromatic (single-wavelength) and polychromatic (multi-wavelength) microdiffraction, producing highly-detailed information of sample microstructure. Using different strain and temperature regimes enabled the researchers to observe the evolution of various crystalline phases in the microcrystals. When combined with other methods (e.g., electron diffraction), these microdiffraction techniques provide new insights into controlling phase formation in VO_2, which in turn should lead to improvements in devices such as field-effect transistors and ultrafast optoelectronic switches.

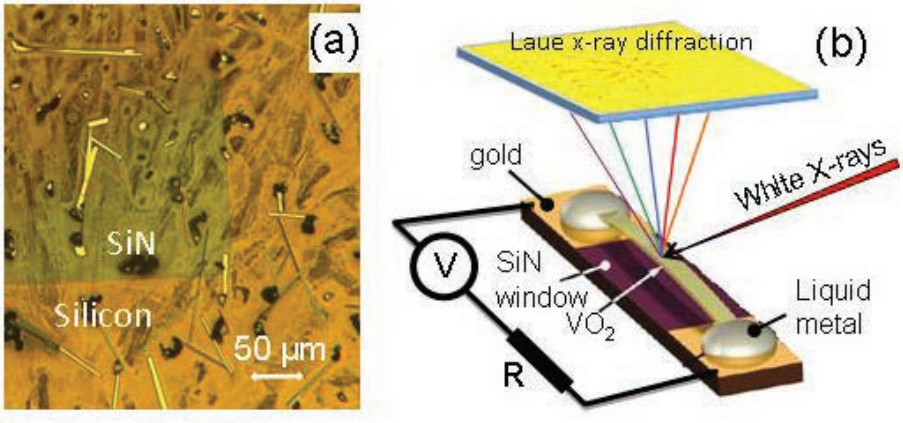

Fig. 1. Three types of VO_2 samples studied using x-ray microdiffraction. (a) Microcrystals grown directly on a SiN membrane and on a rigid silicon support. (b) Microcrystals suspended across gold electrical contacts and attached with liquid metal.

Figures 1(a) and 1(b) illustrate the range of sizes of the VO_2 microcrystals (note the scale bar) and the three different surface types used to hold them. Each surface mounting technique induced a different level of stress within the microcrystals, which in turn influenced their crystal phase formation and distribution. The highest induced stress resulted from situating the microcrystals on a rigid silicon substrate; significantly less stress resulted from mounting them on a flexible silicon nitride (SiN) membrane or by suspension between liquid-metal electrical contacts. For each of the three setups, the temperature was varied to determine the phase stability of the microcrystals near the metal-insulator transition temperature.

Both the monochromatic and polychromatic (white) x-ray experiments were performed at XSD beamline 34-ID-E of the APS. X-ray optics focused the synchrotron x-rays down to a width of ~400 nm. White x-ray measurements produced Laue diffraction patterns that yielded the crystal structure and orientation. Monochromatic x-ray measurements provided the additional information needed to reconstruct the

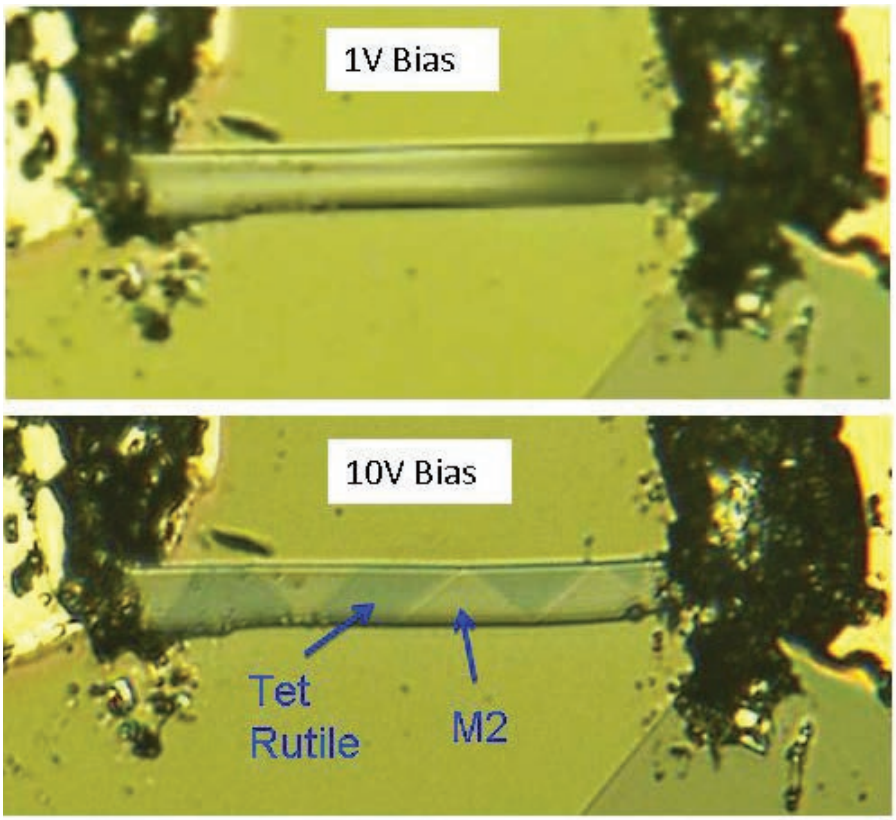

Fig. 2. Different phase behaviors when bias voltage is changed. Top: Single-crystal phase and abrupt phase transition at low-bias voltage. Bottom: Phase separation into triangular monoclinic M2 and tetragonal rutile (Tet Rutile) domains at higher bias voltage. The microcrystal is about 18-μm wide.

local strain distribution to high resolution (less than half-micron spatial resolution).

Three crystal phases were observed in the VO_2 microcrystals: the monoclinic M1 and monoclinic M2 phases, which behave as insulators, and the conducting rutile (R) phase (rutile derives from rutilus, Latin for red; this crystal phase most commonly occurs as a reddish mineral of titanium dioxide, TiO_2). As the temperatures of the microcrystal samples were changed, the phases of the microcrystals transitioned from one type to another. However, these transitions varied markedly according to sample stress. For instance, in the stress-free suspended samples, transitions between the M1 and R phases occurred abruptly following temperature changes as little as 0.003° C. The strain-free samples exhibited another interesting feature: when subjected to a higher threshold electric current, the M2 and R phases co-existed as alternating, triangular domains (regions) within the microcrystals [Fig. 2(b)]. At a lower current, however, these alternating domains disappeared and only an abrupt M1-to-R transition was observed.

In the highly-strained environment of the rigid silicon substrate, coexisting R and M2 phases appeared with a pronounced strain-field (a high-gradient strain pattern) very close to their interface. The highly-strained microcrystals also exhibited submicron-sized M2 twins. Twinning occurs when two domains of the same type of crystalline lattice (in this case the M2 phase) meet and mismatch — i.e., the crystallographic directions of the same crystal phase are misaligned in a symmetric way. For microcrystals on the flexible membrane, transitions between the M1 and R phases occurred abruptly throughout their entire volume.

The researchers demonstrated that a wide variety of crystal domains and phases can be formed in VO_2 microcrystals simply by varying their strain environment. This has significant implications for VO_2 thin films, which constitute the most commonly used form of VO_2 in electronic and sensor devices. The presence of local strain inhomogeneities undoubtedly produces an assortment of crystal phases and domains, which in turn contribute to the broadened and shifted phase transitions observed in these thin films. Controlling the strain profile of VO_2 thin films should lead to better control of their characteristics, with the potential for application to similar metal-oxide-based MIT materials.

— Philip Koth and William A. Atkins

See: J.D. Budai[1]*, A. Tselev[2], J.Z. Tischler[1,3], E. Strelcov[2], A. Kolmakov[2], W.J. Liu[3], A. Gupta[4], and J. Narayan[4], "*In situ* X-ray Microdiffraction Studies Inside Individual VO_2 Microcrystals," Acta Mater. **61**, 2751 (2013). DOI:10.1016/j.actamat.2012.09.074
Author affiliations: [1]Oak Ridge National Laboratory, [2]Southern Illinois University at Carbondale, [3]Argonne National Laboratory, [4]North Carolina State University
Correspondence: * budaijd@ornl.gov

Research by J.D.B. and J.Z.T. was sponsored by the U.S. Department of Energy Office of Science-Basic Energy Sciences, Materials Sciences and Engineering Division. Use of the Advanced Photon Source at Argonne National Laboratory was supported by the U.S. Department of Energy Office of Science under Contract No. DE-AC02-06CH11357.

34-ID-E • XSD • Materials science, physics, environmental science, geoscience • Microdiffraction, Laue crystallography, microbeam • 7-30 keV • On-site • Accepting general users •

Gauging Reaction Velocities in Multilayer Foils

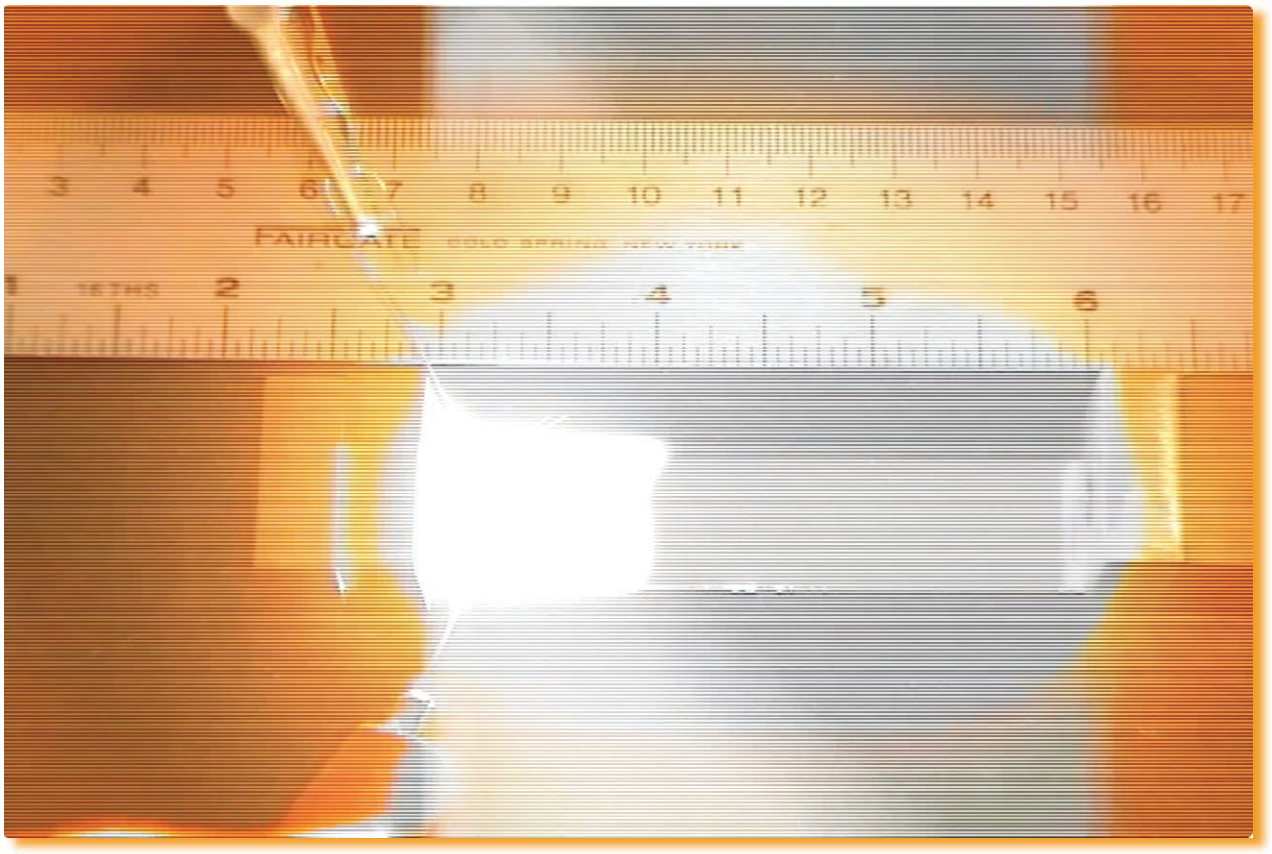

Foils made of nanoscale layers alternating between transition elements such as nickel, niobium, zirconium, or titanium; and light elements such as aluminum, silicon, boron, or carbon can react in a rapid, exothermic wave that burns through the foil at a steady speed (Fig. 1). Such reactive multilayer foils typically consist of hundreds of layers of metal, each layer just a few nanometers thick. A single foil can contain over 500 pairs of layers, known as bilayers. For example, a commercially available reactive multilayer called NanoFoil® contains alternating layers of nickel and aluminum multilayers and is used commercially as a local heat source for soldering. In general, the speed of the foil's reaction front slows as the thickness of a single bilayer increases. But in at least one pair of metals, the speed-thickness dependence breaks down. Researchers used the intensely bright x-rays at the APS to image the reaction front of such an anomalous system, made from layers of aluminum (Al) and zirconium (Zr). Though they still do not know why the speed-thickness dependence breaks down in the Al/Zr foil, the researchers did obtain a detailed view of the crystalline phase transformations that occur during the rapid reaction. Their results could eventually help fine-tune such metal bilayer systems, which are used for precision welding, chemical time delays, and heat sources for bioagent destruction.

The Al/Zr multilayer foils tested in this study have a 3:1 atomic ratio of aluminum to zirconium, and they show an anomalous behavior: The reaction velocity stays a constant 7.7 m/sec even as the bilayer thickness increases from 20 nm to 30 nm. It is a puzzling discrepancy that Johns Hopkins materials scientists have been investigating. A colleague at Lawrence Livermore National Laboratory suggested that the zirconium might undergo a phase change due to the heat given off by the reaction, and this phase change might alter the speed of the reaction front. At room temperature the zirconium has a hexagonal close-packed crystalline phase, but at high temperatures it can shift to a body-centered cubic structure.

To test this idea, the Johns Hopkins researchers with colleagues from Argonne performed *in situ* x-ray microdiffraction at XSD beamline 7-ID-B at the APS. The very bright yet tightly focused x-ray beam allowed them to zoom in on the tiny area in which the reaction was occurring and watch to see if the zirconium crystalline phase changed (Fig. 1). The APS produces a billion times more photons per second than the typical laboratory x-ray source, giving a higher probability that enough photons would interact with the reaction front to accurately picture the crystalline structure of the metal as it passed through the x-ray beam. The experiment worked; it clearly showed that the zirconium did not undergo a phase change at the reaction front prior to mixing with the aluminum.

< Fig. 1. A macroscopic view of the reaction front. The exothermic mixing of aluminum and zirconium heats the foil to white-hot on the left; the unreacted foil is still gray. The reaction front where the two regions meet, at the 4-in. mark on the ruler, is obvious. Photo: Todd Hufnagel, Johns Hopkins University.

While the researchers ruled out this possible explanation, they saw something else. A separate experiment, using the undulator x-ray source at XSD beamline 32-ID-B, revealed that the nature of the reaction front itself shifted in foils with different compositions. Multilayers with the same bilayer thickness but Al:Zr ratios of 1:1 had uneven reaction fronts that propagated through the foil in a step-wise motion. If the 3:1 Al/Zr foils had the same unsteady propagation, this could explain the unexpected speed-bilayer relationship. However, the multilayers with a 3:1 ratio of aluminum to zirconium had steady, planar reaction fronts, foiling this explanation as well.

The researchers are now exploring numerical simulations of reaction propagation with the hopes that they can replicate the speed anomaly. A more precise understanding of reaction propagation in the Zr/Al system will give insight into the thermodynamics of these reactive nanosystems and ultimately could enhance our use of reactive multilayer foils in nanoenergetics-on-a-chip, precision welding of microscopic components and other advanced applications. *— Kim Krieger*

See: S.C. Barron[1], S.T. Kelly[1], J. Kirchhoff[1], R. Knepper[1], K. Fisher[1], K.J.T. Livi[1], E.M. Dufresne[2], K. Fezzaa[2], T.W. Barbee[3], T.C. Hufnagel[1], and T.P. Weihs[1]*, "Self-propagating reactions in Al/Zr multilayers: Anomalous dependence of reaction velocity on bilayer thickness," J. Appl. Phys. **114**, 223517 (2013). DOI:10.1063/1.4840915
Author affiliations: [1]Johns Hopkins University, [2]Argonne National Laboratory, [3]Lawrence Livermore National Laboratory
Correspondence: * weihs@jhu.edu

Research at the APS was supported by the U.S. Department of Energy (Grant No. ESC002509). Use of the Advanced Photon Source at Argonne National Laboratory was supported by the U.S. Department of Energy Office of Science under Contract No. DE-AC02-06CH11357.

7-ID-B,C,D • XSD • Materials science, atomic physics, chemistry • Time-resolved x-ray scattering, time-resolved x-ray absorption fine structure, phase contrast imaging • 6-21 keV • On-site • Accepting general users •

32-ID-B,C • Materials science, life sciences, geoscience • Phase contrast imaging, radiography, transmission x-ray microscopy, tomography • 7-40 keV • On-site • Accepting general users •

Building Better Cathodes for Rechargeable, Earth-Friendly Batteries

A new nanostructured material has qualities necessary for good cathodes in next-generation rechargeable batteries. Researchers at Argonne, The University of Chicago, and the Illinois Institute of Technology mixed iron oxide nanoparticles and carbon nanotubes to create a cathode that allows fast charge transfers and cyclability in a sodium ion battery. Using x-rays from two beamlines at the APS, they monitored the material as ions moved into and out of the cathode's crystal lattice. Because iron oxide, carbon, and sodium are all abundant materials, this is a promising route to developing efficient, cost-effective, rechargeable batteries. These results were the cover subject of *Chemistry of Materials* **25**(7), 2013.

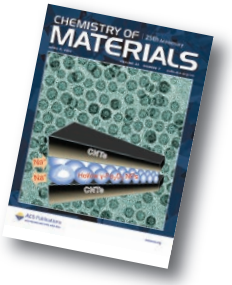

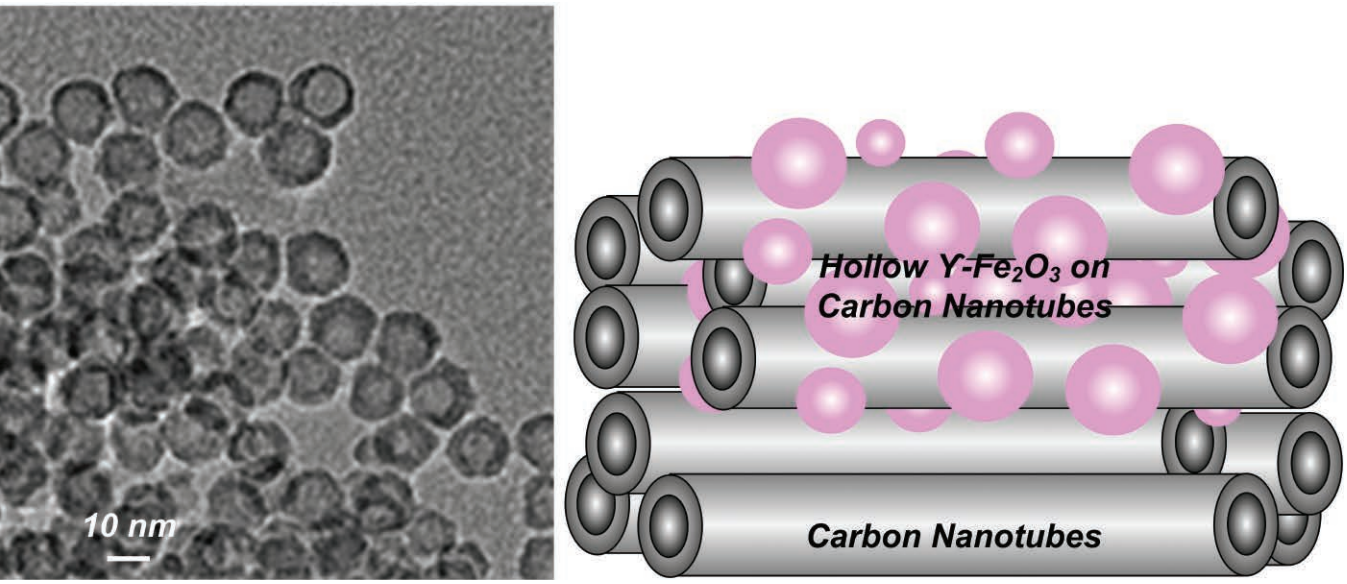

Fig. 1. Transmission electron micrograph of the hollow iron oxide nanoparticles (left) and depiction of the electrode structures (right). The electrodes were used to test the intercalation and deintercalation of Na^+ ions in hollow iron oxide nanoparticles that were found to have a high concentration of iron vacancies.

Portable electronics and hybrid cars are powered by lithium ion (Li-ion) batteries. The technology provides desirable charge capacity and cyclability at a commercially viable price and weight. But Li is a limited resource, whereas the demand for batteries continues to grow. Sodium (Na)-ion batteries utilize materials that are more abundant than Li, but are not as well developed. Many cathodes (which attract positively-charged ions from the electrolyte solution in the battery) designed for Li-ion batteries perform poorly in batteries that use the larger Na ions.

A test battery built using Argonne's Center for Nanoscale Materials (CNM) from a cathode made of hollow iron oxide nanoparticles and carbon nanotubes was subjected to multiple charge and discharge cycles. The researchers then took electron microscope images, again at the CNM, of the materials before and after charging. Using synchrotron x-rays they could also monitor changes in the cathode while the battery cycled.

To understand what happens when the Na ions move into the iron oxide nanoparticles, the researchers used two x-ray absorption spectroscopy methods that allowed them to study the local structure around certain elements in the cathodes: x-ray absorption near edge structure (XANES) and extended x-ray absorption fine structure (EXAFS). They used XANES to figure out the oxidation state of the iron and thus determine the concentration of vacancies (areas into which Na ions could move) in different positions in the crystal lattice. The XANES and EXAFS measurements were conducted at the MR-CAT 10-ID-B beamline at the APS.

The researchers also used x-ray diffraction to study changes in both the crystalline lattices and vacancies. These measurements were performed at the GSECARS beamline 13-ID-C,D at the APS.

Electrodes usually fail because of damage to the material. As ions move into and out of the cathode, delivering charge, the cathode swells or shrinks, which can literally pulverize the oxide electrode. As damage accumulates, the pathways that guide charge out of the battery are also damaged, so over a number of cycles the efficiency of the battery declines. To combat this damage, the researchers used CNM's synthesis facilities to create hollow nanoparticles — which tolerate volume changes well — sandwiched between carbon nanotubes, providing good electrical connectivity even if the charge-accepting material is damaged. Using XANES measurements, they discovered many cation vacancies in the iron-oxide structure, about four times higher than in most cathode materials.

Nanoparticles made up 45% of the electrode by weight. The researchers found that the Na ions enter the vacancies faster than iron oxidizes. Thus, charge transfers from the electrolyte to cathode faster than the chemical reaction that would change the cathode material from an inverse spinel to a rock salt structure. They tested the speed of charging and the electrode's capacity (in other words, how much electric charge can be provided by a certain weight of material). The electrode had a large and reversible capacity of 189 mAh/g. But many good cathodes for Na-ion batteries fade quickly, so how does this one stack up to repeated charging? Strikingly, after 500 cycles of quickly draining a lot of charge (99 mAh/g) from the test cell, the researchers found that the cathode retained its capacity.

They discovered that the Na ions move inside the hollow nanoparticles and do not damage the crystal structure of the cathode. In fact, the crystal structure improved with use. Also, when subjected to many cycles at high current rates, the capacity increased! They believe that the vacancies become organized into channels that make it easier for Na ions to move through the structure.

This is the first Na cathode material that shows high-rate performance while maintaining capacity, to the best of the researchers' knowledge. Therefore, the hollow nanoparticles sandwiched by carbon nanotubes offer an Earth-friendly and efficient cathode material for Na-ion batteries. The researchers continue to investigate the cathode by changing the concentration of vacancies via doping the ferrous oxide with multivalent cations.

— Yvonne Carts-Powell

See: Bonil Koo[1]*, Soma Chattopadhyay[3], Tomohiro Shibata[3], Vitali B. Prakapenka[2], Christopher S. Johnson[1], Tijana Rajh[1], and Elena V. Shevchenko[1], "Intercalation of Sodium Ions into Hollow Iron Oxide Nanoparticles" Chem. Mater. **25**(7), 245 (2013).

Author affiliations: [1]Argonne National Laboratory, [2]The University of Chicago, [3]Center for Synchrotron Radiation Research and Instrumentation-Illinois Institute of Technology

Correspondence:

* bonilkoo79@gmail.com,

** eshevchenko@anl.gov

Use of the Center for Nanoscale Materials was supported by the U.S. Department of Energy (DOE) Office of Science-Basic Energy Sciences under Contract No. DE-AC02-06CH11357. GSECARS is supported by the National Science Foundation-Earth Sciences (EAR-0622171) and DOE-Geosciences (DE-FG02-94ER14466). MR-CAT operations are supported by the DOE and the MR-CAT member institutions. Use of the Advanced Photon Source at Argonne National Laboratory was supported by the U.S. Department of Energy Office of Science under Contract No. DE-AC02-06CH11357.

10-ID-B • MR-CAT • Materials science, environmental science, chemistry • X-ray absorption fine structure, time-resolved x-ray absorption fine structure, micro x-ray absorption fine structure, microfluorescence (hard x-ray) • 4.3-27 keV, 4.3-32 keV, 15-90 keV • On-site • Accepting general users •

13-ID-C,D • GSECARS • Geoscience, environmental science • Inelastic x-ray scattering, micro x-ray absorption fine structure, microdiffraction, x-ray absorption fine structure, microfluorescence (hard x-ray), high-pressure diamond anvil cell, high-pressure multi-anvil press • 4-45 keV • On-site • Accepting general users •

Turning Up the Power in Organic Solar Cells

Solar cells are an important component of renewable energy, and polymer solar cells are particularly attractive for some uses. They're lightweight and flexible, so they're easily integrated with architecture, and they can be manufactured on plastic surfaces using inexpensive roll-to-roll printing. Polymer solar cells, however, lag behind their silicon counterparts in their efficiency at converting sunlight to electricity. Now, based on experiments carried out at the APS, researchers have reported a new approach to boosting that efficiency, potentially making them more practical and cost effective.

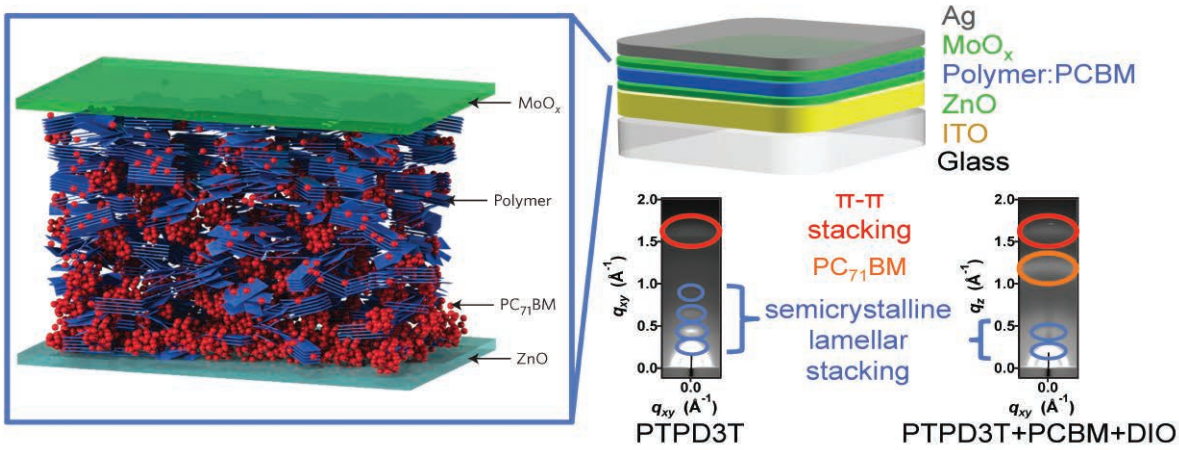

Fig. 1. A schematic of a solar cell (top right) shows a glass substrate coated with indium tin oxide, a layer of polymer sandwiched between zinc oxide and molybdenum oxide, and a silver contact on top. X-ray scattering revealed the organization of the polymer molecules (left) with the blue ribbons of PCBM arranged in stacks that, together with π-π stacking, allows charge to move more easily.

Three factors contribute to the power conversion efficiency of all types of solar cells, including polymer solar cells: the short-circuit current, the open-circuit voltage, and the fill factor. Fill factor is the ratio of the maximum power available from the solar cell to the product of the short-circuit-current and open-circuit voltage.

Although increasing conversion efficiency can be achieved by adjusting the polymer properties to improve either the short-circuit current or the open-circuit voltage, the two properties may compromise each other. Ultimately, raising the fill factor is a key to boost cell power conversion efficiency, but the best result researchers had been able to achieve in the past was 72%, with most polymers falling far short of that.

The team of researchers from Argonne, Northwestern University, South University of Science and Technology of China, the University of Malaga (Spain), and the Polyera Corp. developed polymers that enable the production of solar cells with fill factors of 76 to 80%, the highest ever achieved. That leads to a power conversion efficiency of 8.7%, but the researchers say further adjustments should bring that to above 10%. The eventual goal, they say, would be to create polymer solar cells with 15% power conversion efficiency.

The polymers the researchers created were poly[5-(2-hexyldodecyl)-1,3-thieno[3,4-c]pyrrole-4,6-dione-alt-5,5-(2,5-bis(3-dodecylthiophen-2-yl)-thiophene)] (PTPD3T) and poly[N-(2-hexyldodecyl)-2,2′-bithiophene-3,3′-dicarboximide-alt-5,5-(2,5-bis(3-decylthiophen-2-yl)-thiophene)] (PBTI3T). They combined these electron donating polymers with fullerene ("bucky ball") electron acceptors in films to create bulk heterojunction solar cells. In such solar cells, light striking the material creates excitons in the polymers, which can be split into positive and negative charges at the intersection between the polymer, acting as an electron donor, and fullerene molecules, acting as an electron acceptor. The positive charges in the polymers and the electrons in the fullerene clusters in the films then flow to the solar cell's respective electrodes

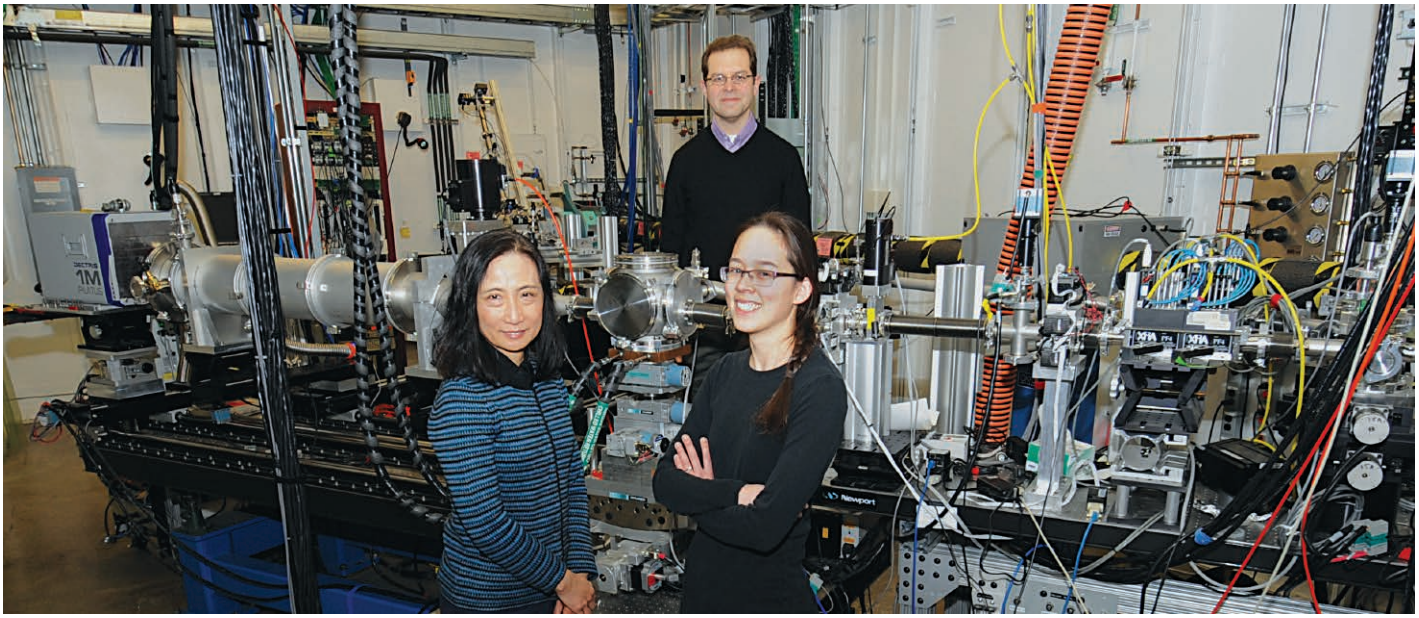

L. to r.: Lin X. Chen (CSE and Northwestern University), Joseph W. Strzalka (XSD), and Sylvia J. Lou (Northwestern University) in the 8-ID-E research station.

to provide power. Enhancing the ease with which excitons split and charge carriers transport through the material and reducing the probabilities for the positive and negative carriers to recombine will improve the fill factor, and hence the solar cell efficiency.

Using XSD beamline 8-ID-E at the APS, the team made grazing incident x-ray scattering measurements that allowed them to study the orientation and arrangement of the molecules in the thin bulk heterojunction films on an electrode substrate. Though the molecules of a polymer are not as ordered as those in a silicon crystal, they were found to be arranged in an orderly enough fashion in one dimension to have polymer aligned at the interface. The polymers, the researchers found, were arranged in ribbons, stacked flat on top of the electrode in an arrangement known as π-π stacking. The arrangement creates a periodic structure that allows positive charge carriers to move from ribbon to ribbon easily, thus improving the carriers' mobility and maximizing the contacts with the electrode to enhance the charge collection efficiency.

The fullerenes, however, tend to form big clusters and interrupt the polymer stacking, so the team looked at what happened when they added 1,8-diiodooctane (DIO) to the mix. The DIO caused the fullerenes to be dispersed more evenly among the polymer ribbons. Because the intersection between fullerenes and polymer is where the charge carriers are most likely to separate into positive and negative, dispersing the fullerene more regularly to create an optimal number of these junctions to allow more excitons to split into charge carriers effectively.

Many parameters of the materials that go into polymer solar cells can be adjusted to improve performance, and not all the mechanisms that work against high efficiency are fully understood, but the researchers say their demonstration that they can enhance the fill factor to record levels means that the devices, which have doubled their efficiency in the last five years, will continue to improve.

– Neil Savage

See: Xugang Guo[1,2], Nanjia Zhou[1], Sylvia J. Lou[1], Jeremy Smith[1], Daniel B. Tice[1], Jonathan W. Hennek[1], Rocío Ponce Ortiz[1,3], Juan T. López Navarrete[3], Shuyou Li[1], Joseph Strzalka[4], Lin X. Chen[1,4*], Robert P. H. Chang[1**], Antonio Facchetti[1,5***], and Tobin J. Marks[1****], "Polymer solar cells with enhanced fill factors," Nat. Photonics **7**, 82 (October 2013). DOI:10.1038/NPHOTON.2013.207

Author affiliations: [1]Northwestern University, [2]South University of Science and Technology of China, [3]University of Málaga, [4]Argonne National Laboratory, [5]Polyera Corporation

Correspondence: * lchen@anl.gov; ** r-chang@northwestern.edu; *** a-facchetti@northwestern.edu; **** t-marks@northwestern.edu

This research was supported as part of the ANSER Center, an Energy Frontier Research Center funded by the U.S. Department of Energy Office of Science, Basic Energy Sciences (award no. DE-SC0001059); by Polyera Corporation; and by the Air Force Office of Scientific Research (FA9550-08-1-0331). X.G. acknowledges financial support from a South University of Science and Technology of China start-up fund. R.P.O. acknowledges the MICINN of Spain for a Ramòn y Cajal research Contract. J.T.L.N. acknowledges financial support from the MICINN (project no. CTQ2012-33733) and the Junta de Andalucía (project no. PO9-4708). D.B.T. is funded by the National Science Foundation-Integrative Graduate Education and Research Traineeship Program. Use of the Advanced Photon Source at Argonne National Laboratory was supported by the U.S. Department of Energy Office of Science under Contract No. DE-AC02-06CH11357.

8-ID-E • XSD • Materials science, polymer science, physics • Grazing incidence small-angle scattering, x-ray photon correlation spectroscopy, intensity fluctuation spectroscopy, grazing incidence diffraction • 7.35-7.35 keV • On-site • Accepting general users •

New Materials for Capturing Carbon Dioxide from Combustion Gases

Carbon dioxide is both a culprit in global warming and also responsible for keeping the Earth warm enough to support life as we know it. It is odorless and colorless, often represented by a smokestack plume trailing into the sky, signifying pollution and greenhouse gases. That plume is actually water vapor, which together with carbon dioxide and nitrogen makes up the majority of the gas exhausted from power plants burning fossil fuels. But water vapor turns out to be an obstacle to removing carbon dioxide from power plant emissions. Studies carried out at the APS support the effort to quantify the ability of new materials to capture carbon dioxide, even while in the presence of water.

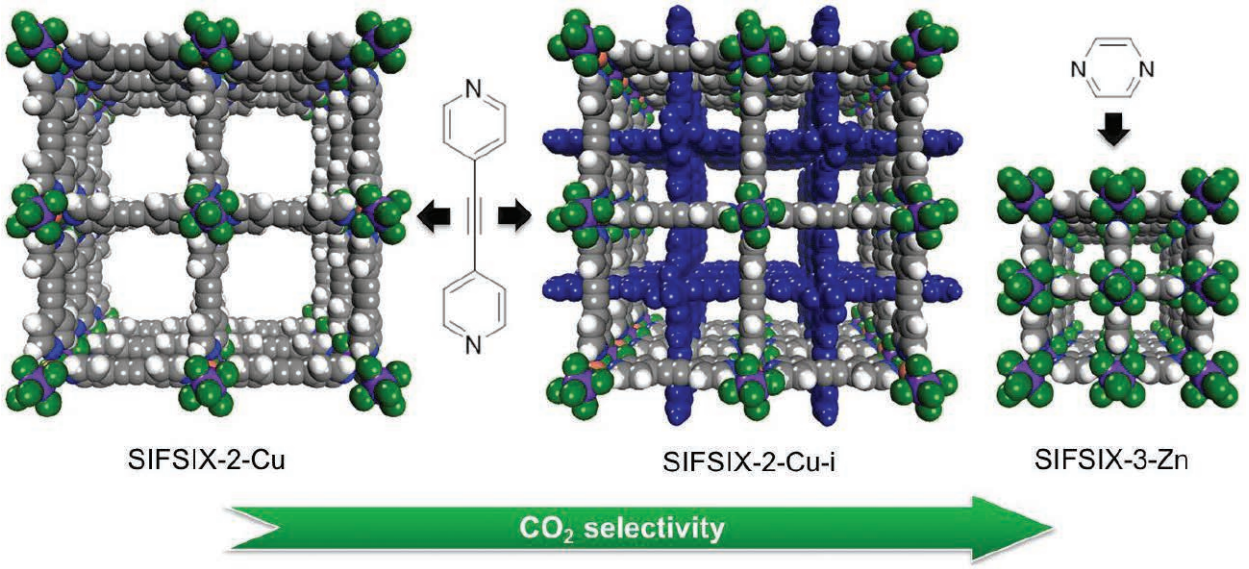

Fig. 1. The SIFSIX materials in order of increasing carbon dioxide selectivity, from left to right. The bright blue spheres in SIFSIX-2-Cu-i represent the interpenetrating network. The nitrogen ring molecules link together the SIFSIX materials; SIFSIX-2-Cu and SIFSIX-2-Cu-i use 4,4'-dipyridylacetylene as a linker while SIFSIX-3-Zn uses pyrazine.

From an engineering perspective, the metal-organic material for a post-combustion chamber must capture carbon dioxide efficiently, it must be reusable, and it must require less energy than existing solutions, which can require as much as 30% of the energy produced by the plant. In materials science terms, this means a high selectivity for carbon dioxide, just enough affinity for carbon dioxide that the gas adsorbs onto the material, but not so much the gas cannot be extracted then sequestered, and a large uptake of carbon dioxide per volume of the material.

Scientists with the University of South Florida and King Abdullah University of Science and Technology (Saudi Arabia) are exploring new materials based on a pre-existing combination of copper, bipyridine $(C_5H_4N)_2$, and the hexafluorosilicate anion SiF_6^{2-}. Previous research by this team showed that the SiF_6^{2-}, which they refer to as SIFSIX, has strong, favorable interactions with carbon dioxide. From this base, they created three materials: SIFSIX-2-Cu, SIFSIX-2-Cu-i, and SIFSIX-3-Zn, described in Fig. 1.

The team's measurements of carbon dioxide uptake for each material allowed them to reject SIFSIX-2-Cu due to its low value. Using the Ideal Adsorbed Solution Theory (IAST) (in solution thermodynamics, a predictive model that does not require any mixture data and is independent of the actual model of physical adsorption) they confirmed that the SIFSIX-2-Cu carbon dioxide selectivity was also low, probably because the SIFSIX anions that line its cell walls are not sufficiently close together to boost each other's potential for attracting carbon dioxide. SIFSIX-2-Cu-i and SIFSIX-3-Zn have uptake values similar to those of benchmark materials.

Single-crystal x-ray diffraction studies at the 15-ID-B,C,D beamline and calculations of the enthalpy of adsorption, which relates to the materials' affinity for carbon dioxide, showed that SIFSIX-2-Cu-i and SIFSIX-3-Zn adsorb carbon dioxide uniformly over a range of carbon dioxide loading. The adsorption is efficient and reversible, meaning that the CO_2 is easily captured but also easily removed from the SIFSIX material, so it can be sequestered. This makes the material reusable.

However, carbon dioxide selectivity is the most important characteristic for a metal-organic material to be used in post-combustion chambers. The high values for SIFSIX-2-Cu-i calculated using IAST — higher than any benchmark material, not just metal-organic materials — surprised the team. They confirmed these results using breakthrough tests. The selectivity of SIFSIX-3-Zn was even higher than SIFSIX-2-Cu-i; the team confirmed those results using both breakthrough tests and by measuring single-gas adsorption isotherms.

Because water is present in the post-combustion gases of fossil fuels, the researchers needed to show that the selectivity of the materials does not decrease in the presence of water. They found that the ability of SIFSIX-3-Zn to preferentially select carbon dioxide was unaffected by water, because the $SiF6^{2-}$ anion attracts polarizable molecules — carbon dioxide is more strongly polarized than other post-combustion gases — making the SIFSIX-3-Zn hydrophobic.

Both SIFSIX-2-Cu-i and SIFSIX-3-Zn have the characteristics necessary to capture carbon selectively and efficiently in a power plant's post-combustion chamber. Both materials keep a firm but not unbreakable hold on the carbon dioxide allowing it to be released through pressure or temperature changes, then sequestered into geological formations or empty oil wells. These materials are an ideal start for engineering a carbon capture solution in post-combustion chambers.

— Mary Alexandra Agner

See: Patrick Nugent[1], Youssef Belmabkhout[2]*, Stephen D. Burd[1], Amy J. Cairns[2], Ryan Luebke[2], Katherine Forrest[1], Tony Pham[1], Shengqian Ma[1], Brian Space[1], Lukasz Wojtas[1], Mohamed Eddaoudi[1,2]*, and Michael J. Zaworotko[1]**, "Porous materials with optimal adsorption thermodynamics and kinetics for CO_2 separation," Nature **495**, 80 (7 March 2013). DOI:10.1038/nature11893

Author affiliations: [1]University of South Florida, [2]King Abdullah University of Science and Technology

Correspondence:

* mohamed.eddaoudi@kaust.edu.sa,

** xtal@usf.edu

This work is supported by King Abdullah University of Science and Technology (KAUST) award number FIC/2010/06 (M.E. and M.J.Z.) and KAUST start-up funds (M.E.). B.S. acknowledges computational resources made available by an XSEDE grant (number TG-DMR090028). ChemMatCARS is principally supported by the National Science Foundation/ Department of Energy under grant number NSF/CHE-0822838. Use of the Advanced Photon Source at Argonne National Laboratory was supported by the U.S. Department of Energy Office of Science under Contract No. DE-AC02-06CH11357.

15-ID-B,C,D • ChemMatCARS • Materials science, chemistry • Single-crystal diffraction, anomalous and resonant scattering (hard x-ray), wide-angle x-ray scattering, microdiffraction, liquid surface diffraction, small-angle x-ray scattering, ultra-small-angle x-ray scattering, high-pressure diamond anvil cell • 6-32 keV, 10-60 keV • On-site • Accepting general users •

A Better Way to Probe Biological Polymorphs

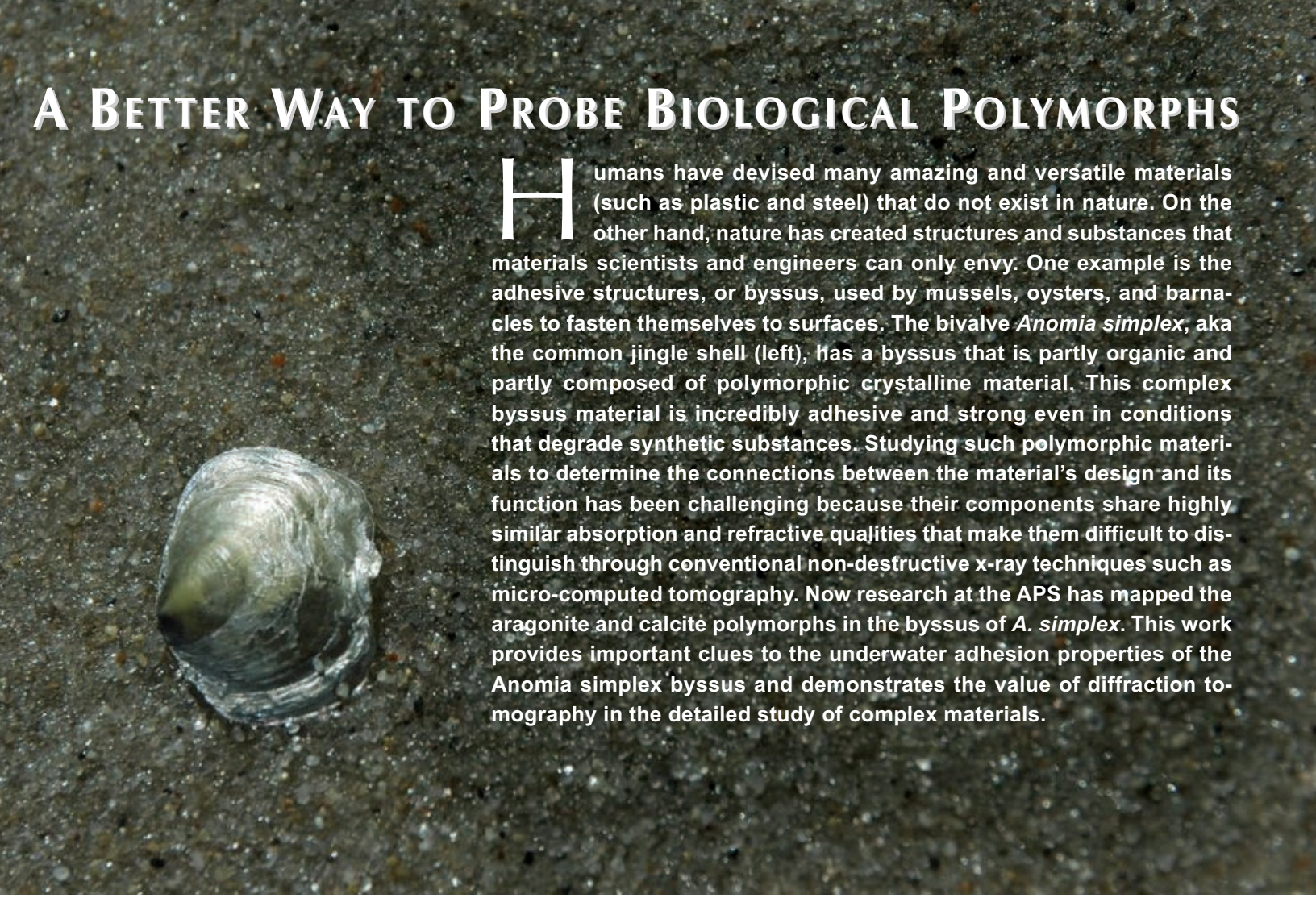

Humans have devised many amazing and versatile materials (such as plastic and steel) that do not exist in nature. On the other hand, nature has created structures and substances that materials scientists and engineers can only envy. One example is the adhesive structures, or byssus, used by mussels, oysters, and barnacles to fasten themselves to surfaces. The bivalve *Anomia simplex*, aka the common jingle shell (left), has a byssus that is partly organic and partly composed of polymorphic crystalline material. This complex byssus material is incredibly adhesive and strong even in conditions that degrade synthetic substances. Studying such polymorphic materials to determine the connections between the material's design and its function has been challenging because their components share highly similar absorption and refractive qualities that make them difficult to distinguish through conventional non-destructive x-ray techniques such as micro-computed tomography. Now research at the APS has mapped the aragonite and calcite polymorphs in the byssus of *A. simplex*. This work provides important clues to the underwater adhesion properties of the Anomia simplex byssus and demonstrates the value of diffraction tomography in the detailed study of complex materials.

The experimenters from Aarhus University (Denmark), Northwestern University, and Argonne examined *A. simplex* specimens at the XSD 1-ID-B,C,E beamline of the APS. They utilized non-destructive x-ray diffraction tomographic methods to reconstruct the distribution of various crystalline phases in the material and determine the degree of local magnesium substitution through analysis of reconstructed powder diffractograms. The specimens were examined whole, without being cut or sectioned in any way.

The *A. simplex* byssus is a highly calcified and complex structure, consisting of a lamellar section that interacts with the musculature and a more porous section that faces the hard surface. The lamellar section is composed of highly crystallized organic material sheets that extend both into the muscles and through the porous part of the byssus all the way to the attachment surface. The byssus begins in a young *A. simplex* as a small lamellar organic plate that slowly mineralizes and increases in size as the animal grows, adding calcified support below.

The researchers collected both absorption and diffraction data simultaneously, obtaining maps with 50-μm resolution. They found that they were able to obtain much more valuable information from the diffraction tomography. The x-ray absorption studies showed macroscopic-scale features with little detail, while the diffraction studies allowed data-rich reconstructions using two different approaches, one examining specific regions of interest in particular diffraction angles consistent with different polymorphs, and the other generating full reconstructed powder diffractograms. The first approach demonstrated that the calcite and aragonite polymorphs were present in quite distinct areas of the byssus: aragonite solely in the lamella, calcite solely in the porous region.

The reconstructed powder diffraction data from the second approach showed the degree of magnesium substitution in the porous calcite areas, where magnesium can substitute into the calcite structure leading to shifts in its diffraction peaks. The investigators found bands of high magnesium content in the porous areas of the byssus, especially near the interface with the lamellar volumes.

They explain that two separate mechanisms could account for the presence of magnesium in the byssus. The first is structural adaptation due to increased mechanical stress (the presence of magnesium strengthens and stiffens the calcite structure of the byssus).

A second possibility is that seawater infiltrates the byssus and magnesium is thus incorporated into it as a byproduct of normal growth. This is supported by the discovery of a generally higher amount of magnesium near the interface between the lamellar and porous regions of the byssus, as magnesium cannot incorporate into the

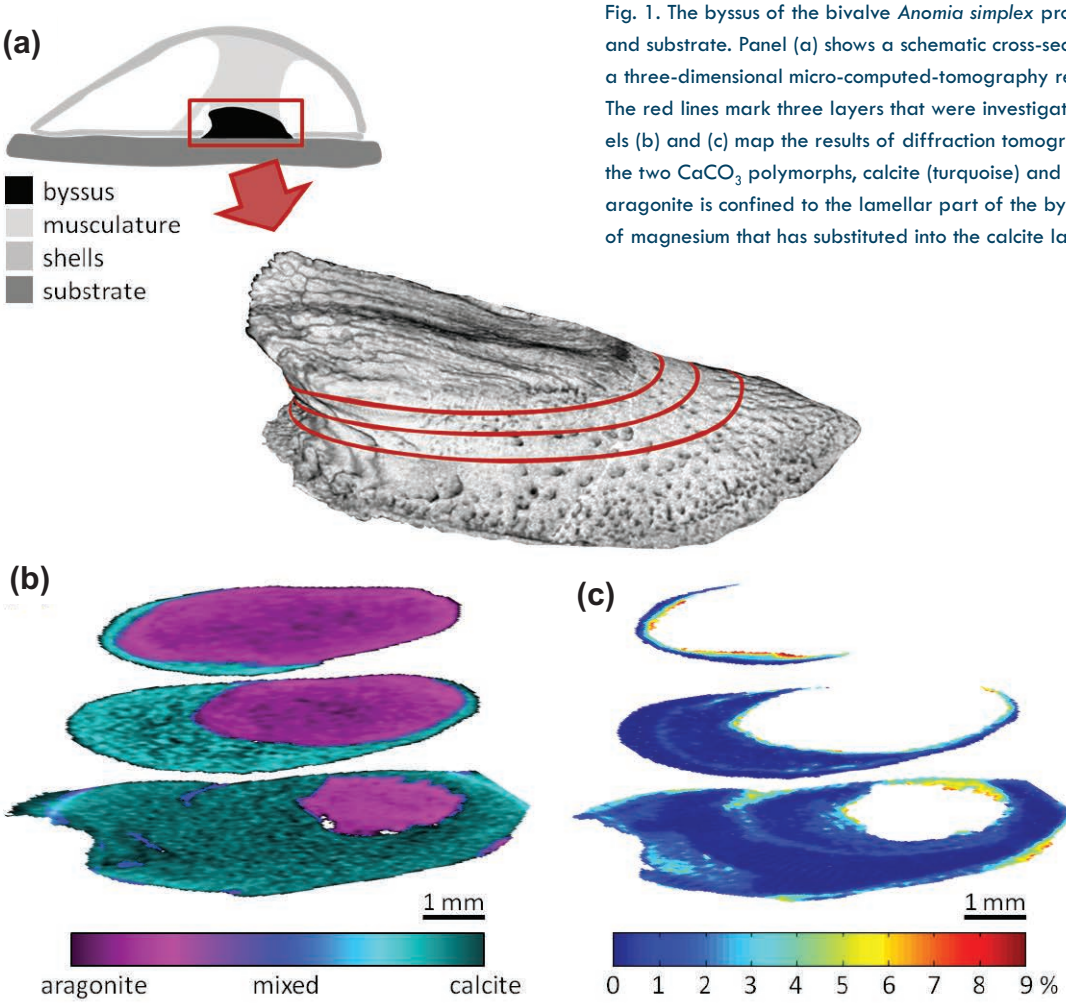

Fig. 1. The byssus of the bivalve *Anomia simplex* provides the anchor between mussel and substrate. Panel (a) shows a schematic cross-section of the animal (left) and (right) a three-dimensional micro-computed-tomography rendering of the mineralized byssus. The red lines mark three layers that were investigated by diffraction tomography. Panels (b) and (c) map the results of diffraction tomography. Panel (b) is the distribution of the two $CaCO_3$ polymorphs, calcite (turquoise) and aragonite (magenta), proving that aragonite is confined to the lamellar part of the byssus. Panel (c) shows the percentage of magnesium that has substituted into the calcite lattice in the place of calcium.

aragonite structure but will be pushed in front of the growth zone, giving an increased magnesium concentration at the interface. The investigators note that the question is still unresolved and bears further investigation.

The ability to map the relative distribution of polymorphs and local variations in the crystalline phases (here giving magnesium substitution in the *A. simplex* byssus) demonstrated in this work provides an impressive example of the value of diffraction tomography in the detailed study of complex materials. Because these techniques are completely non-destructive both mechanically and from a radiation exposure standpoint, the same specimen can later be studied using different methods. Particularly in cases where such concerns are most important, as when dealing with biological specimens, this makes diffraction tomography an invaluable tool. *— Mark Wolverton*

See: Hanna Leemreize[1], Jonathan D. Almer[2], Stuart R. Stock[3]*, and Henrik Birkedal[1]**, "Three-dimensional distribution of polymorphs and magnesium in a calcified underwater attachment system by diffraction tomography," J.R. Soc. Interface **10**(89), 20130319 (2013). DOI:10.1098/rsif.2013.0319

Author affiliations: [1]Aarhus University, [2]Argonne National Laboratory, [3]Northwestern University

Correspondence:

* s-stock@northwestern.edu,

* hbirkedal@chem.au.dk

This work was supported by the Human Frontiers Science Program, the Danish Council for Independent Research—Natural Sciences, and the Graduate School of Science and Technology of Aarhus University. S.R.S. acknowledges support from National Institute of Dental and Craniofacial Research grant no. DE001374 (to Arthur Veis). Use of the Advanced Photon Source at Argonne National Laboratory was supported by the U.S. Department of Energy Office of Science under Contract No. DE-AC02-06CH11357.

1-ID-B,C,E • XSD • Materials science, physics, chemistry • High-energy x-ray diffraction, radiography, small-angle x-ray scattering, fluorescence spectroscopy, pair distribution function • 50-90 keV, 50-150 keV • On-site • Accepting general users •

A Hidden Structure in Amorphous Biomineral Deposits

Amorphous solids lack the long-range, periodic structure of a crystal, but order is still present on short and medium length scales. Materials scientists are interested in amorphous materials because they can be easier to mold into complex shapes than can their crystalline counterparts. This is also the reason that certain organisms use non-crystalline solids, such as amorphous calcium carbonate (ACC). A new study of ACC from a marine lobster finds that it is surprisingly similar in structure to less stable varieties of ACC made in the lab. The results come from x-ray scattering measurements carried out with high-brightness x-rays from the APS. The researchers conclude that observed differences between biogenic and synthetic ACC may come from the state of water molecules intermingled with the calcium carbonate.

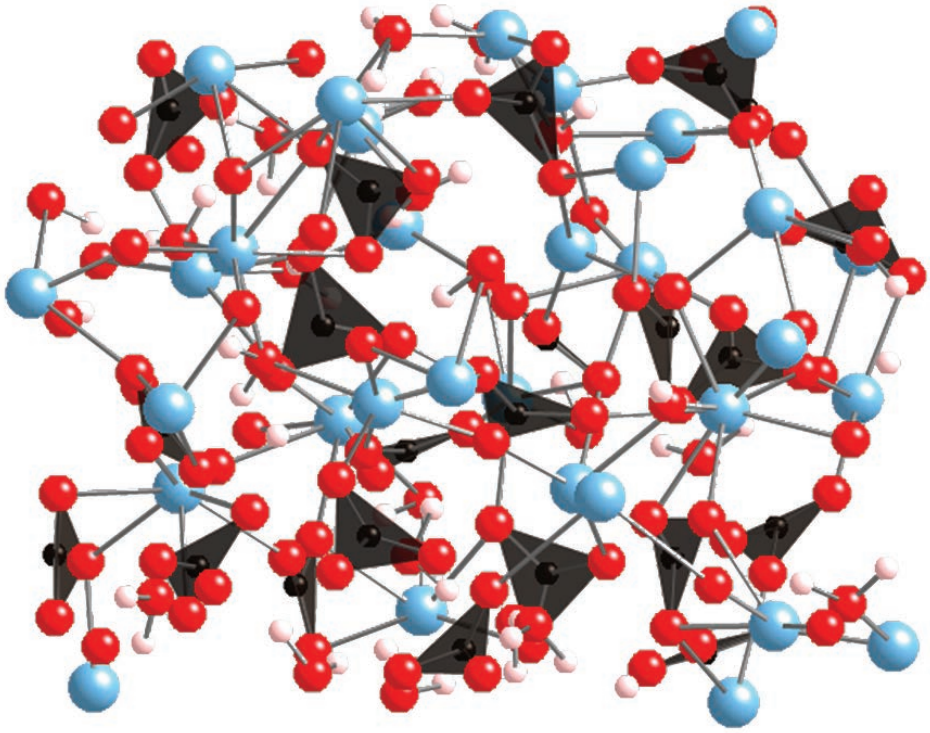

Fig. 1. This structure for amorphous calcium carbonate is based on modeling of the total x-ray scattering data collected at APS. The different atoms are depicted with different colors: calcium = blue; oxygen = red; carbon = black; and hydrogen = white. The black triangles indicate the orientation of the different carbonate groups (CO_3). Image courtesy of R. Reeder (Stony Brook University).

Crystals typically form by nucleating out of solution. However, it is possible to build a crystal by passing through an amorphous phase that acts as an intermediate step. A beautiful example of this comes from the sea urchin, whose long brittle spines are single crystals of calcium carbonate ($CaCO_3$). It would be very hard to grow this shape directly, so the sea urchin instead fashions the spines out of ACC and then lets them transform naturally into a more stable crystalline form.

Scientists would like to mimic organisms like the sea urchin by using ACC or another amorphous solid to create thin films and other complicated structures. However, synthetic varieties don't often perform as well as biogenic ones. To provide some new insight into biogenic ACC, a team of researchers from Stony Brook University and the Lobster Conservancy has performed a series of experiments on ACC samples taken from the American lobster (*Homarus americanus*). Like closely related fresh-water crustaceans, the American lobster uses ACC to store calcium during its molting process. When molting begins, calcium is drawn out of the lobster's shell and stored as ACC in centimeter-wide disks, called gastroliths, located near the stomach. The high solubility of ACC makes this a practical storage medium because the calcium is relatively easy to retrieve later when the lobster reforms its shell.

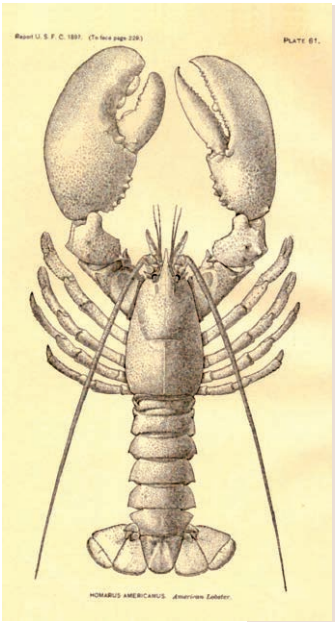

Figure: *Homarus americanus*, the American lobster, from *Report of the United States Commissioner of Fisheries, 1897;* courtesy of the Freshwater and Marine Image Bank. **Why do lobsters turn red when cooked?** A relatively simple explanation for the color change emerged in a study published in 2002 [M. Cianci et al., PNAS **99**(15), 9795 (2002)]: Heat changes the shape of a protein called beta-crustacyanin in the shell, relaxing its bonds with the pigment astaxanthin. The freed pigment reflects wavelengths of light in the red spectrum. But it turned out that the heat-related shape change accounted for only about a third of the color difference, according to a 2005 study by Dutch researchers [A.A.C. van Wijk et al., JACS **127**(5), 1438 (2005)]. The new research pointed to a complex quantum-physics interaction that would account for a much larger shift — and for the living lobster's original color. When the red pigment is fully hidden in the enclosing protein, it absorbs all wavelengths of light, red as well as blue and green, so the lobster appears black. The previous research had found that the red pigment molecules were grouped in pairs within the crustacyanin, crossing each other in a tight X formation. The Dutch researchers calculated that they interfered with one another, causing shifts in their quantum energy states, thus altering the wavelengths of light that are absorbed. C. Claiborne Ray, *The New York Times*, September 16, 2013. ©2013 The New York Times Company.

The research team measured the high-energy x-ray total scattering from collected lobster gastroliths. Total scattering is the method of choice for studying non-crystalline materials, which scatter x-rays diffusely (this in contrast to crystals that mostly scatter at discrete angles defined by Bragg's law). Total scattering measurements, which capture diffuse scattering over a wide range of scattering angles, require high-energy synchrotron light, such as that provided by the XSD 11-ID-B beamline at the APS.

The researchers analyzed their total scattering data to derive the pair distribution function (PDF), which characterizes the distribution of interatomic distances throughout the sample. Peaks in the PDF correspond to structural components in ACC. For example, a peak at a distance of 2.4 Å is readily interpreted as due to calcium-oxygen bonds. The team confirmed this with data collected through the use of the extended x-ray absorption fine structure (EXAFS) technique at the XSD 20-BM-B beamline at APS. These measurements of the calcium *K*-edge absorption spectrum produced the same distance between calcium and oxygen atoms as did the PDF analysis.

Broad peaks in the PDF at 4 and 6 Å correspond to medium-range correlations between second and third neighbors, which were not clearly identified in the EXAFS findings. The team observed similar peaks in synthetic ACC data, implying that the calcium carbonate in both types of ACC has roughly the same structure (Fig. 1).

This begs the question: What distinguishes the different ACC forms?

It turns out that ACC typically contains a large amount of water molecules that are either bound to calcium atoms or in a more mobile (but not liquid) state. The hydrogen atoms in the water do not scatter x-rays significantly, so the team performed nuclear magnetic resonance measurements, which showed that mobile H_2O is largely absent in biogenic ACC.

The team speculates that the relatively slow formation of biogenic ACC gives these mobile molecules an opportunity to re-arrange themselves or escape. The lack of mobile water may possibly explain the greater stability of biogenic over synthetic ACC.

The authors plan to go back to 11-ID-B to perform real-time studies of both biogenic and synthetic ACC samples to see if they transform differently to crystalline calcium carbonate.

— Michael Schirber

See: Richard J. Reeder[1]*, Yuanzhi Tang[1‡], Millicent P. Schmidt[1], Laura M. Kubista[1], Diane F. Cowan[2], and Brian L. Phillips[1], "Characterization of Structure in Biogenic Amorphous Calcium Carbonate: Pair Distribution Function and Nuclear Magnetic Resonance Studies of Lobster Gastrolith," Cryst. Growth Des. **13**, 1905 (2013). DOI:10.1021/cg301653s

Author affiliations: [1]Stony Brook University, [2]The Lobster Conservancy. Present address: ‡Georgia Institute of Technology

Correspondence:
*rjreeder@stonybrook.edu

This research was supported by the U.S. Department of Energy Office of Science, Basic Energy Sciences Grant DE-FG02-09ER16017. APS Sector 20, which is managed by XSD in partnership with the Canadian Light Source (CLS), is funded by the U.S. Department of Energy Office of Science, and by the Natural Sciences and Engineering Research Council of Canada and the University of Washington via the CLS. Use of the Advanced Photon Source at Argonne National Laboratory was supported by the U.S. Department of Energy Office of Science under Contract No. DE-AC02-06CH11357.

11-ID-B • XSD • Chemistry, environmental science, materials science • Pair distribution function • 58-60 keV, 90-91 keV • On-site • Accepting general users •

20-BM-B • XSD • Materials science, environmental science, chemistry • X-ray absorption fine structure, microfluorescence (hard x-ray), micro x-ray absorption fine structure, diffraction anomalous fine structure • 2.7-25 keV, 2.7-30 keV, 2.7-35 keV • On-site • Accepting general users •

Improved Low-Temperature Performance of Catalytic Converters

Toxic vehicle emissions, such as carbon monoxide and unburned hydrocarbons, are chemically converted to benign compounds like carbon dioxide (CO_2) and water by catalytic converters. Although catalytic converters are valuable technology, they are also expensive to produce. To reduce costs, experiments are being done to lessen the amount of platinum (Pt) and substitute palladium (Pd) in converters. The APS played a role in research that indicates a Pd/lanthanum (La)-alumina catalyst may result in a less-expensive catalytic converter with improved low-temperature carbon monoxide (CO) oxidation reactivity.

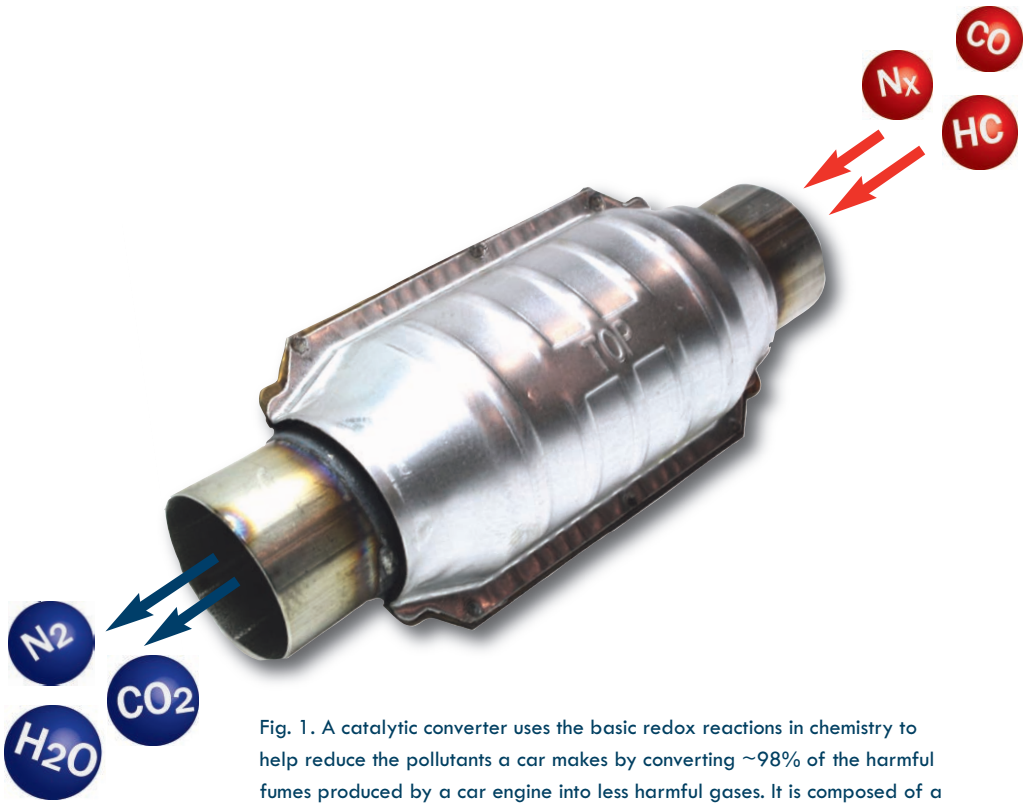

Fig. 1. A catalytic converter uses the basic redox reactions in chemistry to help reduce the pollutants a car makes by converting ~98% of the harmful fumes produced by a car engine into less harmful gases. It is composed of a metal housing that has a ceramic honeycomb-type interior with insulating layers. The honeycomb interior has thin wall channels that are coated with a washcoat of aluminum oxide, which is very porous and increases the surface area, allowing for more reactions to take place. This is where the precious metals are located, including platinum, rhodium, and palladium. These precious metals promote the transfer of electrons and in turn the conversion of toxic fumes. Source: http://chemwiki.ucdavis.edu/Physical_Chemistry/Kinetics/Case_Studies/Catalytic_Converters

Catalytic converters, installed on vehicles with internal combustion and diesel engines, convert the toxic byproducts of combustion to less toxic compounds (Fig. 1). In two-way (lean burn) converters, used primarily on diesel engines, CO and partially burned hydrocarbons are oxidized over a Pt or Pd catalyst to form CO_2 and water. Three-way (stoichiometric) converters, used on internal combustion engines, also reduce nitrogen oxides back to nitrogen. This is tremendously beneficial since nitrous oxide is 300 times more potent as a greenhouse gas than is CO_2. Since diesel exhaust is cooler than gasoline exhaust, the two-way catalyst must perform at low temperatures and also survive severe exothermic reactions when the particulate filter in the catalyst regenerates.

The oxidizing and reducing catalysts in catalytic converters contain precious metals, especially the costly platinum group metals Pt and Pd; a Pt-Pd alloy is more effective than either metal alone. To keep costs down, manufacturers try to minimize the amount of catalyst required, or use less expensive catalysts. The high cost of Pt has led to research to determine the hydrothermal stability of Pd, without the addition of Pt, particularly with La-alumina support.

Researchers from the University of New Mexico and Argonne simulated diesel oxidation catalysts with 2.5% Pd and tested it in two different preparations, one with alumina only and one with La-stabilized alumina. Each catalyst was roasted to 500º C to oxidize the Pd to PdO and then cooled to room temperature. When the temperature was raised to 140º C in the presence of CO, the PdO reduced to Pd metal. Re-

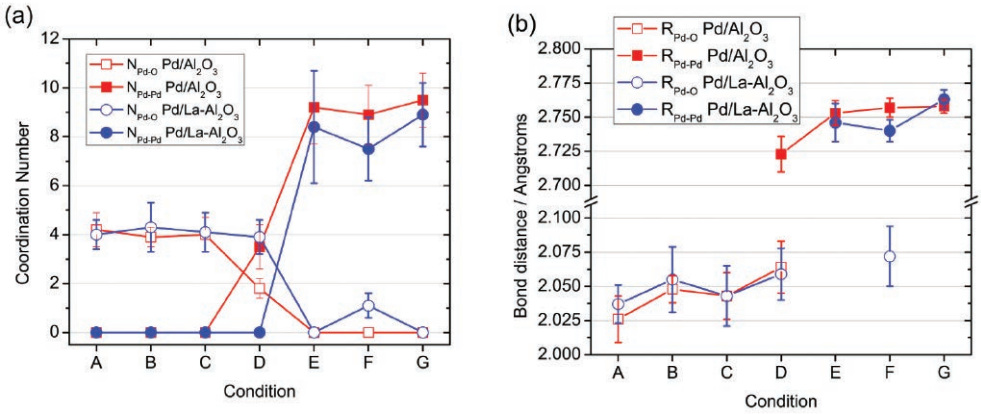

Fig. 2. (a) Coordination numbers and (b) bond distances of Pd-O and Pd-Pd paths for 2.5% catalysts as determined by *ab initio* fitting to the x-ray absorption fine structure spectra obtained at the APS.

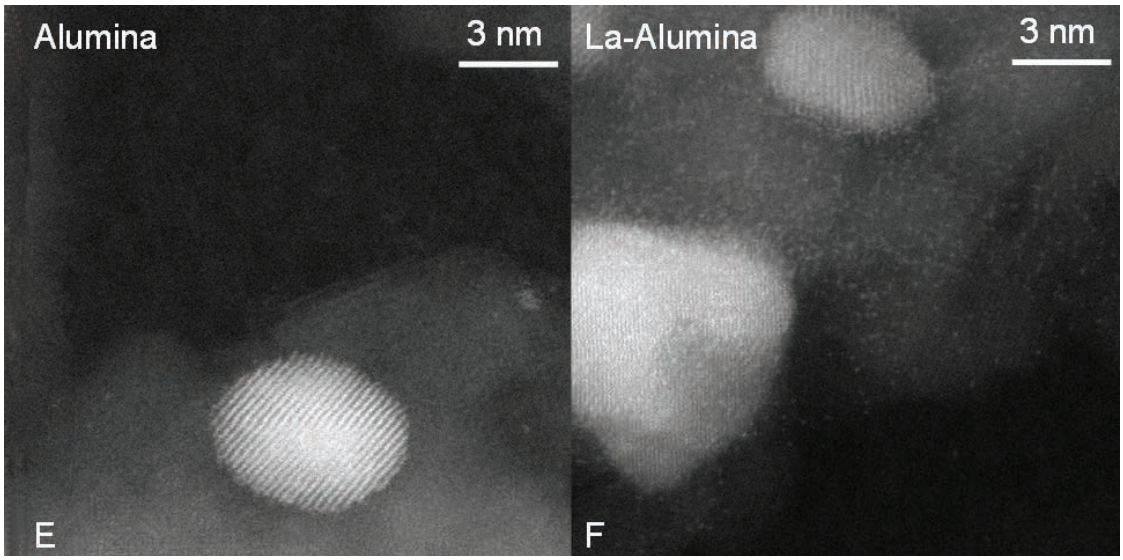

Fig. 3. Atomically dispersed species seen on Pd/La-alumina. Images obtained on the Titan G2 STEM at the Pacific Northwest National Laboratory Environmental Molecular Sciences Laboratory (EMSL).

sults of the experiments were analyzed by x-ray absorption spectroscopy (XAS) and diffuse reflectance Fourier transform infrared spectroscopy (DRIFTS) at the XSD 9-BM-B,C beamline at the APS (Fig. 2).

With the Pd-alumina catalyst, the absorption of CO was found to be irreversible because the catalyst had little reaction with oxygen. With the La-stabilized alumina, the Pd catalyst was more reactive toward oxygen and had higher CO conversion; CO oxidation began at a lower temperature, around 100º C. Pd became oxidized when the gas phase was switched from pure CO to the stoichiometric reaction mixture, and there was a reduction in the surface coverage of CO.

The addition of La to the catalyst had two effects. First, Pd formed small particles and clusters, which increased Pd dispersion from 17% to 26%, since the alumina now contained atomically dispersed La^{+3} (Fig. 3). The increase in dispersion is partially responsible for the improved CO conversion.

Second, the redox reaction was more likely at low temperature, so Pd was less susceptible to CO poisoning. The turnover frequency at 140º C improved 5-fold, due in part to the redox behavior of the Pd/La-alumina catalyst.

In catalytic converters, a Pt-Pd alloy is more stable, more reactive, and less susceptible to aging than Pt metal alone. Adding Pd in the alloy reduces the cost, hence the hydrothermal stability of Pd is important. The use of simultaneous XAS and DRIFTS in this research leads to a greater understanding of the effects of adding La to Pd-based catalysts in catalytic converters to improve the efficiency and decrease the costs of two-way catalytic converters used for diesel engines.

— Dana Desonie

See: Jason R. Gaudet[1‡], Andrew de la Riva[1], Eric J. Peterson[1], Trudy Bolin[2], and Abhaya K. Datye[1*], "Improved Low-Temperature CO Oxidation Performance of Pd Supported on La-Stabilized Alumina," ACS Catal. **3**, 846 (2013). DOI:10.1021/cs400024u

Author affiliations: [1]University of New Mexico, [2]Argonne National Laboratory. ‡Present address: Univ. of Michigan
Correspondence: *datye@unm.edu

This research was supported by the U.S. Department of Energy Office of Science Grant DE-FG02-05ER15712. Electron microscopy was performed at the EMSL, a national scientific user facility sponsored by the Department of Energy Office of Biological and Environmental Research and located at Pacific Northwest National Laboratory. Use of the Advanced Photon Source at Argonne National Laboratory was supported by the U.S. Department of Energy Office of Science under Contract No. DE-AC02-06CH11357.

9-BM-B,C • XSD • Materials science, chemistry • X-ray absorption fine structure • 2.1-23 keV • On-site • Accepting general users •

Cooking Up New Nanoribbons to Make Better White LEDs

As the world moves away from incandescent light bulbs, light-emitting diodes (LEDs) are growing in popularity. They use significantly less energy and have far longer lifetimes than do the traditional incandescent bulbs, and they do not contain mercury, as do compact fluorescents. LEDs do have a drawback, however. The phosphors that convert the single color produced by an LED into white light tend to produce a cool, bluish glow instead of the warmer, yellower color most people prefer. Researchers from Argonne, Oak Ridge National Laboratory, and the University of Georgia are using high-brightness x-rays from the APS to help in the development of new compounds to create nanoribbons that luminesce in different colors, which they can mix together to make a phosphor that provides a more desirable white light that can be tailored for different uses.

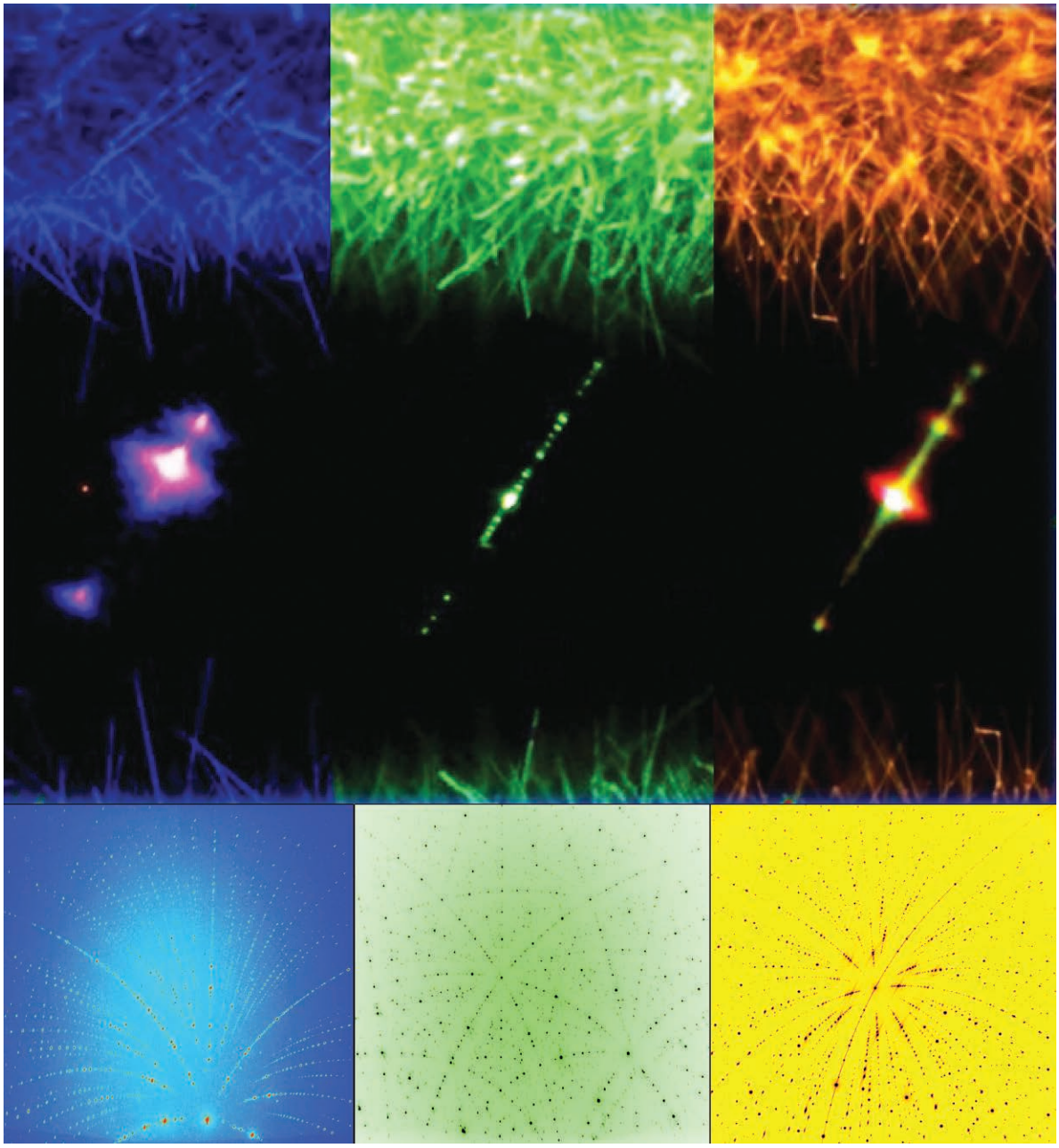

The materials combine the rare-earth element europium with aluminum oxide to form europium aluminate nanoribbons (Fig. 1). Powders of europium oxide (Eu_2O_3) and aluminum oxide (Al_2O_3) were mixed together with graphite powder and heated in a vacuum chamber to temperatures above 1000° C. Powders heated to between 1200° and 1400° C formed nanoribbons that luminesced orange. Those heated to 1000° to 1200° glowed green. When more aluminum oxide powder was added and the pressure in the vacuum chamber was raised, from 5 T to between 10 and 15 T, the resulting nanoribbons shone blue.

It is rare, the researchers say, for a single material to be able to cover the spectrum of visible colors, but it could simplify the creation of phosphors that produce desirable colors when excited by a blue or ultraviolet LED. Scientists would simply have to select the right mix of nanoribbons to get the white light they sought. In a separate experiment, the researchers also produced yellow and red luminescent nanoribbons by adding barium to the europium aluminate.

The researchers first used conventional x-ray powder diffraction to determine the crystal structures of the three types of nanoribbon. They compared the patterns they found to several diffraction databases of known materials and discovered the green nanoribbon was a match for strontium aluminate, so they knew it had a similar crystalline shape.

There was no match for the other two types, though, so they turned to XSD beamline 11-BM-B at the APS to perform high-resolution synchrotron powder diffraction using a single x-ray energy, which provides initial measurements of the spacings between the atomic planes of the crystal. Using a different scattering technique with a wide range of x-ray energies, XSD beamline 34-1D-E, also at the APS, gave them more detailed information, such as the exact angles between different atomic planes and the presence of crystal defects.

Using XSD beamline 20-BM-B at the APS, they performed x-ray absorption near-edge structure measurements, which focused on europium fluorescence and confirmed that the nanoribbons are indeed europium aluminates, and provided their chemical formulas — $EuAl_6O_{10}$ for the blue and $EuAl_2O_4$ for the green and orange. The blue nanoribbons, therefore, are a newly discovered compound. While green photoluminescence at room temperature had been seen before from $SrAl_2O_4$, the orange color was new as well.

Specifically pinning down the complete atomic structure of the crystal and tying it to the observed behavior of the material is a complex undertaking. The team now has an average picture of the local spatial arrangement of the elements and the oxygen vacancies — areas where a missing oxygen atom affects the electrical behavior of the material. They are now trying to refine that picture using the ChemMatCARS 15-ID-B advanced crystallography beamline at the APS to give theorists enough information to explain cause and effect and suggest possible ways to tweak the materials' luminescence properties.

The researchers also found a result they had not been looking for. They discovered that when they hit an individual nanoribbon with a microfocused x-ray beam, it not only produced the x-ray diffraction patterns they were using for their measurements, but also generated strong visible light emission. That light appeared not only at the spot where the beam struck, but also at the ends of the ribbons, showing the ribbons were acting as waveguides. That ability to route light of different colors means the nanoribbons may help in the creation of circuits inside optical devices, which use light beams to perform their functions. *— Neil Savage*

< Fig. 1. The researchers fabricated three types of nanoribbons: (l-r) $EuAl_6O_{10}$ emitting blue light, and two forms of $EuAl_2O_4$ emitting green and orange light. The top row shows microscopic images of the materials. In the middle row, x-rays excite emissions that travel along the ribbons and emerge from end points and defects. On the bottom are x-ray diffraction patterns, which reveal the crystal lattice structures.

See: Feng Liu[1], John D. Budai[2], Xufan Li[1], Jonathan Z. Tischler[2], Jane Y. Howe[2], Chengjun Sun[3], Richard S. Meltzer[1], and Zhengwei Pan[1]*, "New Ternary Europium Aluminate Luminescent Nanoribbons for Advanced Photonics," Adv. Funct. Mater. **23**, 1998 (2013). DOI:10.1002/adfm.201202539
Author affiliations: [1]University of Georgia, [2]Oak Ridge National Laboratory, [3]Argonne National Laboratory
Correspondence: * panz@uga.edu

Z.W.P. acknowledges funding support from the National Science Foundation (CAREER DMR-0955908). J.D.B. and J.Z.T. were supported by the Materials Sciences and Engineering Division, Basic Energy Sciences, U.S. Department of Energy. APS sector 20, which is managed by XSD in partnership with the Canadian Light Source (CLS), is funded by the U.S. Department of Energy Office of Science, and by the Natural Sciences and Engineering Research Council of Canada and the University of Washington via the CLS. The 15-ID-B beamline at the APS is operated by ChemMatCARS and funded by the National Science Foundation. Use of the Advanced Photon Source at Argonne National Laboratory was supported by the U.S. Department of Energy Office of Science under Contract No. DE-AC02-06CH11357.

11-BM-B • XSD • Chemistry, materials science, physics • Powder diffraction • 15-35 keV • On-site, mail-in • Accepting general users •

15-ID-B,C,D • ChemMatCARS • Materials science, chemistry • Single-crystal diffraction, anomalous and resonant scattering (hard x-ray), wide-angle x-ray scattering, microdiffraction, liquid surface scattering, small-angle x-ray scattering, ultra-small-angle x-ray scattering, high-pressure diamond anvil cell • 5-70 keV • On-site • Accepting general users •

20-BM-B • XSD • Chemistry, environmental science, geoscience, materials science • Micro x-ray absorption fine structure, microfluorescence (hard x-ray), x-ray absorption fine structure • 2.7-25 keV, 2.7-30 keV, 2.7-35 keV • On-site • Accepting general users •

34-ID-E • XSD • Materials science, physics • Microdiffraction, Laue crystallography, microbeam • 7-30 keV • On site • Accepting general users •

Electrodes with a Little Extra

In a world ever more dependent on efficient battery technology, finding new ways to squeeze out a little more juice is always important. Sometimes that can be a matter of designing electronic circuits and devices to use less power or to use it more efficiently. But scientists and engineers are also approaching the issue from the other direction by improving battery technology. One way to do so is through a better understanding of new electrode materials and how they operate inside a battery. But the fact that much of the action happens on the nanoscale within buried interfaces in the battery materials makes characterization a challenge. A team from the University of Cambridge, Brookhaven National Laboratory, Stony Brook University, and Argonne investigated the prototypical conversion material RuO_2, which, like some other metal fluoride/oxides, has displayed the intriguing phenomenon of additional capacity beyond its theoretical conversion qualities. The experimenters also managed to disprove one popular explanation for that extra capacity by defining the actual mechanism at work.

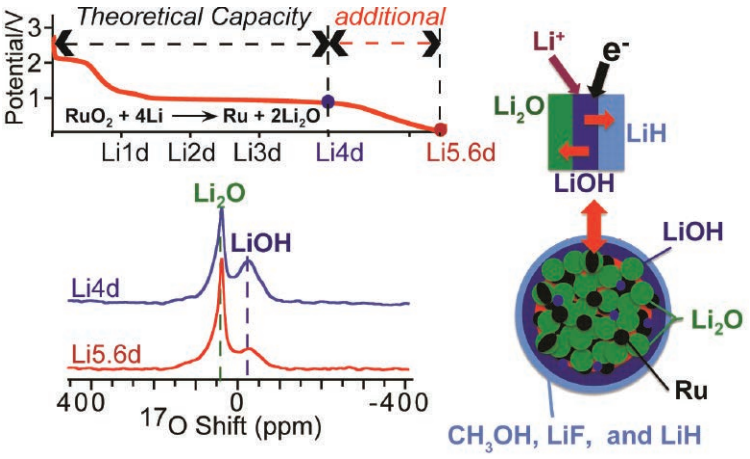

Fig. 1. Origin of additional capacities in RuO_2 lithium-ion battery electrodes.

To characterize and study the mechanism of charge storage in the RuO_2/lithium (Li) system, and particularly to identify the source of the additional capacity, the research team employed various techniques, including x-ray diffraction at the XSD 11-ID-B beamline at the APS, while cycling a RuO_2/Li battery over the course of 30 h.

The suite of x-ray spectroscopic and scattering techniques available at the APS and the National Synchrotron Light Source (Brookhaven) provided deep insight into the electrochemistry of the ruthenium-based processes. Using x-ray absorption near-edge structure and extended x-ray absorption fine-structure as well as pair distribution function methods, the researchers observed three distinct stages involving ruthenium, with lithium insertion into tetragonal ruthenium/oxygen (RuO_2) to form $LiRuO_2$ via an intermediate phase Li_xRuO_2, then the conversion reaction of $LiRuO_2$ to form Li_2O and metallic Ru nanoparticles, and finally an additional-capacity region at low voltage.

Nuclear magnetic resonance (NMR) spectroscopy revealed further details, particularly the Ru-free parts of the cycling process. SEI (solid electrolyte interphase) formation was also seen during the battery discharge process. Previous research work theorized that the major source of the extra capacity in this system arose from the formation of a "space charge" layer at the interface between metal and lithium salts. However, the NMR studies and other theoretical calculations show that the additional capacity is mostly generated by the formation of LiOH and its subsequent conversion to Li_2O and LiH. Another possible source is reversible electrode-electrolyte interphase SEI formation. The present study also demonstrated a particularly effective protocol for NMR studies of SEI formation, the SEI being ubiquitous to all batteries.

Aside from settling a long-standing and much-discussed research question, the team's work has also demonstrated some valuable experimental strategies that can be applied to characterize and understand other promising battery systems. As we continue to demand ever greater versatility, dependability, and capability from our electronic devices, not to mention making them ever smaller and lighter, having a wider range of different types of batteries to choose from will only become more important. *— Mark Wolverton*

See: Yan-Yan Hu[1], Zigeng Liu[1], Kyung-Wan Nam[2], Olaf J. Borkiewicz[3], Jun Cheng[1], Xiao Hua[1], Matthew T. Dunstan[1], Xiqian Yu[2], Kamila M.Wiaderek[3], Lin-Shu Du[4], Karena W. Chapman[3], Peter J. Chupas[3], Xiao-Qing Yang[2], and Clare P. Grey[1,4]*, "Origin of additional capacities in metal oxide lithium-ion battery electrodes," Nat. Mater. **12**, 1130 (December 2013).
DOI:10.1038/NMAT3784
Author affiliations: [1]University of Cambridge, [2]Brookhaven National Laboratory, [3]Argonne National Laboratory, [4]Stony Brook University
Correspondence: * cpg27@cam.ac.uk

This research was supported as part of the North Eastern Center for Chemical Energy Storage, an Energy Frontier Research Center funded by the US Department of Energy Office of Science-Basic Energy Sciences under Award Number DE-SC0001294. Y-Y.H. acknowledges support from a Newton International Fellowship from the Royal Society and a Marie Curie International Incoming Fellowship (PIIF-GA-2011_299341). Use of the Advanced Photon Source at Argonne National Laboratory was supported by the U.S. Department of Energy Office of Science under Contract No. DE-AC02-06CH11357.

Shaking and Baking in Bismuth

Understanding the dynamics of phonon behavior could yield important new information that would help researchers achieve better designs and tailored materials for various commercial applications. Bismuth, commonly used in materials ranging from pharmaceuticals to superconductors, is a semi-metal that provides an ideal system for studying the charge-behavior coupling phenomena at the heart of many important photovoltaic and thermoelectric processes in materials science. While previous work has focused on long-wavelength optical phonons in bismuth, short-wavelength dynamics have been difficult to capture. A team of researchers working at the APS used the newly-developed technique of time-resolved x-ray scattering to study phonon transport in bismuth as it is excited through and above its melting threshold by a laser. The study and understanding of all these processes is valuable not just for its theoretical interest but because of its practical application for the many uses of bismuth, both on its own and in the many ingenious compounds that have been developed in recent years as topological insulators and high-temperature superconductors. The ability to precisely design and refine the characteristics of such materials is the key to making them useful in real-world devices.

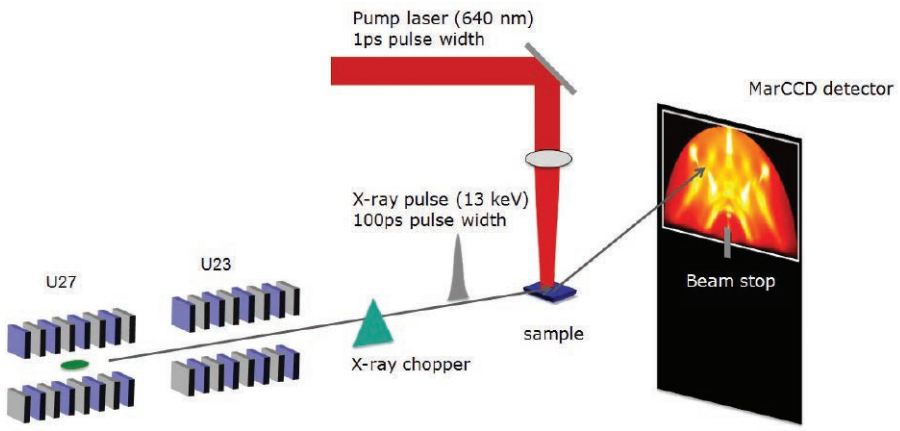

Fig. 1. Experimental setup for time-resolved x-ray diffuse scattering at BioCARS.

Working at the BioCARS 14-ID-B beamline at the APS, the experimenters from the SLAC National Accelerator Laboratory; Stanford University; the University of California, Davis; University College Cork (Ireland); Los Alamos National Laboratory; the University of Michigan; and The University of Chicago subjected a sample of single-crystal bismuth film on sapphire to picosecond laser pulses at 640-nm wavelength and observed x-ray scattering with a charge-coupled device detector. Some of the scattering was due to normal background from static disorder along with Compton and air scattering, but it also contained thermal diffuse scattering from phonons, which can be compared with laser-excited states.

Following the laser pulses, scattering increased for several hundred picoseconds, then decreased after several nanoseconds, and finally returned to an equilibrium state, much like what would be expected with classical thermal transport. The x-ray scattering observations indicate that while thermal transport is dominated by thermal diffusion at first, Kapitza conductance between bismuth and the sapphire layer is more important on the nanosecond time scale.

When the laser exposure was increased above the bismuth melting point, liquid rings began to appear in the samples and persisted for approximately 10 nsec, about the same time interval as the Kapitza conductance seen earlier. Following this, the liquid ring disappeared and long-range order began to return. The researchers attribute this to a temporary laser-induced liquid phase followed by epitaxial regrowth of the crystal lattice back to a single-crystal state.

While the very earliest stages of the phonon generation process could not be observed because of the time-resolution limitations of these particular experiments, the team hopes to conduct further experiments with even shorter time resolution (possible with an x-ray free-electron laser) that will capture all of the events that follow photoexcitation. Time-resolved x-ray diffuse scattering techniques could also capture phenomena such as the decay of high-energy into lower-energy phonons, coupling between different phonon modes, and photo-induced inverse Peierls distortion in bismuth.

— Mark Wolverton

See: J. Chen[1,2*] M. Trigo[1], S. Fahy[3],

"Bismuth" cont'd. on page 68

Reversing Field on Air-Powered Batteries

People who care about battery-powered transportation are getting very excited about rechargeable lithium-oxygen (Li-O_2) batteries. These batteries work much like the ubiquitous lithium-ion batteries in cell phones, laptops, and today's battery-powered cars: both exploit lithium oxidation reactions to create useable electrons. But instead of packing the oxidizing agent into a self-contained but unwieldy package, Li-O_2 batteries use an oxidizer that is light-weight, low-cost, stable, and abundant — the oxygen in air. Promoters note that the energy density of Li-O_2 (also called Li-air) batteries could be ten times greater than their predecessors — almost on par with gasoline — and these devices could extend the range of battery-powered vehicles from the current 100 miles to around 400 miles between charges. But these calculations assume that anodic lithium does not degrade during multiple charge and discharge cycles. In experiments at the APS, researchers peered inside an operating Li-air battery to see if this perfect reversibility is a reality. They found that a degradation layer forms on the anode, but the battery continues to operate through tiny tunnels to the metallic lithium within. Such information is essential to guide future research of Li-air batteries that meet theoretical promise.

The study began with a straightforward experiment. The researchers in this study, from Argonne, built a Li-air battery and charged and discharged the cell until it stopped functioning — about 50 cycles. Then they dissected the battery to figure out what went wrong. Inside, the researchers found plenty of electrolytes, but the previously shiny metal anode was covered with a dark substance. While suspicious, this layer didn't prove that the anode was the culprit, so the researchers built a new battery that incorporated the crusty anode. The rebuilt cell started right up.

The researchers repeated the process, and the dark layer grew thicker. Finally, the metallic shine of the anode disappeared completely and it could no longer support a charge. Clearly the anode was undergoing some kind of irreversible change, but strangely, this change did not interrupt the anode function until the lithium was completely converted. Why?

The property that makes lithium so appealing for energy generation also makes it difficult to study. Because the lithium anode is so reactive, any accidental air exposure will change its chemical state. The researchers needed to look inside the Li-air battery as it operated with a technique that

"Reversing" cont'd. on page 68

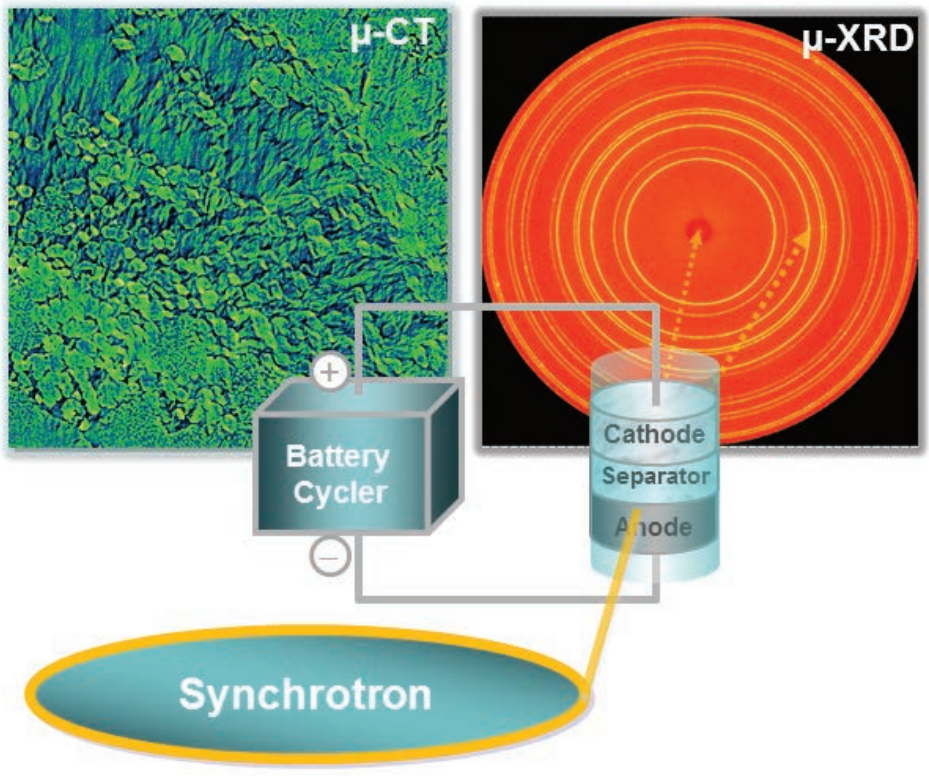

Fig. 1. Shown here is the experimental setup for the lithium-oxygen battery examination. A simple battery is charged and discharged through several cycles. As the battery operates, a high-energy synchrotron x radiation beam scans from the anode to the cathode in tiny increments and records chemical and structural information. This information is used to track chemical changes through space and time with micro x-ray diffraction (μ-XRD, right), and to create a high-resolution three-dimensional structure with a micro-CT scan (μ-CT, left). These scans identified the formation and morphology of the LiOH layer on the anode during cell degradation.

Characterization of the Lattice Rotations and Distortions Due to an Individual Dislocation

Dislocations are crystallographic defects that allow the minimization of strain energy through the localization of crystal lattice distortion. Understanding and controlling the behavior of dislocations is crucial for a wide range of applications, from nanoelectronics and solar cells to structural engineering alloys. Transmission electron microscopy (TEM) revolutionized materials science by allowing the visualization of individual dislocations in thin, electron-transparent samples. However, the "thin sample" requirements of TEM may lead to size effects that modify dislocation behavior. The greater penetration depth of x-rays potentially allows the study of dislocations in samples more representative of the material bulk. But to date, quantitative x-ray measurements of the strain fields surrounding individual dislocations have remained elusive. Researchers utilizing APS x-ray beams achieved the first measurement of the lattice rotations and strain fields due to a single misfit dislocation in a 130-nm-thick, freestanding GaAs/$In_{0.2}Ga_{0.8}As$/GaAs membrane structure. This structure has intrinsic scientific importance, as graded GaAs multilayers are a key ingredient in integrated circuits, light-emitting diodes, and solar cells.

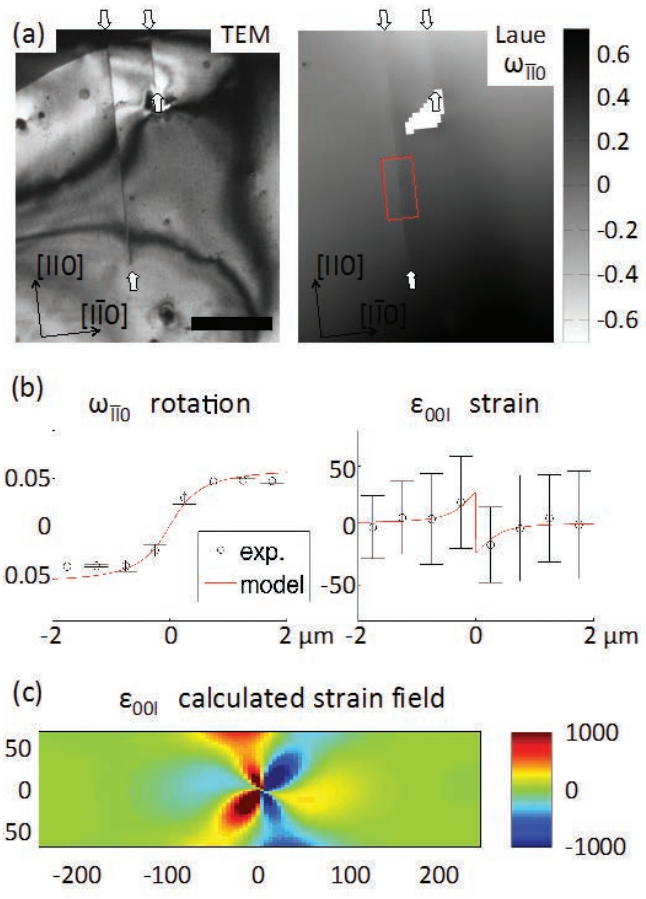

Fig. 1: (a) Transmission electron micrograph and Laue lattice rotation map (in degrees) of the sample showing two misfit dislocations. (b) Lattice rotation (in degrees) and deviatoric elastic strain (x 10^{-6}) as a function of distance from the dislocation line. Measured points and calculated line profiles are shown. (c) Deviatoric elastic strain field (x 10^{-6}) in the sample calculated using an anisotropically elastic model of the structure. x and y axes show sample coordinates in nanometers.

The researchers, from the University of Oxford (UK), LaTrobe University (Australia), and Argonne, overcame the previous experimental limitations by employing the x-ray Laue diffraction microscope at the XSD 34-ID-E beamline of the APS. A key advantage of the membrane geometry is that x-ray measurements could be directly compared to TEM micrographs, which were obtained using Argonne's Center for Nanoscale Materials. Figure 1(a) shows excellent agreement between the Laue and TEM maps. The same dislocations can be unambiguously identified both.

Laue diffraction measurements allow the determination of all three lattice rotation components and the full deviatoric strain tensor at each data point with a single exposure. Figure 1(b) shows measured profiles of lattice rotation and of elastic strain as a function of distance from the dislocation line. These measurements were compared to an anisotropically elastic model of the membrane structure. Figure 1(c) shows one of the calculated deviatoric elastic strain field components due to the misfit dislocation. The anticipated line profiles, determined by performing a virtual diffraction experiment on the computational model, are superimposed on Fig. 1(b) as red lines. Clearly, measurement and calculation

"Lattice" cont'd. on page 68

"Bismuth" cont'd. from page 65
É.D. Murray[4], Y.M. Sheu[5], T. Graber[6], R. Henning[6], Y. J. Chien[7‡], C. Uher[7], and D.A. Reis[1,2], "Time- and momentum-resolved probe of heat transport in photo-excited bismuth," Appl. Phys. Lett. **102**, 181903 (2013). DOI:10.1063/1.4804291
Author affiliations: [1]SLAC National Accelerator Laboratory; [2]Stanford University; [3]University College Cork; [4]University of California, Davis; [5]Los Alamos National Laboratory; [6]The University of Chicago; [7]University of Michigan. ‡Present address: AU Optronics Corporation (Taiwan)
Correspondence:
* chenjian@slac.stanford.edu

J.C., M.T., and D.A.R. acknowledge support from the U.S. Department of Energy Office Science-Basic Energy Sciences through the Division of Materials Sciences and Engineering under Contract No. DE-AC02-76SF00515. S.F. acknowledges support from the Science Foundation Ireland. Time-resolved set-up at Sector 14 was funded in part through a collaboration with Philip Anfinrud (NIH/NIDDK). BioCARS is supported by the National Institute of General Medical Sciences of the National Institutes of Health under grant number R24GM111072. Use of the Advanced Photon Source at Argonne National Laboratory was supported by the U.S. Department of Energy Office of Science under Contract No. DE-AC02-06CH11357.

14-ID-B • BioCARS • Life sciences, materials science, physics, chemistry • Time-resolved crystallography, time-resolved x-ray scattering, Laue crystallography, wide-angle x-ray scattering, biohazards at the BSL2/3 level, macromolecular crystallography • 7-19 keV •

"Reversing" cont'd. from page 66
wouldn't affect the results. High-intensity, microfocused x-ray diffraction (XRD) studies carried out at XSD beamline 1-ID provided an ideal solution (Fig. 1). The researchers created a similar battery to that used in earlier experiments, but with a smaller diameter. As it charged and discharged, the researchers used microfocused XRD to scan its chemical signature, layer by layer, from the anode to the cathode. Initially, the information showed that the anode was pure Li, but as the battery cycled, LiOH (lithium hydroxide) peaks near the separator interface and in the anode indicated that the metal was undergoing irreversible change. As cycling time continued, the strength of LiOH signatures from the anode grew, while metallic lithium grew weaker. The results suggested that lithium was gradually converted to LiOH — a finding that contradicts the assumption of perfect reversibility.

But if the anode grows a layer of LiOH, why did it still work in the rebuilt battery? To answer this question the researchers turned to the non-destructive x-ray technique micro-tomography, also at beamline 1-ID-B,C,E. The technique constructed a very fine 3-D structural image, like a micro-CT scan, for the battery. Micro-tomography results uncovered interconnected holes and cracks in the LiOH layer leading to metallic lithium within. The researchers posit that the anode's lithium reacts with water produced by decomposing electrolyte. Water is a known decomposition by-product of the electrolyte used in this battery.

The study findings contradict the assumption that anodes in today's Li-air batteries are perfectly reversible, and should motivate researchers to develop more stable electrolytes for these devices. Only with this kind of information can the Li-air batteries be better designed for real applications.

— Jenny Morber

See: Jiang-Lan Shui, John S. Okasinski, Peter Kenesei, Howard A. Dobbs, Dan Zhao‡, Jonathan D. Almer, and Di-Jia Liu*, "Reversibility of anodic lithium in rechargeable lithium–oxygen batteries," Nat. Commun. **4**, 2255 (9 August 2013). DOI: 10.1038/ncomms3255
Author affiliation: Argonne National Laboratory. ‡Present address: National University of Singapore
Correspondence: * djliu@anl.gov

This work and the use of Advanced Photon Source at Argonne National Laboratory are supported by the U. S. Department of Energy Office of Science under Contract No. DE-AC02-06CH11357. The financial support from the Grand Challenge program of Argonne National Laboratory is gratefully acknowledged.

1-ID-B,C,E • XSD • Materials science, physics, chemistry • High-energy x-ray diffraction, radiography, small-angle x-ray scattering, fluorescence spectroscopy, pair distribution function • 5-130 keV • On-site • Accepting general users •

"Lattice" cont'd. from page 67
agree well, providing one of few experimental validations of the anisotropic elastic dislocation solutions.

To assess the feasibility of such measurements in thicker bulk samples, a computational model of a misfit dislocation embedded within an infinite medium was established. The strain fields that would be measured using different x-ray beam sizes were computed and compared to the expected experimental uncertainty. These calculations indicate that the strain fields around individual dislocations in the bulk should indeed be measurable, provided polychromatic x-ray beams with sub-200-nm size are available. The findings provide a strong motivation for the development of sub-100-nm polychromatic focusing capabilities for Laue diffraction microscopy. The ability to measure single dislocation strain fields in the bulk with three-dimensional resolution would open revolutionary possibilities for the *in situ* study of dislocation behavior, structure formation, and self-organization. *— Karen Fox*

See: Felix Hofmann[1]*, Brian Abbey[2,3], Wenjun Liu[4], Ruqing Xu[4], Brian F. Usher[2], Eugeniu Balaur[2,3], and Yuzi Liu[4], "X-ray micro-beam characterization of lattice rotations and distortions due to an individual dislocation," Nat. Commun. **4**, 2774 (2013). DOI:10.1038/ncomms3774
Author affiliations: [1]University of Oxford, [2]La Trobe University, [3]Melbourne Centre for Nanofabrication, [4]Argonne National Laboratory
Correspondence:
* felix.hofmann@eng.ox.ac.uk

F.H. acknowledges funding from the John Fell Oxford University Press (OUP) Research Fund. B.A. acknowledges the support of the Australian Research Council Centre of Excellence for Coherent X-ray Science and the Australian Research Council Centre of Excellence for Advanced Molecular Imaging. Use of the Advanced Photon Source and Center for Nanoscale Materials at Argonne National Laboratory was supported by the U.S. Department of Energy Office of Science under Contract No. DE-AC02-06CH11357.

34-ID-E • XSD • Materials science, physics, environmental science, geoscience • Microdiffraction, Laue crystallography, microbeam • 7-30 keV • On-site • Accepting general users •

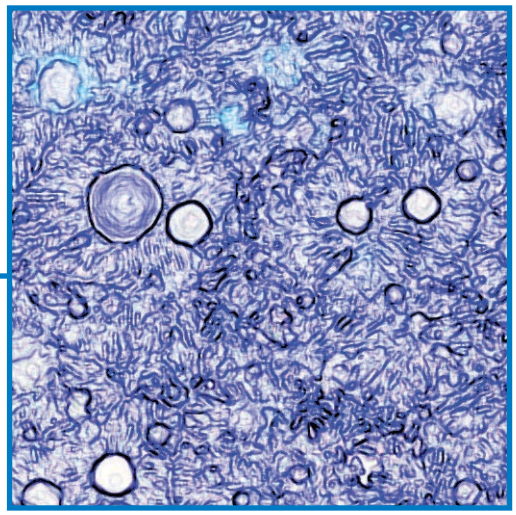

Soft Materials & Liquids

Molten Metal Solidifies into a New Kind of Glass

When a molten material cools quickly, parts of it may have enough time to grow into orderly crystals. But if the cooling rate is too fast for the entire melt to crystallize, the remaining material ends up in a non-crystalline state known as a glass, with atoms caught in place essentially as a frozen liquid. Recently, a group of researchers at the National Institute of Standards and Technology (NIST) and Argonne came across an unexpected reversal of this usual sequence of events. Investigation of the new phase at the XSD beamlines 1-ID-B,C,E and 11-ID-B at the APS suggests that it may be an example of a novel structure, theoretically possible but not seen until now, that is isotropic with infinite rotational symmetry, but lacking any discrete translational symmetry.

After cooling a molten alloy of aluminum, iron, and silicon the researchers found that glassy nodules of a non-crystalline solid phase formed first, growing slowly enough to organize and select some chemical species, rejecting other species into the surrounding melt that, on further cooling, coalesced into crystals.

Direct visual evidence (Fig. 1, facing page) indicates that the nodules formed first, followed by metallic crystals radiating around them. Closer inspection revealed that the radiating white bands are crystalline aluminum with small amounts of iron and silicon. The nodule composition is approximately $Al_{13}Fe_3Si_4$.

The researchers concluded that the nodules formed by nucleation and displaced excess aluminum as they grew; eventually, the aluminum concentration in the surrounding material was high enough that the remaining melt crystallized, pushing residual iron and silicon into the gaps.

Electron microscopy showed that the material in the nodules is isotropic, leading the researchers to call it "*q*-glass," despite the fact that it does not form as glasses normally do.

To investigate its structure further, the team utilized beamline 1-ID-B,C,E to obtain high-energy x-ray scattering data with which to compare samples of the *q*-glass to two other known phases of Al-Fe-Si with composition similar to that of the q-glass: the crystalline cubic α-phase and the quasicrystalline icosahedral phase.

Diffraction of 80-keV x-rays yielded data that the team analyzed using pair distribution function (PDF) methods, which showed a series of peaks corresponding to distances between pairs of atoms.

The PDFs for all three samples were roughly similar up to pair distances of about 12 Å, with the pattern for the *q*-glass closer to that of the α-phase than to the icosahedral phase. Beyond 12 Å, the two crystal phases continued to show peaks corresponding to long-range correlations in atomic position over distances greater than the size of the α-phase unit cell. But the PDF for the *q*-glass mostly fizzled out, showing a lack of longer-range order and therefore an absence of true crystal structure.

That result left open the possibility of the *q*-glass being nanocrystalline, consisting of many tiny and randomly oriented α-phase crystals. To explore that possibility, the researchers went to beamline 11-ID-B, again using high-energy x-ray scattering to study how the x-ray diffraction pattern of the *q*-glass changed as the sample was heated. If the *q*-glass were nanocrystalline, prolonged heating should cause the crystals to coarsen, so that the structure as a whole would come to more closely resemble a polycrystalline α-phase.

That's not what happened. When the *q*-glass was held at 330° C, its diffraction pattern stayed the same for about 40 minutes, at which point it changed rapidly into a pattern characteristic of a new phase, β-$Al_{4.5}$FeSi.

The lesson is that the *q*-glass structure is a true phase that will transform into a different phase at the appropriate temperature.

If the *q*-glass is not crystalline, quasicrystalline, or polycrystalline, what is it?

The researchers point to two general possibilities. One is frustrated growth from an initial seed that results in a structure with clusters that pack stably together, but in a disordered way that breaks up long-range order. More exotically, there are mathematically permissible arrangements of points in three dimensions that are isotropic with neither periodicity nor quasiperiodicity.

The team has sent their data to an expert who maintains a "zoo" of theoretically feasible structures. They want to see if any "animals" exist that fit what they observed. *— David Lindley*

See: Gabrielle G. Long[1,2*], Karena W. Chapman[1], Peter J. Chupas[1], Leonid A. Bendersky[2], Lyle E. Levine[2], Frédéric Mompiou[2,‡], Judith K. Stalick[2], and John W. Cahn[2,‡‡], "Highly Ordered Non-crystalline Metallic Phase," Phys. Rev. Lett. **111**, 015502 (2013). DOI:10.1103/PhysRevLett.111.015502

Author affiliations: [1]Argonne National Laboratory, [2]National Institute of Standards and Technology. Present addresses: ‡CNRS, Toulouse, France, ‡‡University of Washington

Correspondence:

* gglong@aps.anl.gov

Use of the Advanced Photon Source at Argonne National Laboratory was supported by the U.S. Department of Energy Office of Science under Contract No. DE-AC02-06CH11357.

1-ID-B,C,E • XSD • Materials science, physics, chemistry • High-energy x-ray diffraction, radiography, small-angle x-ray scattering, fluorescence spectroscopy, pair distribution function • 50-90 keV, 50-150 keV • On-site • Accepting general users •

11-ID-B • XSD • Chemistry, environmental science, materials science • Pair distribution function • 58-60 keV, 90-91 keV • On-site • Accepting general users •

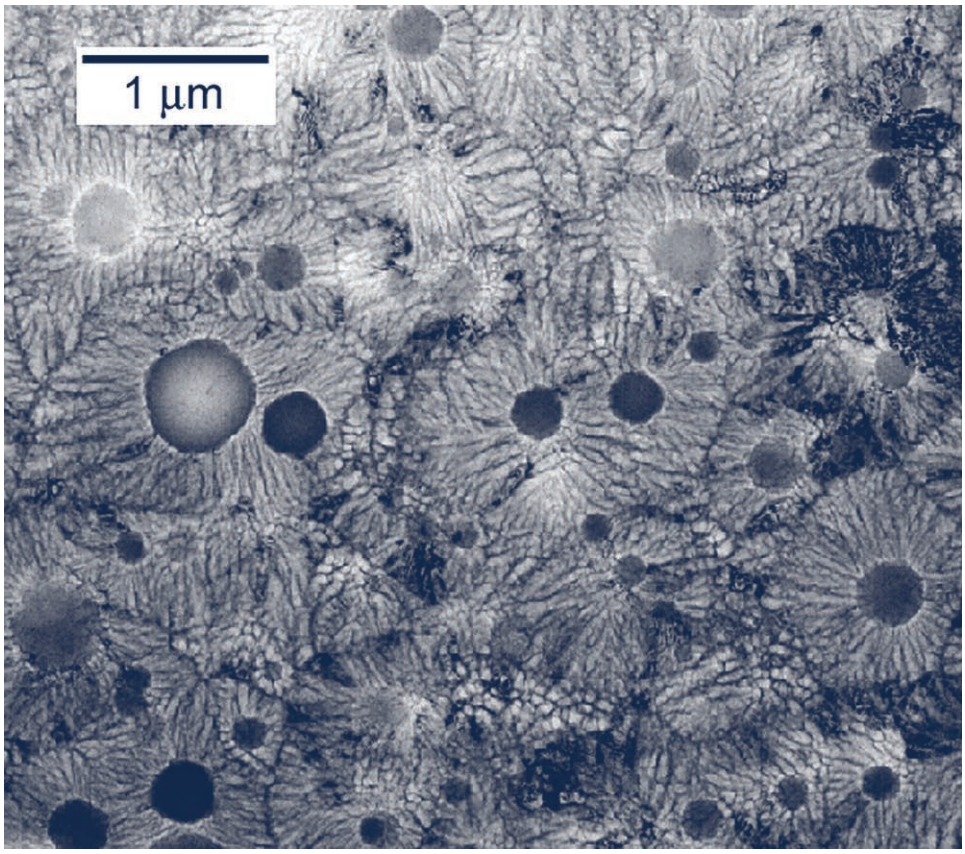

Fig. 1. Microstructure of an $Al_{91}Fe_7Si_2$ alloy after electron beam surface melting with a scan velocity of 50 cm/s. The nodules at the center of radiating patterns of crystallization are q-glass. This morphology indicates that the q-glass was first to solidify from the melt. From G.G. Long et al., Phys. Rev. Lett. **111**, 015502 (2013). © 2013 American Physical Society

Glass Formation from Metal Melts

People have known how to make glass for thousands of years, but how and why glass forms is, remarkably, still only poorly understood. The crucial question is how the atoms in a liquid melt arrange themselves, upon cooling, into the amorphous but somewhat ordered state that constitutes a glass. By combining x-ray scattering measurements at XSD beamline 6-ID-D at the APS and neutron scattering studies carried out at the Institut Laue-Langevin, Instrument D20 (France), scientists have tracked the evolution of atomic order in $PdZr_2$ liquid as it cools toward the glass transition temperature. Their findings hint that this and similar liquids form glasses because the complexity of their short-range atomic ordering hinders crystallization.

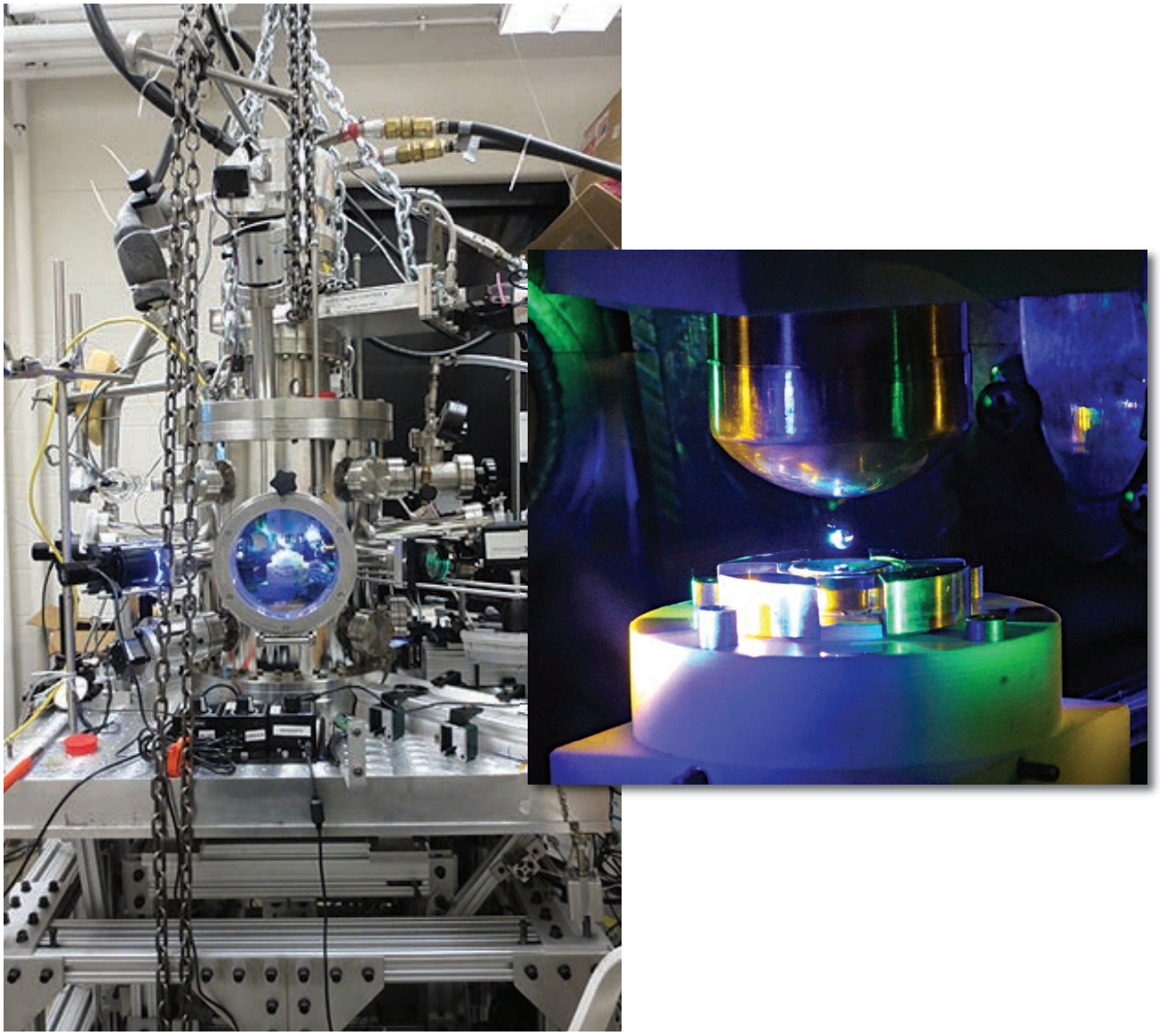

Fig. 1. Left: The experimental setup in the 6-ID-D research station at the APS. Right: Close-up of the levitation stage (visible behind the window in the main photo) and a levitated sphere (solid, not liquid - i.e., before melting). The colors come from the different-color high-intensity light emitting diodes used to record sample position on position-sensitive detectors in order to obtain the feedback signals for adjusting the electrodes used for sample levitation. Photos courtesy of K.F. Kelton (Washington University in St. Louis).

Intermetallic solid phases have fixed stoichiometries and a regular crystal structure, in which atoms of each species in the compound occupy specific lattice positions. Some intermetallic liquids, however, can also form glassy structures. Previous experiments using both x-ray scattering and neutron scattering have shown that on cooling, the atoms in some metallic melts form into small clusters with an icosahedral structure. This short-range order is at odds with the translational symmetry of a crystal lattice, leading to a large activation energy for crystal nucleation and, it has been suggested, a preference for solidification into a glassy state.

In the particular case of zirconium (Zr)-based glass-forming liquids, however, experiments have given conflicting results on the presence and evolution of short-range icosahedral order in samples undercooled below their liquidus temperature. Some measurements on alloy melts of Zr with nickel or copper point to a nearest-neighbor coordination number of 14, rather than the 12 characteristic of icosahedra. Hoping to resolve these discrepancies, scientists from the Deutsches Zentrum für Luft-und Raumfahrt e.V. (DLR, Germany) and Washington University in St. Louis undertook a study of liquid $PdZr_2$.

The team prepared approximately spherical samples of $PdZr_2$ about 2-mm in diameter for x-ray scattering and about 4.5 mm in diameter for neutron scattering studies. To conduct the experiments, they used the electrostatic levitation facilities of Washington University in St. Louis (x-ray scattering) (Fig. 1) and DLR (neutron scattering) to freely suspend the samples in a vacuum while they were heated by high-intensity lasers. The scientists recorded scattering data by holding the samples at temperatures from 1703K down to 1105K, passing through the liquidus temperature of 1358K. X-ray measurements took only about 20 sec, while the neutron measurements required up to an hour.

Because x-rays scatter off an atom's electrons and neutrons scatter off the nucleus, the differences between the two scattering patterns can be used to distinguish the topological order of the liquid (the ordering of its atoms, regardless of identity) from its chemical structure (the relative positioning of the two atomic species). Interpreting the scattering results is not straightforward, however.

Nevertheless, some clear results emerged. Below the liquidus temperature, the team found small but consistent differences in the structure factors deduced from the x-ray and neutron results, indicating that Zr and palladium atoms are not intermixed at random (Fig. 2). The coordination number was roughly 13.8, inconsistent with a dominant icosahedral structure but consistent with results on some other Zr-based alloy liquids. In a detailed analysis of results from a sample undercooled by 250K below the liquidus temperature, the team showed that no single form of short-range ordering, icosahedral or otherwise, could simultaneously fit the measured x-ray and neutron scattering patterns.

It therefore appears that undercooled melts of $PdZr_2$ have a variety of small-scale atomic clusters or aggregates with different geometries, coordination, and packing. This finding is consistent with *ab initio* molecular dynamics calculations of the structure of glass-forming Zr-Cu and Zr-Ni liquids, and with a reverse Monte Carlo analysis of x-ray scattering results from $Zr_{75.5}Pd_{24.5}$, constrained by molecular dynamics.

The team suggests that the different aggregates compete with each other during crystallization, leading to a "frustrated" system that cannot find a unique crystallization pathway. It is the presence of this variety of local clusters, they argue, rather than a pure icosahedral order that blocks crystal nucleation in Zr-based melts and favors glass formation. This mechanism is analogous to what happens with spin glasses. In these magnetically disordered systems, ferromagnetic and antiferromagnetic ordering compete with each other and create a magnetically frustrated system.
— David Lindley

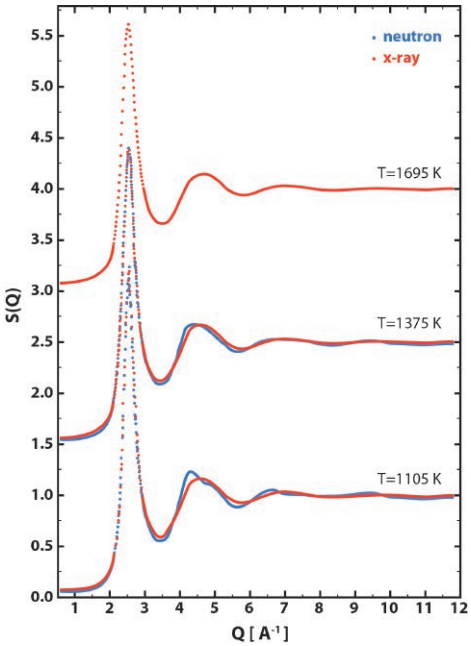

Fig. 2. Comparison of structure factors for $PdZr_2$ derived from x-ray (red) and neutron (blue) scattering, for samples held at temperatures above and below the liquidus temperature of 1358K. In the liquid state (top), the two structure factors are identical, indicating that Zr and Pd atoms are arranged in the same way. At the lower temperatures, small differences arise, indicating the emergence of short-range ordering, in which Pd and Zr are arranged differently.

See: S. Klein[1], D. Holland-Moritz[1], D.M. Herlach[1]*, N.A. Mauro[2], and K.F. Kelton[2], "Short-range order of undercooled melts of $PdZr_2$ intermetallic compound studied by X-ray and neutron scattering experiments," Europhys. Lett. **102**, 36001 (2013). DOI:10.1209/0295-5075/102/36001
Author affiliations: [1]Deutsches Zentrum für Luft-und Raumfahrt e.V., [2]Washington University in St. Louis
Correspondence:
* dieter.herlach@dlr.de

Financial support by the Deutsche Forschungsgemeinschaft within contract No. HE1601/21 is gratefully acknowledged. K.F.K. and N.A.M. gratefully acknowledge the support of the National Science Foundation under Grant DMR-0856199 and NASA under Grants NNX07AK27G, NNX09AJ19H, and NNX10AU19G. Use of the Advanced Photon Source at Argonne National Laboratory was supported by the U.S. Department of Energy Office of Science under Contract No. DE-AC02-06CH11357.

6-ID-D • XSD • Physics, materials science • Magnetic x-ray scattering, high-energy x-ray diffraction, powder diffraction, pair distribution function • 50-100 keV, 70-130 keV • On-site • Accepting general users •

Animatedly Suspended X-ray Observations

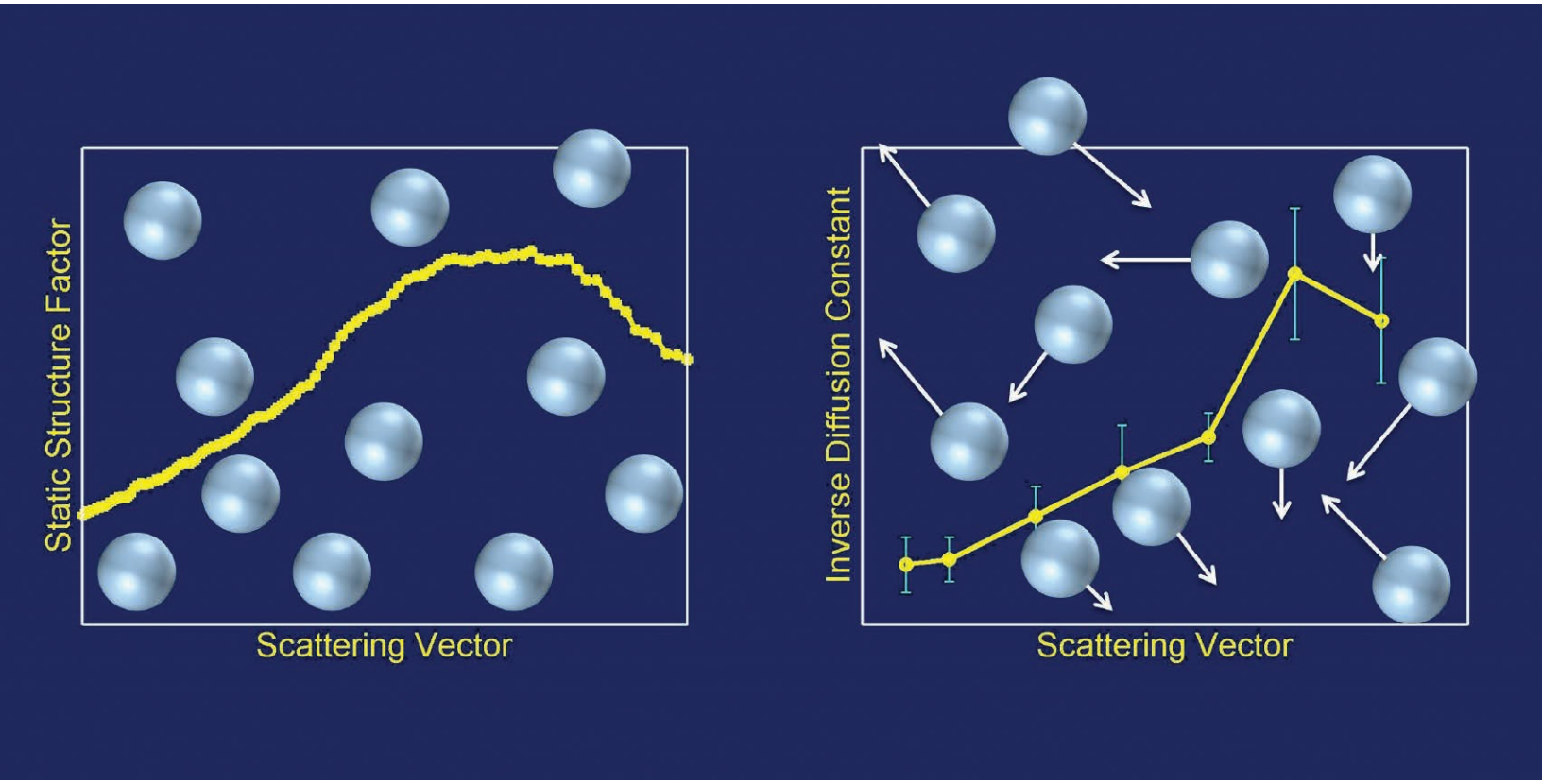

Fig. 1. The static structure factor of the microsphere suspension (left panel) and the effective inverse diffusion constant of microspheres (right panel) show similar dependency on scattering vector, which suggests that the lowest free-energy configuration in the static case also has a long lifetime.

A colloidal suspension is a mixture in which microscopic particles of one substance are dispersed in another and because of its properties, does not "settle" in the way that one might expect a stirred mixture of sand in water to do; nor do the particles dissolve in the fluid as one might expect grains of salt to dissolve in water. More information about colloids could lead to a deeper understanding of complex soft matter, with implications for new or improved materials and polymer science, but we have only an incomplete picture of the structure and dynamics of colloidal suspensions. Utilizing the APS, researchers probed the behavior of colloidal systems in which microscopic particles stay suspended in a fluid indefinitely. Their findings could have applications in new synthetic materials such as paints, coatings and adhesives, foodstuffs, pharmaceutical formulations, and cosmetics.

Colloidal suspensions and the related gels (solid colloidal systems) are of interest because many of them have fundamentally useful properties. Natural systems such as milk, the interior of cells, even atmospheric fog are colloidal systems. Colloidal suspensions never "settle" because the unceasing collisions among the molecules — Brownian motion — that form the suspending fluid and the colloidal particles counteract the effect of gravity on their greater density; they never sink.

If one swirls grains of sand in a beaker of water, the thermal motions of the water molecules will not be sufficient to prevent gravity from causing the sand to eventually form sediment at the bottom of the beaker once it is left to stand for long enough. However, microscopic particles of sand in the mix might remain suspended indefinitely.

The researchers in this study, at the National Institute of Standards and Technology, Northern Illinois University, and Argonne suggest that concentrated colloidal suspensions of microspheres in a liquid are apparently not simple systems. The research team utilized the new synchrotron x-ray technique called ultra-small-angle x-ray scattering (USAXS)–x-ray photon correlation spectroscopy (XPCS) to help them see through colloidal systems in order to reveal inner secrets. This new technique, implemented on the dedicated USAXS beamline (initially the XSD 32-ID beamline, and later the ChemMatCARS 15-ID-B,C,D beamline) at the APS, overcomes the problem of attempting to use light to study such opaque systems because the wavelengths of x-rays are so much shorter than that of visible light and so can resolve details of the particles involved and their behavior on concomitantly shorter length scales.

The team points out that this new approach also overcomes several of the technical limitations of conventional XPCS, allowing larger distances to be observed and so provides data on rapidly moving microspheres. Fundamentally, they can observe particles tenths of a micrometer to several micrometers in diameter.

The team worked with microscopic spheres of the common polymer, polystyrene, and suspended these particles in the colorless and viscous fluid glycerol, which is technically a sugar alcohol compound and is used widely in cosmetics and pharmaceutical formulations. They suspended a range of volumes of polystyrene spheres — from 10% to 20% — in the fluid and used USAXS−XPCS to monitor the motions of the spheres in the fluid.

Their key finding is that the microscopic polystyrene spheres move differently than had been suspected, based on the simple notion of the glycerol molecule buffeting them and preventing them from settling (Fig. 1).

Rather than the apparently simple Brownian motion taking place in this colloidal suspension, it seems that the microspheres move collectively whereby buffeted particles pull along their neighbors. Such behavior implies that, compared with expectations, the suspended particles spend much longer times in close proximity without touching. Potentially, this behavior could be exploited in cases where suspended particles serve as centers for chemical reactions.

Future experimental work is aimed at improving the time resolution of the measurement so that the more industrially and environmentally important aqueous systems can be studied.

— David Bradley

See: Fan Zhang[1,3]*, Andrew J. Allen[1], Lyle E. Levine[1], Jan Ilavsky[2], and Gabrielle G. Long[1,2], "Structure and Dynamics Studies of Concentrated Micrometer-Sized Colloidal Suspensions," Langmuir **29**, 1379 (2013). DOI:10.1021/la3044768

Author affiliations: [1]National Institute of Standards and Technology, [2]Argonne National Laboratory, [3]Northern Illinois University

Correspondence: * fan.zhang@nist.gov

ChemMatCARS Sector 15 is principally supported by the National Science Foundation/Department of Energy under grant number NSF/CHE-0822838. Use of the Advanced Photon Source at Argonne National Laboratory was supported by the U.S. Department of Energy Office of Science under Contract No. DE-AC02-06CH11357.

15-ID-B,C,D • ChemMatCARS • Materials science, chemistry • Single-crystal diffraction, anomalous and resonant scattering (hard x-ray), wide-angle x-ray scattering, microdiffraction, liquid surface diffraction, small-angle x-ray scattering, ultra-small-angle x-ray scattering, high-pressure diamond anvil cell • 6-32 keV, 10-60 keV • On-site• Accepting general users •

Cerium Changes Phases as a Liquid

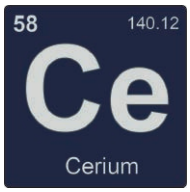

rium (Ce) has long fascinated scientists due to its proclivity for changing phases in unusual ways. Solid Ce, for example, will spontaneously respond to sufficient pressure by changing from a low-density, face-centered-cubic (fcc) crystalline phase to a high-density fcc phase, leading to a volume collapse of up to 17%. This behavior suggests the possibility that Ce may behave similarly when it is a liquid as well. Scientists utilizing the APS achieved the first experimental observation of such a liquid-liquid phase transition. They found that at 13 GPa, liquid Ce does indeed change from a high-density phase to a low-density phase as its temperature is increased from 1550K to 1900K, bringing about a density decrease of 14%. This work revealed new information about the liquid state of metals and opens avenues for research into the physics of the formation of novel and potentially technologically important materials.

The scientists from George Mason University, the Carnegie Institution of Washington, Oak Ridge National Laboratory, and Tohoku University (Japan) studied the melting process and liquid behavior of Ce using *in situ* high-intensity x-ray diffraction (XRD) at the High Pressure Collaborative Access Team's (HP-CAT's) 16-ID-B x-ray beamline at the APS. High pressures were applied using the diamond anvil cell technique, while high temperatures were achieved with a special double-sided laser heating system.

Melting was signaled by the appearance of diffusive halo-like diffraction patterns and the disappearance of sample diffraction lines. The XRD patterns were recorded at various temperatures for pressures of 1.9, 13, and 22 GPa (Fig. 1). The liquid Ce remained in the low-density phase at 1.9 GPa for the temperatures studied, while at 13 GPa, a high-density phase gave way to a low-density phase when the temperature was increased to 1900K. At 22 GPa, the high-density liquid shifted gradually to the low-density phase with increasing temperature.

To investigate why Ce behaves in this manner, the scientists developed theoretical models based on *ab initio* calculations. As part of this study, structure factors corresponding to pure trivalent and tetravalent valence states of Ce were compared with the experimental results.

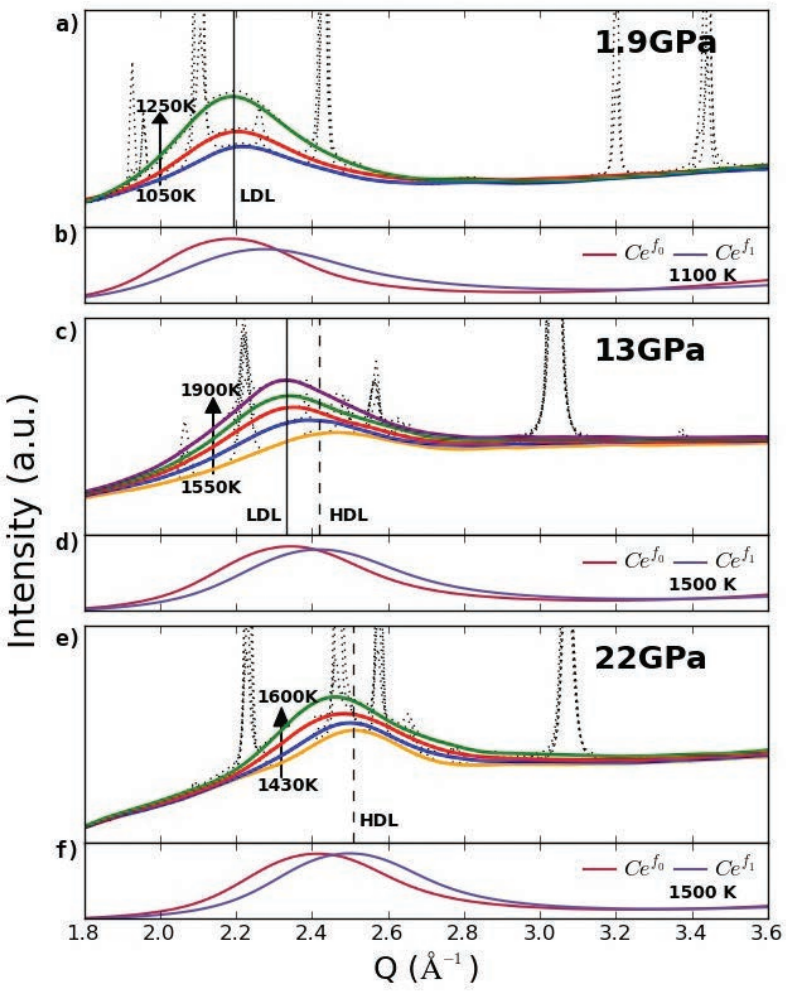

Cerium was discovered by Swedish chemists Jöns Jacob Berzelius and Wilhelm von Hisinger (who named the new element cerium after the asteroid Ceres, which had been discovered two years earlier by Giuseppe Piazzi) and independently by Martin Heinrich Klaproth, a German chemist, in 1803. Cerium is the most abundant of the rare-earth elements and makes up about 0.0046% of the Earth's crust. Pure cerium will ignite if it is scratched with a sharp object, but can be safely used if combined with other materials. Cerium is one of the rare-earth elements used to make carbon arc lights, as a catalyst to refine petroleum, and as an alloying agent to make special metals. The diagram at right is a schematic representation of the atomic shell structure of cerium. Sources: www.chemicool.com/elements/cerium.html, education.jlab.org/itselemental/ele058.html, and www.webelements.com/cerium/atoms.html.

At 1.9 GPa, the structure of the melt was found to be close to that of the pure trivalent Ce liquid over the temperature range studied.

At 13 GPa, the experimentally observed high-density and low-density phases were seen to be similar to the pure tetravalent and trivalent reference structures, respectively.

At 22 GPa, the experimental structure of the Ce liquid was similar to that of the pure tetravalent Ce reference liquid before shifting toward that of the pure trivalent Ce liquid with increasing temperature.

This suggests that under the conditions of the experiment, liquid Ce is in a mixed valence state that can be modeled as a trivalent Ce–tetravalent Ce pseudo-alloy. The researchers made this assumption in their modeling to analyze the thermodynamic conditions for the liquid-liquid phase transition for Ce by assessing the Gibbs free energy of the pseudo-alloy. Such calculations corroborated the experimental observation of a stable low-density phase at 1.9 GPa and a high-density phase at 22 GPa.

< Fig. 1. X-ray diffraction patterns in (a), (c), and (e) show cerium behavior at a range of pressures and temperatures. The dotted black lines are raw experimental data from which the liquid curves (colored lines) are extracted; the crystal peaks present are due to the pressure medium and noninteracting oxides. The diffraction intensities are scaled to better illustrate the phase evolution of liquid Ce. The structure factors from molecular dynamics simulations of the two reference liquids (trivalent Cef0, tetravalent Cef1) are shown in (b), (d), and (f).

At 13 GPa, a calculated first-order liquid-liquid phase transition was observed. The calculations also showed that below 6 GPa the equilibrium low-density and high-density phases are predominantly trivalent and tetravalent Ce, respectively.

The high-density and low-density branches of the free energy were seen to converge as the pressure increases, leading to the occurrence of a critical point at a pressure of 21.3 GPa and a temperature of 2100K.

Above the critical pressure, the free-energy curves always exhibited one minimum, indicating that the first order transition between the low-density and high-density liquid phases no longer exists. The results also implied that the phase transition could be density driven by modulating the pressure under isothermal conditions. That was confirmed by an experiment at about 1100 K when a low-density Ce liquid at 1.9 GPa transformed isothermally to a high-density Ce liquid at 4.0 GPa.

— Vic Comello

See: A. Cadien[1]*, Q.Y. Hu[1], Y. Meng[2], Y.Q. Cheng[3], M.W. Chen[4], J.F. Shu[2], H.K. Mao[2], and H.W. Sheng[1]**, "First-Order Liquid-Liquid Phase Transition in Cerium," Phys. Rev. Lett. **110**, 125503 (2013).
DOI:10.1103/PhysRevLett.110.125503
Author affiliations: [1]George Mason University, [2]Carnegie Institution of Washington, [3]Oak Ridge National Laboratory, [4]Tohoku University
Correspondence: *acadien@gmu.edu, **hsheng@gmu.edu

The work was supported by the U.S. National Science Foundation (NSF) under Grant No. DMR-0907325 and the Office of Naval Research under Grant No. N00014-091-1025A. H.K.M. was supported as part of EFree, an Energy Frontier Research Center funded by the U.S. Department of Energy Office of Science, Basic Energy Sciences (DOE-BES), under Award No. DE-SC0001057. Y.Q.C. was supported at Oak Ridge National Laboratory by the Scientific User Facilities Division, DOE-BES. HP-CAT operations are supported by DOE-National Nuclear Security Administration under Award No. DE-NA0001974 and DOE-BES under Award No. DE-FG02-99ER45775, with partial instrumentation funding by NSF. Use of the Advanced Photon Source at Argonne National Laboratory was supported by the U.S. Department of Energy Office of Science under Contract No. DE-AC02-06CH11357.

16-ID-B • HP-CAT • Materials science, geoscience, chemistry, physics • Microdiffraction, single-crystal diffraction, high-pressure diamond anvil cell • 24-35 keV • On-site • Accepting general users •

Building Better Catalysts for Splitting Water

The dream of a hydrogen economy — a world run on H_2 gas, free from the pollution and politics of fossil fuels — may depend on developing an energy-efficient strategy for splitting water into oxygen and hydrogen. The problem is that water bonds are very stable, requiring hefty energy inputs to break. Scientists are eagerly developing catalysts to lower the energy demands, and thus the cost, of H_2 production. Yet, science still struggles with the basics, such as what structural properties make a good water-splitting catalyst. Using measurements from two APS beamlines, researchers analyzed the stability and composition of three small clusters of palladium — Pd_4, Pd_6, and Pd_{17} — which are under investigation as potential water-splitting catalysts. They then generated structural models of the catalysts. By combining information about the identity and structure of each cluster with its catalytic activity, the researchers identified a particular Pd-Pd bond that appears to be essential for catalytic function, thus allowing scientists to design better water-splitting catalysts.

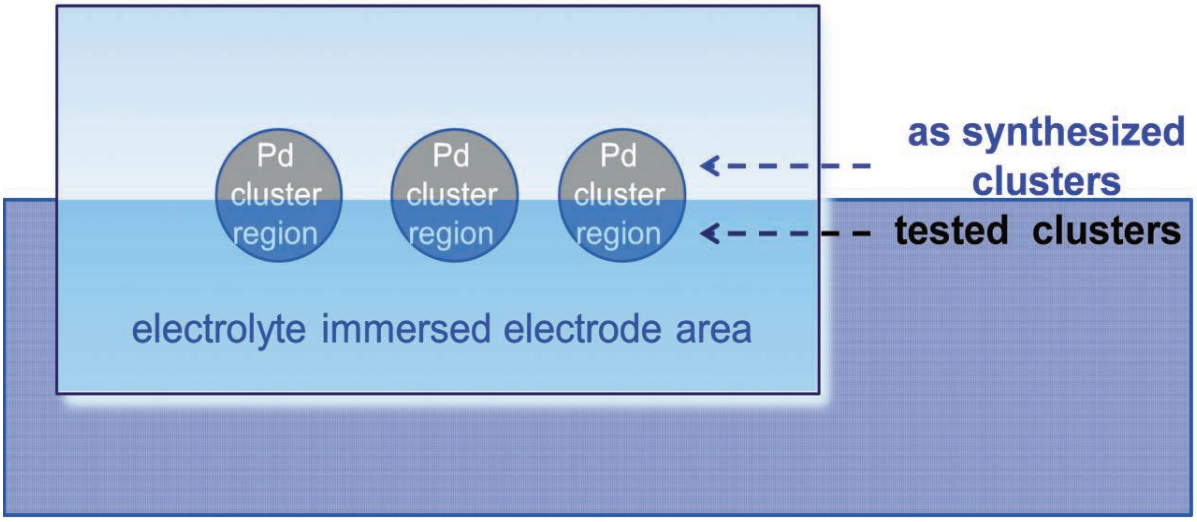

Fig. 1. A schematic of the x-ray experiment used to determine cluster stability and composition (i.e., oxidation state).

Electrochemical water splitting occurs in two distinct reactions: the hydrogen evolution reaction (HER), and the oxygen evolution reaction (OER). In this study, the researchers, from Argonne National Laboratory, the University of Birmingham (United Kingdom), and Yale University focused on the OER, which is currently the least efficient part of the water-splitting process. Past studies showed that platinum metal can catalyze OER, but those materials require a high load of the expensive metal, usually present as large nanoparticles.

In search of more cost-efficient, more energy-efficient, and more active options, the current study focuses on palladium catalysts with sizes of less than a nanometer.

Typically, metallic catalysts are spread somewhat haphazardly onto support surfaces, resulting in unknown distributions of single atoms, clusters, and larger particles. For this study, the researchers isolated size-specific clusters by sending a molecular beam of palladium ions through a mass spectrometer, filtering out all sizes of particles except the clusters of interest: Pd_4, Pd_6, and Pd_{17}. The clusters were then immediately deposited, separately, on an electrode consisting of a silicon wafer coated with a thin nanodiamond film (Fig. 1).

To test the catalytic prowess of the small palladium clusters, the cathodes were dipped, halfway, into a basic solution, which is the standard medium used in OER. Then, the researchers performed voltammetry, using current as a measure of the turnover rate of the OER reaction. The current generated by the cathode containing Pd_4 clusters was no better, and perhaps a little worse, than the electrode alone. However, the Pd_6 and Pd_{17} clusters showed significant activity, with turnover rates that beat those from previous work on Pd metal surfaces and are comparable to those for iridium, the most active metal catalyst for OER.

The next step was to characterize the cluster samples. The researchers

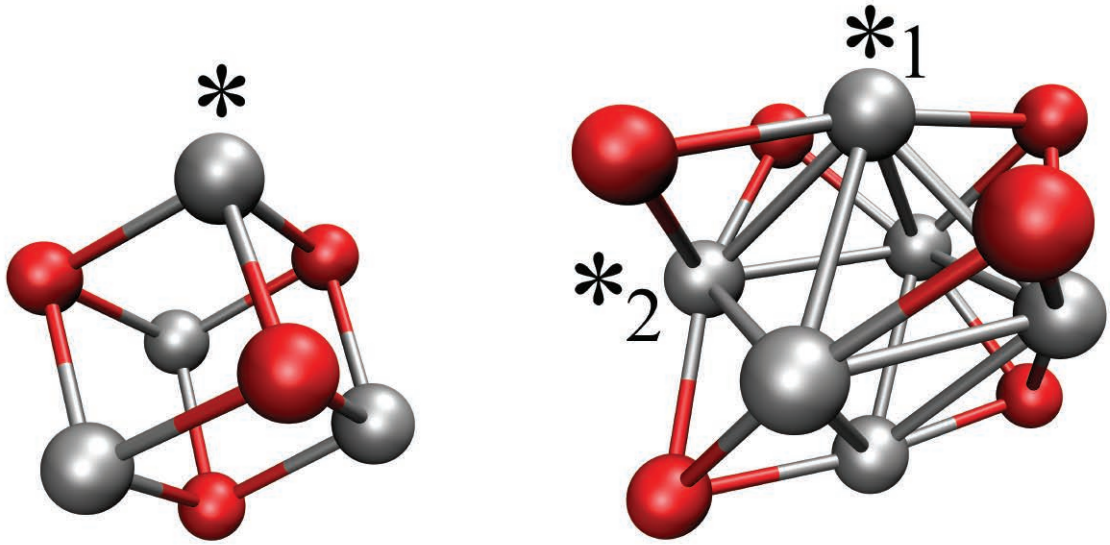

Fig. 2. Possible structures of Pd_4O_4 (left) and Pd_6O_6 (right) generated by density functional calculations.

brought the same cluster-coated electrodes used in the voltammetry studies to the APS for characterization by grazing incidence x-ray absorption spectroscopy (GIXAS) at MR-CAT beamline 10-ID-B and grazing incidence small angle x-ray scattering (GISAXS) at XSD beamline 12-ID-C,D.

One important observation was that immersed clusters look practically identical to those which were not subject to the water oxidation reaction, suggesting that neither catalysis nor the harsh basic environment changed the structure of the clusters. That stability is key to developing durable catalysts. The measured oxidation states of the Pd_4 and Pd_6 clusters was used in density functional calculations which determined, for each cluster, the structural configurations (Fig. 2) as well as the free energy for each step of the OER.

Theoretical calculations performed using the high-performance computing cluster at Argonne's Center for Nanoscale Materials suggest that bridging Pd-Pd sites are active for the oxygen evolution reaction (OER) in Pd_6O_6. Overall, a key descriptor for an efficient OER Pd catalyst is a balancing of binding energy differences with respect to liquid water for each of the important reaction intermediates (O, OH, and OOH). For these Pd clusters, OOH is more strongly bound than the other species, resulting in the observed overpotential. DFT packages Quantum Espresso and VASP were exploited to gain this insight, along with cluster global optimization using the Birmingham Cluster Genetic Algorithm.

The researchers concluded that the pertinent difference between the clusters was the presence of particular Pd-Pd bonds in the two larger clusters, but not in the smaller cluster. They suspect that this bond may be necessary for OER catalysis, suggesting that catalytic surfaces may be hindered by inactive species. The hope is that, with the knowledge of what constitutes an active species, researchers can focus on making water-splitting catalysts using only the best clusters.

— Erika Gebel Berg

See: Gihan Kwon[1], Glen A. Ferguson[1], Christopher J. Heard[2], Eric C. Tyo[3], Chunrong Yin[1], Janae DeBartolo[1], Sönke Seifert[1], Randall E. Winans[1], A. Jeremy Kropf[1], Jeffrey Greeley[1], Roy L. Johnston[2], Larry A. Curtiss[1]***, Michael J. Pellin[1]**, and Stefan Vajda[1]*, "Size-Dependent Subnanometer Pd Cluster (Pd_4, Pd_6, and Pd_{17}) Water Oxidation Electrocatalysis," ACS Nano. **7**(7), 5808 (2013). DOI:10.1021/nn400772s

Author affiliations: [1]Argonne National Laboratory, [2]University of Birmingham, [3]Yale University

Correspondence: *vajda@anl.gov, **pellin@anl.gov, ***curtiss@anl.gov

This work was supported by the U.S. Department of Energy (DOE) Basic Energy Sciences Materials Sciences and Engineering, under Contract No. DE-AC-02-06CH11357, with UChicago Argonne, LLC, operator of Argonne National Laboratory. J.G. acknowledges support through a DOE Early Career Award. R.J. and C.H. acknowledge the University of Birmingham North America fund for travel to Argonne. Use of the Center for Nanoscale Materials was supported by the U. S. Department of Energy Office of Science, Basic Energy Sciences, under Contract No. DE-AC02-06CH11357. MR-CAT operations are supported by the Department of Energy and the MR-CAT member institutions. Use of the Advanced Photon Source at Argonne National Laboratory was supported by the U.S. Department of Energy Office of Science under Contract No. DE-AC02-06CH11357.

10-ID-B • MR-CAT • Materials science, environmental science, chemistry • X-ray absorption fine structure, time-resolved x-ray absorption fine structure, micro x-ray absorption fine structure, microfluorescence (hard x-ray) • 4.3-27 keV, 4.3-32 keV, 15-90 keV • On-site • Accepting general users •

12-ID-C,D • XSD • Chemistry, physics, materials science • Small-angle x-ray scattering, grazing incidence small-angle scattering, wide-angle x-ray scattering, surface diffraction • 4.5-36 keV • On-site • Accepting general users •

The Water-Like Properties of Soft Nanoparticle Suspensions

The unusual properties of water, including its anomalous thermal expansion and density anomaly, have intrigued researchers for decades. These properties are notoriously hard to investigate experimentally owing to the inherently small length scales and complex interactions that appear to govern the physics of these materials. Studies of small particles (colloids) dispersed in solvents, known as colloidal suspensions, used as models for atomic and molecular liquids have shown that some of these anomalies can be engineered in colloidal suspensions of soft particles. Research carried out at the APS elucidates the arrangements and mobility of soft nanoparticles in dense suspensions that mirror the anomalies observed in complex liquids like water. This discovery, which is the first instance of experimental observation of such behavior in a colloidal suspension, allows for an extension of the toolbox of the experimental physicist interested in employing suspensions to mimic molecular liquids, with the added advantage of readily accessible length and time scales.

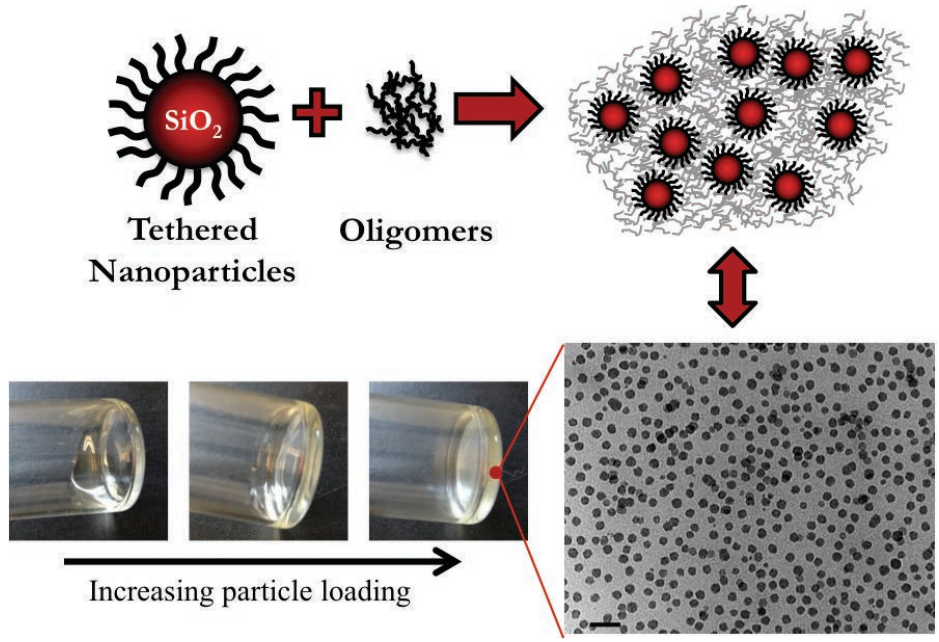

Fig. 1. A schematic of soft nanocolloidal suspensions composed of soft polyethylene glycol (PEG) tethered silica nanoparticles suspended in PEG oligomers. The pictures show the variation in physical characteristics with increasing particle loading. The electron micrograph shows the well-dispersed particles in these suspensions.

The research team, with members from Cornell University and Argonne, synthesized soft nanoparticles by densely tethering small polymers onto the surface of silica nanoparticles. Small-angle x-ray scattering (SAXS) and x-ray photon correlation spectroscopy (XPCS) measurements were carried out at XSD beamlines 8-ID-I and 12-ID-B at the APS to reveal the equilibrium structure and the characteristics of particle motion, respectively.

The particle arrangements become more disordered and move faster when more particles are added into the suspension beyond a critical particle volume fraction, coinciding with a sharp increase in the resistance by the system of grafted nanoparticles to physical deformations (Fig. 1).

This is in contrast to the usual situation where increasing the concentration of particles in a dilute suspension decreases the space available for placing new particles, thus increasing particle ordering and slowing them down. It becomes easier for any particle in these suspensions to diffuse when they are more surrounded by their neighbors.

The anomalous behavior of particles suspended in water and other complex liquids has been long argued to exist for systems with soft repulsion, which is characterized by a potential energy that exhibits a finite width over which particle interaction occurs. These empirical findings lend support to an emerging consensus from simulations and provide for a model system for studying systems with soft repulsive interactions. *— Suresh Narayanan*

See: Samanvaya Srivastava[1], Lynden A. Archer[1]*, and Suresh Narayanan[2], "Structure and Transport Anomalies in Soft Colloids", Phys. Rev. Lett. 1**10**, 148302 (2013).
DOI: 10.1103/PhysRevLett.110.148302
Author affiliations: [1]Cornell University, [2]Argonne National Laboratory
Correspondence: *laa25@cornell.edu

This work was supported by the National Science Foundation, Award No. DMR-1006323 and by Award No. KUS-C1018-02, made by King Abdullah University of Science and Technology (KAUST). Use of the Advanced Photon Source at Argonne National Laboratory was supported by the U.S. Department of Energy Office of Science under Contract No. DE-AC02-06CH11357.

8-ID-I • XSD • Polymer science, materials science, physics • X-ray photon correlation spectroscopy, intensity fluctuation spectroscopy, small-angle x-ray scattering • 6-12.5 keV, 7.35-7.35 keV, 7.35 keV • On-site • Accepting general users •

12-ID-B • XSD • Chemistry, materials science, life sciences, geoscience, polymer science • Small-angle x-ray scattering, grazing incidence small-angle scattering, wide-angle x-ray scattering • 7.9-14 keV • On-site • Accepting general users •

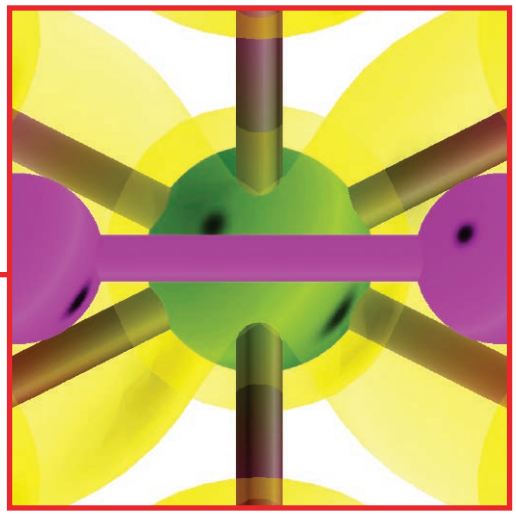

Chemical Science

Making Uncommon Salt

Salt is common in our kitchens and common in chemistry, too. Made of a sodium atom combined with a chlorine atom, salt molecules have been well studied, so scientists understand how they behave at day-to-day temperatures and pressures. Classical chemistry states that the only way sodium and chlorine can combine is in a one-to-one ratio, but new research carried out at Stony Brook University shows there is a wealth of unexpected new configurations for this common molecule. These predictions were verified at the APS and at the Deutsches Elektronen-Synchrotron (DESY, Germany). Moreover, the scientists in this study have demonstrated the feasibility of predicting an unexpected compound and creating it, which opens the door for revolutionary materials science.

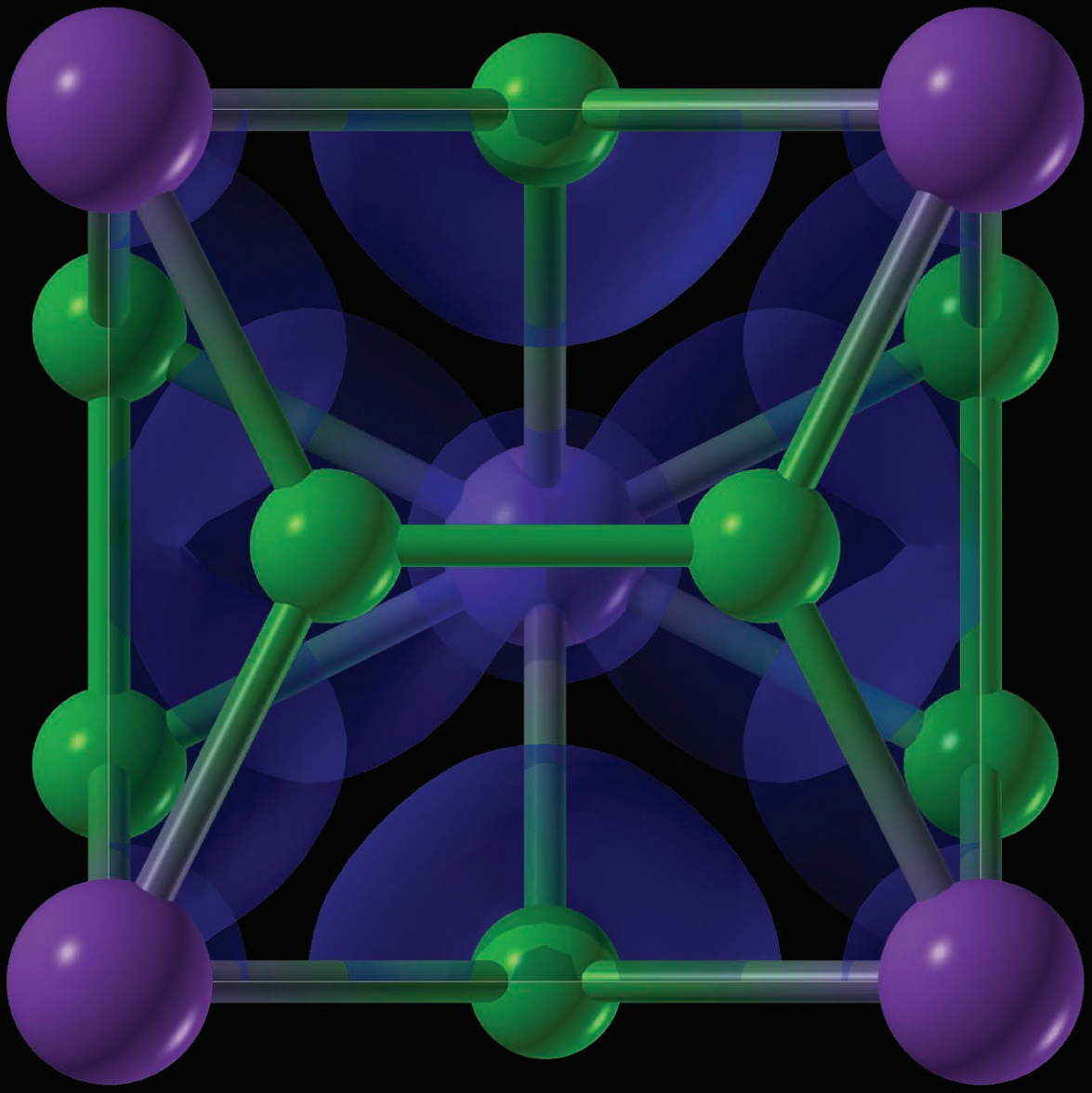

The researchers, from the China Agricultural University, Stony Brook University, the Carnegie Institution of Washington, The University of Chicago, and the Deutsches Elektronen-Synchrotron combined theoretical and experimental techniques to create this new sodium chloride combination.

The process began with an algorithm called USPEX (Universal Structure Predictor: Evolutionary Xtallography) created by Artem R. Oganov at Stony Brook University. The algorithm can be used to design stable materials on the computer and, it turns out, is able to devise predictions that are forbidden by traditional chemistry.

According to classical chemistry, which details just how electrons can help bind different atoms, the only way that sodium and chlorine atoms can fit together is with an equal amount of each type of atom. At higher pressures, the arrangement of the atoms changes, but the basic ratio remains the same.

However, members of the research team worked with the USPEX algorithm and discovered something unexpected. USPEX predicted that certain compounds thought to be forbidden might, in fact, be stable at high pressures — compounds that had three sodium and one chlorine, for example, or one sodium and seven chlorines. These results, if correct, would lead to major rethinking of chemical rules and models.

The team decided to tackle creating two of the new compounds that were accessible at relatively lower pressures: the one with three sodium atoms for every chlorine atoms, and material with one sodium atom for every three chlorine atoms.

The researchers took room-temperature rock salt, added extra sodium or chlorine as appropriate, then compressed the material in a diamond anvil cell and heated it with lasers. The laser heating was performed using the GSECARS x-ray diffraction beamline 13-ID-C,D at the APS, and at the Extreme Conditions Beamline P02.2 at the Deutsches Elektronen-Synchrotron. The resulting materials were stable, never-before seen new sodium chloride compounds. X-ray diffraction data were also collected on the quenched samples using the bending magnet beamlines at GSECARS and HP-CAT at the APS.

< Fig. 1. The structure of a novel sodium chloride compound with one sodium atom for every three chlorine atoms. The purple spheres are sodium, the green spheres are chlorine and the blue surface shows distribution of the electron localization function.

Not only were the researchers able to create these counterintuitive compounds, but they discovered interesting properties. The sodium chloride with three sodiums and one chlorine, for example, had a layered structure made of alternating layers of pure sodium and common sodium chloride (Fig. 1). The sodium chloride does not conduct electricity, but the sodium by itself does, making this what is known as a "two-dimensional metal": It can conduct electricity horizontally, but not vertically. In the high-tech world of semi-conductors, any material with unique properties like this could turn out to be useful.

Exotic chemistry means exotic properties, and the potential for unusual applications. The team's methods show that one can design new materials with desired properties on a computer, which dramatically decreases the time and cost.

This research suggests that other counterintuitive compounds may exist as well, in almost any chemical system, such as in certain compounds thought to help form planets. Planetary science, therefore, could also benefit from learning that the classical rules of chemistry are not necessarily complete. The interiors of planets, with their intense heat and pressures, may not be made of the materials traditionally believed.

— Karen Fox

See: Weiwei Zhang[1,2*], Artem R. Oganov[2,3,4*], Alexander F. Goncharov[5,6], Qiang Zhu[2], Salah Eddine Boulfelfel[2], Andriy O. Lyakhov[2], Elissaios Stavrou[5], Maddury Somayazulu[5], Vitali B. Prakapenka[7], and Zuzana Konôpková[8], "Unexpected Stable Stoichiometries of Sodium Chlorides," Science **342**, 1502 (20 December 2013).

DOI:10.1126/science.1244989

Author affiliations: [1]China Agricultural University, [2]Stony Brook University, [3]Moscow Institute of Physics and Technology, [4]Northwestern Polytechnical University, [5]Carnegie Institution of Washington, [6]Chinese Academy of Sciences, [7]The University of Chicago, [8]Deutsches Elektronen-Synchrotron
Correspondence:
* zwwjennifer@gmail.com,
** artem.oganov@sunysb.edu

Supported by the Young Teachers Development Project in China Agricultural University (W.Z.); National Science Foundation (NSF) grants EAR-1114313 and DMR-1231586, Defense Advanced Research Projects Agency grants W31P4Q1210008 and W31P4Q1310005, Government of the Russian Federation grant 14.A12.31.0003, China's Foreign Talents Introduction and Academic Exchange Program grant B08040 (A.R.O.); NSF, the Army Research Office, and EFREE, a U.S. Department of Energy (DOE)-Energy Frontier Research Center at Carnegie (A.F.G.); and German Federal Ministry of Education and Research grant 05K10RFA (Z.K.). M.S. acknowledges support from the Carnegie/DOE Alliance Center (National Nuclear Security Administration). GeoSoilEnviroCARS is supported by NSF Earth Sciences grant EAR-1128799 and DOE Geosciences grant DE-FG02-94ER14466. HP-CAT operations are supported by DOE-National Nuclear Security Administration under Award No. DE-NA0001974 and DOE-Basic Energy Sciences under Award No. DE-FG02-99ER45775, with partial instrumentation funding by NSF. Use of the Advanced Photon Source at Argonne National Laboratory was supported by the U.S. Department of Energy Office of Science under Contract No. DE-AC02-06CH11357.

13-ID-C,D • GSECARS • Geoscience, environmental science • Inelastic x-ray scattering, micro x-ray absorption fine structure, microdiffraction, x-ray absorption fine structure, microfluorescence (hard x-ray), high-pressure diamond anvil cell, high-pressure multi-anvil press • 4-45 keV • On-site • Accepting general users •

16-BM-D • HP-CAT • Materials science, geoscience, chemistry, physics • Powder angular dispersive x-ray diffraction, x-ray absorption near-edge structure, single-crystal diffraction, high-pressure diamond anvil cell • 6-70 keV • On-site • Accepting general users •

Metal Model Mimics Metalloenzymes

Metal ions play critical roles throughout biochemistry, often facilitating the cleavage of the bond between the two atoms in an oxygen molecule in metalloenzymes. They are the key to oxidizing organic molecules and, in the case of photosynthesis, water. An international team of scientists carrying out research at the XSD 20-BM beamline at the APS has homed in on the role of metal ions in a wide range of biological processes, from metabolism to photosynthesis. The work presents the first example of a non-heme (manganese) Mn(IV)−oxo (oxygen atom) complex binding redox-inactive metal ions, and is a demonstration of the diverse effects of a redox-inactive metal ion on the reactivities of high-valent metal−oxo (an oxygen atom bound only to one or more metal centers) species in oxidation reactions. These results were the cover article for J. Am. Chem. Soc. **135** (2013).

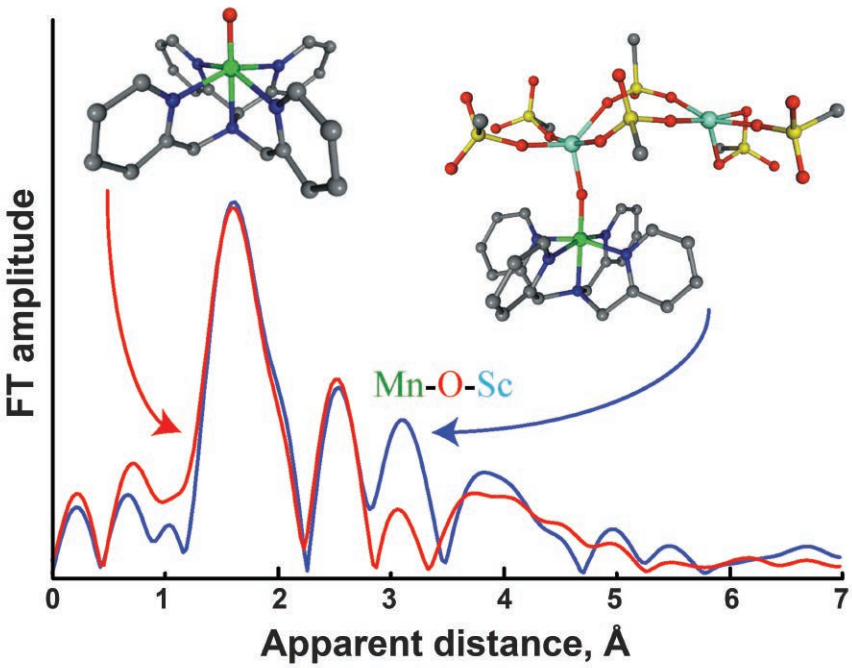

me·tal·lo·en·zyme n. An enzyme having a metal, usually an ion, linked to its protein component. The American Heritage® Medical Dictionary Copyright © 2007, 2004 by Houghton Mifflin Company.

The metal ions in question are not themselves redox active, meaning they can grab a single oxygen atom without suffering interfering side reactions. Commonly, these species are hooked up to a heme-type porphyrin molecule, the central unit in the blood protein hemoglobin and the light-sensitive unit in chlorophyll at the heart of photosynthesis.

The researchers from Ewha Womans University (Korea), Purdue University, Osaka University (Japan), and the Japan Science and Technology Agency built a simplified model of the natural metal-oxo compound (an oxygen atom bound only to one or more metal centers) using manganese in the IV oxidation state to which is attached a chemical group, or ligand, containing five nitrogen atoms — *N*,*N*-bis(2-pyridylmethyl)-*N*-bis(2-pyridyl)methylamine — which allow it to bond to the manganese(IV) through five points, with the final bonding point available for the oxo. Linking scandium ions to this unit completes the structure.

The team used various analytic methods, including electrospray ionization mass spectrometry (ESI-MS), electron paramagnetic resonance spectroscopy, and x-ray crystallography at beamline 20-BM-B to investigate the structure of their model in detail (Fig. 1). They also experimented with its chemical reactivity.

The binding of the scandium ions accelerates oxidation reactions by as much as 2200 times in the oxidation reaction of thioanisole, an oxygen atom transfer akin to those seen in many enzyme reactions in which the bond between two oxygen atoms is cleaved. The same metal model slows the rate of hydrogen atom transfer in activation of the organic compound 1,4-cyclohexadiene; this also emulates the behavior of the metal-oxo units in the metalloenzymes that the team hopes to understand.

The researchers explain that the precise behavior of their metal-oxo model is tuned by the presence or otherwise of the scandium ions. This simulates the tuning behavior of metalloenzymes by calcium ions in biology, for instance. The presence of calcium ions is essential in the photosynthetic oxidation of water, but their exact role is not entirely clear. The team's demonstration of this tuning process by scandium ions hints at one possible explanation.

A mechanism for why the oxygen atom transfer reaction is accelerated so substantially hints at the involvement of a fast-moving electron transfer pathway, the team explains. Conversely, the slower rate of the hydrogen atom transfer they interpret as being due to the bulk of the scandium(III) ions hindering movement of the hydrogen atoms, which are themselves much, much slower moving than electrons.

The work demonstrates that Mn(IV)-O reactivity in oxidation reactions can be altered by binding Sc(III) ions. This provides insight into the role of redox inactive metal ions in modulating the activity of Mn-oxo species, which may inform the ongoing discussion about the role of the Ca(II) ion in the Mn_4CaO_5 oxygen evolving center in photosystem II (PSII).

— David Bradley

< Fig. 1. Fourier transforms of the Mn *K*-edge extended x-ray absorption fine structure show peaks corresponding to Mn-O-Sc interactions, which modifies chemical properties of this reactive Mn(IV)=O center.

See: Junying Chen[1], Yong-Min Lee[1], Katherine M. Davis[2], Xiujuan Wu[1], Mi Sook Seo[1], Kyung-Bin Cho[1], Heejung Yoon[1], Young Jun Park[1], Shunichi Fukuzumi[3]*, Yulia N. Pushkar[2]**, and Wonwoo Nam[1]***, "A Mononuclear Non-Heme Manganese(IV)–Oxo Complex Binding Redox-Inactive Metal Ions," J. Am. Chem. Soc. **135**, 6388-6391 (2013). DOI:10.1021/ja312113p

Author affiliations: [1]Ewha Womans University, [2]Purdue University, [3]Japan Science and Technology Agency

Correspondence:
*fukuzumi@chem.eng.osaka-u.ac.jp,
**ypushkar@purdue.edu,
***wwnam@ewha.ac.kr

This research was supported by the National Research Foundation of Korea through CRI, WCU (R31-2008-000-10010-0), GRL (2010-00353), Basic Research Program (2010-0002558) (to M.S.S.); and by a Grant-in-Aid (20108010) and a Global COE Program from MEXT, Japan, (to S.F.). The research at Purdue was supported by DOE-BES (DE-FG02-10ER16184 to Y.N.P.) and a National Science Foundation Graduate Research Fellowship (0833366 to K.M.D.). APS sector 20, which is managed by XSD in partnership with the Canadian Light Source (CLS), is funded by the U.S. Department of Energy Office of Science, and by the Natural Sciences and Engineering Research Council of Canada and the University of Washington via the CLS. Use of the Advanced Photon Source at Argonne National Laboratory was supported by the U.S. Department of Energy Office of Science under Contract No. DE-AC02-06CH11357.

20-BM-B • XSD • Materials science, environmental science, chemistry • X-ray absorption fine structure, microfluorescence (hard x-ray), micro x-ray absorption fine structure, diffraction anomalous fine structure • 2.7-25 keV, 2.7-30 keV, 2.7-35 keV • On-site • Accepting general users •

A Bimetallic Catalyst That Helps Turn Plants into Plastic

Petroleum does more than fuel our vehicles. Many of the chemicals that supply industrial processes are also derived from petroleum, a limited resource that will likely become more expensive over time. In preparation for that cost increase, scientists are developing new sources for the chemicals typically provided by petroleum. One option is to extract valuable chemicals from biomass, such as plants or microbes, and convert these precursors into useful end-products. Biomass chemicals, however, have significantly more oxygen than petroleum-derived chemicals and require extensive, and expensive, processing. To ease the complex conversions of biomass precursors, catalysts are being developed that include an oxophilic ("oxygen loving") metal alongside a hydrogenation metal (a metal that has been treated with hydrogen). These bimetallic catalysts are promising, but little is known about how they work. In this study, researchers used APS x-rays to unravel the catalytic mechanism. Their discoveries may help make biomass a viable chemical source

The researchers, from the University of Wisconsin–Madison, Purdue University, and Argonne, were initially interested in the reaction that converts 2-hydroxymethyl-tetrahydropyran into 1,6 hexanediol, a 6-carbon chain with two hydroxyl groups at opposite ends. This highly-sought after compound is used in the production of polymers and is typically sourced from petroleum. While it can be produced from biomass, the problem is conversion reactions often result in the improper placement of hydroxyl groups.

In a previous study, a catalyst made from a carbon support, rhenium, an oxophilic promoter, and rhodium, a reducible metal, selectively produced 1,6 hexanediol from 2-hydroxymethyl-tetrahydropyran (Fig. 1). They hypothesized that this specificity stems from the two metals working in concert. The rhenium helps open the ring of 2-hydroxymethyl-tetrohydroparyn at the C-O bond, then, the rhodium does its work, avoiding the production of unwanted side products while hydrogenating the opened ring. Questions remained, however, as to the bimetallic catalyst's mechanism, but these could be answered at the APS.

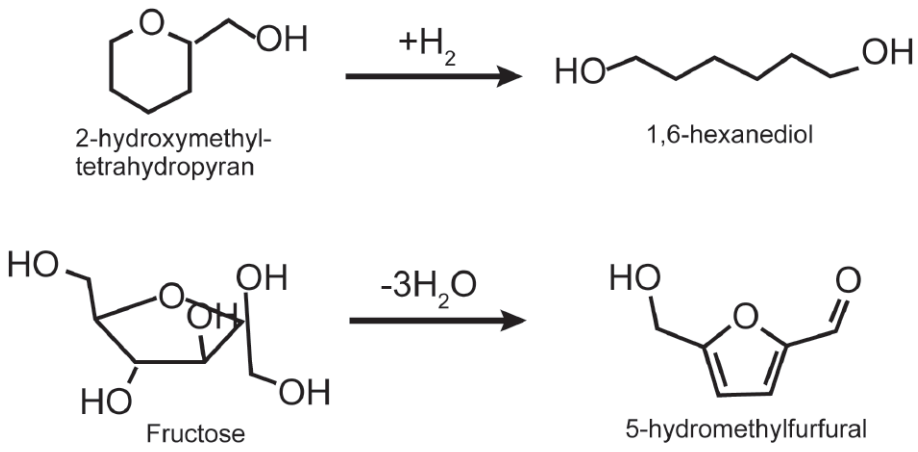

Fig. 1. Researchers studied the catalytic mechanism of two model reactions at the APS: the hydrogenolysis of 2-hydroxymethyl-tetrahydropyran to 1,6-hexanediol and the dehydration of fructose to 5-hydroxymethylfurfural. The reactants can be derived from plant biomass sources and the products, usually obtained from petroleum, have commercial value.

The MR-CAT 10-BM-A,B and 10-ID-B beamlines at the APS, where these studies were carried out, include custom equipment that allowed the research team the unique opportunity to study the catalyst *operando*, that is, during the reaction. The researchers performed x-ray absorption spectroscopy (XAS), which detects bonds between atoms in the catalyst. They observed that rhenium had fewer bonds on average, suggesting that the metal mostly occupied the nanoparticle surface. They interpreted this and other data as evidence that rhenium likely interacts strongly with oxygen in the surrounding water molecules, such that the hydrogen part of the water molecule acts like an acid. The researchers therefore suspected that the bimetallic catalyst may catalyze reactions by be-

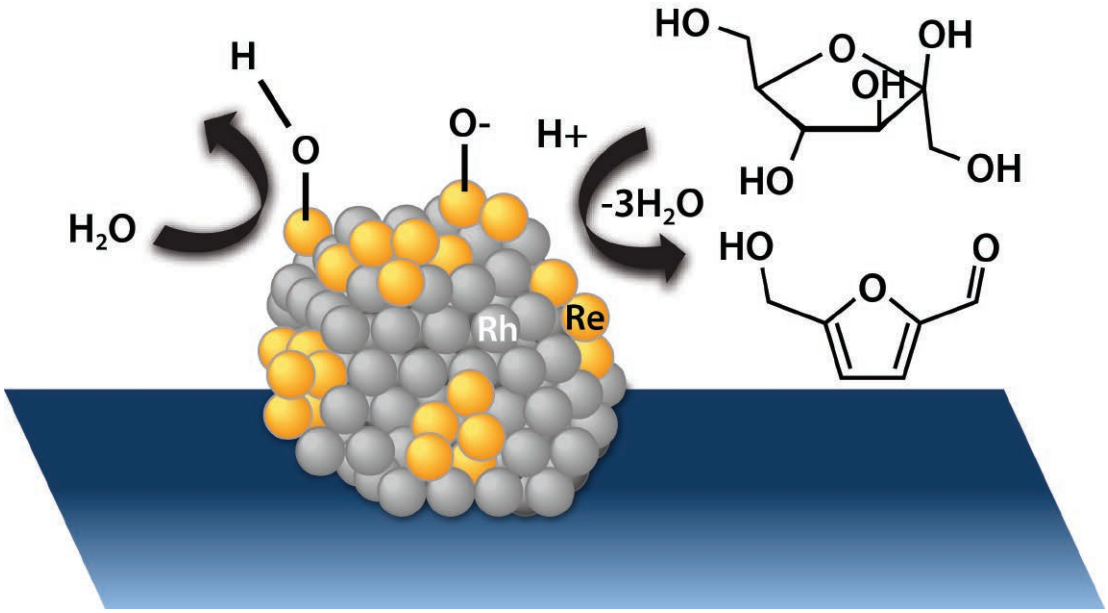

Fig. 2. An increase in reduction temperature results in a decrease in activity of a RhRe/C catalyst for C-O hydrogenolysis and fructose dehydration. XAS measurements and other data indicate that an increase in pretreatment temperature results in a decrease in surface Re on particles with an Rh core. Re atoms on the surface of Rh particles likely activate water, thereby promoting an acid catalysis mechanism.

having like a solid acid. This mechanism was supported by experiments showing that the reaction failed to work without water.

To further test the acid catalysis hypothesis, the researchers studied a second reaction: the conversion of fructose — another chemical that is derived from plant biomass — to 5-hydroxymethyl furfural, which is a chemical way station for several important end products (Fig. 1). This reaction can only be catalyzed by an acid-catalyzed mechanism. They found that 30% of the fructose was converted by the bimetallic catalyst to the desired product, with 50% selectivity, similar to what is achieved with other solid acid catalysts at those conditions.

In additional experiments, the researchers began to study factors that affect catalytic activity, such as pretreatment temperature. Tests on a series of catalysts revealed that higher pretreatment temperatures resulted in lower catalytic activity. Based on XAS data, the researchers found that higher pretreatment temperatures caused rhenium atoms to migrate into the core of nanoparticles (Fig. 2). This may explain the lower activity, as the acid-based catalytic mechanism requires that the rhenium be on the nanoparticle surface, exposed to water.

In future studies, the researchers will continue to test various factors in an attempt produce better catalysts, bringing the dream of biomass-derived polymers and other materials closer to reality. *— Erika Gebel Berg*

See: Mei Chia[1], Brandon J. O'Neill[1], Ricardo Alamillo[1], Paul J. Dietrich[2], Fabio H. Ribeiro[2], Jeffrey T. Miller[3], James A. Dumesic[1]*, "Bimetallic RhRe/C catalysts for the production of biomass-derived chemicals," J. Catal. **308** (2013) 226. DOI:10.1016/j.jcat.2013.08.008
Author affiliations: [1]University of Wisconsin–Madison, [2]Purdue University, [3]Argonne National Laboratory
Correspondence:
* dumesic@engr.wisc.edu

X-ray adsorption spectroscopy studies were supported by the Institute for Atom-efficient Chemical Transformations (IACT), an Energy Frontier Research Center funded by the U.S. Department of Energy Office of Science, Basic Energy Sciences. The research was also supported by the National Science Foundation under Award No. EEC-0813570. R.A. acknowledges support from the National Science Foundation Graduate Research Fellowship Program under Grant No. -DGE-0718123. MR-CAT operations are supported by the Department of Energy and the MRCAT member institutions. Use of the Advanced Photon Source at Argonne National Laboratory was supported by the U.S. Department of Energy Office of Science under Contract No. DE-AC02-06CH11357.

10-BM-A,B • MR-CAT • Materials science, chemistry, environmental science, physics • X-ray absorption fine structure, x-ray lithography, tomography • 3-200 keV, 4-32 keV • On-site • Accepting general users •

10-ID-B • MR-CAT • Materials science, environmental science, chemistry • X-ray absorption fine structure, time-resolved x-ray absorption fine structure, micro x-ray absorption fine structure, microfluorescence (hard x-ray) • 4.3-27 keV, 4.3-32 keV, 15-90 keV • On-site • Accepting general users •

Catalysts Caught in the Act Undergo Radical Rearrangements During Reactions

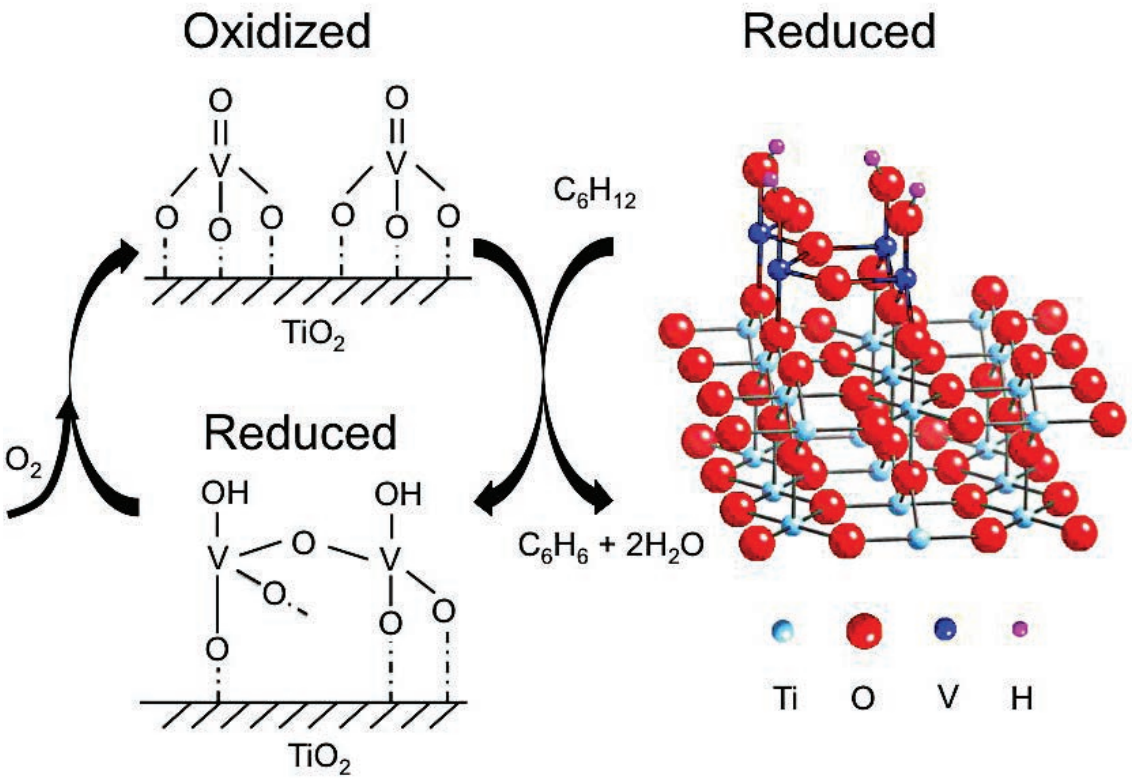

Fig. 1. Left: Oxidized vanadium V^{5+} supported on a single titanium oxide crystal (top) catalyzes the dehydration reaction of cyclohexane (C6H12) to become reduced vanadium V^{4+} (bottom). The addition of oxygen returns vanadium to its oxidized form. Right: An atomic-scale model of reduced vanadium4+ based on data from XSW experiments.

Chemists who develop catalysts are always trying to improve catalytic efficiency or create novel reaction pathways, but they're doing so largely in the dark. The atomic-scale structure and chemical properties of catalysts remain surprisingly mysterious, despite the critical roles that catalysts play in a variety of industrial and environmental applications. Heterogeneous catalysts — which differ in phase from their substrates — are used, for example, to convert toxic nitric oxide from automotive emissions to less harmful gases. Hoping to shed some light on how catalysts behave, and connect these behaviors to catalysts' activity and selectivity, researchers working at the APS teased out structural and chemical information about a single layer of vanadium oxide, a catalyst, supported on the surface of a titanium oxide crystal. The data revealed that vanadium oxide undergoes a dramatic and reversible change in chemical states and structure during a redox reaction cycle, providing unprecedented insight into how vanadium oxide catalyzes reactions. This research will make it possible for scientists to improve catalysts by strategically altering their structures.

Supported vanadium oxide is currently under investigation as a catalyst for the oxidative dehydration of ethanol, propane, and cyclohexane. For example, low-density arrangements of supported vanadium oxide have shown greater catalytic efficiency than supported vanadium oxide at higher densities or bulk vanadium oxide. In this study, researchers from Northwestern University, the Massachusetts Institute of Technology, and Argonne examined the oxidative dehydration of cyclohexane by monolayer vanadium oxide on a titanium oxide scaffold as a model system.

To make the sample, the researchers atomically engineered a layer of vanadium oxide on the surface of a single rutile (10 mm x 10 mm x 1 mm) titanium oxide crystal. The researchers created vanadium atomic density maps relative to the rutile substrate lattice using x-ray standing wave (XSW) *in situ* analysis at the DND-CAT 5-ID-B,C,D beamline at the APS.

The key to XSW is that it uses the x-rays generated by the APS beamline in two ways: single-crystal x-ray diffraction and x-ray fluorescence. The x-ray diffraction provides the basic structural outline, while the fluorescence distinguishes between vanadium and titanium.

To run the *in situ* XSW experiments, the researchers placed the sample in the path of the x-ray beam inside a beryllium dome. The dome, which is "transparent" to x-rays, is used to create the environment for vanadium to catalyze chemical reactions, supplying the proper temperature, pressure and reaction gases. To generate a three-dimensional image, the researchers rotated the crystal with a 5-circle diffractometer. They gathered structural data on the catalyst in three states: oxidized by oxygen, reduced by cyclohexane, and reoxidized by oxygen. This strategy can effectively track the behaviors of catalysts during a chemical reaction.

In addition to structural information, the researchers wanted to assess the chemical oxidation state of the catalyst under the same conditions as studied by XSW. For this, the researchers used a low-energy x-ray source provided by the Keck-II facility at Northwestern University.

X-ray photoelectron spectroscopy (XPS) detected the oxidation state of vanadium and any bound oxygen atoms under oxidized and reduced conditions. By combining the XPS and XSW data, the researchers developed an atomic-scale model for the reduced catalyst in a 4+ oxidation state (Fig. 1, right). Its structure strongly resembles that of the titanium oxide support, which was expected, the researchers say, because titanium also has a 4+ oxidation state.

Things got more interesting when it came to the analysis of the oxidized state. This structure was uncorrelated to that of the underlying titanium oxide, indicating that the catalyst significantly changes upon oxidation. The disharmony between the oxidized vanadium oxide and titanium oxide support made it impossible for the researchers to develop a structural model for the oxidized state.

However, using the information from XPS data as well as from infrared spectroscopy, they figured out that oxidized vanadium is in a 5+ oxidation state, with three single bonds to oxygen and one double bond (Fig. 1, top left). The oxidized and reoxidized states looked the same, suggesting that the reaction is reversible. In future research, the researchers plan to nail down the oxidized structure by combining structural and oxidation state information. *— Erika Gebel Berg*

See: Zhenxing Feng[1,2], Junling Lu[3], Hao Feng[3], Peter C. Stair[1], Jeffrey W. Elam[3], and Michael J. Bedzyk[1]*, "Catalysts Transform While Molecules React: An Atomic-Scale View," J. Phys. Chem. Lett. **4**, 285 (2013). DOI:10.1021/jz301859k

Author affiliations: [1]Northwestern University, [2]Massachusetts Institute of Technology, [3]Argonne National Laboratory

Correspondence:
*bedzyk@northwestern.edu

This work was supported by the Institute for Catalysis in Energy Processes (U.S. Department of Energy Office of Science-Basic Energy Sciences [DOE SC-BES], Chemical Sciences Grant DE-FG02-03ER15457). J.L. and J.W.E. were supported as part of the DOE SC-BES, Chemical Sciences under the Hydrogen Fuel Initiative program. DND-CAT is supported by E.I. DuPont de Nemours & Co., The Dow Chemical Company and Northwestern University. Use of the Advanced Photon Source at Argonne National Laboratory was supported by the U.S. Department of Energy Office of Science under Contract No. DE-AC02-06CH11357.

5-ID-B,C,D • DND-CAT • Materials science, polymer science • Powder diffraction, x-ray standing waves, x-ray optics development/techniques, small-angle x-ray scattering, surface diffraction, x-ray reflectivity, wide-angle x-ray scattering • 6-17.5 keV • On-site • Accepting general users •

Fueling Surface Studies for Catalytic Science

Coating platinum (Pt) nanoparticles with a sub-monolayer of ruthenium converts the normally bulk-sensitive x-ray absorption spectroscopy into a surface-sensitive technique. This new approach can then reveal critical details about the mechanisms of catalytic reactions at the surface, simulating Pt/ruthenium (Ru) catalysts, and allowing researchers to see how the catalyst accelerates the electrochemical oxidation of methanol in a fuel cell with a view to boosting catalyst efficiency. This important process could underpin future electricity generation for portable devices and vehicles.

Fuel cells were first invented in the nineteenth century and use the reaction of an energy-rich organic molecule such as methanol or ethanol, flowing over a catalytic metal reacting with oxygen to produce an electric current as well as releasing water and carbon dioxide as byproducts with no toxic pollutants. Essentially, a fuel cell is a battery with a chemical fuel supply. As such, these devices have become the focus of twenty-first-century clean power technology. They might one day displace the internal combustion engine or allow us to recharge mobile devices, such as cell phones and computer tablets, with a canister of liquid fuel as simply and easily as one might refill a cigarette lighter without the need to connect to an electrical power outlet.

Direct methanol fuel cells (DMFCs) are among the most promising class of these devices. However, their wider adoption for commercial applications has been stymied somewhat by the Pt catalysts used in experimental designs. Platinum is an expensive noble metal. Moreover, the two-step reaction that converts methanol to water and carbon dioxide leads to poisoning of the catalyst as carbon monoxide and methanol intermediates are formed that fill up the reactive sites on the catalyst surface. It was known that addition of a less expensive metal might impede this poisoning process. The most effective additive is Ru metal, which almost wholly precludes the poisoning reaction and so maintains the catalytic activity of the Pt almost indefinitely.

In order to develop the optimal approach to incorporating Ru as an additive to work with the Pt catalyst requires new insights into how different arrangements of the two metals might affect the catalytic process and electricity generation in a DMFC. Researchers from the Illinois Institute of Technology and at Argonne have investigated platinum nanoparticles coated with submonolayers of Ru as a model catalyst for x-ray absorption spectroscopy (XAS) studies of the methanol oxidation mechanisms. They collected *in situ* XAS data at Ru-K edge on the MR-CAT beamline 10-ID- B at the APS. Because of the low concentration of Ru in the sample, they had to use fluorescence mode with a Lytle detector ion chamber in continuous scan mode.

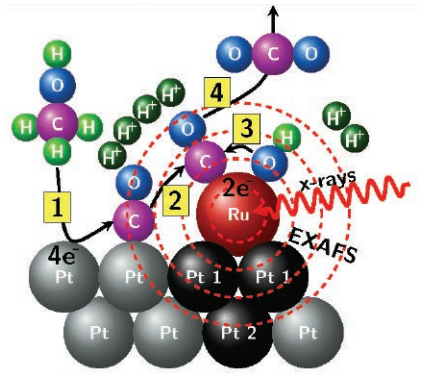

Fig. 1. A novel experimental setup allows *in situ* Ru *K*-edge XAS to be carried out using a sparse layer of Ru atoms coating nanoparticles Pt electrocatalyst in order to study the mechanism of methanol oxidation in a fuel cell. Graphic: C. Pelliccione (IIT) et al.

The team's unique way of coating the Pt nanoparticles with Ru lent itself to a clear view using XAS of the methanol electrochemical oxidation reaction. Specifically, the layer of Ru atoms is very thin — approximately a single atom thick and covering a little less than a third of the platinum surface, simulating the surface of bimetallic catalyst. Having Ru only at the surface of the catalyst, the team explains, means that whereas XAS is usually a "bulk" analytical technique for investigating solids by correlating the x-ray absorption fine structure data at the Ru *K*-edge of the spectra, the team was able to exploit it as a surface analytical technique instead. This provided a unique view of the methanol oxidation process. (The team also investigated the morphology and atomic distribution of as-prepared Ru@Pt catalyst using scanning electron microscopy at the Argonne Electron Microscopy Center [EMC]).

The team recorded data at various oxidation potentials, with a solution of methanol and with background electrolyte lacking methanol as a control experimental setup. This revealed significant differences between the behaviors of the Ru-metal ions in those environments. In the methanol system, the Ru exists as metal and Ru(III) ions regardless of potential. In this state, it absorbs and processes the unwanted carbon monoxide and keeps the Pt active. By contrast, in the control experiments, the metallic Ru was all oxidized to a mixture of Ru(III) and (IV) oxides. The results suggest how to optimize the catalysts for optimal use in DMFC (Fig. 1). *— David Bradley*

See: Christopher J. Pelliccione[1], Elena V. Timofeeva[2], John P. Katsoudas[1], and Carlo U. Segre[1]*, "*In Situ* Ru K-Edge X-ray Absorption Spectroscopy Study of Methanol Oxidation Mechanisms on Model Submonolayer Ru on Pt Nanoparticle Electrocatalyst," J. Phys. Chem. C **117**, 18904 (2013). DOI:10.1021/jp404342z
Author affiliations: [1]Illinois Institute of Technology, [2]Argonne National Laboratory
Correspondence: * segre@iit.edu

C.J.P. was supported by a Department of Education GAANN Fellowship, award P200A090137. MR-CAT operations are supported by the Department of Energy and the MR-CAT member institutions. Use of the Argonne National Laboratory Advanced Photon Source and EMC was supported by the U.S. Department of Energy Office of Science under Contract No. DE-AC02-06CH11357.

A Solid Bulks Up under Pressure

Chemists have spent decades searching for stable materials that have a porous internal structure. Such solids exist in nature in the form of clay-like zeolites, which have vast internal surface areas that can soak up small molecules from liquids and gases. But there are a limited number of zeolites available, with a limited range of pore sizes and shapes. Building new porous materials, such as metal-organic framework (MOF) materials, could allow chemists to design specific pores that can select out particular molecules. Such materials could be used to separate gases, sequester the greenhouse carbon dioxide from combustion exhaust fumes, or act as highly selective catalysts and sensors. Scientists from Argonne have investigated the non-porous material zinc cyanide — $Zn(CN)_2$ — which can double in size when under pressure as it forms a new "porous" crystalline structure resembling a sponge. This new form, studied by researchers utilizing the APS, can soak up water, methanol, ethanol, and other fluids. It also forms other shape-shifting materials that could lead to the design of new high-density gas storage systems, powerful chemical catalysts, and filters for separating or absorbing greenhouse gases.

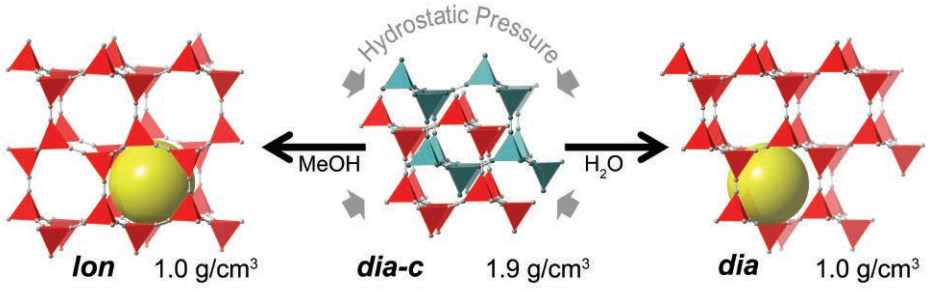

Fig. 1. Applying pressure causes the material to expand as new fluid-filled pores form within. Graphic: Karena W. Chapman (XSD).

$Zn(CN)_2$ is known to contract when heated, something that only water and very few other substances do; most materials expand when heated. The changes occur as bonds between atoms in the material are broken and reformed to make a more compact structure.

If temperature can play an important role in the structure of a material, then so too can applying pressure. Despite being non-porous, zinc cyanide is highly compressible. Moreover, applying high pressure to this material can change its physical properties, making the temperature effect of its contraction on heating even more pronounced.

However, astoundingly, the research team in this study has found that when they apply pressure to this material it undergoes a different internal shape-shifting as bonds break and reform; in this case the material expands rather than contracting, forming a more open, porous material that doubles the volume of the material (see the figure). The team used the powerful analytical technique known as synchrotron powder diffraction to test their samples and elucidate the precise structures formed, in a series of experiments carried out at the XSD beamlines 1-BM-B,C, 11-ID-B, and 17-BM-B of the APS.

The team demonstrated that five new phases can be produced using applied pressure on zinc chloride. Four of those phases have a regular, crystalline structure and one is irregular, or amorphous. The structures were characterized based on the synchrotron data using high-power computational techniques to determine the exact positions of each atom within the structure.

The team points out that the different phases, or polymorphs, are generated depending on what fluid is used to apply the pressure to the original compound. The team used one of three liquids — isopropanol, ethanol, or fluorinert — to put the squeeze on the zinc cyanide and each produces a different internal structure as the molecules of each fluid act as a template for the pores that are formed as the pressure is applied. The researchers note that water, methanol, ethanol, or mixtures of those liquids can cause further shifts to the crystal structures.

The new applied pressure approach to morphing solids between different crystal forms could open not only pores in otherwise non-porous materials, but also provide chemists with the means to generate novel porous solids with pores of different size and shape for specific applications, the researchers suggest.

The approach could allow materials that are not available to the conventional synthetic methods used to build MOFs and so could increase the diversity of materials available. Such increased diversity boosts the chances of finding the optimal material for a given industrial separation or catalytic process. *— David Bradley*

See: Saul H. Lapidus, Gregory J. Halder, Peter J. Chupas, and Karena W. Chapman*, "Exploiting High Pressures to Generate Porosity, Polymorphism, and Lattice Expansion in the Nonporous Molecular Framework $Zn(CN)_2$," J. Am. Chem. Soc. **135**, 7621 (2013). DOI:10.1021/ja4012707

Author affiliation:
Argonne National Laboratory
Correspondence:
*chapmank@aps.anl.gov

Work done at Argonne and at the Advanced Photon Source was supported by the U.S. Department of Energy Office of Science under Contract No. DE-AC02-06CH11357.

1-BM-B,C • XSD • Materials science, physics • Single-crystal diffraction, white Laue single crystal-diffraction, energy dispersive x-ray diffraction • 6-30 keV, 50-120 keV • Accepting general users •

11-ID-B • XSD • Chemistry, environmental science, materials science • Pair distribution function • 58.66 keV, 86.7 keV • On-site • Accepting general users •

17-BM-B • XSD • Chemistry, materials science, powder diffraction • 15-18 keV • On-site • Accepting general users •

A Pinch and a Wrinkle Reveal Behavior of Nanoscopic Layers

Pinch the sides of a thin layer of gold particles just a few billionths of a meter thick and the material will wrinkle up before doubling over and then folding again to form a triple layer. X-ray studies at the APS reveal a short-lived intermediate phase between the initial state and the final triple layer that could provide insights into how chemical surfactants behave in nature and the laboratory, as well as how biological membranes such as those that enclose our body's cells form and behave.

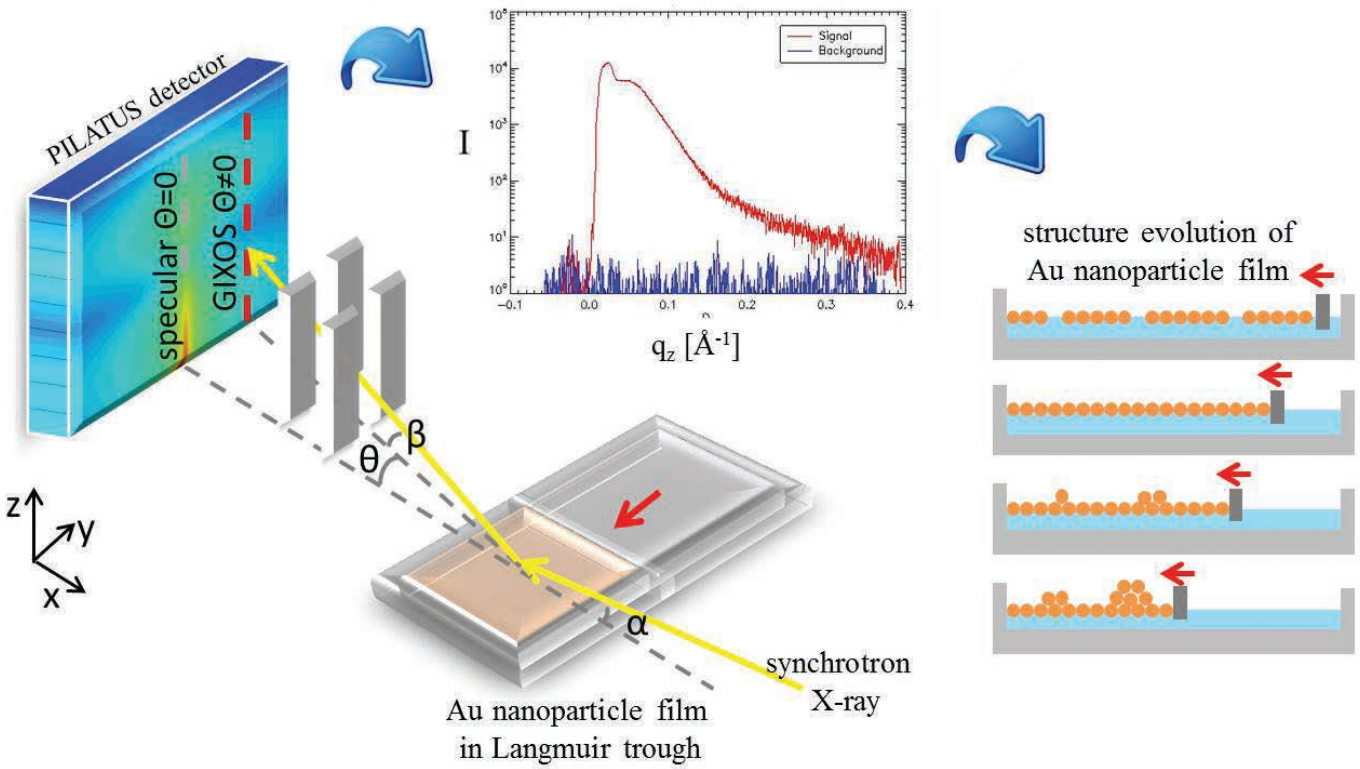

Fig. 1. Lateral pressure applied to a thin film of gold nanoparticles will cause it to wrinkle as revealed by a novel application of GIXOS. Image courtesy of Oleg Shpyrko (UCSB) et al.

Researchers from the University of California, San Diego; The University of Chicago; and Cornell University carried out grazing incidence x-ray off-specular scattering (GIXOS) studies on the ChemMatCARS liquid surface scattering station on beamline 15-ID-C at the APS with monochromatic x-rays (wavelength of 1.24 Å.) to help them investigate what are known as interfacial nanostructures. In such materials a thin layer exists between a liquid and the air above it. Until now, it was not possible to obtain detailed insights into the behavior of such layers under compression, because the consequent wrinkling of the layer and the formation of multiple-layered films occurs too quickly. The GIXOS studies can tease apart the details of the process because the X-ray scattering occurs on a much shorter timescale (Fig. 1).

The team created a monolayer of gold nanoparticles on a liquid surface through a process of self-assembly in which the structure of the particles and their interactions with the molecules in the liquid's surface lead them to form an organized layer. The researchers could then probe this so-called "Langmuir monolayer" using GIXOS with a spatial resolution of nanometers and time resolution of 10s of seconds.. As a result, their data reveals much more than would be visible to conventional x-ray scattering or atomic force microscopy. Indeed, as the team applied a compressive force laterally to the layer with trough barriers, the GIXOS data revealed the initial wrinkling of the layer and the formation of a previously unseen "hash" formation of the nanoparticles. This intermediate structure then crinkled further as the team applied squeezes to the layer more and more until it folded into a double layer and then a triple layer (Fig. 2).

The crinkling mechanism, from initial monolayer to bilayer, is a revelation not previously considered. Given that the gold Langmuir monolayer is acting as a representative model of any nanoscopic layer, the findings could have implications for understanding how multiple-layers cell membranes and other chemical thin films form from simple monolayers in nature. The crinkles that formed are not much bigger than the nanoparticles and so do not represent a high-energy barrier to the formation of the triple layer. Indeed, the crinkles represent the only plausible route in terms of the energy calculations the team has carried out that explains how an intermediate bilayer and then a triple layer can form.

The calculations do suggest that the leap to a quadruple- or even a quintuple-layer from the triple layer is not so energetically favorable and so apparently does not occur. The nanoparticles would have to climb much higher to form the necessarily crinkles that would allow the triple layer to fold still further and so the only possible route would be for the whole layer to fold in concert. As the team has already demonstrated with GIXOS, the crinkling mechanism is the only plausible route to add an extra layer and so this perhaps explains why quadruple and quintuple layers have not been seen in natural or synthetic membranes to date.

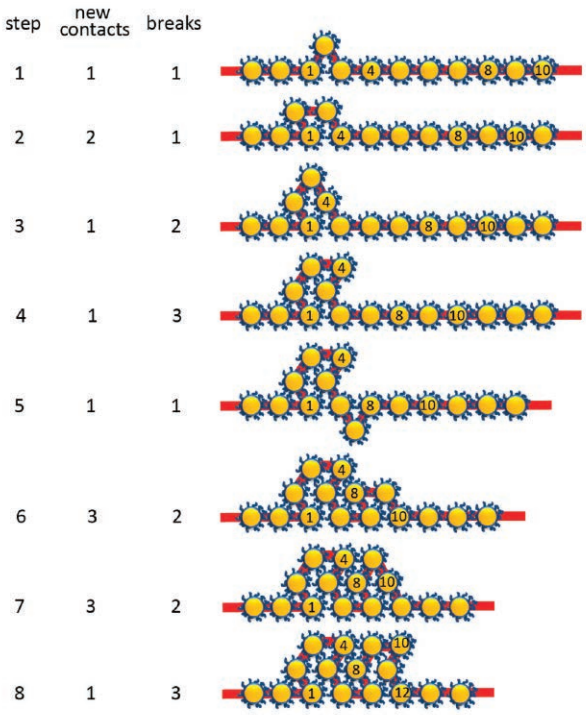

Fig. 2. Steps in a hypothetical crinkle-folding mechanism. Row 1: monolayer viewed in cross section after one buckling event. Horizontal direction is the compression direction; vertical direction is the normal to the liquid surface. Particles 1, 4, 8, 10, and 12 along the monolayer are labeled. Rows 2–8: subsequent steps in the trilayer formation. Colored stripe follows the original sequence of particles in the monolayer. Columns at left indicate the number of new particle–particle contacts formed in the step and total number of contacts that must be broken or weakened to make the step move, including interfacial contacts. Further crinkling after step 8 proceeds as in step 5. From Y. Dai et al., Langmuir **29**, 104050 (2013). © 2013 American Chemical Society.

With the appropriate APS beamline and the newly developed GIXOS technique, the team has demonstrated the wider application of this approach for obtaining snapshots of rapidly evolving systems of nanoparticles.

— David Bradley

See: Yeling Dai[1], Binhua Lin[2]*, Mati Meron[2], Kyungil Kim[2], Brian Leahy[3], Thomas A. Witten[2], and Oleg G. Shpyrko[1]**, "Synchrotron X-ray Studies of Rapidly Evolving Morphology of Self-Assembled Nanoparticle Films under Lateral Compression," Langmuir **29**, 14050 (2013). DOI:10.1021/la403252d

Author affiliations: [1]University of California, San Diego; [2]The University of Chicago; [3]Cornell University

Correspondence:

* b-lin@uchicago.edu,

** oshpyrko@physics.ucsd.edu

This research is supported by the National Science Foundation CAREER Award Grant 0956131. T.W. and B.L. thank for the support from The University of Chicago, Materials Research Science and Engineering Center, NSF-DMR Grant 0820054. ChemMatCARS is principally supported by the National Science Foundation/Department of Energy under Grant CHE0087817. Use of the Advanced Photon Source at Argonne National Laboratory was supported by the U.S. Department of Energy Office of Science under Contract No. DE-AC02-06CH11357.

15-ID-B,C,D • ChemMatCARS • Materials science, chemistry • Single-crystal diffraction, anomalous and resonant scattering (hard x-ray), wide-angle x-ray scattering, microdiffraction, liquid surface diffraction, small-angle x-ray scattering, ultra-small-angle x-ray scattering, high-pressure diamond anvil cell • 6-32 keV, 10-60 keV • On-site • Accepting general users •

THE 2013 THREE-WAY MEETING
APS, ESRF, PETRA III, SPRING-8

Attendees at the 2013 Three-Way Meeting. In the front row, left to right, are Edgar Weckert, Director, Photon Sciences, DESY; APS Director Brian Stephenson; Tetsuya Ishikawa, Director, RIKEN Harima Institute, SPring-8; and Francesco Sette, Director General, ESRF.

The 2013 Three-Way Meeting was held at the APS from July 30 through August 2. This was the 14th meeting in a long history dating back to the early years of the hard x-ray synchrotron (circa 1993). The meeting takes place approximately every 18 months, alternately hosted by the current four large, hard x-ray light sources: the APS; the European Synchrotron Radiation Facility (ESRF, France); the newest member, PETRA III at the Deutsches Elektronen-Synchrotron (DESY, Germany); and SPring-8 (Japan). The next Three-Way Meeting host is SPring-8 in 2015.

The meeting is attended by the facility directors from the four synchrotrons, optics and detector scientists, and user program administrators. The meeting fosters communication and collaboration between the laboratories and provides a forum for discussion of instrument, scientific, and organizational issues common. Fifteen exhibitor companies and more than 150 participants made this year's meeting an opportunity to share insights and information among the organizations.

A reception for meeting attendees was held on the eve of the start of the main meeting sessions. The main meeting opened with a welcome from APS Director Brian Stephenson followed by facility reports from Francesco Sette, Director General, ESRF; Tetsuya Ishikawa, Director, RIKEN Harima Institute, SPring-8; Edgar Weckert, Director, Photon Sciences, DESY; and Stephenson for the APS.

Two days of optics, detector, and user services workshops featured presentations by speakers from the four facilities. The optics workshop (organized by Lahsen Assoufid, XSD) spanned the topics of crystal, thin-film, and nanofocusing optics; metrology; and optics simulation, modeling, and coherence. Detector workshop organizers Antonino Miceli and Robert Bradford (XSD) hosted two sessions focused on current projects and future directions across the four facilities and more in-depth technical talks. There were stimulating discussions, including conversations with the DESY group regarding testing XFEL detectors at the APS Optics and Detector Test Beamline.

The user services workshop (organized by Susan Strasser, XSD) began with overview presentations from the managers of the four user programs, followed by presentations and discussions on publications, databases, proposal and scheduling systems, user portals, governmental and facility issues, user organizations, and outreach.

Plenary sessions included talks on facility upgrades and future plans.

Plans for facility upgrades, a common theme among all of the facilities, were woven through the presentations.

The social event highlight was a meeting banquet held at the Art Institute of Chicago, which included guided tours of various museum galleries.

Visitors were offered a choice of two tours of the APS: an accelerator/sources tour or a beamlines tour that took in the soft x-ray beamline for scattering and photo-emission spectroscopy as well as the new Dynamic Compression Sector.

The full meeting agenda and links to presentations are at http://aps.anl.gov/Users/3Way/.

Contact: Susan White De Pace, swd@aps.anl.gov

Life Science

Looking Inside a Living Frog Embryo

An embryo goes through several radical changes on its way to becoming a complex organism. One of the critical moments in this development is gastrulation, when the embryo forms the primary germ layers out of which different tissues and organs will arise. Common experimental techniques give only a limited view of this important transformation. But now a research team has employed x-ray phase-contrast microtomography to produce three-dimensional (3-D) movies of gastrulation. The researchers exposed frog embryos to high-brightness x-rays from the APS to reveal where cellular motion may be arising and how parts of the embryo grow in size, important new information about embryonic development.

Once an egg is fertilized, the resulting embryo grows into a larger and larger ball of cells. But after about 10 h, the ball begins to contort into a donut shape. Gastrulation is the first step in this "topological" change, with the initial opening in the gastrointestinal tract, called the blastopore, developing on one side of the embryo. At the same time, other cells begin congregating into separate structures that will eventually form the main organ cavity. One of the main questions biologists have is what drives cellular movement during gastrulation.

Previous work has studied gastrulation using a wide variety of methods, such as fluorescence microscopy and magnetic resonance imaging. However, none of these techniques have been able to provide high-resolution images of the interior of an opaque, still-living embryo. X-ray phase-contrast microtomography, wherein hard x-rays pass through the embryo and are imprinted with a small phase change that can be used to reconstruct the embryo's internal structures, offers this capability.

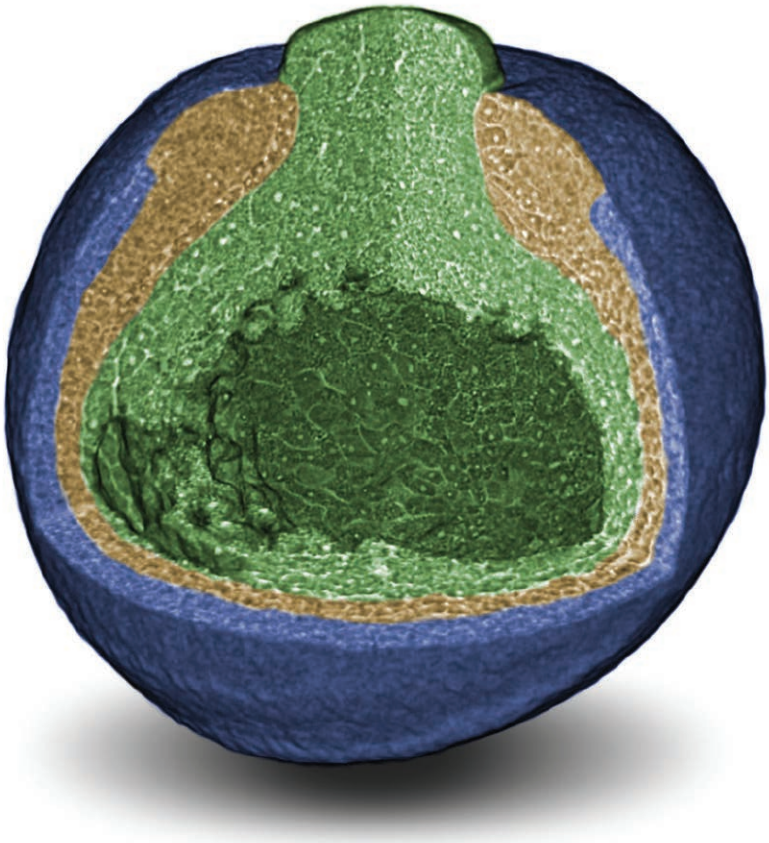

Fig. 1. X-ray phase-contrast tomography provides a detailed look at a frog embryo during gastrulation. The image above shows the embryo's multiple layers as well as particular structures, such as the blastopore opening at the top. The graphic on the next page depicts cell and tissue motion as captured by flow analysis software. Graphic: Alexey Ershov (KIT).

For their subject matter, the scientists from the Karlsruhe Institute of Technology (Germany), the Tomsk Polytechnic University (Russia), Northwestern University, and Argonne National Laboratory chose embryos of the South African clawed frog, *Xenopus laevis*. Exposing the 1-mm-wide embryos to a typical x-ray scan, which relies on absorption, would quickly kill them. But phase-contrast is a milder form of imaging that works well with soft tissues. In phase-contrast, x-rays travel through a given embryo, accumulating a phase change that depends on cell type and density along the light path. To detect the phase change, the typical strategy is to record the light intensity at several different positions behind the sample.

However, the embryo in this case was not going to sit still long enough for an x-ray detector to be moved back and forth. Working at the XSD 2-BM-A,B beamline at the APS, the researchers instead fixed their detector at a propagation distance of 60 cm and used sophisticated computer algorithms to retrieve the phase information. By rotating the embryo and taking 1200 different projections, the team produced a 3-D map of the embryo with sub-cellular spatial resolution of 2 μm (Fig. 1). (Another XSD beamline, 32-ID-B,C, was utilized to check for systematic errors, i.e., to confirm that the data looked the same on a different beamline.)

To view changes during gastrulation, the researchers made a movie with multiple "snapshots" taken one after the other over a 2-h period. Each 3-D image took 20 sec to complete — fast enough to avoid blurring from cell

Xenopus laevis, the African clawed frog, lacks a tongue and a visible ear; the males lack vocal cords. They have the ability to change their appearance to match their background. During the 1940s, female African clawed frogs were injected with the urine of a female human. If the human was pregnant, then the injected frog would start producing eggs. This was the first vertebrate cloned in the laboratory. Source: The Smithsonian National Zoo Park, http://nationalzoo.si.edu/Animals/ReptilesAmphibians/Facts/FactSheets/Africanclawedfrog.cfm

movement that averages about 2-µm per minute — and a time lapse of 10 min was used until the next tomogram was recorded. A computer program tracked the direction that individual cells moved into and at what speed.

The team was able to identify certain regions where some cells individually "crawled" along a fixed surface. In other places, a unified effort was made by cells moving in opposite transverse directions in order to extend the length of a particular tissue along the longitudinal direction (convergent extension).

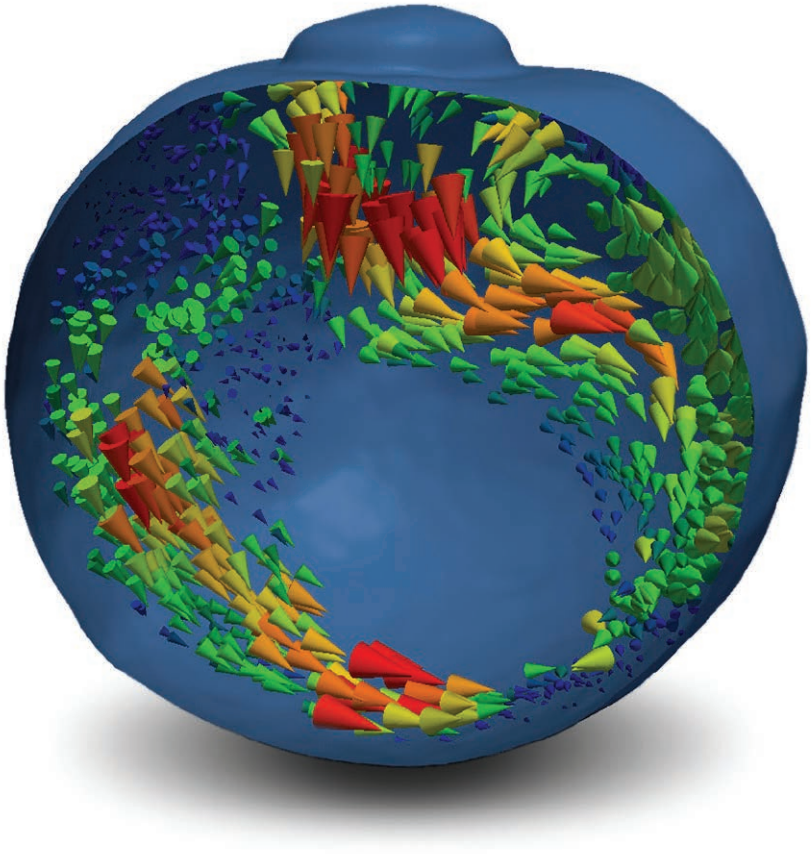

One of the main results of these observations concerns the growth of the archenteron, a small pocket that later develops into the gut cavity. By accurately measuring the volumes inside the embryo, the team showed that the inflation of the archenteron is due to water being pumped in from outside. This contradicts recent work that assumed the archenteron grew by stealing material from other parts of the embryo.

The researchers also discovered a cusp, or bump, that develops on one of the linings inside the embryo when different layers collide with each other. To determine what affect this cusp might have, future studies with x-ray phase-contrast microtomography will look at different mutant frog embryos to see if they behave in an alike fashion.

— Michael Schirber

See: Julian Moosmann[1], Alexey Ershov[1,2], Venera Altapova[1], Tilo Baumbach[1], Maneeshi S. Prasad[4], Carole LaBonne[3], Xianghui Xiao[4], Jubin Kashef[1]**, and Ralf Hofmann[1]*, "X-ray phase-contrast *in vivo* microtomography probes new aspects of Xenopus gastrulation," Nature **497**, 374, (16 May 2013). DOI: 10.1038/nature12116

Author affiliations: [1]Karlsruhe Institute of Technology, [2]National Research Tomsk Polytechnic University, [3]Northwestern University, [4]Argonne National Laboratory

Correspondence: *ralf.hofmann2@kit.edu, **jubin.kashef@kit.edu

J.K.'s Young Investigator Group received financial support from the "Concept for the Future" program of Karlsruhe Institute of Technology within the framework of the German Excellence Initiative. This research was partially funded by the German Federal Ministry of Education and Research under grant numbers 05K12CK2 and 05K12VH1. Use of the Advanced Photon Source at Argonne National Laboratory was supported by the U.S. Department of Energy Office of Science under Contract No. DE-AC02-06CH11357.

2-BM-A,B • XSD • Physics, life sciences, geoscience, materials science • Tomography, phase contrast imaging • 10-170 keV, 11-35 keV • On-site • Accepting general users

32-ID-B,C • XSD • Materials science, life sciences, geoscience • Phase contrast imaging, radiography, transmission x-ray microscopy, tomography • 7-40 keV • On-site • Accepting general users •

Fishing for Viral RNA

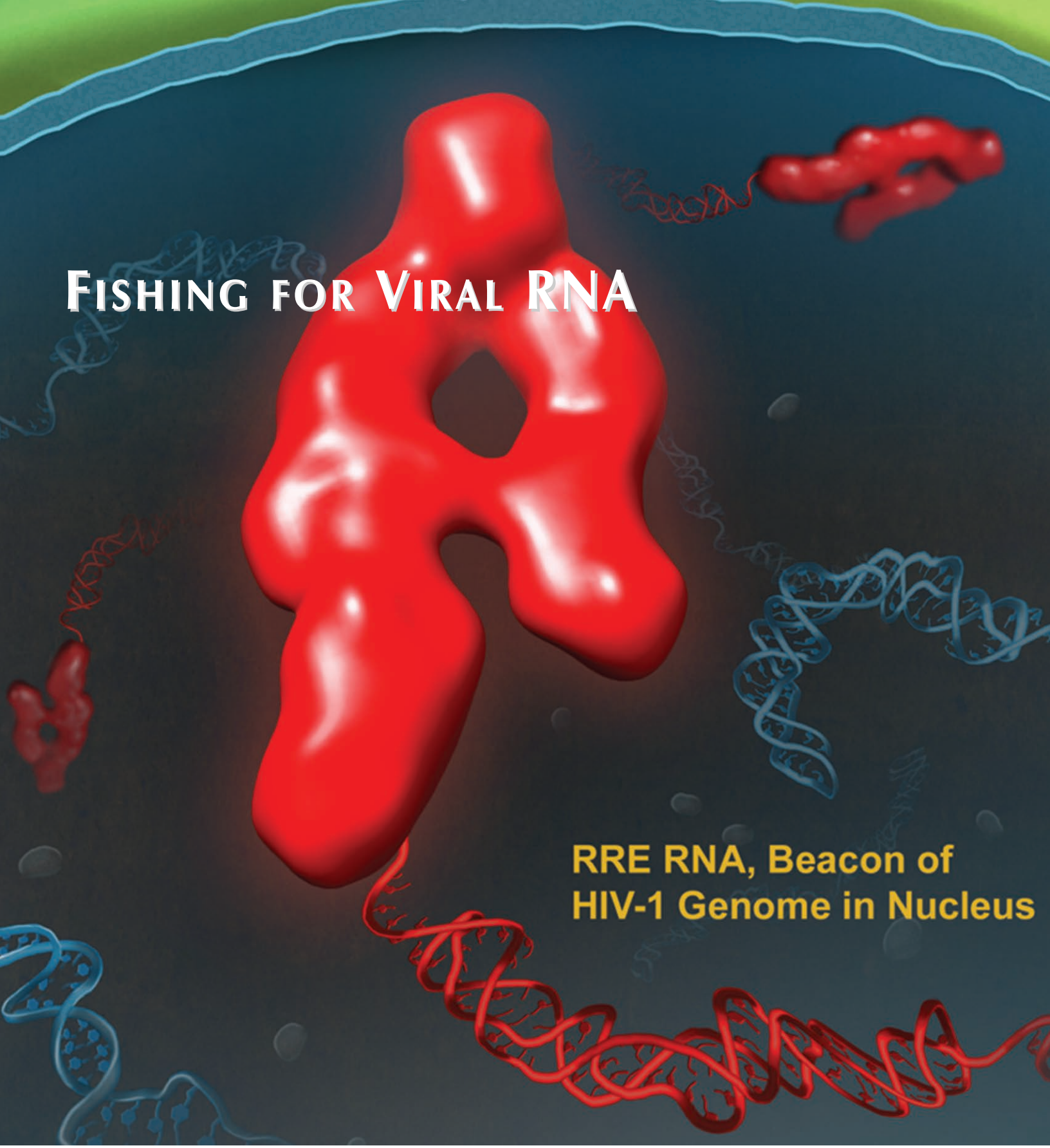

Fig. 1. Elucidation of the structure of the Rev Response Element in the HIV-1 RNA genome reveals how HIV-1 uses the "A-like" structure as a molecular beacon for fishing its RNA out of the RNA-rich cell nucleus and provides a new potential target for AIDS treatment.

12-ID-B • XSD • Chemistry, materials science, life sciences, geoscience, polymer science • Small-angle x-ray scattering, grazing incidence small-angle scattering, wide-angle x-ray scattering • 7.9-14 keV • On-site • Accepting general users •

12-ID-C,D • XSD • Chemistry, physics, materials science • Small-angle x-ray scattering, grazing incidence small-angle scattering, wide-angle x-ray scattering, surface diffraction • 4.5-40 keV • On-site • Accepting general users •

Retroviruses go to a lot of trouble to replicate themselves in our cells and further their infectious cycle. The human immunodeficiency virus-1 (HIV-1), which causes acquired immunodeficiency syndrome (AIDS), is a good example. HIV-1 is an RNA virus that must synthesize DNA from its RNA genome, transport its DNA into the nucleus, transcribe it back to RNA, transport the new RNA out of the nucleus again, and then make proteins from the RNA that will be assembled with new viral RNA genomes and released from the cell as new infectious particles. While the molecular details of many of these steps are known, one mystery that remains is how HIV-1 recognizes and fishes out its own RNA from among all the other RNAs in the nucleus, an essential step in viral replication. Now, the structural basis for this recognition has been defined by researchers carrying out a small-angle x-ray scattering (SAXS) study at the APS. Their work may also provide information that will help in the design of a completely new class of drugs that target HIV-1 genomic RNA for treatment of patients with AIDS.

In normal cells, uninfected with retroviruses, messenger RNAs are transcribed from DNA and then processed before being transported out of the nucleus to be translated into protein. The problem for HIV-1 is that it must get some of its RNA genomes out of the nucleus without being processed so they can be packaged into new viral particles and it must recognize its own RNA genome from among the more abundant host RNAs in the nucleus. It does this using a protein called Rev that recognizes a Rev response element (RRE) in the viral RNA.

Rev works in pairs, as a dimer, to bind the RRE, then recruits more Rev molecules and host proteins that are responsible for getting RNA out of the nucleus. The binding sites for Rev on the RRE have been identified but are curiously vague. The site on the RNA is not sequence-specific and is defined by purine-rich grooves that could easily be found in many other RNA molecules. Attempts to understand this in more depth through solution of the three-dimensional structure of the RRE using nuclear magnetic resonance imaging or x-ray crystallography have been unsuccessful for the past two decades. So to learn more about these interactions, the researchers from the National Cancer Institute, National Institutes of Health, and Argonne turned to SAXS analysis to get structural information and then confirmed their findings with biochemical and functional analyses to figure out how this very specific RNA fishing trick is done.

The three-dimensional structure of the RRE determined from the SAXS data obtained at the XSD 12-ID-B and -C beamlines at the APS showed that the RNA forms an extended "A" with one leg shorter than the other (Fig. 1). The legs are about 50 to 60 Å apart and position the known binding sites for Rev on either arm of the A. The higher affinity binding site is on the lower part of the short arm and the lower affinity site is on the lower part of the longer arm, placing them about 55 Å from each other. This finding is consistent with previous studies that have shown that when two Rev molecules form a dimer, their interaction domains are oriented 55 Å apart.

Next, the team studied different mutants of the RRE to identify important structural elements for Rev binding and nuclear transport function. They made two truncated mutants that contained either one arm or the other of the A. These mutants had either the high- or low-affinity binding site for Rev, but not both.

The team also made three insertion mutants that increased the distance between the arms of the A by adding to the crossbar. Biochemical assays of Rev binding showed that neither the insertion nor the truncation mutants could form the higher order complexes with multiple Rev proteins required for proper functioning. Nuclear transport assays confirmed these results. The truncation mutants were completely incapable of performing nuclear transport and the insertion mutants had greatly reduced activity.

Taken together, these results provide an explanation for how HIV-1 specifically identifies the HIV-1 RNA genome using RRE as a molecular beacon. As nuclear transport is essential for HIV-1 replication, this makes it a potential target for antiviral therapy.

These new results open the door for design of antiviral strategies blocking this step in the viral life cycle by targeting the viral RNA. Targeting the viral RNA has not been possible because the viral RNA structure was unknown until now.

The Wang and Rein laboratories at the National Cancer Institute, National Institutes of Health, are now beginning to test some of these strategies. One of the possible outcomes of targeting the viral RNA is the development of a new class of agents that destroy the viral RNA genome. Another is development of ultra-sensitive probes for viral detection and diagnosis. *— Sandy Field*

See: Xianyang Fang[1], Jinbu Wang[1], Ina P. O'Carroll[1], Michelle Mitchell[1], Xiaobing Zuo[1‡], Yi Wang[1], Ping Yu[1,2], Yu Liu[1], Jason W. Rausch[1], Marzena A. Dyba[2], Jørgen Kjems[3], Charles D. Schwieters[1], Soenke Seifert[4], Randall E. Winans[4], Norman R. Watts[1], Stephen J. Stahl[1], Paul T. Wingfield[1], R. Andrew Byrd[1], Stuart F.J. Le Grice[1], Alan Rein[1]*, and Yun-Xing Wang[1]**, "An Unusual Topological Structure of the HIV-1 Rev Response Element," Cell **155**, 594 (October 24, 2013). DOI:10.1016/j.cell.2013.10.008

Author affiliations: [1]National Institutes of Health, [2]SAIC-Frederick, [3]University of Aarhus, [4]Argonne National Laboratory. ‡Present address: Argonne National Laboratory

Correspondence: *reina@mail.nih.gov, **wangyunx@mail.nih.gov

This work was supported in part by the Intramural Research Program of the National Institutes of Health, National Cancer Institute Center for Cancer Research; National Institute of Arthritis, Musculoskeletal and Skin Diseases; Center for Information Technology; and SAIC-Frederick under contract HHSN26120080001E. Use of the Advanced Photon Source at Argonne National Laboratory was supported by the U.S. Department of Energy Office of Science under Contract No. DE-AC02-06CH11357.

Cool Muscles:
Storing Elastic Energy for Flight

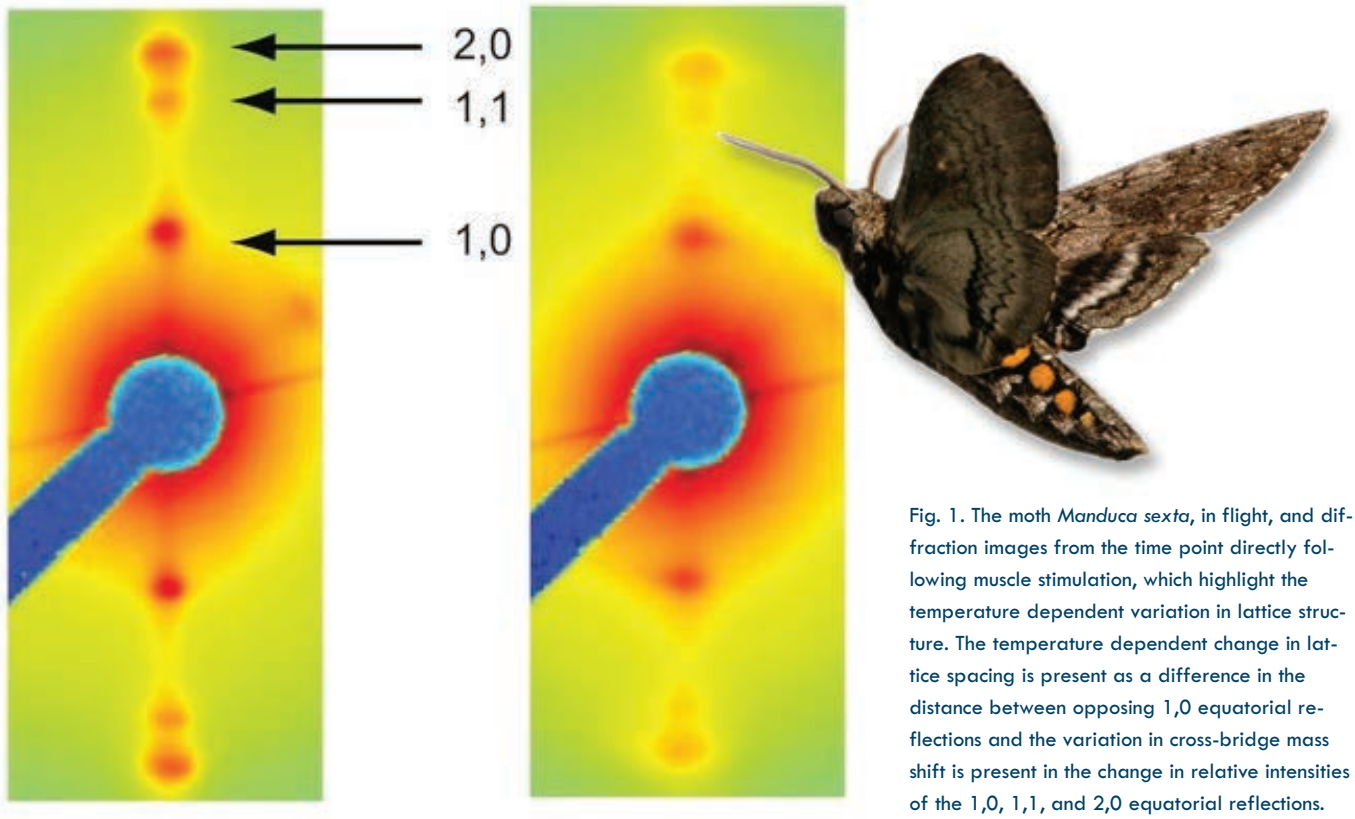

Fig. 1. The moth *Manduca sexta*, in flight, and diffraction images from the time point directly following muscle stimulation, which highlight the temperature dependent variation in lattice structure. The temperature dependent change in lattice spacing is present as a difference in the distance between opposing 1,0 equatorial reflections and the variation in cross-bridge mass shift is present in the change in relative intensities of the 1,0, 1,1, and 2,0 equatorial reflections. Diffraction patterns from N.T. George et al., Science **340**(6137), 1217 (7 June 2013).

Movie S1 @
http://www.sciencemag.org/content/suppl/2013/04/24/science.1229573.DC1/1229573s1.mov
View an animation consisting of 5-frame x-ray diffraction movies (on the right) paired with their respective mechanical measures of force and length (creating a work-loop, on the left), one from the 25° C condition and one from the 35° C condition. X-ray diffraction images from concurrent points in the contraction cycle highlight the temperature dependent variation in muscle lattice structure.

Flying has always fascinated humans, probably because we are so relentlessly Earthbound. One of the things that fascinates researchers who study flight is the question of how animals that do it can generate the energy required. Flying is an intensely power-hungry activity that is less than 10% efficient. Some studies have suggested that physical properties of the molecules involved in insect flight might contribute small amounts of energy to the flight "power grid" through potential energy savings in the form of elastic strain energy. Insight into this question has been provided by research completed at the Bio-CAT beamline 18-ID at the APS. These results provide important information about how flying species meet the energy needs of their powerful adaptation, new knowledge that may have implications for locomotion in general.

The study, by researchers from the University of Washington, the Illinois Institute of Technology, and Harvard University combined time-resolved small-angle x-ray diffraction with measurements of mechanical energy-exchange in the wing muscle of the moth *Manduca sexta* to create high-speed video of muscle motion at the molecular level. Their results show that temperature differences between the dorsal (top) and ventral (bottom) sides of the wing create an opportunity for elastic strain energy to be stored in the cooler regions of the muscle and then released during the transitions between contraction and relaxation to assist with the inertial power costs associated with accelerating and decelerating the wings.

The breakthrough in this work was the development of an apparatus that allowed the team to make high-speed x-ray diffraction measurements at the same time as they measured wing-muscle motion mechanics.

To do this, the researchers first fixed the body and flight muscle of the moth onto a "work-loop" apparatus that allowed them to stimulate muscle contractions in a controlled manner that simulated flight while measuring the forces of those contractions.

Next, the work-loop apparatus was aligned to the 18-ID x-ray beam and a custom shutter was installed to allow for high-speed measurements. The team recorded 5 diffraction images per wing-beat cycle, 1 every 8 msec, for 100 cycles at 25° C and at 35° C — temperatures that cover the range observed for *M. sexta* wing muscle.

The force generated during muscle contraction is known to result from the ratcheting of cross-bridge proteins along other muscle filament proteins. As the cross-bridge proteins bind, move, and release the filament, they generate force. As with all molecular interactions, the cross-bridges move faster at higher temperatures. These researchers had already shown that the temperature of the muscle on the dorsal and ventral sides of the moth wing can differ by as much as 6.9° C during flight.

By taking their x-ray diffraction images at 25° C and 35° C they were able to see what was going on at each temperature at the molecular level.

The x-ray diffraction data showed differences in the spacing of the molecules involved in muscle contraction depending on the temperature (Fig. 1). This indicated that the cross-bridges cycled faster at the warmer temperature and slower at the cooler temperature.

These results support a model in which the cross-bridges that drive the muscles on the warmer, underside of the wing cycle quickly during flight, while cross-bridges on the cooler, top side of the wing remain bound to filaments longer, building up strain until it is released as elastic energy as the muscle advances into its next phase of shortening or lengthening.

The combination of advanced technologies at the APS and the x-ray expertise of Tom Irving, Director of Bio-CAT and a collaborator on this project, made possible a new view of how temperature, strain, and molecular motors conspire to produce a range of functions in a single muscle: from an actuator to a spring, and provides important information about how flying species meet the energy needs of their powerful adaptation and may have implications for locomotion in general.

— Sandy Field

See: N.T. George[1], T.C. Irving[2], C.D. Williams[1,3], and T.L. Daniel[1]*, "The Cross-Bridge Spring: Can Cool Muscles Store Elastic Energy?," Science **340**(6137), 1217 (7 June 2013). DOI:10.1126/science.1229573
Author affiliations: [1]University of Washington, [2]Illinois Institute of Technology, [3]Harvard University
Correspondence: *danielt@uw.edu

This research was supported by the National Science Foundation (NSF) Graduate Research Fellowship under Grant No. DGE-0718124 to N.T.G., an NSF Grant (IOS-1022471) to T.L.D and T.C.I., NSF Grant (EEC 1028725) to T.L.D., and the University of Washington Komen Endowed Chair to T.L.D. Bio-CAT is supported by Grant 5 P41 GM103622 from the National Institute of General Medical Sciences of the National Institutes of Health. Use of the Advanced Photon Source at Argonne National Laboratory was supported by the U.S. Department of Energy Office of Science under Contract No. DE-AC02-06CH11357.

18-ID-D • Bio-CAT • Life sciences • Fiber diffraction, microdiffraction, small-angle x-ray scattering, time-resolved x-ray scattering, micro x-ray absorption fine structure • 3.5-35 keV • On-site • Accepting general users •

Fleshing Out Skeletal Growth with Strontium

As sea urchin embryos grow, they transform amorphous calcium carbonate (ACC) into skeletons of orderly crystalline calcite. Getting a close-up look at that biological process has been difficult, because imaging techniques that can resolve matter on the scale of atoms and molecules have trouble characterizing disordered materials such as amorphous calcium carbonate. Capturing a moment inside a living organism is more difficult still. Last year, researchers devised a clever way to probe the shift from disorder to order. They pulsed artificial sea water (ASW) containing strontium into the sea urchin embryos' environments for a short time, and then withdrew it. The sea urchins incorporated the occasional strontium atom into their skeletons in lieu of calcium. The researchers then used two different beamlines at the APS to probe the atomic structure around the strontium atoms, getting unique insights into the evolution of order in the skeleton over time. The results have the potential to illuminate the biomineralization processes of not just sea urchins, but all creatures that build skeletons with calcium.

Transparent, small, and rapidly developing, the sea urchin embryo is beloved of developmental biologists. It is a model organism for studying how anatomy emerges from information encoded in genes. Its transparency makes it easy to see the skeleton at any given moment of development. But how the sea urchin transforms amorphous calcium carbonate into a single crystalline structure of intricate shape has been mysterious.

Researchers from Northwestern University wanted a marker that would show them how the skeletal structure evolved over time. Strontium, which sits just below calcium in the same column of the periodic table, seemed like the perfect choice. It is heavier than calcium, but its electronic structure is very similar and the occasional strontium atom can easily substitute for calcium in calcium carbonate. It also interacts more efficiently with x-rays than does calcium.

The researchers from Northwestern and Argonne pulsed sea water enriched with strontium into the sea urchin embryo's culture medium for two hours, and then withdrew it. They then flash-froze the embryos and probed the skeletons with x-rays from the APS.

Every element has a minimum "edge" energy at which an incoming x-ray is absorbed, kicking out an electron in the process. Strontium interacts with x-rays at higher energies than does calcium, and more efficiently, resulting in a better signal-to-noise ratio. The researchers used a focused x-ray beam 1-μm wide at XSD beamline 2-ID-D to perform a micro x-ray absorption near edge structure (micro-XANES) scan. The tightly focused beam recorded strontium *K*-edge spectra from select areas of the sea urchin skeletons (Fig. 1). These spectra, which show how efficiently x-rays of a particular energy are absorbed, are affected by the atoms close to the strontium atoms, hinting at the mineral structure of the skeleton in the immediate vicinity. Normally, samples to be examined by micro-XANES are dry, but removing the water from the sea urchin embryo could have ruined the sample. Instead, nitrogen cryo-jets were utilized to keep the samples frozen.

The researchers also performed bulk x-ray absorption spectroscopy on frozen whole sea urchin embryos at XSD beamline 20-BM-B. The data gathered at this beamline allowed the researchers to get more precise information regarding the number and distance of atoms surrounding individual strontium atoms, providing more detailed information on the progression of the ordering process in the skeletons after the strontium was incorporated.

The experiment "allows us to resolve events happening in the skeleton itself in both time and space. We single out a specific volume of the skeleton, and watch it evolve over time," said Derk Joester, a materials scientist at Northwestern University, who led the work. Their results indicate that sea urchins initially use amorphous calcium carbonate for their skeletons, but that short-range calcite crystalline order develops within the first three hours of skeletal construction. Long-range crystalline order slowly follows over the next 24 h. Most creatures on the planet that use minerals to form shells or bones use either calcium carbonate or, as humans do, calcium phosphate. The strontium techniques pioneered at the APS may eventually illuminate how all of them build their bones.

— Kim Krieger

See: Chantel C. Tester[1], Ching-Hsuan Wu[1], Minna R. Krejci[1], Laura Mueller[1], Alex Park[1], Barry Lai[2], Si Chen[2], Chengjun Sun[2], Mahaling Balasubramanian[2], and Derk Joester[1]*, "Time-Resolved Evolution of Short- and Long-Range Order During the Transformation of Amorphous Calcium Carbonate to Calcite in the Sea Urchin Embryo," Adv. Funct. Mater. **23**, 4185 (2013). DOI:10.1002/adfm.201203400
Author affiliations: [1]Northwestern University, [2]Argonne National Laboratory
Correspondence:
* d-joester@northwestern.edu

This work was supported in part by the National Science Foundation (NSF) (DMR-0805313 and DMR-1106208), the International Institute for Nanotechnology, and the MRSEC program of the NSF (DMR-1121262) at the Materials Research Center of Northwestern University. APS Sector 20, which is managed by XSD in partnership with the Canadian Light Source (CLS), is funded by the U.S. Department of Energy Office of Science, and by the Natural Sciences and Engineering Research Council of Canada and the University of Washington via the CLS. Use of the Advanced Photon Source at Argonne National Laboratory was supported by the U.S. Department of Energy Office of Science under Contract No. DE-AC02-06CH11357.

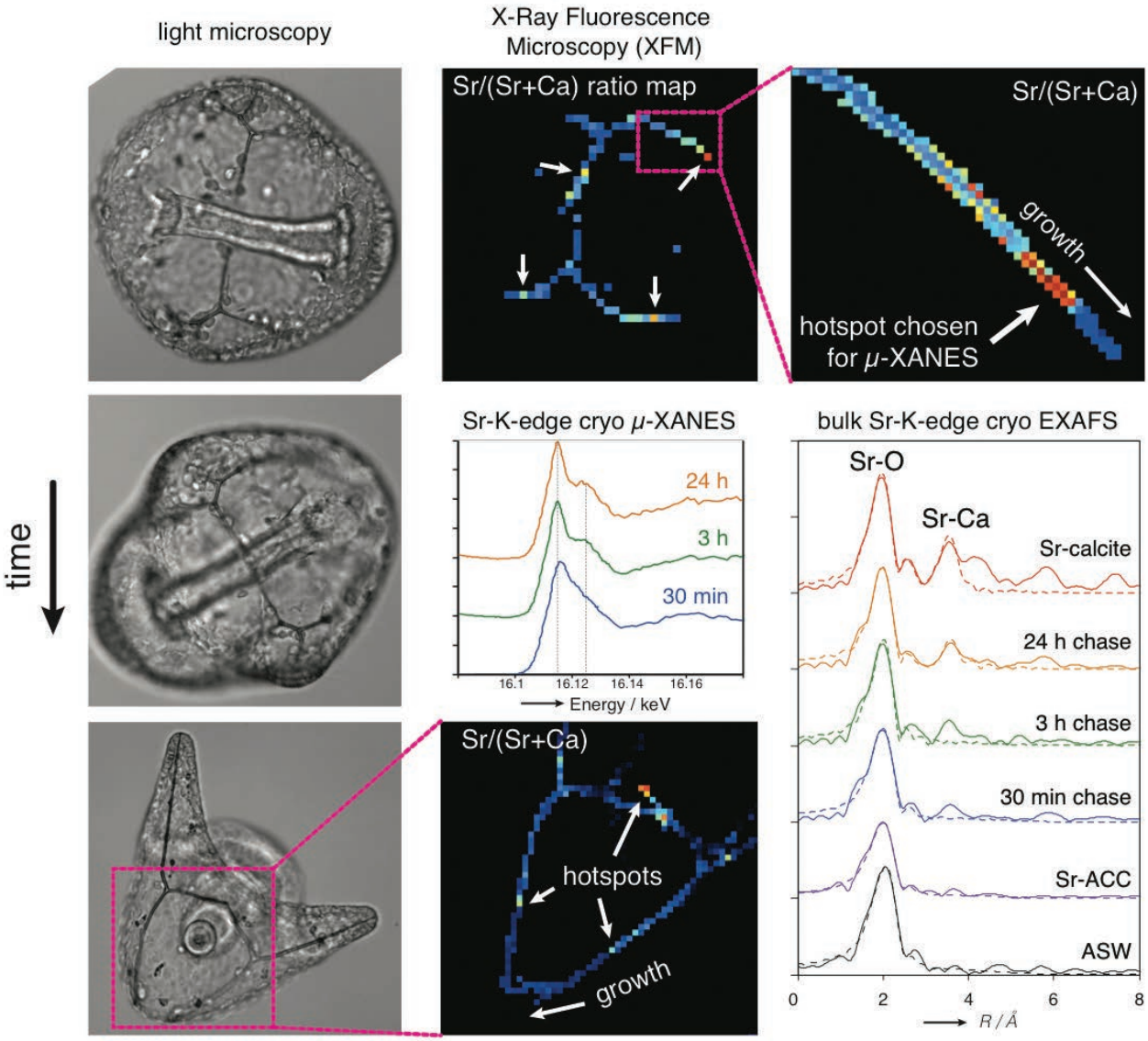

Fig. 1. The left-hand column shows light microscopy images of sea urchin larval spicules (skeletal structures) after 30 min, 3 h, and 24 h from the end of the strontium pulse. X-ray fluorescence microscopy identified strontium-enriched areas (black background images), which were then examined by cryo micro-XANES. The peaks on XANES spectra give clues to the mineral structure surrounding the strontium atoms. Using bulk cryo-extended x-ray absorption fine structure, atomic distances surrounding the strontium atom were determined.

2-ID-D • Life sciences, materials science, environmental science, geoscience • Microfluorescence (hard x-ray), microdiffraction, micro x-ray absorption fine structure • 5-30 keV • On-site • Accepting general users •

20-BM-B • XSD • Materials science, environmental science, chemistry • X-ray absorption fine structure, microfluorescence (hard x-ray), micro x-ray absorption fine structure, diffraction anomalous fine structure • 2.7-25 keV, 2.7-30 keV, 2.7-35 keV • On-site • Accepting general users •

Heavy Metal Trafficking

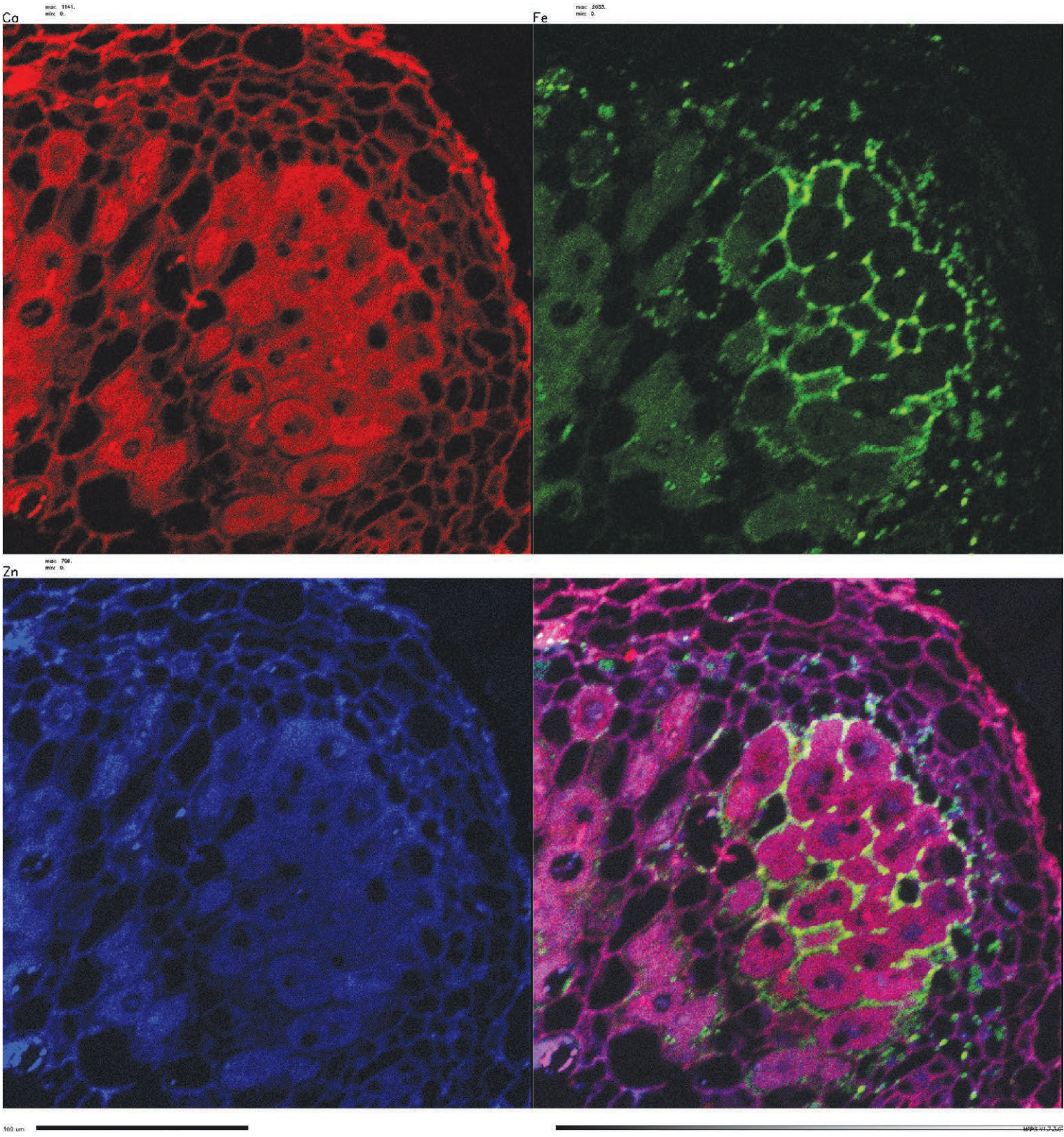

Fig. 1. Element distribution in the *Medicago truncatula* root nodule. Calcium is indicated in red (upper left panel), iron in green (upper right panel), and zinc in blue (lower left panel). The overlay of the distribution of the three elements is shown in the lower right panel.

Legumes — the family of plants that includes beans and lentils — are the primary source of plant protein in our diet, making them a vital part of the global food supply. Key to their success is their endosymbiotic relationship with abacteria known as rhizobia. These microorganisms colonize nodules in the legume's root system and allow the plants to fix atmospheric nitrogen, reducing their need for nitrogen fertilizer. A plentiful supply of iron for the synthesis of a variety of ferroproteins is critical to nitrogen fixation. But the mechanism for maintaining an adequate supply of this scarce metal within the legume's nodules is unknown. Researchers used synchrotron-based x-ray fluorescence (S-XRF) at the APS to capture high-resolution images of the distribution of iron and other elements in the nodule of the legume *Medicago truncatula* throughout the nodule's development. Their work illuminates the source of iron in legumes, laying the groundwork for discovering the mechanism by which the metal is transported, and demonstrates the utility of S-XRF in characterizing the role of metals in a variety of important physiological processes in plants and microbes.

Nitrogen is essential for the synthesis of life's building blocks, including chlorophyll, nucleic acids, and amino acids. But its pure form is relatively inert, requiring that nitrogen be fixed, or combined with other elements, before plants can put it to use. In nature, nitrogen is fixed in the maelstrom of lightning strikes or by microorganisms such as rhizobia. In a form of symbiosis, rhizobia infect the root system of legumes, causing the formation of nodules on the root within which atmospheric nitrogen is converted to ammonia, a form of nitrogen that can be utilized by the plant. Iron is a necessary cofactor of the primary enzymes responsible for nitrogen fixation, yet how the metal is transported within nodules has largely remained a mystery.

The first step in describing iron trafficking is pinning down where the metal comes from. The researchers from the Universidad Politécnica de Madrid, Consejo Superior de Investigaciones Científicas (both Spain) and Argonne, scanned the nodules of *Medicago truncatula* with S-XRF at XSD beamlines 2-ID-E and 8-BM-B at the APS to narrow down three hypothesized sources of iron: pre-existing stores in the primordial root nodule; uptake through the nodule epidermis; and delivery through the root system vasculature. This powerful imaging technique measures submicromolar concentrations of a variety of elements with subcellular resolution. In addition to iron, the team kept track of potassium, calcium, and zinc, and identified hotspots of these elements in expected locations (Fig. 1). For example, calcium was concentrated in cell walls, consistent with its capacity for minimizing oxygen permeability and its role in strengthening cell wall structure; and zinc was concentrated in the nucleus, consistent with the role of zinc-finger domain proteins in DNA transcription.

As for iron, low concentrations were found in the outermost region of the nodule, called zone I, as well as in the nodule's epidermal layers, effectively ruling out the first two hypothetical sources of iron. The S-XRF images revealed dense dotted-line patterns of iron threading through the spaces between the rhizobia-infected cortical cells in the more proximal zone II of the nodule. The ribbons of iron appeared to emanate from vascular bundles—the primary structures of plants' transport systems—suggesting that iron is delivered to the rhizobia-bearing cells via the vasculature.

Iron hot spots were also found in globular shapes near the vascular bundles of zone III, leading the research team to speculate that iron is recycled back to the vasculature via zone III vesicles. In addition, upon nodule senescence, iron appears concentrated in a thread-like pattern near the vasculature of zone IV, the zone closest to the root stem, providing further support for the recycling of iron. Because nodule senescence is coupled to flowering, the recovery of iron from the nodules to the plant's shoots could facilitate flower development.

The researchers' observations helped identify the source of iron in legume root system nodules, laying the groundwork for discovering the mechanism by which the metal is transported. This work also demonstrates the power of S-XRF to track the movement of physiologically important metals and other elements within developing plants and microbes with subcellular resolution. *— Chris Palmer*

See: Benjamín Rodríguez-Haas[1], Lydia Finney[2], Stefan Vogt[2], Pablo González-Melendi[1], Juan Imperiala[3], and Manuel González-Guerrero[1]*, "Iron distribution through the developmental stages of Medicago truncatula nodules," Metallomics **5**(9), 1247 (2013). DOI:10.1039/C3MT00060E

Author affiliations: [1]Universidad Politécnica de Madrid, [2]Argonne National Laboratory, [3]Consejo Superior de Investigaciones Científicas

Corresponding author:

* manuel.gonzalez@upm.es

This work was supported by the Ramón y Cajal Fellowship RYC-2010-06363, and the Marie Curie International Reintegration Grant MENOMED (both to M.G.G.). Use of the Advanced Photon Source at Argonne National Laboratory was supported by the U.S. Department of Energy Office of Science under Contract No. DE-AC02-06CH11357.

2-ID-E • XSD • Life sciences, environmental science, materials science • Microfluorescence (hard x-ray) • 7-10.5 keV, 11-17 keV • On-site • Accepting general users •

8-BM-B • XSD • Chemistry, life sciences, environmental science • Microfluorescence (hard x-ray) • 5.5-20 keV, 9-18 keV • On-site • Accepting general users •

Exploring Natural Product Biosynthesis through Halogenation by an Iron Enzyme

Non-heme iron enzymes perform a variety of reactions, including halogenation, hydroxylation, oxygenation, ring cleavage, and desaturation. Studies of these enzymes are therefore important in understanding phenylalanine metabolism, the production of neurotransmitters, the hypoxic response, the demethylation of DNA, the biosynthesis of secondary metabolites, and other important processes in the human body. Researchers using high-brightness x-rays from the APS have elucidated the key Fe(IV)=O intermediate in the catalytic cycle of a non-heme iron enzyme, the halogenase SyrB2. The research used synchrotron-based nuclear resonance vibrational spectroscopy (NRVS) to probe the vibrational modes involving iron motion and thus define the nature of the Fe(IV)=O active site. Understanding this reaction mechanism is important both for medical advances and for industrial purposes.

In general, α-ketoglutarate-dependent enzymes harness the reducing power of α-ketoglutarate to catalyze oxidative reactions for processes such as natural product biosynthesis, the mammalian hypoxic response, and DNA repair. These enzymes couple the decarboxylation of α-ketoglutarate with the formation of a high-energy Fe(IV)=O intermediate that acts as a hydrogen-abstracting species. SyrB2 is an α-ketoglutarate-dependent halogenase that catalyzes the chlorination of L-threonine in syringomycin E biosynthesis.

The researchers, from Stanford University, Pennsylvania State University, Argonne, SPring-8 (Japan), Kyoto University (Japan), and the SLAC National Accelerator Laboratory extracted samples of SyrB2 from the bacterium *Pseudomonas syringae* pv. *Springae*, trapped the oxygen intermediate in this enzyme. They examined the samples using NRVS, a proven technique for detailed structural characterization of iron active sites, at XSD beamline 3-ID-B,C,D at the APS and beamline BL09XU at the SPring-8 light source. NVRS is a site-selective technique allowing the observation of only normal modes involving iron motion, which makes it ideal for studying iron-dependent enzymes without interference from protein backbone modes (Fig.1).

This methodology, coupled with spectroscopically-calibrated density functional theory (DFT) calculations, was used to determine the specific frontier molecular orbitals responsible for hydrogen-atom abstraction that can selectively lead to halogenation or hydroxylation, depending on the positioning of the substrate. The substrate directs the orientation of the Fe(IV)=O intermediate formed during the catalytic cycle, resulting in the availability of different frontier molecular orbitals which can activate the selective halogenation versus hydroxylation reactivity.

The researchers found the Fe(IV)=O intermediate to possess a five-coordinate trigonal bipyramidal geometry, with an axial Fe–oxo bond. The native-substrate-bound O_2 reaction coordinate reproduces this structure, and gives an intermediate with its Fe–oxo vector perpendicular to the substrate carbon-hydrogen bond. After the initial hydrogen-atom abstraction, the substrate radical is positioned favorably for chlorine rebound, thus defining a selective mechanism in halogenases for halogenation of the native substrate. Alternatively, with a non-native substrate, variation in the O_2 reaction coordinate can result in an intermediate with its Fe–oxo vector parallel to the substrate carbon-hydrogen bond, leading to a substrate radical positioned favorably for hydroxylation.

Halogenated natural products, including chlorinated organic molecules of therapeutic interest such as vancomycin, chlortetracyclin, etc., are frequently produced by microorganisms. Enzymatic incorporation of halogens during complex biosyntheses is of great interest due to its potential application in the pharmaceutical industry for the clean, environmentally friendly development of new protein inhibitors. The halogenase SyrB2 is a prototypical example of such an effective catalyst that controls functionalization of aliphatic substrates with high (but tunable) selectivity through the highly reactive non-heme Fe(IV)=O intermediate.

— Catherine Foster

See: Shaun D. Wong[1], Martin Srnec[1], Megan L. Matthews[2‡], Lei V. Liu[1], Yeonju Kwak[1], Kiyoung Park[1], Caleb B. Bell, III[1], E. Ercan Alp[3], Jiyong Zhao[3], Yoshitaka Yoda[4], Shinji Kitao[5], Makoto Seto[5], Carsten Krebs[2], J. Martin Bollinger, Jr.[2], and Edward I. Solomon[1,6], "Elucidation of the Fe(IV) = O intermediate in the catalytic cycle of the halogenase SyrB2," Nature **499**, 320 (2013). DOI:10.1038/nature12304.

Author affiliations: [1]Stanford University, [2]Pennsylvania State University, [3]Argonne National Laboratory, [4]SPring-8, [5]Kyoto University, [6]SLAC National Accelerator Laboratory. ‡Present address: The Scripps Research Institute

Correspondence:

*edward.solomon@stanford.edu

Funding was provided by the National Institutes of Health (GM-40392 to E.I.S. and GM-69657 to J.M.B. and C.K.) and the National Science Foundation (MCB-0919027 to E.I.S., and MCB-642058 and CHE-724084 to J.M.B. and C.K.). Sector 3 operations are partially supported by COMPRES (NSFEAR06-49658). Use of the Advanced Photon Source was supported by the U.S. Department of Energy Office of Science under Contract No. DE-AC-02-06CH11357.

3-ID-B,C,D • XSD • Physics, nuclear resonant scattering, inelastic x-ray scattering, high-pressure diamond anvil cell • 7-27 keV, 14.41-14.42 keV • On-site • Accepting general users •

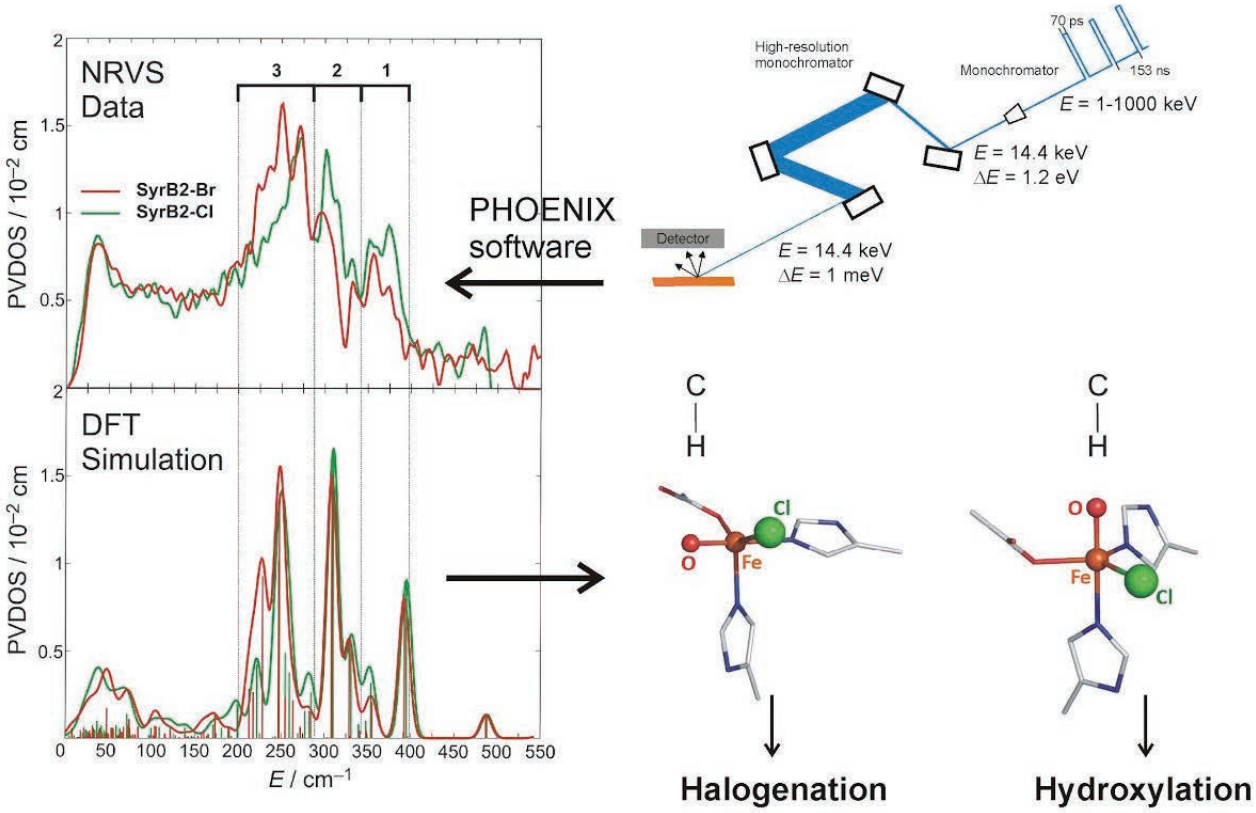

Fig. 1. The synchrotron-based experimental set-up used for NRVS experiments allowed measurement of spectra of two Cl/Br-Fe(IV) = O intermediates in SyrB2 that were correlated with DFT calculations to define the geometric structure of the Fe(IV)=O intermediate. These NRVS-calibrated DFT calculations were employed to provide insight into the frontier molecular orbitals of Fe(IV)=O that control halogenation vs. hydroxylation selectivity.

Membrane Structure Made Crystal Clear

In an ideal world, medications would be delivered straight to their target, whether it is a tumor or other disease-afflicted tissue, increasing potency and minimizing side effects. Some scientists are developing vesicles that encapsulate drugs within fatty membranes for delivery, but they are typically made from flexible lipid bilayers. Crystalline membranes, however, may offer a sturdier barricade to protect drugs in the body and release them at the right time. To make a crystalline drug vehicle, researchers must first understand how different conditions and lipid constituents affect the membranes. In this study, researchers determined the structure of crystalline membranes at the DND 5-ID-D and XSD 12-ID-C undulator beamlines at the APS. They found that changes in pH and molecular tail length alter the membrane's structure, an insight that may help with targeted drug delivery.

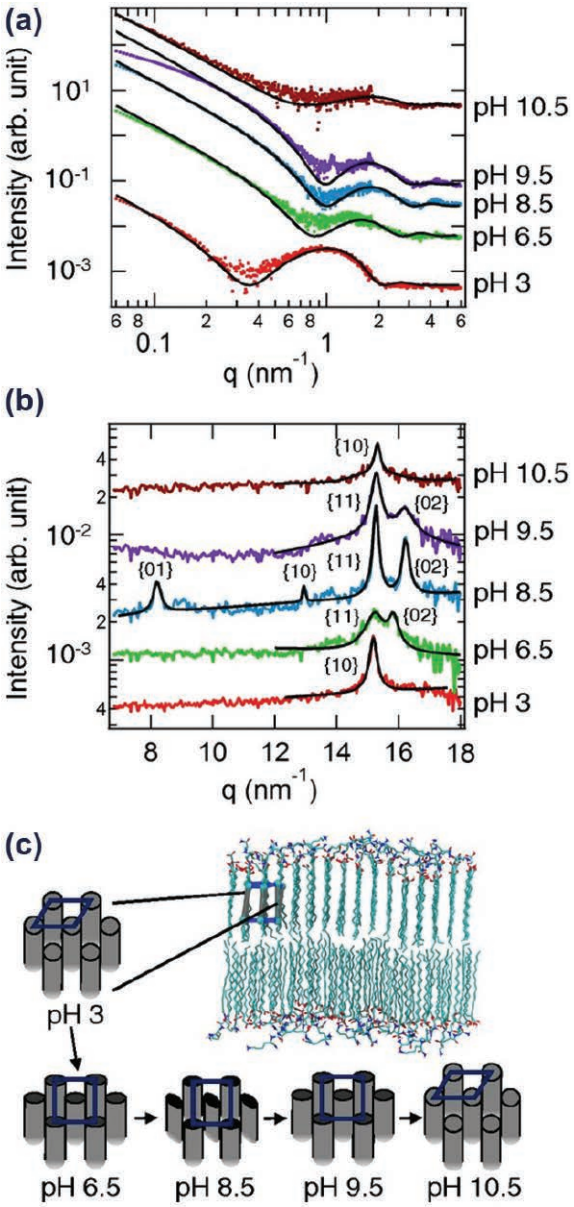

Membranes are assembled from amphiphiles, molecules that contain both hydrophilic and hydrophobic elements. The electrostatic interaction forces between these molecules drive membrane assembly. In this study, the researchers from Northwestern University built membranes from hydrophobic lipids with two different hydrophilic headgroups: a 2+ dilysine headgroup and a -1 carboxylic headgroup. They mixed the positive and negative amphiphiles to form lipid bilayers, and analyzed their structures at the APS.

The 5-ID-D and 12-ID-D beamlines are unique in that they offer both a wide-angle x-ray scattering (WAXS) detector and a small-angle x-ray scattering (SAXS) detector. This combination allowed the researchers to gather structural information from the membranes on two different spatial scales simultaneously — the nanoscale and the atomic scale. The SAXS data reports on the global bilayer structure while the WAXS data hones in on the periodic spacing of the molecular tails.

The researchers tested samples of bilayers formed and maintained at different levels of pH. The scattering data revealed that pH, which affected the electrostatic interactions between lipid head groups, had a strong effect on the structure of the crystalline membrane. In particular, the pH affected the packing of the fatty tails. At pH 3 and pH 10.5, the tails associated in a hexagonal geometry, a low density orientation. At pH 6.5, 8.5, and 9.5, the tails packed more densely together in a rectangular geometry.

These observations are explained by the fact that the carboxylic headgroups are mostly neutral at low pH, while the dilysine headgroups are positively charged. At high pH, the reverse happens. Thus, under both scenarios, the electrostatic forces are expected to be weak, allowing the fatty acid tails to intermingle in a rotationally disordered low-density organization. At a more neutral pH, positive and negative charges mix, generating stronger electrostatic interactions and restricting the movement of the tails.

To test the effect of lipid length, the researchers generated a series of each type of amphiphile, varying the length of the lipid chain between 14 and 22 carbons. The longer the chain, the greater the van der Waals attraction between chains. At pH 3, the membranes maintained a hexagonal loose structure until the chain length reached 22. At that point, the geometry switched to a rectangle, suggesting that, at that length, interactions between the alkyl tails begin to dominate, leading to dense packing of lipid tails.

One interesting observation came from looking at how the molecular structure, as gleaned from the WAXS data, related to the SAXS- and transmission electron microscopy-derived bilayer structure and to the global structure of assembly. The hexagonal molecular tail geometries lead to buckled membrane shapes, while the rectangular orientation resulted in flat membrane configurations. Thus, it is possible to change the global structure of assembly by tuning the environmental conditions (pH). This may be important in the development of drug-carrying vesicles because it suggests that a medication could be delivered in a pH-dependent fashion. As the membrane shifted from a buckled closed structure to a flatter state, the vesicle would open to release the precious cargo. *— Erika Gebel Berg*

< Fig. 1. (a) *In situ* SAXS and (b) WAXS data showing the background-subtracted scattered intensity versus the scattering vector q for mixtures of palmitic acid (C_{15}-COOH) and cationic *N*-palmitoyl dilysine (C_{16}-K_2) as the pH is increased from 3 to 10.5. The datasets are offset vertically for clarity. The black lines are the fits. Deviations in the SAXS fits are likely due to sample polydispersity. (c) Schematic representations for the bilayer model at pH 3, 6.5, 8.5, 9.5, and 10.5. Changes are observed in the packing of the alkyl tails into a hexagonal, rectangular-C, or rectangular-P lattice. From Cheuk-Yui Leung et al., Proc. Natl. Acad. Sci. USA **110**(41), 16309 (October 8, 2013). Copyright © 2013 National Academy of Sciences.

See: Cheuk-Yui Leung, Liam C. Palmer, Sumit Kewalramani, Baofu Qiao, Samuel I. Stupp, Monica Olvera de la Cruz*, and Michael J. Bedzyk**, "Crystalline polymorphism induced by charge regulation in ionic membranes," Proc. Natl. Acad. Sci. USA **110**(41), 16309 (October 8, 2013). DOI:10.1073/pnas.1316150110

Author affiliation:
Northwestern University
Correspondence:
* m-olvera@northwestern.edu,
** bedzyk@northwestern.edu

C.-Y.L., M.O.d.l.C. and M.J.B. were funded by the U.S. Department of Energy (DOE)–Basic Energy Sciences DE-FG02-08ER46539. S.K. was funded by Air Force Office of Scientific Research (FA9550-11-1-0275), and B.Q. was funded by the Office of the Director of Defense Research and Engineering National Security Science and Engineering Faculty Fellowship award (FA9550-10-1-0167). L.C.P. and S.I.S. thank the National Science Foundation (DMR-1006713) for financial support. DND-CAT is supported by E.I. DuPont de Nemours & Co., The Dow Chemical Company, and Northwestern University. Use of the Advanced Photon Source was supported by the U.S. Department of Energy Office of Science under Contract No. DE-AC-02-06CH11357.

5-ID-B,C,D • DND-CAT • Materials science, polymer science • Powder diffraction, x-ray standing waves, x-ray optics development/techniques, small-angle x-ray scattering, surface diffraction, x-ray reflectivity, wide-angle x-ray scattering • 6-17.5 keV • On-site • Accepting general users •

12-ID-C,D • XSD • Chemistry, physics, materials science • Small-angle x-ray scattering, grazing incidence small-angle scattering, wide-angle x-ray scattering, surface diffraction • 4.5-36 keV • On-site • Accepting general users •

How Do Bacteria Repair Damage from the Sun?

From bacteria to plants to humans, all organisms have mechanisms that they use to repair DNA damaged by ultraviolet (UV) light. This fundamental maintenance function is critical to our health because damaged DNA can lead to diseases such as cancer. So, of course, we know all about how it works. Or so scientists thought. New research shows that we must reworked the current model for how UV-repair functions. At issue is the number of molecules of the important proteins in the complex, UvrA and UvrB. This study, conducted by researchers from Harvard University utilizing the APS, promises to provide new insights into the fundamental mechanisms of DNA repair and into diseases that are caused by mutations in these genes such as xeroderma pigmentosum (an autosomal recessive genetic disorder of DNA repair in which the ability to repair damage caused by UV light is deficient), Cockayne syndrome (a disorder characterized by short stature and an appearance of premature aging), and trichothiodystrophy (an inherited condition in which hair is brittle, sparse, and easily broken).

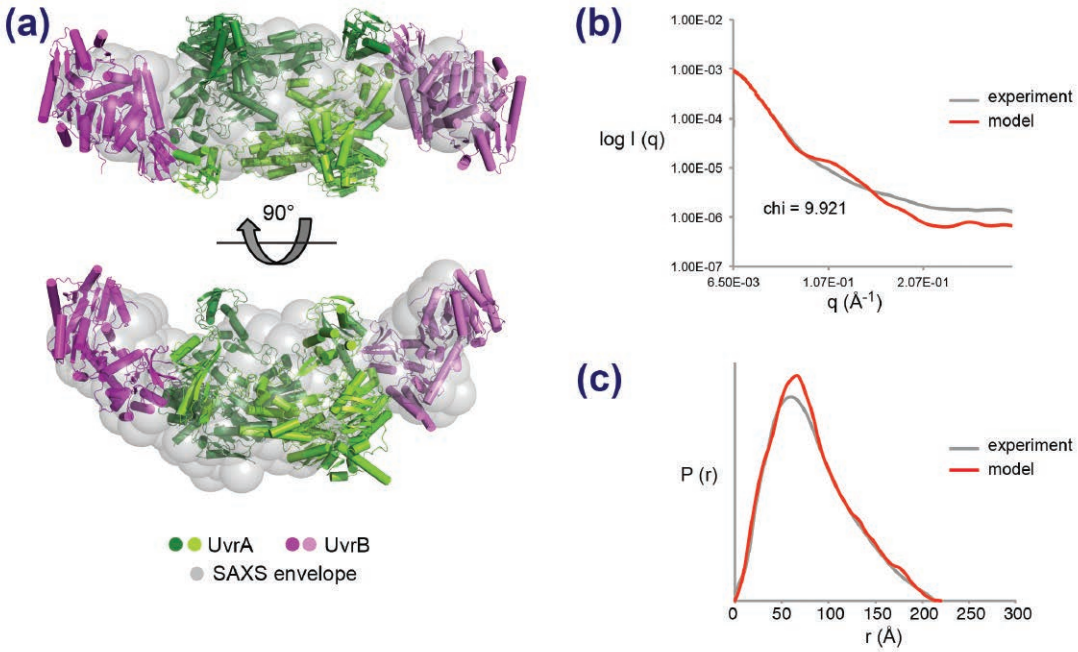

Fig. 1. Modeling of UvrA/UvrB SAXS data. Panel (a) shows the bead model of the elongated structure of the A_2B_2 complex calculated from SAXS data overlaid with the structure of the complex. Panels (b) and (c) show the comparison of SAXS data to the A_2B_2 model data.

Previous work had shown that the bacterial DNA repair mechanism involved three proteins, UvrA, UvrB, and UvrC. The model was that two copies of UvrA traveled around with one copy of UvrB (A_2B_1) and scanned the DNA for places where damage had occurred. When a spot was identified that needed repair, the A_2B_1 stopped and waited at the spot that needed repair. At this point UvrC would come in and displace UvrA and form a complex with UvrB (B_1C_1) that conducted the repair. This model explained how the complex could scan both DNA strands but then orient to repair just one strand. The asymmetric A_2B_1 fit perfectly.

The only problem was, data from various structural methods started to pile up that were not consistent with this model and suggested that the initial complex might actually be A_2B_2. In addition, the Harvard research team solved the crystal structure of the UvrA/UvrB complex and it was consistent with the A_2B_2 model. They proposed that A_2B_2 identified the damage and then the UvrA and one of the UvrB molecules were released when UvrC arrived to repair the problem. However, outstanding questions remained

"Bacteria" cont'd. on page 112

Stepping from Two Dimensions to Three

Protein folding has fascinated biologists since it was first understood that DNA is transcribed to make RNA, which is then translated into the amino acid sequence that makes up proteins. Of particular interest is how the relatively simple linear amino acid sequence dictates the formation of the highly complex three-dimensional (3-D) structure of a protein. While much is now known about how amino acids interact with each other in the 3-D protein, less is known about the folding process. In new studies, structural intermediates in the folding process have been revealed. This work, conducted at the Bio-CAT beamline 18-ID-D at the APS, and at the Photon Factory at KEK (Japan), provides much-needed data for improving computer simulations of protein folding and brings biologists another small step closer to answering the fundamental question about protein folding.

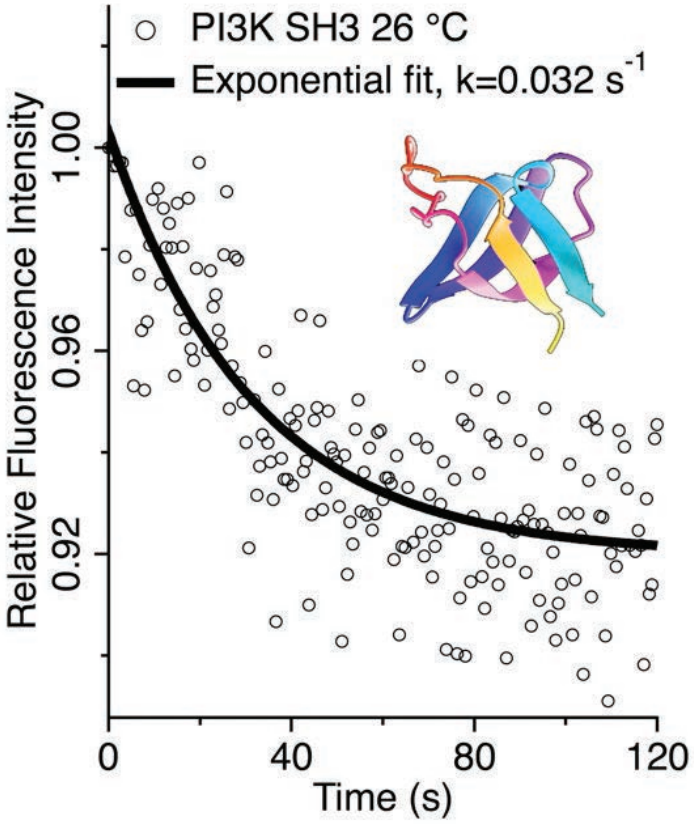

Fig. 1. Generic SH3 fold ribbon structure and intrinsic tyrosine fluorescence of PI3K SH3 domain refolding by GuHCl-jump at 26° C (aqueous buffer without ethylene glycol). The solid curve is a single exponential fit. Copyright © 2013 American Chemical Society.

Most protein folding is thought to occur via a spontaneous process that is dependent on the amino acid sequence of the protein. Models of the process suggest that the final stable structure of the protein adopts the lowest free-energy state, but there have been experimental indications that the structure may sample other low free-energy intermediates on the way to the final structure. In particular, researchers have looked at the formation of the two main types of protein secondary structures called “alpha helices” and “beta sheets.”

A number of proteins have now been shown to adopt alpha-helical intermediates, with excess helix compared to the final folded state. These intermediates have been hypothesized to assist in folding by protecting the new amino acid sequence from aggregation, and by reducing the search for the lowest free-energy conformation.

Interestingly, one protein domain, the src SH3 domain, trans-

“Dimensions” cont’d. on page 112

"Bacteria" cont'd. from page 110
about whether there might be other configurations in the crystal structure consistent with the longstanding model.

The group decided to answer these questions by evaluating the complex using small-angle x-ray scattering (SAXS). Their thinking was that low-resolution structural data collected on the protein complex in solution would be ideal for comparison modeling of various protein configurations. In addition, they hoped to find evidence for structural changes associated with how these proteins bind to ATP and use its energy for their activities.

SAXS analysis of a solution of UvrA and UvrB in complex carried out at the Bio-CAT beamline 18-ID-D at the APS showed an elongated structure (Fig. 1).

Modeling of the SAXS data against five possible configurations, four A_2B_2 options and one A_2B_1 option, showed that the data was consistent with one of the A_2B_2 configurations observed in the crystal structure but ruled out the others. Further analysis of the SAXS data by five other methods also supported this conclusion.

Unfortunately, when the team added ATP or ADP to the complex, they were not able to see any significant changes. This may require further experiments with different versions of the protein that allow them to keep the proteins bound to either ATP or ADP. For now, the Harvard researchers will be working on their new model to explain how bacteria perform this universal function. *— Sandy Field*

See: Danaya Pakotiprapha and David Jeruzalmi*, "Small-angle X-ray scattering reveals architecture and A_2B_2 stoichiometry of the UvrA–UvrB DNA damage sensor," Proteins 81,132 (2013). DOI: 10.1002/prot.24170
Author affiliation: Harvard University
Correspondence: *dj@ccny.cuny.edu

This research was funded by National Science Foundation Grant number MCB 0918161 (D.J.); National Institutes of Health Grants number GM084162 (D.J.) and CA100742 (Gregory L. Verdine). Bio-CAT is supported by Grant 5 P41 GM103622 from the National Institute of General Medical Sciences of the National Institutes of Health. Use of the Advanced Photon Source at Argonne National Laboratory was supported by the U.S. Department of Energy Office of Science under Contract No. DE-AC02-06CH11357.

18-ID-D • Bio-CAT • Life sciences • Fiber diffraction, microdiffraction, small-angle x-ray scattering, time-resolved x-ray scattering, micro x-ray absorption fine structure • 3.5-35 keV • On-site • Accepting general users •

Dimensions" cont'd. from page 111
itions through the alpha helix on its way to forming a beta sheet. To determine whether this is unique to src SH3 or may represent a paradigm for folding of these beta-sheet structures, the researchers from the University of Illinois at Urbana-Champaign, Kansai Medical University (Japan), Hokkaido Blood Center (Japan), Ritsumeikan University (Japan), and Nagoya University (Japan), looked at two other SH3 domains from the phosphatidyl inositol-3-kinase (PI3K) and the src-related protein Fyn.

Using circular dichroism (CD) and small angle x-ray scattering (SAXS) at the Bio-CAT 18-ID-D beamline at the APS and the 15A beamline at KEK, their experiments were done under cryogenic conditions (-5° C for PI3K and -28° C for Fyn) to slow down the folding process enough to detect intermediates. Using a technique called "denaturant jumps," the researchers observed the formation of alpha helical or beta sheet structures by CD. The method involves maintaining the protein in the unfolded state in a high concentration of denaturing solution and then jumping it to a low concentration of denaturant that favors folding.

The data for PI3K showed that it formed an alpha helical intermediate at 6 msec after the jump and that this slowly converted to the final beta sheet structure. SAXS analysis confirmed this observation, showing that the intermediate was only about 20% larger than the final state, suggesting a very compact, low free-energy intermediate (Fig. 1).

For the Fyn protein, the results were similar but with some important differences. The compact alpha helical intermediate was also formed very quickly (< 6 msec), but the structure then adopted an additional alpha helical intermediate before settling down to the final native protein structure.

These findings suggest that these SH3 domains contain some intrinsic propensity in their amino acid sequence that drives them to form an alpha helical intermediate on the way to folding, but that the intermediate structure is not always the same for each SH3 domain. Different SH3 proteins follow different paths while folding.

The detection of these alpha helical intermediates opens the door for investigation of the evolutionary forces that may favor or preclude their formation and that may ultimately result in new stable protein folds.

Finally, alpha helical intermediates have been detected in computational simulations of protein folding for a long time and have been considered a nuisance to be avoided through technical adjustments. But now that they have been observed experimentally, these alpha helical intermediates have become more than just simulation artifacts, and they can be incorporated into computational models to improve their real-world applicability. *— Sandy Field*

See: Yoshitaka Matsumura[1], Masaji Shinjo[1]*, Seung Joong Kim[2], Nobuyuki Okishio[3], Martin Gruebele[2], and Hiroshi Kihara[1,4,5], "Transient Helical Structure during PI3K and Fyn SH3 Domain Folding," J. Phys. Chem. B **117**, 4836 (2013). DOI:10.1021/jp400167s
Author affiliations: [1]Kansai Medical University, [2]University of Illinois at Urbana-Champaign, [3]Japanese Red Cross Hokkaido Blood Center, [4]Ritsumeikan University, [5]Nagoya University
Correspondence:
*shinjom@hirakata.kmu.ac.jp

This study was supported by a Grant-in-Aid for Scientific Research (no. 20540400) from the Ministry of Education, Culture, Sports, Science, and Technology (Japan). M.G. and S.J.K. were supported by National Institutes of Health grant R01- GM093318. Bio-CAT is supported by Grant 5 P41 GM103622 from the National Institute of General Medical Sciences of the National Institutes of Health. Use of the Advanced Photon Source at Argonne National Laboratory was supported by the U.S. Department of Energy Office of Science under Contract No. DE-AC02-06CH11357.

High-Resolution Tracking of Large-Protein Folding

In order for proteins to perform their varied roles within the cell, these complex macromolecules must fold into their native, functional conformation. With the use of small-angle x-ray scattering (SAXS), in conjunction with other highly sensitive biophysical methods, work from the lab of S. Walter Englander at the University of Pennsylvania's Perelman School of Medicine unveils how large denatured proteins refold into their native state. This research addresses the biophysical nature of protein folding, and uses the maltose binding protein (MBP) as a model to demonstrate that proteins form an obligate structural intermediate en route to their fully native state, rather than folding through varied paths to reach the same native fold. The work is a valuable tool for interpreting a large body of preexisting biophysical data on protein folding.

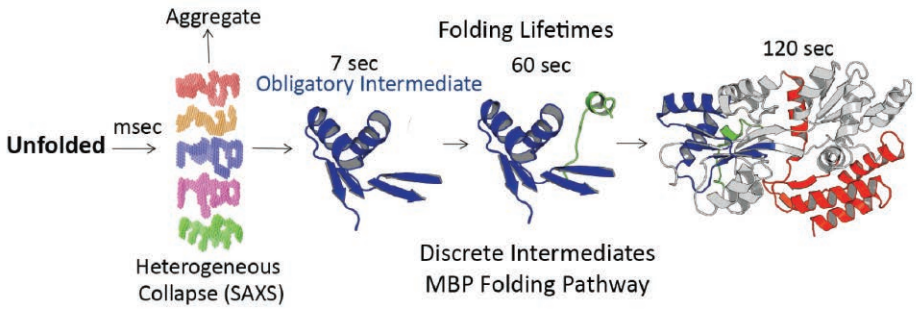

Fig. 1. Pathway of MBP folding. The completely denatured protein (far left), once placed into native conditions, adopts a heterogeneous collapsed state (second from left) capable of forming aggregates (top left) or continuing along the folding pathway to form an obligatory intermediate and subsequent folding intermediates (center) as it folds to reach its native conformation (far right). Folding lifetimes of each state are indicated at each step in the pathway. Intermediates are shown in blue alone and within the context of fully folded MBP.

Proteins carry out a vast array of cellular functions of critical importance. Synthesized in a linear fashion from their building blocks, amino acids, these macromolecules carry out enzymatic reactions in metabolic pathways, regulate processes such as cell growth, orchestrate finely tuned responses to the cellular environment, and perform structural roles required for maintenance of tissue integrity. Central to any protein's ability to coordinate a given cellular process is the way in which its chain of amino acids is folded; it is the resultant three-dimensional structure that largely dictates functionality.

Folding can bring sequentially distant amino acids into close proximity to one another, allowing the formation of active sites that carry out biochemical reactions or stabilizing the protein structure required for proper function. Being able to understand the biophysical determinants of this process lends valuable insight into how proteins fold into their correct conformation in the cell. Improper protein folding can have disastrous consequences in many disease states. For example, in neurodegenerative disorders such as Alzheimer's and Parkinson's disease, misfolded proteins aggregate forming plaques that damage nervous tissue and along with the symptoms associated with these diseases.

It has long been appreciated that chemically denatured (unfolded) proteins, when returned to native (cell-like) conditions, refold back into their original form. In this work, researchers from the University of Pennsylvania and The University of Chicago used SAXS at Bio-CAT beamline 18-ID-D to characterize the unfolded protein in native conditions, and advanced hydrogen exchange mass spectroscopy (HX-MS) to monitor MBP, a large multi-domain protein, as it folded to its native state. Their findings demonstrate that proteins fold through an invariant predetermined track, and pass through an obligate structural intermediate. This is in direct contrast to the "funnel-like" mechanism hypothesis in which proteins are proposed to reach the native state though varied multiple pathways from the collapsed, unfolded state.

Although this research uses MBP as a model system for exploring protein folding, the findings here are consistent with established biophysical principles, and may be applied to other proteins, making this work a valuable lens through which to view and interpret a large body of preexisting biophysical data on protein folding.

— Emma Nichols

See: Benjamin T. Walters[1], Leland Mayne[1], James R. Hinshaw[1], Tobin R. Sosnick[2], and S. Walter Englander[1]*, "Folding of a large protein at high structural resolution," Proc. Natl. Acad. Sci. **110**(47), 18898 (November 19, 2013). DOI:10.1073/pnas.1319482110
Author affiliations: [1]University of Pennsylvania, [2]The University of Chicago
Correspondence:
* engl@mail.med.upenn.edu

This work was supported by National Institutes of Health (NIH) Research Grants R01 GM031847 (to S.W.E.), R01 GM055694 (to T.R.S.), a Structural Biology Predoctoral Training Grant GM08275 (to B.T.W.), and a National Science Foundation Research Grant MCB1020649 (to S.W.E.). Bio-CAT is supported by Grant 5 P41 GM103622 from the National Institute of General Medical Sciences of the NIH. Use of the Advanced Photon Source at Argonne National Laboratory was supported by the U.S. Department of Energy Office of Science under Contract No. DE-AC02-06CH11357.

18-ID-D • Bio-CAT • Life sciences • Fiber diffraction, microdiffraction, small-angle x-ray scattering, time-resolved x-ray scattering, micro x-ray absorption fine structure • 3.5-35 keV • On-site • Accepting general users •

Optimized Energy Recovery at the APS: Closing the Loop on Recycling Waste Heat

The Site Operations Office of the AES Division in the APS has implemented some unique system designs that expand the range and application of low-grade waste heat recovery to the 16 commercial-grade office and laboratory buildings that comprise the APS conventional facilities. These new designs shift the heat-recovery systems from seasonal-only applications to year-round usage, and also from winter heating to space temperature control. The overwhelming majority of electricity consumed by commercial buildings eventually turns into low-temperature waste heat at or below 32° C (90° F). While this waste heat can be recycled during cold weather for preheating outdoor air, its low temperature makes recycling and reusing it for other purposes extremely difficult. Typically, the majority of this waste heat is rejected to the outdoors. The Department of Energy reports, "Commercial buildings represent just under one-fifth of U.S. energy consumption, with office space, retail space, and educational facilities representing about half of commercial sector energy consumption. In aggregate, commercial buildings consumed 17.9 quads of primary energy in 2009, representing 46.0% of building energy consumption and 18.9% of U.S. energy consumption." [1]

Facility engineers at Argonne have worked to expand the reach of this underused energy source by focusing on applications that integrate other portions of a building heating system including reheat and exterior-wall heating. The goal is to maximize the recycling of building waste-heat. Building reheat systems typically operate continuously all year to provide interior space temperature control. This is especially true in the case of laboratories, hospitals, and related facilities. Many large office buildings also employ reheat for space temperature control. In mild climates, the energy utilized by space reheat will dominate a building's heating energy usage, making it a prime candidate for recycled sources of energy.

Marvin Kirshenbaum (AES) checks one the modified high-efficiency reheat coils installed in laboratory/office module 438F at the APS.

Reheat systems take cool air supplied by the building ventilation system, in the range of 10° C (50° F) to 14° C (56° F), and heat it locally at each individual space with small heat-transfer coils to maintain the space temperature control. Since the temperature difference between the cool building supply air and a typical waste-heat stream is small, extracting adequate heat and being able to warm the supply air to a sufficient temperature has impeded the cost-effective use of this energy source. Conventional heat transfer coils (reheat coils) usually are not up to the task; they tend to be limited to heating air only to within 4° C (7° F) of the temperature of the waste heat source. In order to achieve the necessary air temperatures the waste-heat temperature must be elevated using a heat pump, or the effectiveness of the heat transfer at the coils must be dramatically improved. Such "high-efficiency" heat transfer coils are manufactured as large single units for outdoor air preheat. Argonne, working with a leading manufacturer of these coils, has dramatically reduced the coil size to test their efficacy as space-reheat coils.

At the APS, a new building, laboratory/office module 438 F, is a 5300 sq ft building with 17 HVAC zones. Each zone has been fitted with the modified high-efficiency reheat coils. The building, in operation since November of 2013, has cycled through both mild and extreme cold weather conditions. Data collected to date show an average of better than 20 kW of recycled energy usage under extreme weather conditions (-20° C) and 15 kW during mild weather conditions. It is projected that the building will recycle an average 10 kW of waste heat continuously, equal to 88 MW hours of energy per year, providing an energy savings of about 16 kW-hrs/sq ft /yr and yielding an operating cost savings of over $1.00/sq ft/yr while saving an estimated 20 metric tons of carbon per year. To gain a perspective on the impact on potential energy savings: applying this technology to one of the larger lab/office buildings (150,000 sq ft) at the APS would realize a yearly savings of $150,000 per year and over 550 metric tons of carbon.

The ability to provide space reheat with systems operating at these lower temperatures opens a whole new avenue for low-grade waste heat recycling through both direct heat transfer and in the creation of hybrid heat-pump systems. With direct heat transfer, systems can provide heating without supplementation of heat pumps or other external energy consuming devices. Through this dramatic lowering of the required heating source operating temperature, we can significantly decrease the heat pump's energy consumption increasing system coefficient of performance by a factor of 2 or greater.

Contact: Marvin Kirshenbaum, kirshen@aps.anl.gov

Reference

[1] Building Energy Data Book, "US Department of Energy Office of Energy Efficiency & Renewable Energy," (March 2010). http://buildingsdatabook.eren.doe.gov/ChapterIntro3.aspx

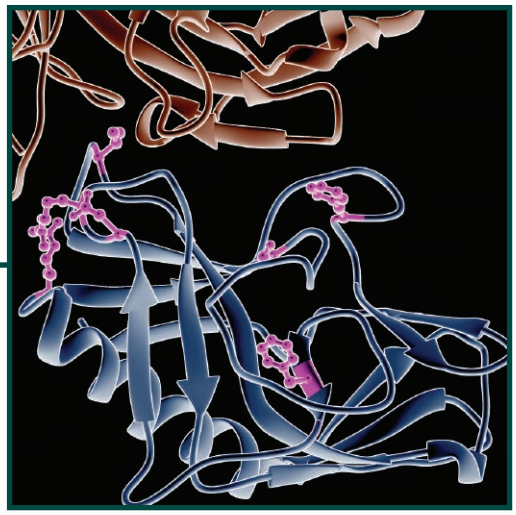

Structural Biology

The Balancing Act We Call Life

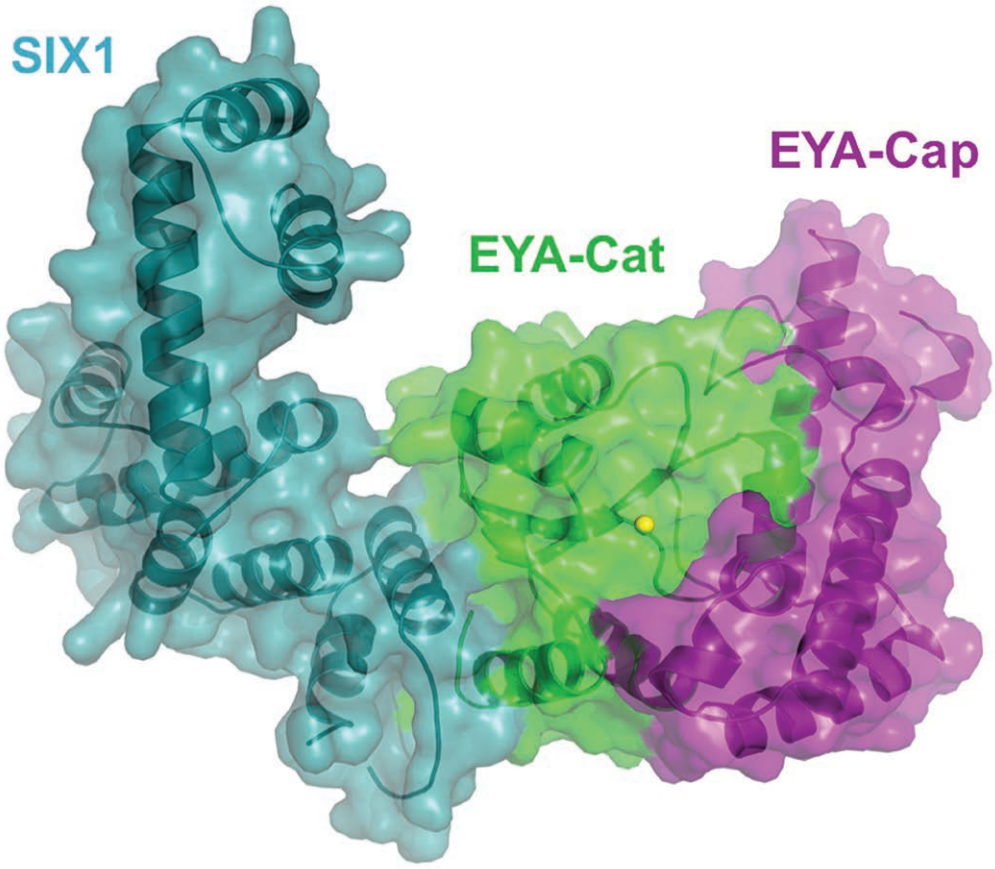

Fig. 1. Structure of the SIX1-EYA complex. SIX1 (teal) binds to the catalytic domain of EYA (green) using a single alpha helix. The EYA cap domain (non-catalytic domain) is shown in magenta.

As we learn more about how genes are regulated throughout development and our lives, one thing becomes very clear: Gene expression is a balancing act. This is certainly the case for the SIX family of proteins that regulate how some genes are activated during embryonic development. The SIX1 protein works with a partner, the EYA protein, to regulate genes involved in the proper formation of organs. However, if these partners don't function correctly during development, a condition known as branchio-oto-renal (BOR) syndrome can result in which children are born with hearing loss, kidney problems, and skin problems. Conversely, inappropriate reactivation of SIX1 and EYA later in life can contribute to the development of metastatic cancer. Now, in work by researchers conducted at the APS, the structure of this complex has been solved. The work provides insight into how SIX1-EYA mutations are important in causing BOR syndrome and highlights the importance of the SIX1-EYA complex in the development of metastatic cancer. Their findings also suggest that the SIX1-EYA complex could be a target for intervention in cancers where it has been inappropriately expressed.

The SIX1 protein is a member of the highly conserved homeodomain family of proteins that is responsible for the proper regulation of gene expression during embryonic development. The DNA binding activity of SIX1 is enhanced by EYA and EYA also has enzymatic activity of its own, as a protein tyrosine phosphatase. Together, these proteins form a transcription factor that tells cells what to do. However, in some cases either EYA or SIX1 gets mutated and does not work properly and BOR syndrome develops. In other cases, the complex, which is turned off in adults, gets reactivated by aberrant cellular processes and cells are told to grow when they are not supposed to. This, of course, is cancer.

In order to learn more about the delicate balance between abnormal development, normal organ formation, and cancer, the researchers from the University of Colorado Anschutz Medical Campus, and the University of Southern California, Los Angeles, sought to learn more about the interaction between SIX1 and EYA by solving the structure of these proteins in complex at the SBC-CAT 19-ID-D beamline at the APS.

The 2.0-Å structure of the complex shows that SIX1 has two domains joined by a flexible linker, one that binds DNA and one that binds EYA. The domain that binds DNA resembles other homeobox proteins that regulate gene expression during development but has unique characteristics that suggest that there might be additional regulation of DNA binding by the other domain. This will be investigated in a future structure that will include DNA as well. As for the other domain, SIX1 binds EYA in an unexpected manner through the interaction of an alpha helix in SIX1 with a groove on the catalytic domain of EYA (Fig. 1).

A number of discoveries follow from this finding. First, this study shows that mutations that disrupt formation of the SIX1-EYA complex also disrupt the ability of SIX1 to activate cancer signaling pathways and to enhance metastatic spread of cancer cells. This suggests that therapies that target the complex might be effective in fighting cancers caused by its re-activation. This is good news because it has historically been difficult to target the interactions of gene regulators with DNA for therapies.

Also fortuitously, the structure of the interaction between SIX1 and EYA resembles that of two other protein complexes that have been targeted in cancer therapy, suggesting that it might be possible to target the SIX1-EYA interaction with similar small molecule inhibitors.

Finally, analysis of the structure to identify the location of mutations found in BOR syndrome showed that some of them were located on the SIX1-EYA binding interface and important for the formation of the active complex.

Taken together, the team has uncovered answers about how BOR syndrome mutations affect protein function during development, how reactivation of SIX1 and EYA can lead to cancer spread, and how cancers driven by SIX1 and EYA reactivation might be targeted therapeutically. *— Sandy Field*

See: Aaron N. Patrick[1], Joshua H. Cabrera[1], Anna L. Smith[1], Xiaojiang S. Chen[2], Heide L. Ford[1]*, and Rui Zhao[1]**, "Structure-function analyses of the human SIX1–EYA2 complex reveal insights into metastasis and BOR syndrome," Nat. Struct. Mol. Biol. **20**(4), 447 (April 2013).
DOI:10.1038/nsmb.2505
Author affiliations: [1]University of Colorado Anschutz Medical Campus; [2]University of Southern California, Los Angeles
Correspondence:
** rui.zhao@ucdenver.edu,
* heide.ford@ucdenver.edu

This work was supported by grants from the US National Cancer Institute (2R01-CA09 5277 and R01CA157790) to H.L.F. and from the U.S. Department of Defense Synergistic IDEA award (W81XWH-09-1-0253), Breast Cancer Research Foundation–American Association for Cancer Research, State of Colorado (2009 and 2011) and National Institutes of Health (R03DA030559 and R03DA033174) to H.L.F. and R.Z. A.N.P. was supported by a Pediatric Hematology/Oncology Postdoctoral Fellowship (2T32082086-11A1). SBC-CAT is funded by the U.S. Department of Energy (DOE) Office of Biological and Environmental Research. Use of the Advanced Photon Source at Argonne National Laboratory was supported by the DOE Office of Science under Contract No. DE-AC02-06CH11357.

19-ID-D • SBC-CAT • Life sciences • Macromolecular crystallography, multi-wavelength anomalous dispersion, subatomic (<0.85 Å) resolution, microbeam, ultra-low-temperature (15K), large unit cell crystallography, single-wavelength anomalous dispersion • 6.5-19.5 keV • On-site, remote, mail-in • Accepting general users •

The Pathway to HIV Vaccination

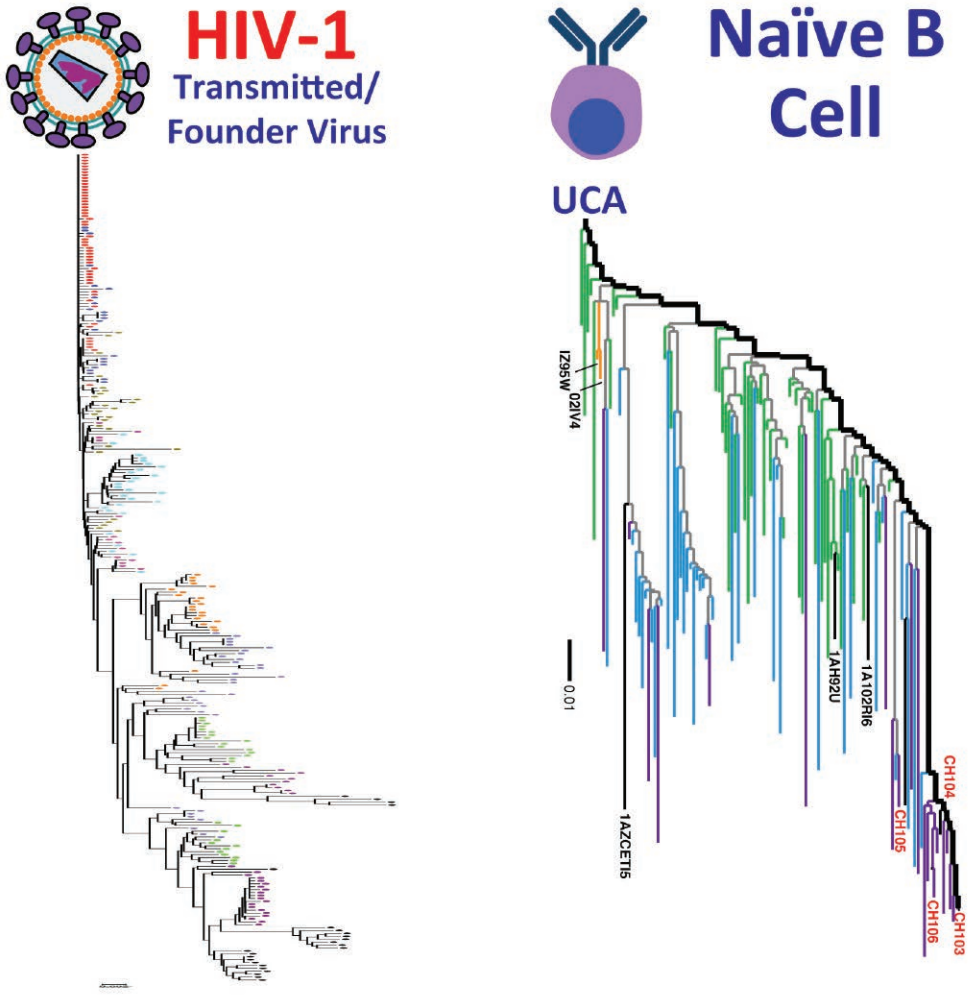

Fig. 1. Co-evolution of HIV-1 T/F virus and antibodies developed from an HIV-1 infected individual in response to the virus and its mutating variants, leading to the development of a clonal lineage of BnAbs.

Human immunodeficiency virus-1 (HIV-1) causes most cases of HIV worldwide. Developing an effective vaccine against this virus has proven difficult since it can rapidly mutate and avoid the immune system. But more recently, broadly neutralizing antibodies (BnAbs), produced by a minority of HIV-infected patients, have risen to the fore in HIV vaccine research, due to their ability to target many strains of the virus. Researchers in this study aimed to determine the sequence of events that occurs between HIV-1 infection and generation of BnAbs. The results tracked the evolution of a BnAb from a patient who was followed from the time of infection, and showed that the mature form of the antibody neutralized more than half of the HIV-1 isolates. They also used the high-brightness x-rays from the APS to collect data in order to evaluate the crystal structure of the antibody bound to the viral envelope. This helped them identify a new method of defining how antibody neutralization evolves. The results demonstrate, for the first time, the evolutionary pathway of HIV-1 and BnAb in a HIV-1-infected individual from the time of infection to the development of BnAbs.

There are two types of HIV, HIV-1 and HIV-2, but the predominant type responsible for the current worldwide pandemic is HIV-1. Additionally, most HIV-1 infections result from the transmission of just one virus variant, known as the transmitted/founder (T/F) virus.

Whereas non-cross-reactive antibodies are specific for individual strains of a virus, BnAbs are cross-reactive, and can neutralize multiple strains. However, these only arise in about a fifth of individuals infected with HIV-1. Since HIV is a retrovirus with the ability to mutate quickly, often as soon as it enters the body, an effective vaccine will need to stimulate production of more than one type of antibody to prevent infection. Consequently, generation of BnAbs represents the biggest hope to date for successful HIV vaccine development. They recognize and target antigens such as HIV envelope glycoprotein gp120, which is found on the surface of the virus, and is the site where CD4 white blood cells bind. These cells play an important role in generating an effective immune response to foreign pathogens, but are destroyed by HIV. Since the viral envelope glycoprotein is needed for the infection process, it is less likely to mutate, and is typically similar even in different HIV strains.

However, stimulating production of BnAbs by human cells has proven difficult, because they typically do not become potent against HIV until its infection has been established in the body for some time.

In this study, researchers aimed to investigate the series of events that lead to production of BnAbs after a person is infected with HIV-1. They found a BnAb, which they called CH103, in an African individual within three years of infection, and then evaluated samples of the individual's blood that had been previously taken. In this way, they were able to follow the evolution of the virus, as well the evolution of antibodies produced in response to the mutating virus after it infected the body (Fig. 1). They identified the un-mutated common ancestor or germline precursor of the antibody —– its earliest form — and detailed the sequence of events that led to its maturation into a BnAb. The researchers also used x-ray diffraction data sets collected at the SER-CAT beamline 22-ID-D at the APS to evaluate the three-dimensional crystal structure of antibody CH103 bound to the HIV-1 gp120.

They demonstrated that the CH103 line of BnAbs is less mutated than most other BnAbs, and can be detected as early as 14 weeks after a person has been infected with HIV-1. They also found that the mature form of the antibody neutralized more than half of HIV-1 isolates, and that the T/F envelope glycoprotein can stimulate, and bind to, a potent BnAb. Evaluation of the crystal structure of the CH103 in complex with HIV-1 gp120 also showed a novel loop-based method of antibody neutralization. *— Nicola Parry*

See: Hua-Xin Liao[1,2]*, Rebecca Lynch[3]*, Tongqing Zhou[3], Feng Gao[1,2], S. Munir Alam[1,2], Scott D. Boyd[4], Andrew Z. Fire[4], Krishna M. Roskin[4], Chaim A. Schramm[5], Zhenhai Zhang[5], Jiang Zhu[3], Lawrence Shapiro[3,5], NISC-Comparative Sequencing Program†, James C. Mullikin[3], S. Gnanakaran[6], Peter Hraber[6], Kevin Wiehe[1,2], Garnett Kelsoe[1,2], Guang Yang[1,2], Shi-Mao Xia[1,2], David C. Montefiori[1,2], Robert Parks[1,2], Krissey E. Lloyd[1,2], Richard M. Scearce[1,2], Kelly A. Soderberg[1,2], Myron Cohen[7], Gift Kamanga[8], Mark K. Louder[3], Lillian M. Tran[3], Yue Chen[1,2], Fangping Cai[1,2], Sheri Chen[1,2], Stephanie Moquin[3], Xiulian Du[3], M. Gordon Joyce[3], Sanjay Srivatsan[3], Baoshan Zhang[3], Anqi Zheng[3], George M. Shaw[9], Beatrice H. Hahn[9], Thomas B. Kepler[10], Bette T. M. Korber[6], Peter D. Kwong[3], John R. Mascola[3], and Barton F. Haynes[1,2]**, "Co-evolution of a broadly neutralizing HIV-1 antibody and founder virus," Nature **496**, 469 (25 April 2013). DOI:10.1038/nature12053

Author affiliations: [1]Duke University School of Medicine, [2]Duke Center for HIV/AIDS Vaccine Immunology and Immunogen Discovery, [3]National Institutes of Health, [4]Stanford University, [5]Columbia University, [6]Los Alamos National Laboratory, [7]University of North Carolina, [8]Kamuzu Central Hospital, [9]University of Pennsylvania, [10]Boston University. †A full list of participants and their affiliations appears at the end of the paper.

Correspondence: * hliao@duke.edu, ** barton.haynes@duke.edu

This study was supported by the National Institutes of Allergy and Infectious Diseases (NIAID) and by intramural National Institutes of Health (NIH) support for the NIAID Vaccine Research Center, by grants from the NIH, NIAID, AI067854 (the Center for HIV/AIDS Vaccine Immunology) and AI100645 (the Center for Vaccine Immunology-Immunogen Discovery). SER-CAT is supported by the member institutions found at www.ser-cat.org/members.html. Use of the Advanced Photon Source at Argonne National Laboratory was supported by the U.S. Department of Energy Office of Science under Contract No. DE-AC02-06CH11357.

22-ID-D • SER-CAT • Life sciences • Macromolecular crystallography, multi-wavelength anomalous dispersion, microbeam • 6-20 keV • On-site, remote • Accepting general users •

Broadening the Approach to HIV Vaccination

Developing an effective vaccine against human immunodeficiency virus (HIV) has so far proven elusive. In particular, it has been difficult to produce a vaccine that can target the variety of strains of HIV that result from its ability to mutate readily to evade the host's immune response. Researchers in this study aimed to engineer an immunogen that could stimulate VRC01-class antibodies — broadly neutralizing antibodies (bNAbs) capable of neutralizing most strains of HIV. They used the APS and the Stanford Synchrotron Radiation Lightsource (SSRL) to collect data to evaluate the crystal structures of the immunogen, a germline VRC01 antibody, and the eOD-GT6 immunogen bound to the antibody. The results showed that the immunogen activated B cells expressing either germline, or mature, VRC01-class antibodies. They also determined which HIV mutations were responsible for its reactivity with germline VRC01 antibodies. These results demonstrate that the eOD-GT6 immunogen shows promise as a prime for HIV vaccine development, This will be important in guiding future studies to investigate application of germline-targeting strategies in vaccine development against HIV and other pathogens.

Fig. 1. Crystal structure of the complex of eOD-GT6 bound to germline VRC01.

HIV causes acquired immunodeficiency syndrome, a condition that affects the immune system, leaving infected people more susceptible to other infections and diseases. And since more than 34 million people worldwide live with HIV, development of an effective, safe, and lasting vaccine for the virus remains a priority.

Most vaccines currently licensed for use help protect against disease by promoting antibody production. However, viruses like HIV with high antigenic diversity can change their surface proteins to evade the host's immune response. Because this highly variable virus can mutate readily, there are many HIV strains in existence, even within an infected person. This makes HIV somewhat of a moving target with respect to attempts to develop effective vaccines against it. So, one of the main problems has been developing a vaccine able to stimulate the immune system to respond by producing antibodies that allow protection against numerous strains of HIV.

VRC01 antibodies are known as broadly neutralizing antibodies (bNAbs) because they can neutralize most strains of HIV. They target a specific site on a glycoprotein found on the surface of HIV which is known as gp120, and is where CD4 cells of the immune system bind. These are white blood cells that are important in achieving a regulated, effective immune response to pathogens, but are attacked by HIV. However, although VRC01 class antibodies have been found in people infected with HIV, vaccination has not yet been able to induce them.

In this study, the researchers from The Scripps Research Institute; the University of Washington; the Seattle Biomedical Research Institute; and the Ragon Institute of Massachusetts General Hospital, Massachusetts Institute of Technology, and Harvard aimed to develop a new method for producing vaccine immunogens, the substances that provoke an immune response, in the hope of generating a response that would be effective against many HIV strains via production of bNAbs. They developed an immunogen that binds to multiple VRC01-class bNAbs and germline precursors, and named it eOD-GT6.

Vaccines induce protective antibodies by first stimulating germline B-cells and then selecting for mutated, higher affinity antibodies during the process of somatic hypermutation. Typically, vaccine developers are not concerned with the particular germline B cells that are used to start the process. In the case of VRC01-class bNAbs against HIV, however, native HIV gp120 proteins have no detectable affinity for VRC01-class germline antibodies. The researchers therefore hypothesized that this presented a barrier to reliable vaccine induction of VRC01-class bNAbs. Consequently, they designed a modified HIV protein that could bind and activate VRC01-class germline B cells, eliminating the barrier.

The researchers used data sets collected from experiments to investigate eOD-GT6 and its interaction with germline antibodies, using the GM/CA beamline 23-ID-D at the APS and at the SSRL. They determined the three-dimensional atomic structures of this immunogen, a germline VRC01 antibody, and the compound formed by binding of the immunogen to the antibody (Fig. 1).

This immunogen was shown to activate B cells expressing germline or mature VRC01-class bNAbs, and data from this study were also able to determine which HIV mutations were important for its reactivity with germline VRC01 antibodies. *— Nicola Parry*

See: Joseph Jardine[1,4], Jean-Philippe Julien[1], Sergey Menis[1,2], Takayuki Ota[1], Oleksandr Kalyuzhniy[1,2], Andrew McGuire[3], Devin Sok[1], Po-Ssu Huang[2], Skye MacPherson[1,2], Meaghan Jones[1,2], Travis Nieusma[1], John Mathison[1], David Baker[2], Andrew B. Ward[1], Dennis R. Burton[1,4], Leonidas Stamatatos[2,3], David Nemazee[1], Ian A. Wilson[1], William R. Schief[1,2], "Rational HIV Immunogen Design to Target Specific Germline B Cell Receptors," Science **340**, 711 (10 May 2013). DOI:10.1126/science.1234150

Author affiliations: [1]The Scripps Research Institute, [2]University of Washington, [3]Seattle Biomedical Research Institute, [4]Ragon Institute of Massachusetts General Hospital, Massachusetts Institute of Technology, and Harvard

Corresponding author:

* schief@scripps.edu

This work was supported by IAVI Neutralizing Antibody Center, CHAVI-ID (UM1 AI100663); National Institutes of Health (NIH) grants AI84817 (I.A.W.), AI094419 (L.S.), and AI33292 (D.R.B.); NIH National Research Service Award Training Grant fellowship T32CA080416 (J.J.); Canadian Institutes of Health Research fellowship (J.-P.J.); Creative and Novel Ideas in HIV Research grant P30 AI027767-24 (T.O.); NIH Interdisciplinary Training Program in Immunology 5T32AI007606-10 (D.S.); and the Ragon Institute. (J.H., K.H., J.W.). GM/CA-XSD is funded in whole or in part with Federal funds from the National Cancer Institute (Y1-CO-1020) and the National Institute of General Medical Sciences (Y1-GM-1104). Use of the Advanced Photon Source at Argonne National Laboratory was supported by the U.S. Department of Energy Office of Science under Contract No. DE-AC02-06CH11357.

23-ID-D • GM/CA-XSD • Life sciences • Macromolecular crystallography, microbeam, large unit cell crystallography, subatomic (<0.85 Å) resolution, multi-wavelength anomalous dispersion, single-wavelength anomalous dispersion • 5-20 keV • On-site, remote • Accepting general users •

A Case of Nonspecific Substrate Specificity

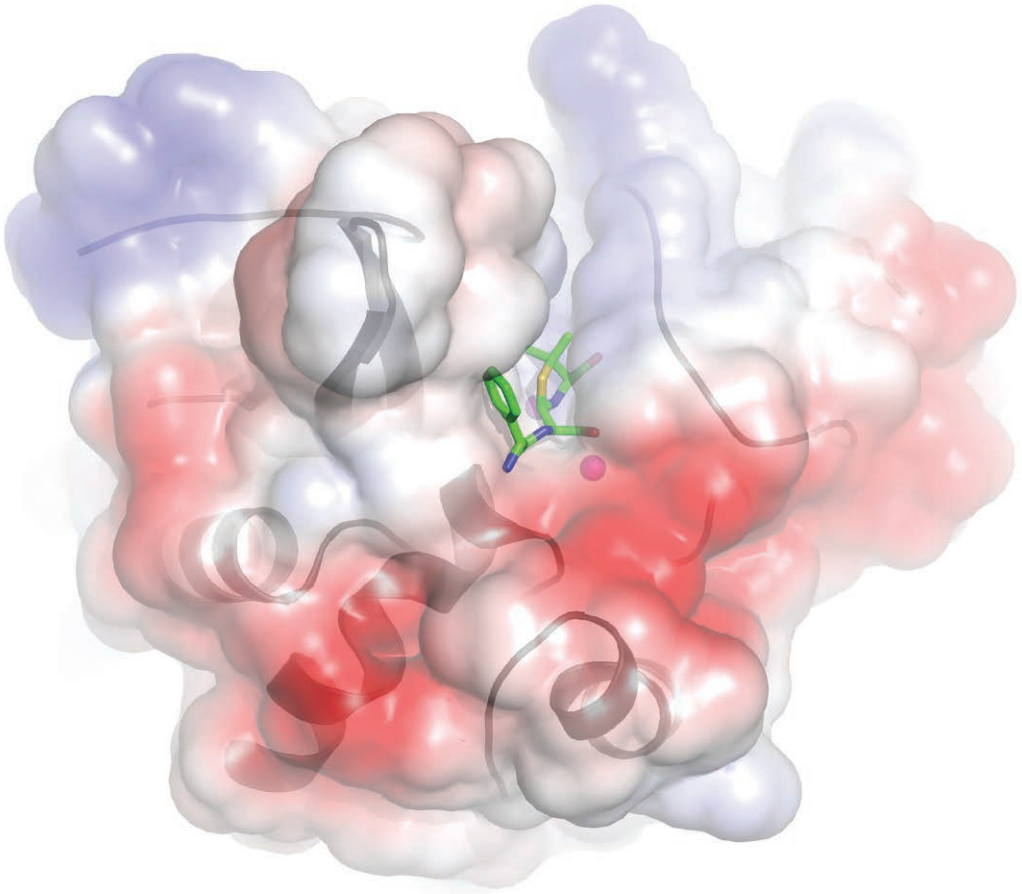

Fig. 1. Space-filling model of NDM-1 active site with hydrolyzed ampicillin substrate containing broken β-lactam moiety and zinc atoms bound. Major structural elements of NDM-1 are shown in gray ribbons. Zinc atoms are shown as pink balls and hydrolyzed ampicillin is shown in colored stick representation with green for carbon, red for oxygen, blue for nitrogen, and yellow for sulfur atoms.

Enzymes are known for their specific recognition of the molecules they act on and for the speed of their reactions. Much of the work done by researchers who study protein structure is devoted to discovering the precise architecture of enzyme catalytic sites in order to uncover the exact features responsible for this specificity and speediness. The recent discovery of a bacterial enzyme, called New Delhi metallo-β-lactamase, or NDM-1, that can neutralize nearly all of the β-lactam antibiotics, suggests that promiscuity, rather than specificity, may also be an effective strategy. In an effort to understand exactly how NDM-1 can work on so many different antibiotics, researchers solved the structure of NDM-1 in four different configurations using data collected at the APS. Then they used their structural data as a basis for modeling the energetics of possible catalytic pathways. While the evolution of ever more promiscuous microbial enzymes is not surprising, it is hardly good news in this era of increasing antibiotic resistance. Efforts to inhibit the action of this enzyme have thus far been unsuccessful but insights from this work provide important information that will be used to guide the rational design of future drugs to control the spread of bacteria that harbor the NDM-1 enzyme.

NDM-1 is capable of hydrolyzing (inactivating) the β-lactam ring present in over 60% of antibiotics used in clinics and of working with more than one metal to catalyze the enzymatic reaction. Indeed, NDM-1 has proven to be the ultimate example of a promiscuous enzyme. But the question is, how does it work? Previous studies suggested that the reaction occurs in multiple steps and involves two zinc (or other metal) ions that catalyze the reaction. However, only the first and last steps of the reaction had been visualized by previous structures and the available studies reported different distances between the two metal ions, leaving open the possibility of a number of alternative catalytic mechanisms. The researchers in this study, from Argonne, the University of Texas-Pan American, and Texas A&M University, sought to learn more about the precise catalytic mechanism of NDM-1 by using high-brightness x-rays on the SBC-CAT 19-ID-D beamline at the APS to solve four structures of the enzyme in complex with β-lactam antibiotics and either zinc, manganese, or cadmium ions.

The structure of NDM-1 in complex with ampicillin plus zinc (Fig. 1) and computer-modeling experiments reveal the basis for the promiscuity of NDM-1. The enzyme makes only two main contacts with the substrate, between oxygen molecules on the β-lactam ring and the active site containing the zinc ions. Any additional structural elements on the antibiotic that come off the β-lactam ring are neatly annexed to a spacious and flexible area adjacent to the active site and do not appear to participate in recognition by the enzyme or in catalysis. This allows for catalysis of a wide variety of β-lactam antibiotics without regard to molecular variation beyond the β-lactam ring.

Using a combination of the information gained from the structures and molecular modeling calculations, the team discovered an explanation for the reported discrepancies in the distance between zinc molecules in the NDM-1 active site and learned more about how the catalytic reaction proceeds. Modeling showed that variations in pH result in the presence of either a water molecule (lower pH) or hydroxide ion (higher pH) oriented between the zinc ions and that the differences created by this change can account for the different distances reported in previous NDM-1 structures, which were solved at different pHs. Calculation of the energies involved in the hydrolysis reaction based on the new structures allowed the team to discard the previous hypothesis for catalysis and propose a new mechanism for catalysis that is more energetically favorable and explains differing enzyme efficiencies observed with different metals.

NDM-1 has proven to be difficult to inhibit due to its promiscuous ability to inactivate multiple β-lactam-based antibiotics. However, the knowledge gained in this study has led the team to believe that development of new inhibitors for NDM-1 that focus on structures that contain oxygen molecules that mimic the distance found in β-lactam antibiotics could be successful. The work continues on the discovery of NDM-1 specific inhibitors that will take advantage of the β-lactam recognition by the enzyme. Some promising compounds have been identified already. The race is on as 12 variants of NDM have been found in 15 different strains of pathogenic bacteria all over the world. *— Sandy Field*

See: Youngchang Kim[1], Mark A. Cunningham[2]**, Joseph Mire[3], Christine Tesar[1], James Sacchettini[3], and Andrzej Joachimiak[1]*, "NDM-1, the ultimate promiscuous enzyme: substrate recognition and catalytic mechanism," FASEB J. **27**, 1917 (May 2013). DOI:10.1096/fj.12-224014
Author affiliations: [1]Argonne National Laboratory, [2]University of Texas-Pan American, [3]Texas A&M University
Correspondence: * andrzejj@anl.gov, ** cunningham@utpa.edu

This research was funded in part by a grant from the National Institutes of Health GM094585 (A.J.), GM094568 (J.S.), and by the U.S. Department of Energy Office of Biological and Environmental Research (DOE-BER), under contract DE-AC02-06CH11357. M.A.C. has also received support through the National Science Foundation's FaST program (HRD-0703584), administered by the Department of Educational Programs at Argonne. SBC-CAT is funded by the DOE-BER. Use of the Advanced Photon Source at was supported by the U.S. Department of Energy Office of Science under Contract No. DE-AC02-06CH11357.

19-ID-D • SBC-CAT • Life sciences • Macromolecular crystallography, multi-wavelength anomalous dispersion, subatomic (<0.85 Å) resolution, microbeam, ultra-low-temperature (15K), large unit cell crystallography, single-wavelength anomalous dispersion • 6.5-19.5 keV • On-site, remote, mail-in • Accepting general users •

Does a Yeast Protein Hold the Key to Preventing Premature Aging?

Post-translational lipid modification modulates the function of newly synthesized proteins. A prominent example is the CAAX processing pathway, where a series of enzymes, among them the endoprotease Ste24p, convert immature substrates into functionally active forms. Lipid modification also represents a method to target proteins to membranes, and many classes of drugs are now being developed that target membrane proteins like Ste24p. A number of mutations in this protease cause premature-aging diseases in humans. Also, data suggest that some of the severe side effects in patients receiving certain antiretroviral medications for treatment of acquired immune deficiency syndrome may arise from adverse drug interactions with Ste24p. These proteases therefore represent promising new therapeutic targets. Researchers in this study investigated Ste24p from yeast, using the APS to collect data to solve its crystal structure and to provide a first view of its catalytic site. They showed that Ste24p possesses a new protein fold, consisting of a ring of seven helices that span the membrane and surround a large cavity containing the enzyme's active site and substrate-binding region. These results will be important in guiding future studies in treatment of premature-aging diseases, and in providing insights into the side effects of certain antiretroviral medications for patients with AIDS.

Post-translational modification is a step in protein synthesis that increases the functional diversity of proteins. One type of modification involves the addition of a lipid moiety to the protein. Isoprenoids, a specific class of lipids, are attached to cysteine amino acids near the carboxy termini of specific proteins. These proteins contain a CAAX acceptor sequence for the lipid, which directs the post-translational modification. In this CAAX sequence, C is a cysteine residue, AA represents two aliphatic residues (amino acids with a hydrocarbon side chain), and X is the C-terminal residue. Additional processing steps follow isoprenoid attachment, including cleavage of the AAX amino acids, and carboxymethylation of the now-terminal cysteine.

The CAAX protease Ste24p is a zinc-requiring enzyme that was first identified in yeast, due to its role in the maturation of the yeast mating pheromone a-factor. A similar zinc-requiring protease, ZMPSTE24, is also present in humans. ZMPSTE24 is involved in the processing of prelamin A, a protein which forms a mesh at the inner surface of the nuclear membrane. This mesh, the nuclear lamina, provides mechanical support for the nucleus, and serves to localize protein complexes responsible for transcription, DNA repair, and replication, among other functions. Mutations in ZMPSTE24 lead to improper processing and assembly of prelamin A, leading to a group of diseases called laminopathies which include various premature-aging diseases in humans, the severity of which correlates with the degree of loss of protease activity.

Some antiviral drugs commonly used to treat patients with AIDS also interact with ZMPSTE24, which may lead to some of the severe side effects of these drugs, such as insulin resistance and diabetes.

However, the specific interactions between Ste24p and its substrates, responsible for the proper physiological function of the protease, remained essentially unknown. Consequently, in this study, the researchers from the University of Virginia; the University of Rochester; the Hauptman Woodward Institute; the State University of New York at Buffalo; and the Membrane Protein Structural Biology Consortium, USA, determined the structure of Ste24p from the yeast *Saccharomyces mikatae*, closely related to *Saccharomyces cerevisiae*, common baker's yeast.

Using data collected at the SER-CAT 22-ID-D beamline at the APS, they determined the crystal structure of Ste24p, allowing an initial view of its catalytic site (Fig. 1). They demonstrated that the core structure of Ste24p is a ring of seven helices that span the membrane, surrounding a large cavity containing the enzyme's active site and substrate-binding groove. This cavity is accessible to the membrane via gaps between the transmembrane helices; however, the exact function of the large cavity remains to be determined.

These results provide new information that will be important in guiding future work to investigate the role of lipid modification of proteins in aging processes related to prelamin A processing, and to help develop drugs to treat premature-aging diseases. They will also improve understanding of the

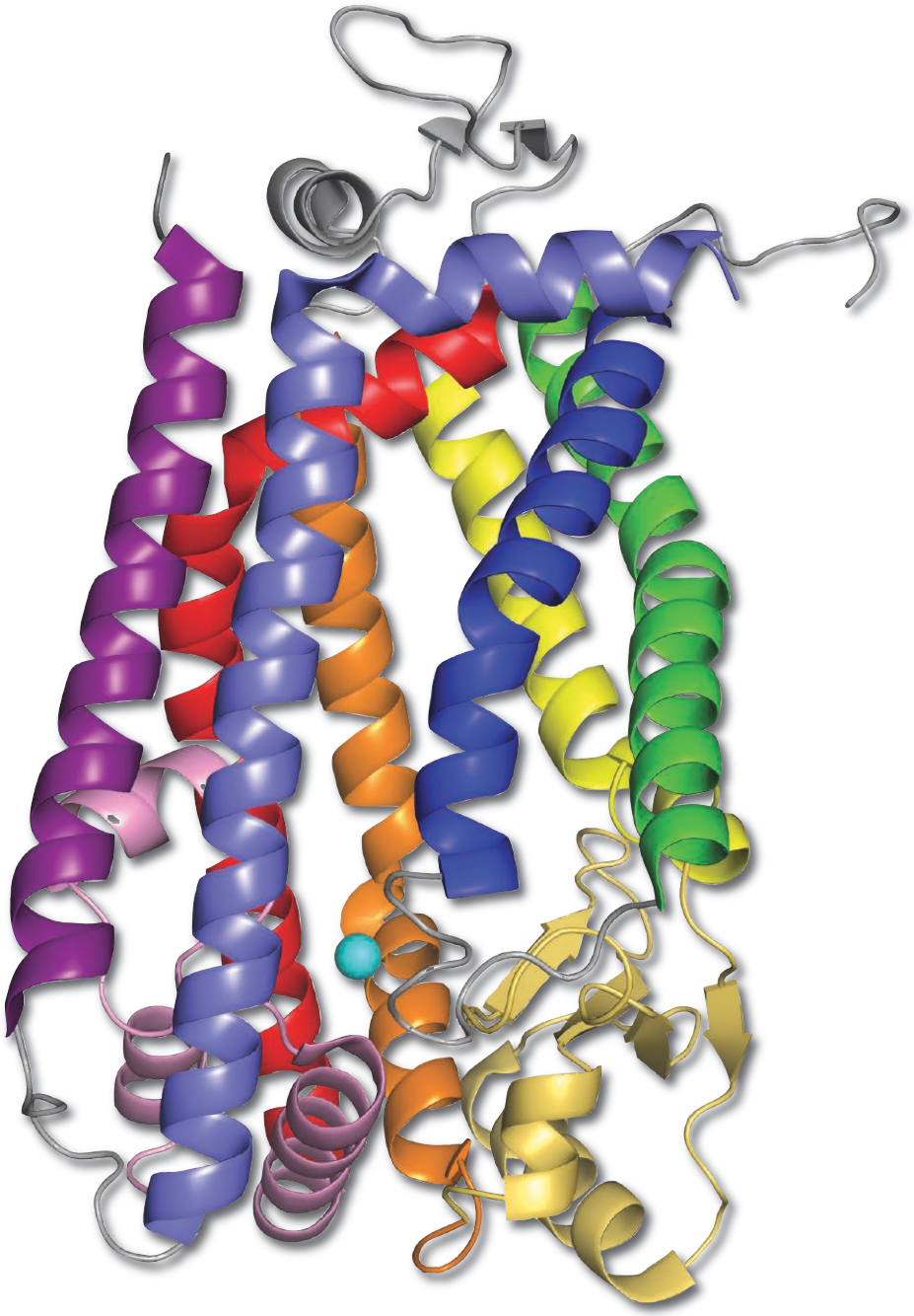

Fig. 1. The overall structure of Ste24p, depicted as a ribbon diagram. The catalytic zinc atom is shown as a cyan sphere.

basis for side effects of some HIV antiviral drugs. – *Nicola Parr*y

See: Edward E. Pryor, Jr.[1,2], Peter S. Horanyi[1,2], Kathleen M. Clark[1,3], Nadia Fedoriw[1,3], Sara M. Connelly[1,3], Mary Koszelak-Rosenblum[1,4], Guangyu Zhu[1,4], Michael G. Malkowski[1,4,5], Michael C. Wiener[1,2*], Mark E. Dumont[1,3,5**], "Structure of the Integral Membrane Protein CAAX Protease Ste24p," Science **339**, 1600 (29 March 2013). DOI:10.1126/science.1232048

Author affiliations: [1]Membrane Protein Structural Biology Consortium, USA; [2]University of Virginia; [3]University of Rochester School of Medicine and Dentistry; [4]Hauptman-Woodward Institute; [5]State University of New York at Buffalo

Corresponding authors:

* mwiener@virginia.edu

** mark_dumont@urmc.rochester.edu

This work was supported by Protein Structure Initiative: Biology grant U54 GM094611 (NIH) for membrane protein structural genomics. SER-CAT is supported by the member institutions found at www.ser-cat.org/members.html. Use of the Advanced Photon Source at Argonne National Laboratory was supported by the U.S. Department of Energy Office of Science under Contract No. DE-AC02-06CH11357.

22-ID-D • SER-CAT • Life sciences • Macromolecular crystallography, multi-wavelength anomalous dispersion, microbeam • 6-20 keV • On-site, remote • Accepting general users •

A Promising Vaccine to Contend against a Fatal Childhood Virus

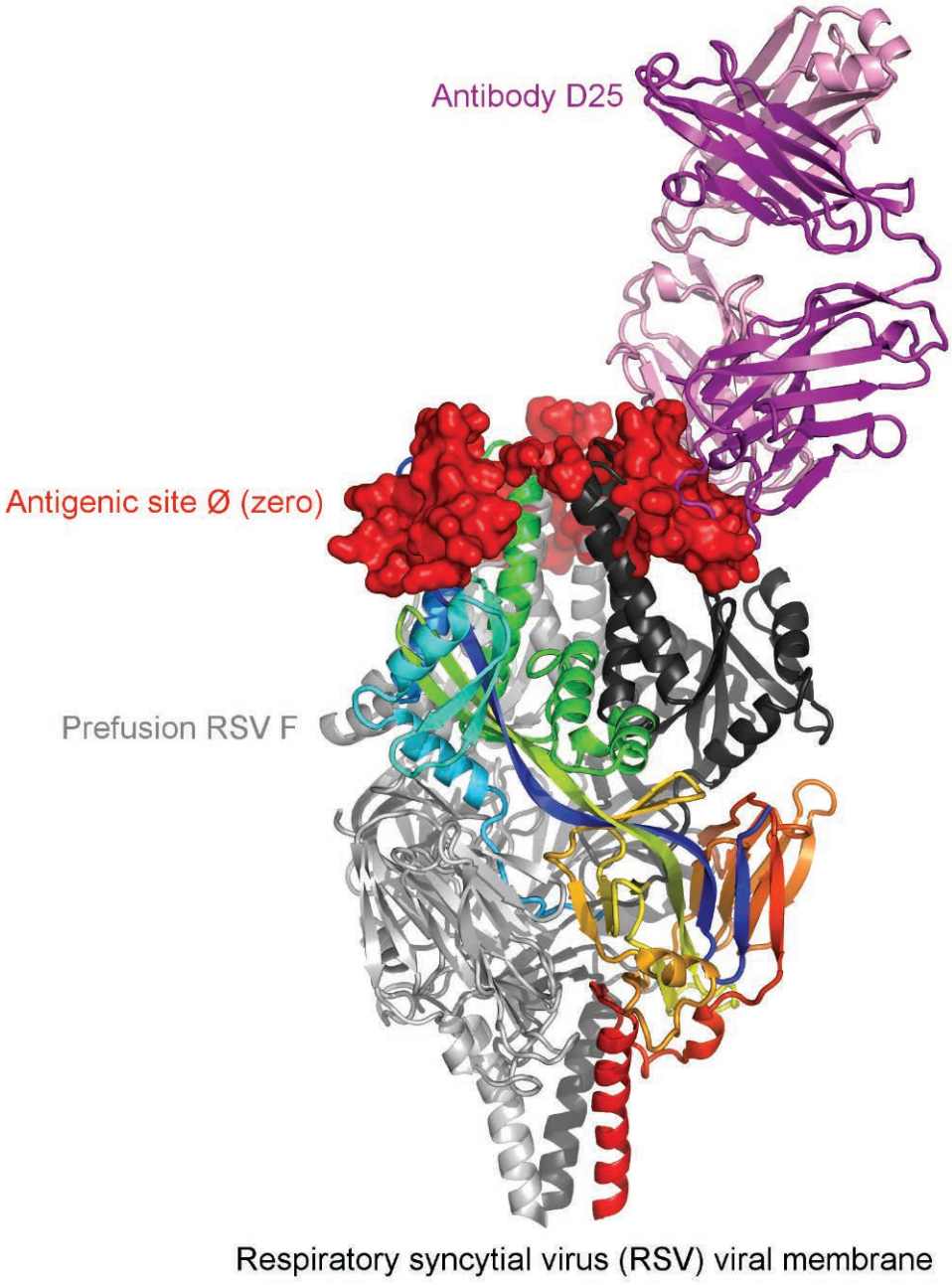

Fig. 1. Structural definition of a neutralization-sensitive site of viral vulnerability. X-ray crystal structure of the human antibody D25 (antigen-binding fragment or Fab, purple) in complex with prefusion respiratory syncytial virus (RSV) F protein (light gray, dark gray, and rainbow) at antigenic site Ø (red).

Respiratory syncytial virus (RSV) is a major cause of respiratory illnesses such as bronchiolitis (inflammation of the small airways in the lung) and pneumonia in infants and children under five years of age. RSV infections are highly contagious and result in 132,000 to 172,000 pediatric hospitalizations per year in the United States alone. Moreover, RSV is an important cause of respiratory illness in adults older than 65 years of age. For almost two decades, structural biologists have actively investigated the design of new, highly potent vaccines against skillfully evasive viruses such as human immunodeficiency virus, hepatitis C, dengue, West Nile, and RSV. Now, a research team utilizing the APS has collected x-ray diffraction data on the fusion (F) glycoprotein of RSV and determined the structure of its prefusion conformation — both by itself and in complex with an antibody called "D25," which binds to antigenic site Ø, a critical antigenic site on RSV F. This approach allowed the team to preserve the display of antigenic site Ø and to elicit neutralizing antibody responses many fold greater than postfusion forms of RSV F protein. Their breakthrough provides a new paradigm for structure-based vaccine design as well as a promising RSV vaccine candidate.

Scientists at the National Institute of Allergy and Infectious Diseases recognized that conformational stability of vaccine immunogens might play a dominant role in vaccine efficacy. Armed with this knowledge, the research group focused on antigenic site Ø. Because antigenic site Ø is exposed on the RSV F protein during the viral prefusion state, before the virus' membrane fuses with the host-cell's membrane, the researchers set out to capture RSV F in its prefusion state (Fig. 1).

The researchers designed several variations of prefusion-stabilized RSV F proteins in the absence of an antibody. They discovered that a few amino acid mutations — S155C-S290C, S190F-V207L, and D486H-E487Q-F488W-D489H — were able to freeze RSV F into its prefusion structure. Utilizing x-ray diffraction data collected at SER-CAT beamline 22-ID-D, the research group from the National Institutes of Health, Frederick National Laboratory for Cancer Research, the Academic Medical Center (The Netherlands), and Xiamen University (China) found three RSV F variants, DS, Cav1, and TriC, that continuously displayed antigenic site Ø and retained binding of the site Ø-specific antibody, D25. Furthermore, creating different combinations of the three variants demonstrated further improvements in D25 binding to antigenic site Ø as well. However, one combination variant in particular, DS-Cav1, proved to be the best, exhibiting reasonable levels of production and good physical stability against changes in pH, temperature, osmality, and freeze-thaw cycles.

The stability of site Ø and its ability to generate highly potent antibodies against RSV were assessed in animals that develop respiratory illnesses similar to humans. Sera from mice and rhesus macaques immunized with the prefusion form of RSV F variant DS-Cav1 were extracted after several weeks to measure its ability to thwart RSV infection in a human cell line. To the researchers' delight, DS-Cav1 showed promise by generating an antibody response that was 40 times higher and 80 times higher (from mice and primates, respectively) than what is considered protective levels in infants.

Although antigenic site Ø is not the only key site on RSV, it appears to be the site most suitable for eliciting neutralizing antibodies against RSV. Therefore, future attempts to design novel vaccines must thoroughly examine all key sites on other evasive viruses to find regions similar to site Ø that are suitable for vaccine design.

— Candice A. Shaifer

See: Jason S. McLellan[1], Man Chen[1], M. Gordon Joyce[1], Mallika Sastry[1], Guillaume B.E. Stewart-Jones[1], Yongping Yang[1], Baoshan Zhang[1], Lei Chen[1], Sanjay Srivatsan[1], Anqi Zheng[1], Tongqing Zhou[1], Kevin W. Graepel[1], Azad Kumar[1], Syed Moin[1], Jeffrey C. Boyington[1], Gwo-Yu Chuang[1], Cinque Soto[1], Ulrich Baxa[2], Arjen Q. Bakker[3], Hergen Spits[3], Tim Beaumont[3], Zizheng Zheng[4], Ningshao Xia[4], Sung-Youl Ko[1], John-Paul Todd[1], Srinivas Rao[1], Barney S. Graham[1]*, and Peter D. Kwong[1]**, "Structure-Based Design of a Fusion Glycoprotein Vaccine for Respiratory Syncytial Virus," Science **342**(6158) 592 (2013). DOI:10.1126/science.1243283

Author affiliations: [1]National Institutes of Health, [2]Frederick National Laboratory for Cancer Research, [3]Academic Medical Center, [4]Xiamen University

Correspondence: * bgraham@nih.gov, ** pdkwong@nih.gov

See also: Jason S. McLellan et al., "Structure of RSV Fusion Glycoprotein Trimer Bound to a Prefusion-Specific Neutralizing Antibody," Science **340**(6136), 1113 (31 May 2013). DOI:10.1126/science.1234914

Support for this work was provided by the Intramural Research Program (National Institute of Allergy and Infectious Diseases) and the National Natural Science Foundation of China (81161120419 and 812111615). Supporting institutions for SER-CAT may be found at www.ser-cat.org/members.html. Use of the Advanced Photon Source at Argonne National Laboratory was supported by the U.S. Department of Energy Office of Science under Contract No. DE-AC02-06CH11357.

22-ID-D • SER-CAT • Life sciences • Macromolecular crystallography, multi-wavelength anomalous dispersion, microbeam • 6-20 keV • On-site, remote • Accepting general users •

Oxygen's Dark Side

We know that fruits and vegetables, green tea, and even wine are healthy for us because they are full of antioxidants. But what do they actually do once we eat them? It turns out that many of the antioxidant compounds found in these health foods activate a pathway in our cells that protects us from cellular damage caused by reactive oxygen species (ROS) that are a normal byproduct of oxygen metabolism. In times of environmental stress, levels of ROS increase, damaging our proteins and DNA, and, sometimes, causing disease. The stress protection pathway is regulated by a protein called Nrf2 that activates over 600 genes that ameliorate the damage caused by ROS. Due to its central role in this important protective process, Nrf2 has been the focus of efforts to find drugs that can treat diseases caused by environmental and oxidative stress. A research team screened more than 250,000 compounds to identify small molecules that activate the Nrf2 pathway. Their work, conducted via x-ray diffraction studies at the LRL-CAT 31-ID-D beamline at the APS, provides new hope for the development of drugs for the treatment of a wide array of diseases including cancer, Alzheimer's disease, cystic fibrosis, asthma, and chronic kidney disease in type 2 diabetes.

Nrf2 is a transcription factor that regulates the expression of genes in the nucleus of the cell. However, it spends most of its time outside of the nucleus in a complex with the Keap1 protein. Keap1 maintains Nrf2 in an inactive state until ROS are detected. If there is no need for activation, Keap1 sends the Nrf2 to the cellular trash removal system, the proteasome, for degradation. If ROS are present, they are able to react irreversibly with cysteine amino acids in the Keap1 molecule and this leads to release of Nrf2 so it can enter the nucleus and activate genes to neutralize the ROS threat.

A number of molecules have been identified that mimic this activation of Nrf2 but, because they also react irreversibly with cysteines (a semi-essential amino acid), these drugs can react with other proteins and this results in off-target interactions that can cause toxic side effects for patients. Therefore, the research team sought to identify small molecules that activate Nrf2 through a new mechanism.

In order to find new compounds that might inhibit the Nrf2/Keap1 interaction, the researchers from Biogen Idec, NoValiX (France), and Evotec AG (Germany), Merrimack Pharmaceuticals, the Celgene Corporation, and Keimyung University (South Korea) screened 267,551 compounds from a chemical library. For their test assay, they measured whether the candidate compounds could inhibit the interaction between the small pieces of Nrf2 and Keap1 that had previously been identified as essential for their interaction. After library screening, 18 possible compounds were identified that fell into two main chemical subclasses, and two promising representatives, compounds 15 and 16, were further investigated.

Compound 15 was co-crystallized with the Keap1 domain and found to bind in a 2:1 stoichiometry (Fig. 1). Also, as they had hoped, the structure revealed that the two molecules of compound 15 interacted through reversible hydrophobic and electrostatic interactions, not through covalent binding to Keap1 reactive cysteines.

Compound 16, which inhibited the Nrf2/Keap1 interaction more strongly in the test assay, was also the only compound found to activate Nrf2 in a cell-based assay. This suggests that, with some molecular tinkering, compound 16 could become an effective drug candidate. Also encouraging was the fact that the crystal structure of the Keap1 domain with compound 16 showed that the interaction was mediated in a manner that involved hydrophobic and electrostatic interactions, but did not involve covalent binding to the active Keap1 cysteine amino acids. The structure also showed that they bound in a 1:1 stoichiometry and identified features of the interaction that explained its improved performance compared to compound 15 and suggested design strategies to improve its inhibitory activity further.

These results are an important first step in identification of the molecular features of chemical inhibitors that might be used to treat a number of conditions where failure to protect cellular components from the damaging effects of oxidative stress is an important factor in the disease. The researchers hope that what they have learned from small molecules like compound16 can be used to develop a specific, effective, and safe Nrf2-activating drug.

— Sandy Field

See: Douglas Marcotte[1], Weike Zeng[1], Jean-Christophe Hus[1], Andres McKenzie[1], Cathy Hession[1], Ping Jin[1], Chris Bergeron[1], Alexey Lugovskoy[1,4], Istvan Enyedy[1], Hernan Cuervo[1,5], Deping Wang[1], Cédric Atmanene[2], Dominique Roecklin[2], Malgorzata Vecchi[1], Valérie Vivat[2], Joachim Kraemer[3], Dirk Winkler[3], Victor Hong[1,6], Jianhua Chao[1], Matvey Lukashev[1], and Laura Silvian[1]*, "Small molecules inhibit the interaction of Nrf2 and the Keap1 Kelch domain through a non-covalent mechanism," Bioorgan. Med. Chem. **21**, 4011 (2013). DOI:10.1016/j.bmc.2013.04.019

Author affiliations: [1]Biogen Idec, [2]NoValiX, [3]Evotec AG, [4]Merrimack Pharmaceuticals, [5]Celgene Corporation, [6]Keimyung University

Correspondence:

* laura.silvian@biogenidec.com

Use of the LRL-CAT beamline was provided by Eli Lilly Company, which operates the facility. Use of the Advanced Photon Source at Argonne National Laboratory was supported by the U.S. Department of Energy Office of Science under Contract No. DE-AC02-06CH11357.

31-ID-D • LRL-CAT • Life sciences • Macromolecular crystallography, single-wavelength anomalous dispersion, single-crystal diffraction • 4.7-28 keV • Mail-in • Accepting general users •

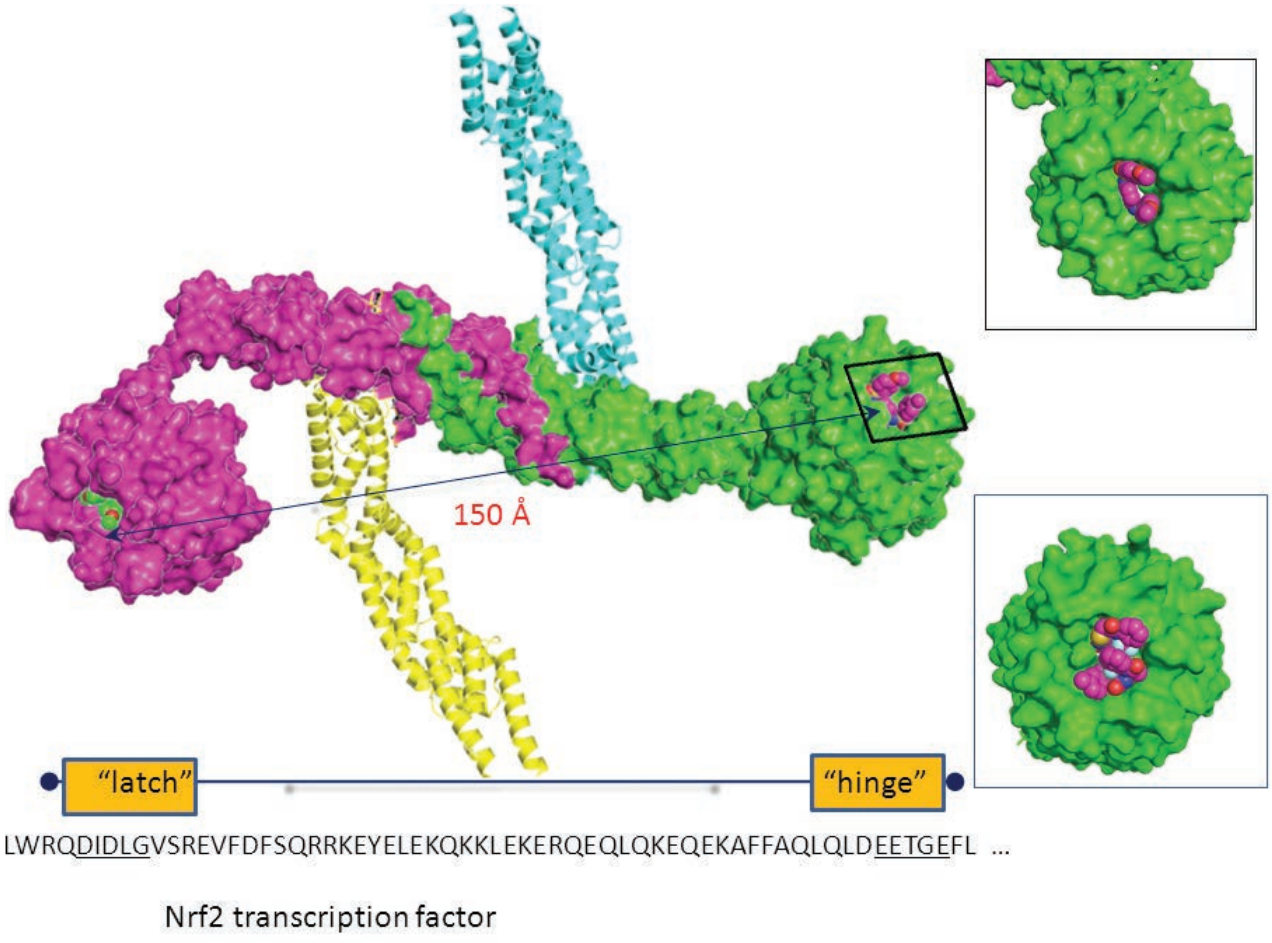

Fig. 1. Model of how compounds 15 and 16 inhibit Nrf2/Keap1 interaction. The full length Keap1 dimer (magenta and green) bound to proteasomal targeting proteins (yellow and blue ribbons) is shown. The insets show how compounds 16 (top) and 15 (bottom) are thought to bind to the Keap1 dimer at each end to block the binding of the "hinge" and "latch" peptide regions within the Nrf2 transcription factor (sequence shown at bottom). The predicted distance between the Keap1 domains (150 Å) matches the distance between the Nrf2 hinge and latch regions. Figure was made using Pymol (The PyMOL Molecular Graphics System, Version 1.7 Schrödinger, LLC.)

The Mechanism of Processive DNA Digestion by Exonuclease I

Enzymes that processively digest single-stranded DNA (ssDNA) and RNA are critical for genome maintenance and gene regulation. The chemistry of the nuclease reaction is understood, but what is not clear is how processive nucleases are able to use energy from digested phosphodiester bond cleavage as fuel. Studies at the LRL-CAT x-ray beamline at the APS are helping to clear up the mystery. Their work adds to the discussion on how ExoI is able to rapidly motor along ssDNA tracks to remove mismatched 3′ bases before it separates.

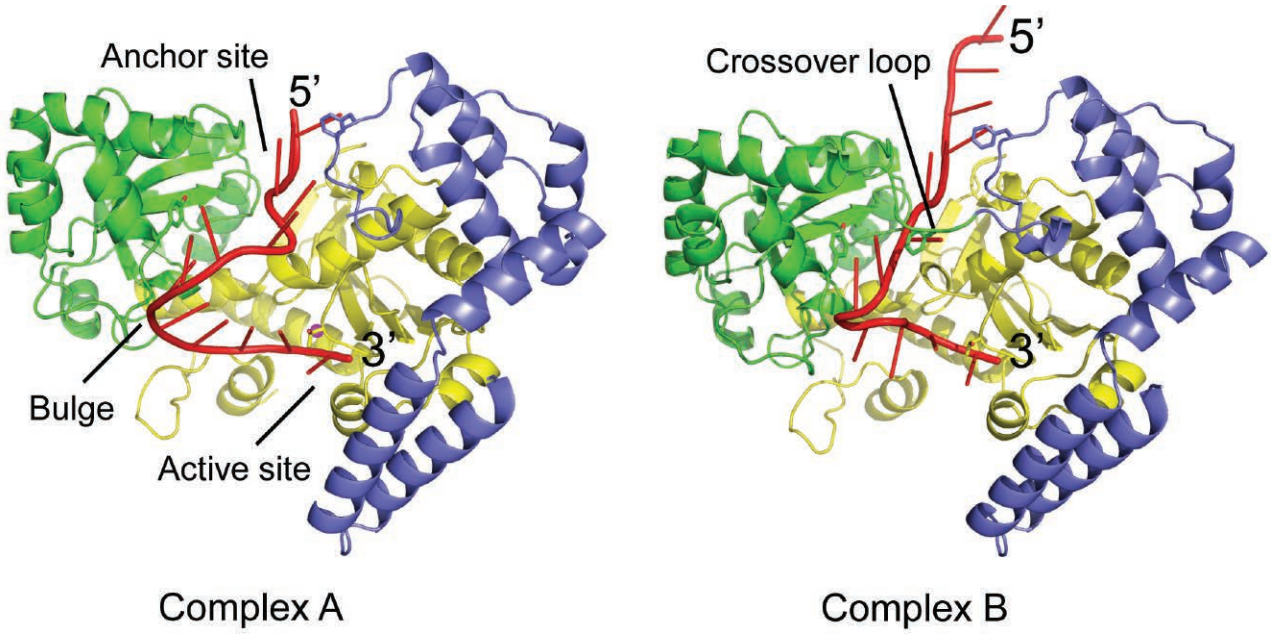

Fig. 1. The structure of the ExoI-dT13 complex reveals two distinct binding modes. The exonuclease domain is yellow, the SH3-like domain green, the C-terminal domain blue, and the ssDNA red. Notice that in Complex A all 13 nucleotides of the dT13 are bound in the groove, whereas in Complex B it is only the first 10.

Previously, scientists have reported that processive digestion of ssDNA by *Escherichia coli* Exonuclease I (ExoI) is so efficient that it occurs at a rate of approximately 275 nucleotides per second. Within the past few decades, researchers have proposed various mechanisms on how ExoI is able to achieve high levels of processivity. Earlier x-ray crystallography studies showed that ExoI is a C-shaped molecule with a large central channel for binding the ssDNA substrate. A loop on the enzyme that crosses over the groove, effectively giving the enzyme an O shape, was proposed to encircle the ssDNA substrate, to account for processivity.

Recently, a research group used the LRL-CAT 31-ID-D beamline at the APS to study ExoI bound to different ssDNA substrates. One ssDNA substrate in particular revealed two separate binding modes of ExoI.

The research team, from The Ohio State University, employed the hanging drop vapor diffusion method, using EDTA (Ethylenediaminetetraacetic acid, a colorless, water-soluble solid utilized to sequester metal ions) to inhibit the enzyme's nuclease activity in order to crystallize ExoI bound to four different Cy5-labeled and unlabeled oligonucleotides. By using this approach, ExoI crystals associated with ssDNA would appear blue and therefore be easily recognized from ExoI not associated with DNA.

One oligonucleotide substrate in particular, 5′-Cy5 labeled-dT13, produced the most detailed x-ray diffraction images of ExoI interacting with ssDNA and was used for the bulk of this study. While the ssDNA bound to the enzyme in more or less the expected manner, with the 3′-end in the active site and the downstream (5′-) end threaded under the crossover loop, a surprising result was that the two independent copies of the structure seen in the crystal, referred to as Complexes A and B, revealed remarkably distinct binding modes.

The difference between complexes A and B was found only in the shape of the DNA when bound to ExoI — the conformation of the ExoI itself was essentially unchanged.

In complex A, all 13 nucleotides are in contact with the ExoI DNA-binding groove, but in complex B, only the first 10 nucleotides enter the groove. In both complexes, the downstream (5′-) end of the ssDNA is bound by an extensive and equivalent set of interactions to an "anchor" site on the enzyme.

However, due to the difference in registration, in complex A nucleotides 11-13 are bound to the anchor site, while in complex B, it is nucleotides 8-10 (counting from the 3′-end) (Fig. 1). In complex A, the 3′-end of the ssDNA inserts into the active site, where the phosphate that is cleaved binds to a Mg^{2+} ion in a near catalytic-configuration. In complex B, however, the 3'-end does not reach fully into the active site, and there is no Mg^{2+}. The researchers thus proposed that complex A is likely to represent a catalytic state, while complex B represents a post-catalytic state.

Based on these structures, the authors propose a mechanism in which, starting with complex A, three rounds of cleavage from the 3′-end, without displacement of the nucleotides bound to the anchor site, results in the structure seen in complex B. Since the ssDNA in complex B is too short to reach the active site, further rounds of cleavage would require forward movement of the enzyme along the ssDNA, to generate a new complex A. The model thus predicts a "stepping" mechanism, in which a translocation step of 3 nucleotides forward alternates with three rounds of cleavage.

A plausible mechanism for ExoI's processivity has thus been established. However, the proposed stepping mechanism will require further studies for validation. In particular, whether or not both of the complexes observed in the crystal are likely to be biologically relevant remains to be determined.

— Candice A. Shaifer

See: Sai Krishna C. Korada, Trevor D. Johns, Christopher E. Smith, Nathan D. Jones, Kimberly A. McCabe and Charles E. Bell*, "Crystal structures of *Escherichia coli* exonuclease I in complex with single-stranded DNA provide insights into the mechanism of processive digestion," Nucleic Acids Res. **41**(11), 5887(June 2013). DOI:10.1093/nar/gkt278.

Author affiliation:
The Ohio State University
Correspondence: * bell.489@osu.edu

This research was funded by the National Science Foundation (MCB-1021066 to C.E.B.). Use of the Lilly Research Laboratories Collaborative Access Team beamline was provided by Eli Lilly Company, which operates the facility. Use of the Advanced Photon Source at Argonne National Laboratory was supported by the U.S. Department of Energy Office of Science under Contract No. DE-AC02-06CH11357.

31-ID-D • LRL-CAT • Life sciences • Macromolecular crystallography, single-wavelength anomalous dispersion, single-crystal diffraction • 4.7-28 keV • Mail-in • Accepting general users •

How Receptors Work

Without complex biochemical pathways and their component molecules, the human body could not function. Yet the extremely intricate nature of these systems can both baffle researchers and take decades to characterize. A driving force for understanding the structure and function of cellular pathways is that many drug therapies and much medical progress depend upon acquiring this knowledge. Persistence and advances in methodology are key tools in unraveling the components of protein systems, especially when it comes to the receptors that activate those proteins. Both of these tools were used by a research team to greatly advance what we know about a G-protein-coupled receptor (GPCR) important to a wide array of human metabolic reactions. The research team used structural data collected at the APS to gain important new insights that will aid in developing drugs to treat many diseases, especially those involving the central nervous system and metabolic disorders.

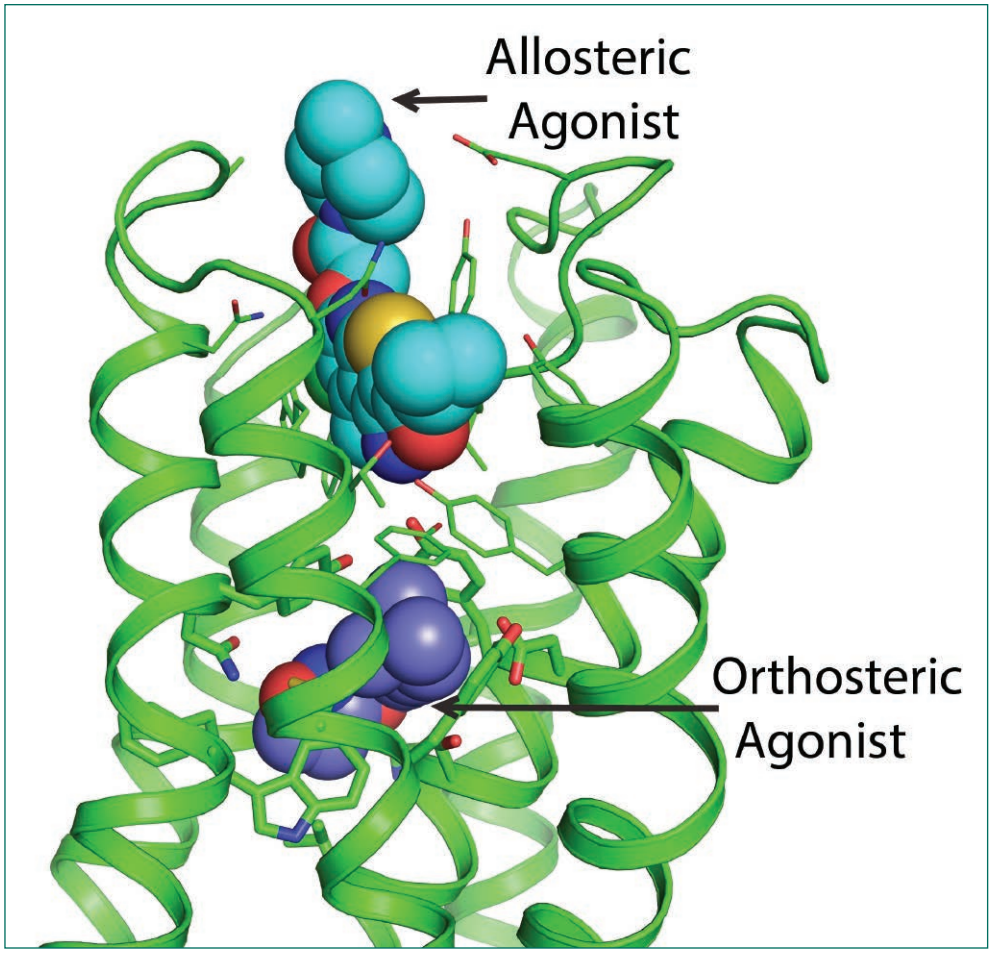

Fig. 1. Binding pockets for the M2 muscarinic receptor, occupied by orthosteric and allosteric agonists.

The researchers from Stanford University, the National Institute of Diabetes and Digestive and Kidney Diseases, Friedrich Alexander University (Germany), Vrije Universiteit Brussel (Belgium), VIB (Belgium), Monash University (Australia), and Eli Lily & Co. focused on a class of GPCRs called muscarinic acetylcholine receptors because of their key roles as activators of G proteins in many different human biochemical pathways. In particular they studied the M2 muscarinic receptor, which is important to cardiac functions, cognition, and pain perception. The M2 receptor — one of the first GPCRs identified — had been previously studied in some detail because it binds small molecules, an important attribute for using it to develop new drug therapies. Though the structure of the M2 receptor was known, this was only when it was in the inactive state. So the research team set out to answer the following questions: What does the M2 receptor look like when it is active and bound to a drug? What changes in shape occur to allow the receptor to achieve this structure and activate the appropriate cascade of subsequent reactions?

To find answers to these questions, the team had to overcome methodological problems created by the flexibility and instability of the crystallized receptor, problems that had impeded earlier characterization of the active M2 receptor. The GM/CA-XSD 23-ID-B and 23-ID-D microfocus beamlines at the APS were essential for obtaining diffraction data integral to solving these structures. The researchers were able to stabilize the M2 structures in an active state by binding them to a high-affinity G protein mimetic camelid antibody fragment as well as a high-affinity agonist, and by doing so they obtained definitive crystal structures.

Several seminal details arose from the structural analyses of the M2 receptor in its active state bound to a drug-like molecule. All three regions of the receptor (the extracellular vestibule, the binding pocket, and the intracellular surface) are involved. Expected changes in the intracellular structure were observed but unexpected were the significant extracellular shape changes that occurred. By carefully analyzing details of the binding site, the researchers were able to propose a mechanism for binding of the orthosteric agonist that includes contraction of the outer binding pocket, thereby forming the binding pocket for the allosteric agonist (Fig. 1). Details such as these are critical to designing drugs that effectively and efficiently reach their targets and thereby constitute a major breakthrough for use of the M2 receptor in therapeutics.

Future research will include identifying new orthosteric and allosteric drugs and understanding how their binding influences both the dynamics and conformations of the receptor. Achieving the latter goal will require developing strategies for applying EPR and NMR spectroscopy to studying muscarinic receptor dynamics.

By developing ways to observe the muscarinic receptor bound to drug-like molecules, the research team was able to observe more pronounced shape changes than had been previously observed, underscoring how important it is to study particular interactions when asking how receptor binding occurs. The team's work is key to progress in drug design and therapeutics for treating human diseases. *— Mona Mort*

See: Andrew C. Kruse[1], Aaron M. Ring[1], Aashish Manglik[1], Jianxin Hu[2], Kelly Hu[2], Katrin Eitel[3], Harald Hübner[3], Els Pardon[4,5], Celine Valant[6], Patrick M. Sexton[6], Arthur Christopoulos[6], Christian C. Felder[7], Peter Gmeiner[3], Jan Steyaert[4,5], William I. Weis[1], K. Christopher Garcia[1], Jürgen Wess[2], and Brian K. Kobilka[1]*, "Activation and allosteric modulation of a muscarinic acetylcholine receptor," Nature **504**, 101 (5 December 2013). DOI:10.1038/nature12735

Author affiliations: [1]Stanford University School of Medicine, [2]National Institute of Diabetes and Digestive and Kidney Diseases, [3]Friedrich Alexander University, [4]Vrije Universiteit Brussels, [5]VIB, [6]Monash University, [7]Eli Lilly & Co.
Correspondence:
* kobilka@stanford.edu

This research was supported by the National Science Foundation (graduate fellowship to A.C.K., and Award 1223785 to B.K.K.), the Stanford Medical Scientist Training Program(A.M., A.M.R.), the American Heart Association (A.M.), the Ruth L. Kirschstein National Research Service Award (A.M.R.), National Institutes of Health (NIH) Grants NS02847123 and GM08311806 (B.K.K.), the Mathers Foundation (B.K.K., W.I.W., K.C.G.), the Deutsche Forschungsgemeinschaft for the Grant GM13/10-1 (K.E., H.H., P.G.), the National Health and Medical Research Council (NHMRC) of Australia program Grant 519461 (P.M.S., A.C.), NHMRC Principal Research Fellowships (P.M.S., A.C.), and the Howard Hughes Medical Institute (K.C.G.). This work was supported in part by the Intramural Research Program, the National Institute of Diabetes and Digestive and Kidney Diseases, NIH, and the U.S. Department of Health and Human Services (J.H., K.H., J.W.). GM/CA-XSD is funded in whole or in part with Federal funds from the National Cancer Institute (Y1-CO-1020) and the National Institute of General Medical Sciences (Y1-GM-1104). Use of the Advanced Photon Source at Argonne National Laboratory was supported by the U.S. Department of Energy Office of Science under Contract No. DE-AC02-06CH11357.

23-ID-B • GM/CA-XSD • Life sciences • Macromolecular crystallography, microbeam, large unit cell crystallography, subatomic (<0.85 Å) resolution, multi-wavelength anomalous dispersion, single-wavelength anomalous dispersion • 3.5-20 keV • On-site, remote • Accepting general users •

23-ID-D • GM/CA-XSD • Life sciences • Macromolecular crystallography, microbeam, large unit cell crystallography, subatomic (<0.85 Å) resolution, multi-wavelength anomalous dispersion, single-wavelength anomalous dispersion • 5-20 keV • On-site, remote • Accepting general users •

Unveiling the Complexities of Hairpin Telomere Formation

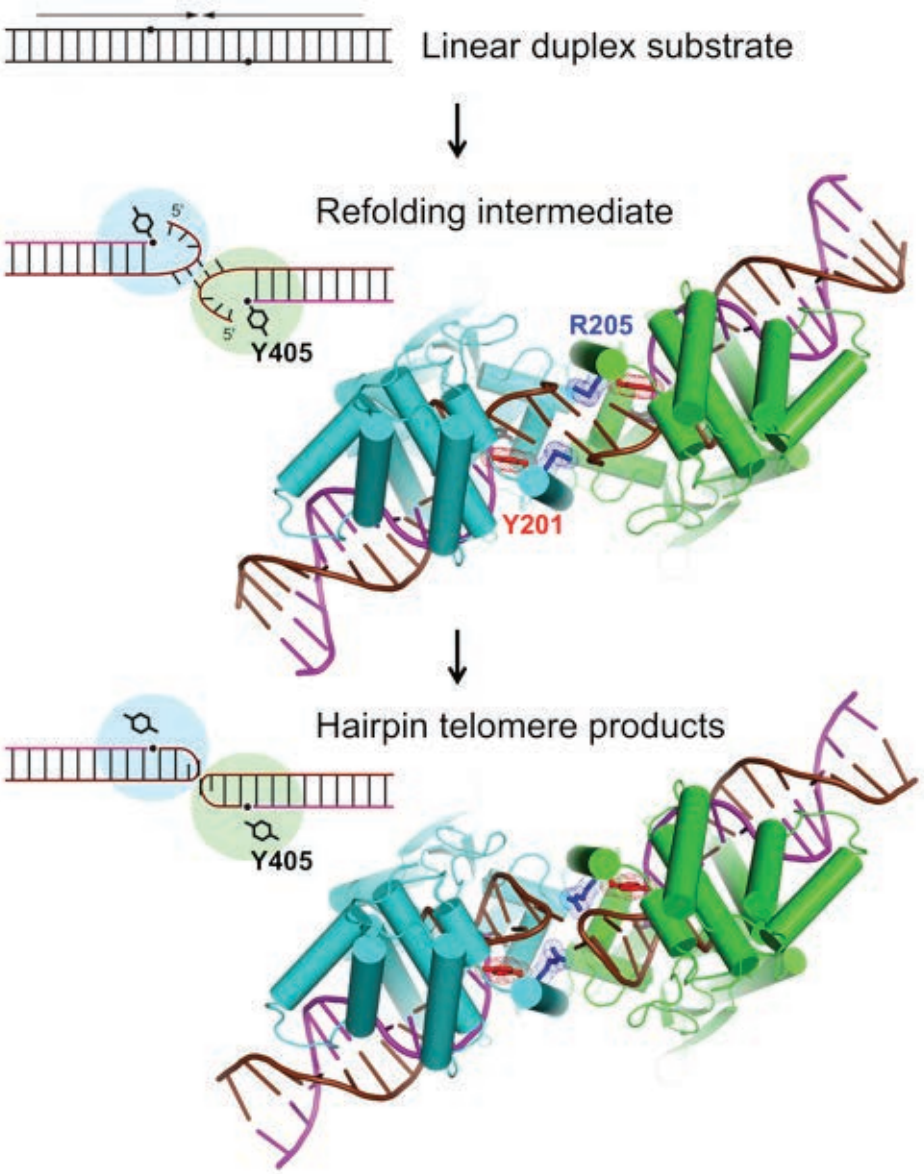

In order for a bacterial cell to survive, it must be able to maintain the integrity of its genetic information, as well as ensure the stability of replicated chromosomes (compact structures of tightly packed genomic DNA), which are distributed between daughter cells during cell division. Bacteria that package their genomic DNA in the form of linear chromosomes face a particular challenge in that the ends of these structures are especially prone to damage from DNA degradation or from aberrant repair reactions. In these bacteria, the ends of the chromosomes, also known as "telomeres," are folded into tight hairpins that protect the DNA while permitting accurate replication of genetic material at the chromosome's ends. Research at the APS has produced a clearer understanding of this process, which is important for the development of protelomerase inhibitors that may be useful in treating certain bacterial infections.

Replication of linear chromosomes in bacteria such as Borrelia spirochetes, the causative agent of Lyme disease, begins in the center of the chromosome and proceeds in two directions, forming a single circular DNA molecule composed of two identical chromosomes. This "concatamer" must then be "resolved" by a specialized enzyme, protelomerase, yielding two intact chromosomes with hairpin ends, or telomeres.

Researchers from the University of Minnesota and the University of Utah Health Sciences Center utilized x-ray crystallography on the Agrobacterium protelomerase, TelA, to define the unique mechanism by which protelomerase actively stabilizes transitional DNA structural states as it refolds linear DNA into highly structured hairpin telomeres. Diffraction data of several DNA: TelA complexes, in which TelA is trapped in different stages of hairpin formation (Fig. 1), were collected at the BioCARS 14-BM-C and 14-ID-B beamlines and the Northeastern Collaborative Access Team 24-ID-C beamline of the APS.

During cell division, the linear bacterial chromosome begins the process of duplication in its center, which proceeds bi-directionally, toward the ends. This mode of replication results in a circular DNA molecule composed of two complete chromosomes joined at their ends. Before they can be distributed between daughter cells, however, the chromosomes must be separated. The enzyme, protelomerase, cuts the DNA concatamer at the appropriate position, yielding two identical chromosomes, and folds the resulting DNA ends into highly compact, hairpin structures.

The current study employs x-ray crystallography to understand how the protelomerase present in *Agrobacterium tumefaciens*, TelA, is able to carry out this reaction. Researchers were able to trap TelA at various stages in this ordered reaction by solving several crystal structures of TelA bound to different DNA folding intermediates and hairpin products. Atomic structures of each enzymatic step allowed researchers to propose a model for TelA activity in which the enzyme facilitates formation of energetically strained hairpins through stabilizing folding intermediate with a set of DNA: TelA interactions entirely different from those that stabilize the end product hairpins. The role of specific protein residues were confirmed through mutagenesis based experiments.

The mechanism proposed here, in which TelA cleaves and refolds its substrate through active stabilization of folding intermediates, is novel, and may be conserved among protelomerases in other bacterial species, or between enzymes involved in reshaping molecules in other cellular contexts. *— Emma Hitt*

< Fig. 1. Model for hairpin telomere formation by protelomerase TelA (left), based on crystallographic data (right). Linear duplex DNA (brown and magenta) is bound by a TelA dimer (cyan and green), which cleaves the DNA and folds its ends into hairpin structures. TelA amino acids arginine (R) 205 (blue) and tyrosine 201(red) are dispensable for DNA cleavage, but required for formation of the folding intermediate and hairpin formation.

See: Ke Shi[1], Wai Mun Huang[2], and Hideki Aihara[1]*, "An Enzyme-Catalyzed Multistep DNA Refolding Mechanism in Hairpin Telomere Formation," PLoS Biol. **11**(1), e1001472 (2013). DOI:10.1371/journal.pbio.1001472
Author affiliations: [1]University of Minnesota, [2]University of Utah Health Sciences Center
Correspondence: * aihar001@umn.edu

This work was supported by National Institutes of Health grant R01 GM095558 (H.A.) and National Science Foundation grant MCB-0213124 (W.M.H.). BioCARS is supported by the National Institute of General Medical Sciences of the National Institutes of Health under grant number R24GM111072. The NE-CAT beamlines are funded by NE-CAT member institutions and by the National Institute of General Medical Sciences of the National Institutes of Health. Use of the Advanced Photon Source, at Argonne National Laboratory was supported by the U.S. Department of Energy Office of Science under Contract No. DE-AC02-06CH11357.

14-BM-C • BioCARS • Life Sciences, macromolecular crystallography, fFiber diffraction, biohazards at the BSL2/3 level, subatomic (<0.85 Å) resolution, large unit cell crystallography • 8-14.9 keV • On-site • Accepting general users •

14-ID-B • BioCARS • Life sciences, materials science, physics, chemistry • Time-resolved crystallography, time-resolved x-ray scattering, Laue crystallography, wide-angle x-ray scattering, biohazards at the BSL2/3 level, macromolecular crystallography • 7-19 keV • On-site • Accepting general users •

24-ID-C • NE-CAT • Life sciences • Macromolecular crystallography, microdiffraction, single-wavelength anomalous dispersion, single-crystal diffraction, microbeam • 6.5-23 keV • On-site, remote • Accepting general users •

Shedding Light on Cyanobacterial Photoreceptors

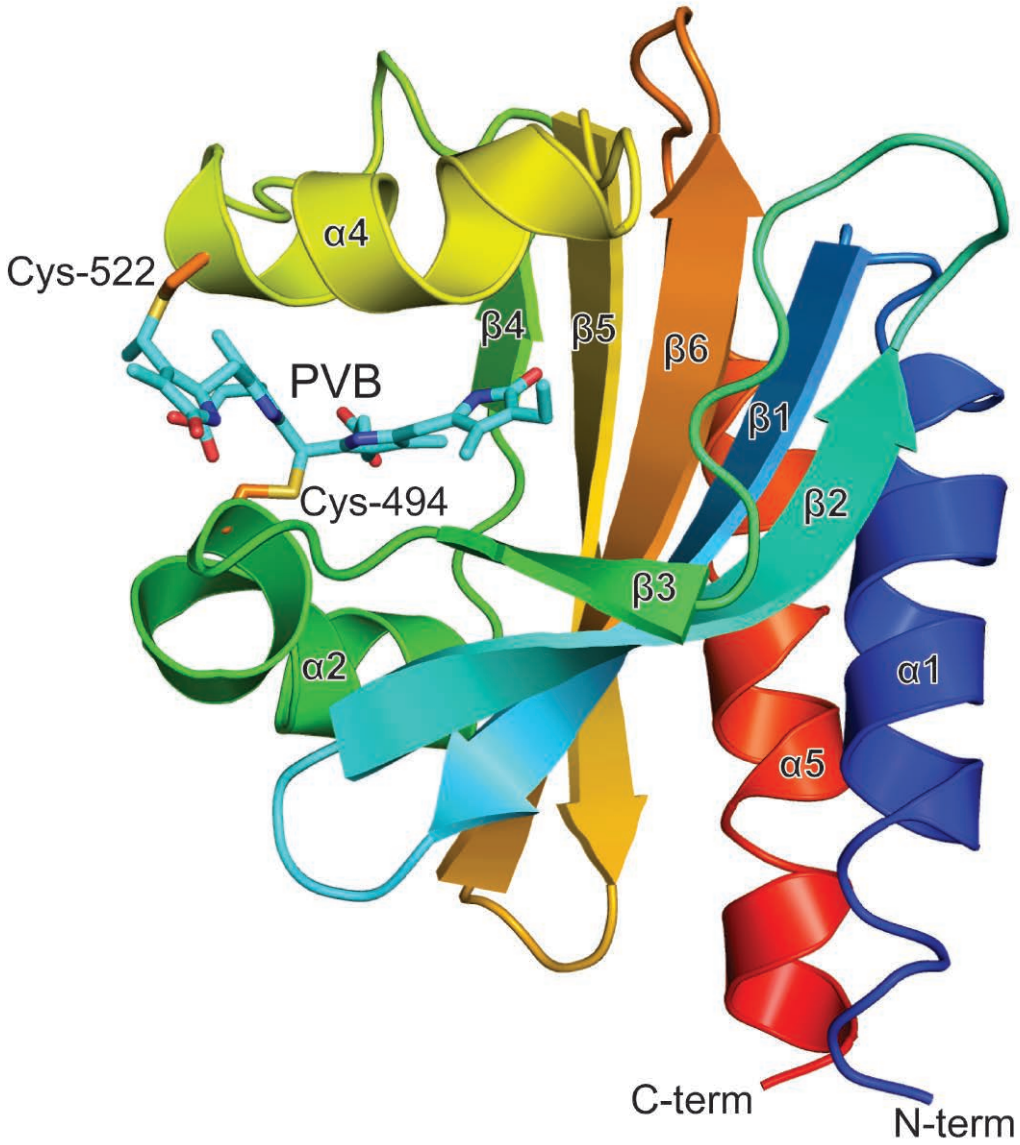

Fig. 1. Structure of the *Thermosynechococcus elongatus* PixJ GAF-domain. A ribbon diagram of the polypeptide chain of the PixJ GAF-domain is colored from blue to red to show the progression of the polypeptide chain from the N-terminal to C-terminal ends. The phycoviolobilin chromophore and covalently bound cysteine side chains are shown as sticks. For the stick diagram, the phycoviolobilin carbons are colored cyan and the cysteine side chain carbons are colored orange. Additionally, nitrogens, oxygens, and sulfurs are colored blue, red, and yellow, respectively. α-helices and β-strands are numbered, and the cysteines 494 and 522, which form thioether bonds with phycoviolobilin, are labeled.

Plants and photosynthetic microorganisms rely on light as their chief energy source and utilize photoreceptors to provide information to the cell about light duration, spectral distribution, and light intensity. Among these remarkable photoreceptors are the phytochromes. Most phytochromes work by reversibly converting between a red-light absorbing ground state and a far-red-light-absorbing active state. However, recent work has shown that some cyanobacteria have specialized light sensors, called cyanobacteriochromes (CBCRs), which are able to absorb additional colors of light. In fact, some species contain many CBCRs that collectively can detect the entire visual spectrum of light. Work at the APS has provided the first structure of a CBCR, called *Te*PixJ. Solution of the three-dimensional structure of this CBCR illustrates how cyanobacteria have tinkered with nature to alter the spectral sensitivity of these unique photoreceptors. In addition, the work verified a new model for how this family of CBCRs works and resulted in the discovery of possible new role for CBCRs: the ability to act as temperature sensors. Understanding the basic biochemistry of these unique phytochromes will impact work in human health, food production, and renewable energy production where possible uses of cyanobacteria are being explored.

Phytochromes house light-sensitive bile pigments (bilins) that absorb light by virtue of their ability to change shape when they absorb light. Light-activated changes in bilin shape are propagated via a photosensory module to the phytochrome output module and result in changes in plant function and development including chloroplast formation and energy production, seed germination, flowering, and position-sensing.

The CBCR photosensory module is more varied than that of typical phytochromes. The common feature among CBCRs is the presence of at least one GAF domain. CBCR GAF domains incorporate the chromophore phycocyanobilin (PCB). But distinct structural or chemical differences among the CBCR GAF-domains permit responses to wavelengths of light that differ from each other and from the red/far-red photocycles of typical phytochromes. The photosensory modules of CBCRs may contain one GAF domain, several GAF domains that are daisy-chained together, or GAF domains positioned in series with other domains. For photosensory modules containing multiple GAF domains, the photocycles of the individual GAF domains might occur independently from each other, giving them exquisite sensitivity to light, and potentially yielding specific responses to multiple light conditions.

*Te*PixJ belongs to the DXCF family of CBCRs, and is photoconvertible between blue and green light-absorbing states. Its photosensory module contains one GAF domain that is linked to the output module. Studies have suggested that DXCF CBCRs convert PCB into phycoviolobilin and additionally form a second linkage between the bilin and the protein. However, it was unclear where the second cysteine linked to the bilin, how the novel features of phycoviolobilin were utilized, and thus, how *Te*PixJ and other DXCF-type CBCRs work mechanistically.

Thanks to diffraction data collected at the LS-CAT 21-ID-G beamline at the APS, researchers from the University of Wisconsin-Madison were able to determine the location of the second cysteine linkage between the protein and the chromophore, and verified structural features consistent with a phycoviolobilin-like chromophore. Remarkably, the structure shows that the second cysteine linkage subdivides the chromophore so one side absorbs blue light and the other absorbs ultraviolet. Breaking the bond modifies the chromophore so that it absorbs green light.

The structural data coupled with further biochemical studies support a hypothesis in which irradiation of the ground state with blue light leads to rupture of the second cysteine linkage and produces a bilin with a photoreceptor system that absorbs green light. The associated bilin-dependent structural changes then presumably cause reciprocal changes in the GAF domain that are propagated throughout the molecule leading to signal transduction.

Interestingly, data collected in this study also showed that reversion to the CBCR ground state is temperature dependent, suggesting that responses to light might be more favored at low temperatures and may diminish at higher than optimal temperatures. This unexpected result means that the CBCRs like *Te*PixJ might also serve as temperature sensors. This discovery will be the subject of future research.

— Sandy Field

See: E. Sethe Burgie, Joseph M. Walker, George N. Phillips, Jr.‡, and Richard D. Vierstra*, "A Photo-Labile Thioether Linkage to Phycoviolobilin Provides the Foundation for the Blue/Green Photocycles in DXCF-Cyanobacteriochromes," Structure **21**(1), 88 (January 8, 2013). DOI:10.1016/j.str.2012.11.001

Author affiliation: University of Wisconsin-Madison. ‡Present address: Rice University

Corresponding author:
vierstra@wisc.edu

This work was supported by grants from the National Science Foundation (MCB 1022010) and the University of Wisconsin College of Agricultural and Life Sciences (Hatch) to R.D.V. LS-CAT is supported by the Michigan Economic Development Corporation and the Michigan Technology Tri-Corridor (Grant 085P1000817). Use of the Advanced Photon Source at Argonne National Laboratory was supported by the U.S. Department of Energy Office of Science under Contract No. DE-AC02-06CH11357.

21-ID-G • LS-CAT • Life sciences • Macromolecular crystallography • 12.7 keV • On-site, remote, mail-in • Accepting general users •

The Protein is Greater Than the Sum of Its Domains

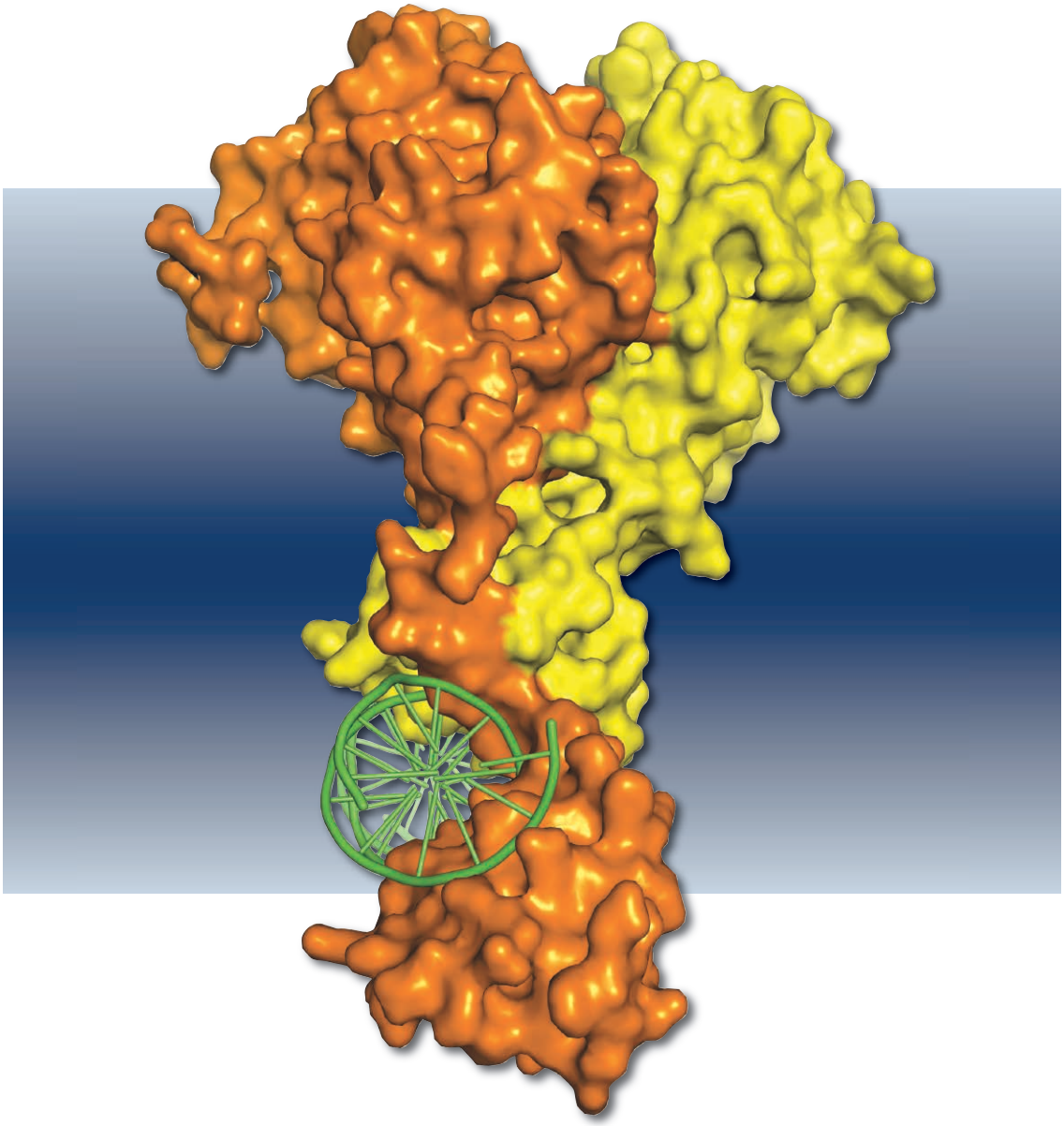

Fig. 1. The multi-domain structural organization of the homodimeric HNF-4α nuclear receptor; each member of the dimer is shown, one in yellow, one in orange bound to its DNA response element (green).

Over the past few decades, eliminating technical obstacles has allowed researchers to solve the three-dimensional structures of ever-larger molecules. Now, it is possible to solve the structures of large complexes and understand the subtleties of the interactions between the different parts of the complex. This is exemplified in recent studies by researchers from the Sanford-Burnham Medical Research Institute and Argonne. In work completed at the APS, they solved the structure of the hepatocyte nuclear factor 4α (HNF-4α) in complex with its DNA recognition site and activating cofactors. Elucidation of the structure of the HNF-4α complex provides new insights into how protein domains interact with each other over large molecular distances and suggests ways in which the HNF-4α protein complex could be targeted for treatment of metabolic conditions, such as maturity-onset diabetes of the young, type 1, a rare type of diabetes; and a condition called hyperinsulinemic hypoglycemia, both of which are caused by mutations in this gene.

HNF-4α is an important regulator of genes involved in the way our bodies metabolize lipids and sugars. This is highlighted by the fact that the DNA sequence that HNF-4α recognizes is present in an estimated 40% of liver genes and 11% of pancreatic genes. Mutations in HNF-4α have been associated with a rare form of diabetes called maturity onset diabetes of the young (MODY) and a condition known as hyperinsulinemic hypoglycemia in which the body makes too much insulin.

HNF-4α acts as a complex that consists of two copies of the protein, each one with a DNA-binding domain and an activator-binding domain. What is not clear, however, is how the complex is regulated by the metabolic events that it responds to. In order to address this question, Rastinejad's team crystallized HNF-4α in a complex with a small piece of DNA containing the HNF-4α recognition site and its required activator peptides.

What they found was surprising.

First, although the three-dimensional structure derived from x-ray diffraction data collected at the SBC-CAT 19-ID-D beamline shows that the two DNA-binding domains interact with the DNA recognition elements as expected, complex interactions between one of the DNA-binding domains and the two activator-binding domains results in an asymmetric organization of the complex that straddles only one of the DNA binding sites rather than both as previously thought (Fig. 1). Further experiments showed that high-affinity DNA binding is only possible when these three domains are present.

Second, when the research team looked at two amino acids that are known to act as "on/off" switches for HNF-4α binding to DNA, they found that the sites were curiously distant from DNA in the complex. The structure of the complex shows that when the on switch, Arg 91, is modified, it acts at the cooperating surface between the two activator-binding domains to "glue" them to the DNA binding domain and ensure high affinity binding. The off switch, Ser 78, is located on the "wrong" side of the DNA-binding domain to interfere directly with DNA binding, but acts at a distance by interfering with an amino acid involved in the cooperation between the activator-binding domains and DNA-binding domain.

The team hypothesize that the interface between the four domains of the dimer creates a domain convergence center that receives and propagates signals to finely control gene expression. Their work shows that the three-dimensional configuration of the protein on DNA creates a setting in which identical subunits act within unique environments, a finding that would never have been possible with the structures of individual subunits.

This highlights the idea that, although previous structures of the domains of these proteins were informative, one cannot simply extrapolate that the domains work in a linear "domains-on-a-string" orientation in the full complex.

More practically, examination of mutations that have been identified in patients with maturity-onset diabetes of the young, type 1, and hyperinsulinemic hypoglycemia showed that some of them also appear to act from a distance through the domain convergence center. *— Sandy Field*

See: Vikas Chandra[1], Pengxiang Huang[1], Nalini Potluri[1], Dalei Wu[1], Youngchang Kim[2], and Fraydoon Rastinejad[1]*, "Multidomain integration in the structure of the HNF-4α nuclear receptor complex," Nature **495**, 394 (21 March 2013). DOI:10.1038/nature11966

Author affiliations: [1]Sanford-Burnham Medical Research Institute, [2]Argonne National Laboratory

Correspondence:

* frastinejad@sanfordburnham.org

This work was supported by National Institutes of Health grants R01 DK094147 and R01 DK097475. SBC-CAT is funded by the U.S. Department of Energy Office of Biological and Environmental Research. Use of the Advanced Photon Source, at Argonne National Laboratory was supported by the U.S. Department of Energy Office of Science under Contract No. DE-AC02-06CH11357.

19-ID-D • SBC-CAT • Life sciences • Macromolecular crystallography, multi-wavelength anomalous dispersion, subatomic (<0.85 Å) resolution, microbeam, ultra-low-temperature (15K), large unit cell crystallography, single-wavelength anomalous dispersion • 6.5-19.5 keV • On-site, remote, mail-in • Accepting general users •

How Bacteria Use Their Metabolism to Compete in Nature

Most bacteria use multiple compounds as carbon sources for growth. Carbon catabolite repression (CCR) is a regulatory mechanism used by bacteria to establish a hierarchy of sugar utilization, ensuring that carbohydrate sources are selected for use in an optimal sequence. This mechanism is important to allow bacteria to compete in their natural environments, because selection of the preferred carbon source is a key factor affecting growth rate. Researchers utilized the APS to collect data that will be important in guiding future studies to evaluate the processes used by bacteria to regulate their metabolism and compete successfully with other microorganisms in their environment.

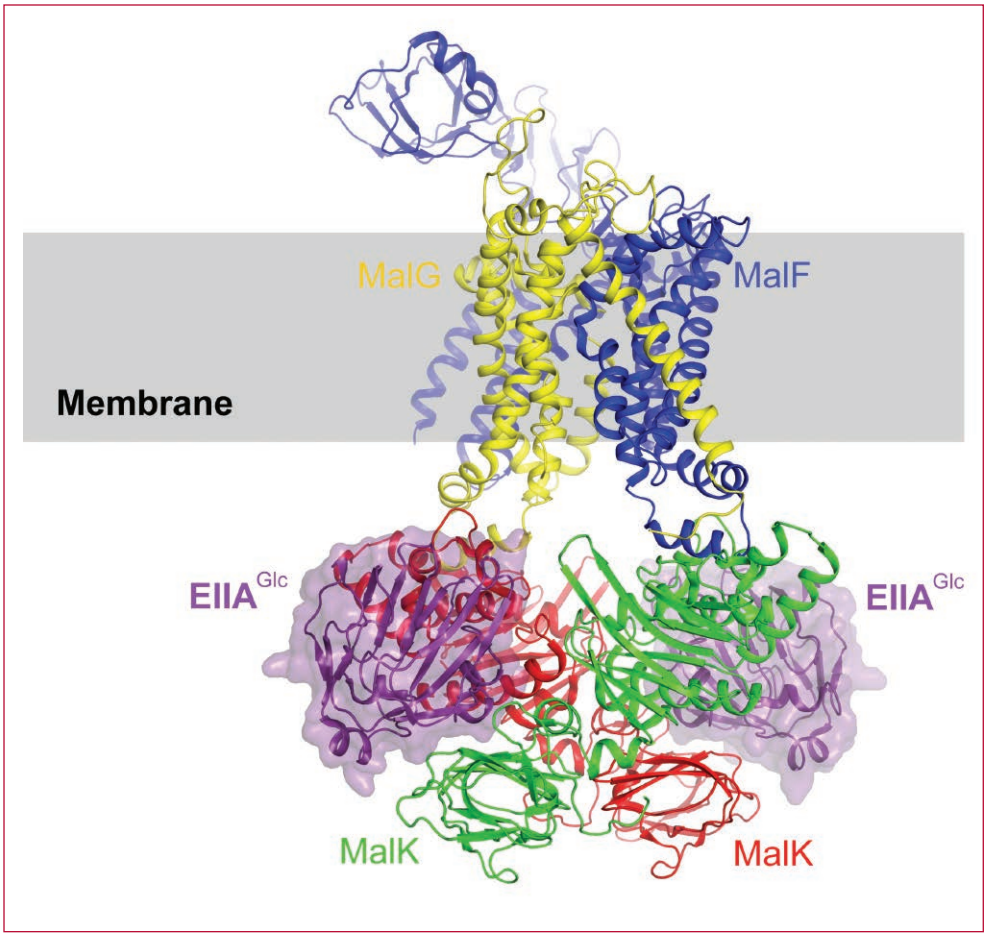

Fig. 1. Crystal structure of the $EIIA^{Glc}$-maltose transporter complex.

In order to compete and survive in their environment, bacteria must optimize their energy usage. To achieve this, many have developed a system that enables them to select substrates from a mixture of carbon sources, and preferentially take up carbohydrates that allow rapid growth.

CCR is one of the most important mechanisms of genetic regulation in bacteria. This is where products accumulate in the cell after a substance is broken down, and inhibit the formation of enzymes involved in the breakdown of other substances. In this way, they can select carbon sources with high nutritional value first.

This selection mechanism occurs mainly at the level of carbohydrate-specific induction. Most genes involved in carbohydrate breakdown are regulated by specific control proteins and inducers, so they can be silenced by direct control of these proteins and inducers.

In intestinal bacteria such as *Escherichia coli*, glucose-specific enzyme IIA ($EIIA^{Glc}$) is a central regulator of CCR. It forms part of the glucose-specific phosphotransferase system (PTS), a cascade of processes that controls carbohydrate transport via phosphorylation reactions. In its unphosphorylated state, $EIIA^{Glc}$ binds to and inhibits various transporters when glucose or other PTS substrates are available for use. One of these transporters is the maltose transporter, a transmembrane protein that uses energy from breakdown of adenosine triphosphate (ATP), the cell's energy currency, to carry out biological processes. Unphosphorylated $EIIA^{Glc}$ also prevents glycerol utilization by binding to glycerol kinase, an enzyme important in glycerol metabolism. These carbohydrates or their derivatives serve as inducers to control the production of transporters and enzymes. Consequently, binding of $EIIA^{Glc}$ with the transporter directly prevents secondary carbon source uptake, and also dampens the expression of the corresponding breakdown system by reducing the levels of the inducer.

However, the underlying molecular mechanism involved in this process has remained unclear due to the lack of known crystal structures for $EIIA^{Glc}$ in combination with transporter molecules.

In this study, researchers from Purdue University and the Howard Hughes Medical Institute aimed to investigate the crystal structure of the maltose transporter bound with $EIIA^{Glc}$. The researchers performed crystallization experiments using different combinations of cofactors, to determine whether the *Escherichia coli* $EIIA^{Glc}$ binds to the transporter in the resting state, or an intermediate conformation induced by maltose-binding protein (MBP) and/or ATP. MBP is part of the system involved in uptake and breakdown of maltodextrins which are carbohydrates made up of glucose chains.

Using data sets collected from x-ray diffraction studies at the GM/CA-XSD 23-ID-D and NE-CAT 24-ID-C beamlines at the APS, they determined the crystal structure of *Escherichia coli* $EIIA^{Glc}$ in complex with the maltose transporter (Fig. 1), showing how 2 unphosphorylated $EIIA^{Glc}$ molecules bind to the cytoplasmic subunits of ATPase, the enzyme responsible for breakdown of ATP. This stabilizes the transporter in its resting state, an inward-facing configuration, and prevents structural changes needed for ATP breakdown, thus preventing maltose transport when glucose is available. Upon glucose depletion, $EIIA^{Glc}$ becomes phosphorylated and can no longer bind to the maltose transporter. To start maltose uptake, MBP and ATP bind, and a structural change in the transporter produces an outward-facing configuration that allows transfer of maltose to the transporter, and positions ATP at the enzyme's catalytic site for hydrolysis. Maltose is then released into the cytoplasm, returning the transporter to its resting state.

This study is the first to demonstrate the crystal structure of the regulatory enzyme $EIIA^{Glc}$ in complex with a carbohydrate transporter, and suggest a model of how preventing structural changes in this transporter can prevent maltose uptake in *Escherichia coli*. The results will be important in guiding future work to investigate the mechanisms by which bacteria coordinate their metabolism, and how they can degrade compounds in nature. They may also have implications in the design of biotechnological processes.

— Nicola Parry

See: Shanshuang Chen[1], Michael L. Oldham[2], Amy L. Davidson[1], and Jue Chen[1,2], "Carbon catabolite repression of the maltose transporter revealed by X-ray crystallography," Nature **499**, 364 (18 July 2013).
DOI:10.1038/nature12232
Author affiliations: [1]Purdue University, [2]Howard Hughes Medical Institute
Correspondence:
* chenjue@purdue.edu

This work was supported by a National Institutes of Health grant (GM070515 to J.C. and A.L.D.). 085P1000817). GM/CA-XSD is funded in whole or in part with Federal funds from the National Cancer Institute (Y1-CO-1020) and the National Institute of General Medical Sciences (Y1-GM-1104). NE-CAT is supported by a grant from the National Institute of General Medical Sciences (P41 GM103403) from the National Institutes of Health. Use of the Advanced Photon Source at Argonne National Laboratory was supported by the U.S. Department of Energy Office of Science under Contract No. DE-AC02-06CH11357.

23-ID-D • GM/CA-XSD • Life sciences • Macromolecular crystallography, microbeam, large unit cell crystallography, subatomic (<0.85 Å) resolution, multi-wavelength anomalous dispersion, single-wavelength anomalous dispersion • 5-20 keV • On-site, remote • Accepting general users •

24-ID-C • NE-CAT • Life sciences • Macromolecular crystallography, microdiffraction, single-wavelength anomalous dispersion, single-crystal diffraction, microbeam • 6.5-23 keV • On-site, remote • Accepting general users •

A Novel Mechanism for $GABA_B$ Receptor Activation

Electrical signaling in the brain requires a delicate balance of excitatory and inhibitory messages. Disrupting this balance can have disastrous consequences. For example, malfunctioning $GABA_B$ receptors, a G-protein-coupled receptor for GABA — the primary inhibitory neurotransmitter in the central nervous system — can lead to serious neurological disorders such as spasticity and epilepsy. Numerous drugs with closely related physical structures can target the $GABA_B$ receptor to regulate nervous system function. Whether a drug activates or inactivates the receptor depends on subtle structural characteristics. Knowing the precise physical anatomy of the $GABA_B$ receptor will help researchers identify molecules that can target the receptor more efficiently. Studies carried out at the APS provided the first x-ray crystal structures of the extracellular portion of the $GABA_B$ receptor, in both its resting and active states. The receptor's two subunits were found to remain open at rest, while just one of the subunits closed upon agonist binding. These results yield insights about a novel mechanism for the activation of a G-protein-coupled receptor.

The $GABA_B$ receptor belongs to a distinct class of receptors called "metabotropic G-protein-coupled receptors." When an agonist ligand, such as GABA or the muscle relaxant Baclofen, binds and activates the $GABA_B$ receptor, a cascade of intracellular chemical events is kicked off. The result is the opening of K+ channels embedded in the neuronal membrane. In most cases, potassium rushes out of the cell, leaving it in a hyperpolarized state and thereby reducing the probability of future action potentials. Other kinds of ligands, called antagonists, bind the receptor but fail to activate it due to small variations in their molecular composition. Therefore, the structural match between drugs and the $GABA_B$ receptor determines ligand function.

Most of the knowledge about the architecture of metabotropic receptors comes from x-ray crystallography of glutamate receptors. Those receptors are assembled from homomeric, or structurally identical, subunits, whereas the $GABA_B$ receptor is assembled from heterodimeric, or structurally unique, subunits. Researchers from Columbia University working at the NE-CAT 24-ID-C and 24-ID-E beamlines at the APS captured x-ray crystal structures of the heterodimeric complex between GBR1 and GBR2 subunits, bound with various agonists and antagonists, as well as in the absence of ligands. Having snapshots of these various configurations provides researchers with valuable information about the molecular mechanisms underlying ligand recognition, receptor activation, and the assembly of heterodimeric receptor subunits.

The team discovered that the GBR1 and GBR2 subunits have very similar overall structures, consistent with their 33% sequence homology. However, only GBR1 subunits were able to bind ligands, likely due to small differences in the molecular connections between the two lobes comprising each of the subunits. While GBR2 always assumed an open configuration, the lower lobe of GBR1 folded inward into a closed configuration when bound by an agonist, like one half of a Venus flytrap attempting to ensnare a fly. At rest, with no ligand bound to the receptor, both subunits assumed an open configuration. The same open-open configuration was maintained when each of six different antagonists was bound to the receptor, consistent with its inactivated state.

Further analysis of the $GABA_B$ receptor structure indicated that interactions between the lower lobes of GBR1 and GBR2 caused GBR1 to bind agonists more tightly. Mutagenesis of various inter-lobe residues revealed that these interactions were, in fact, necessary for receptor activation. Other mutagenesis experiments identified the roles of various residues in regulating agonist and antagonist binding. Additionally, small molecular variations in the lower lobe of GBR1 were found to affect the receptor's affinity for different antagonists.

The high-resolution morphological details of the $GABA_B$ receptor captured with x-ray crystallography can help researchers identify both agonists and antagonists that more efficiently target the receptor. In addition, the discovery of the $GABA_B$ receptor's novel mechanism for activation adds to the overall understanding of metabotropic receptor composition and function.

— Chris Palmer

See: Yong Geng, Martin Bush, Lidia Mosyak, Feng Wang, and Qing R. Fan*, "Structural mechanism of ligand activation in human $GABA_B$ receptor," Nature **504**, 254 (12 December 2013). DOI:10.1038/nature12725

Author affiliation: Columbia University
Correspondence: * qf13@columbia.edu

This work was supported by the American Heart Association grant SDG0835183N and the National Institute of Health grant R01GM088454 (both to Q.R.F.). Q.R.F. is an IrmaHirschl Career Scientist, Pew Scholar, McKnight Scholar and Schaefer Scholar. Health. NE-CAT is supported by a grant from the National Institute of General Medical Sciences (P41 GM103403) from the National Institutes of Health. Use of the Advanced Photon Source at Argonne National Laboratory was supported by the U.S. Department of Energy Office of Science under Contract No. DE-AC02-06CH11357.

24-ID-C • NE-CAT • Life sciences • Macromolecular crystallography, microdiffraction, single-wavelength anomalous dispersion, single-crystal diffraction, microbeam • 6.5-23 keV • On-site, remote • Accepting general users •

24-ID-E • NE-CAT • Life sciences • Macromolecular crystallography, microbeam, microdiffraction, single-wavelength anomalous dispersion, single-crystal diffraction • 12.68 keV • On-site, remote • Accepting general users •

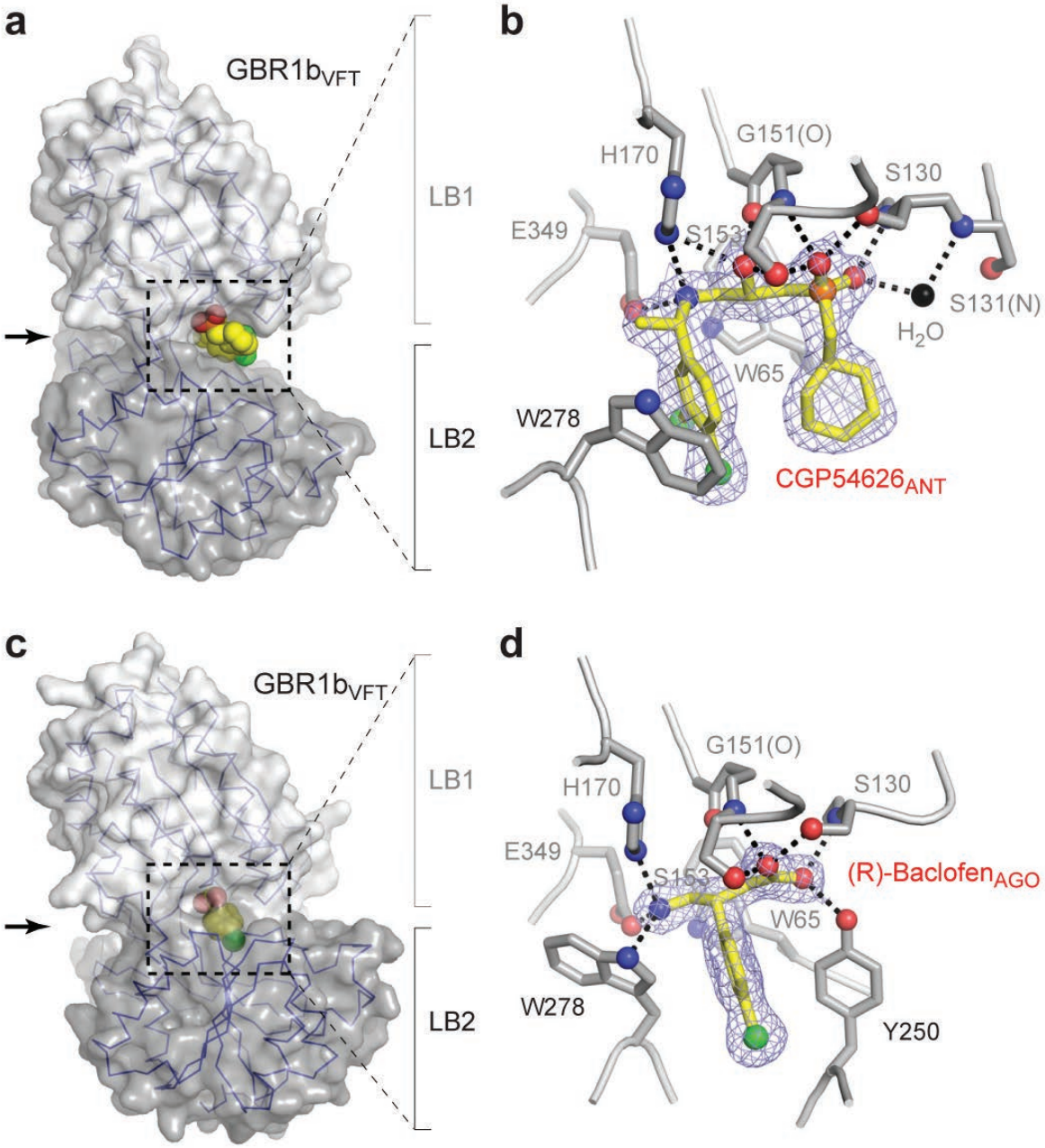

Fig. 1. Ligand recognition by the GBR1b$_{VFT}$ subunit of the GABA$_B$ receptor. Upper: The antagonist CGP54626 binds the subunit in a crevice between its two lobes, LB1 and LB2. Upon binding, the subunit maintains an open, or inactivated, configuration. Lower: Binding by the agonist (R)-Baclofen causes the lower lobe to swing into a closed position, activating the receptor.

Taking a Snapshot of Mammalian Translation

Protein synthesis, specifically its initiation, is a multifaceted process within the cell that is often affected in a variety of cancers, degenerative diseases, and viral infections. Researchers carrying out studies at the APS revealed the molecular mechanism involved in this process. This work uncovers details of the molecular mechanisms specific to efficient translation initiation in eukaryotes, provides a model system for crystallographic studies of mammalian translation, and may help in the development of therapeutics for the treatment of diseases that involve disruption of these processes.

The researchers from Yale University determined the way in which the ribosomal pre-initiation complex scans mRNA as it searches for a start codon (a signal within the mRNA for translation to start), and the associated structural changes that occur once translation from RNA to protein begins. Using low-resolution x-ray crystallography, the Yale researchers were able to identify snapshots of initiation complexes that helped define interactions between the ribosome, translation initiation factors, initiator tRNAi, and mRNA at critical points of translation initiation.

This work uncovers details of the molecular mechanisms specific to efficient translation initiation in eukaryotes (cells with a nucleus) and provides a model system for crystallographic studies of mammalian translation. The research may also help in the development of therapeutics for the treatment of diseases that involve disruption of these processes.

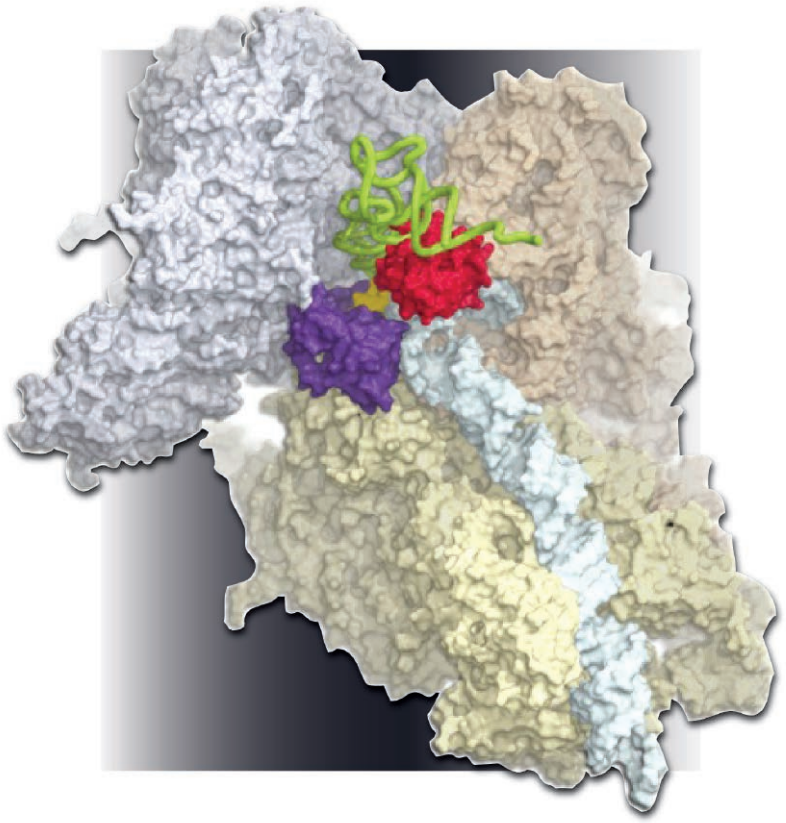

Fig. 1. Structure of the rabbit 48S pre-initiation complex. Initiation factor eIF1A (violet), initiator tRNAi (green), and mRNA (yellow) are shown bound to the 40S ribosomal subunit (grey and tan). The position of initiation factor eIF1 (red), crystallized with 40S in the absence of other factors is shown in this model, demonstrating the steric clash that occurs with tRNAI in the P-site as the base pairing interactions with the mRNA start codon are established. This clash forces eIF1 dissociation from the ribosome, promoting attachment of the large ribosomal subunit and subsequent peptide synthesis.

Proteins are made within the cell through a process in which DNA is transcribed to mRNA, and then mRNA is translated into proteins. In eukaryotes, translation initiation occurs when a preinitiation complex consisting of the small ribosomal 40S subunit, initiation factors, and initiator tRNAi are recruited to one end of an mRNA molecule. This pre-initiation complex scans the mRNA until it locates a certain sequence called the start codon. tRNAi then pairs with the mRNA, after which the large ribosomal subunit joins the complex, and translation of the encoded protein begins. Marilyn Kozak first proposed the so-called "scanning hypothesis" of eukaryotic translation initiation in 1978, and the intervening years have yielded a wealth of biochemical data that has helped further refine this model. However, the exact molecular mechanisms underlying mRNA scanning and initiation complex formation are not fully known.

To further define these interactions, the researchers obtained diffraction data utilizing the NE-CAT 24-ID-C beamline at the APS. They determined three separate crystal structures of the rabbit 40S ribosomal subunit in complex with the initiation factors eIF1, eIF1, and eIF1A, and with mRNA, tRNAi, and eIF1A (Fig. 1). These structures showed the interactions in each functional state and highlighted their differences.

In the proposed model, mRNA is

"Snapshot" cont'd. on page 147

The Structural Complexities of tRNA Transcriptional Regulation

Transfer RNAs (tRNAs) are non-coding, highly structured RNA molecules responsible for delivering amino acids, the building blocks of proteins, to the cell's protein biosynthetic machine, the ribosome. Maintaining appropriate cellular levels of amino-acid-carrying tRNAs (i.e., "charged" tRNA) is important for optimal cellular function. Many bacterial species, including pathogens, use structured RNAs, or "riboswitches," to specifically sense cellular amino acid levels and guide the production of amino-acid metabolic genes accordingly. A team of researchers utilized x-ray crystallography at the APS and another U.S. Department of Energy Office of Science synchrotron light source to examine the interaction between $tRNA^{Gly}$ (the tRNA that carries the amino acid glycine) and the stem I domain of the *glyQ* T-box riboswitch (Fig. 1). Findings from this research may be applied to understanding other T-box riboswitches, which are widespread in transcriptional control of amino acid metabolism, and are prevalent in pathogens such as *Listeria* and *Staphylococcus*. An increased understanding of these mechanisms may contribute to development of antibiotics that target RNA-RNA interactions, aiding in the fight against increasingly problematic drug-resistant bacterial infections.

The researchers from the National Heart, Lung and Blood Institute of the National Institutes of Health determined the structural basis for riboswitch recognition of tRNA. High-resolution diffraction data of the tRNA: riboswitch co-crystal was collected at a resolution of 3.2 Å, and was acquired at the NE-CAT 24-ID-C and 24-ID-E beamlines at the APS using an x-ray wavelength of 0.9729 Å. Additional data were collected at beamlines 5.0.1 and 5.0.2 of the Advanced Light Source (Lawrence Berkeley National Laboratory).

Transcription is the cellular process by which DNA is copied into RNA. Transcribed RNA is often mRNA (messenger RNA that encodes a protein sequence to be translated by the ribosome), but it can also be functional non-coding RNA (regulatory RNA that does not encode protein). Finely controlled transcription is an important aspect of bacterial adaptation to stress and environmental change, and the cell has evolved numerous ways to guide transcription appropriately.

One widespread and abundant control mechanism is through riboswitches, non-coding RNA domains at the beginning of mRNA transcripts, which determine whether continued

"Complexities" cont'd. on page 147

Fig. 1. Structure of the T-box stem I domain (blue) in complex with $tRNA^{Gly}$ (green) and the K-turn binding protein YbxF (grey). The interaction between the highly structured 102 nucleotide stem I and the L-shaped tRNA is surprisingly extensive.

A Structural Basis for Metabolic Advantage in Cancer

Cancerous cells face an increased demand for the nutrients and the cellular building blocks required to support rapid growth and proliferation. A team of researchers utilized x-ray crystallography at an APS beamline to uncover a mechanistic basis for an increase in glycolytic metabolism observed in many types of cancers. Study of the crystal structures of the metabolic enzyme phosphoglycerate mutase 1 (PGAM1) allowed researchers to determine how switching on PGAM1, through phosphorylation (addition of a phosphate), promotes conformational changes that lead to hyperactivity of this protein, and thus an increase in glycolytic metabolism. The highly active version of this protein is found in diverse cancers, including leukemia and solid tumors, suggesting a widespread mechanism by which cancer cells can sustain a metabolic advantage, as well as a potential for the use of phosphorylated PGAM1 detection as a cancer diagnostic marker and potentially a target for cancer therapeutics.

Many normal human proteins can contribute to cancer development when the genes that encode them are mutated. These oncogenes produce proteins with altered activity, leading to overproduction of growth signals, or underproduction of factors that keep cell growth under control.

One of the ways in which cancer cells are able to grow more quickly than their normal counterparts is through a shift in their metabolic pathways, sequential chemical reactions in the cell used to generate energy, to favor those pathways that produce energy at a level that would be excessive for a healthy cell. One example of this type of shift is the Warburg effect, the observation that even when oxygen is available to cancer cells, a condition that normally mandates the use of a metabolic pathway known as oxidative phosphorylation, cancer cells will continue to utilize glycolysis, a metabolic pathway generally reserved for times when the cell does not have access to oxygen. These cancer cells also take up more glucose from the environment than normal tissue.

Proteins that add phosphate groups, called tyrosine kinases, promote proliferation of many types of cancer; however, the way in which they

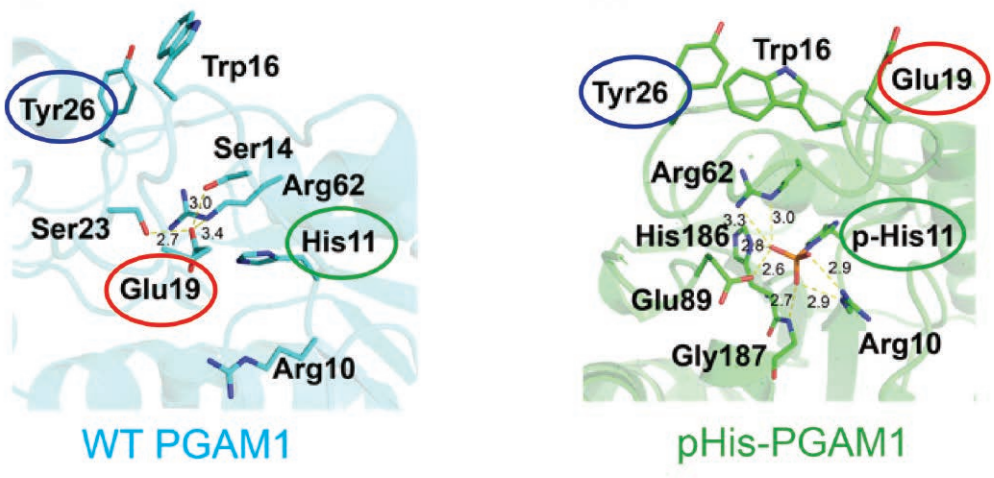

Fig. 1. Structures of normal, or "wild-type," un-phosphorylated, and thus inactive, PGAM1 (blue), and active PGAM1 (green) phosphorylated at His11 (green circle). The relative positions of Glu19 (red circle) in the inactive and active forms of PGAM1 indicates that binding of activating metabolite 2,3-bisphosphoglycerate is blocked by this residue, and suggests that phosphorylation of Tyr26 (blue circle) may stabilize the active conformation of Glu19, promoting hyperactivity of this enzyme in cancer cells.

mediate the cancer-related changes in cellular metabolism is not well understood. In this study, researchers from the Emory University School of Medicine, The University of Chicago, Cell Signalling Technology, Inc., Princeton University, the Chinese Academy of Sciences, and the Yale University School of Medicine investigated the enzyme phosphoglycerate mutase 1 (PGAM1), a protein that is activated through the transfer of a phosphate to one of the tyrosine amino acids contained within PGAM1, called Tyr26.

Using x-ray crystallography at the LS-CAT 21-ID-F and NE-CAT 24-ID-C beamlines at the APS, the researchers compared the structures of the active phosphorylated form of PGAM1 to that of the unmodified, inactive version of the protein.

Based on these data, researchers proposed a model in which phosphorylation of PGAM1 Tyr26 induces a conformational change in the protein that

"Basis" cont'd. on page 147

"Snapshot" cont'd. from page 144
threaded through the tunnel formed by the 40S latch, keeping it unstructured as it is inspected by tRNAi. As tRNAi passes over the mRNA, the initiation factor eIF1 competes with initiator tRNAi for a specific location (the P-site) within the 40S subunit, preventing non-specific base pairing between the tRNAi and mRNA. Once the tRNAi locates the start codon, however, the interaction between the tRNAi and mRNA is strong enough to displace eIF1, halting scanning and locking the initiator tRNAi in place. This locking of the tRNAi in the ribosomal P-site, accompanied by rotation of the 40S head domain, completes the process. *— Emma Nichols*

See: Ivan B. Lomakin and Thomas A. Steitz*, "The initiation of mammalian protein synthesis and mRNA scanning mechanism," Nature **500**, 307 (15 August 2013).
DOI:10.1038/nature12355
Author affiliation: Yale University
Correspondence:
* thomas.steitz@yale.edu

This work was supported by the National Institutes of Health grant GM022778 (to T.A.S.). NE-CAT is supported by a grant from the National Institute of General Medical Sciences (P41 GM103403) from the National Institutes of Health. Use of the Advanced Photon Source at Argonne National Laboratory was supported by the U.S. Department of Energy Office of Science under Contract No. DE-AC02-06CH11357.

"Complexities" cont'd. from page 145
production of the rest of the RNA is required. The alternate structures of these RNA switches can promote continued transcription, or its termination. In this work, the T-box riboswitch that regulates transcription of an important cellular enzyme that links glycine to $tRNA^{Gly}$ binds specifically to this tRNA. This is the same type of interaction that occurs between $tRNA^{Gly}$ and mRNA during translation (i.e., in the ribosome) when the RNA sequence in the anti-codon loop of the $tRNA^{Gly}$ matches the codon in the mRNA.

When the *glyQ* T-box riboswitch interacts with $tRNA^{Gly}$ that is uncharged (not carrying its amino acid due to lack of glycine, as a signal of cellular starvation), it adopts a structural conformation that promotes further transcription, because the cell needs to attach more glycine onto their carrier tRNAs to ensure continued protein synthesis.

If the riboswitch interacts with $tRNA^{Gly}$ that is charged with glycine, it will form a structure that halts transcription, as there is more than enough glycine present on $tRNA^{Gly}$ so there is no need for more linking enzymes. In this study, biochemical data demonstrated that the stem I domain of the T-box riboswitch is both the determinant of tRNA binding specificity and primarily responsible for binding affinity.

To define the basis for these observations, high-quality x-ray diffraction data were required. A crystal structure of $tRNA^{Gly}$ bound to stem I of the *GlyQ* T-box riboswitch provided a rare glimpse of interaction between two non-coding RNAs, and revealed a surprisingly extensive interaction between tRNA and the T-box, suggesting how shape-based complementarity enhances the cognate interaction between these structured RNAs.

— Emma Nichols

See: Jinwei Zhang and Adrian R. Ferré-D'Amaré*, "Co-crystal structure of a T-box riboswitch stem I domain in complex with its cognate tRNA" Nature **500**, 363 (2013). DOI:10.1038/nature12440
Author affiliation:
National Institutes of Health
Correspondence:
* adrian.ferre@nih.gov

This work was supported in part by the intramural program of the National Heart, Lung, and Blood Institute, National Institutes of Health. NE-CAT is supported by a grant from the National Institute of General Medical Sciences (P41 GM103403) from the National Institutes of Health. Use of the Advanced Photon Source at Argonne National Laboratory was supported by the U.S. Department of Energy Office of Science under Contract No. DE-AC02-06CH11357.

24-ID-C • NE-CAT • Life sciences • Macromolecular crystallography, microdiffraction, single-wavelength anomalous dispersion, single-crystal diffraction, microbeam • 6.5-23 keV • On-site, remote • Accepting general users •

24-ID-E • NE-CAT • Life sciences • Macromolecular crystallography, microbeam, microdiffraction, single-wavelength anomalous dispersion, single-crystal diffraction • 12.68 keV • On-site, remote • Accepting general users •

"Basis" cont'd. from page 146
lowers the energetic threshold for binding to its activator (2,3-bisphosphoglycerate), a normal component of the glycolytic pathway, causing increased activity of PGAM1 in the presence of its substrate. *— Emma Nichols*

See: Taro Hitosugi[1], Lu Zhou[2], Jun Fan[1], Shannon Elf[1], Liang Zhang[2], Jianxin Xie[3], Yi Wang[3], Ting-Lei Gu[3], Masa Alečković[4], Gary LeRoy[4], Yibin Kang[4], Hee-Bum Kang[1], Jae-Ho Seo[1], Changliang Shan[1], Peng Jin[5], Weimin Gong[6], Sagar Lonial[1], Martha L. Arellano[1], Hanna J. Khoury[1], Georgia Z. Chen[1], Dong M. Shin[1], Fadlo R. Khuri[1], Titus J. Boggon[7], Sumin Kang[1], Chuan He[2], and Jing Chen[1]*, "Tyr26 phosphorylation of PGAM1 provides a metabolic advantage to tumours by stabilizing the active conformation," Nat. Commun. **4**, 1790 (30 April 2013).
DOI:10.1038/ncomms2759
Author affiliations: [1]Emory University School of Medicine; [2]The University of Chicago; [3]Cell Signalling Technology, Inc.; [4]Princeton University; [5]Emory University School of Medicine; [6]Chinese Academy of Sciences; [7]Yale University School of Medicine
Correspondence: *jchen@emory.edu

This work was supported in part by National Institutes of Health grants CA120272 (J.C.), CA140515 (J.C.), and GM071440 (C.H.); Department of Defense grant W81XWH-12-1-0217 (J.C.); the Pharmacological Sciences Training Grant T32 GM008602 (S.E.); and the National Natural Science Funds of China No. 20902013 (L. Zhou). LS-CAT is supported by the Michigan Economic Development Corporation and the Michigan Technology Tri-Corridor (Grant 085P1000817). NE-CAT is supported by a grant from the National Institute of General Medical Sciences (P41 GM103403) from the National Institutes of Health. Use of the Advanced Photon Source at Argonne National Laboratory was supported by the U.S. Department of Energy Office of Science under Contract No. DE-AC02-06CH11357.

21-ID-F • LS-CAT • Life sciences • Macromolecular crystallography • 12.7 keV • On-site, remote, mail-in • Accepting general users •

24-ID-C • NE-CAT • Life sciences • Macromolecular crystallography, microdiffraction, single-wavelength anomalous dispersion, single-crystal diffraction, microbeam • 6.5-23 keV • On-site, remote • Accepting general users •

Real-Time Capture of Intermediates in Enzymatic Reactions

Successful development of new pharmaceuticals could be the payoff from five-dimensional crystallography, a new experimental technique employed by researchers carrying out studies at the APS. X-ray crystallography uses x-rays to investigate protein structure, and has played an increasingly important role in drug discovery in recent decades. This new technique essentially represents a type of extremely high-resolution microscopy for investigating the molecular structure of proteins with near-atomic resolution. This facilitates improved understanding of their function, and provides vital structural information on specific protein targets. In this way it can contribute to the design of new drugs that target specific proteins, or to the engineering of enzymes for specific industrial processes.

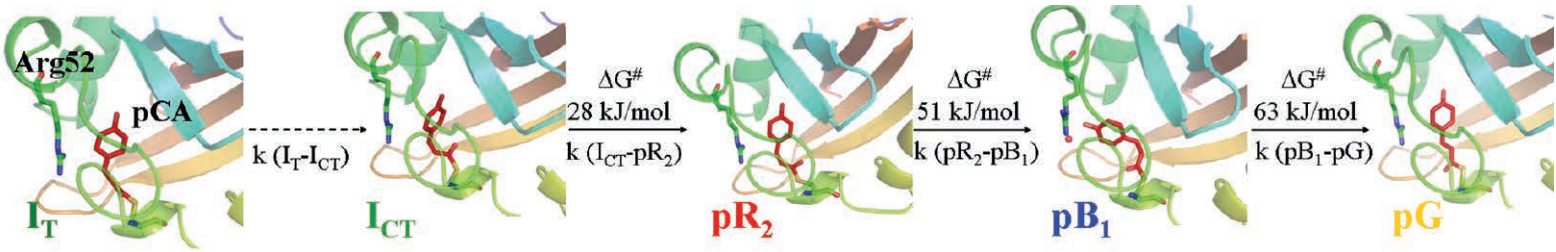

Fig. 1. Structures of the intermediates I_T, I_{CT}, pR_2, pB_1 and the dark resting state of photoactive yellow protein on the main reaction pathway. Barriers of activation between the intermediates are determined by 5-D crystallography.

Protein folding is the process by which a protein takes on a specific three-dimensional (3-D) structure essential for it to function. Many proteins, called enzymes, promote or catalyze specific chemical reactions. The 3-D structures of these proteins change during the course of the reactions. Free energy landscapes represent multidimensional hyper-surfaces that determine the progress of catalyzed reactions, and characterization of these landscapes allows the reaction to be described and visualized.

In time-resolved crystallography (TRX), x-ray diffraction by crystals is utilized to examine in real time the structures of proteins as they are changing and therefore improve understanding of their function and gain important structural information on specific protein targets.

Five-dimensional (5-D) crystallography is a specific form of the TRX technique where, in addition to space and time, temperature is a variable as well. It allows complete characterization of all features of a chemical reaction, including the structure of its intermediate compounds, and the reaction kinetics, and barriers of activation between the intermediates. It provides an essential and direct link between the structural changes and energy changes in the chemical reaction.

In this study, researchers from the University of Wisconsin-Milwaukee, The University of Chicago, The Institute for Basic Science (Republic of Korea), and the Korea Advanced Institute of Science and Technology (Republic of Korea) employed the photocycle reaction of photoactive yellow protein (PYP), a bacterial photosensor protein, as a model for 5-D crystallography. In this reaction, a sequence of light-induced structural changes in the protein produces distinct intermediate structures. Using data sets collected from TRX experiments conducted on crystals of PYP at the BioCARS 14-ID-B beamline at the APS, the researchers investigated the effect of changing temperature on the kinetics of inter-conversion between intermediates formed during the photocycle. By lowering the temperature below 0° C, the rate of the chemical reactions slowed down, allowing an early intermediate like IT to be observed on the nanosecond time-scale (Fig. 1), whereas it had previously only been evident using picosecond TRX.

The study also showed that from -40º C to +50º C, the reaction proceeded in a temperature-dependent manner. However, above 50º C, the optimum temperature for the reaction was exceeded, and its rate slowed down again. Most importantly, such temperature-dependent data allowed

"Capture" cont'd. on page 150

The Crystallized Catalytic Domain of Human SIRT1

Scientists have been eager to find out how the structure and catalytic function of sirtuins, proteins that regulate cellular homeostasis and play a role in human-related diseases, are able to influence certain physiological outcomes. Researchers utilizing the APS studied the catalytic domain of a human sirtuin to better understand the mechanisms of its inhibition. This breakthrough allows scientists to directly and clearly observe the actual binding mode of a SIRT1 inhibitor, which, within the past three years, had only been achieved using computational models. This provides an opportunity for scientists to develop new drugs that selectively control SIRT1's function when its activity is exploited by cancer cells.

Sirtuins (SIRTs) are a family of proteins that regulate cellular homeostasis and have been well-documented to play a role in human-related diseases including diabetes, cancer, and cardiovascular disease. Given this, scientists have been eager to find out how the structure and catalytic function of sirtuins are able to influence certain physiological outcomes. Of the seven human sirtuins (SIRT1-7), which occupy various cellular compartments such as the nucleus, cytoplasm, and the mitochondria, crystal structures have only been determined for SIRT2, SIRT3, SIRT5, and SIRT6. Recently, a collaborative research team studied the catalytic domain of human SIRT1 at the LRL-CAT beamline 31-ID-D to better understand the mechanisms of its inhibition.

Researchers from the Lilly Biotechnology Center and the Lilly Corporate Center collaborated to use the hanging drop vapor diffusion and limited proteolysis mass spectrometry (LP/MS) techniques to engineer the crystallized human SIRT1 protein to determine the boundaries of its catalytic domain. The authors screened several different SIRT1 catalytic domain constructs in the presence of nicotinamide adenine dinucleotide (NAD^+) and a variety of SIRT1 inhibitors to identify molecules that granted the highest thermal stabilization and affinity for SIRT1. The research group found that the crystal structure of human SIRT1 bound to an inhibitor, known as compound 35; (SIRT1/NAD^+/35 complex) produced

"Crystallized" cont'd. on page 150

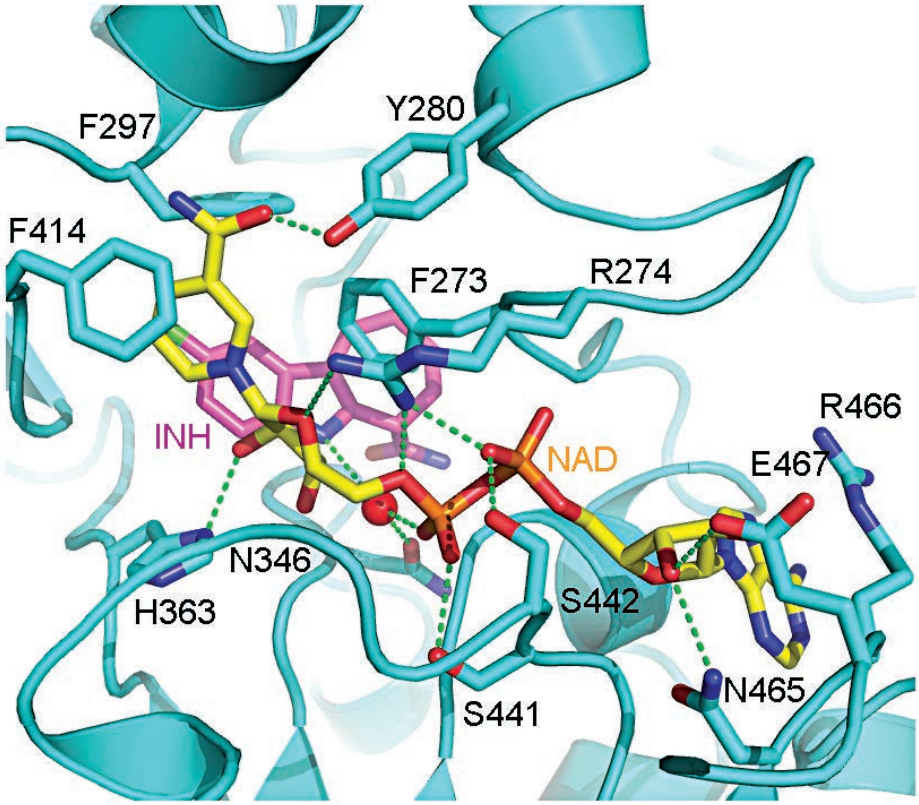

Fig. 1. Schematic representation of the NAD^+/35/SIRT1 crystal structure. SIRT1, depicted by ribbons, has interacting side chains shown as colored sticks (cyan, red, and blue). The inhibitor 35 (magenta sticks) is buried deep in the back of SIRT1 with a bridging water molecule (red sphere) positioned between the indole nitrogen of 35 and the 2′ phosphate. NAD^+ (yellow sticks) is bound diagonally across the opening of the catalytic site starting from right to left.

"Capture" cont'd. from page 148
energies of activation between intermediates to be determined directly from x-ray data.

Using the BioCARS beamline, time-resolved high-resolution Laue crystallographic data with 100-psec time resolution can be collected and analyzed swiftly with novel data collection and data processing strategies.

Data from this study showed how 5-D crystallography may demonstrate energy changes associated with barriers of activation in the photocycle reaction of PYP. The results will be important in guiding future work to investigate changing energy landscapes of other enzymatic reactions, and may contribute to the development of novel drugs that target a specific protein.

— Nicola Parry

See: Marius Schmidt[1]*, Vukica Srajer[2], Robert Henning[2], Hyotcherl Ihee[3,4], Namrta Purwar[1], Jason Tenboer[1], and Shailesh Tripathi[1], "Protein Energy Landscapes Determined by 5-Dimensional Crystallography," Acta Cryst. D **69**, 2534 (2013).

Author affiliations: [1]University of Wisconsin-Milwaukee, [2]The University of Chicago, [3]Institute for Basic Science, [4]Korea Advanced Institute of Science and Technology

Correspondence: * m-schmidt@uwm.edu

M.S. is supported by National Science Foundation (NSF) CAREER grant 0952643 and NSF STC 1231306. H.I. is supported by Institute for Basic Science in Korea. Use of BioCARS was supported by the National Institutes of Health, National Institute of General Medical Sciences grant R24GM111072. The time-resolved set-up at Sector 14 was funded in part through a collaboration with Philip Anfinrud (National Institutes of Health/ National Institute of Diabetes and Digestive and Kidney Diseases). Use of the Advanced Photon Source at Argonne National Laboratory was supported by the U.S. Department of Energy Office of Science under Contract No. DE-AC02-06CH11357.

14-ID-B • BioCARS • Life sciences, materials science, physics, chemistry • Time-resolved crystallography, time-resolved x-ray scattering, Laue crystallography, wide-angle x-ray scattering, biohazards at the BSL2/3 level, macromolecular crystallography • 7-19 keV • On-site • Accepting general users •

"Crystallized" cont'd. from page 149
(yielded) the highest resolution (Fig.1).

Using yeast sir2/H4/carabNAD crystal structure as the molecular replacement search model, the team revealed the manner in which 35 halts SIRT1's activity. There is a dual mechanism of inhibition by compound 35 and it requires binding of both the inhibitor and the cofactor NAD^+. First, the binding of 35 mimics the binding of NAD^+ nicotinamide, thereby displacing NAD^+ and forcing it into an inactive conformation that splays NAD^+ across the outer edge of the binding groove. This occurs when the F273 side chain of SIRT1 rotates closer to the indole of compound 35 creating a steric impediment to NAD^+ in the proper kinked active conformation. Then, the resultant extended conformation of NAD^+ prevents substrates such as NFkB, p53, PPAR gamma, and FOXO from binding to SIRT1 by closing up the access channel.

Although the structure and role of other human SIRTs in age-related diseases and cellular homeostasis are well-known, thanks to compound 35 the structural basis of SIRT1 inhibition is established. *— Candice A. Shaifer*

See: Xun Zhao[1], Dagart Allison[1], Bradley Condon[1], Feiyu Zhang[1], Tarun Gheyi[1], Aiping Zhang[1], Sheela Ashok[1], Marijane Russell[1], Iain MacEwan[1], Yuewei Qian[2], James A. Jamison[2], and John Gately Luz[2]*, "The 2.5 Å crystal structure of the SIRT1 catalytic domain bound to nicotinamide adenine dinucloetide (NAD^+) and an indole (EX527 analogue) reveals a novel mechanism of histone deacetylase inhibition," J. Med. Chem. **56**(3),963 (February 2013). DOI:10.1021/jm301431y.

Author affiliations: [1]Lilly Biotechnology Center, [2]Lilly Corporate Center

Correspondence: *luz_john@lilly.com

Use of the LRL-CAT beamline was provided by Eli Lilly Company, which operates the facility. Use of the Advanced Photon Source at Argonne National Laboratory was supported by the U.S. Department of Energy Office of Science under Contract No. DE-AC02-06CH11357.

31-ID-D • LRL-CAT • Life sciences • Macromolecular crystallography, single-wavelength anomalous dispersion, single-crystal diffraction • 4.7-28 keV • Mail-in • Accepting general users •

Ordering Issues of *APS Science*

Issues of *APS Science* (2002-2013) can be downloaded in .pdf format at:

www.aps.anl.gov/Science/Reports/

To order a CD containing a particular issue of *APS Science* and/or a four-color printed copy, send an email to apsinfo@aps.anl.gov. Include your mailing address and contact information, and please specify which issue or issues you are requesting (2002 is available in print only).

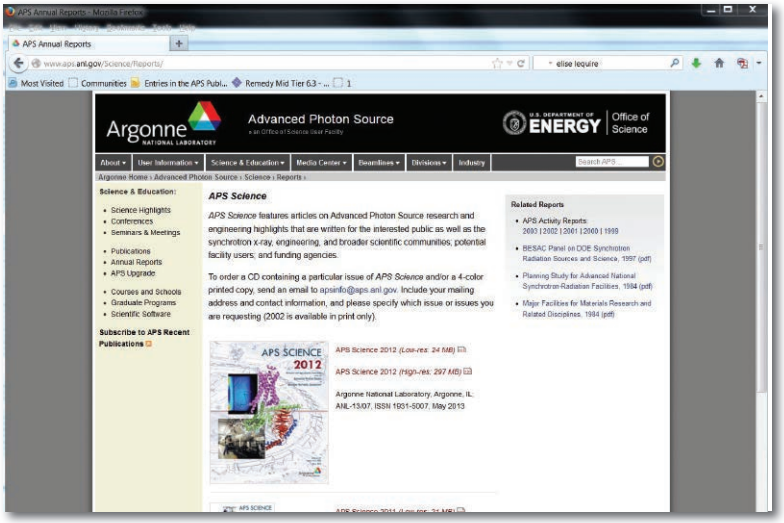

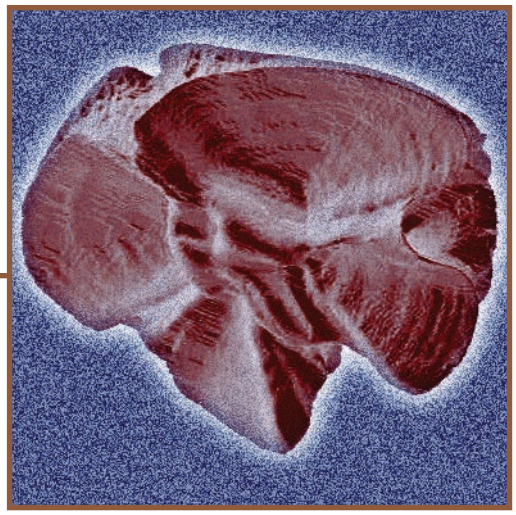

Environmental, Geological & Planetary Science

The Fate of Bioavailable Iron in Antarctic Coastal Seas

Science is exploring many options for carbon dioxide sequestration in order to mitigate the climatological impact of CO_2. One of these is geoengineering: deliberate, large-scale intervention in the Earth's natural systems to counteract climate change. Understanding all of the possible effects of geoengineering, such as the results of iron fertilization on marine ecosystems, is vital. In iron fertilization, which has been discussed as a way to sequester carbon dioxide from the atmosphere, iron is introduced to the surface ocean to stimulate a phytoplankton bloom in locations where iron is the limiting nutrient. Carbon taken up by the phytoplankton is later sequestered in deep sea sediments. Researchers using the APS found that iron was incorporated into biogenic silica in diatoms from the Southern Ocean and was then lost from the ecosystem. The loss of bioavailable iron could favor the growth of phytoplankton species that are less efficient at assimilating carbon, the opposite of the desired result of iron fertilization.

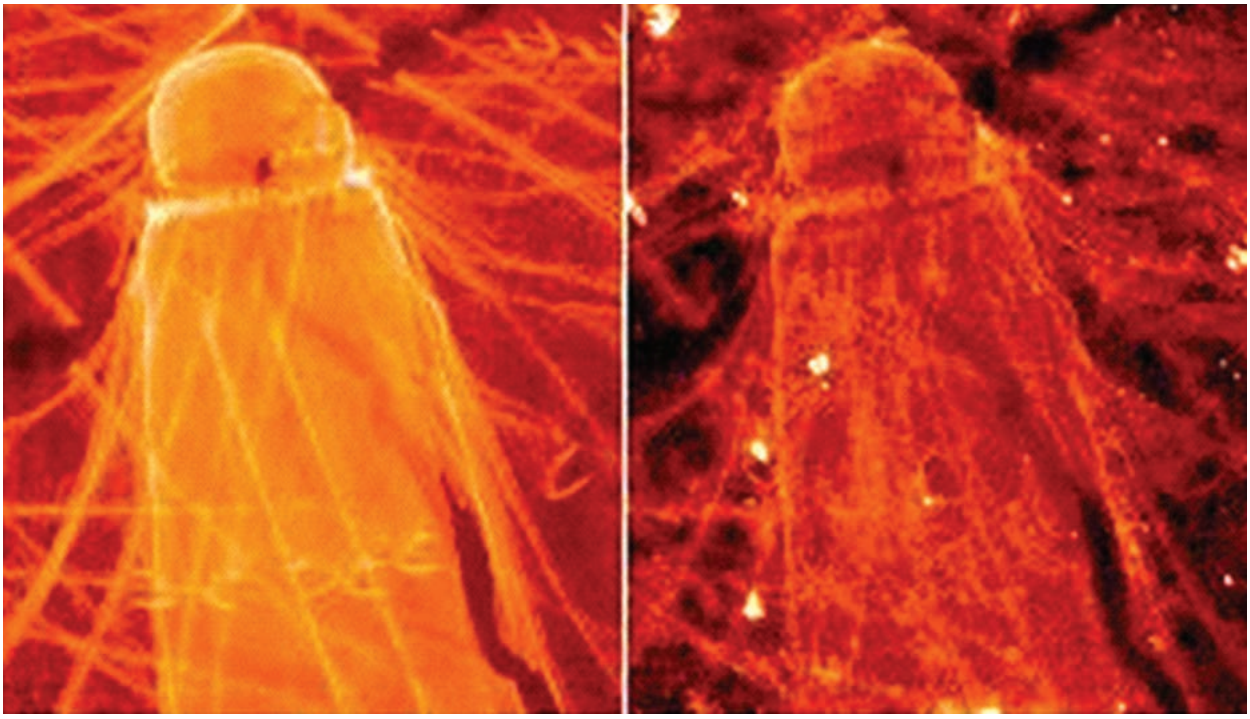

Fig. 1. On the left is an XRF micrograph map of silicon distribution in the diatom Corethron spp. On the right is a map of the distribution of iron in the same diatom. (The images are 66-μm in width.) Lighter colors indicate higher concentrations. Note how the distribution of iron mirrors the distribution of silicon.

Diatoms, single-celled algae that have a cell wall of silica, account for nearly half of the annual marine carbon fixation worldwide, and dominate many phytoplankton communities in Antarctic coastal seas. After the organisms die, their dense siliceous shells descend into the deep ocean. The sequestration of carbon in deep sea sediments is a crucial sink for carbon dioxide, an important greenhouse gas. Iron is a limiting nutrient in phytoplankton communities in these seasonally ice-covered seas, which include some of the most biologically productive regions of the Southern Ocean, like the Ross Sea. Bioavailable iron limits biological

A decision by the International Hydrographic Organization in the spring of 2000 delimited a fifth world ocean — the Southern Ocean — from the southern portions of the Atlantic Ocean, Indian Ocean, and Pacific Ocean. The Southern Ocean extends from the coast of Antarctica north to 60° south latitude, which coincides with the Antarctic Treaty Limit. The Southern Ocean is now the fourth largest of the world's five oceans (after the Pacific, Atlantic, and Indian, but larger than the Arctic Ocean). The Southern Ocean has the unique distinction of being a large circumpolar body of water totally encircling the continent of Antarctica. Source: http://adventure443.blogspot.com/2010/10/southern-ocean.html

production and also affects the composition of the phytoplankton community.

The availability of iron, therefore, can limit uptake of atmospheric carbon dioxide, with important implications for the climate. Understanding iron cycling in Antarctic phytoplankton is crucial for determining whether iron fertilization can be an effective strategy for reducing atmospheric carbon dioxide.

In the Ross Sea, bioavailable iron enters the area through snow melt and dust deposition. Iron removal is calculated to be about equal to iron input. Fertilizing the surface ocean with iron increases biological productivity, but the resulting carbon dioxide removal will be much less than expected due to the increased productivity of diatoms, which incorporate and remove the bioavailable iron.

The resultant decrease in iron favors plankton communities with lower iron requirements. *Phaeocystis antarctica*, a non-siliceous prymnesiophyte, dominates some Southern Ocean phytoplankton communities, but loses out to diatoms when bioavailable iron is low. *P. antarctica* assimilates more carbon dioxide than diatoms, so a shift to a diatom-rich phytoplankton community may reduce carbon dioxide sequestration, the opposite of the desired effect.

In this investigation, the researchers from the Georgia Institute of Technology, the University of Georgia, the Bigelow Laboratory for Ocean Sciences, the Skidaway Institute of Oceanography, and Argonne National Laboratory discovered an important sink for iron in some marine systems. Utilizing XSD beamlines 2-ID-D and 2-ID-E at the APS the researchers performed x-ray fluorescence (XRF) microscopy and x-ray absorption near-edge structure spectroscopy on samples of the diatom genera *Fragilariopsis* and *Corethron* from the Ross Sea.

Two morphologically distinct forms of iron were discovered: one reduced form was structurally incorporated into the biogenic silica; the second form was hot spots of iron that were more oxidized (Fig. 1).

The researchers conclude that the iron was incorporated into the biogenic silica because iron in contact with seawater would become at least partially oxidized. This incorporated organic iron has a better chance of surviving diagenesis (the conversion, as by compaction or chemical reaction, of sediment into rock) deep in a frustule (the two-valved siliceous shell of a diatom) than it would in a surface coating or in the protoplasm. When the siliceous diatoms sink to the seafloor, the iron is sequestered from the marine ecosystem. The loss of iron from the surface may reduce biological productivity in locations where iron is limiting.

This research leads to a greater understanding of the dynamics of iron cycling in the Southern Ocean with possible implications for improving carbon sequestration. *— Dana Desonie*

See: Ellery D. Ingall[1]*, Julia M. Diaz[1‡], Amelia F. Longo[1], Michelle Oakes[1‡‡], Lydia Finney[2], Stefan Vogt[2], Barry Lai[2], Patricia L. Yager[3], Benjamin S. Twining[4], and Jay A. Brandes[5], "Role of biogenic silica in the removal of iron from the Antarctic seas," Nat. Comm. **4**, 1981 (2013). DOI:10.1038/ncomms2981

Author affiliations: [1]Georgia Institute of Technology, [2]Argonne National Laboratory, [3]University of Georgia, [4]Bigelow Laboratory for Ocean Sciences, [5]Skidaway Institute of Oceanography. Present addresses: ‡Woods Hole Oceanographic Institution, ‡‡National Center of Environmental Assessment.
Correspondence:
*ingall@eas.gatech.edu

This research was supported by National Science Foundation (NSF) grants 0849494(E.D.I.), 0836144 (P.L.Y.) and 1060884 (E.D.I.), the NSF Graduate Research Fellowship Program (J.M.D.), and the Ford Foundation Fellowship Program (J.M.D.). Thanks to the Swedish Antarctic Research Programme and the colleagues and crew aboard the 2008/2009 expedition of the icebreaker *Oden*. Use of the Advanced Photon Source at Argonne National Laboratory was supported by the U.S. Department of Energy Office of Science under Contract No. DE-AC02-06CH11357.

2-ID-D • XSD • Life sciences, materials science, environmental science • Microfluorescence (hard x-ray), microdiffraction, micro-x-ray absorbtion fine structure • 5-30 keV • On-site • Accepting general users •

2-ID-E • XSD • Life sciences, environmental science, materials science • Microfluorescence (hard x-ray) • 7-10.5 keV, 11-17 keV • On-site • Accepting general users •

The Meaning of Ossicle Dissolution Off Antarctica

Brittle stars (*Ophionotus victoriae*) are marine invertebrates that live on spiny sponges and other sessile animals in massive fields on the muddy seafloor, as well as by themselves or in abundance directly on the seafloor. The discrepancy between the abundance of *O. victoriae* in the Antarctic marine (benthic) ecosystems, and its abundances in sediment cores from the region that date as far back as the Cenozoic period 65 million years ago needs an explanation. During a two-year experiment, brittle stars were suspended above or placed on samples of the sediment, during which time the small bones, or ossicles, in the brittle stars began to show dissolution features. The conclusions from this study, namely that ossicle dissolution begins soon after death, suggest that their scarcity in sediment cores means these organisms cannot be used to understand the region's geologic and biologic past. This work also provides baseline information for understanding ocean acidification.

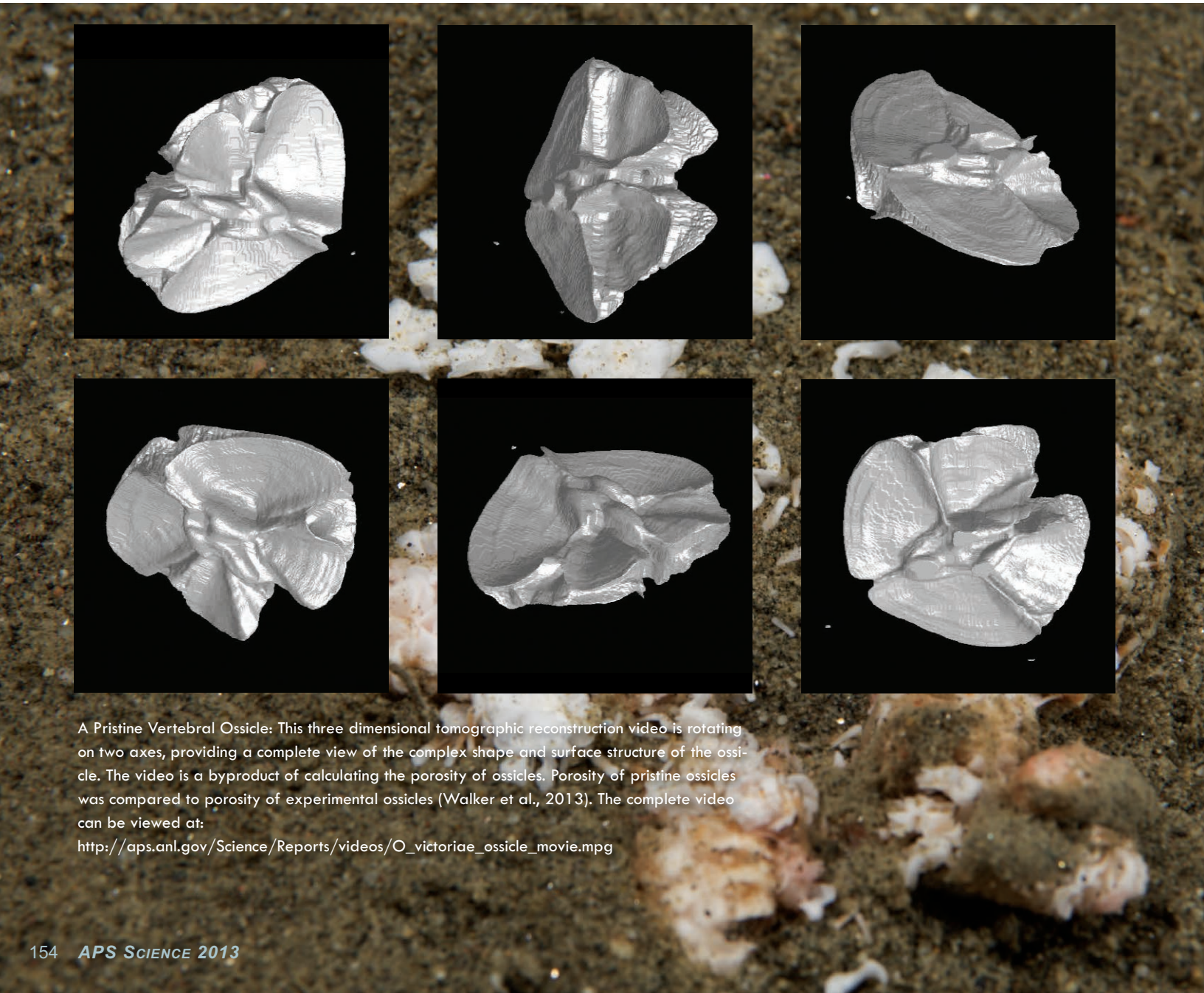

A Pristine Vertebral Ossicle: This three dimensional tomographic reconstruction video is rotating on two axes, providing a complete view of the complex shape and surface structure of the ossicle. The video is a byproduct of calculating the porosity of ossicles. Porosity of pristine ossicles was compared to porosity of experimental ossicles (Walker et al., 2013). The complete video can be viewed at:
http://aps.anl.gov/Science/Reports/videos/O_victoriae_ossicle_movie.mpg

Fig. 1. Ossicles from *Ophionotus victoriae* in sediment at Explorers Cove, Antarctica. Photo: Shawn Harper.

Besides raising global temperatures, increasing atmospheric CO_2 is predicted to lower ocean pH, a phenomenon referred to as ocean acidification. The ocean absorbs about one-quarter of the annual output of CO_2 resulting from human activity; the resultant increase in acidity is predicted to impede calcification by organisms that build carbonate shells or skeletons or cause carbonate in existing shells to dissolve. The effects of ocean acidification on calcareous marine organisms are the object of much study.

The distinctive benthic fauna of the Antarctic continental shelf are rich in some life forms and poor in others, but overall biodiversity and biomass of the fauna are high. *Ophionotus victoriae* can be found from shelf to ocean depths of 600 to 6000 ft (180 to 1800 m). The ophiuroid is composed of an internal skeleton of around 1500 ossicles made of high-magnesium (Mg) calcite that are connected and protected by organic tissue while the organism is alive. With few exceptions, sediment cores drilled on the Antarctic continental shelf contain almost none of these ossicles.

The discrepancy between the abundance of living fauna and their remains is the subject of this study by researchers from Vanderbilt University and the New York Department of Health. The goals of the study were to 1) determine if the fossil record accurately reflects the abundance and distribution of benthic fauna at the time of deposition, 2) evaluate if the fossil record is of paleoclimatic significance, and 3) assess *in situ* dissolution over a short period of time to provide a baseline for future ocean acidification studies.

To determine what happened to the *O. victoriae* remains, the researchers sacrificed ophiuroids and suspended them in mesh bags above the seafloor or embedded them in aquaria within the sediment in Explorers Cove, offshore of Taylor Valley in Antarctica. After two years, the researchers analyzed the recovered ossicles by scanning electron microscopy to determine the chemical and physical damage, and utilized x-ray tomography at the GSECARS 13-BM-D beamline at the APS to create a three-dimensional map for calculating the total volume of the ossicles.

The results showed that the soft tissue disintegrated rapidly. Without its protection, the ossicles dissolved very rapidly. At the rates calculated, complete dissolution is projected to occur in just 6 to 105 years. Contributing to the rapid dissolution and degradation of the ossicles are factors such as the composition of the ossicles, the abiotic conditions in Explorers Cove, and the reworking (or bioturbation) of the sediment by animals. High-Mg calcite dissolves in polar seawater because it is less saturated in carbonate, meaning that the ossicles are close to a dissolution threshold. In addition, researchers have observed that two epifaunal animals, an ophiuroid and a scallop, churn and suspend the upper 5 cm of sediment, creating a thick, active-sediment zone that affects decay processes. Bioturbation keeps the ossicles in the zone where they are more likely to dissolve, which in turn means that the ossicles are not a good source of paleoenvironmental or paleoecological information in the region, nor is the fossil record complete enough to indicate the evolutionary history of these benthic fauna.

The rapid dissolution of the ossicles in Explorers Cove suggests that high-Mg calcite of the *O. victoriae* ossicles is currently metastable in high-latitude seawater. This stability will decrease as ocean pH lowers. Ocean acidification is predicted to affect the ability of ophiuroids to develop and grow as they are challenged to secrete high-Mg calcite ossicles. On a larger scale, ocean acidification will affect all benthic ecosystems, but especially those in high-latitude regions in organisms that secrete high-Mg calcite.

— Dana Desonie

See: Beverly J. Walker[1]*, Molly F. Miller[1], Samuel S. Bowser[2], David J. Furbish[1], and Guilherme A.R. Gualda[1], "Dissolution of Ophiuroid Ossicles on the Shallow Antarctic Shelf: Implications for the Fossil Record and Ocean Acidification," PALAIOS **28**, 317 (2013). DOI:10.2110/palo.2012.p12-100r

Author affiliations: [1]Vanderbilt University, [2]New York Department of Health

Correspondence:

* bevjwalk@gmail.com

This research was supported by National Science Foundation (NSF) ANT0739496 (M.F.M.) and NSF ANT0739583 (S.S.B.). GSECARS is supported by the National Science Foundation - Earth Sciences (EAR-1128799) and Department of Energy-GeoSciences (DE-FG02-94ER14466). Use of the Advanced Photon Source at Argonne National Laboratory was supported by the U.S. Department of Energy Office of Science under Contract No. DE-AC02-06CH11357.

13-BM-D • GSECARS • Geoscience, environmental science • Tomography, high-pressure diamond anvil cell, high-pressure multi-anvil press, x-ray absorption fine structure • 4.5-70 keV • On-site • Accepting general users •

Gauging the Levels of Strontium in Rusted Pipes

Tap water contains many substances of which we are usually unaware. These impurities are for the most part harmless, but the effects of some, like the metal strontium, are still unclear. Recently, water utilities have begun monitoring how much strontium we ingest from drinking water. A new study shows that this monitoring may need to factor in the release of strontium from rusted pipes. Researchers using two beamlines at the APS have identified high levels of strontium in corrosion products taken from different water supply pipes. This bound strontium can eventually be released back into the water, presumably causing the strontium concentration to occasionally spike above the monitoring reporting limit.

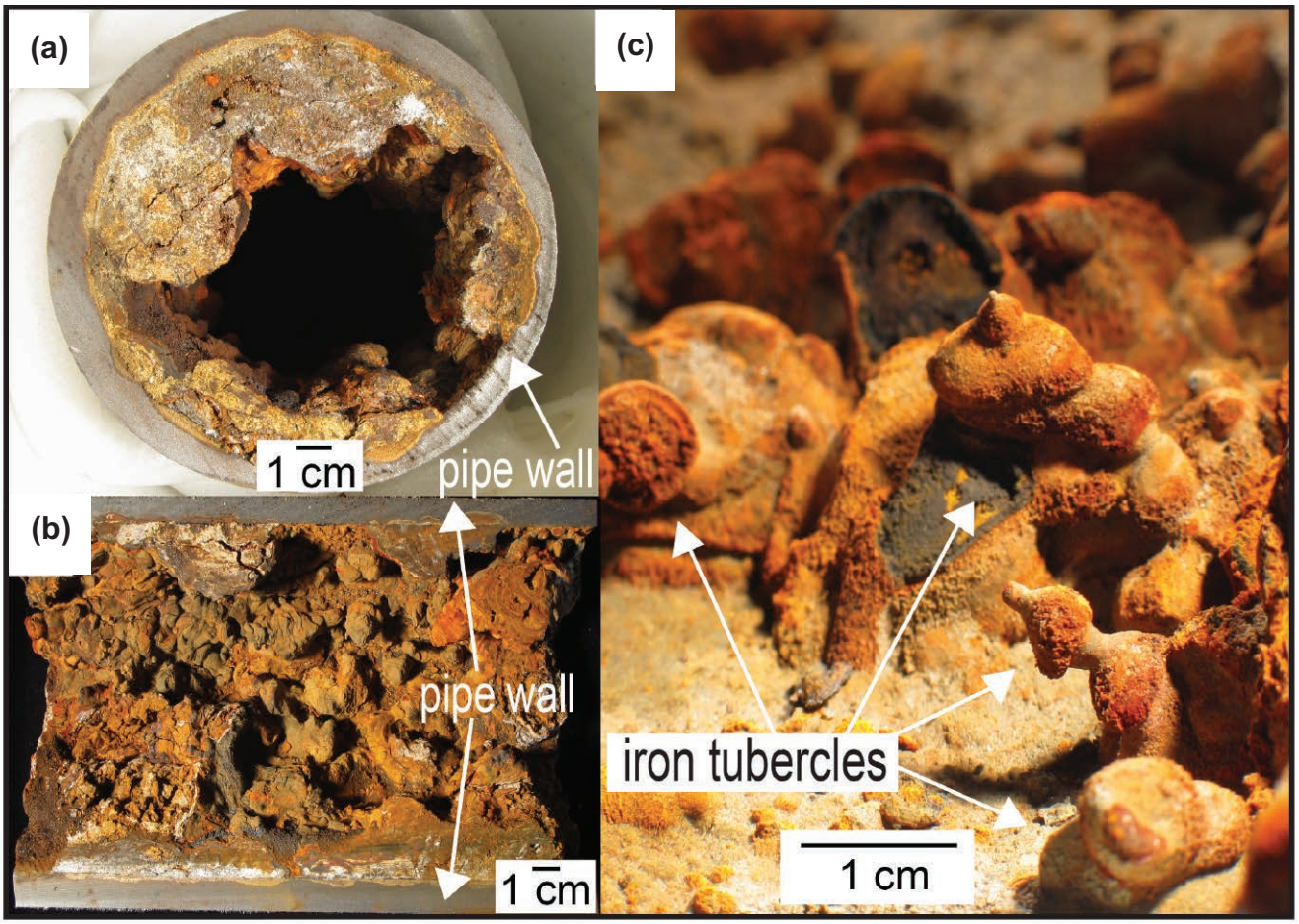

Fig. 1. Images (a) and (b) show iron corrosion products inside a cast-iron service drinking water pipe recovered from a water supply system in the Midwest. Image (c) is a close-up view of an iron corrosion product from a 15-cm-wide cast-iron service drinking water pipe from a system in New England. The mound features, called tubercles, can be seen in the photo. Images: M.K. DeSantis. Graphic: T.L. Gerke (U. Cincinnati).

The average concentration of strontium in our drinking water is around 1 mg/l. Because strontium is chemically similar to calcium, some of this strontium ends up in our bones and teeth. This may be beneficial, as certain drugs containing strontium have been shown to improve bone density. However, other studies suggest that too much strontium may lead to bone weakness. The U.S. Environmental Protection Agency (U.S. EPA) does not presently regulate strontium, but since January 2013 the agency has required certain water utilities to monitor strontium (as well as other contaminants) in their water supplies.

One unresolved issue is where best to check the strontium concentration. Strontium monitoring occurs at the point-of-entry and point-of-maximum stagnation in a water distribution system. However, this may not reflect what comes out of the faucets at the other end. Previous work has shown that the metal vanadium binds to, and later releases from corrosion products inside of water pipes. Now researchers from Miami University, the University of Cincinnati, the Naval Research Laboratory at the Stennis Space Center in Mississippi, and the U.S. EPA have investigated whether similar binding and release occurs with strontium.

The researchers looked specifically at iron corrosion products, as possible locations where strontium may concentrate. These rust concentrations, which are found in iron pipes, consist of multiple mounds of iron oxides/oxyhydroxides (Fig. 1). They are composed not only iron but other metals and minerals that have adsorbed onto iron corrosion products or precipitated from the drinking water. This "filtering" can, during normal operations, reduce the amount of contaminants that reach the tap. However, a disturbance in the water flow or in the water chemistry can cause some of the metals to be desorbed or dislodge small pieces of the surface layers of iron corrosion products.

To evaluate if strontium is a metal that adsorbs to iron corrosion product surfaces, the research team collected iron corrosion product samples from four different water distribution systems. Using x-ray fluorescence measurements, they found strontium concentrations ranging from 3 to 128 mg/kg in the surface layers of the products. But these measurements by themselves did not reveal how easily strontium can be desorbed from the surfaces of the iron corrosion products. For this, the team performed micro-x-ray adsorption near edge structure spectroscopy (μ-XANES) at the MR-CAT 10-ID-B beamline and the XSD beamline 20-ID-B,C, both at the APS.

Sample spectra were compared to several standards that contained strontium in different configurations. The comparisons revealed that strontium was primarily bound in calcite ($CaCO_3$) crystals, replacing calcium atoms. This is a fairly stable configuration with regard to release. However, they also found that a portion of the strontium was simply adsorbed on the surface of iron oxides/oxhydroxides or calcite crystals. A disturbance in the flow or in the water chemistry could cause this adsorbed strontium to release back into the drinking water.

To verify that this release happens, the team analyzed a water filter from a single home connected to one of the utilities in the study. They found that the particulates caught by the filter had the same iron and strontium concentrations as the iron corrosion products they analyzed.

The researchers surmise that sudden releases of iron corrosion particulates could potentially expose water drinkers to strontium levels above the U.S. EPA Health Reference Level of 4 mg of strontium per liter of water.

— Michael Schirber

See: Tammie L. Gerke[1‡*], Brenda J. Little[2], Todd P. Luxton[3], Kirk G. Scheckel[3], and J. Barry Maynard[1], "Strontium Concentrations in Corrosion Products from Residential Drinking Water Distribution Systems," Environ. Sci. Technol. **47**, 5171 (2013). DOI:10.1021/es4000609

Author affiliations: [1]University of Cincinnati, [2]Naval Research Laboratory, [3]U.S. Environmental Protection Agency. ‡Present address Miami University

Correspondence:

* gerketl@miamioh.edu

This research has not been subject to U.S. EPA review and, therefore, does not necessarily reflect the views of the U.S. EPA. MR-CAT operations are supported by the Department of Energy and the MR-CAT member institutions. APS Sector 20, which is managed by XSD in partnership with the Canadian Light Source (CLS), is funded by the U.S. Department of Energy Office of Science, and by the Natural Sciences and Engineering Research Council of Canada and the University of Washington via the CLS. Use of the Advanced Photon Source at Argonne National Laboratory was supported by the U.S. Department of Energy Office of Science under Contract No. DE-AC02-06CH11357.

10-ID-B • MR-CAT • Materials science, environmental science, chemistry • X-ray absorption fine structure, time-resolved x-ray absorption fine structure, micro x-ray absorption fine structure, microfluorescence (hard x-ray) • 4.3-27 keV, 4.3-32 keV, 15-90 keV • On-site • Accepting general users •

20-ID-B,C • XSD • Materials science, environmental science, chemistry • X-ray absorption fine structure, surface diffraction, x-ray Raman scattering, micro x-ray absorption fine structure, microfluorescence (hard x-ray), time-resolved x-ray absorption fine structure, x-ray emission spectroscopy • 4.3-27 keV, 7-52 keV • On-site • Accepting general users •

Tracing the Path of Contaminants in Alaskan Streams

Historic mining in the Kantishna district of Denali National Park, Alaska, has left its mark with high levels of toxic antimony and arsenic in some of the park's creeks. The impact of these metals on Alaskan wildlife is not fully understood. One open question is where the contaminants end up as they are carried downstream. New research using an APS beamline has revealed that the antimony and the arsenic bind primarily to iron oxide particulates, which eventually settle in the stream beds. The results offer new insights into the physical, as well as chemical, path that these elements take through the environment and will help in building geochemical models that can predict how antimony behaves in general environmental settings.

Fig. 1. The waste rock pile from mining near Stampede Creek. Photo: Seth Mueller (Boliden Mineral).

Map outlining the Tintina Gold Province (shaded area), major faults, and the Stampede Creek and Slate Creek study areas. Modified from Eppinger et al., U.S Geological Survey Professional Paper, 1662 (2000).

Fig. 2. Sample collection in Slate Creek. Photo: Tom Trainor (U. Alaska Fairbanks).

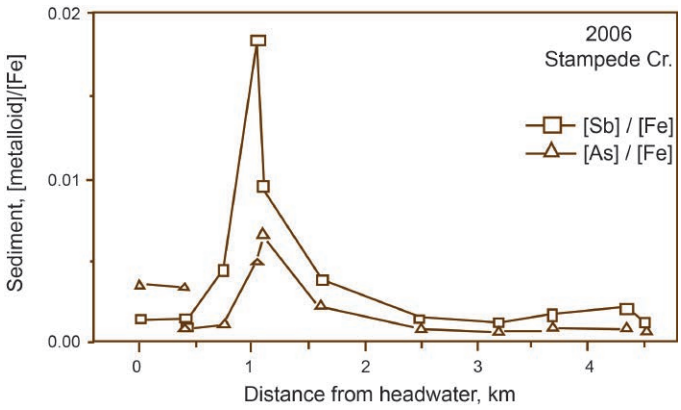

Fig. 3. The concentration of antimony (Sb) and arsenic (As) relative to iron (Fe) in sediments taken from Stampede Creek in Denali National Park, Alaska. The peaks occur near the location of the Stampede Mine, which was the largest producer of antimony in Alaska's history. From Vanessa J. Ritchie et al., Chem. Geol. **335**, 172 (2013).

The Kantishna Hills of the northwestern part of Denali National Park are home to several antimony deposits, which were extensively mined up through the mid-1980s. As a result of this mining, some of the nearby streams, such as Stampede Creek and Slate Creek (see Figs. 1 and 2), have concentrations of antimony and the related element arsenic (As) around 100 µg per liter of water. These levels are roughly 10 times higher than the drinking water limits set by the U.S. Environmental Protection Agency. Both antimony and arsenic are toxic to humans, so there is a concern over the effects these contaminants will have on the Alaskan ecosystem.

Arsenic is a common contaminant associated with mineral deposits, so its environmental interactions have been intensely studied. By contrast, antimony chemistry is not well-understood. Antimony is typically found in nature in the form of the sulfide mineral stibnite (Sb_2S_3). In the mining process, stibnite and other sulfide minerals (some containing arsenic) are exposed to oxidative weathering.

An important question is how fast des antimony oxidizes, since the oxidization state is related to the toxicity. Moreover, oxidization makes antimony more water soluble, so it can enter runoff. Once it reaches streams, there are uncertainties about how long it stays in the water. Does it react with something and become immobilized or does it float downstream and become diluted by more water?

To answer these questions, researchers from Fairbanks Environmental Services, the University of Alaska Fairbanks, the Swedish company Boliden Mineral, and the U.S. Geological Survey collected samples of stream water and sediments from the Kantishna mining district during field expeditions between 2005 and 2007.

From their water analysis, the team found that the concentrations of antimony and arsenic near the mining sites reached peaks of 720 and 239 µg per liter, respectively. These levels were around 100 times higher than the normal levels recorded upstream of the mines. This data suggests that antimony oxidizes quickly when exposed to weathering. The water samples from downstream sites showed that the arsenic concentration dropped back to normal after about 1.5 km. The antimony concentration also dropped down, but not as quickly. The level of antimony in the water remained above normal for more than 8 km downstream from the mining operations.

To see where the metals go when they leave the water, the researchers used the GSECARS 13-BM-D beamline at the APS for a number of x-ray studies. They analyzed sediments from the bottom of the streams using x-ray absorption spectroscopy (XAS). They exposed samples to x-ray energies near the K edge of antimony (30 keV), as well as arsenic (12 keV). X-ray absorption near edge structure (XANES) spectra revealed oxidized forms of antimony and arsenic in the sediments. The greatest amounts appeared just downstream of the mining sites (Fig. 3). Following up with extended x-ray absorption fine structure measurements, the team found that both antimony and arsenic are associated with iron oxides in the sediments. The researchers concluded that the contaminants bind to the surface of amorphous iron oxide particulates, which are readily transported downstream before settling out. The x-ray experiments showed that the antimony forms a fairly strong chemical bond to the iron oxide particulates. The implication is that the antimony incorporated into the stream sediments. The team is continuing their XAS studies to better understand the binding of antimony to iron-oxide substrates.

— Michael Schirber

See: Vanessa J. Ritchie[1,2], Anastasia G. Ilgen[2 ‡], Seth H. Mueller[3], Thomas P. Trainor[2*], and Richard J. Goldfarb[4], "Mobility and chemical fate of antimony and arsenic in historic mining environments of the Kantishna Hills district, Denali National Park and Preserve, Alaska," Chem. Geol. **335**, 172 (2013). DOI:10.1016/j.chemgeo.2012.10.016
Author affiliations: [1]Fairbanks Environmental Services, Inc.; [2]University of Alaska Fairbanks; [3]Boliden Mineral; [4]U.S. Geological Survey. ‡Present address: Sandia National Laboratories
Correspondence:
* tptrainor@alaska.edu

This research was financially supported by the U.S. Geological Survey Mineral Resources External Research Program grant MRERP-06HQGR0177, National Science Foundation grants CBET-0404400 and CHE-0431425, Strategic Environmental Research and Development Program grant SERD-PER-1770, and the Discover Denali Research Fellowship (funded by the National Park Service and the Denali Education Center). GSECARS is supported by the National Science Foundation - Earth Sciences (EAR-1128799) and Department of Energy-Geo-Sciences (DE-FG02-94ER14466). Use of the Advanced Photon Source at Argonne National Laboratory was supported by the U.S. Department of Energy Office of Science under Contract No. DE-AC02-06CH11357.

13-BM-D • GSECARS • Geoscience, environmental science • Tomography, high-pressure diamond anvil cell, high-pressure multi-anvil press, x-ray absorption fine structure • 4.5-70 keV • On-site • Accepting general users •

Defining the Line: Melting Curve for Iron Helps Characterize the Earth's Core

The Earth's core is 16% of the planet by volume. It is composed primarily of iron, but includes a quantity of lighter elements whose presence, but not identity, is inferred from geophysical measurements. The core consists of a solid inner section surrounded by a convecting, liquid outer layer. It creates Earth's magnetic field, protecting the planet from space weather events such as solar flares, and provides the heat for plate tectonics as the liquid core freezes. The core begins approximately 2900 km below the Earth's surface, making it difficult to determine its exact composition and temperature profile, so scientists rely on laboratory experiments and an evolving model to infer core characteristics. For example, they use experiments to populate data points on the melting curve of iron, a key descriptor of the core because the liquid outer core and solid inner core coexist at a temperature below the melting point of pure iron. Now, utilizing the APS in a new application of the Mössbauer effect, scientists are refining the temperature range of the Earth's inner core/outer core border to increase our understanding of geophysical processes and the Earth's formation.

A team of scientists, from the California Institute of Technology, Argonne, the Carnegie Institution of Washington, and the University of Illinois at Urbana-Champaign, utilized synchrotron Mössbauer spectroscopy at XSD beamline 3-ID-B to determine the melting points of iron at pressures representative of the core's environment. Mössbauer spectroscopy leverages the Mössbauer effect: that for some isotopes, including ^{57}Fe, resonant absorption, and re-emission of a gamma ray can occur without the nuclei recoiling when the isotope is bound in a solid. This effect vanishes if the isotope is bound in a liquid. This recoil-free characteristic of ^{57}Fe means that x-rays absorbed and re-emitted will continue on in their original direction to be detected on the opposite side of the sample where the Mössbauer signal is determined by the scattering strength and ^{57}Fe density of the sample.

Figure 1 shows the team's experimental setup, with the left-to-right horizontal arrow indicating the direction of the x-rays; the detector is to the right of the diamond anvils. The Mössbauer signal that scatters from the sample prior to melting is sensitive to the movement of the iron nuclei. As the sample transitions from solid to liquid, the iron nuclei move more; this enhanced freedom of motion results in fewer recoil-free scattering events, and the Mössbauer signal drops markedly.

The team heated compressed samples of ^{57}Fe with an infrared laser system, measured the integrated synchrotron Mössbauer signal intensity as each sample transitioned from solid to liquid, then determined the scattering strength from the integrated intensity. The marked drop in scattering strength indicated when the solid iron melted. They determined the temperatures at the first measurement of the molten state and the final measurement of the

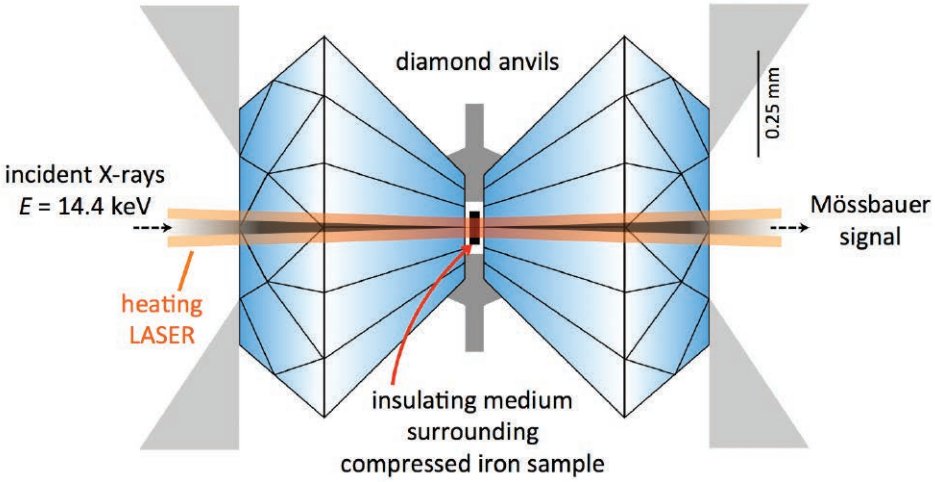

Fig. 1. Diagram of the experimental setup for the synchrotron Mössbauer spectroscopy experiments. This approach is unique because the dynamics of only the iron atoms are monitored. Image: Jennifer M. Jackson (Caltech).

solid state, defining the melting point to be the mean of the two.

The resulting temperatures agreed well with the existing literature at low pressures, but above 60 GPa this new technique yielded higher melting temperatures than other published results. This difference might be explained by disparities in the determination of exactly when the material melted, methods of accounting for thermal pressure, or temperature determination. The strength of the synchrotron Mössbauer spectroscopic technique is that it monitors the solid-to-liquid transition using the dynamics of the atoms themselves, unlike other melt-monitoring techniques, so it is possible the disparity is due to this alternative diagnostic of melting. The researchers have begun incorporating *in situ* x-ray diffraction measurements of hot ^{57}Fe to refine the thermal pressure estimates used in this study and remove it as a possible discrepancy.

This application of synchrotron Mössbauer spectroscopy to the melting curve of iron allows for greater scientific scrutiny of the temperatures in the environment of Earth's core, yielding new data which characterizes the inner core/outer core border, and broadens the palette of tools available to probe the workings of Earth's inaccessible core. *— Mary Alexandra Agner*

See: Jennifer M. Jackson[1], Wolfgang Sturhahn[2], Michael Lerche[2], Jiyong Zhao[2], Thomas S. Toellner[2], E. Ercan Alp[2], Stanislav V. Sinogeikin[3], Jay D. Bass[4], Caitlin A. Murphy[1], and June K. Wicks[1], "Melting of compressed iron by monitoring atomic dynamics," Earth Planet. Sci. Lett. **362**, 143 (2013). DOI:10.1016/j.epsl.2012.11.048

Author affiliations: [1]California Institute of Technology, [2]Argonne National Laboratory, [3]Carnegie Institution of Washington, [4]University of Illinois at Urbana-Champaign,

Correspondence:

* jackson@gps.caltech.edu

This research was supported by the National Science Foundation and Caltech. APS Sector 3 operations are partially supported by COMPRES (NSFEAR06-49658). Use of the Advanced Photon Source at Argonne National Laboratory was supported by the U.S. Department of Energy Office of Science under Contract No. DE-AC02-06CH11357.

3-ID-B,C,D • XSD • Physics, nuclear resonant scattering, inelastic x-ray scattering, high-pressure diamond anvil cell • 7-27 keV, 14.41-14.42 keV • On-site • Accepting general users •

Inge Lehmann: Discoverer of the Earth's Inner Core

Seismic waves — shock waves generated by earthquakes and explosions that travel through Earth and across its surface — reveal the structure of the interior of the Earth. The waves important for understanding the Earth's interior are P-waves, (primary, or compressional waves) and S-waves (secondary, or shear waves), which travel through solid and liquid material in different ways. The seismograph, which detects and records the movement of seismic waves, was invented in 1880. At the time, geophysicists believed Earth to be made up of a liquid core surrounded by a solid mantle, itself surrounded by a crust, all separated by abrupt density changes in the Earth called "discontinuities."

In 1929 a large earthquake occurred near New Zealand. Danish seismologist Inge Lehmann, "the only Danish seismologist," as she once referred to herself, studied the shock waves and was puzzled by what she saw. A few P-waves, which should have been deflected by the core, were recorded at seismic stations. Lehmann theorized that these waves had traveled some distance into the core and then bounced off some kind of boundary. Her interpretation of this data was the foundation of a 1936 paper in which she theorized that Earth's center consisted of two parts: a solid inner core surrounded by a liquid outer core, separated by what has come to be called the Lehmann Discontinuity. Lehmann's hypothesis was confirmed in 1970 when more sensitive seismographs detected waves deflecting off this solid core.

Born in Denmark in 1888, Lehmann was a pioneer among women and scientists. Her early education was at a progressive school where boys and girls were treated exactly alike. This was a sharp contrast to the mathematical and scientific community she later encountered.

A critical and independent thinker, Lehmann subsequently established herself as an authority on the structure of the upper mantle. When Lehmann received the William Bowie medal in 1971, the highest honor of the American Geophysical Union, she was described as "the master of a black art for which no amount of computerizing is likely to be a complete substitute." Lehmann lived to be 105.

Excerpted from EARTH: INSIDE AND OUT, edited by Edmond A. Mathez, a publication of the New Press. © 2000 American Museum of Natural History, http://www.amnh.org/education/resources/rfl/web/essaybooks/earth/p_lehmann.html

Determining the Structure of Postperovskite

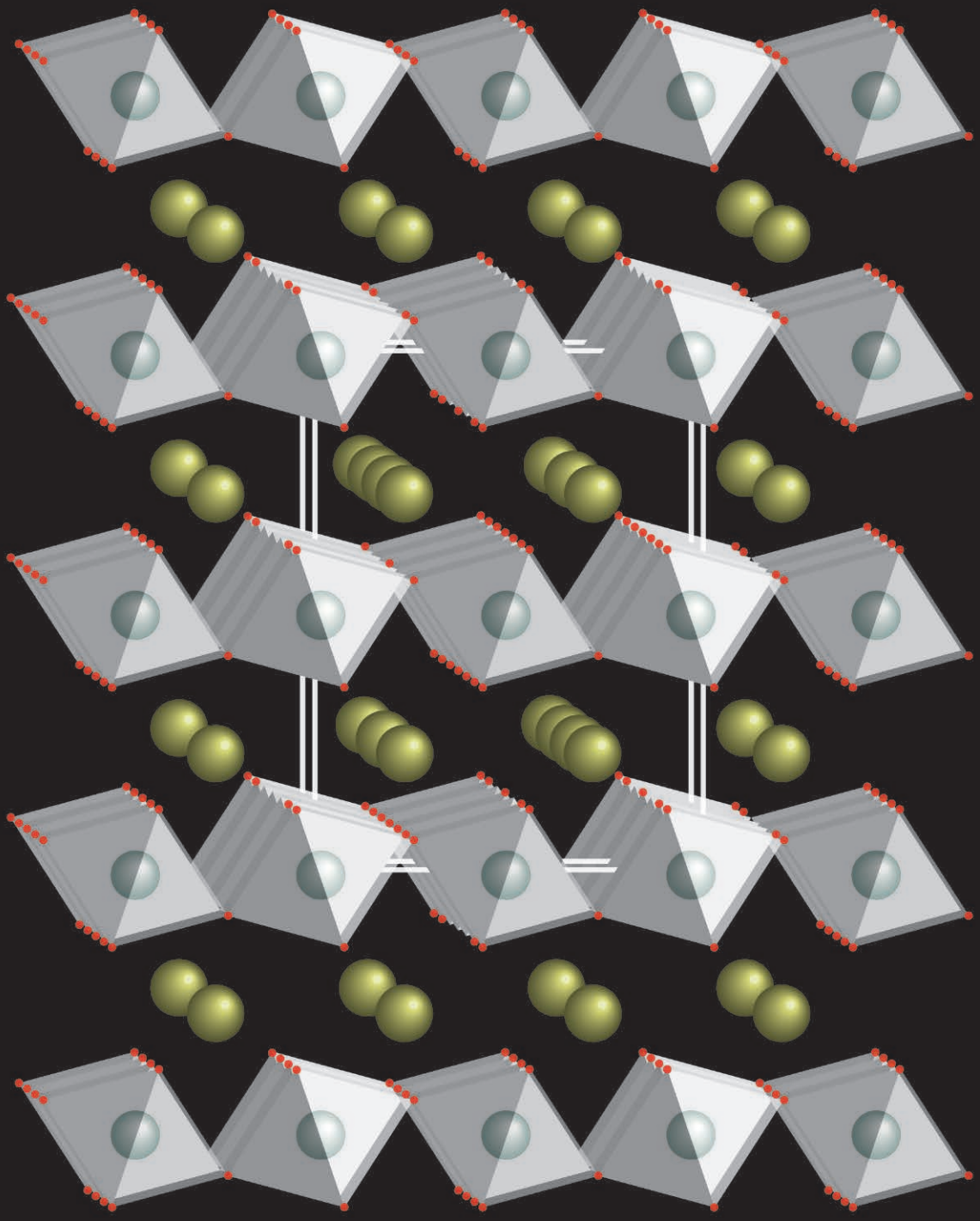

Earth's mantle is divided by seismic discontinuities, places where seismic waves traveling through the planet abruptly change speed. The lowermost ~200 km of the mantle (and also the top of the deepest portion of the mantle) called the D″ layer, presents a first-order seismic discontinuity. The discontinuity is likely caused by a phase change between the two magnesium-iron silicate minerals, perovskite and its higher pressure phase, postperovskite (ppv), a high-pressure mineral that makes up most of this region. To better understand the seismic discontinuity, scientists study the crystal structure of postperovskite because understanding the seismic features of the lowermost mantle requires precise knowledge of the effects of pressure and composition on the crystal structure of postperovskite at the tremendous pressures and temperatures in the region. Powder x-ray diffraction experiments indicate that magnesium or iron may alter the crystal structure of the postperovskite phase. But a new technique, as applied by a research team carrying out studies at the APS, is yielding insights into the crystal structure of postperovskite at the perovskite-postperovskite transition.

The new technique employs multigrain single-crystal x-ray diffraction (XRD) analysis in a diamond anvil cell. It was used in a study by researchers from the Center for High Pressure Science and Technology Advanced Research (China), the Carnegie Institution of Washington, The University of Chicago, the Hawaii Institute of Geophysics and Planetology, Stanford University, and SLAC National Accelerator Laboratory. In this work, polycrystalline samples of (Mg,Fe)SiO_3 postperovskite were synthesized in a diamond anvil cell at pressures and temperatures typical of the D″ layer. Then the newly developed single-crystal x-ray diffraction technique was performed *in situ*. Utilizing the HP-CAT 16-ID-B beamline at the APS, the crystallographic orientations were be simultaneously determined for over 100 individual submicron crystals at one beam position. Advanced computation methods then separated the signals from different grains into a single-crystal structure. The individual crystallites were also mapped across the x-ray beam using the focused polychromatic and monochromatic x-ray beam available at XSD beamline 34-ID-E, aldo at the APS. The intensity of the diffraction spot dropped by more than half after moving one step in both directions, indicating that the sizes of crystallites in the sample were ~0.5 μm (FWHM) or less.

Fig. 1. Crystal structure of (Mg,Fe)SiO_3 postperovskite. Polyhedra of O atoms around Si atoms are shown as octahedra, and ~10% Fe^{2+} ions substitute Mg^{2+}, shown as spheres.

In the diamond anvil cell, postperovskite became the dominant phase at 120 GPa. The volume difference between perovskite and postperovskite, which have the same composition but different structure, is 1.1%. This value is approximately the same as the volume difference of 1.0% to 1.2% in $MgSiO_3$. The result is that Fe-partitioning is not distinguishable between the perovskite and postperovskite phases, an outcome that is in good agreement with the powder diffraction data of previous studies.

Models of Earth's deep interior have been built upon the assumption that the lower mantle mainly consists of iron-bearing magnesium silicate with nominally 10% iron. The analysis in this study reveals that replacing 10% of the magnesium with iron in postperovskite barely alters its crystal structure. But at the base of the deepest mantle, the core-mantle boundary contains ultra-low velocity zones that may be enriched in iron from interactions with the molten metal outer core. In this case, postperovskite might be structurally different.

This new, single-crystal XRD technique has many advantages over powder diffraction methods, such as insights into rigorous three-dimensional angular and symmetric relations. Indexing aggregates of several hundred submicron crystallites and performing structural analysis on each allows for *in situ* single-crystal studies in high-P conditions that were not previously possible. Single-crystal XRD provides structural analysis and refinement methods that, when applied for a few ppv crystals, demonstrate the feasibility of the *in situ* study of crystal structures of submicron crystallites in a multiphase polycrystalline sample in a high-P device. *— Dana Desonie*

See: Li Zhang[1,2]*, Yue Meng[2], Przemyslaw Dera[3,4], Wenge Yang[2], Wendy L. Mao[5,6], and Ho-kwang Mao[1,2]*, "Single-crystal structure determination of (Mg,Fe)SiO_3 postperovskite," Proc. Natl. Acad. Sci. U.S.A. **110**(16), 6295 (April 16, 2013). DOI:10.1073/pnas.1304402110

Author affiliations: [1]Center for High Pressure Science and Technology Advanced Research, [2]Carnegie Institution of Washington, [3]The University of Chicago, [4]Hawaii Institute of Geophysics and Planetology, [5]Stanford University, [6]SLAC National Accelerator Laboratory

Correspondence:

* zhangli@hpstar.ac.cn,

* hmao@ciw.edu.

This research was supported by National Science Foundation (NSF) Grants EAR-0911492, EAR-1055454, and EAR-1119504. High Pressure Synergetic Consortium (HPSynC) is supported as part of EFree, an Energy Frontier Research Center funded by the U.S. Department of Energy (DOE) Office of Science -Basic Energy Sciences under Grant DE-SC0001057. HP-CAT operations are supported DOE-National Nuclear Security Administration under Award No. DE-NA0001974 and DOE-Basic Energy Sciences under Award No. DE-FG02-99ER45775, with partial instrumentation funding by the NSF. Use of the Advanced Photon Source at Argonne National Laboratory was supported by the U.S. Department of Energy Office of Science under Contract No. DE-AC02-06CH11357.

16-ID-B • HP-CAT • Materials science, geoscience, chemistry, physics • Microdiffraction, single-crystal diffraction, high-pressure diamond anvil cell • 14-42 keV • On-site • Accepting general users •

34-ID-E • Materials science, physics, environmental science, geoscience • Microdiffraction, Laue crystallography, microbeam • 7-30 keV • On-site • Accepting general users •

Mimicking Earth's Magnesite Formation in the Lab

A photograph of a sample of Mg_2SiO_4 and carbon dioxide together, as seen from above. Multiple experiments can be made using the same sample. Each dark spot in the (roughly) rectangular region is where the sample has been irradiated by infrared lasers while the sample is held at successively higher pressures and synchrotron x-ray diffraction measurements are being made simultaneously.

The mineral magnesite – rich in carbon, magnesium, and oxygen – is thought to be common in Earth's mantle and is believed to play a large role in how carbon cycles through the Earth, the oceans, and the environment. But studying the materials present in the intense heat and pressure of the mantle, which extends down to some 1800 miles below the Earth's surface, is not easy. Scientists must rely on a variety of remote techniques to probe these inaccessible regions, many of which involve trying to recreate the extreme environment found there and observing what happens. Research at the APS observed how, under such extreme conditions, magnesite can be made from magnesium oxide and carbon dioxide. The work strongly supports the model of magnesite's prevalence in and import to the Earth's mantle.

The mineral magnesite – rich in carbon, magnesium, and oxygen – is thought to be common in Earth's mantle and is believed to play a large role in how carbon cycles through the Earth, the oceans, and the environment. But studying the materials present in the intense heat and pressure of the mantle, which extends down to some 1800 miles below the Earth's surface, is not easy. Scientists must rely on a variety of remote techniques to probe these inaccessible regions, many of which involve trying to recreate the extreme environment found there and observing what happens. Research at the APS observed how, under such extreme conditions, magnesite can be made from magnesium oxide and carbon dioxide. The work strongly supports the model of magnesite's prevalence in and import to the Earth's mantle.

Inside the Earth, magnesite likely serves as the main storage phase for carbon. The magnesite contains carbon bonded to oxygen. When magnesite breaks down in the mantle it may release carbon dioxide. Much evidence exists to suggest that magnesite is the primary storage mineral for carbon deep inside the Earth, and that it is stable under very high pressures and temperatures. Previous studies have focused, however, on already formed magnesite. In contrast, this work — carried out by researchers from Indiana University South Bend (IUSB), Northern Illinois University, and The University of Texas at Austin — examined the process of how magnesite is formed to establish how easily or not it might arise in the mantle.

The team compressed magnesium oxide and carbon dioxide within a diamond anvil cell (DAC). In addition to the high pressures from the DAC, the samples were heated using lasers at the APS. Diamond anvil cells are useful not only for putting samples under pressure, but also because they are clear, allowing the sample to be examined directly. The crystalline structure of the sample was observed with synchrotron x-rays from three different beamlines at the APS: 16-ID-B and 16-BM-D of HP-CAT, and 13-ID-D of GSECARS. Examining the samples showed that magnesite forms quite easily from magnesium oxide and carbon dioxide at the pressures and temperatures expected in Earth's mantle. Moreover, during the experiments, the team didn't witness other materials forming. The ease of formation, and the material's stability support the model that much of the oxidized carbon in Earth's mantle is stored in magnesite.

When magnesite breaks down and releases carbon dioxide it may help melt other rocks or even precipitate diamonds. The next step for these researchers will be to look at more complicated chemical systems to see if other carbon-bearing minerals form and also to place additional constraints on the conditions for which magnesite becomes unstable, thus releasing carbon.

— Karen Fox

See: Henry P. Scott[1]*, Vincent M. Doczy[1], Mark R. Frank[2], Maggie Hasan[2], Jung-Fu Lin[3], and Jing Yang[3], "Magnesite formation from MgO and CO_2 at the pressures and temperatures of Earth's mantle," Am. Mineral. **98**, 1211 (2013).DOI:10.2138/am.2013.4260

Author affiliations: [1]Indiana University South Bend, [2]Northern Illinois University, [3]The University of Texas at Austin
Correspondence: * hpscott@iusb.edu

This research was partially supported by COMPRES, the Consortium for Materials Properties Research in Earth Sciences under U.S. National Science Foundation Cooperative Agreement EAR 11–57758. H. Scott thanks the IUSB R&D committee for faculty research support and the SMART committee for supporting several undergraduate researchers who helped with this project. J.F. Lin acknowledges supports from NSF-EAR Geophysics, CDAC (Carnegie-DOE Alliance Center), and EFree (Energy Frontier Research in Extreme Environments). GSECARS is supported by the National Science Foundation-Earth Sciences (EAR-1128799) and U.S. Department of Energy (DOE)-GeoSciences (DE-FG02-94ER14466). HP-CAT operations are supported by the DOE-National Nuclear Security Administration under Award No. DE-NA0001974 and DOE-Basic Energy Sciences under Award No. DE-FG02-99ER45775, with partial instrumentation funding by the NSF. Use of the Advanced Photon Source at Argonne National Laboratory was supported by the U.S. Department of Energy Office of Science under Contract No. DE-AC02-06CH11357.

13-ID-C,D • GSECARS • Geoscience, environmental science • Inelastic x-ray scattering, micro x-ray absorption fine structure, microdiffraction, x-ray absorption fine structure, microfluorescence (hard x-ray), high-pressure diamond anvil cell, high-pressure multi-anvil press • 4-45 keV • On-site • Accepting general users •

16-BM-D • HP-CAT • Materials science, geoscience, chemistry, physics • Powder angular dispersive x-ray diffraction, x-ray absorption near-edge structure, single-crystal diffraction, high-pressure diamond anvil cell • 6-70 keV • On-site • Accepting general users •

16-ID-B • HP-CAT • Materials science, geoscience, chemistry, physics • Microdiffraction, single-crystal diffraction, high-pressure diamond anvil cell • 14-42 keV • On-site • Accepting general users •

Iron's Electronic Transition under Pressure

Iron and its alloys are used in applications ranging from industry to electronics, and even superconductor research. In addition to their importance *on* our planet, these materials are found *in* our planet as well — high-pressure iron-nickel alloy is the primary ingredient in the Earth's core and perhaps the cores of other planets. The Earth and space sciences thus require a thorough understanding of iron and iron-nickel alloys under pressure, but although scientists have studied these materials for many years, mysteries still remain. For example, early studies found discrepancies in iron's behavior when the pressure reached 40 GPa. Was this signal mere noise or the sign of a significant electronic transition? Now a research team has solved the mystery of this anomaly and gathered clues about iron's superconductivity by studying iron and the iron-nickel alloy $Fe_{0.9}Ni_{0.1}$ at multiple facilities including the APS.

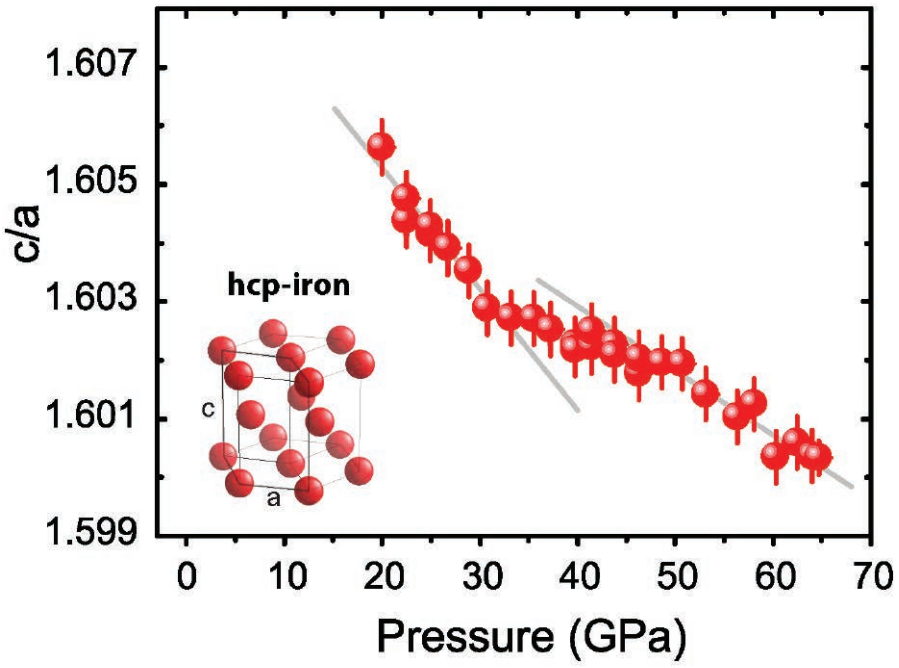

Fig. 1. Pressure dependence of the c/a ratio, the lattice parameter of hexagonal close-packed iron and iron-nickel. Inset: unit cell of a hexagonal close-packed structure.

To find the origin of the anomaly at 40 GPa, an international team of researchers first had to prove the signal was real. It was crucial to show a change in the material's compressional behavior when the pressure reached this point.

The compressional behavior of iron and the iron-nickel alloy $Fe_{0.9}Ni_{0.1}$ can be seen by looking at changes in the lattice parameters. At the range of pressures around 40 GPa, both pure iron and its nickel alloy shift into the phase known as hexagonal close packed, or hcp. The hcp unit cell (see the first figure) can be described by the ratio of c to a. Changes in this lattice parameter under various pressures were thus important indications of the material's compressional behavior.

Using the diamond anvil cell at GeoSoilEnviroCARS beamline 13-ID-D at the Argonne National Laboratory APS, the researchers measured how the c/a ratio changed as the pressure rose from 12 to about 65 GPa. At about 40 GPa, they noticed an anomaly (second figure). The phenomenon was confirmed by independent measurements taken at the European Synchrotron Radiation Facility (France) on beamline ID09A.

To understand the physical nature of the phenomenon, the researchers also ran two independent experiments under a similar range of pressures. Using beamline ID18 at the European Synchrotron Radiation Facility, they performed nuclear resonant inelastic x-ray scattering to measure the Debye sound velocity. At the University of Bayreuth's Bavarian Research Institute of Experimental Geochemistry and Geophysics (Germany), they used Mössbauer spectroscopy to measure the Mössbauer center shift.

Both of these experiments observed similar anomalies around 40 GPa. The Debye sound velocity softened slightly around 42 to 52 GPa, and the Mössbauer center shift showed a strong anomaly around 40 to 45 GPa.

These results proved the existence of a signal at 40 GPa. However, previous papers on hcp iron and iron-nickel had shown no changes in the crystal structure at this pressure. In addition, hcp iron has shown no evidence of ordered magnetic structure. If the signal does not stem from physical or magnetic changes, it must indicate a change in the electronic state.

To learn more, members of the researcher team, from Linköping University (Sweden) calculated the theoretical electronic structure of iron in the 12 to 70 gigapascal pressure range. Their technique combined local density approximation with dynamical mean-field theory.

According to the theoretical model the topology of the Fermi surface (which describes the electronic band structure of the metal) changes under

"Transition" cont'd. on page 168

Earth's Core Reveals an Inner Weakness

The word "core" conjures up images of something strong. However, new experiments show that the iron found in the Earth's core is relatively weak. This finding is based on x-ray spectroscopy and diffraction measurements performed at high pressure and utilizing several x-ray beamlines at two U.S. Department of Energy Office of Science light sources including the APS. The researchers in these studies extrapolated their results to core conditions and found that the strength of iron deep within the Earth is lower than previously thought. This weakness may explain how the crystal structure in the Earth's core has transformed over geological time scales.

The extreme conditions of the Earth's core are very difficult to reproduce in a laboratory. The pressure rises above 3 million (320-370 GPa), and the temperature is comparable to that on the surface of the Sun (over 5000° C). Seismologists have learned about the core by studying seismic waves that travel through the Earth's interior.

One discovery is that core-traversing seismic waves travel 3% faster along the polar axis as compared to those moving through the equatorial plane. Researchers assume that this seismic-wave anisotropy is due to iron crystals aligning their lattice structures, which requires a certain amount of "flow" through the solid core, and this has yet to be explained.

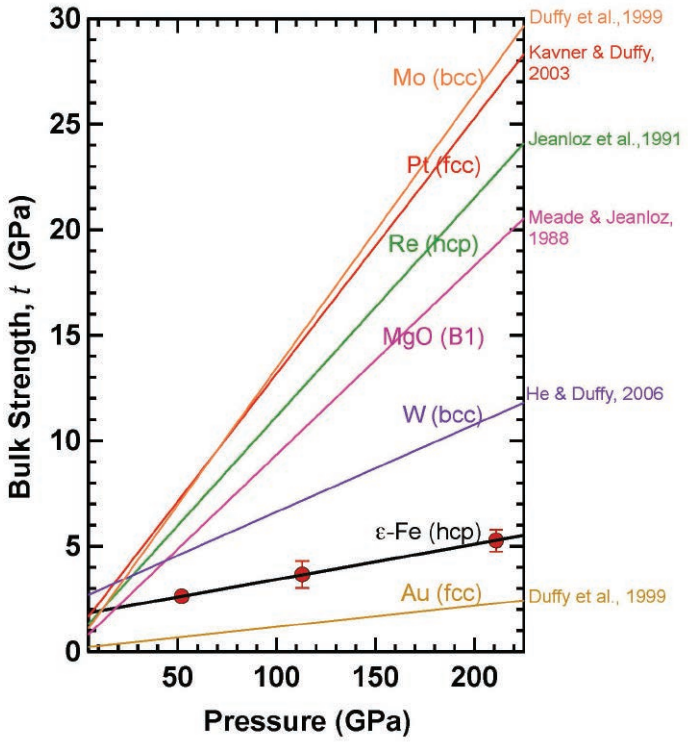

Fig. 1. The strength of several different metals, extrapolated to high pressure. Plot courtesy of A.E. Gleason (Stanford U.).

Deep inside the Earth, iron has a different structure than at the surface. For objects like horseshoes and tea kettles, the iron atoms are packed together in a pattern called body-centered cubic (bcc). However, when the pressure rises above 12 GPa, the iron atoms rearrange into a hexagonally close-packed (hcp) structure.

To better understand hcp iron, researchers from Stanford University and the SLAC National Accelerator Laboratory have made new strength measurements at high pressure, as described in *Nature Geoscience*. Strength, which is a material's resistance to flow, is characterized by the pressure at which the material begins to deform. Previous studies of iron's strength have typically applied pressure in a non-uniform (or non-hydrostatic) way.

To reproduce the hydrostatic conditions of the Earth's interior, the researchers here loaded their foil-shaped samples of iron into a gasket filled with a pressure-transmitting medium of neon or helium gas. This gasket was then placed in a diamond-anvil cell, where pressures as high as 200 GPa could be applied.

For their study of the material properties of hydrostatically compressed iron, the team first performed nuclear resonant inelastic x-ray scattering (NRIXS) experiments at two APS x-ray beamlines: 3-ID-B (operated by XSD) and16-ID-D (operated by HP-CAT). The spectrum of the scattered x-rays contained information about shear waves that travel through the iron like seismic waves. From their data analysis, the team derived the shear modulus — a measure of the rigidity of a material — and found it to be slightly lower than previous measurements of iron taken in non-hydrostatic environments.

The team then performed radial x-ray diffraction (rXRD) experiments at the HP-CAT 16-BM-D beamline, as well as with another x-ray beamline at the Advanced Light Source at Lawrence Berkeley National Laboratory. These measurements showed a shift in iron

"Weakness" cont'd. on page 168

"Transition" cont'd. from page 166
pressure. At 40 GPa, the material undergoes an electronic topological transition, a change of electronic configuration. This transition is due to the interactions of multiple electrons, also known as correlation effects.

The existence of this topological transition must be taken into account by solid-state physicists. The correlation effects that cause the transition also play an important role in the properties of other transition metals. Iron, however is particularly interesting because at certain pressures and temperatures, pure iron in the hcp phase can become superconducting. Describing its properties, including the correlation effect, may provide clues about iron's superconductivity. *— Sophie Bushwick*

See: K. Glazyrin[1,2]*, L.V. Pourovskii[3,4], L. Dubrovinsky[1], O. Narygina[5], C. McCammon[1], B. Hewener[6], V. Schünemann[6], J. Wolny[6], K. Muffler[6], A.I. Chumakov[7], W. Crichton[7], M. Hanfland[7], V.B. Prakapenka[8], F. Tasnádi[3], M. Ekholm[3], M. Aichhorn[9], V. Vildosola[10], A.V. Ruban[11], M.I. Katsnelson[12], and I.A. Abrikosov[3], "Importance of Correlation Effects in hcp Iron Revealed by a Pressure-Induced Electronic Topological Transition," Phys. Rev. Lett. **110**, 117206 (2013). DOI:10.1103/PhysRevLett.110.117206
Author affiliations: [1]Universität Bayreuth, [2]Yale University, [3]Linköping University, [4]Polytechnique, [5]University of Edinburgh, [6]Technische Universität Kaiserslautern, [7]European Synchrotron Radiation Facility, [8]The University of Chicago, [9]Institute of Theoretical and Computational Physics, [10]Comisión Nacional de Investigaciones Científicas y Técnicas, [11]Royal Institute of Technology, [12]Radboud University Nijmegen
Correspondence:
*konstantin.glazyrin@desy.de

This research was supported by funding from the Swedish e-Science Research Centre, the Swedish Research Council via Grant No. 621-2011-4426, and the Swedish Foundation for Strategic Research programs SRL Grant No. 10-0026 and "Multifilms," as well as financial support from the German Science Foundation (DFG) and German Ministry for Education and Research (BMBF). GeoSoilEnviroCARS is supported by the National Science Foundation-Earth Sciences (EAR-1128799) and Department of Energy-Geosciences (DE-FG02-94ER14466). Use of the Advanced Photon Source at Argonne National Laboratory was supported by the U.S. Department of Energy Office of Science under Contract No. DE-AC02-06CH11357.

13-ID-C,D • GSECARS • Geoscience, environmental science • Inelastic x-ray scattering, micro x-ray absorption fine structure, microdiffraction, x-ray absorption fine structure, microfluorescence (hard x-ray), high-pressure diamond anvil cell, high-pressure multi-anvil press • 4-45 keV • On-site • Accepting general users •

"Weakness" cont'd. from page 167
diffraction lines due to a squeezing (or strain) of the lattice separation when the sample was under pressure. The researchers combined the observed strain and shear modulus values to obtain the strength of iron at high pressures. Surprisingly, the derived strength was 60% lower than previous estimates, making iron one of the weakest metals at high pressures (Fig. 1).

> The researchers estimated that iron's strength is around 1 GPa at the pressure and temperature of the Earth's core. This low value has implications for how the material in the core deforms, or "creeps," over time.

The team estimated that iron's strength is around 1 GPa at the pressure and temperature of the Earth's core. This low value has implications for how the material in the core deforms, or "creeps," over time. Previous models assumed that this creep was a very slow process, based mostly on diffusion of atoms. However, a lower strength for iron means that creep could occur through the movement of defects, or "dislocations," in the crystal structure. This faster dislocation creep would imply that the observed seismic-wave anisotropy developed relatively early in the Earth's history. To explore this idea further, the team plans to perform a new set of iron experiments at high temperature as well as high pressure.

— Michael Schirber

See: A.E. Gleason[1]* and W.L. Mao[1,2], "Strength of iron at core pressures and evidence for a weak Earth's inner core," Nat. Geo. **6**, 571 (July 2013). DOI:10.1038/NGEO1808
Author affiliations: [1]Stanford University, [2]SLAC National Accelerator Laboratory
Correspondence:
*ariannag@stanford.edu

The authors are supported by the Geophysics Program at the National Science Foundation (NSF, EAR0738873). Sector 3 operations are partially supported by COMPRES (NSFEAR06-49658). HP-CAT operations are supported by the U.S. Department of Energy (DOE)-National Nuclear Security Administration under Award No. DE-NA0001974 and DOE-Basic Energy Sciences under Award No. DE-FG02-99ER45775, with partial instrumentation funding by the NSF. Use of the Advanced Photon Source at Argonne National Laboratory was supported by the U.S. Department of Energy Office of Science under Contract No. DE-AC02-06CH11357.

3-ID-B,C,D • XSD • Physics, nuclear resonant scattering, inelastic x-ray scattering, high-pressure diamond anvil cell • 7-27 keV, 14.41-14.42 keV • On-site • Accepting general users •

16-BM-D • HP-CAT • Materials science, geoscience, chemistry, physics • Powder angular dispersive x-ray diffraction, x-ray absorption near-edge structure, single-crystal diffraction, high-pressure diamond anvil cell • 6-70 keV • On-site • Accepting general users •

16-ID-D • HP-CAT • Materials science, geoscience, chemistry, physics • Nuclear resonant scattering, inelastic x-ray scattering (1 eV resolution), x-ray Raman scattering, x-ray emission spectroscopy, high-pressure diamond anvil cell • 5-35 keV, 14.41-14.42 keV • On-site • Accepting general users •

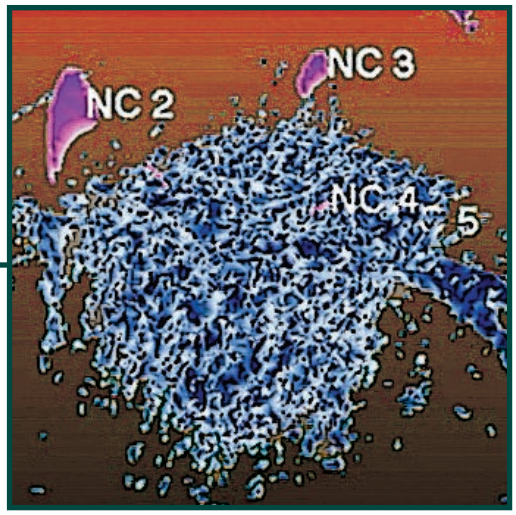

Nanoscience

Anti-Cancer Nanoparticle Therapy Heats Up

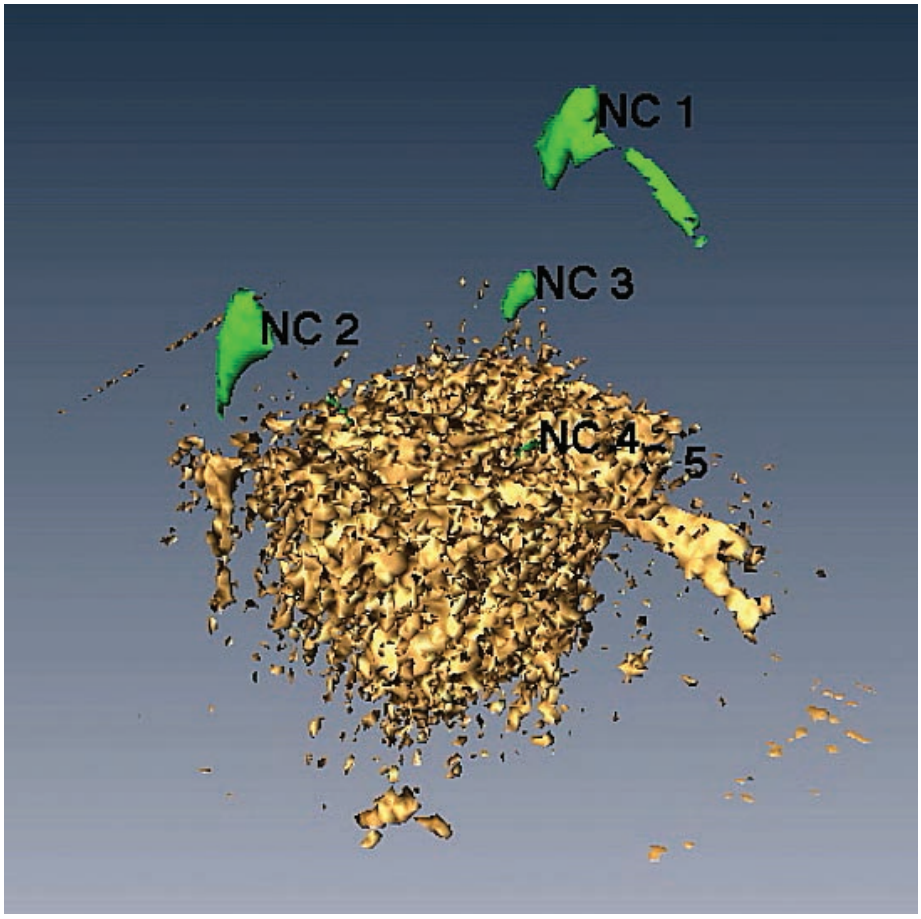

Fig. 1. A tomographic reconstruction of the material signatures produced by x-ray fluorescence microscopy shows a position of zinc (gold color) that indicates the cell's nucleus, and green patches representing the titanium of the nanoparticles. Part of the nucleus has been "cut away" in this image to show that the nanoparticles are located within the nucleus.

Oncologists are striving to focus their therapies more directly on cancer cells, both to increase therapeutic effectiveness in fighting cancer and to minimize damage to healthy tissue. One approach uses photoactivated nanoparticles, which enter a cell and, when excited by ultraviolet or ionizing radiation, produce a cloud of ions that destroys the cancer cell. The trouble lies in making sure the nanoparticles reach the right target; often they enter a cell but remain in the cytoplasm, where they are ineffective. Scientists from Northwestern University, Argonne, the Northwestern Synchrotron Research Center, and Carl Zeiss X-ray Microscopy have created and followed the cellular fate of nanoparticles targeted toward a particular receptor on a cell's surface. When they tracked these nanocomposites, using the APS, they found the particles in fact traveled all the way to the cancer cell's nucleus, where they could do the most damage.

The team created nanoparticles averaging approximately 7 nm in diameter, with a Fe_3O_4 core and TiO_2 shell. The titanium oxide is the photoactive material, while the ferric oxide lets the nanoparticle show up in a magnetic resonance image. The ferric oxide also changes the bandgap of the titanium oxide so it can be activated by white light, though in practice ionizing radiation would probably be used because it can penetrate tissue to a greater depth. The team attached several different peptides to the nanoparticles, creating nanocomposites, and tested to see which ones would bind to the epidermal growth factor receptor (EGFR). EGFR is overexpressed in many types of cancer, so nanoparticles that target it should attach to cancer cells more than normal tissue. It turned out that the B-loop peptide — a portion of the protein for epidermal growth factor — bound to the EGFR.

The researchers mixed their B-loop nanocomposites and other nanoparticles with HeLa cancer cells. Using flow cytometry and confocal fluorescent microscopy, they indirectly determined that the B-loop particles bound to EGFR and to a nuclear transport protein, karyopherin-β, and accumulated in the nucleus, while other particles stayed in the cytoplasm. In order to directly image and quantify the nanocomposites, the team turned to the LS-CAT beamline 21-ID-D at the APS, where the Bionanoprobe instrument has been installed. This is the first and only x-ray fluorescent microscopy (XFM) instrument that can focus hard x-rays down to a 30-nm spot size to image frozen hydrated biological samples. It allows researchers to look at intact and hydrated cells, whereas other techniques require cutting the cells, then dehydrating and labeling them, which alters them and makes it difficult to see some natural processes.

The x-rays induce x-ray fluorescence in the particles' iron and titanium, making them easy to see by XFM without adding an additional fluorescent label. XFM can also map the distribution of elements that occur naturally within the cell, such as phosphorus and sulfur, and trace metals such as zinc and copper. Inside the Bionanoprobe, the sample can be rotated, allowing pictures from multiple angles to be combined into one three-dimensional image. In a two-dimensional image it would be hard to see if the particles were underneath the cell or nucleus or on its surface. By looking from different angles, the team could see that the particles were indeed located within the cells. They could see that, 30 min after they were served to the cells, the nanoparticles had moved to the nucleus, where they would do the most damage when activated.

In a second test, the researchers attached gold to an antibody that binds to EGFR. They used the XSD beamline 2-ID-D at the APS to image the gold-labeled antibodies in cells that had also been exposed to the nanocomposites, which allowed them to confirm that the nanocomposites and the EGFR were in the same place.

Though the researchers demonstrated that the nanoparticles reached their target and degraded nuclear DNA, they did not test the dynamics with which the nanoparticles destroyed the cancer cells. That will be the next step in developing these potential cancer therapies. *— Neil Savage*

See: Ye Yuan[1], Si Chen[2], Tatjana Paunesku[1], Sophie Charlotte Gleber[2], William C. Liu[1], Caroline B. Doty[1], Rachel Mak[1], Junjing Deng[1], Qiaoling Jin[2], Barry Lai[2], Keith Brister[3], Claus Flachenecker[4], Chris Jacobsen[1,2], Stefan Vogt[2], and Gayle E. Woloschak[1]*, "Epidermal Growth Factor Receptor Targeted Nuclear Delivery and High-Resolution Whole Cell X-ray Imaging of Fe_3O_4@TiO_2 Nanoparticles in Cancer Cells," ACS Nano **7**(12), 10502 (2013). DOI:10.1021/nn4033294

Author affiliations: [1]Northwestern University, [2]Argonne National Laboratory, [3]Northwestern Synchrotron Research Center, [4]Carl Zeiss X-ray Microscopy

Correspondence:

* g-woloschak@northwestern.edu

This research was supported by the National Institutes of Health under the grant numbers CA107467, EB002100, U54CA119341, and GM104530. Y.Y. was supported in part by National Institutes of Health/National Cancer Institute training grant T32CA09560. LS-CAT is supported by the Michigan Economic Development Corporation and the Michigan Technology Tri-Corridor (Grant 085P1000817). funding by the U.S. National Science Foundation. Use of the Advanced Photon Source at Argonne National Laboratory was supported by the U.S. Department of Energy Office of Science under Contract No. DE-AC02-06CH11357.

2-ID-D • XSD • Life sciences, materials science, environmental science • Microfluorescence (hard x-ray), microdiffraction, micro-x-ray absorbtion fine structure • 5-30 keV • On-site • Accepting general users •

21-ID-D • LS-CAT • Life sciences • Macromolecular crystallography, microfluorescence (hard x-ray), nano-fluorescence imaging, nanotomography • 6.5-20 keV • On-site, remote, mail-in • Accepting general users •

A Layered Nanostructure Held Together By DNA

Dreaming up nanostructures that have desirable optical, electronic, or magnetic properties is one thing. Figuring out how to make them is another. A new strategy uses the binding properties of complementary strands of DNA to attach nanoparticles to each other and builds up a layered thin-film nanostructure through a series of controlled steps. Investigation at the APS has revealed the precise form that the structures adopt, and points to ways of exercising still greater control over the final arrangement.

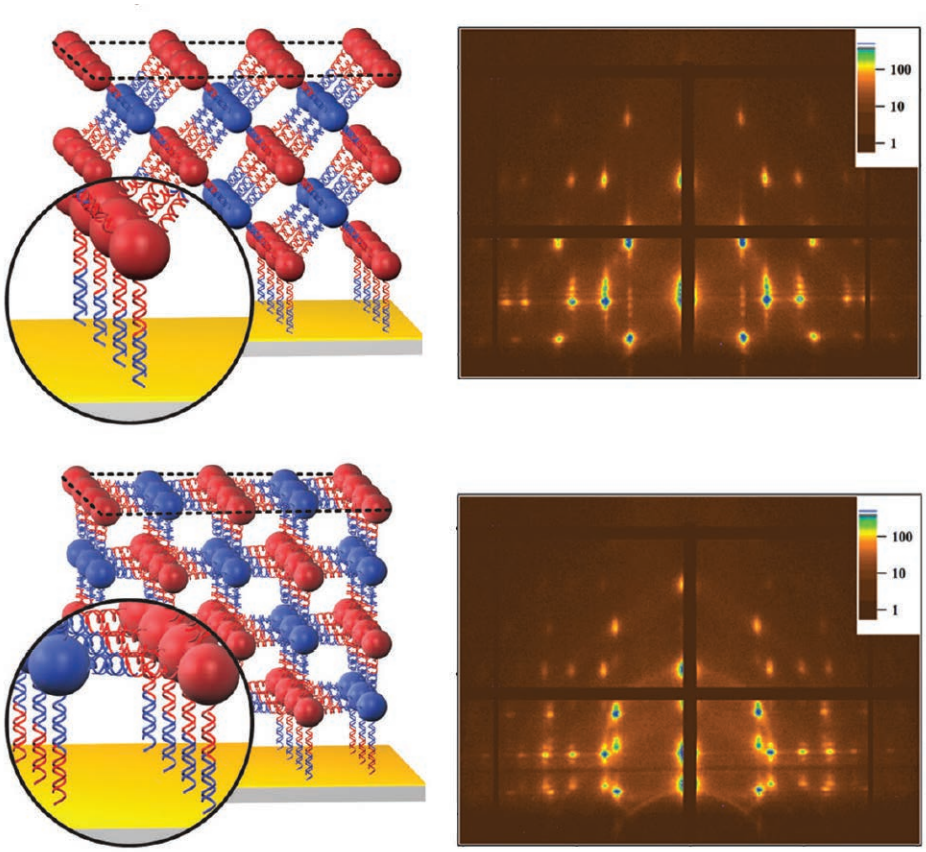

Fig. 1. Nanoparticles linked by complementary DNA-strands form a bcc superlattice when added layer-by-layer to a DNA coated substrate. When the substrate DNA is all one type, the superlattice forms at a different orientation (top left) than if the substrate has both DNA linkers (bottom left). Top right image is a two-dimensional GISAXS scattering pattern of (100)-oriented bcc superlattices. Bottom right shows a two-dimensional GISAXS scattering pattern (110)-oriented bcc superlattices.

The idea of using DNA to hold nanoparticles was devised more than 15 years ago by Chad Mirkin and his research team at Northwestern University. They attached short lengths of single-stranded DNA with a given sequence to some nanoparticles, and then attached DNA with the complementary sequence to others. When the particles were allowed to mix, the "sticky ends" of the DNA hooked up with each other, allowing for reversible aggregation and disaggregation depending on the hybridization properties of the DNA linkers.

Recently, this DNA "smart glue" has been utilized to assemble nanoparticles into ordered arrangements resembling atomic crystal lattices, but on a larger scale. To date, nanoparticle superlattices have been synthesized in well over 100 crystal forms, including some that have never been observed in nature.

However, these superlattices are typically polycrystalline, and the size, number, and orientation of the crystals within them is generally unpredictable. To be useful as metamaterials, photonic crystals, and the like, single superlattices with consistent size and fixed orientation are needed.

The Northwestern researchers and a colleague at Argonne National Laboratory have devised a variation on the DNA-linking procedure that allows a greater degree of control.

The basic elements of the superlattice were gold nanoparticles, each 10 nm across. These particles were made in two distinct varieties, one adorned with approximately 60 DNA strands of a certain sequence, while the other carried the complementary sequence.

The researchers built up thin-film superlattices on a silicon substrate that was also coated with DNA strands. In one set of experiments, the substrate DNA was all of one sequence — call it the "B" sequence — and it was first dipped into a suspension of nanoparticles with the complementary "A" sequence.

When the A and B ends connected, the nanoparticles formed a single layer on the substrate. Then the process was repeated with a suspension of the B-type nanoparticles, to form a second layer. The whole cycle was repeated, as many as four more times, to create a multilayer nanoparticle superlattice in the form of a thin film.

Grazing incidence small-angle x-ray scattering (GISAXS) studies carried out at the XSD 12-ID-B beamline at the APS revealed the symmetry and orientation of the superlattices as they formed. Even after just three half-cycles, the team found that the nanoparticles had arranged themselves into a well-defined, body-centered cubic (bcc) structure, which was maintained as more layers were added.

In a second series of experiments, the researchers seeded the substrate with a mix of both the A and B types of DNA strand. Successive exposure to the two nanoparticle types produced the same bcc superlattice, but with a different vertical orientation. That is, in the first case, the substrate lay on a plane through the lattice containing only one type of nanoparticle, while in the second case, the plane contained an alternating pattern of both types (Fig. 1).

To get orderly superlattice growth, the researchers had to conduct the process at the right temperature. Too cold, and the nanoparticles would stick to the substrate in an irregular fashion, and remain stuck. Too hot, and the DNA linkages would not hold together.

But in a temperature range of a couple of degrees on either side of about 40° C (just below the temperature at which the DNA sticky ends detach from each other), the nanoparticles were able to continuously link and unlink from each other. Over a period of about an hour per half-cycle, they settled into the bcc superlattice, the most thermodynamically stable arrangement.

GISAXS also revealed that although the substrate forced superlattices into specific vertical alignments, it allowed the nanoparticle crystals to form in any horizontal orientation. The researchers are now exploring the possibility that by patterning the substrate in a suitable way, they can control the orientation of the crystals in both dimensions, increasing the practical value of the technique.

— David Lindley

See: Andrew J. Senesi[1], Daniel J. Eichelsdorfer[1], Robert J. Macfarlane[1], Matthew R. Jones[1], Evelyn Auyeung[1], Byeongdu Lee[2]*, and Chad A. Mirkin[1]**, "Stepwise Evolution of DNA-programmable Nanoparticle Superlattices," Angew. Chem. Inter. Ed. **52**, 6624 (2013).
DOI:10.1002/anie.201301936
Author affiliations: [1]Northwestern University, [2]Argonne National Laboratory
Correspondence: *blee@anl.gov, **chadnano@northwestern.edu

C.A.M. acknowledges support from Air Force Office of Scientific Research Awards FA9550-11-1-0275 and FA9550-09-1-0294; Asian Office of Aerospace. Research Development Award FA2386-10-1-4065; Department of the Navy/Office of Naval Research Award N00014-11-1-0729; Department of Defense (DOD)/ National Security Science and Engineering Faculty Fellowships / Naval Postgraduate School Awards N00244-09-1-0012 and N00244-09-1-0071; and the Non-Equilibrium Energy Research Center, an Energy Frontier Research Center funded by the U.S. Department of Energy Office of Science, Basic Energy Sciences Award DE-SC0000989. D.J.E. and E.A. acknowledge support from the DOD, Air Force Office of Scientific Research, National Defense Science and Engineering Graduate (NDSEG) Fellowship, 32 CFR 168a. M.R.J. acknowledges a Graduate Research Fellowship from the National Science Foundation. Use of the Advanced Photon Source at Argonne National Laboratory was supported by the U.S. Department of Energy Office of Science under Contract No. DE-AC02-06CH11357.

12-ID-B • XSD • Chemistry, materials science, life sciences, geoscience, polymer science • Small-angle x-ray scattering, grazing incidence small-angle scattering, wide-angle x-ray scattering • 7.9-14 keV • On-site • Accepting general users •

Probing Large Wave Vector Phonons in Silicon Nanomembranes

Nanoscience is bringing about a revolution in the design and creation of materials having fundamental properties that are dramatically different from those of bulk materials. As engineered dimensions shrink to the nanoscale, long-understood materials take on novel mechanical, optical, electronic, and thermal characteristics that present challenges to both empirical measurement and theoretical understanding. Large wave vector vibrational (phonon) modes, for example, which play important roles in determining the thermal and electronic properties of nanoscale materials, possess symmetries and frequencies that have proven difficult to characterize completely. Researchers from the University of Wisconsin-Madison and Argonne, utilizing the high brilliance of the APS, adapted the technique of synchrotron x-ray thermal diffuse scattering (TDS) to probe phonons with wave vectors spanning the entire Brillouin zone of nanoscale silicon membranes.

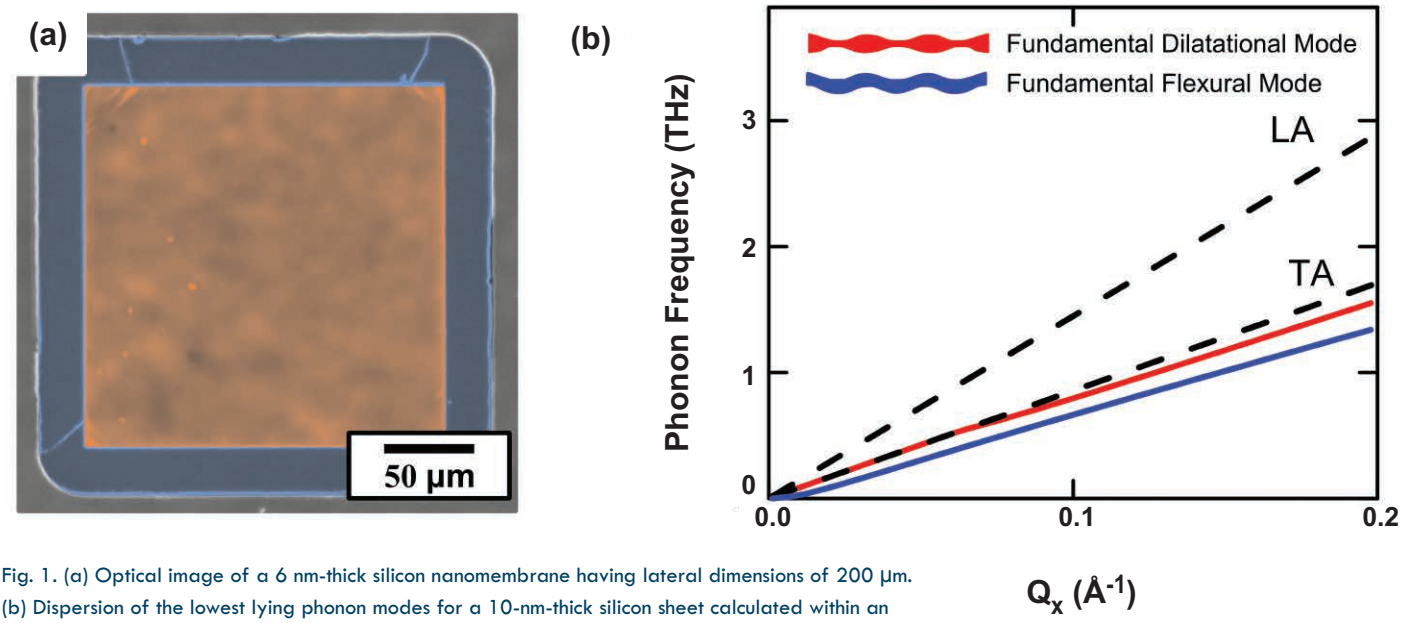

Fig. 1. (a) Optical image of a 6 nm-thick silicon nanomembrane having lateral dimensions of 200 μm. (b) Dispersion of the lowest lying phonon modes for a 10-nm-thick silicon sheet calculated within an elastic continuum approximation. For comparison, the dispersion of the acoustic branches of bulk silicon are shown as dashed lines.

The TDS signals from the flat silicon nanomembranes, with thicknesses from 315 nm to 6 nm and sample volumes as small as 5 μm^3, were found to scale linearly with membrane thickness and exhibit excess intensity at large wave vectors, which is consistent with the scattering signature expected from low-lying phonon modes of the membranes.

Efforts to understand the role of phonons in determining the properties of nanoscale materials have faced a fundamental obstacle in that full phonon dispersions in nanostructures have proved difficult to measure. Advances in nanoscale fabrication and synchrotron radiation instrumentation, including the development of highly stable nanoprobe beamlines, have now made it possible to address this issue.

Flat, ultrathin nanomembranes were fabricated from silicon-on-insulator (SOI) wafers, with thicknesses down to 6 nm and lateral dimensions of 200 μm, at the Wisconsin Center for Applied Microelectronics at the University of Wisconsin-Madison and at the Argonne Center for Nanoscale Materials, shown in Fig. 1(a).

The TDS measurements were conducted at the CNM/XSD 26-ID-C beamline at the APS in vacuum with a 10-keV x-ray beam incident on suspended nanomembranes. A charge-coupled device detected TDS signals from the small amounts of material in the nanomembranes that were orders of magnitude lower than the typical amounts required for neutron and inelastic x-ray scattering.

Two sets of measurements were performed to acquire TDS intensity distributions: (1) a measurement of the TDS intensity from the suspended sili-

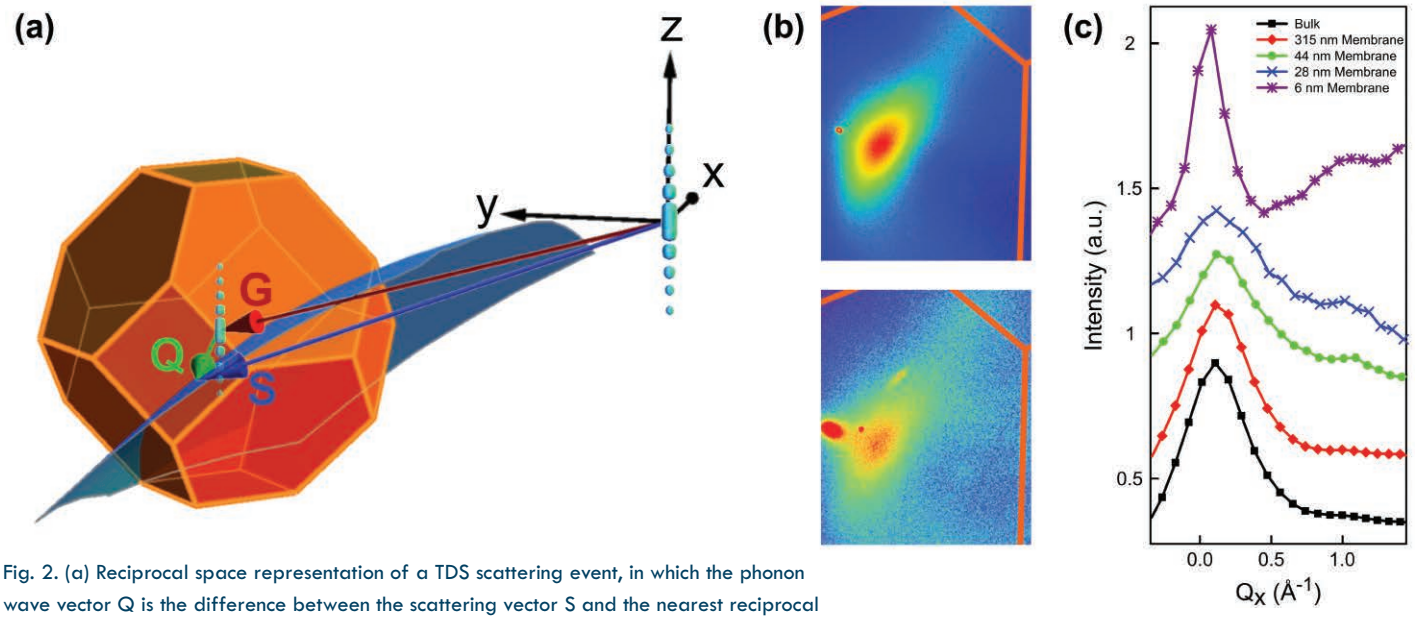

Fig. 2. (a) Reciprocal space representation of a TDS scattering event, in which the phonon wave vector Q is the difference between the scattering vector S and the nearest reciprocal lattice vector G. The truncated octahedron is the first Brillouin zone of silicon, the blue surface represents the detector plane, and zone centers are occupied by truncation rods arising from the finite thickness of the nanomembranes. (b) Detector images showing the TDS intensity distributions measured from 315-nm- and 44-nm-thick membranes. (c) Line profiles of TDS intensity for membranes having different thicknesses.

con membrane with the x-ray beam directed through its center and (2) a bulk measurement with the x-ray beam passing through a thickness of approximately 100-μm of the SOI handle wafer. Each series of measurements involved several consecutive repetitions of a pair of exposures that were double-correlated to eliminate random events. An averaged background image was subtracted from the averaged membrane or bulk image to remove contributions to the detected x-ray intensity arising from sources outside the sample.

Synchrotron x-ray TDS extends the experimental study and engineering of phonons in nanostructures beyond the low wave vector regime typically probed by optical techniques, contributing to an expanded toolset for the design of novel thermal and electronic devices. This capability allows new vibrational modes be probed, such as the dilatational and flexural distortions shown in (b) in Fig. 1.

Differences between bulk and membrane TDS signals were observed at large wave vectors, as shown in Fig. 2, suggesting that the dispersion of large wave vector phonons in thin silicon nanomembranes is substantially different than that in bulk silicon. A thorough comparison of the experimental results with theory will require the computation of phonon dispersions based on atomistic rather than continuum theories. Such predictions are not yet available for silicon nanomembranes.

In addition to silicon material systems, TDS can be used to probe large wave vector acoustic phonons at the nanoscale in systems for which phonons determine phase transformations and thermal transport phenomena where experimental insight has been available only in bulk-scale samples.

Further advances in x-ray nanobeam techniques will allow TDS studies to be conducted on individual nanostructures in these emerging materials through the use of tightly focused, highly intense x-ray beams.

— Vic Comello

See: Gokul Gopalakrishnan[1,‡,*], Martin V. Holt[2], Kyle M. McElhinny[1], Josef W. Spalenka[1], David A. Czaplewski[2], Tobias U. Schülli[3], and Paul G. Evans[1,**], "Thermal Diffuse Scattering as a Probe of Large-Wave-Vector Phonons in Silicon Nanostructures," Phys. Rev. Lett. **110**, 205503 (2013). DOI:10.1103/PhysRevLett.110.205503

Author affiliations: [1]University of Wisconsin-Madison, [2]Argonne National Laboratory, [3]European Synchrotron Radiation Facility. ‡Present address: University of Wisconsin-Platteville

Correspondence:

* gopalakrishg@uwplatt.edu;

** evans@engr.wisc.edu

G.G., K.M., and P.E. acknowledge support from the U.S. Air Force Office of Scientific Research, through Contract No. FA9550-10-1-0249, and support from the European Synchrotron Radiation Facility for initial synchrotron radiation measurements. J.S. acknowledges support from the University of Wisconsin Materials Research Science and Engineering Center, NSF Grant No. DMR-1121288. M.H. and D.C., as part of the Center for Nanoscale Materials core research program, and use of the Center for Nanoscale Materials was supported by the U. S. Department of Energy, Office of Science, Basic Energy Sciences, under Contract No. DE-AC02-06CH11357. Use of the Advanced Photon Source was supported by the U.S. Department of Energy Office of Science under Contract No. DE-AC02-06CH11357.

26-ID-C • CNM/XSD • Physics, materials science • Nanofluorescence imaging, microdiffraction, nanotomography • 8-12 keV • On-site • Accepting general users •

Probing the Palladium Nanocatalyst Poisoning Pathway

The noble metal palladium (Pd) is commonly used as a catalyst in automotive catalytic converters. In nanoparticle form, it is also finding increasing use in manufacturing, particularly to catalyze the Heck and Suzuki reactions in industrial chemical processes (the palladium-catalyzed C-C coupling between aryl halides or vinyl halides and activated alkenes in the presence of a base, and the organic reaction that is classified as a coupling reaction where the coupling partners are a boronic acid with a halide catalyzed by a palladium complex, respectively). Those unique catalytic properties, however, can be greatly compromised by the presence of organo-sulfur contaminants in the reactions. Researchers from Brown University and Argonne combined a number of advanced spectroscopy techniques at the APS to elucidate how Pd nanoparticles undergo sulfidation in the presence of 1-octadecanethiol under high temperatures, making it possible to better understand the behavior of Pd nanocatalysts in many industrial chemical processes.

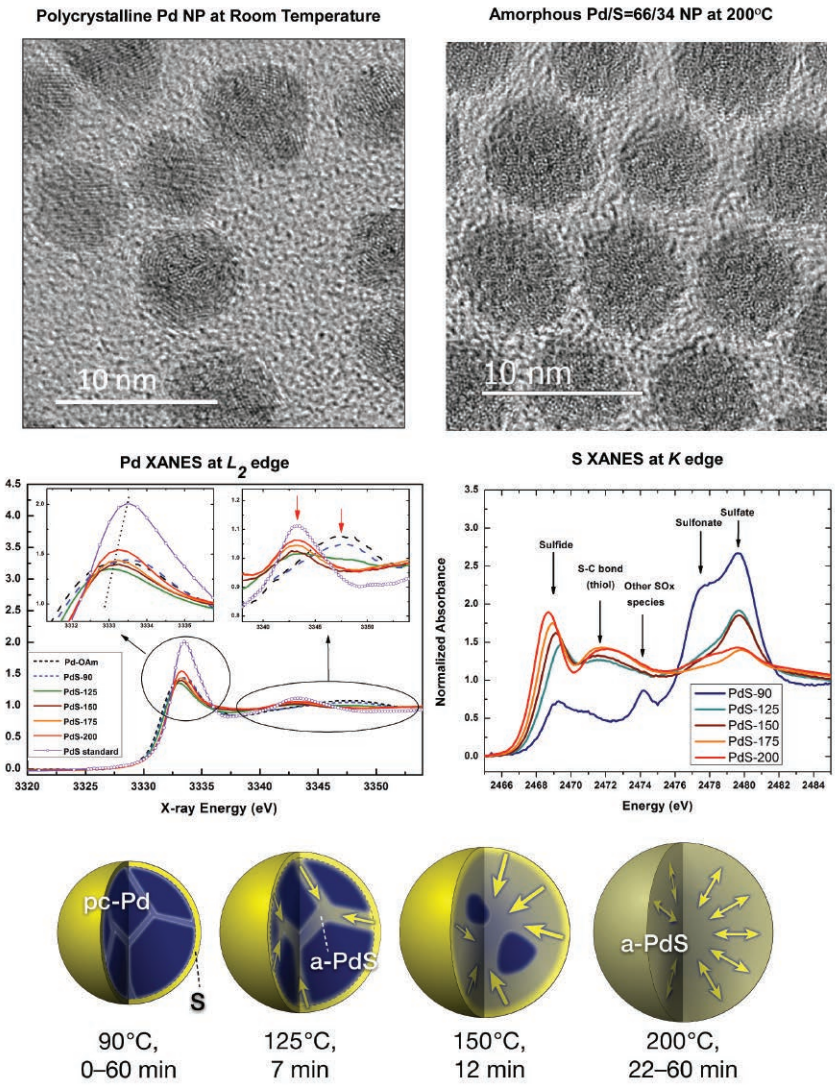

Experiments have shown that alkanethiols can interact with Pd nanoparticles and produce a sulfur-containing interlayer beneath the nanoparticle surface. But the stoichiometry, depth, and extent of this PdS_x layer have remained elusive, apparently due to differences in the processes used to form the nanoparticles and resultant variations in particle sizes and degrees of sulfidation. The current work set out to better characterize and thus better understand the entire process.

Researchers at Argonne's Center for Nanoscale Materials (CNM) developed the synthesis protocol, which involved preparing Pd nanoparticles capped with with oleylamine (OAm), then introduced 1-octadecanethiol while heating the mixture to a temperature of 200˚ C and maintained that temperature for 30 min. The nanoparticles were designated PdS-200A. Samples were also taken at four additional temperatures during heating (90˚ C, 125˚ C, 150˚ C, and 175˚ C, each named for the corresponding quenching temperature) to provide a range of intermediate states for analysis. This allowed the sulfidation process to be captured in various stages with increasing temperature.

Studied with various transmission electron microscopy (TEM) techniques at the Argonne Electron Microscopy Center (EMC), the Pd-OAm nanoparticles showed multiple twinning and an overall polyhedral shape before the introduction of thiol, while the PdS-200A nanoparticles were more spherical. They also displayed a distinct change from a polycrystalline to an amorphous state, confirmed with both electron and x-ray diffraction studies (Fig. 1). The Pd/S ratio of 66/34 in the PdS-200A nanoparticles also implies that sulfur has diffused into the particles rather than merely forming a surface layer. This high sulfur content inside the particles was verified with energy-filtered transmission electron microscopy (EFTEM) and high-angle annular dark-field scanning transmission electron microscopy (HAADF-STEM), which indicates a more or less uniform sulfur distribution within the nanoparticles.

The nanoparticles samples taken at intermediate temperatures showed a progressive increase of sulfur content upon increasing temperature. For example, while the PdS-90 sample Pd/S ratio was 96:4, the PdS-125 particles showed a 91:9 ratio, and the sulfur content of the PdS-150 particles was even higher with a 84:16 ratio.

To probe the surface oxidation, bond structure, and electronic states of the Pd nanoparticles in greater detail, the experimenters performed x-ray absorption near-edge spectroscopy (XANES) studies of the Pd L_2- and L_3-edges using the XSD 9-BM-B,C beamline at the APS; these revealed a shift toward higher energies as the nanoparticles become increasingly sulfurized, indicating formation of Pd-S bonds. Meanwhile, XANES spectra of the sulfur *K*-edge (the shape of which is strongly influenced by sulfur oxidation states and chemical specifications) show peaks associated with various species of oxidized sulfur, which can be used to trace the diffusion of sulfur into the nanoparticles.

The team also conducted Pd *K*-edge extended x-ray absorption fine structure studies at the XSD 20-ID-B beamline to investigate the local atomic environment of Pd. Increased first-shell coordination number (CN) of Pd-S with a corresponding decreased CN of Pd-Pd indicates increasing sulfidation as temperatures are raised, and that sulfur is steadily diffusing from the nanoparticle surfaces into the interior.

With the findings from these various studies, the research team was able to devise a clear model of how Pd-OAm nanoparticles become sulfurized under high temperature conditions.

At first, as octadecanethiol is introduced, a thin surface layer of sulfuric species forms on the nanoparticles, and then, beginning at about 125˚ C, sulfur atoms begin to migrate into the particle. However, these sulfur atoms tend to congregate mostly along grain boundaries, moving into the Pd lattice of the nanoparticle only at higher temperatures. Finally, at around 200˚ C, the particle becomes mostly amorphous, with the atomic concentration saturated at a Pd/S ratio of 66:34, close to the cubic phase of $Pd_{16}S_7$. This also indicates that this Pd poisoning process by thiol is self-limiting, driven by Pd catalyzed C-S bond breakage of the thiol molecule.

With the new insight into the Pd nanoparticle catalyst poisoning pathway provided by the team's work, it is now possible to better understand the behavior of Pd nanocatalysts in many industrial chemical processes.

— Mark Wolverton

< Fig. 1. Polycrystalline Pd-oleylamine nanoparticles (NP) undergo a structural transformation to amorphous state when exposed to 1-octadecanethiol at progressively higher temperatures. The combination of electron microscopy and x-ray absorption spectroscopy shows that the sulfidation process starts from the Pd-catalyzed S-C bond breakage, goes through the polycrystalline boundary at intermediate temperatures, and eventually self-limits at a chemical stoichiometry close to $Pd_{16}S_7$.

See: Yi Liu[1], Chengjun Sun[1], Trudy Bolin[1], Tianpin Wu[1], Yuzi Liu[1], Michael Sternberg[1], Shouheng Sun[2], and Xiao-Min Lin[1]*, "Kinetic Pathway of Palladium Nanoparticle Sulfidation Process at High Temperatures," Nano Lett. **13**, 4893 (2013). DOI:10.1021/nl402768b
Author affiliations: [1]Argonne National Laboratory, [2]Brown University
Correspondence: * xmlin@anl.gov

X.M.L. thanks partial support from the University of Chicago MRSEC, supported by NSF DMR-0820054. The work at Brown University was supported in part by Exxon Mobil. APS Sector 20, which is managed by XSD in partnership with the Canadian Light Source (CLS), is funded by the and the EMC was supported by the U. S. Department of Energy Office of Science , and by the Natural Sciences and Engineering Research Council of Canada and the University of Washington via the CLS. Use of the Advanced Photon Source, the CNM, and the EMC was supported by the U. S. Department of Energy Office of Science under Contract No. DE-AC02-06CH11357.

9-BM-B,C • XSD • Materials science, chemistry • X-ray absorption fine structure • 2.1-23 keV • On-site • Accepting general users •

20-ID-B,C • XSD • Materials science, environmental science, chemistry • X-ray absorption fine structure, surface diffraction, x-ray Raman scattering, micro x-ray absorption fine structure, microfluorescence (hard x-ray), time-resolved x-ray absorption fine structure, x-ray emission spectroscopy • 4.3-27 keV, 7-52 keV • On-site • Accepting general users •

Artificial Crystals Come of Age

In recent years, scientists have produced a variety of structures using DNA-coated nanoparticles (NPs). When placed in solution, these "functionalized" NPs can assemble into periodic structures, including superlattices (sometimes called artificial crystals). However, these binary (two-part) superlattices, featuring NPs coated with short DNA segments, cannot match the complex compositions and phase-change behaviors of many natural and manmade crystals. Researchers have custom-designed and synthesized several ternary (three-part) DNA/NP superlattices and analyzed them at an APS beamline to explore whether additional complexity and functionality can be found in these systems. Their results move the assembly of nanoparticle-based materials in the direction of atom- or molecule-based materials found in nature. Moreover, changing crystal structure at will makes the superlattices useful as materials for new devices that require the ability to switch between different states. Taken together, these qualities point toward the development of novel, tunable structures not attainable with current methods of materials synthesis.

The researchers from Northwestern University and Argonne found that not only do these three-dimensional superlattices self-assemble, but their temperature-dependent structures can be deliberately toggled between different hierarchical states: heating transforms the three-part superlattice into a binary structure, while cooling completely restores it.

The structural and temperature characteristics of the ternary superlattices were confirmed using x-ray measurements performed at the DND-CAT beamline 5-ID-B,C,D. Compared to their binary cousins, ternary superlattices possess a greater potential for exhibiting unusual magnetic, light harvesting, catalytic, and other important properties; furthermore, their temperature-dependent nature could lead to applications as temperature sensors or nanoscale switches.

Each ternary superlattice in the experiment began as a binary superlattice with precisely sized and aligned voids, or pockets, into which "daughter" nanoparticles were infused. This process is called topotactic intercalation.

Assembling ternary superlattices follows a basic sequence: First, the NPs are functionalized (i.e., coated with short DNA segments). Next, longer DNA-linkers are attached to the functionalized gold nanoparticles (this is hybridization). The third step in formation of the parent (binary) superlattice. And finally, hybridized daughter nanoparticles are inserted into the parent superlattice to form the ternary superlattice.

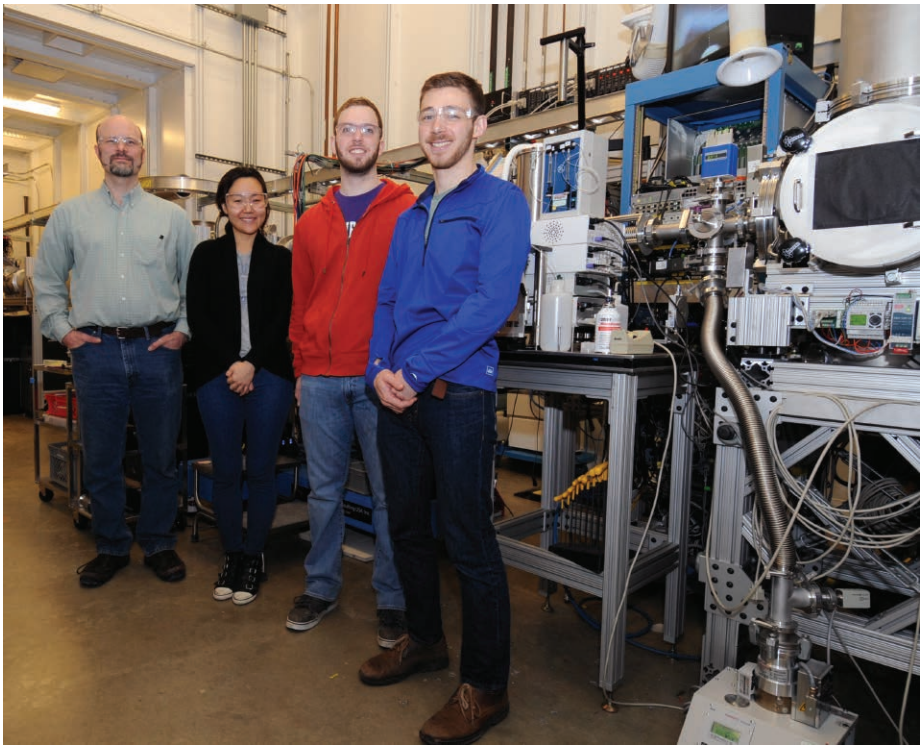

In the DND-CAT 5-ID-D beamline station. Left to right: Steve Weigand (DND-CAT), Youngeun Kim, Ryan Thaner, and Matthew O'Brien (all Northwestern U.). Kim, Thaner, and O'Brien are all Ph.D. candidates in the Mirkin group at Northwestern. They run small-angle x-ray scattering experiments at the APS for the purpose of observing the crystal structures of DNA-mediated assembly of inorganic nanoparticles, such as the ones described in this article.

The attachment of DNA segments to the parent nanoparticles is depicted in (a) of Fig. 1 (top left); these DNA-covered gold nanoparticles act like individual units, and are called programmable atom equivalents (PAEs). Attached to

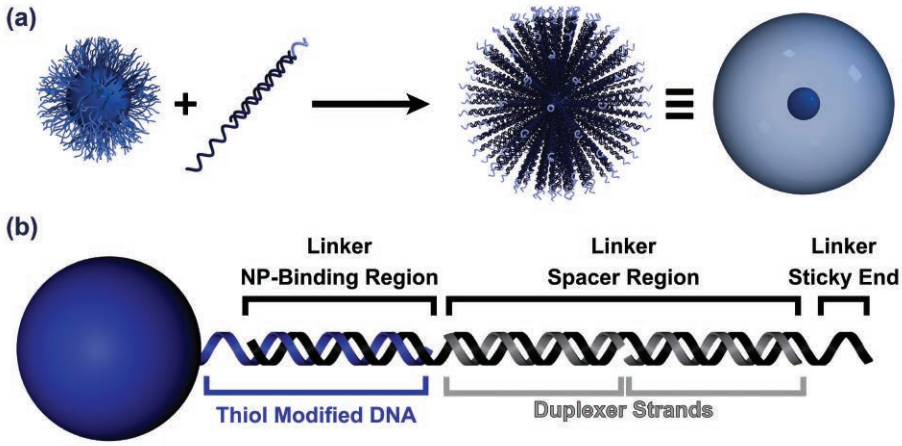

Fig. 1. DNA-based scheme for assembling nanoparticles into ternary superlattices. All figures from R.J. Macfarlane et al., Science **341**, 1222 (2013). © 2013 American Association for the Advancement of Science.

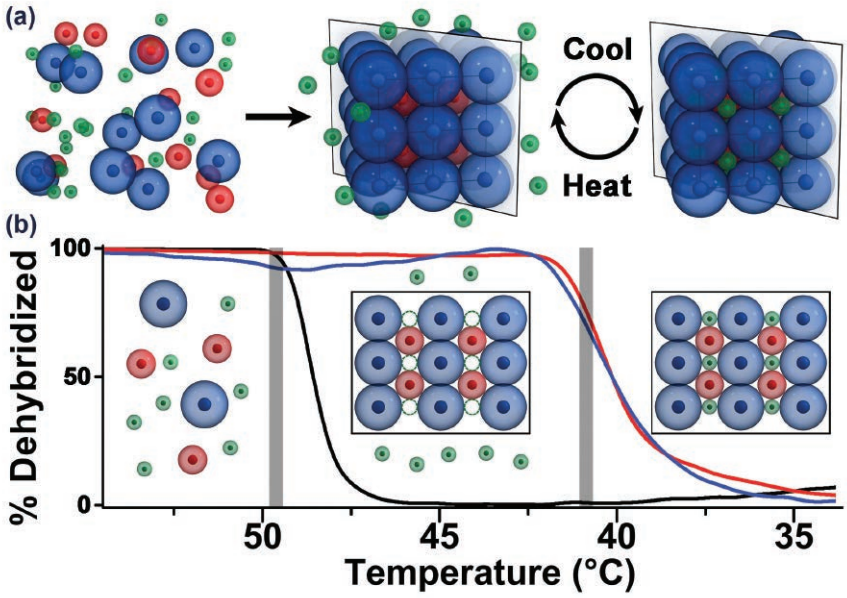

Fig. 2. Assembly of ternary nanoparticle superlattices. A "parent structure," consisting of blue and red nanoparticles linked via relatively strong DNA interactions, is first assembled by cooling the superlattice from a high temperature. Once this parent lattice has formed, daughter particles, which possess relatively weak binding interactions to the parent lattice, intercalate into the parent structure by cooling the system to a temperature at which the daughter particle-to-parent lattice DNA connections are stable. By specifically designing the sizes of the DNA strands and nanoparticles, these daughter particles can be directed to very specific sites within the parent lattice (see dashed outlines and filled holes in the bottom inset images), thereby generating a specific ternary lattice by design. Moreover, these lattices can be toggled between the parent and daughter states by heating the ternary lattice above or below the temperature at which the daughter-to-parent DNA connections break.

each PAE are lengthier DNA-linkers (Fig. 1(a), top right) that radiate from the core (gold nanoparticle diameters in these lattices were typically 10-20 nm).

The scheme depicted in Fig. 1(b) of the figure illustrates the distinct sequences of the DNA-linker: a nucleobase sequence complementary to the PAEs, then a middle spacer sequence, terminating in a sticky end.

In the same way that the double-stranded DNA in our chromosomes is joined together via base pairing — T with A, C with G — the single-stranded ends of the DNA-linker molecule joins, or hybridizes, with the base pairs of other single-stranded DNA segments. Specifically, one end of the DNA-linker hybridizes with the DNA-functionalized nanoparticle (left side of Fig. 1(b)), while the sticky end is furthest from the nanoparticle. The binary superlattice forms when the sticky ends of parent nanoparticles hybridize with one another, forming an ordered structure (see Fig. 2).

The capability to design superlattices like the one shown in Fig. 2(a) of the second figure, with its precisely arranged and sized pockets, is made feasible by the complementary contact model (CCM), a set of rules developed by the researchers to prepare targeted structures on demand. These rules eliminate trial-and-error methods in favor of an *a priori* design approach.

This means that scientists can visualize a DNA-based nanoparticle system, e.g., a superlattice, and use CCM to determine the DNA linkers and NPs needed to realize the system.. The researchers relied on CCM to guide the synthesis of the DNA-linkers that correctly attached to the functionalized nanoparticles, yielding the desired parent superlattice.

The CCM was also enlisted to determine the appropriate DNA-linkers for the daughter nanoparticles (daughter gold-core diameters were 10 nm). The hybridized daughter nanoparticles — shown filling the pockets of their parent superlattice in the far right-side of Figs. 2(a) and 2(b) — possessed relatively weak bonds with the parent superlattice, as compared to the bonds between the parent nanoparticles.

Five distinct ternary superlattices were synthesized, three of which possessed lattices unlike those of any known natural or manmade crystal (Fig. 3). In confirming the structures of these superlattices at the DND-CAT beamline at the APS, the researchers employed small-angle x-ray scattering (SAXS) to obtain measurements that were essential for identifying the precise crystalline arrangements of the ternary superlattices, and for confirming the temperature-dependent phase shift between the binary and ternary forms.

In one experimental run, the temperature of a superlattice sample was

"Crystals" cont'd. on page 180

"Crystals" cont'd. from page 179

cycled three times. The real-time SAXS measurements revealed that beyond the melting transition temperature for the daughter particles (42º C), a binary lattice appeared, indicating daughter nanoparticle dispersal into solution. In each instance, subsequent cooling restored the original ternary superlattice.

Ternary superlattices constitute a major step toward developing DNA/nanoparticle structures that rival the phase and lattice complexities of natural and manmade atom- or molecule-based crystals. Additionally, the ability to reversibly change superlattice symmetry with simple external stimuli presents the opportunity to generate novel nanoparticle-based materials whose physical properties can be dynamically altered at will.

— Philip Koth

See: Robert J. Macfarlane[1], Matthew R. Jones[1], Byeongdu Lee[2], Evelyn Auyeung[1], and Chad A. Mirkin[1]*, "Topotactic Interconversion of Nanoparticle Superlattices," Science **341**, 1222 (2013). DOI:10.1126/science.1241402

Author affiliations: [1]Northwestern University, [2]Argonne National Laboratory

Correspondence:

* chadnano@northwestern.edu

This material is based on work supported by the Air Force Office of Scientific Research awards FA9550-11-1-0275, FA9550-12-1- 0280, and FA9550-09-1-0294; Defense Advanced Research Projects Agency/Microsystems Technology Office award HR0011-13-2-0002; National Science Foundation (NSF)-Materials Research Science and Engineering Center program DMR-0520513; and the Non-Equilibrium Energy Research Center, an Energy Frontier Research Center funded by the U.S. Department of Energy Office of Science-Basic Energy Sciences award DE-SC0000989. M.R.J. acknowledges a Graduate Research Fellowship from the NSF; E.A. acknowledges a Graduate Research Fellowship from the National Defense Science and Engineering Graduate Fellowship. DND-CAT is supported by E.I. DuPont de Nemours & Co., The Dow Chemical Company and Northwestern University. Use of the Advanced Photon Source at Argonne National Laboratory was supported by the U.S. Department of Energy Office of Science under Contract No. DE-AC02-06CH11357.

5-ID-B,C,D • DND-CAT • Materials science, polymer science • Powder diffraction, x-ray standing waves, x-ray optics development/techniques, small-angle x-ray scattering, surface diffraction, x-ray reflectivity, wide-angle x-ray scattering • 6-17.5 keV • On-site • Accepting general users •

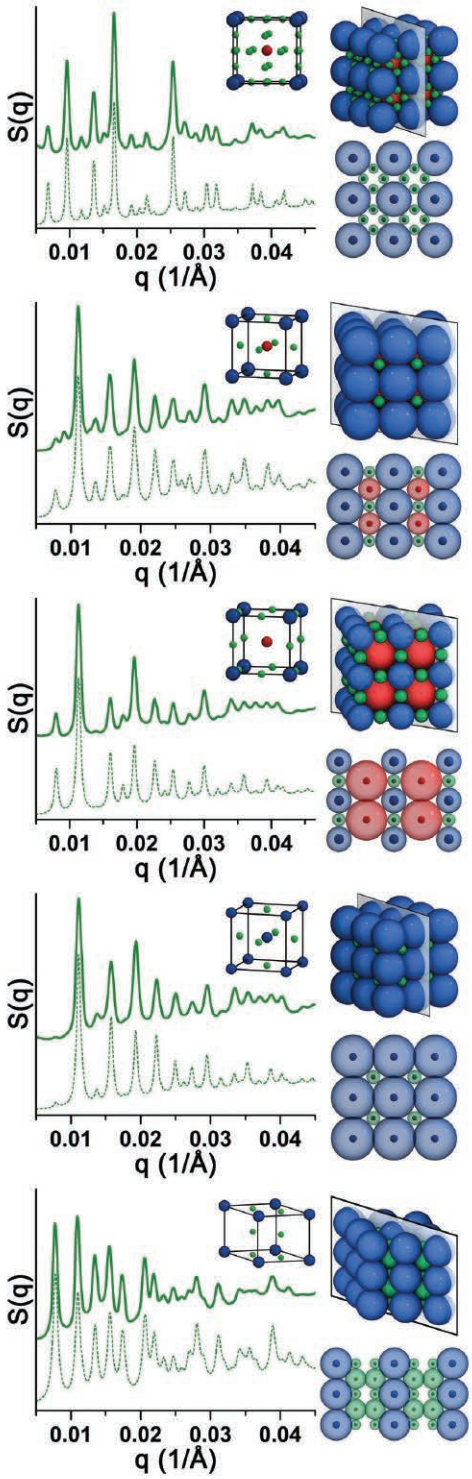

Fig. 3. Five unique ternary NP superlattices synthesized and then analyzed at the DND-CAT beamline. The SAXS data obtained experimentally (solid traces) confirms the structure of the ternary lattices when compared to predicted scattering patterns (dashed traces) for these lattices. From the top, these lattices correspond to: ABC_{12}-type, "face"-type perovskite, "edge"-type perovskite, A_2B_3-type, and AB_4-type lattices. Note that the ABC_{12}-, A_2B_3-, and AB_4-type lattices have no naturally occurring or man-made equivalent. The insets correspond to: (top left) the positions and relative sizes of the gold nanoparticles, (top right) the positions and sizes of the full DNA-NP constructs, and (bottom right) the relative DNA and NP sizes of nanoparticles in the plane shown in each top right inset.

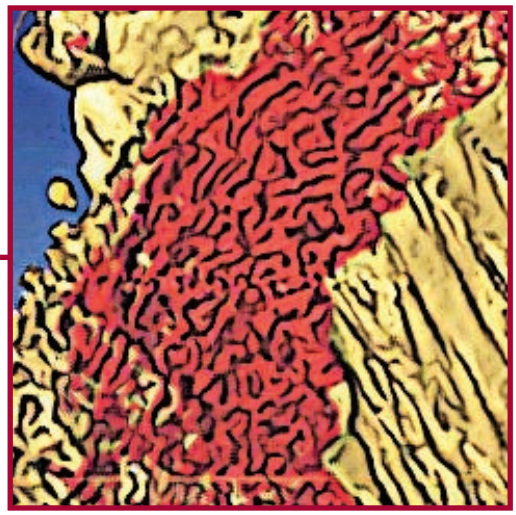

Novel X-ray Techniques & Instrumentation

New Microscopy Techniques Peer inside Even Thick Tissue

In the world of microscopy, each technique brings advantages for particular samples — some are better for live samples, some better for looking at certain kinds of molecules, some better for looking at single cells. Scientists seek, therefore, to improve each technique to the highest resolution. Hard-x-ray microscopy has lagged behind other techniques due to the difficulty of resolving the internal structure of cells within tissues, a crucial need for studying larger systems such as neurological networks, for example. New results based on work at the APS has resulted in dramatically improved hard-x-ray microscopy reaching resolutions on the order of 20 nm, small enough to see sub-cellular structures such as organelles and vesicles inside even fairly thick, mammalian tissue. This work opens a door for hard-x-ray microscopy to become an important technique within biology for potentially observing real-time movement of cells, or organelles within cells.

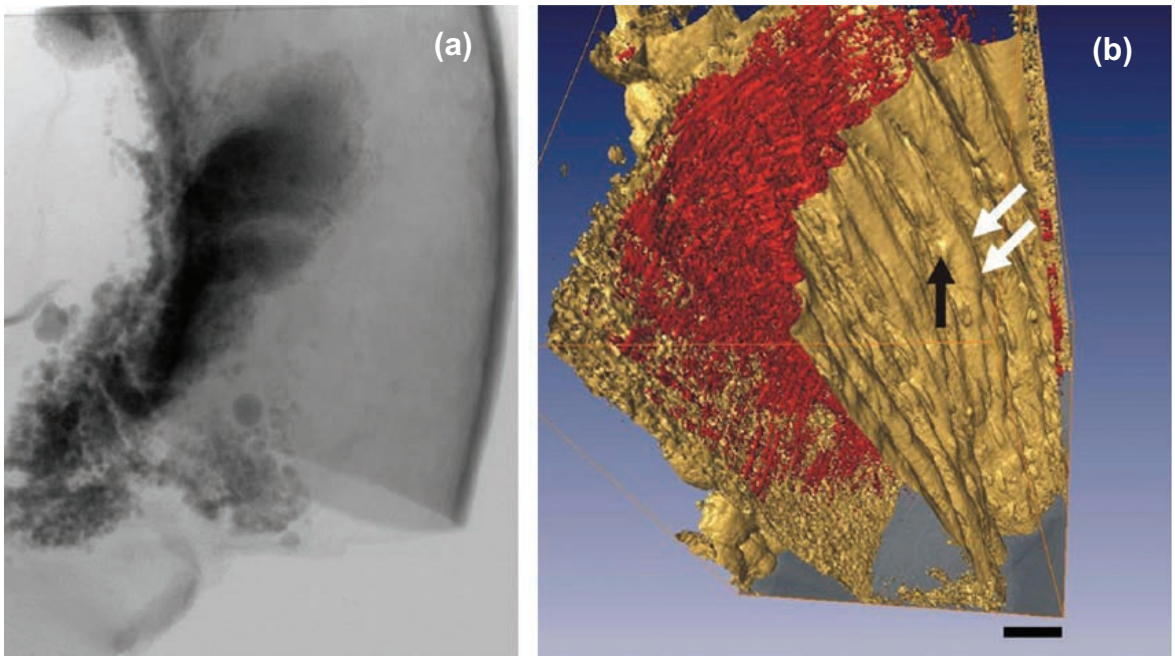

Fig. 1. (a) hard-x-ray micrographs of a mouse aorta specimen fixed in resin; the overall specimen dimension, including the resin, was ~5 × 7 × 10 mm^3. Bar: 1 mm. (b) Tomographic volume-rendered structure of the same aorta specimen; scale bar: 50 μm. From C.C. Chien et al., Biotech. Adv. **31**, 375 (2013).

Such record-breaking resolution was provided by an international team of researchers who combined a host of techniques to improve resolution and contrast, as well as specimen preparation and analysis of the data. The team set out to test their techniques on a range of biologically important specimens, including tumors, plant cells, zebra fish, and a mouse aorta (Fig. 1).

Improving hard-x-ray microscopy has been hindered by two basic — indeed, fundamental — constraints: resolution and contrast. Contrast has been greatly improved over the last two decades with the introduction of phase contrast x-ray imaging, where observing and analyzing interference patterns from the light waves can provide enough detectible contrast to form an image of a biological specimens.

The team made use of two additional factors to improve resolution: coherent synchrotron x-rays and additional magnification via Fresnel plates. The experiments were performed on the XSD 32-ID-B,C beamline of the APS, beamlines 01A and 01B of the National Synchrotron Radiation Research Center (NSRRC) in Taiwan, and the 7B2 beamline of the Pohang Light Source (Republic of Korea). Tests with high spatial resolution were implemented on the NSRRC 01B and APS 32-ID-B,C beamlines, while the two other beamlines were used for experiments with less resolution but faster image gathering.

Using a high-brightness synchrotron such as APS is crucial for achieving high lateral and temporal resolution. X-ray optical microscopes alone could not do the job. An additional magnification technique helped the team observe their specimens down to 16.7-nm resolution, which is a world record for multi-kiloelectronvolt hard x-rays. The x-ray microscopes at the APS, for example, were outfitted with Fresnel zone focusing plates that the team developed utilizing nanofabrication techniques.

For the zebra fish specimen, the team could resolve down to 5 μm, the size of an *in vivo* cell. Another sample, of a mosquito abdomen, reached 1-μm resolution. At such performance levels, hard-x-ray observations could become increasingly important in biological and biomedical investigations. For one thing, the hard x-rays penetrate deeply into thick tissue, greater than 300 μm, allowing for three-dimensional reconstructions.

The highest resolution imagery took some time, however. Fast image taking is important when observing cells in their natural environment, so the team also looked at what optical resolution could be achieved at faster speeds. In their tests, they obtained millisecond-resolution images by removing the amplifying Fresnel zone plate and using unmonochromatized x-rays. These speeds are suitable for real-time biology experiments, and still produce high resolution.

This approach has been routinely performed at other APS beamlines operated by XSD, reaching very high time resolution on non-biological samples. This team, on the other hand, concentrated on biology specimens: They could observe the opening and closing movement of the stoma cells in plant cells that regulate its opening and closure, and serve as the site for gas exchange. High-resolution tomographic image processing — which requires thousands of raw images to create a three-dimensional image, and so also requires quick image speeds — was successful down to micron-level resolution.

High-speed imaging offers another advantage in that it minimizes the chances for radiation damage to the sample from the x-rays. Indeed, the team found no detectable radiation damage when experiments were performed quickly.

Providing hard-x-ray microscopy with fast speeds and high visual resolution opens the door to taking advantage of one of the technique's key strengths: the capability to nondestructively examine thick specimens. The minimal prepping needed for hard-x-ray microscopy, therefore, can allow the sample to be kept in a natural environment, making it possible to examine entire cells, multicellular structures or tissues without sectioning and distorting the specimen. However, the technique cannot yet be used on a living specimen.

— Karen Fox

See: C.C. Chien[1,2], P.Y. Tseng[1], H.H. Chen[1], T.E. Hua[1], S.T. Chen[1], Y.Y. Chen[1], W.H. Leng[1], C.H. Wang[1], Y. Hwu[1,2,3,4]*, G.C. Yin[5], K.S. Liang[6], F.R. Chen[2], Y.S. Chu[7], H.I. Yeh[8], Y.C. Yang[8], C.S. Yang[9], G.L. Zhang[10], J.H. Je[11], and G. Margaritondo[12], "Imaging cells and sub-cellular structures with ultra-high resolution full-field X-ray microscopy," Biotech. Adv. **31**, 375 (2013). DOI:10.1016/j.biotechadv.2012.04.005

Author affiliations: [1]Academia Sinica, [2]National Tsing Hua University, [3]Taiwan Ocean University, [4]Cheng Kung University, [5]National Synchrotron Radiation Research Center, [6]National Chiao Tung University, [7]Brookhaven National Laboratory, [8]Mackay Memorial Hospital, [9]National Health Research Institutes, [10]Chinese Academy of Sciences, [11]Pohang University of Science and Technology, [12]Ecole Polytechnique Fédérale de Lausanne

Correspondence:

*phhwu@sinica.edu.tw

This work was supported by the National Science and Technology Program for Nanoscience and Nanotechnology, by the Academia Sinica, by Mackay Memorial Hospital (MMH-E-94003) (Taiwan), by the MOST (KOSEF) through National Core Research Center for Systems Bio-Dynamics (Korea), by the Fonds National Suisse de la Recherche Scientifique, and by the Ecole Polytechnique Fédérale de Lausanne. Use of the Advanced Photon Source at Argonne National Laboratory was supported by the U.S. Department of Energy Office of Science under Contract No. DE-AC02-06CH11357.

32-ID-B,C • XSD • Materials science, life sciences, geoscience • Phase contrast imaging, radiography, transmission x-ray microscopy, tomography • 7-40 keV • On-site • Accepting general users •

High-Energy Diffraction Microscopy at APS Sector 1

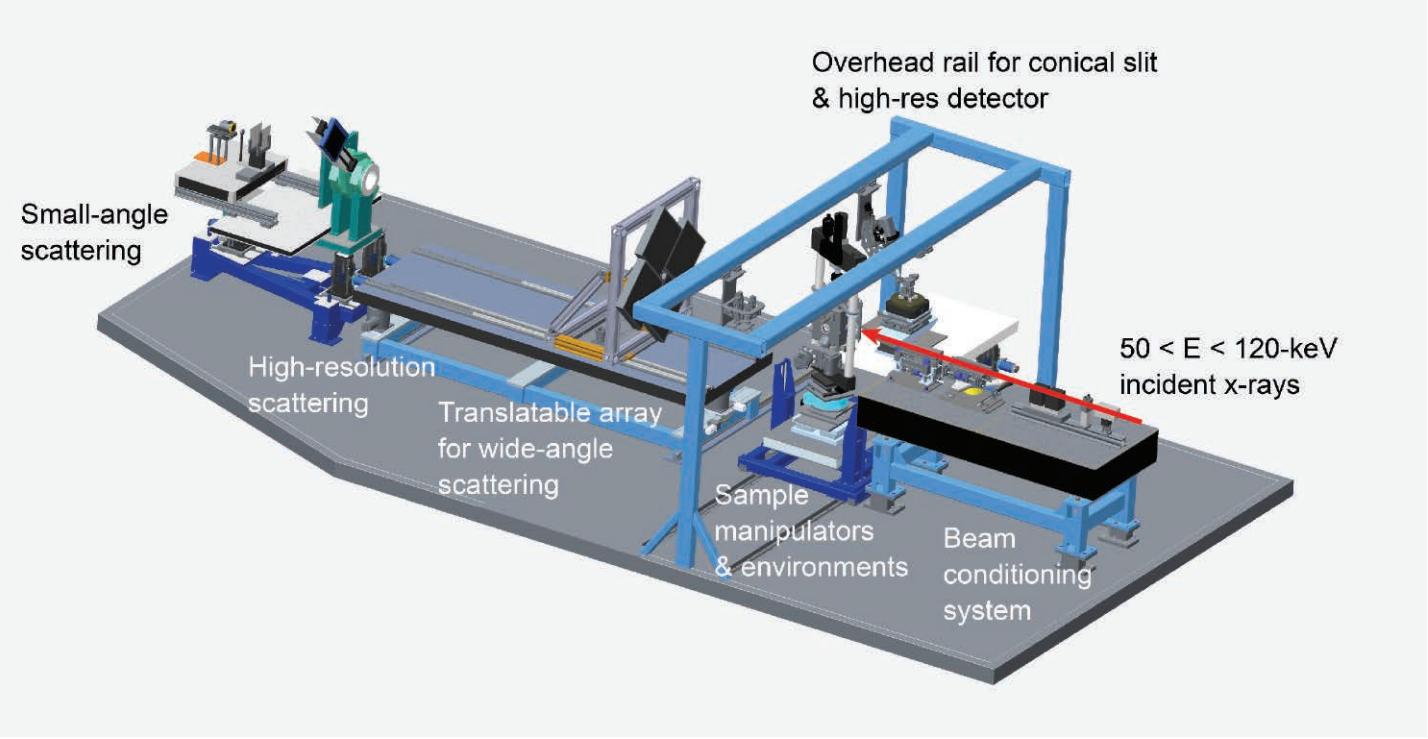

Fig. 1. The 1-ID-E hutch at the APS, constructed for high-energy diffraction microscopy measurements, with beam shown incident on a vacuum furnace used for thermo-mechanical studies of irradiated materials, and key components labeled.

The strategic development of new engineering materials with improved performance rests on establishing computational models that link materials processing, microstructure, properties, and performance. Scientists and engineers have long sought these linkages, but without access to experimental data at the relevant length scales, validated models capable of predicting complex phenomena such as fatigue crack initiation and deformation in polycrystals have remained elusive. Developing such models is at the heart of integrated computational materials science efforts as well as the recently launched Materials Genome Initiative. These efforts promise to speed up the design, development, and deployment of new materials for a variety of applications, with broad economic implications. For example, higher-temperature operation associated with the successful implementation of SiC/SiC composites and associated coatings for turbine blades would lead to a 15% increase in engine efficiency, translating to $1M/yr/airplane or $7B to the U.S. airline fleet alone.

The use of experimental methods capable of validating materials models over the appropriate processing or service conditions — i.e., length/time scales and deformation/temperature regimes — are essential to these efforts. The development of cutting-edge characterization techniques capable of exploring the links between processing, microstructure, and properties/performance has been accelerated by coordinated efforts at high-energy synchrotron x-ray beamlines. Over the past decade, this has led to the development of high-energy diffraction microscopy (HEDM, also known as 3DXRD) at the APS (beamline 1-ID); the European Synchrotron Radiation Facility in France (beamline ID11); and, more recently, the Deutsches Elektronen-Synchrotron (DESY)/PETRA in Germany and the Cornell High Energy Synchrotron Source facilities. The result of these efforts is a suite of nondestructive techniques to characterize and monitor evolving material states, including sub-grain orientations, void/crack formation, and the stress states of individual grains. HEDM development has reached a tipping point where these experiments can be combined to produce an unparalleled tool for probing the grain-scale response to external stimuli including thermo-mechanical deformation.

At the APS, the recently built hutch at beamline 1-ID-E houses near- and far-field HEDM, tomography, and small-angle x-ray scattering (SAXS) capabilities (Fig. 1). The beamline is fed by a high-energy undulator, a brilliance-preserving monochromator, and refractive focusing lenses to provide a high flux of 50 < E < 120-keV x-rays with beam sizes down to a micron. Specialized user environments have

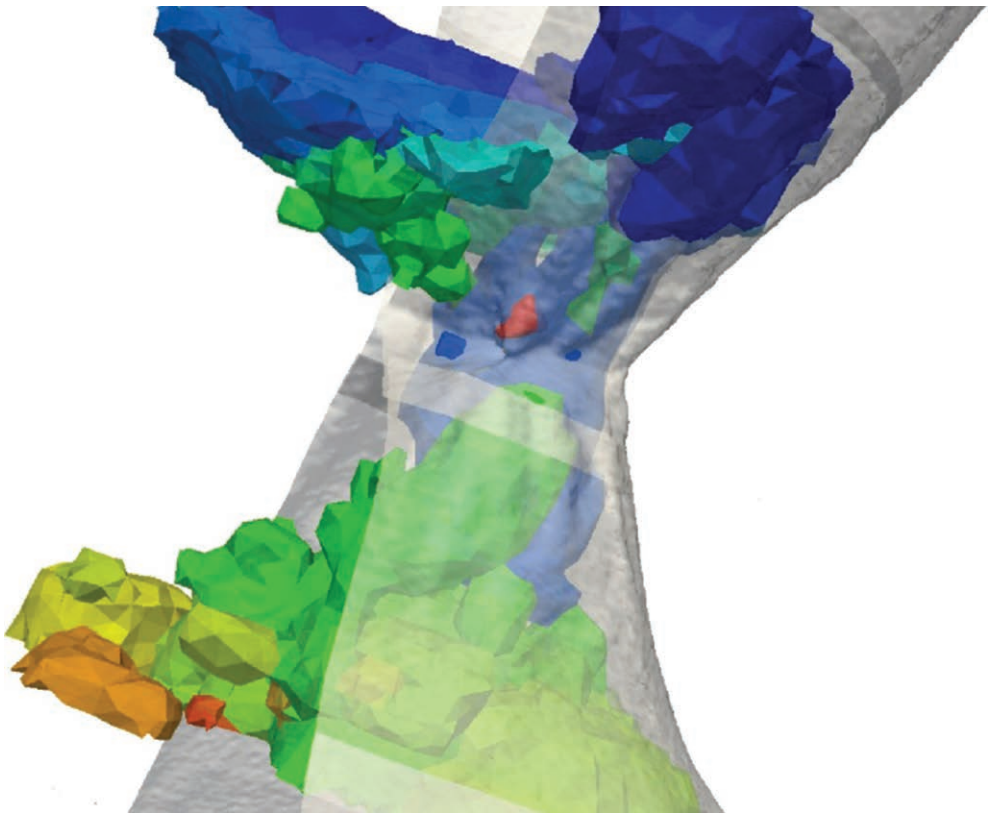

Fig. 2. Example of HEDM data in necked Cu wire (250-μm neck diameter) subjected to tensile strain, with tomography contour (gray) and HEDM grain mesh (color) illustrated. Courtesy of R.M. Suter et al. (Carnegie Mellon U.).

been developed through collaborations with external partners including the Air Force Research Laboratory for a high-precision apparatus allowing *in situ* measurements of samples undergoing a variety of mechanical loading conditions at ambient and high temperatures, and the Argonne Nuclear Engineering Division for a vacuum furnace which enables *in situ* thermo-mechanical measurements on irradiated materials. A variety of specialized area detectors are available, including high-spatial-resolution "near-field" diffraction/tomography systems, an array of flat-panel detectors (GE 41-RT) for "far-field" diffraction, and a SAXS detector with medium-resolution placed at the back of the hutch (ScintX). Detectors can also be mounted on a specialized rotation-translation system near the back of the hutch for high-q-resolution measurements over a large range of range of q-space. These detection modes allow a single sample to be probed on length scales from nanometers to millimeters, simultaneously or sequentially, fully leveraging the development and use of complex *in situ* environments.

HEDM datasets are inherently multi-dimensional (three-dimensional space and orientation, six-dimensional strain tensor, several time/processing steps), which results in large data volumes and the need for correlated data analysis. For example, HEDM grain maps, such as that shown in Fig. 2, require ~30,000 area detector images with each image being roughly 8 MB in size, or 240 GB for this particular *in situ* loading condition; several load steps are desired to observe material evolution. Algorithms are in active development to reduce, analyze, image, and fuse these large, high-dimensionality data sets using cluster and supercomputing resources. Finally, active involvement of the modeling community is being fostered in order to take full advantage of these unique data sets.

Contacts: Jonathan D. Almer (XSD, almer@aps.anl.gov), Erika Benda (AES, benda@aps.anl.gov), Robert M. Suter (Carnegie Mellon University, suter@andrew.cmu.edu), Jay C. Schuren (Air Force Research Laboratory, jay.schuren@wpafb.af.mil)

Rapid-Acquisition Powder Diffraction at APS Beamline 17-BM-B

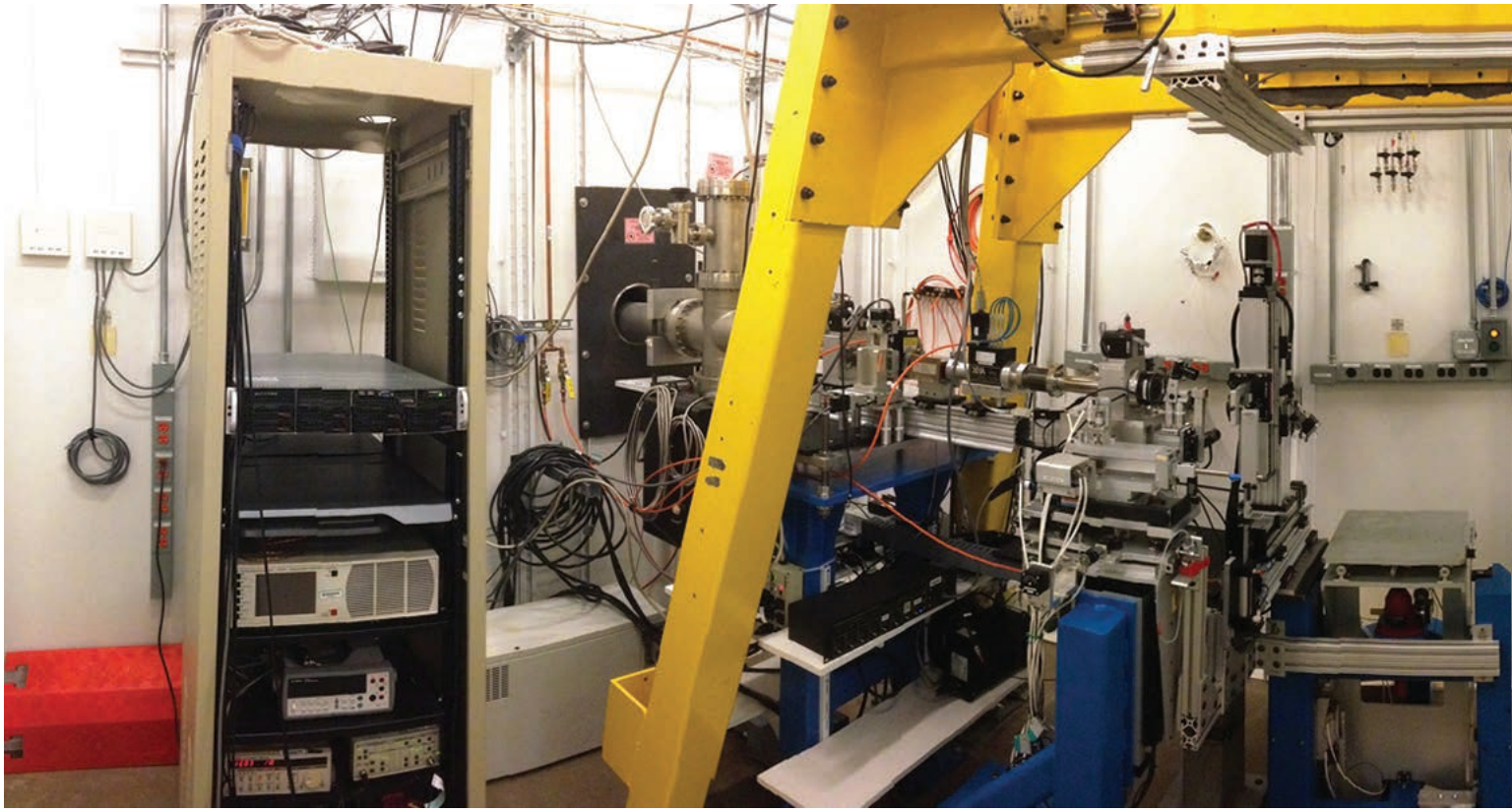

Fig. 1. Panoramic view of the interior of the reconfigured 17-BM-B research station. Photo: Greg Halder (XSD).

2013 saw expansion of powder diffraction capabilities within XSD. The rapid-acquisition (or "area detector") powder diffraction program, formerly one of several programs operating out of beamline 1-BM, was relocated to a dedicated beamline at 17-BM-B (previously operated as a macromolecular crystallography instrument by the Industrial Macromolecular Crystallography Association Collaborative Access Team, which operates beamline 17-ID-B). The initial phase of the relocation was completed in less than two months, allowing uninterrupted user access critical to satisfying the rapidly growing demand for powder diffraction capabilities at the APS. The relocation of the program has since generated a three-fold in increase in the general user subscription rates, while the legacy of the program has resulted in the highest ever annual publication total for beamline 1-BM during calendar year 2013 (30 papers for calendar year 2013 as of April 30, 2014).

At 17-BM-B, the combination of sagittal focused, high-flux bending magnet radiation and a state-of-the-art area detector delivers moderate resolution powder diffraction data in as little as 1/10 of a second. A highly flexible and spacious experimental station set-up, featuring an agile A-frame-mounted detector support, makes 17-BM-B uniquely well suited to a wide variety of *in situ* measurements. In addition to the now increased accessibility through a dedicated beamline, the reconfigured 17-BM-B location offers a number of critical improvements, including improved optics reliability and stability, streamlined gas handling system, and more readily interchangeable experimental set-ups.

The instrument utilizes a Perkin-Elmer amorphous silicon flat-panel area detector, allowing rapid collection of high-quality powder diffraction data ($\Delta d/d$: ~1 x 10^{-3}; typical data collection times: 0.1-30 sec). The 17-BM-B energy range is 10 to 18 keV at the time of writing, with plans to increase this to >30 keV (based on user demand) under way. All standard experimental capabilities for on-site users offered at 1-BM have been retained in the new location, including a high-throughput sample changer (more than 100 unique samples can be measured in under an hour); variable temperature options (100-1200K), a compact flowcell apparatus for controlled atmospheres that can be coupled with all temperature options; and high-pressure diamond anvil cell experiments, specifically targeting accurate pressures in ranges appropriate for industrially important applications (<10 GPa) of energy-related materials, such as gas storage and separation materials (e.g., zeolites and metal-organic frameworks).

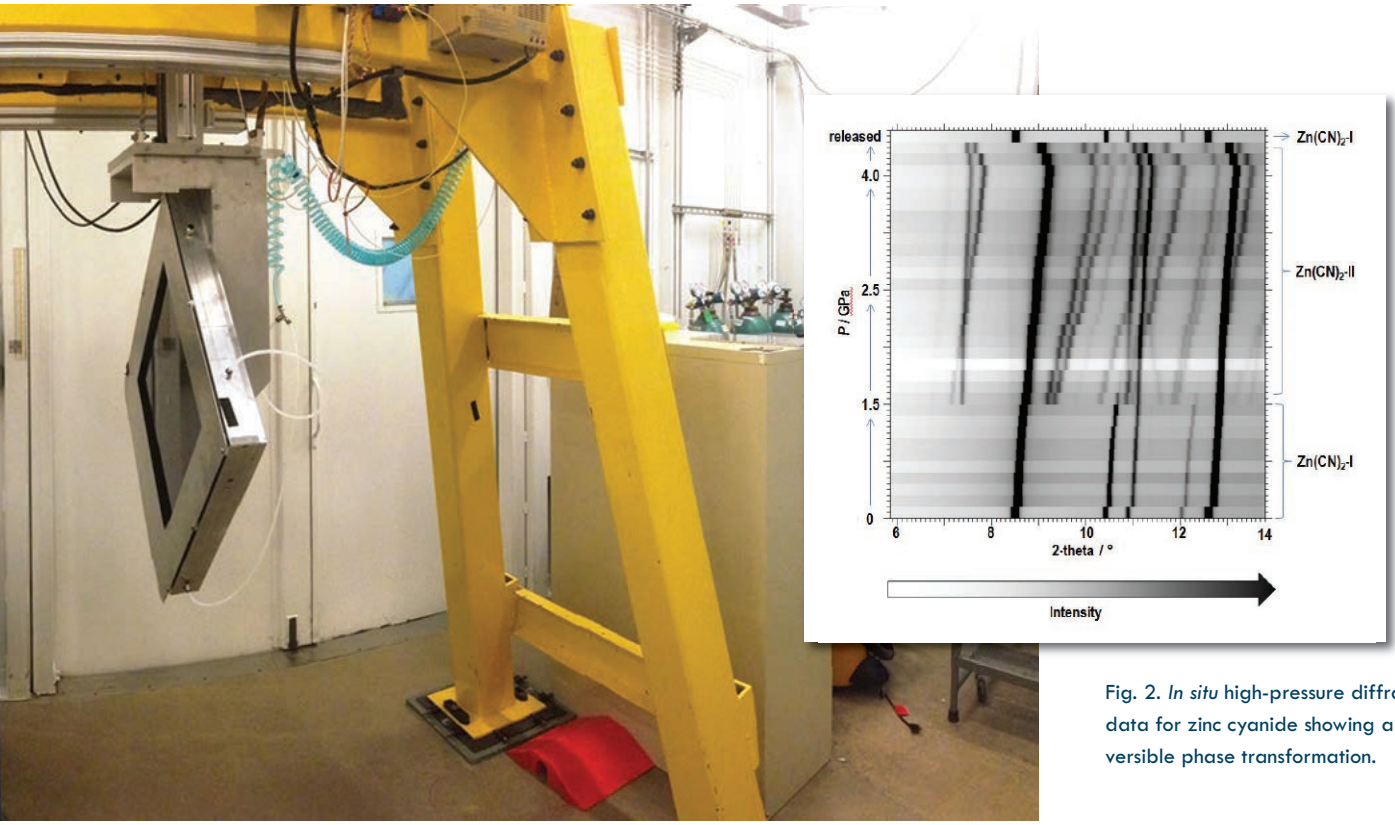

Fig. 2. *In situ* high-pressure diffraction data for zinc cyanide showing a reversible phase transformation.

The new location has already generated several publications, including work carried out by beamline staff that led to a novel discovery reported in the Journal of the American Chemical Society; see "Exploiting High Pressures to Generate Porosity, Polymorphism, and Lattice Expansion in the Nonporous Molecular Framework Zn(CN)2" by Lapidus et al., 135, 7621 (2013), DOI:10.1021/ja4012707. By applying pressure, a dense non-porous phase was transformed into a range of new porous materials with half the density; this is akin to squeezing a rock and forming a sponge (see "A Solid Bulks Up under Pressure" on page 91).

The enhanced powder diffraction program at 17-BM-B complements the capabilities of the APS beamline 11-BM, which is dedicated to high-resolution powder diffraction measurements. Beamline 11-BM operates over the energy range 15-35 keV, and uses multiple Si crystal analyzers to achieve exceptional resolution and sensitivity ($\Delta d/d$: ~2 x 10^{-4}; typical data collection times: 10-60 min). Beamline 11-BM offers a unique mail-in service for rapid access, and supports on-site user experiments for non-routine powder diffraction measurements. The success of 11-BM, which has been one of the most productive beamlines at the APS over the past 2-3 years with more than 100 publications in 2013 alone, has greatly contributed to the increased awareness and demand for synchrotron powder diffraction in the U.S. and beyond. However, not all experiments demand the world-class resolution of this instrument and would benefit more from the improved sampling statistics (i.e., full diffraction cone imaging) and the increased temporal resolution available with an area detector at 17-BM-B. Combining these factors with the highly flexible experimental station set-up allows for highly interactive experiments to be performed in "real" time and under "real" conditions. In some cases, utilizing both powder diffraction techniques may even be critical to fully characterize a system's structural properties, for example see "Chemical ordering rather than random alloying in SbAs" by D. P. Shoemaker et al. (Phys. Rev. B **87**, 094201 (2013), DOI:10.1103/PhysRevB.87.094201) .

Both dedicated powder diffraction beamlines are operated by the Structural Sciences (SRS) Group within XSD. More information on SRS beamlines can at: www.aps.anl.gov/Xray_Science_Division/Structural_Science/ or by emailing beamline staff at 17-BM@aps.anl.gov.

Contact: Gregory J. Halder, halder@aps.anl.gov

Funded by the U.S. Department of Energy Office of Science under Contract No. DE-AC02-06CH11357.

17-BM-B • XSD • Chemistry, materials science • Powder diffraction • 15-18 keV • On-site • Accepting general users •

The New RIXS Beamline at APS Sector 27

Richard Krakora (left) and Thomas Gog (both XSD) at 27-ID, under construction, April 2, 2014.

In the past two decades, inelastic x-ray scattering (IXS) techniques have become very powerful spectroscopic tools at synchrotron radiation facilities all over the world. The resonant variety of this class of techniques, RIXS, is uniquely suited to the study of electron dynamics in complex materials by probing the energy-, momentum- and polarization dependence of elementary excitations in these systems.

RIXS at the APS, established in the early 2000s, is one of the world's leading programs of its kind. It is currently spread over two time-shared beamlines of varying sophistication, with many significant milestones achieved and many important discoveries made. Among them were numerous comprehensive studies of 3*d* transition metal oxides (particularly the cuprates), which shed light on many novel phenomena such as high-T_c superconductivity.

In 2008 a bi-magnon excitation in a cuprate was observed experimentally at the APS for the first time, an important step in establishing RIXS as an inelastic scattering probe for not only electronic but also magnetic excitations [1]. At the same time, however, it was recognized that the impact and utility of the RIXS technique would be dramatically enhanced if its energy resolution was substantially improved to become comparable to inelastic neutron scattering. Most recently great strides towards this goal have been made with the implementation of an x-ray optical set-up, combining special near-backscattering monochromators with a matching diced, spherical crystal analyzer and appropriate beam focusing to achieve an unprecedented energy resolution of 30 meV.

Advancing the energy resolution at the iridium L_3 edge enabled the observation of scattering from single magnon excitations (spin waves) [2] and immediately led to the discovery of a new magnetic excitation, a spin orbit exciton, as shown in Fig. 1. This was a major advance in the field, which spurred enormous interest in the community and a

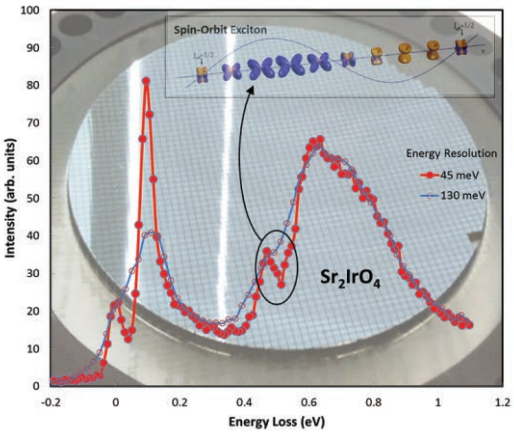

Fig. 1. A dramatic improvement in energy resolution (30 meV) for RIXS measurements at the iridium absorption edge immediately led to the discovery of a novel magnetic excitation, a spin-orbit exciton. Shown in the background of the figure is a diced, spherical crystal analyzer, the centerpiece of the RIXS x-ray optics.

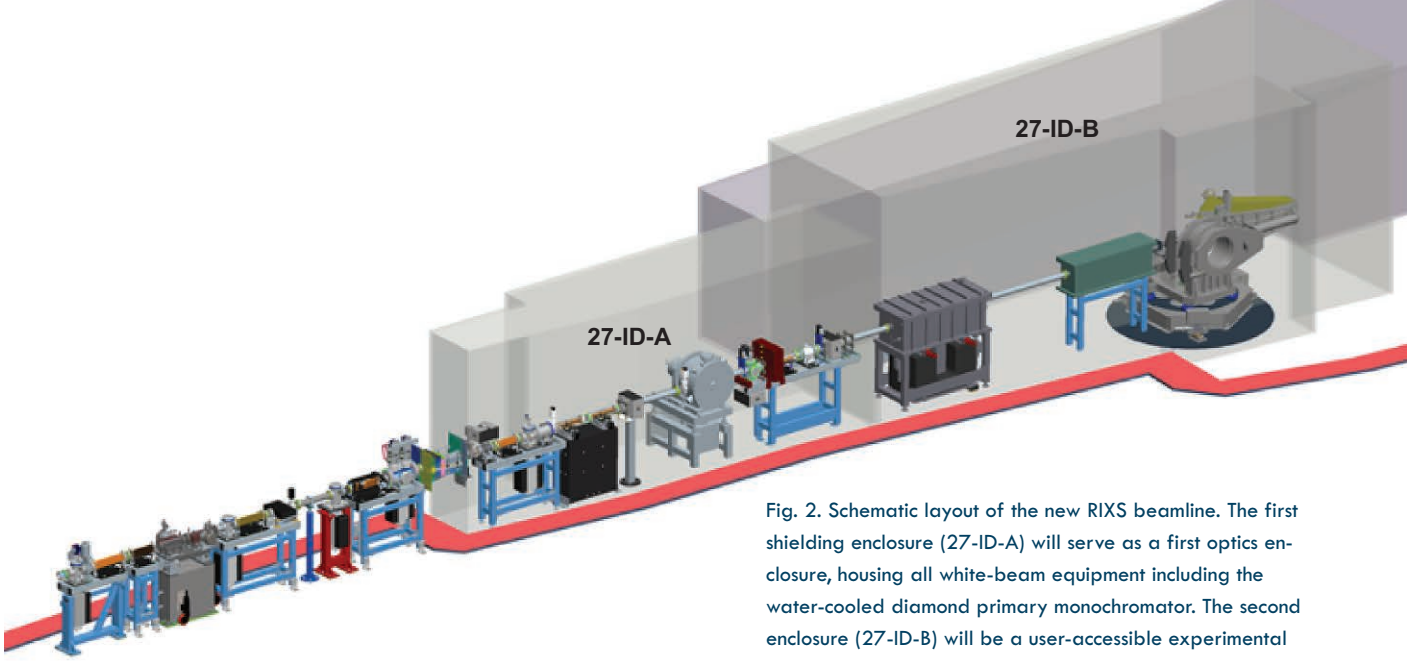

Fig. 2. Schematic layout of the new RIXS beamline. The first shielding enclosure (27-ID-A) will serve as a first optics enclosure, housing all white-beam equipment including the water-cooled diamond primary monochromator. The second enclosure (27-ID-B) will be a user-accessible experimental station, housing a set of high-resolution secondary monochromators, focusing mirrors, and the RIXS spectrometer.

rapid burst in high-impact publications. Indeed, since 2012 this set-up has generated six high-impact articles in the *Physical Review* [2-6], studying novel magnetic phenomena in various iridium-containing transition metal oxides.

Inspired by the success story surrounding the iridates, a new RIXS beamline is being constructed at Sector 27 of the APS. It will consolidate all RIXS efforts at the APS on one dedicated, optimized, state-of-the-art insertion device beamline, offering enhanced energy resolution and x-ray intensities, combined with advanced beam focusing and a comprehensive suite of sample environments for meaningful *in situ* experimentation. It will be possible to study complex materials of high technological and fundamental importance, including 5*d*-transition-metal-oxides, iridates, osmates, rheniates, and others where a treasure trove of novel phenomena are expected, such as topological band or Mott insulators, quantum spin liquids, field-induced topological order, and topological superconductors.

The beamline, shown schematically in Fig. 2, will be powered by two 2.4-m-long, in-line, 30-mm-period undulators, providing full tunability between 4.9 and 23 keV, thereby allowing access to the most important transition metal absorption edges. It will feature a water-cooled diamond high-heat-load monochromator combined with flexible-configuration, high-resolution secondary monochromators. Advanced single-stage focusing to beam sizes down to 5 x 10 μm^2 at the sample position will be accomplished with a dynamically figured pair of Kirkpatrick-Baez mirrors. Beam focusing would be further improved dramatically with the implementation at the APS of a multi-bend achromat-lattice storage ring.

A wide selection of diced, spherical, crystal analyzers will be made available. In the past, silicon and germanium were the preferred material choices for these analyzers; however, with advances in crystal growth, other materials are becoming very viable, such as quartz, sapphire, and lithium niobate. These materials open a multitude of possibilities for new analyzers, capable of matching resonance energies with greatly improved energy resolution and/or throughput. Fabrication of such crystal analyzers is being pursued by a dedicated R&D program in the context of the new RIXS beamline.

Contact: Thomas Gog, gog@aps.anl.gov

Funded by the U.S. Department of Energy Office of Science under Contract No. DE-AC02-06CH11357.

References

[1] J.P. Hill, G. Blumberg, Young-June Kim, D. S. Ellis, S. Wakimoto, R. J. Birgeneau, Seiki Komiya, Yoichi Ando, B. Liang, R. L. Greene, D. Casa, and T. Gog, "Observation of a 500 meV Collective Mode in $La_{2-x}Sr_xCuO_4$ and Nd_2CuO_4 Using Resonant Inelastic X-Ray Scattering," Phys. Rev. Lett. **100**, 097001 (2008).

[2] Jungho Kim, D. Casa, M. H. Upton, T. Gog, Young-June Kim, J. F. Mitchell, M. van Veenendaal, M. Daghofer, J. van den Brink, G. Khaliullin, and B. J. Kim "Magnetic Excitation Spectra of Sr_2IrO_4 Probed by Resonant Inelastic X-Ray Scattering: Establishing Links to Cuprate Superconductors," Phys. Rev. Lett. **108**, 177003 (2012).

[3] X. Liu, Vamshi M. Katukuri, L. Hozoi, Wei-Guo Yin, M. P. M. Dean, M. H. Upton, Jungho Kim, D. Casa, A. Said, T. Gog, T. F. Qi, G. Cao, A. M. Tsvelik, Jeroen van den Brink, and J. P. Hill, "Testing the Validity of the Strong Spin-Orbit-Coupling Limit for Octahedrally Coordinated Iridate Compounds in a Model System Sr_3CuIrO_6," Phys. Rev. Lett. **109**, 157401 (2012).

[4] Jungho Kim, A. H. Said, D. Casa, M. H. Upton, T. Gog, M. Daghofer, G. Jackeli, J. van den Brink, G. Khaliullin, and B. J. Kim, "Large Spin-Wave Energy Gap in the Bilayer Iridate $Sr_3Ir_2O_7$: Evidence for Enhanced Dipolar Interactions Near the Mott Metal-Insulator Transition," Phys. Rev. Lett. **109**, 157402 (2012).

[5] H. Gretarsson, . P. Clancy, X. Liu, J. P. Hill, Emil Bozin, Yogesh Singh, S. Manni, P. Gegenwart, Jungho Kim, A. H. Said, D. Casa, T. Gog, M. H. Upton, Heung-Sik Kim, J. Yu, Vamshi M. Katukuri, L. Hozoi, Jeroen van den Brink, and Young-June Kim, "Crystal-Field Splitting and Correlation Effect on the Electronic Structure of A_2IrO_3," Phys. Rev. Lett. **110**, 076402 (2013).

[6] Wei-Guo, X. Liu, A. M. Tsvelik, M. P. M. Dean, M. H. Upton, Jungho Kim, D. Casa, A. Said, T. Gog, T. F. Qi, G. Cao, and J. P. Hill, "Ferromagnetic Exchange Anisotropy from Antiferromagnetic Superexchange in the Mixed 3d−5d Transition-Metal Compound Sr_3CuIrO_6," Phys. Rev. Lett. **111**, 057202 (2013).

Full-Field Diffraction Microscopy of Surfaces and Interfacial Structures

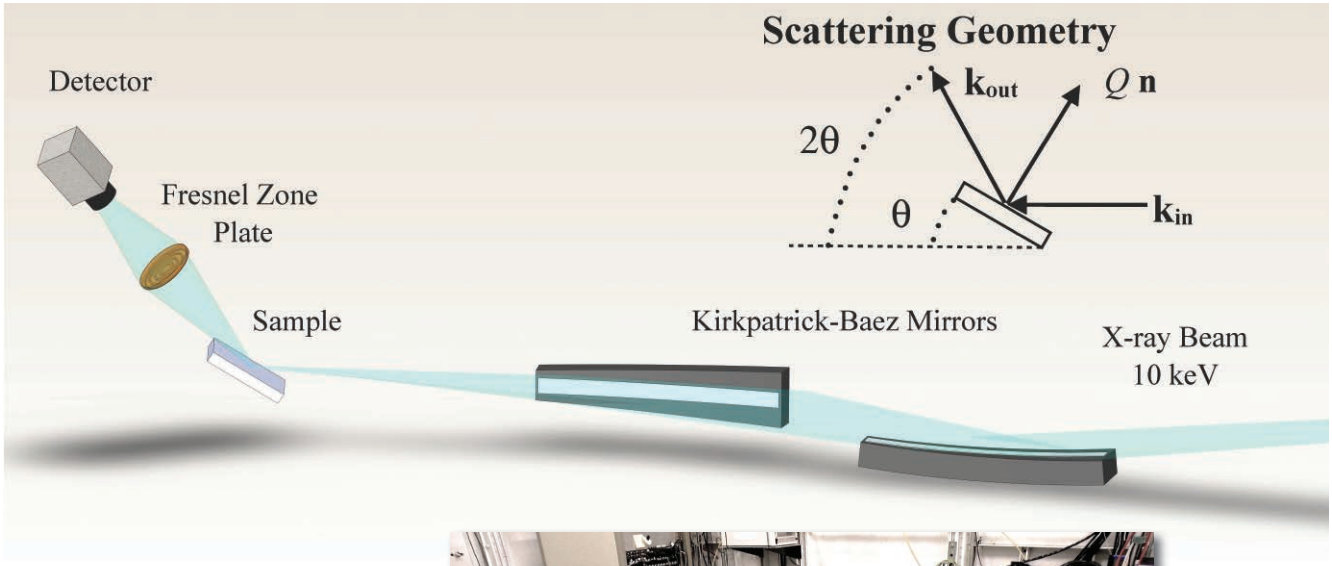

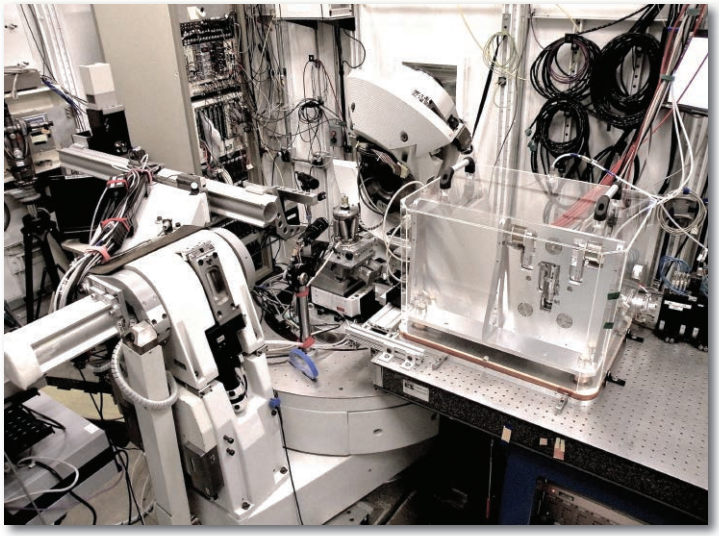

Fig. 1. Schematic (top) and photograph (right) of the optical configuration of XRIM-2 (distances and components not drawn to scale). Inset at upper right: specular diffraction geometry indicating sample rotation (θ), lens/detector rotation (2θ), and scattering transfer Q. The photograph shows the instrument during its implementation at beamline 33-ID-D.

Over the past century, x-ray diffraction has excelled at revealing the structures of a multitude of systems, from crystals and interfaces to thin films and nanoparticles, by averaging the diffracted signal over the entire system. Meanwhile, the ever-increasing need to obtain local, spatially-resolved, structural information on systems from the nano- through the meso-scale has led to significant development of hard x-ray imaging techniques. Furthermore, the inherent complexity of many processes (growth, dissolution, etc.) demands experimental probes that can investigate phenomena *in situ* and in real-time, with structural (and often, elemental) sensitivities. This article describes efforts to establish a new instrument that combines these capabilities to image interfaces in complex environments and in real-time: the X-ray Reflection Interface Microscope (XRIM).

The XRIM operates in a reflection geometry that spatially resolves the structure of systems using diffraction contrast. The optical configuration of XRIM (Fig. 1) is composed of a condenser lens to illuminate the sample, an objective lens to image the sample using the diffracted x-ray wave, and an x-ray area detector with 20x optical magnification. The upgraded instrument is currently hosted at APS beamline 33-ID-D. The initial implementation (XRIM-1) demonstrated imaging of sub-nanometer high interfacial topography [1] and identified the corresponding contrast mechanism [2]. The microscope was also applied to the observation of interfacial reactivity (through both *ex situ* [3] and *in situ* observations [4]). These initial investigations clarified the significant limitations of the XRIM-1 system, which include resolution (~170 nm), image acquisition time, and beam-induced damage for *in situ* studies [4].

Improvements to the XRIM-1 system were necessary to make it a robust research tool, and to balance the various competing requirements for stability, resolution, and throughput. The use of diffraction contrast requires large angular motions of the sample (and its cell or chamber), the objective

lens, and detector while also placing severe constraints on the mechanical stability requirements of all the components in a diffractometer.

The current implementation, XRIM-2 [5], has achieved sub-100-nm lateral resolution, a ~2-fold improvement over the resolution of the first implementation, chiefly due to the design of a dedicated sample stage that is mechanically decoupled from the rest of the instrument. Moreover, a 10-fold increase in the illumination flux has been achieved by using a high-efficiency reflective condenser (the previous version used diffractive optics), leading to a substantial reduction in the acquisition time. Further increases in the resolution, to 30 nm – 50 nm, and throughput, will require a dedicated instrument and improvements in the objective lens efficiency; alternatives to achieve these goals are currently being pursued.

The XRIM-2 system has been utilized to image a number of interfacial systems, including: dislocation networks and associated strain fields at a solid/solid interface, ferroelectric/ferroelastic domains in buried epitaxial thin films in a capacitor configuration, real-time changes to mineral/water interfaces, and the mapping of the lateral variation of thin-film thicknesses. This latter application nicely illustrates the versatility of this technique.

Bi_2Se_3 films (Fig. 2a) are grown by molecular beam epitaxy (Lian Li; University of Wisconsin-Milwaukee) on epitaxial graphene /6H-SiC(0001) (synthesized by Kurt Gaskill, U.S. Naval Research Laboratory by sublimation of SiC). Conventional surface x-ray diffraction characterizes the average film thickness, but reveals neither its spatial variation nor its relationship to the substrate topography. This is important in the case of Bi_2Se_3, where a critical thickness of approximately six quintuple layers (QL, corresponding to a Se-Bi-Se-Bi-Se layer with ~1-nm thickness) is required for surface conduction, while the bulk material is insulating. Moreover, one-dimensional conducting channels through the bulk are predicted and are associated with bulk line defects.

Using the diffraction contrast at the Bi_2Se_3 film (0,0,9) Bragg condition (Qz = 1.32 Å^{-1}), the lateral distribution of the QL thickness (NQL is the number of QLs) was spatially resolved as shown in Fig. 2c, revealing a ~50% variation of the film thickness with >100-nm-sized lateral domains. Imaging of the same sample area at a different scattering condition (Fig. 2b, at Qz = 2.43 Å^{-1}) provides sensitivity to the underlying surface topography of SiC, even though it is located ~27 nm beneath the film surface (additional measurements can probe the graphene layer morphology as well), so that the structural controls over the film growth can be elucidated.

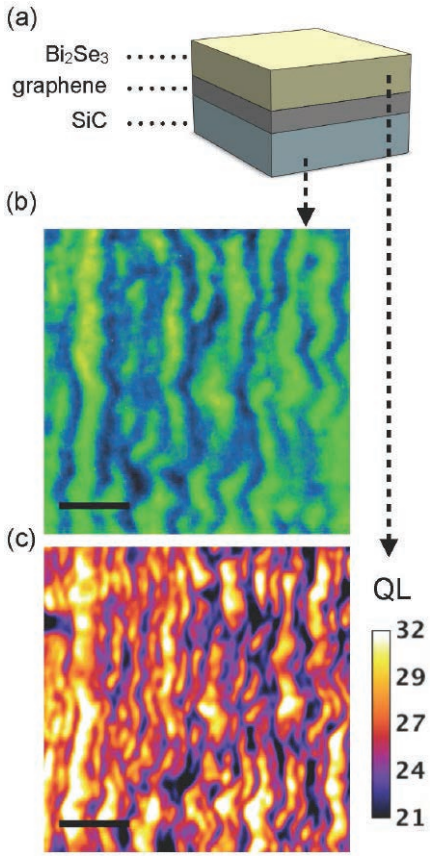

Fig. 2. Imaging of buried structures in the Bi_2Se_3/graphene/SiC system at different scattering conditions. a) Schematic representation of the film structure. b) XRIM image at Q = 2.43 Å^{-1} that is sensitive to the SiC surface topography, shown in false color. Bright and dark regions can be qualitatively interpreted as terraces and steps. c) XRIM image at Q(009) = 1.32 Å^{-1} revealing the lateral distribution of the thin-film thickness of Bi_2Se_3. This image is taken at the same spot as that in (b) (as indicated by the oval). The image intensity scale in (c) refers to the number of quintuple layers (QL) of Bi_2Se_3 as derived from the intensity of the thin-film Bragg peak. The scale bar in both images is 1.5 μm.

This full-field x-ray diffraction microscope will be an invaluable tool in meso-scale structural studies of condensed-matter systems, materials science, and interfacial chemistry, specifically when used in settings that require real-time monitoring of a system's properties as a function of varying thermodynamic potentials.

This work was supported by the U.S. Department of Energy Office of Science, Basic Energy Sciences, Geoscience Research Program, and the APS through the Partner User Program. We thank Kurt Gaskill (Naval Research Laboratory) and Lian Li (University of Wisconsin-Milwaukee) for providing the grapheme-coated SiC substrates and for growing the Bi_2Se_3 films, respectively; Peter Eng (GeoSoilEnviroCARS, University of Chicago) for setting up the Kirkpatrick-Baez mirror system; Jonathan Tischler (XSD) for his invaluable advice and suggestions during the design of the microscope, and Joan Vila-Comamala (Diamond Light Source, UK) for making the Fresnel zone plate objective lenses.

Nouamane Laanait, Zhan Zhang, Christian M. Schlepütz, and Paul Fenter***

Author affiliation:
Argonne National Laboratory

Correspondence: * nlaanait@anl.gov, ** fenter@anl.gov

References

[1] P. Fenter, C. Park, Z. Zhang, and S. Wang, "Observation of subnanometre-high surface topography with X-ray reflection phase-contrast microscopy," Nat. Phys. **2**(10), 700 (2006).

[2] P. Fenter, C. Park, V. Kohli, and Z. Zhang, "Image contrast in X-ray reflection interface microscopy: Comparison of data with model calculations and simulations," J. Synchrotron Rad. **15**, 558 (2008).

[3] P. Fenter, S.S. Lee, C. Park, J.G. Catalano, Z. Zhang, and N.C. Sturchio, "Probing interfacial reactions with X-ray reflectivity and X-ray reflection interface microscopy: Influence of NaCl on the dissolution of orthoclase at pOH 2 and 85º C," Geochim. Cosmochim. Acta **74**(12), 3396 (2010).

[4] P. Fenter, S.S. Lee, Z. Zhang, and N.C. Sturchio, "*In situ* imaging of orthoclase-aqueous solution interfaces with x-ray reflection interface microscopy," J. Appl. Phys. **110**(10), 102211 (2011).

[5] N. Laanait, Z. Zhang, C.M. Schleputz, and P. Fenter, "Full-field Diffraction Microscopy of Surfaces and Interfacial Structures," in preparation (2014).

Coherent Diffraction Reveals 3-D Nano-Strain

The diamond anvil cell (DAC) is the most widely used research device for subjecting materials to high pressures over extended periods. A promising technique for probing materials within the DAC environment is coherent x-ray diffraction imaging (CXDI). The advantage of using CXDI is that high-energy x-rays — optimally derived from the APS or similar facilities — can penetrate the DAC while (theoretically) providing unsurpassed high-resolution spatial and strain information. Unfortunately, the x-ray beam required by CXDI partially loses coherence (i.e., the x-ray photons' phase relationships change) after passing through the environment of the DAC device. To address this "coherence problem," a team of scientists employed the recently-developed mutual coherence function (MCF) method. Utilizing this new method, the research team used CXDI to probe a gold nanocrystal at high pressures within a DAC, achieving three-dimensional (3-D) spatial resolutions 100 times better than previous results, and with a ten-fold improvement in strain resolution.

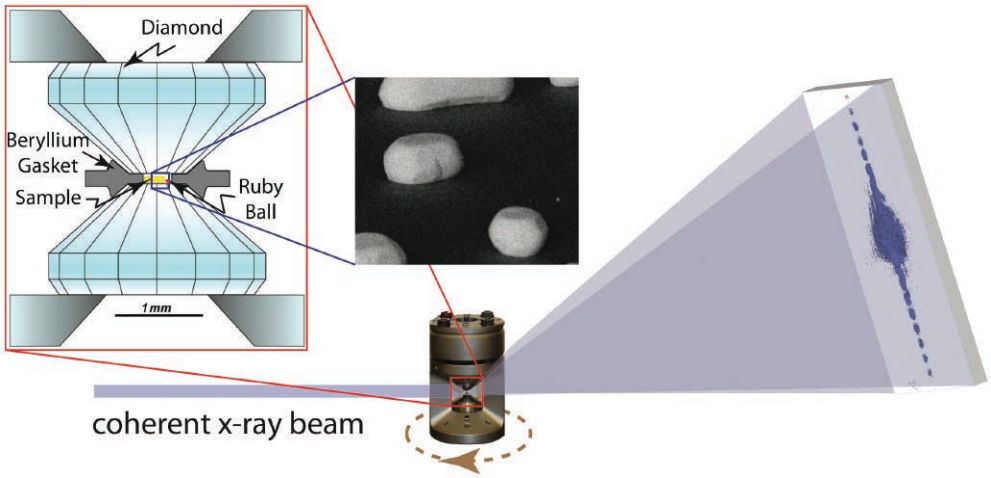

Fig. 1. Overall schematic of the experimental setup. A large-opening panoramic DAC is used to compress the gold nanocrystal, positioned at the rotation center of the diffractometer. An x-ray-sensitive CCD is placed 1 m away on the right side to collect far-field diffraction patterns. Far left: A zoomed-in diagram of the DAC depicts details of the nanocrystal's environment. Inset micrograph: scanning-electron microscopy picture shows gold nanoparticles — similar to the nanocrystal used in the experiment — distributed on a silicon substrate.

The researchers, from the Carnegie Institution of Washington, the Center for High Pressure Science and Technology Advanced Research (P.R. China), Argonne, University College London, and the Research Complex at Harwell (UK) believe that applying the MCF method will lead to new insights into the chemical nature, phase change behavior, structural stability, and other physical properties of materials under extreme conditions.

The basic experimental layout depicted in the first figure shows highly coherent and collimated x-rays, derived from the XSD 34-ID-C beamline at the APS, directed to a gold nanocrystal held within the DAC. The diffracted x-rays are registered by a charge-coupled device. The zoomed-in part of the figure shows the two diamond anvils. A high-pressure liquid along with the sample are sealed by a beryllium gasket situated between the two diamond anvils. The x-ray beam is aimed along the gasket/anvil interface, not through the common axis of the diamonds (the diamonds would excessively absorb the x-ray beam).

CXDI is a lens-less technique that, instead of focusing the diffracted x-rays, utilizes the sophisticated processing of algorithms to reconstruct phase and intensity information from the diffraction pattern. If the DAC apparatus was removed, standard CXDI techniques would produce highly-detailed images of the gold nanocrystal. However, the presence of the DAC alters both the phase and scattering intensity of the initially-coherent x-ray photons. These changes occur due to scattering of the x-rays as they pass through the DAC's beryllium gasket, high-pressure liquid, and other components. For this experimental configuration, recovering the degraded phase and intensity information (called de-convolution) required special treatment.

In the case of fully-coherent diffraction, the so-called direct phase retrieval method is used for CXDI. However, the altered intensity-and-phase relations in

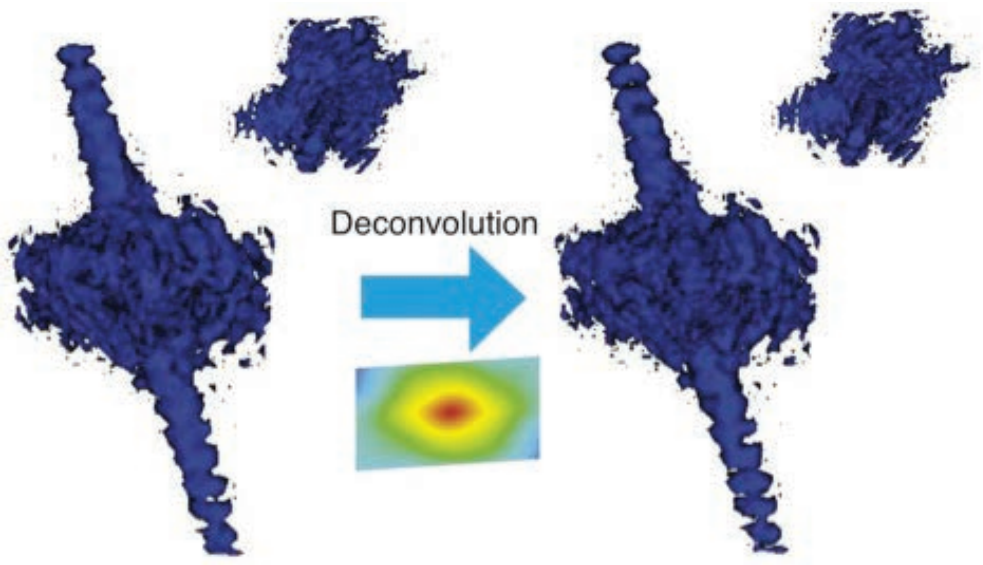

Fig. 2. Comparison of the diffraction intensity distribution before and after de-convolution. The measured diffraction intensity distribution, which is only partially coherent, is shown on the left. The fully coherent, de-convoluted intensity distribution is shown on the right. For this measurement the nanocrystal was under a pressure of 0.8 GPa.

this experiment led to partially coherent x-ray radiation. For this situation, a mathematical formula is used that relates the diffracted x-ray intensity to both the mutual coherence function and a complex-valued wavefield. The principal idea is that as the phase information is retrieved from the recorded diffraction pattern, both the MCF and wavefield are updated in an iterative process — aided by constraints on the sample, such as the nanocrystal's size and shape — until their two values converge. The second figure shows the effect of using the MCF method to recover the coherent diffraction intensity information.

The gold nanocrystal examined in this research was synthesized by melting a thin layer of gold film and then forming it to a facetted shape, with its largest dimension around 400 nm. Within the DAC, the gold nanocrystal was subjected to a range of pressures. Multiple x-ray diffraction measurements of the nanocrystal were performed at five pressures: 0.8, 1.7, 2.5, 3.2, and 6.4 GPa. Applying the MCF method to these diffraction measurements produced 3-D electron density and strain distributions with spatial resolutions of 30 nm and strain accuracies of 1 x 10^{-4}. At the lowest pressure of 0.8 GPa, strain within the nanocrystal was relatively low. At 1.7 GPa, a sharp corner formed in the nanocrystal, accompanied by an increased level of strain. At all higher pressures, both the pronounced corner and strain were significantly reduced.

These findings, involving a single nanocrystal, stand in stark contrast to earlier high-pressure studies using powder x-ray diffraction, which employs large numbers of nanocrystals. While powder diffraction methods indicated that nanocrystal strain rises with pressure, this single-nanocrystal study actually demonstrates that low strain levels accompany these higher pressures. The scientists hypothesize that the disparity arises from the inter-nanocrystal effects inherent in powder diffraction.

The researchers envision that CXDI, augmented by the MCF method, will be applied to experimental conditions beyond the confines reported here, such as imaging nanocrystals at ultra-high pressures, in the terapascal range (1 terapascal = 1,000 GPa). Another expected research avenue involves applying these same methods to larger objects and with an even higher spatial resolution, as typified by the new field of ptychography, which aims to solve the diffraction-pattern phase problem by interfering adjacent Bragg reflections coherently and thereby determine their relative phase.

— Philip Koth

See: Wenge Yang[1,2*], Xiaojing Huang[1], Ross Harder[3], Jesse N. Clark[4], Ian K. Robinson[4,5], and Ho-kwang Mao[1,2], "Coherent Diffraction Imaging of Nanoscale Strain Evolution in a Single Crystal under High Pressure," Nat. Commun. **4**, 1680 (9 April, 2013). DOI:10.1038/ncomms2661

Author affiliations: [1]Carnegie Institution of Washington, [2]Center for High Pressure Science and Technology Advanced Research, [3]Argonne National Laboratory, [4]University College London, [5]Research Complex at Harwell

Correspondence: * wyang@ciw.edu

This work was supported by EFree, an Energy Frontier Research Center funded by the U.S. Department of Energy Office of Science, Basic Energy Sciences, under grant number DE-SC0001057 and by the European Research Council "nanosculpture" advanced grant 227711. Use of the Advanced Photon Source at Argonne National Laboratory was supported by the U.S. Department of Energy Office of Science under Contract No. DE-AC02-06CH11357.

34-ID-C • XSD • Materials science, physics • Coherent x-ray scattering • 5-15 keV, 7-25 keV • On-site • Accepting general users •

The Dynamic Compression Sector at the Advanced Photon Source

Far left: The 35-ID-D impact facility. Center: Brendan Williams (left) and Erik Zdanowicz testing an impact driver at Washington State University. Right: The exterior of the DCS laboratory/office module.

Over the past year, the Dynamic Compression Sector (DCS) located at APS Sector 35 has made a transition from concept to reality with the construction of four in-line experimental stations (Fig. 1) and a laboratory office module (LOM). The DCS is a National Facility that is funded by the Department of Energy's (DOE's) National Nuclear Security Administration (NNSA) in support of its Stockpile Stewardship Science Mission. This first-of-a-kind user facility is being developed through a partnership between Washington State University and the APS, in strong collaboration with NNSA laboratories, Department of Defense laboratories, and other institutions. The DCS will provide a unique experimental capability that will be dedicated to time-resolved (~nanosecond resolution), multi-scale x-ray measurements in dynamically compressed materials.

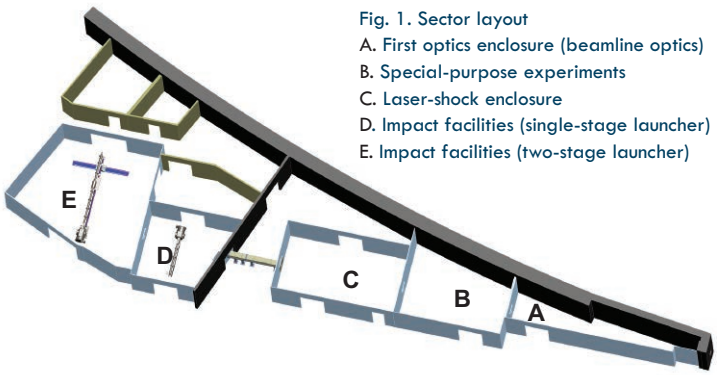

Fig. 1. Sector layout
A. First optics enclosure (beamline optics)
B. Special-purpose experiments
C. Laser-shock enclosure
D. Impact facilities (single-stage launcher)
E. Impact facilities (two-stage launcher)

Understanding the real-time, atomistic-level response of materials under extreme dynamic conditions is central to fundamental science frontiers in numerous fields and to advanced technology. To address this key scientific need, the DCS will couple a variety of dynamic compression platforms to a state-of-the-art undulator beamline at Sector 35. The APS is ideally suited for these measurements due to its high brightness and its unique storage ring fill patterns, in which adjacent hard x-ray pulses are separated in time by minimum of 2.8 to hundreds of nanoseconds.

Dynamic compression experiments will utilize both x-ray diffraction and imaging measurements, simultaneously with continuum measurements, to observe time-dependent changes in materials subjected to a broad range of stress amplitudes (~5 GPa to >200 GPa) and time-durations (~10 nsec to ~1 μs). For example, as a shock wave propagates through a material, time-resolved x-ray diffraction will measure changes in crystallographic properties while time-resolved, high-spatial-resolution, phase contrast imaging will be employed to obtain a sequence of spatially resolved images.

A crucial element of the DCS experiments will be an area detector capable of capturing a series of images (diffraction patterns) generated by consecutive x-ray pulses. Initially, scintillator-based indirect-detection detectors will be deployed that are optimized for the APS storage ring 24-bunch mode fill pattern, and are capable of recording four frames per experiment with a minimum interframe spacing of 153.4 nsec.

The 35-ID-E and 35-ID-D research stations will contain a two-stage, light-gas gun (2SLGG) and a single-stage gas gun (SSGG), respectively (Fig. 1). These impact launchers will be mounted on motion control systems to precisely align samples to the x-ray beam in both position and angle. The 35-ID-C station will house a laser-shock facility and the 35-ID-B station will be used for special-purpose and non-single-event experiments. Continuum diagnostics, such as laser interferometry (e.g., Velocity Interferometry System for Any Reflector and Photonic Doppler Velocimetry) to measure shock wave histories with nanosecond and sub-nanosecond resolution, will be available in all four stations.

The DCS took beneficial occupancy of its LOM in October 2013 and began to configure the space with the infrastructure needed for on-site sample characterization and experimental component fabrication. In the upcoming year, the DCS looks forward to installation and commissioning of x-ray optics in 35-ID-A; the SSGG and 2SLGG installation in the 35-ID-D and 35-ID-E stations, respectively; and design/development of the laser in 35-ID-C. Commissioning experiments will commence in the first run of 2014 and continue throughout the year. A revolver undulator, a new device that allows switching between two magnetic lattices, with periods of 27 and 30 mm will be installed during the third APS run in 2014.

Contact: Yogendra M. Gupta, ymgupta@wsu.edu

X-ray Topography of Threading Dislocations in Aluminum Nitride

Wide bandgap (WBG) semiconductors are essential to our technology future [1]. Power electronics made with WBG components overcome the upper limits on temperature, frequency, and voltage that apply to silicon-based electronics and can help to eliminate up to 90% of present-day power losses in electric conversion. They are foreseen as essential for the future development of electric vehicles, industrial motors, laptop power converters and inverters for connecting wind turbines, and solar panels to the power grid [1]. A wide bandgap also makes them ideal for ultraviolet (UV) detectors that must be blinded from visible light in the solar spectrum, so-called "solar-blind detectors." Another application is to UV laser diodes. These applications, in general, require single-crystal material, and device performances are degraded by crystalline defects such as dislocations. Dislocations are also deleterious for reliability and lifetimes of devices. X-ray topography is a potent and non-invasive technique for imaging dislocation arrays in crystals, and work to characterize dislocation arrays in aluminum nitride, a WBG semiconductor, by means of x-ray topography has been carried out at the APS by researchers from Stony Brook University. Their work was published in a recent paper [2].

The wurtzite III-V nitride binary compounds of indium nitride (InN), gallium nitride (GaN), and aluminum nitride (AlN) have bandgaps of 1.9 eV, 3.4 eV, and 6.2 eV, respectively. They form a continuous range of compounds useful for optoelectronic sources and detectors at UV wavelengths, much like the III-V arsenides and III-V phosphides are useful at visible and infrared wavelengths [3]. Heteroepitaxy is a widely applied technology for device fabrication, but because lattice parameters do not match those of readily available substrates (e.g., sapphire), mismatch dislocations in epitaxial layers occur. Consequently, single-crystal boules of III-V nitrides are much desired to provide substrate wafers, and crystal growth of III-V nitride boules is an important technological effort. The melting temperature of InN, GaN, and AlN also follows an upward progression, with a melting temperature of AlN in excess of 3000° C. Such a high melting point is problematic for crystal growth from the melt [4]. This dilemma is finessed by the technique of physical vapor transport (PVT). For PVT, powdered AlN is sublimed in one chamber and transported with gaseous N_2 to a second chamber that is held at a temperature that is approximately 1000° C lower [4]. The AlN studied at APS beamline 1-BM was grown by PVT from an AlN seed placed in the growth chamber.

A remaining technological emphasis is to grow crystals with very low dislocation densities. Dislocation densities need to be low so that devices fabricated on wafers cut from boules achieve an optimum performance. A readily applied method to characterize threading dislocations is to etch the surface to reveal etch pits. But one cannot determine the orientation of the displacement vector that characterizes the dislocation this way [2]. The displacement vector of a dislocation is determined by schematically making an atom-to-atom circuit around a region of crystal that contains the dislocation. Without the dislocation this circuit would be closed, but because of the dislocation there is a displacement vector between start and end. This is the displacement vector that characterizes the dislocation. However, a novel technique was able to determine the entire displacement vector for threading dislocations [2]. This technique combines grazing incidence x-ray topography with ray tracing simulations. Dislocations thread along the c-axis of the wurtzite crystal structure. There are six possible types of threading edge dislocations (TEDs) and two possible types of threading screw dislocations (TSDs). With grazing incidence x-ray topography, accompanied by ray tracing simulations, for the first time it was possible to sort out which of these possible dislocations were prevalent in the PVT-grown material [2]. TEDs were found to occur in arrays of two kinds: 1) oriented along <1 -1 0 0>, and 2) oriented along <1 1 -2 0>. The most prevalent was type 1). This characterization of the line defects occurring in PVT-grown AlN provides a bench mark against which future improvements in crystal quality can be judged. *Contact: Al Macrander, atm@aps.anl.gov*

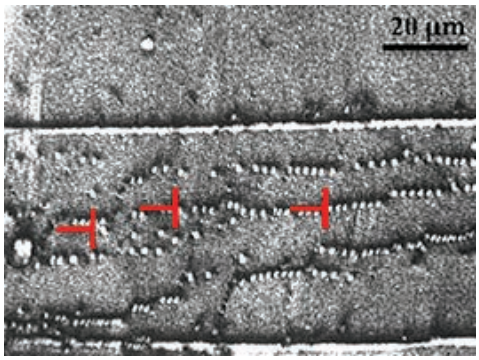

Fig. 1. Monochromatic x-ray topographic image for the (1 1 -2 4) reflection in grazing incidence showing a TED array along the <1 -1 0 0> direction [2]. Three edge dislocations are schematically depicted in red. This image was obtained at XSD beamline 1-BM of the APS.

References

1] http://energy.gov/articles/wide-bandgap-semiconductors-essential-our-technology-future

[2] T. Zhou et al., "Characterization of Threading Dislocations in PVT-Grown AlN Substrates via x-Ray Topography and Ray Tracing Simulation," J. Electron. Mater. **43**(4), 838 (2014).

[3] S. Strite and H. Morkoc, J. Vac. Sci. Tech. B **10**, 1237 (1992).

[4] G. Dhanaraj, K. Byrappa, V. Prasad, and M. Dudley, "Handbook of Crystal Growth," (Springer, 2010).

Financial support from DARPA via HexaTech, Inc. Monochromatic x-ray topography was carried out at the 33-BM-C and 1-BM-B,C beamlines of the APS, which is supported by the U.S. Department of Energy (DOE) Office of Science under Contract No. DE-AC02-06CH11357. The published work was in part also based on white-beam x-ray topography carried out at the Stony Brook Topography Facility (Beamline X19C) at the National Synchrotron Light Source, Brookhaven National Laboratory, supported by the DOE under Contract No. DE-AC02-76CH00016.

A New Multilayer-Based Grating for Hard X-ray Grating Interferometry

A new kind of x-ray multilayer grating that could open a pathway for high-sensitivity, hard x-ray phase contrast full-field imaging of large samples has been developed by researchers at the National Institutes of Health, Argonne, and Pennsylvania State University. The device produced phase-contrast images of vascular structures in a mouse kidney specimen (Fig. 1) that rival those obtained with magnetic resonance imaging [1]. Such soft-tissue structures were previously invisible to conventional attenuation-based x-ray imaging methods.

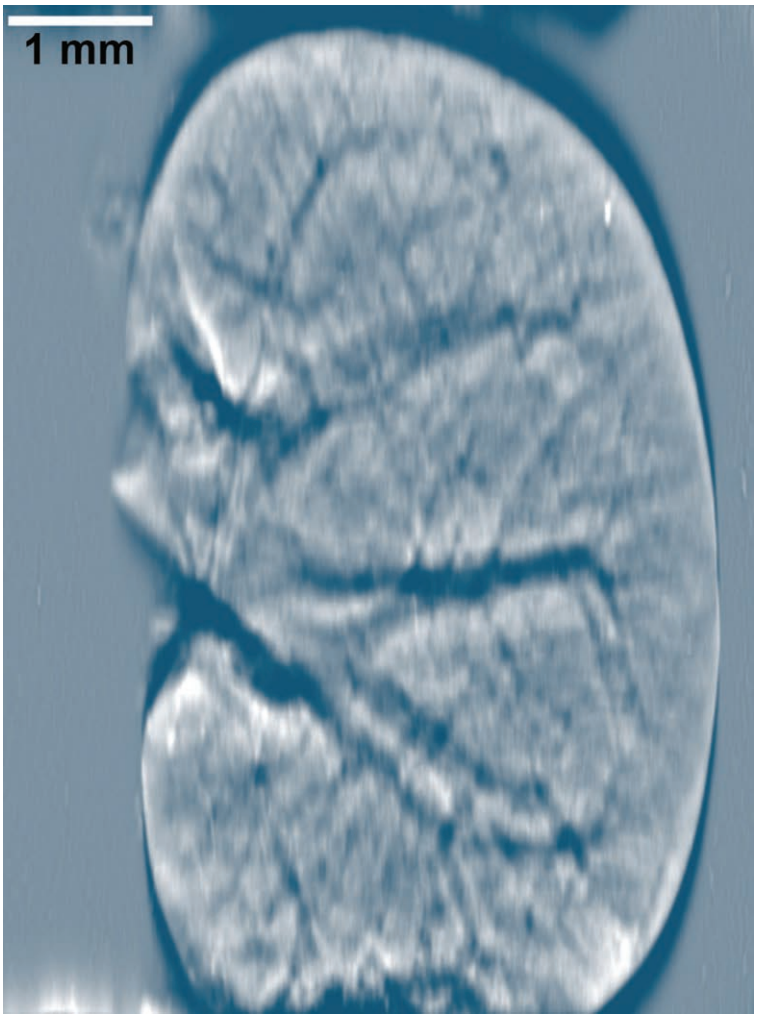

Fig. 1. An image of the phase shift in the mouse kidney, from a Bonse-Hart interferometer built utilizing the new micro-multilayer grating, provides a projection view of the blood vessels. From Han Wen et al., Nat. Commun. **4**, 2659, (November 5, 2013). © 2013 Macmillan Publishers Limited.

The new grating (Fig. 2), with an ultra-small period and theoretically unlimited depth-to-period ratios, is based on a multilayer thin-film-deposition technique utilizing an anisotropic wet-etched staircase on an off-cut silicon (Si) wafer as the substrate. It has a very small grating period that is equal to the bilayer thickness of the multilayer. It also features a large area of the whole staircase with thousands of steps.

The multilayer grating consists of an array of micro-gratings of multilayer sitting on the floor of steps of a staircase Si substrate. The grating period equals the bilayer thickness, and the grating area covers the whole staircase with thousands of steps.

Details of fabrication processes were published in the *Journal of Micromechanics and Microengineering* [2]. The paper has been selected for inclusion in the Highlights 2012 collection of the journal, based on referee endorsement, novelty, scientific impact, and broad appeal.

Grating-based interferometry for x-ray phase-contrast imaging has advanced rapidly thanks to its potential for better image contrast and lower radiation dose over conventional absorption radiography and computed tomography. Phase-contrast imaging is hundreds of times more sensitive than conventional x-ray imaging techniques based solely on absorption contrast. It is especially useful for imaging soft tissue with hard x-rays from synchrotron light sources like the Advanced Photon Source.

Gratings are used to diffract an incident x-ray beam into two beams that pass through a sample and produce an interference pattern at the detector

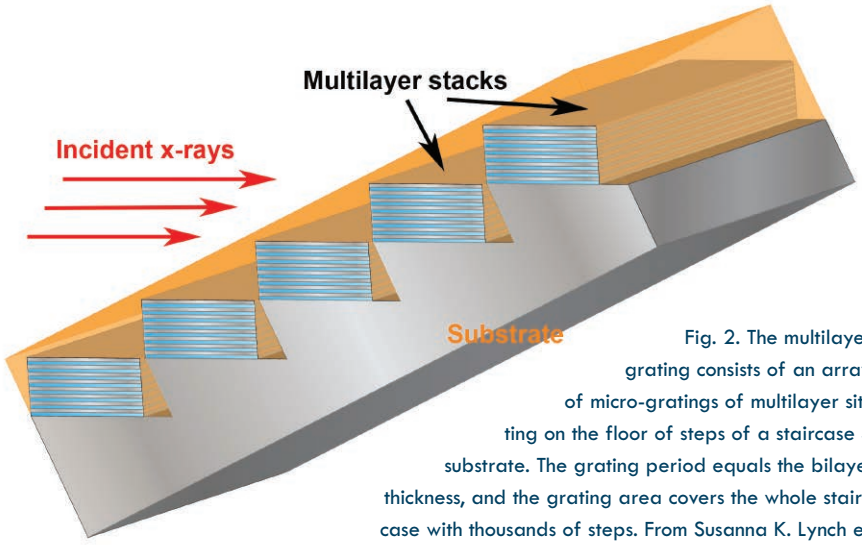

Fig. 2. The multilayer grating consists of an array of micro-gratings of multilayer sitting on the floor of steps of a staircase Si substrate. The grating period equals the bilayer thickness, and the grating area covers the whole staircase with thousands of steps. From Susanna K. Lynch et al., J. Micromech. Microeng. **22,** 105007 (2012).

plane. Variations of the refractive index in the sample lead to a relative difference in the path length, or phase delay, between the interfering beams, which is detectable as a shift of the fringe pattern. Additionally, random scattering of the beams in the sample reduces their mutual coherence, resulting in decreased amplitudes of the interference fringes. A grating interferometer is thus able to detect both x-ray refraction and diffraction in the sample.

A small grating period, which splits and diffracts light into several beams travelling in different directions, will lead to a larger separation between the diffracted beams and thus higher interferometer sensitivity.

Hard x-rays have great penetration power. The interferometer gratings require a sufficient thickness to produce the desired phase shift and absorption. Traditional hard x-ray gratings are fabricated using lithography processes; the grating period is relatively large, and the attainable aspect ratio of the grating is limited.

Multilayer gratings can easily solve the aspect ratio problem. The layers can be as thin as a few nanometers, and the grating can be sliced to many millimeters. However, if a flat substrate is used, the limited height of a single multilayer stack (<50 μm) precludes full-field imaging of large samples.

The new grating with multilayers grown on a staircase substrate, on the other hand, promises both large area detection and small, dense periods. With each stair surface supporting a multilayer as a micro grating and an x-ray beam shining through the layers at an oblique angle to the substrate and parallel to the layer surfaces, the result is a large-area transmission-grating array with small grating periods. This method enables large-area imaging with unprecedented resolution.

Multilayer grating wafers were successfully fabricated at the Advanced Photon Source deposition lab. A 200-nm-period multilayer of tungsten/silicon (W/Si) bilayers was grown on a 20-mm × 20-mm Si staircase substrate with a 28° blaze-angle. The fabricated multilayer grating has a depth-to-period ratio of more than 100:1. The multilayer thickness matches the stair height so that the continuity between adjacent micro-gratings is achieved. A nitride layer was coated before multilayer deposition so that the backside of the Si substrate could be etched away after deposition to reduce x-ray attenuation. The major portion of the multilayer was parallel to the stair surface with a minimal amount on the sidewall. The sample was tilted during multilayer deposition so that the stair surfaces faced the target. Deposition collimators were used to direct the coating flux. Good uniformity of the multilayer was achieved using a profile-coating technique with specific masks made for each sputter gun. A protective epoxy layer was spun onto the multilayer surface after the multilayer was deposited.

Slit diffraction patterns and contact radiography images obtained at XSD beamline 2-BM-B of the APS demonstrated successful intensity modulation by the new grating of a 25-keV x-ray beam. Contact radiography showed intensity modulation at a 200-nm period. The slit diffraction pattern showed 69% of the beam energy diffracted into the ±1 and higher diffraction orders. For comparison, a perfect absorption grating diffracts 50% of the beam energy, while an ideal π phase shift grating with no absorption loss diffracts 100% of the beam energy.

This method opens a pathway for compact x-ray systems to deliver the full benefit of phase contrast to a broad range of applications, such as high-sensitivity x-ray microscopy of pathology specimens that are opaque to optical microscopes, pre-clinical imaging of animal disease models, and non-invasive detection in industrial and material science areas.

Lahsen Assoufid, assoufid@aps.anl.gov;
Francesco De Carlo, decarlo@aps.anl.gov;
Chian Liu, cliu@aps.anl.gov;
Xianghui Xiao, xhxiao@aps.anl.gov
(all Argonne);
Han Wen, han.wen@nih.gov
(National Institutes of Health)

References

[1] Han Wen[1], Andrew A. Gomella[1], Ajay Patel[1], Susanna K. Lynch[1], Nicole Y. Morgan[1], Stasia A. Anderson[1], Eric E. Bennett[1], Xianghui Xiao[2], Chian Liu[2]*, and Douglas E. Wolfe[3], "Subnanoradian X-Ray Phase-Contrast Imaging Using a Far-Field Interferometer of Nanometric Phase Gratings," Nat. Commun. 4, 2659, (November 5, 2013).

[2] Susanna K. Lynch[1], Chian Liu[2]*, Nicole Y. Morgan[3], Xianghui Xiao[2], Andrew A. Gomella[1], Dumitru Mazilu[1], Eric E. Bennett[1], Lahsen Assoufid[2], Francesco De Carlo[2], and Han Wen[1], "Fabrication of 200 Nanometer Period Centimeter Area Hard X-Ray Absorption Gratings by Multilayer Deposition," J. Micromech. Microeng. **22**, 105007 (2012).

Work at the Advanced Photon Source at Argonne National Laboratory was supported by the U.S. Department of Energy Office of Science under Contract No. DE-AC02-06CH11357.

BORLAND OF ASD AWARDED ACFA-IPAC'13 PRIZE FOR ACCELERATOR SCIENCE

• Argonne physicist Michael D. Borland has been awarded the Asian Committee for Future Accelerators ACFA-IPAC'13 Prize for recent, significant contribution to the field of accelerator science. Borland, who is the Associate Division Director in ASD, was cited for "his original contributions in creating the program **elegant** [ELEctron Generation ANd Tracking], and the SDDS [Self-Describing Data Sets] platform, which has marvelous impact on the design and analysis of circular accelerators, energy-recovery linacs, and free-electron lasers [FELs]. Using **elegant**, he predicted, for the first time, the coherent synchrotron radiation-driven microbunching instability in FELs that triggered an active on-going field of research." **elegant** is used by physicists around the world in the design and operation of storage rings, short-wavelength FELs, and other accelerator-based facilities. With **elegant**, accelerator physicists can carry out easily performed simulated experiments that mimic those one might perform on a real accelerator. SDDS offers access to a suite of about 70 generic data processing and display tools that can be used, together with scripting languages like Tcl, to compose customized postprocessing commands. This permits, for example, users of **elegant** to perform an arbitrary number of similar simulations without additional effort in postprocessing. The prize was presented during the Awards Session at the Shanghai International Convention Center during IPAC'13 on May 16, 2013. The ACFA was formed to strengthen regional collaboration in accelerator-based science. In particular, ACFA seeks cooperative ways to facilitate efficient utilization of existing human and material resources, bring up scientists of the next generation, and encourage future projects in Asia and to make recommendations for them to governments. *Contact: borland@aps.anl.gov*

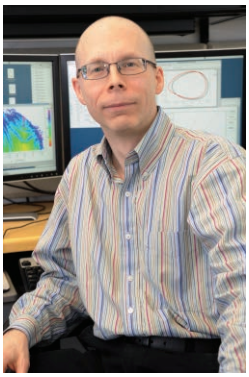

Harkay of ASD Elected American Physical Society Fellow

• Katherine Harkay has been elected to Fellowship in the American Physical Society. Harkay, of the Accelerator Operations and Physics Group in ASD, was cited for "significant contributions to the understanding of the physics of electron cloud effects and the experimental investigation and understanding of collective effects, as well as for playing leading roles in development of photocathodes and superconducting undulator technology." Among the professional accomplishments leading to her Fellowship, Harkay was (with Richard Rosenberg, then of ASD, now with XSD) the first to characterize the electron cloud distribution in a positron storage ring using retarding field analyzers (RFAs) designed by Rosenberg. Through their many collaborations, RFAs are now a standard electron cloud diagnostic in high-energy storage rings, and play a key role in benchmarking electron cloud simulation codes. *Contact: harkay@aps.anl.gov*

USPAS ACHIEVEMENT IN ACCELERATOR PHYSICS AWARD TO KIM OF ASD

• Argonne Distinguished Fellow Kwang-Je Kim of ASD was the recipient of the prestigious 2013 U.S. Particle Accelerator School (USPAS) Prize for Achievement in Accelerator Physics and Technology. Kim was presented with the award for "... a life-time of leadership in beam physics and for significant theoretical contributions improving our understanding of photocathode electron guns, synchrotron radiation and free- electron lasers, and for his work educating young scientists." The USPAS prize honors individuals by recognizing their outstanding achievements over the full range of accelerator physics and technology. The prizes are awarded on a competitive basis without bias to race, sex, and/or nationality. Two USPAS achievement prizes are awarded every two years; this year one of the prizes, awarded to a young scientist under 45 years of age, went to Jean Luc Vay of Lawrence Berkeley National Laboratory. The awards were presented at the 2013 North American Particle Accelerator Conference held in Pasadena, California. *Contact: kwangje@aps.anl.gov*

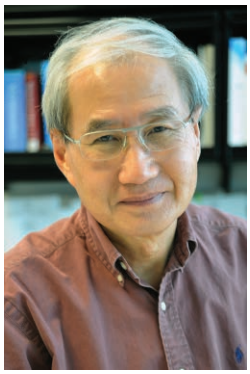

VON DREELE OF XSD RECEIVES HANAWALT AWARD

• Argonne Senior Physicist Robert B. Von Dreele of XSD was awarded the prestigious Hanawalt Award by the International Centre for Diffraction Data (ICDD) "For his insight, courage and creativity in bringing powder diffraction to the macromolecular community." Von Dreele's research focuses on the development of x-ray and neutron powder diffraction and its application to a wide variety of scientific problems. He pioneered the General Structure Analysis System program suite for Rietveld analysis, an exceptionally valuable method for structural analysis of nearly all classes of crystalline materials not available as single crystals. He has been using the Rietveld Method since 1972. His current research is in further extensions of protein powder diffraction including investigation of crystal growth, phase transformations, radiation damage, and exploring possible routes to de novo protein structure determination from powder data. The Award was presented on August 7, 2013, during the Plenary Session of the 62nd Annual Denver X-ray Conference. The J.D. Hanawalt Award is named for Professor J. Donald Hanawalt, whose pioneering work in the 1930s led to the development of the pair distribution function database structure and search/ match procedures still in use today. The award is presented every three years for an important, recent contribution to the field of powder diffraction.

Contact: vondreele@aps.anl.gov

National School on Neutron and X-ray Scattering • August 10-24 • The main purpose of the National School on Neutron and X-ray Scattering is to educate graduate students on the utilization of major neutron and x-ray facilities. Lectures, presented by researchers from academia, industry, and national laboratories, include basic tutorials on the principles of scattering theory and the characteristics of the sources, as well as seminars on the application of scattering methods to a variety of scientific subjects. Students conduct short experiments at Argonne's APS and Oak Ridge's Spallation Neutron Source and High Flux Isotope Reactor facilities to provide hands-on experience for using neutron and synchrotron sources. The target Audience is graduate students attending North American universities majoring in physics, chemistry, materials science, or related fields. The school is jointly conducted by Argonne's Communications, Education and Public Affairs Division; Materials Science Division; and the APS; and Oak Ridge National Laboratory's Biology and Soft Matter, Chemical and Engineering Materials, and Condensed Matter divisions. *Contact: nxschool@dep.anl.gov*

CCP4/APS School in Macromolecular Crystallography: From Data Collection to Structure Refinement and Beyond • June 18-26 • Organized with the National Institute of General Medical Sciences and the National Cancer Institute Structural Biology (GM/CA) facility at the APS, the course is intended mainly for graduate students and postdoctoral researchers in the area of structural biology from across the globe. In some cases, assistant-professor-level applicants can be accepted. The school is designed for applicants with reasonable expertise in crystallography and experience with the CCP4 suite. The purpose of the school is to address specific problems that the applicants face while collecting diffraction data, and while solving and refining novel structures. Applicants with crystals for data collection or with already collected data are given strong consideration, although these are not mandatory requirements. Several of the leading protein crystallography software developers from around the world present lectures and tutorials on their software and are available to help with problems during hands-on sessions of the workshop. *Contact: rsanishvili@anl.gov, garib@ysbl.york.ac.uk, ronan.keegan@stfc.ac.uk*

Revealing the Physics of Nuclei, Atoms, and Molecules with Past, Present, and Future Facilities • April 19 • This symposium brought together international experts in atomic, molecular, optical, and nuclear physics to discuss how a broad variety of scientific facilities, including heavy-ion accelerators, synchrotron storage rings, and free-electron lasers have been exploited to solve a wide range of problems in those fields. The speakers discussed highlights of such past research revealing structures and dynamics of atoms, molecules, and nuclei as well as ongoing research and suggestions for opportunities with future facilities. They showed how a variety of novel experimental techniques were developed to explore the newly accessible parameter space generated by new facilities — the cumulative effect being an evolution of scientific thinking and problem selection. *Contact: young@anl.gov*

Paris-Edinburgh Cell Workshop 2013 • May 23 - 24 • A new program utilizing the Paris-Edinburgh Cell (PEC)-type large-volume press has been developed at the HP-CAT 16-BM-B beamline at the APS. A range of techniques have been integrated for physical property measurements with the HP-CAT existing multi-angle, energy-dispersive, x-ray diffraction capability for structure measurement, to promote comprehensive studies of structure-property correlations in liquids. These include white x-ray radiography, ultrasonic velocity, and falling sphere viscometry techniques. The integrated facility now allows users to make simultaneous observations of the macroscopic phenomena as direct manifestation of the microscopic structure. The new instrumental setup provides a unique opportunity for characterization of liquid and amorphous solid materials at high pressures and high temperatures using synchrotron white x-rays. The Paris-Edinburgh Cell Workshop 2013 is an outreach to potential users in earth science, materials science, physics and chemistry, especially to students, post-doctoral, and young researchers. Emphasis was be on hands-on trainings for those who are interested in using the PEC in their current and future research. A series of talks and a poster session were held to address the current status and potential opportunities in this field.

Contact: pecworkshop2013@hpcat.aps.anl.gov

The 2013 APS/CNM/EMC Users Meeting

Nobel Laureate Brian Kobilka (main photo and inset) gave the keynote address at the 2013 users meeting.

The 2013 meeting of U.S. Department of Energy user facilities at Argonne (officially the 2013 APS/CNM/EMC Users Meeting) was held jointly by the APS, the Center for Nanoscale Materials, and the Electron Microscopy Center on May 6-9. More than 625 attendees representing 42 different countries took in 20 different workshops, plenary sessions, and satellite meetings; more than 160 posters at the poster session; 54 exhibitor companies; and a Nobel Prize winner giving the keynote address.

The meeting, with the theme "Building on Success: Focus on the Future," was opened by Pamela Focia (Northwestern Univ.), Chair of the APS Users Organization (APSUO) Steering Committee. Argonne Director Eric Isaacs welcomed the participants and introduced The Honorable Bill Foster (11th Congressional District of Illinois) and the Honorable Daniel Lipinski (3rd Congressional District of Illinois). Foster and Lipinski represent districts that each claim part of Argonne and both gave enlightening talks on the role of scientific research in furthering the national interest.

In his keynote address, Professor Brian K. Kobilka (Stanford Univ. School of Medicine), co-winner, with Robert J. Lefkowitz (Howard Hughes Medical Institute and Duke Univ. Medical Center), of the 2012 Nobel Prize in Chemistry, discussed the G-protein-coupled receptors research that earned them the Prize. Much of that research was carried out by Kobilka and his team utilizing the National Institute of General Medical Sciences and National Cancer Institute Structural Biology (GM/CA-XSD) facility at the APS (see "The 2012 Nobel Prize in Chemistry: Shining a Bright Light on G-Protein-Coupled Receptors," by Janet Smith, Scientific Director of GM/CA-XSD; and Robert Fischetti, GM/CA-XSD Associate Division Director and Group Leader, in *APS Science 2012*, page 6, http://www.aps.anl.gov/Science/Reports/). As APS Director Brian Stephenson said in his introduction, "Kobilka's work demonstrates the best of what basic research can achieve: the willingness and ability of APS scientists to remove roadblocks so that research demonstrates the best of what light sources can provide."

The cross-facility meeting themes included: "Driving Discovery: Visualization, Data Management, and Workflow Techniques;" "Nanoscale Imaging of Next-generation Materials;" and "Pushing the Boundaries of Energy Technology: Materials Design for Battery Applications." APS plenary sessions included Peter Abbamonte (Univ. of Illinois at Urbana-Champaign) on "Whither Inelastic X-ray Scattering?;" Mark Stalzer (Caltech) on "Trends in Scientific Discovery Engines;" Jay Schuren (Air Force Research Lab.) on "Changing the Paradigm for Engineering Design by Merging High Energy X-ray Data with Materials Modeling;" Paul G. Evans (Univ. Wisconsin–Madison) on "Opportunities for Picosecond Science in the APS Upgrade;" and the invited student talk by Christopher M. Dettmar (Purdue Univ.) on "Second Harmonic Generation for Monitoring X-ray Damage."

Pamela Focia, APSUO Chair, opened the 2013 user meeting.

Argonne Director Eric Isaacs welcomed the attendees on behalf of the Laboratory, and introduced U.S. Representatives Bill Foster, (Ill. 11th) and Daniel Lipinski (Ill. 3rd).

Contact: Susan White De Pace, swd@aps.anl.gov

2013 APSUO Compton Award to Borland, Emery, Galayda, and Moncton

APS Associate Laboratory Director Brian Stephenson (left) with the 2013 Compton Award winners: (left to right) John N. Galayda, David E. Moncton, Louis Emery, and Michael D. Borland.

Top-up operation of synchrotrons has substantially improved both the intensity and the quality of x-ray beams for experiments at light sources. The APS Users Organization (APSUO) 2013 Arthur H. Compton Award presented at the 2013 APS/CNM/EMC Users Meeting to Michael D. Borland (Argonne), Louis Emery (Argonne), John N. Galayda (SLAC National Accelerator Laboratory), and David E. Moncton (MIT) recognized the recipients' visionary leadership and technical ingenuity in introducing top-up operation to the synchrotron radiation community. Top-up is now used in most third-generation light sources worldwide and is integral to the design of new facilities such as the Diamond Light Source (UK) and the National Synchrotron Light Source II at Brookhaven National Laboratory.

Top-up addresses the loss of stored electron beam, or current, in a storage ring. In the original APS operating modes, current was injected every 12 h and then decreased 35% between injections, causing the x-ray intensity to decrease as well, resulting in thermal errors and intensity variations that often limited the length of an experiment and lost x-rays during injection. With top-up, injection is done every 2 min, the current drops only 1%, thermal and intensity transients are minimal, and x-ray production is never interrupted.

In their respective roles as Director of the APS and Director of ASD, Moncton and Galayda identified the critical developments for implementing and verifying top-up operation and advocated for it to users. Borland, a member of ASD, carried out a massive tracking study of the injection process, co-opting many employee workstations after hours. Emery, also a member of ASD, did analytical studies of top-up safety as an independent confirmation, and led the technical effort to implement quiet, automated top-up, overseeing major improvements to many APS accelerator systems. Borland and Emery also collaborated to reduce the electron beam emittance (a measure of beam size) from about 8 nm to about 3 nm, employing top-up to compensate for the attendant lifetime reduction.

The impact of top-up has been important across the spectrum of the APS research program. Protein crystallography and extended x-ray absorption fine structure experiments have particularly benefited from stable beam intensity. Data collected soon after the implementation of top-up mode provided crucial information for solving ribosomal structures, work that was recognized with the Nobel Prize in Chemistry in 2009. The reduction of systematic errors has been important for low-count-rate experiments, such as inelastic and magnetic scattering. Finally, top-up allows the APS to offer unique operating modes (such as 24-bunch and hybrid) that would be impossible without the improvements made to the injection process.

Contact: Susan White De Pace, swd@aps.anl.gov

APS Award for Excellence in Beamline Science to Ilavsky

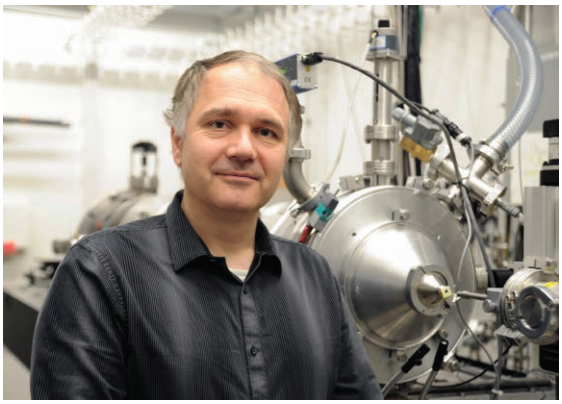

Jan Ilavsky

The inaugural Award for Excellence in Beamline Science at the Advanced Photon Source was presented at the 2013 APS/CNM/EMC Users Meeting to Argonne Physicist Jan Ilavsky, an XSD beamline scientist working in partnership with ChemMatCARS at APS Sector 15. The award recognizes Ilavsky's work in creating the world-leading APS ultra-small-angle x-ray scattering (USAXS) facility for the exploration of materials-based phenomena in pure and applied science.

Under his direction, USAXS has evolved from a "niche" technique to a mainstream capability enabling forefront research in static microstructure relationships as well as dynamics. Areas include nanoparticle formation, growth, aggregation, and stabilization; correlation of microstructure and properties in thermal barrier coatings, xerogels and aerogels, fuel cells, elastomeric materials and superalloys; and dynamics of particle interactions in inaccessible time and size ranges.

The Award for Excellence in Beamline Science at the Advanced Photon Source is intended to recognize beamline scientists who have made significant scientific contributions in their area of research or instrumentation development and have promoted the user community in this area.

This award is conferred each year on an active APS beamline scientist, regardless of employer or rank. It may recognize a career of meaningful, sustained contribution; a body of recent important work; and/or a single work of particular importance. Potential nominees are limited to full-time beamline scientists at the APS with at least half of their time spent on user operations or instrument development.

Contact: Susan White De Pace, swd@aps.anl.gov

Data

X-ray Availability and Reliability

In fiscal year 2013* the APS x-ray source continued to function as a highly reliable delivery system for synchrotron x-ray beams for research. Several factors support the overall growth in both the APS user community and the number of experiments carried out by that community. But there is a direct correlation between the number of x-ray hours available to users; the success of the APS experiment program; and the physicists, engineers, and technicians responsible for achieving and maintaining optimum x-ray source performance. Below are definitions of important measures for the delivery of x-ray beam to users (latest data shown graphically).

Storage Ring Reliability: A measure of the mean time between beam losses (faults), or MTBF, calculated by taking the delivered beam and dividing by the total number of faults. The APS targets, and routinely exceeds, 70 h MTBF. A fault is defined as complete unavailability of beam either via beam loss or removal of shutter permit not related to weather. A fault also occurs when beam has decayed to the point where stability and orbit can no longer be considered reliable. At the APS, this threshold is 50 mA.

APS storage ring reliability (MTBF), fiscal years 1999-2013.

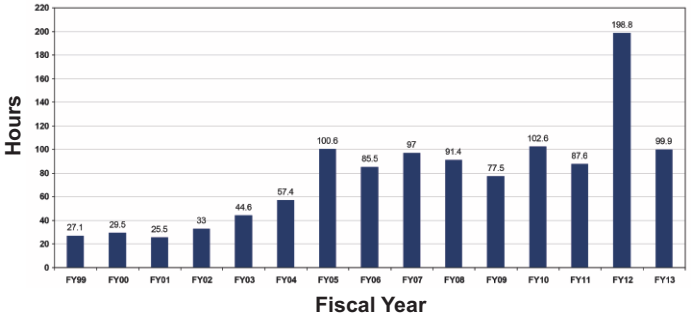

X-ray Availability: The number of hours that the beam is available to the users divided by the number of hours of scheduled beam delivery prior to the beginning of a run. The specific definition of available beam is that the APS Main Control Room has granted permission to the users to open their shutters, *and* there is more than 50-mA stored beam in the storage ring.

APS x-ray availability, fiscal years 1999-2013.

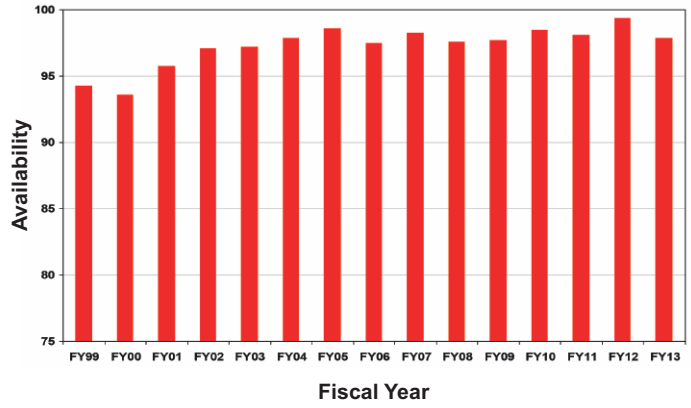

* While the highlights in, and title of, this report cover calendar year 2013, data on accelerator performance and user statistics are measured on the basis of fiscal years.

APS funding levels, fiscal years 2003-2013.

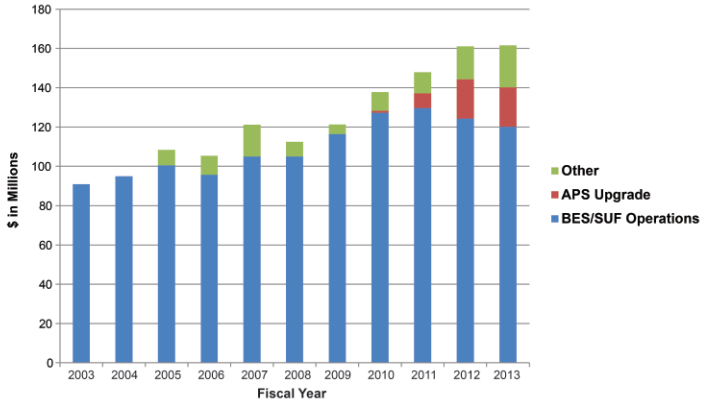

APS staffing levels, fiscal years 2003-2013.

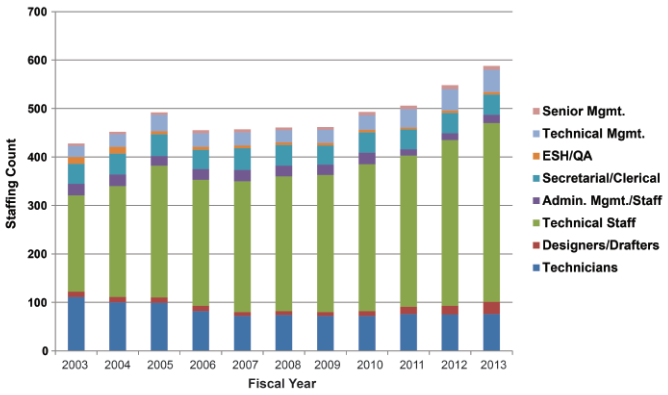

Number of APS publications, calendar years 1998-2012, as of 5.1.14.

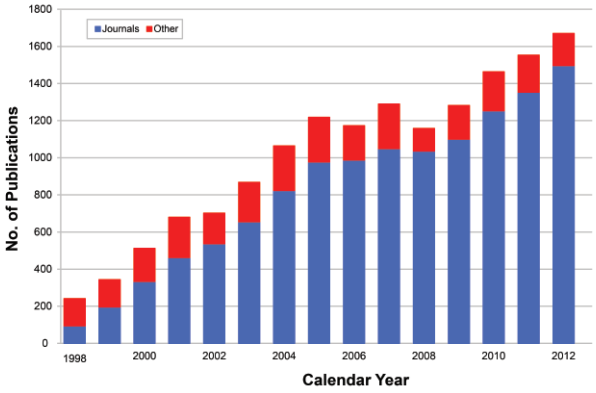

For lists of APS publications see http://www.aps.anl.gov/Science/Publications/

Deposits in Protein Data Bank from research at the APS, calendar years 1998-2012, as of 5.1.14.

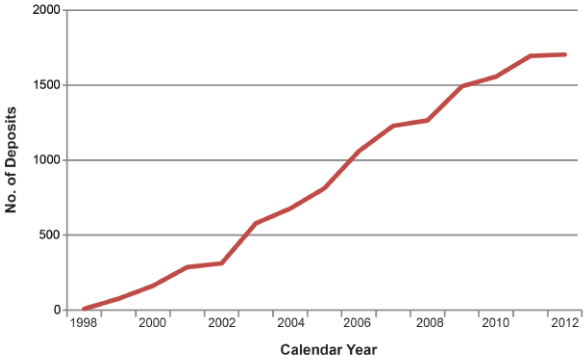

APS users by institution type, fiscal year 2013.

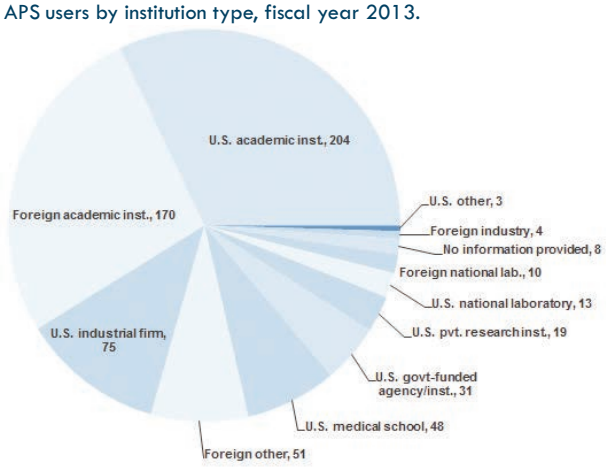

APS users by experiment subject, fiscal year 2013.

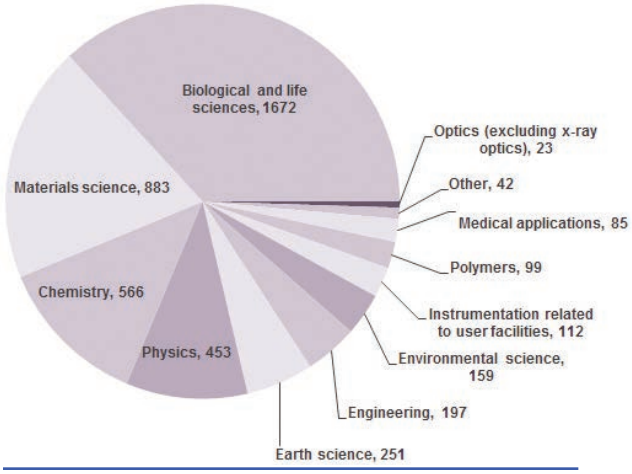

APS users by source of support, fiscal year 2013.

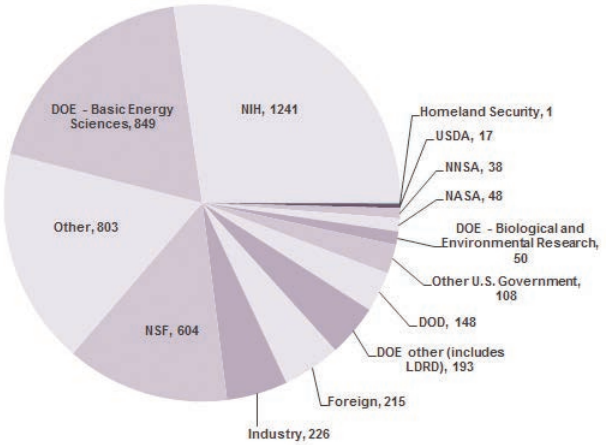

APS users by employer, fiscal year 2013.

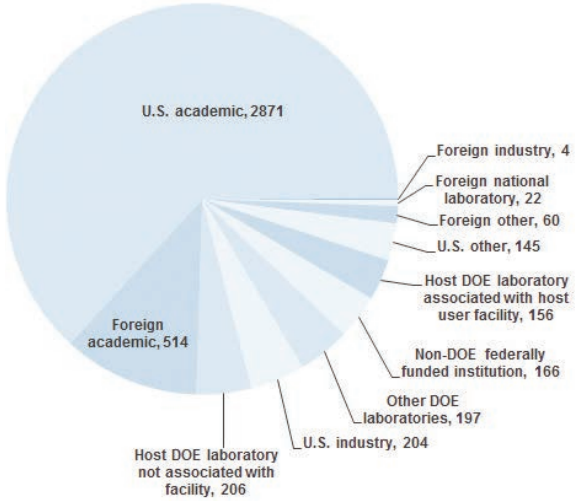

APS users by user type, fiscal year 2013.

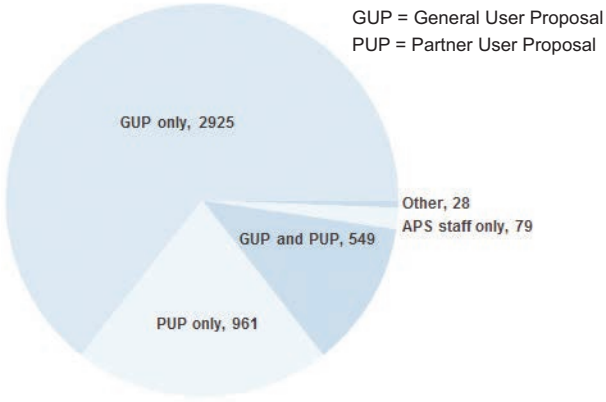

Number of unique on-site & off-site APS users, fiscal years 1998-2013).

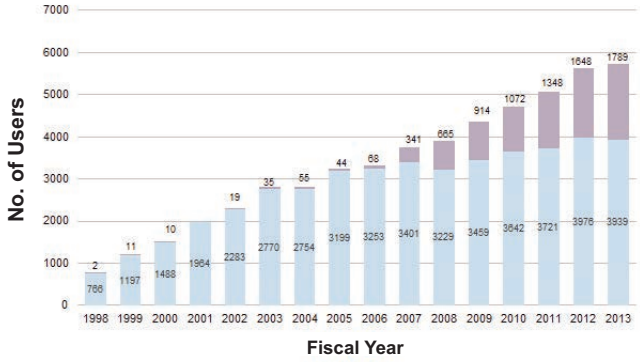

Number of experiments at the APS, fiscal years 1998-2013.

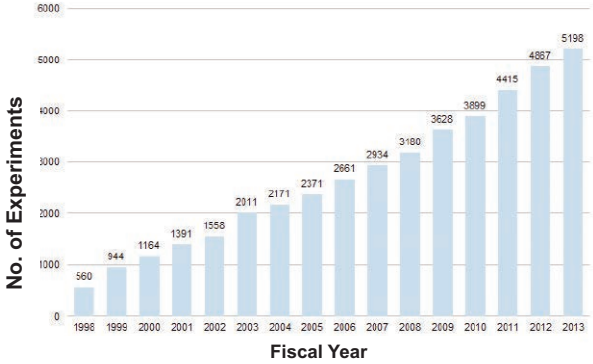

APS users by institutional geographic distribution, fiscal year 2013.

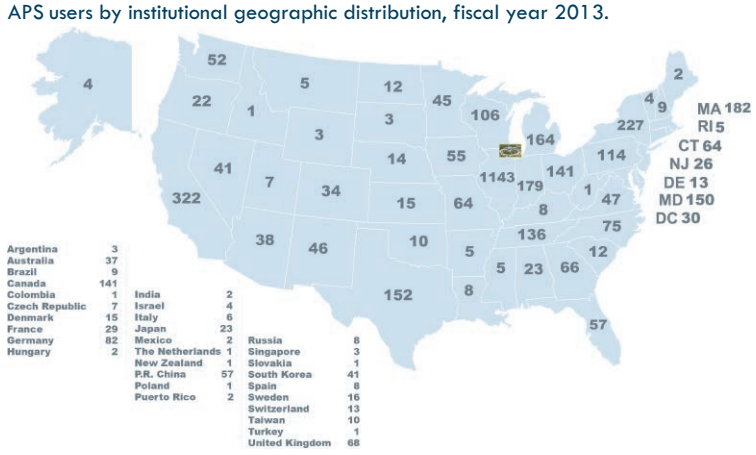

Typical APS Machine Parameters

Linac

Output energy	375 MeV
Maximum energy	450 MeV
Output beam charge	1–3 nC
Normalized emittance	10–20 mm-mrad
Frequency	2.856 GHz
Modulator pulse rep rate	30 Hz
Gun rep rate (1–6 pulses, 33.3 ms apart every 0.5 s)	2–12 Hz
Beam pulse length	8–15 ns
Bunch length	1–10 ps FWHM

Particle Accumulator Ring

Nominal energy	375 MeV
Maximum energy	450 MeV
Circumference	30.66 m
Cycle time	500 ms
Fundamental radio frequency (RF1)	9.77 MHz
12th harmonic RF frequency (RF12)	117.3 MHz
RMS bunch length (after compression)	0.34 ns

Injector Synchrotron (Booster)

Nominal extraction energy	7.0 GeV
Injection energy	375 MeV
Circumference	368.0 m
Lattice structure	10 FODO cells/ quadrant
Ramping rep rate	2 Hz
Natural emittance	69 nm-rad (actual)
	92 nm-rad (nominal)
Radio frequency	351.930 MHz

Storage Ring System

Nominal energy	7.0 GeV
Circumference	1104 m
Number of sectors	40
Length available for insertion device	5.0 m
Nominal circulating current, multibunch	100 mA
Natural emittance	2.5 nm-rad
RMS momentum spread	0.096%
Effective emittance	3.1 nm-rad
Vertical emittance	0.040 nm-rad
Coupling	1.5%
Revolution frequency	271.554 kHz
Radio frequency	351.930 MHz
Number of bunches	24 to 1296
Time between bunches	153 to 2.8 ns
RMS bunch length	40 ps to 22 ps
RMS bunch length of 16 mA in hybrid mode	50 ps

APS Source Parameters

Undulator A (28 insertion devices [IDs])

Period: 3.30 cm
Length: 2.1 m in sectors 16, 21, 23, 24, 34; 2.3 m in Sector 6; 2.4 m in others
Minimum gap: 10.5 mm
B_{max}/K_{max}: 0.892 T/2.75 (effective; at minimum gap)
Tuning range: 3.0–13.0 keV (1st harmonic)
3.0–45.0 keV (1st–5th harmonic)
On-axis brilliance at 7 keV (ph/s/mrad^2/mm^2/0.1%bw):
4.1 x 10^{19} (2.4 m), 4.0 x 10^{19} (2.3 m), 3.3 x 10^{19} (2.1 m)
Source size and divergence at 8 keV:
Σ_x: 276 μm Σ_y: 11 μm
$\Sigma_{x'}$: 12.7 μrad (2.4 m), 12.8 μrad (2.3 m), 12.9 μrad (2.1 m)
$\Sigma_{y'}$: 6.7 μrad (2.4 m), 6.8 μrad (2.3 m), 7.1 μrad (2.1 m)

2.30-cm Undulator (3 IDs in sectors 1, 11, 14)

Period: 2.30 cm
Length: 2.4 m
Minimum gap: 10.5 mm
B_{max}/K_{max}: 0.558 T/1.20 (effective; at minimum gap)
Tuning range: 11.8–20.0 keV (1st harmonic)
11.8–70.0 keV (1st-5th harmonic, non-contiguous)
On-axis brilliance at 12 keV (ph/s/mrad^2/mm^2/0.1%bw): 6.9 x 10^{19}
Source size and divergence at 12 keV:
Σ_x: 276 μm Σ_y: 11 μm
$\Sigma_{x'}$: 12.3 μrad $\Sigma_{y'}$: 5.9 μrad

2.70-cm Undulator (4 IDs in sectors 3, 12, 14)

Period: 2.70 cm
Length: 2.1 m in Sector 12; 2.4 m in others
Minimum gap: 10.5 mm
B_{max}/K_{max}: 0.698 T/1.76 (effective; at minimum gap)
Tuning range: 6.7–16.0 keV (1st harmonic)
6.7–60.0 keV (1st-5th harmonic, non-contiguous)
On-axis brilliance at 8.5 keV (ph/s/mrad^2/mm^2/0.1%bw):
5.7 x 10^{19} (2.4 m), 4.7 x 10^{19} (2.1 m)
Source size and divergence at 8 keV:
Σ_x: 276 μm Σ_y: 11 μm
$\Sigma_{x'}$: 12.7 μrad (2.4 m), 12.9 μrad (2.1 m)
$\Sigma_{y'}$: 6.7 μrad (2.4 m), 7.1 μrad (2.1 m)

3.00-cm Undulator (8 IDs in sectors 12, 13, 16, 21, 23, 30, 34)

Period: 3.00 cm
Length: 2.1 m in sectors 12, 13, 16, 21, 23, 34; 2.4 m in Sector 30
Minimum gap: 10.5 mm
B_{max}/K_{max}: 0.787 T/2.20 (effective; at minimum gap)
Tuning range: 4.6–14.5 keV (1st harmonic)
4.6–50.0 keV (1st-5th harmonic)
On-axis brilliance at 8 keV (ph/s/mrad^2/mm^2/0.1%bw):
4.8 x 10^{19} (2.4 m), 3.9 x 10^{19} (2.1 m)
Source size and divergence at 8 keV:
Σ_x: 276 μm Σ_y: 11 μm
$\Sigma_{x'}$: 12.7 μrad (2.4 m), 12.9 μrad (2.1 m)
$\Sigma_{y'}$: 6.7 μrad (2.4 m), 7.1 μrad (2.1 m)

3.50-cm SmCo Undulator (Sector 4)

Period: 3.50 cm
Length: 2.4 m
Minimum gap: 9.75 mm
B_{max}/K_{max}: 0.918 T/3.00 (effective; at minimum gap)
Tuning range: 2.4–12.5 keV (1st harmonic)
2.4–42.0 keV (1st-5th harmonic)
On-axis brilliance at 7 keV (ph/s/mrad^2/mm^2/0.1%bw): 3.7 x 10^{19}
Source size and divergence at 8 keV:
Σ_x: 276 μm Σ_y: 11 μm
$\Sigma_{x'}$: 12.7 μrad $\Sigma_{y'}$: 6.7 μrad

3.60-cm Undulator (Sector 13)

Period: 3.60 cm
Length: 2.1 m
Minimum gap: 11.0 mm
B_{max}/K_{max}: 0.936 T/3.15 (effective; at minimum gap)
Tuning range: 2.2–11.8 keV (1st harmonic)
2.2–40.0 keV (1st-5th harmonic)
On-axis brilliance at 6.5 keV (ph/s/mrad^2/mm^2/0.1%bw): 2.8 x 10^{19}
Source size and divergence at 8 keV:
Σ_x: 276 μm Σ_y: 11 μm
$\Sigma_{x'}$: 12.9 μrad $\Sigma_{y'}$: 7.1 μrad

5.50-cm Undulator (Sector 2)

Period: 5.50 cm
Length: 2.4 m
Minimum gap: 14.0 mm
B_{max}/K_{max}: 0.965 T/4.96 (effective; at minimum gap)
Tuning range: 0.64–7.0 keV (1st harmonic)
0.64–25.0 keV (1st-5th harmonic)
On-axis brilliance at 4 keV (ph/s/mrad^2/mm^2/0.1%bw): 1.7 x 10^{19}
Source size and divergence at 4 keV:
Σ_x: 276 μm Σ_y: 11 μm
$\Sigma_{x'}$: 13.9 μrad $\Sigma_{y'}$: 8.8 μrad

IEX 12.5-cm Quasi-Periodic Polarizing Undulator (Sector 29)

Period: 12.5 cm
Length: 4.8 m
Circular polarization mode:
Max. currents: horizontal coils 34.4 A, vertical coils 20.7 A
K_{max}: 2.73 (effective; at max. currents)
B_{max}: 0.27 T (peak; at max. currents)
Tuning range: 0.44–3.5 keV (1st harmonic)
On-axis brilliance at 1.8 keV (ph/s/mrad^2/mm^2/0.1%bw): 1.4 x 10^{19}
Linear horizontal polarization mode:
Max. current: vertical coils 47.6 A
K_{max}: 5.39 (effective; at max. current
B_{max}: 0.54 T (peak; at max. current)
Tuning range: 0.24–3.5 keV (1st harmonic)
0.24–11.0 keV (1st–5th harmonic)
On-axis brilliance at 2.1 keV (ph/s/mrad^2/mm^2/0.1%bw): 1.1 x 10^{19}
Linear vertical polarization mode:
Max. current: horizontal coils 50.3 A
K_{max}: 3.86 (effective; at max. current)
B_{max}: 0.37 T (peak; at max. current)
Tuning range: 0.44–3.5 keV (1st harmonic)
0.44–11.0 keV (1st–5th harmonic)
On-axis brilliance at 2.1 keV (ph/s/mrad^2/mm^2/0.1%bw): 1.1 x 10^{19}
Fast polarization switching not required
Source size and divergence at 2 keV:
Σ_x: 276 μm Σ_y: 13 μm
$\Sigma_{x'}$: 13.9 μrad $\Sigma_{y'}$: 8.8 μrad

APS Source Parameters

12.8-cm Circularly Polarizing Undulator (Sector 4)

Period: 12.8 cm
Length: 2.1 m
Circular polarization mode:
Max. currents: horizontal coils 1.34 kA, vertical coils 0.40 kA
K_{max}: 2.85 (effective; at max. currents)
B_{max}: 0.30 T (peak; at max. currents)
Tuning range: 0.4–3.0 keV (1st harmonic)
On-axis brilliance at 1.8 keV (ph/s/mrad^2/mm^2/0.1%bw): 3.1 x 10^{18}
Linear horizontal polarization mode:
Max. current: vertical coils 0.40 kA
K_{max}: 2.85 (effective; at max. current)
B_{max}: 0.30 T (peak; at max. current)
Tuning range: 0.72–3.0 keV (1st harmonic)
0.72–10.0 keV (1st–5th harmonic)
On-axis brilliance at 2.1 keV (ph/s/mrad^2/mm^2/0.1%bw): 2.3 x 10^{18}
Linear vertical polarization mode:
Max. current: horizontal coils 1.60 kA
K_{max}: 3.23 (effective; at max. current)
B_{max}: 0.34 T (peak; at max. current)
Tuning range: 0.58–3.0 keV (1st harmonic)
0.58–10.0 keV (1st–5th harmonic)
On-axis brilliance at 2.1 keV (ph/s/mrad^2/mm^2/0.1%bw): 2.3 x 10^{18}
Switching frequency (limited by storage ring operation): 0–0.5 Hz
Switching rise time: 50 ms
Source size and divergence at 2 keV:
Σ_x: 276 μm Σ_y: 12 μm
$\Sigma_{x'}$: 16.7 μrad $\Sigma_{y'}$: 12.7 μrad

SCU0 Superconducting Undulator (Sector 6)

Period: 1.60 cm
Length: 0.34 m
Gap: 9.5 mm (fixed)
Max. current: 650 A
B_{max}/K_{max}: 0.774 T/1.15 (effective; at maximum current)
Tuning range: 17.5–26 keV (1st harmonic)
17.5–100.0 keV (1st-5th harmonic, non-contiguous)
On-axis brilliance at 87.5 keV (ph/s/mrad^2/mm^2/0.1%bw): 5.3 x 10^{17}
Source size and divergence at 87.5 keV:
Σ_x: 276 μm Σ_y: 11 μm
$\Sigma_{x'}$: 12.3 μrad $\Sigma_{y'}$: 5.8 μrad

APS Bending Magnet

Critical energy: 19.51 keV
Energy range: 1–100 keV
On-axis brilliance at 16 keV (ph/s/mrad^2/mm^2/0.1%bw): 5.4 x 10^{15}
On-axis angular flux density at 16 keV (ph/s/mrad^2/0.1%bw): 9.6 x 10^{13}
Horizontal angular flux density at 6 keV (ph/s/mradh/0.1%bw): 1.6 x 10^{13}
Source size and divergence at the critical energy:
Σ_x: 92 μm Σ_y: 31 μm
$\Sigma_{x'}$: 6 μrad $\Sigma_{y'}$: 47 μrad

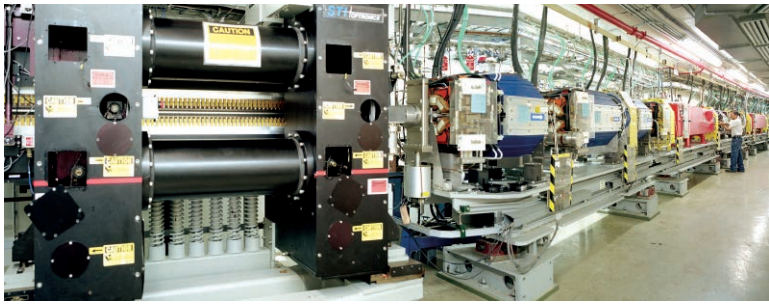

Acknowledgments

***APS Science 2013* Editorial Board:**

Cele Abad-Zapatero (University of Illinois at Chicago), Mark A. Beno (ANL-XSD), Rodney E. Gerig (ANL-PSC), Jonathan C. Lang (ANL-XSD), Dennis M. Mills, (ANL-PSC), William G. Ruzicka (ANL-AES), George Srajer (ANL-PSC), G. Brian Stephenson (ANL-PSC), Linda Young (ANL-XSD), Alexander A. (Sasha) Zholents (ANL-ASD)

The research highlights in this report were written by:

Mary Alexandra Agner (marymary@gmail.com)
William Arthur Atkins (waarc@grics.net)
Erika Gebel Berg (erikagebel@gmail.com)
David Bradley (david@sciencebase.com)
Sophie Bushwick (smbushwick@gmail.com)
Yvonne Carts-Powell (yvonne.cartspowell@gmail.com)
Vic Comello (ANL-CEP, vcomello@anl.gov)
Dana Desonie (desonie@cox.net)
Sandy Field (sfield@fieldscientific.com)
Catherine Foster (scatherinefoster@gmail.com)
Karen Fox (kfox@nasw.org)
Jenny Morber (jenny.morber.business@gmail.com)
Emma Nichols (emma@hittmedicalwriting.com)
Philip Koth (philkoth@comcast.net)
Kim Krieger (mskrieger@gmail.com)
David Lindley (dxlindley@gmail.com)
Mona A. Mort (monasbox@gmail.com)
Chris Palmer (crpalmer2009@gmail.com)
Nicola Parry (nicola@parrymedicalwriting.com)
Neil Savage (neil@stefan.com)
Candice Shaifer (shaiferca@gmail.com)
Michael Schirber (mschirber@gmail.com)
Mark Wolverton (exetermw@earthlink.net)

Photography: Wes P. Agresta, Mark L. Lopez (both ANL-CEP), George Joch (ANL-CEP, ret.)
Aerial photograph of the APS: John Hill (Tigerhill Studio, http://www.tigerhillstudio.com)
Publications, contracts, rights and permissions, circulation: Jessie L. Skwarek (ANL-PSC)
Printing oversight: Gary R. Weidner (ANL-CEP)
CD production: Lorenza M. Salinas and Janet Barrett (both ANL-CEP)
Editorial, project coordination, design, photography: Richard B. Fenner (ANL-PSC)

Our thanks to the corresponding authors and others who assisted in the preparation of the research highlights, to the users and APS personnel who wrote articles for the report, and our apologies to anyone inadvertently left off this list. To all: your contributions are appreciated.

We note with deep sadness the passing of our colleague, Elise LeQuire, on December 9, 2013. Elise was one of the first freelance science writers engaged to produce highlights for *APS Science*. From TheDailyTimes.com (Maryville, TN): “Elise was a graduate of Webb School (Knoxville, 1966). She held degrees from Emory University (B.A., French and humanities, 1970, Vanderbilt University (Ph.D., French, 1977), University of Tennessee (M.S., journalism, 1997). After studies in Paris and living in the south of France, Elise taught French literature and language at Randolph-Macon Woman's College, Lynchburg, Va., 1978-1984. Then, she began a career as feature writer for a number of scientific journals as well as editing others. She was employed by the Argonne National Laboratory, Department of Energy. She was the editor and managing editor for *Forum for Applied Research and Public Policy* from 1995-2001 and the recipient of awards for various journals she edited. She was also an award-winning poet.” Elise was a true professional and her passion for science was evident in her writing. She is missed.

ON THE FRONT COVER: *Clockwise from top:* A high-energy x-ray diffraction pattern from a single grain of icosahedral rare-earth-cadmium quasicrystal, taken with x-ray beam from the APS superconducting undulator at X-ray Science Division (XSD) beamline 6-ID-D and used on the cover of *Nature Materials*; *see page 32*. The structure of the bacterial enzyme NDM-1, determined at the Structural Biology Center Collaborative Access Team beamline 19-ID-D; *see page 122*. A close-up of the levitation stage and a levitated sphere (solid, not liquid - i.e., before melting) in the XSD 6-ID-D research station, used to track the evolution of atomic order in $PdZr_2$ liquid as it cools toward the glass transition temperature; *see page 72*. A three-dimensional tomographic reconstruction of a Pristine Vertebral Ossicle imaged at the GSECARS 13-BM-D beamline; *see page 154*.

ON THE BACK COVER: *Clockwise from top:* Overlay of the distribution of elements calcium, iron, and zinc in the *Medicago truncatula* root nodule, from data obtained at XSD beamlines 2-ID-E and 8-BM-B; *see page 104*. Fluorescence maps obtained at the Center for Nanoscale Materials/XSD 26-ID-C beamline, showing the correlation of zinc oxide pigments (labeled Zn) and iron (Fe) impurities in the house paint "Ripolin blanc de neige," originally sold in France in the early 20th century and used by Pablo Picasso in some of his artwork; *see page 10*. X-ray diffraction patterns obtained at XSD beamlines 11-BM-B, 20-BM-B, and 34-ID-E, showing the crystal lattice structure of three types of light-emitting nanoribbons; *see page 62*.

COVERS BACKGROUND: The interior of the APS storage ring. An Undulator A, source of the APS high-brightness x-rays, is at left. The electromagnets and other instrumentation utilized for circulating electrons at nearly the speed of light can be seen at right. For a color version of this photo see page 205.

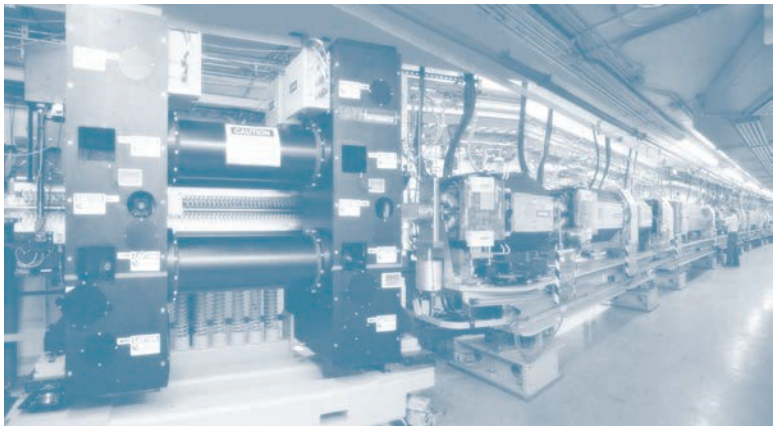

Argonne NATIONAL LABORATORY

Advanced Photon Source
Argonne National Laboratory
9700 S. Cass Ave.
Argonne, IL 60439 USA

www.anl.gov
www.aps.anl.gov

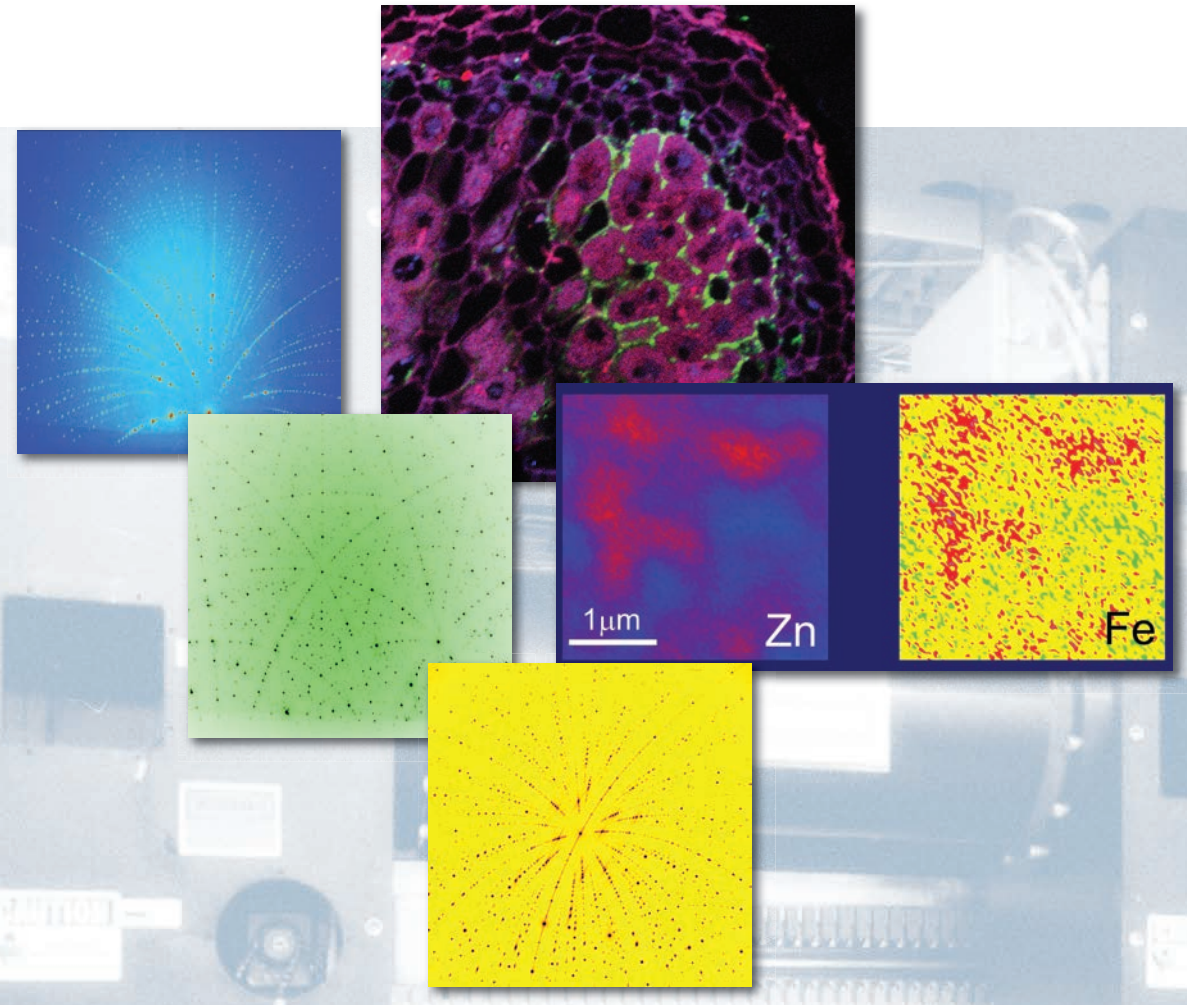

U.S. DEPARTMENT OF ENERGY
Office of Science